AVERAGE ATOMIC NUMBER AND ELECTRON DENSITY ANALYSIS WITH COMPUTERIZED AXIAL TOMOGRAPHY - EXPERIMENTAL AND COMPUTATIONAL FEASIBILITY STUDIES

by

DAVID BRUCE LANING
B.S., University of Wisconsin - Madison
(1975)

S.M., Massachusetts Institute of Technology
(1978)

SUBMITTED IN PARTIAL FULFILLMENT
OF THE REQUIREMENTS FOR THE
DEGREE OF
DOCTOR OF SCIENCE

at the

MASSACHUSETTS INSTITUTE OF TECHNOLOGY
June 1980

Vol I

Signature of Author _____
Department of Nuclear Engineering
June, 1980

Certified by _____
Gordon L. Brownell
Thesis Supervisor

Certified by _____
David D. Lanning
Thesis Supervisor

Accepted by _____
Chairman, Departmental Committee on Graduate Students

AVERAGE ATOMIC NUMBER AND ELECTRON DENSITY ANALYSIS WITH COMPUTERIZED AXIAL TOMOGRAPHY - EXPERIMENTAL AND COMPUTATIONAL FEASIBILITY STUDIES

by

DAVID BRUCE LANING

Submitted to the Department of Nuclear Engineering
on June 19, 1980 in partial fulfillment of the
requirements for the Degree of Doctor of Science

ABSTRACT

Computational and experimental studies of "tomochemistry" were performed. These studies involve the investigation of the feasibility of photoelectric + Rayleigh and Compton attenuation coefficient imaging of a head-like target through the modification of a single-scan computerized axial tomography (CT) scanner. Compositional (tomochemical) information is obtained from these images since the photoelectric + Rayleigh and the Compton attenuation coefficients of a substance are directly related to the weighted-average atomic number and electron density of that substance respectively.

Photon transport studies were performed and design models developed to determine the x-ray tube voltage and spectral filtration of the two incident spectra which could be used to determine the tomochemical information with the maximum accuracy while minimizing the dose to the patient. It was found that in the above context alternated 120 kVp/2.16 mm Fe-filtered and 120 kVp/130 μm Ta-filtered spectra are the best when filter modulation alone is used, while 150 kVp/2.16 mm Fe-filtered and 120 kVp/130 μm Ta-filtered spectra are the best when simultaneous kVp/filtration modulation is used. For a single 10 second/fixed 120 kVp/30 mA scan with the above filtrations the absorbed surface dose was determined to be about 1.8 Rad.

The results of the photon transport studies served as a basis for the design of the proof-of-principle experiment. A conventional CT scanner was modified to perform tomochemistry by adding a device which modulated the x-ray filtration so as to obtain the required x-ray transmission information. Also, calibration and data processing methods were developed to reconstruct photoelectric + Rayleigh and Compton attenuation coefficient images from the two spectra x-ray transmission measurements.

Proof-of-principle experiments were performed to test the performance of the integrated tomochemistry scanner system. From experimental measurements it was found that the theoretical minimum of the statistical uncertainty of the reconstructed attenuation coefficients in the center of the image is about 0.2% for the conventional image, 7.5% for the photoelectric + Rayleigh image and 0.6% for the Compton image when measurements are averaged over a 5mm x 5mm pixel area. It was also found that at a spatial resolution of 4 mm tomochemistry measurements could accurately predict the photoelectric + Rayleigh and Compton attenuation coefficients near the edge of the image. However, it was found that due to systematic errors of the polynomial fits at large solution thicknesses the accuracy of the reconstructions were poorer in the center of the images. Finally, it was found that tomochemical measurements could be used to distinguish between material properties that normal CT do not readily image.

Thesis Supervisor:	Dr. Gordon L. Brownell
Title:	Professor of Nuclear Engineering
Thesis Supervisor:	Dr. David D. Lanning
Title:	Professor of Nuclear Engineering

Dedication

To Anita Sarosiek for adding a new dimension to my life.

Acknowledgments

I would like to thank all those people who aided in bringing this research project to a successful completion. In particular I would like to thank Professors Gordon L. Brownell and David D. Lanning for their advice and direction throughout this research project. Professor Brownell was particularly effective at aiding the author in maintaining an overview of this research project and in attaining an appreciation of the relevance of this work to the medical research community. Conversely, Professor Lanning was highly effective at making sure that the author did not overlook the engineering details which were crucial to the success of this research project.

I would like to thank Tim Walters, Dave Kaufman, Charlie Burnham, Dave Chesler, Joel Lazewatsky, and Wesley Akutagawa of the MGH Physics Research Laboratory for their aid with much of the technical work in this thesis. Tim Walters deserves special mention for his invaluable insight into the mechanics of the MGH scanner software. Without his truly professional help it would have been extremely difficult to understand most of the peculiarities of the pre-thesis software or to develop the new software required in this project. Dave Kaufman was also very helpful as an extra pair of skilled hands to help put the experiment together as well as to help find the gremlins that always seem to sneak into electronics systems.

The author would also like to acknowledge the financial support of the Nuclear Engineering Department as well as the two years of support received from the Whitaker Health Sciences Fellowship Fund.

Thanks are also extended to Priscilla Kelly and Jane Patterson for typing the manuscript and taking the time to do the job right. Priscilla Kelly deserves special mention for the excellent way in which she layed out the format of the text, formulas, tables, and figures.

Particular appreciation is expressed to Greg Greeman, Kord Smith, Neil Novich, Mark Broussard, Mark Gottlieb, Kim Kearfott, Manzar Ashtari, Owen Deutsch, Bob Zammenhof, Sue Best, Tommy Thomas, Steve Herring, Dave Boyle and all the other students and faculty I have met at MIT for their encouragement, friendship, and camaraderie during my studies in the Nuclear Engineering Department. I will certainly remember with fondness the student-faculty dinners, the semi-annual picnics, the post-generals parties, and all the other 'educational' experiences within the department.

I would also like to thank my parents and my brothers and sisters for their continuing confidence and optimism throughout my education. Also, I would like to thank my friends who went to school with me at the University of Wisconsin. In particular, I would like to thank Robert Wood, Jeff Archibald, Mike Cain, Tom Prijic, and Nick Sharrow for their continuing encouragement and friendship. To have friends like these make me feel like a rich man.

Finally, I would like to thank my wife, Anita Sarosiek. It was her love, friendship, understanding, patience, humor, and affection that gave me hope when there was no hope, new enthusiasm when things were going wrong, and strength when I needed it the most.

Biographical Note

The author was born in Milwaukee, Wisconsin on September 18, 1953. He was raised in Milwaukee and his high school education was within the public school system. In high school he was active in athletics, student government and other activities. In his senior year he was the gymnastics team captain and he placed second and seventh in the city and state gymnastics championships, respectively. He graduated from John Marshall High School with the highest academic honors and he was chosen as the outstanding high school athletic-scholar of 1971 by the Common Council and Mayor of the City of Milwaukee.

In September of 1971 he entered the University of Wisconsin-Madison. There he was supported by a combination of state scholarships and work-study jobs within the experimental physics research laboratories at the University. The experimental physics work included a two year term as a visiting scientist at the Fermi National Accelerator Laboratory in Batavia, Illinois. Besides the commitment to academics the author was for two years active within the University as a University cheerleader. In 1975 he graduated from Wisconsin Summa Cum Laude with a B.S. in Engineering Physics and Applied Mathematics.

The author entered the Massachusetts Institute of Technology in September of 1975. He was supported for the first three semesters as a teaching assistant in the Nuclear Engineering Department and for the following two years the author was the recipient of the Whitaker Health Sciences Fellowship. In June of 1978 the author received an S.M. in Nuclear Engineering from M.I.T.

After completion of his S.M. degree the author was married to Anita Sarosiek in August of 1978.

Upon completion of his thesis, the author plans to work at the Oak Ridge National Laboratory in Oak Ridge, Tennessee where the author will work within the Instrumentation and Controls Division as a Eugene Wigner Fellow.

The author is a member of the American Nuclear Society, the American Physical Society, the Institute for Electrical and Electronics Engineers, Phi Beta Kappa, Phi Kappa Phi, and Sigma Xi.

Table of Contents

Page

Page

List of Figures

List of Tables

1.0 Introduction

With the development of computerized axial tomography by Godfrey Hounsfield (H.1) a new dimension has been added to the fields of radiology and non-destructive examination. Computerized axial tomography (CT) scanners scan thin cross sectional slices of the body yielding two dimensional grey scale images of the spectrum averaged x-ray attenuation coefficients versus position within those slices. CT scanning is a very accurate radiographic method with typical CT scanners capable of determining the spectrum averaged attenuation coefficients with an error of less than 0.5% at a resolution of 1-2 mm.

Within the diagnostic energy region (0-150 keV) there are three basic physical processes which cause the attenuation of photons in matter: Compton scattering, Rayleigh scattering, and photoelectric absorption. Furthermore, the magnitudes of these processes depend upon the "average" atomic number and electron density of the target being scanned as well as the energy of the incident x-rays. Hounsfield was the first to suggest (H.1) that if two different CT scans are performed on the target at two different x-ray energies it is possible to obtain a grey scale image of the electron density as a function of position and another grey scale image of the "average" atomic number. This method of obtaining composition information through the use of computerized axial tomography is commonly referred to as tomochemistry.

The principle objective of this thesis is to determine experimentally and theoretically the engineering considerations which go into the design of a scanner which can perform tomochemistry in a

single scan. At this point it should be made clear that no attempt will be made to determine the medical efficacy of tomochemistry. The intent rather is to present the methods and results of an optimal experiment design, the new data processing methods developed, and the results of the proof-of-principle experiments. As will be seen later, the fundamental physical assumptions, hardware design, and software methods all in some way limit the quantitative accuracy of tomochemistry.

1.1 General Description of a CT Scanner and Its Images

Since shortly after the discovery of x-rays by Roentgen in 1895, x-rays have been used to image the internal structure of the body. Typical radiographs are projection images of the transmission of x-rays through the body (Fig. 1.1.1). A broad beam of x-rays incident upon the patient is attenuated by the body. Some of those x-rays which are transmitted by the body are detected by a film detection medium on the opposite side of the body. The internal structure image is formed by the relative attenuation of the x-rays along different paths. Hence, in those paths where the photon attenuation is high, such as with the presence of bone, the radiographic film is less exposed than in those paths where the photon attenuation is low, due to the presence of air cavities or soft tissue.

The radiographic projection method has become widely used in the medical profession because it has two advantages. The first is that film radiography can give spatial information on internal structures of the body noninvasively at a relatively acceptable risk to the patient. With spatial resolutions of $\sim$5 line pairs per millimeter (J.1), the images are sufficiently sharp for imaging most structures of the body. The second advantage of film radiography is that radiographs of the patient can be made in a few seconds and then developed in a matter of minutes so that the physician can make a diagnostic assessment of the patient rapidly and accurately.

However, in spite of projection radiography's simplicity and ease of use, there are two main problems with the simple radiographic method. First, the x-ray projection method may mask important

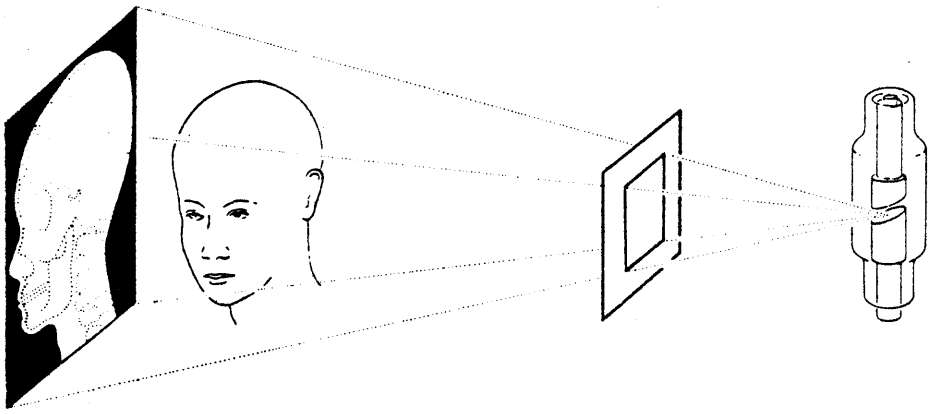

Figure 1.1.1 Illustration of the typical x-ray projection radiographic method (J.1).

information the physician needs for diagnosis. In particular, overlying or underlying tissue may mask the desired information because the depth dimension is lost when one compresses three dimensional information into two dimensions. The second main problem of film radiography is that the photographic density of a developed image is a nonlinear function of the x-ray exposure. Thus, accurate quantitative radiography is difficult to perform with film systems.

To help suppress undesirable image structures the method of linear tomography was developed. In this method, as illustrated in Fig. 1.1.2, the x-ray tube and film move simultaneously in opposite directions. This motion causes blurring of the structures to occur in all planes except the one to be visualized. By moving the imaging system up or down one can then observe structures in different planes within the patient. Although linear tomography improves the capability of radiologists to determine spatial information, it uses a film system; therefore quantitative radiography is still difficult to perform with linear tomographic scanners. Furthermore, linear tomographic scanners cannot improve the radiographic situation when the soft tissue of interest is enclosed within bone (as in the case of the brain).

In 1971 the first radiographic system which could unravel the radiographic projection information was introduced by EMI Limited: the computerized axial tomographic (CT) scanner. The original clinical

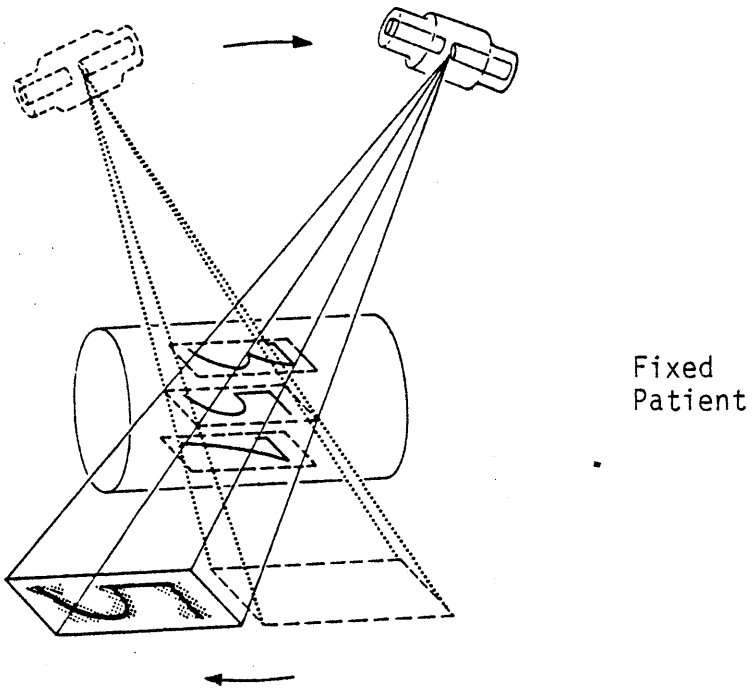

Figure 1.1.2 Schematic illustration of the linear tomographic method (J.1).

CT scanner, invented by Godfrey Hounsfield* (H.1), was intended for head scanning only. In Hounsfield's first machine the patient was positioned within a gantry holding an x-ray tube and a single detector as shown in Fig. 1.1.3. The scan would be performed by translating the x-ray tube and detector past the head at a fixed gantry angle. At about 200 discrete positions along the line of the translation a pencil x-ray beam was used as a probe to measure the line integral of photon attenuation given by the expression (monochromatic source of energy E):

$$\frac{I}{I_o} = \exp\left[- \int_A \mu(\bar{r},E)\, d\ell \right] \qquad (1.1.1)$$

where:

$\mu(\bar{r},E)$ is the macroscopic photon cross section (attenuation coefficient) for photons of energy E at vector position $\bar{r}$ which lies on ray A

I/I_o is the ratio of the current measured by the detector when the patient is within the x-ray beam to that current measured with no patient in the beam

As shown in Fig. 1.1.4, after one translational measurement was completed the gantry would then be rotated by 1° and the machine

*It is interesting to note that Hounsfield was not the first to come up with the idea of computerized axial tomography (D.2). However, he alone was successful in developing a clinical machine because he was able to synthesize a practical design by drawing upon the fields of mechanical and electrical engineering, computer science, and diagnostic radiology.

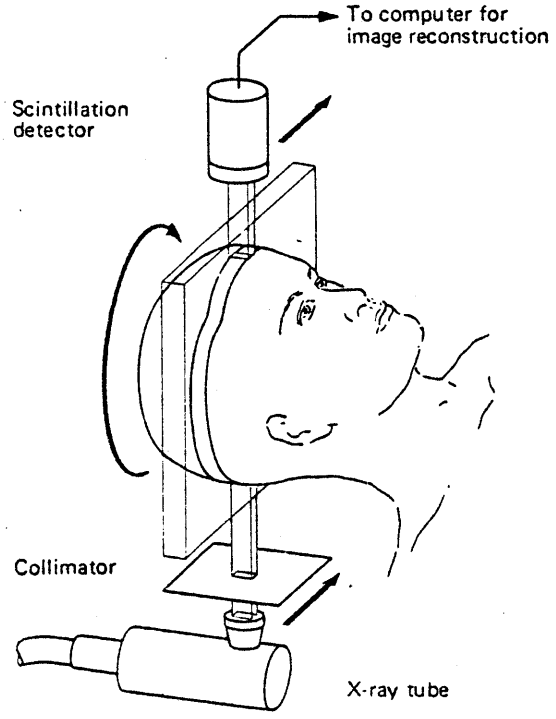

Figure 1.1.3 Diagram of the pencil x-ray beam arrangement used to measure the attenuation coefficient line integral (J.1).

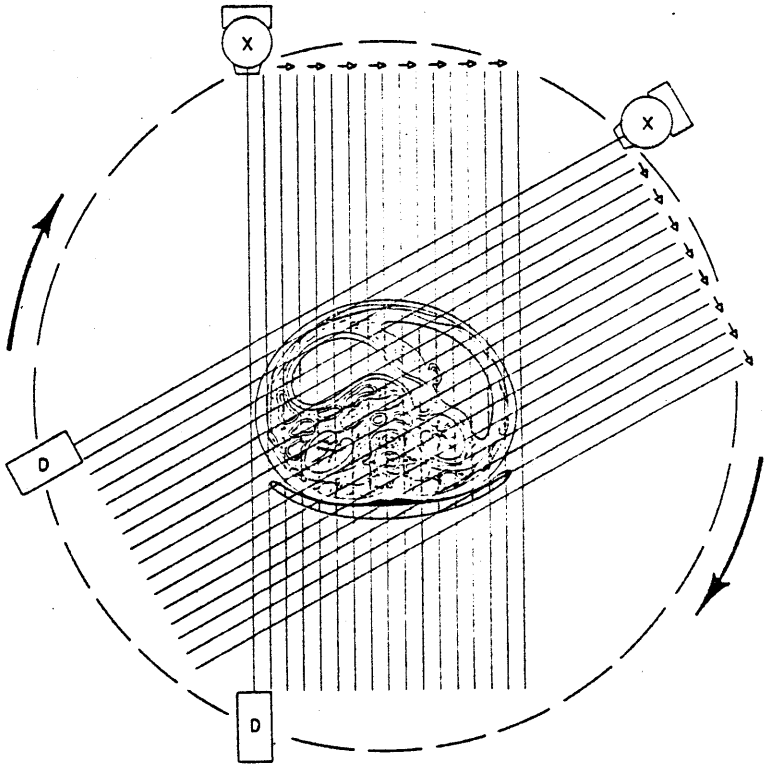

Figure 1.1.4 Schematic diagram of the translate-rotate scan method used in the first commercial CT scanner.

would commence another translational measurement. This process would be repeated for 180 translational measurements so that when the scan was completed the gantry would be rotated by one-half of a turn. The entire scanning process took about 5 minutes. By scanning the head using the above method 180 sets of 200 parallel ray measurements of photon attenuation were obtained. These measurements, digitized and stored in a computer, then served as the basic data set of the tomographic reconstruction.

The reconstruction of the image, as performed by the first scanner, was done by a matrix inversion of the basic data set. Conceptually, the computer reconstruction program would ask the rhetorical question: "Which two dimensional matrix of attenuation coefficients versus position would yield the set of line integrals measured in the scan?".

Once the two-dimensional matrix of attenuation coefficients* had been determined, they were displayed on a cathode ray tube (CRT) using a grey scale format as illustrated in Fig. 1.1.5. The reconstruction

---

*A more common unit used by CT scanners is the Hounsfield unit which is defined as:

$$H(\bar{r}) = \frac{(\bar{\mu}(\bar{r}) - \bar{\mu}_{water})}{\bar{\mu}_{water}} * 1000$$

where:

$H(\bar{r})$ is the Hounsfield unit determined at point $\bar{r}$

$\bar{\mu}(\bar{r})$ is the spectrum averaged attenuation coefficient at point $\bar{r}$ in the body for the incident spectrum used.

$\bar{\mu}_{water}$ is the spectrum averaged attenuation coefficient for water for the incident spectrum used.

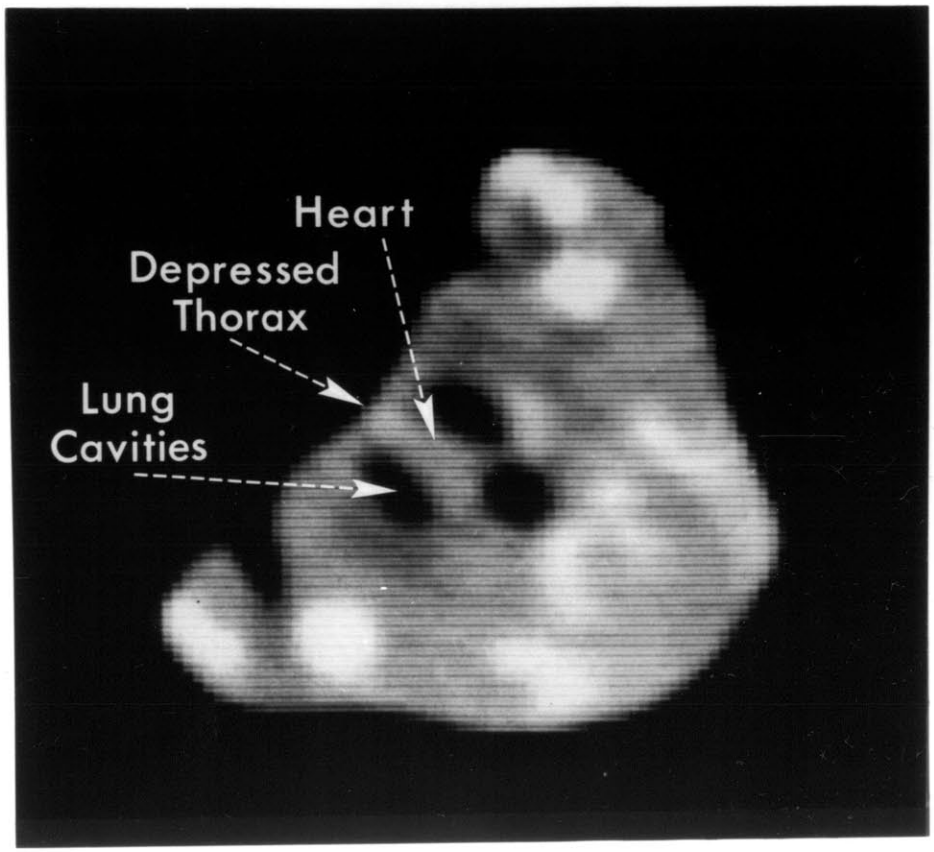

Figure 1.1.5 Illustration of the CRT grey scale format display of a reconstructed image.

in Fig. 1.1.5 is that of a slice of a kitten scanned in the thoracic region. Note that one can clearly see the lung cavities, bones, and other anatomical features. In this image a window of reconstructed attenuation coefficients is chosen for display. Those reconstructed attenuation coefficients which are less than the window minimum are displayed as black. Similarly, reconstructed attenuation coefficients greater than the window maximum are displayed as white. Those attenuation coefficients which lie between the window minimum and maximum are displayed by linearly relating them to the grey level scale.

Since the introduction of Hounsfield's first machine in 1971, a large number of technological developments have occurred which have increased the speed, accuracy, and spatial resolution of CT scanners. By increasing the number of detectors, using more powerful x-ray tubes, developing faster and more sophisticated image reconstruction methods, and improving the mechanical design, 5 second scanners were developed which could scan any anatomical section of the body. Figure 1.1.6 shows the relative dimensions of these higher generation machines with respect to the patient.

One of the main features of these higher generation machines, as seen in Fig. 1.1.7, is the continuous rotation scan method. In this setup a collimated fan beam of x-rays is incident upon the patient. The photon attenuations within the slice being scanned are then measured by a bank of $\sim$250 detectors on the opposite side of the patient. Typically, these scanners measure about 360 views in one full revolution of the gantry. The x-ray tube used for these scanners is most commonly a rotating anode x-ray tube. These tubes are used

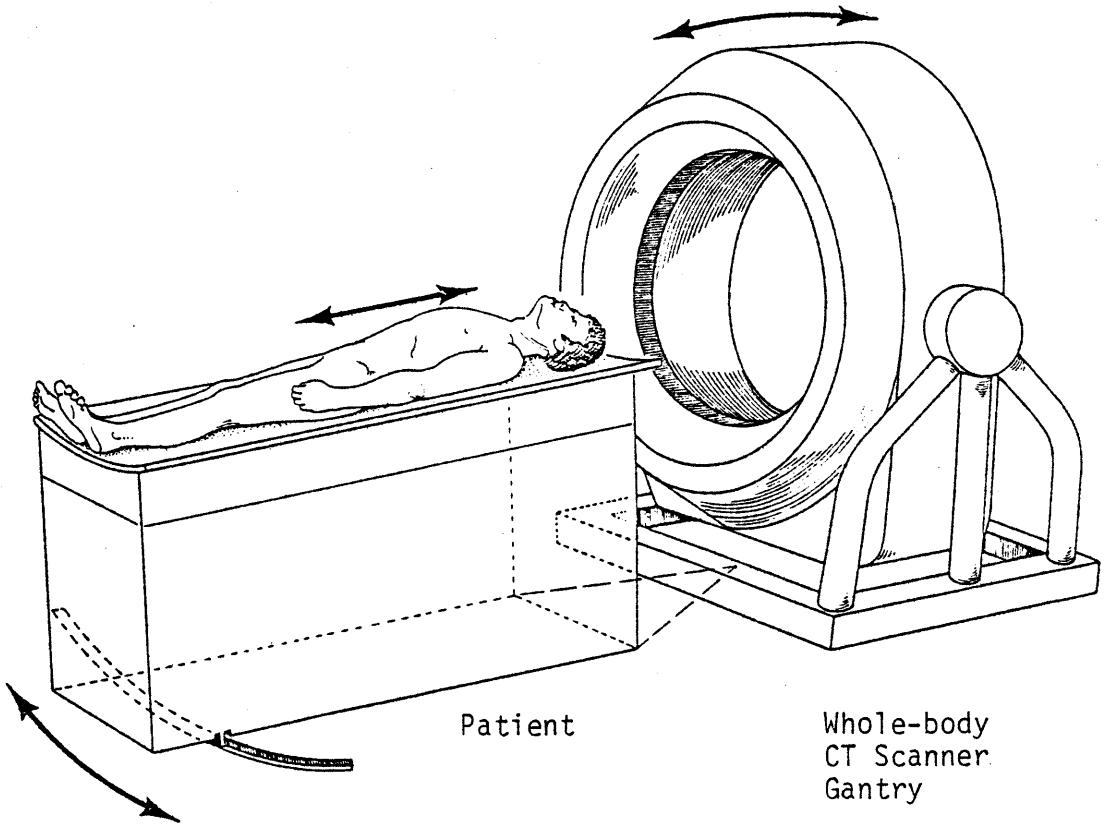

Figure 1.1.6 Typical relative dimensions of a whole-body CT scanner.

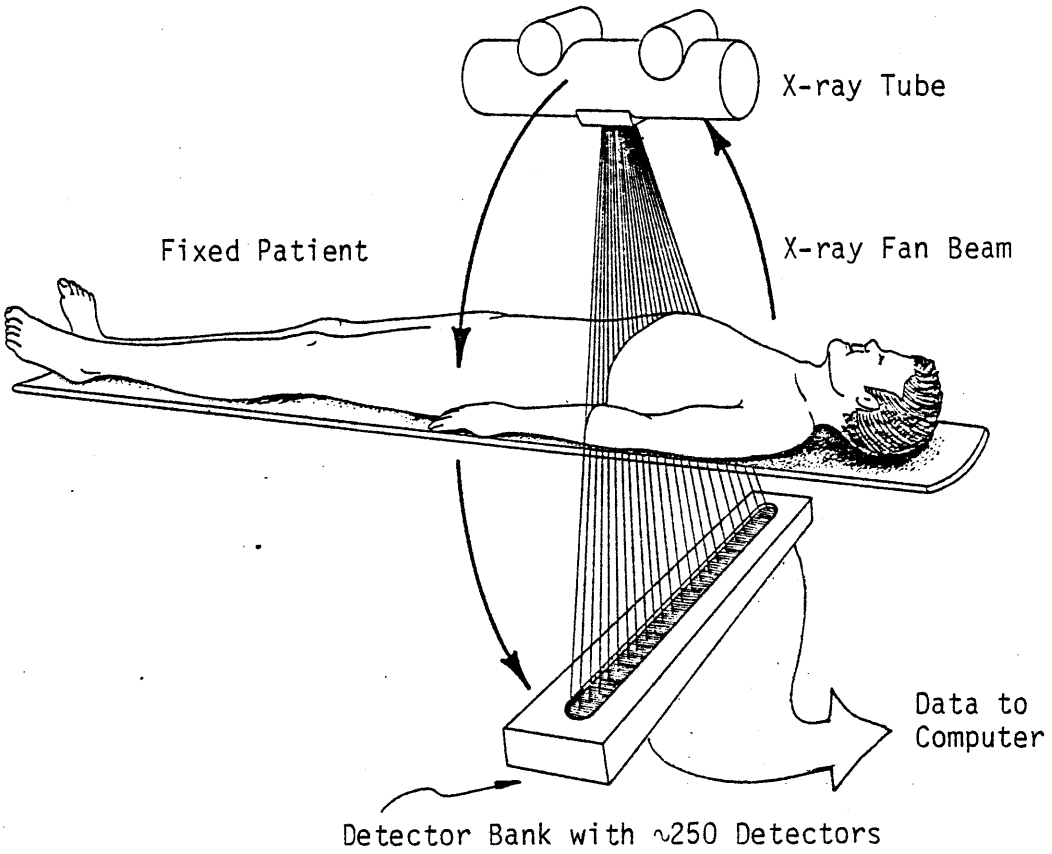

Figure 1.1.7 Illustration of the continuous rotation method of scanning used in whole-body CT scanners.

because they can be run at about 100 mA electron current on the anode target at kilovoltage potentials between 100 and 150 peak kilovolts (kVp). Furthermore, these tubes have a small ($\sim$ 1 mm^2) focal spot size which is important when trying to perform high resolution radiographic imaging. The 250 detectors, which simultaneously measure the photon transmission along the different ray paths, are either of the ionization chamber type or of the scintillation crystal-photon multiplier type. Both of these detector types are run in the current mode in CT scanners due to the high photon-flux rate. These detectors are then interfaced to a dedicated minicomputer which controls the detector data input and output (I/O) and also stores and reconstructs the measured data. With this improved design these CT scanners can scan the body in 3 to 20 seconds - depending upon the manufacturer. Figure 1.1.8 summarizes the major characteristics of present generation CT scanners.

Because of the highly competitive nature of CT scanner manufacturing, research and development of scanners is of a proprietary nature. Hence, in an effort to bring pertinent research information into the public domain a fundamental research project was initiated at the Massachusetts General Hospital's Physics Research Laboratory. In this project a benchtop device was developed which could be used to investigate the fundamental limitations and abilities of CT scanners. In this device, a schematic of which is given in Fig. 1.1.9, the x-ray tube and detector bank are fixed while the unknown target of interest is rotated in 10 seconds on a rotating table. The major characteristics of this device are listed in Table 1.1.1.

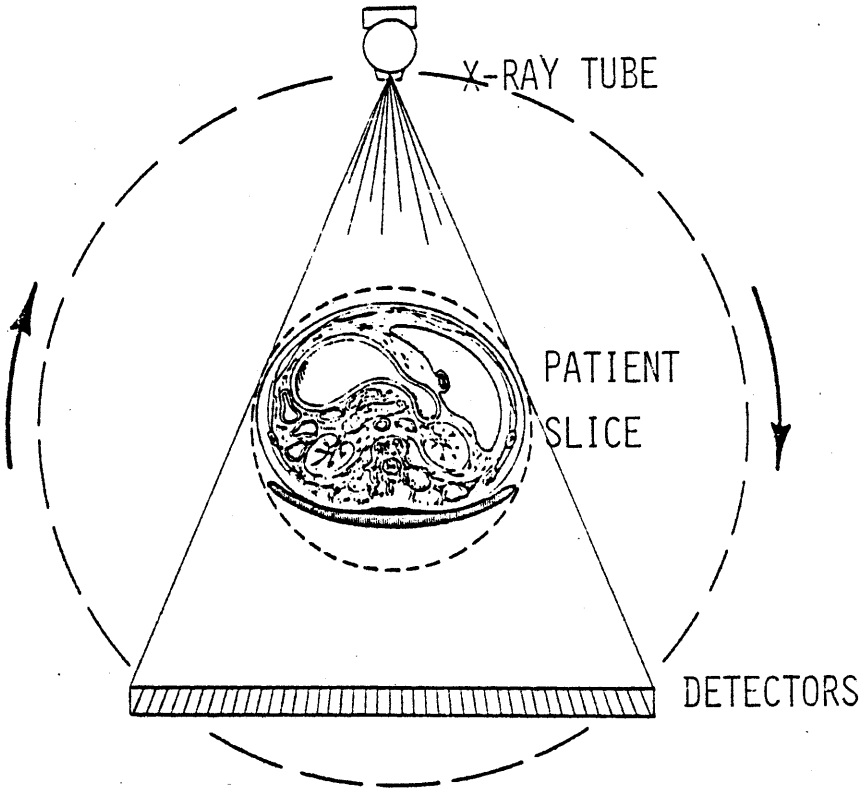

Key Characteristics:

Fan x-ray beam intersects a slice of the body. 256 detectors make simultaneous measurements. X-ray tube is used due to high photon flux and point source requirements. Rotate source and detector around in 5 seconds.

Figure 1.1.8 Summary of the major characteristcs of fan beam whole-body CT scanners.

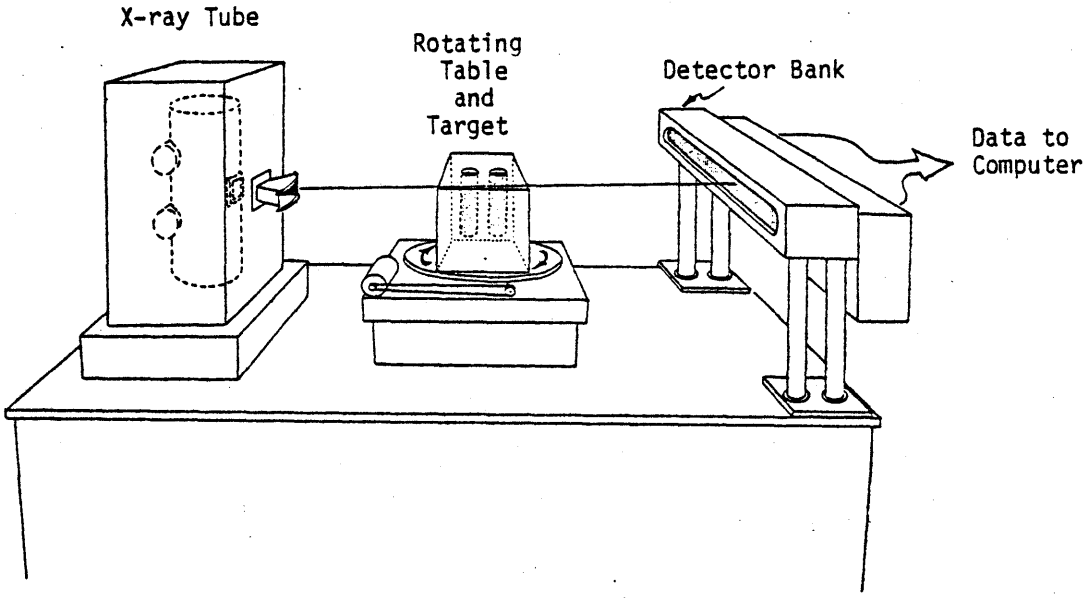

Figure 1.1.9 Schematic diagram of the MGH benchtop CT scanner.

Table 1.1.1

Typical Physical Parameters
in a CT Scanner

MGH X-Ray Scanner:

Scan Time	5 seconds
Detectors per Slice	256 detectors
Number of Slices	1
Slice Thickness	5 - 10 mm
Angle of Rotation	360 degrees
Matrix Format	320 x 320
X-Ray Source	140 kVp
X-Ray Absorption Accuracy	0.5%
Spatial Resolution	2 mm
Data Set (No. Detectors x No. Samples)	256 x 600 = 154,000

The use of this scanner for fundamental research has two main advantages over commercial machines. First, this device is not committed to a clinical schedule and therefore studies can be performed without interferring with clinical use. Second, due to the non-proprietary nature of this device, changes can be made to any part of the scanner system (hardware or software) without conflict with a manufacturer. Because of the relative ease with which hardware and software changes could be made with this machine, all of the experimental and theoretical development work described in this thesis was performed with this scanner.

1.2 Underlying Physical Principles of, and Motivation for, Composition Analysis CT (Tomochemistry)

This thesis deals with an intriguing extension of CT called tomochemistry. Tomochemistry, first mentioned by Hounsfield (H.1) and developed further by Alvarez and Macovski (A.1), refers to the analysis of CT data to obtain images of the electron density and the weighted-average elemental composition within the scanned body slice. To understand the principle of tomochemistry, it is easiest to first consider the methodology for monochromatic photons. When a monochromatic diagnostic energy (0-150 keV) photon is attenuated by matter, it interacts with that matter in one of three ways:

(1) photoelectric absorption

(2) Compton scattering

(3) Rayleigh scattering.

Furthermore, it has been shown (W.1, W.2, W.3) that in a limited energy range one can express the total attenuation coefficient, μ_{total}, of biological tissue as a function of: (1) the electron density of the tissue, (2) a weighted average atomic number of the tissue, and (3) the energy of the incident monochromatic x-ray. More specifically, the total attenuation coefficient is given by the expression (R.2):

$$\mu(E) \cong \underbrace{K_p\, E^{-3.28}\, \rho_e\, Z^{-3.6}}_{\text{Photoelectric Absorption}} + \underbrace{\sigma_{KN}(E)\, \rho_e}_{\text{Compton Scatter}} + \underbrace{K_{coh}\, \rho_e\, E^{-2.0}\, Z^{-1.8}}_{\text{Rayleigh (coherent) Scatter}} \qquad (1.2.1)$$

where the weighted-average elemental composition, $\overline{Z}$, is given by the expression:

$$\overline{Z} \equiv \left[\sum_i \rho_i Z_i^{4.6} \Big/ \sum_j \rho_j Z_j \right]^{1/3.6}$$

ρ_i is the number of atoms per cc of element i

ρ_e is the electron density in electrons per cc

E is the photon energy in keV

σ_{KN} is the Klein-Nishina cross section

K_p, K_{coh} are constants for the photoelectric and coherent scattering respectively.

The basic principle of tomochemistry is that if one performs two CT scans of the body using sufficiently different monochromatic photon energies, one can uniquely determine the electron density and atomic composition profiles. As seen in Fig. 1.2.1, one would use a low energy photon beam to furnish information on the photoelectric and Rayleigh cross sections (and hence the atomic composition), and a high energy photon beam to furnish information about the Compton cross section (and hence the electron density). By using the appropriate software one could then determine the electron density and atomic composition profiles from the two photon measurements, and then display these profiles using a grey scale format similar to normal CT scanners.

In practice polychromatic bremsstrahlung spectra are used in CT scanners and not monochromatic photons. The complications of using polychromatic spectra for tomochemistry is one of the central problems

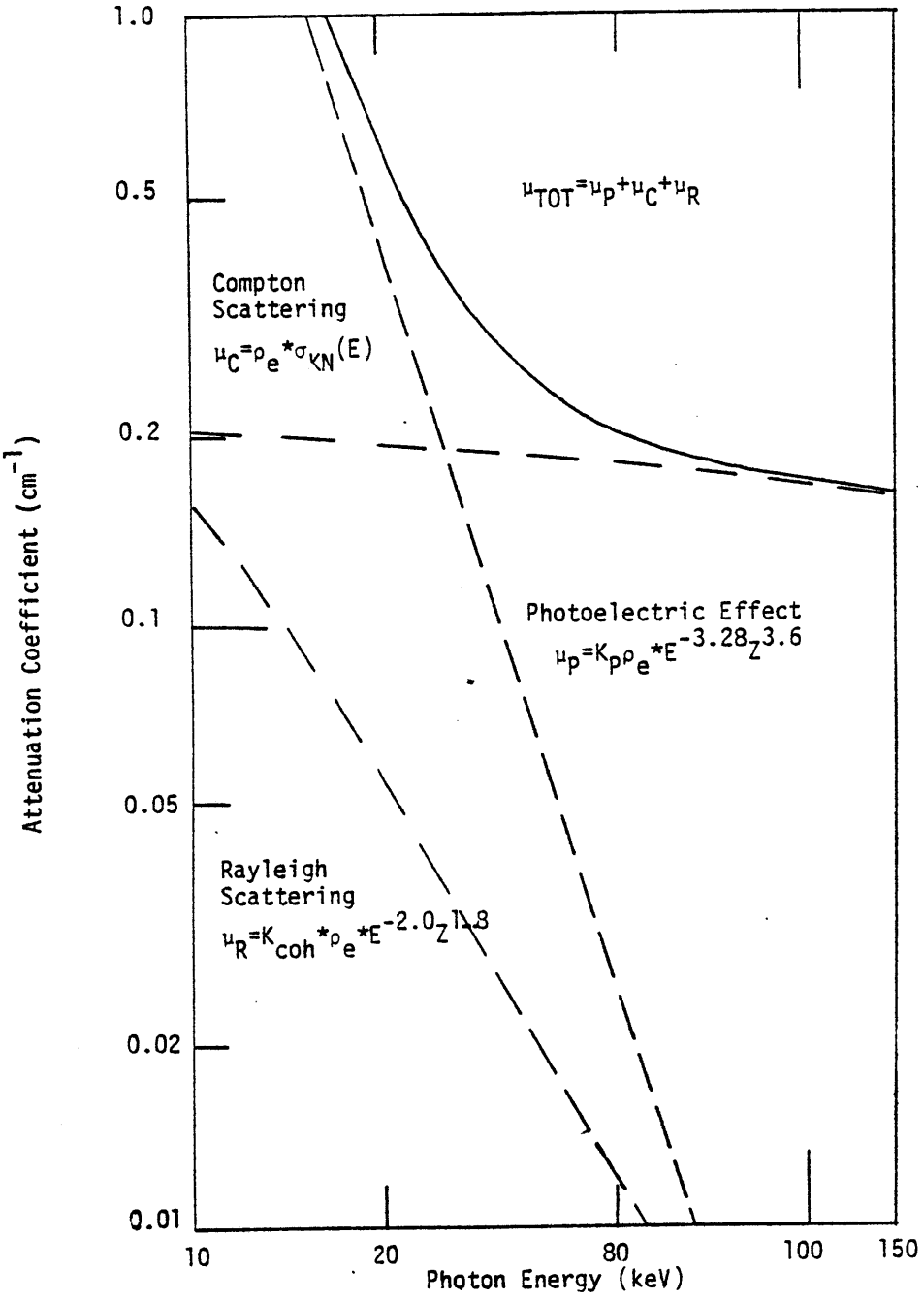

Figure 1.2.1 Attenuation coefficients for photons in water.

addressed in this thesis. The problem of polychromatic spectra is considered in the next chapter when the design of an optimal tomochemical scanner is considered.

There are several potential applications of tomochemistry technology which are of interest to both the medical and nonmedical communities. A few of the medical applications are:

(1) Use the electron density information for radiation therapy planning of high energy ($\sim$ 1 MeV) photons. In a great number of hospitals in the United States and elsewhere Co^{60} is used as a radiation source for photon therapy. When Co^{60} decays it predominantly emits photons at 1.33 MeV and 1.17 MeV. At these energies the photons interact with body tissues primarily via the Compton effect. Hence, accurate (< 5% error) distributions of electron density versus position from tomochemistry would aid in the determination of dose distributions in a patient undergoing radiation therapy (F.1).

(2) Perform in-vivo bone mineral and bone density analysis. Efforts have been made (W.5, G.1, R.1, E.1) to use CT for bone composition analysis. The thrust of these efforts has been to distinguish between, and determine the extent of, osteoporosis and osteomalacia. In osteoporosis there is a general decrease in the bone density (ρ_e decreases) during the progression of the disease, with the relative concentration of the mineral contents remaining constant. In osteomalacia there is a general loss of phosphorous and calcium ($\bar{Z}$ decreases) during the progression of the disease, with the bone density remaining approximately constant. Radiographically or with standard CT the diseases are difficult to distinguish. However, tomochemistry can make the determination of the disease state simply and directly.

(3) Distinguish between normal and diseased tissue. It is known (H.3) that one indicator of cancerous tissue is the presence of calcium deposits near to, or within, the cancerous tissue. It may be possible that with tomochemical analysis one can determine whether a tissue being investigated has a higher average atomic number due to a potential tumor and the presence of calcium, or an increase in the tissue density or atomic number because of another pathological problem (such as the presence of a hematoma).

(4) Reduce the required concentration of contrast agents in radiographic contrast enhancement studies (K.1, K.2). A common technique used by radiologists is the injection into the blood stream of iodinated compounds, commonly known as contrast agents. These agents are radiographically more opaque than soft tissue. Thus, when radiographic procedures are performed on the patient, the blood vessels within the body become highly visible within the radiograph. With the use of tomochemistry it may be possible to reduce the required concentration of these agents because the technique of tomochemistry enhances those regions with higher average atomic number.

There are a few non-medical applications of tomochemistry which may be of interest to various industries. For example, the nondestructive evaluation of complicated machinery or components is one possible application of composition analysis CT. In particular, it has been mentioned (H.2) that tomochemical methods may be used for the nondestructive assay of spent fuel rods from nuclear reactors. More exactly, the determination of uranium and plutonium inventories within

these rods would be important for non-proliferation reasons. Hopefully, more applications would be found with the cross fertilization of the methods developed in this thesis into other scientific and engineering areas.

1.3 Methodologies Used for Tomochemical Analysis

There are two basic methods by which the tomochemical parameters, "average" atomic number and electron density, can be determined from CT scanning. In both these methods a low energy scan and a high energy scan are performed on the body slice of interest. However, once the scan data is obtained, the way in which it is processed is very different. The first of the two methods, the "effective energy" - postreconstruction method, is the most widely used of the two procedures (I.1, P.3, M.4, B.1, B.2, D.1, R.2, R.3). In this method the two sets of x-ray transmission data from the CT scans are reconstructed separately before performing the tomochemistry data processing. One of the reconstructed images contains the distribution of the high-energy-spectrum-averaged attenuation coefficient versus position, $\bar{\mu}$(HIGH ENERGY SPECTRUM), and the other image contains the distribution of the low-energy-spectrum-averaged attenuation coefficient versus position, $\bar{\mu}$(LOW ENERGY SPECTRUM). By then assuming (1) a functional dependence for the photoelectric, Compton, and Rayleigh cross sections, and also assuming (2) that the two incident spectra can each be parameterized by an "effective energy", once can write:

$$\bar{\mu}\left(\bar{E}_{\substack{\text{LOW} \\ \text{EFFECTIVE}}}\right) = K_p \bar{E}_{\substack{\text{LOW} \\ \text{EFF}}}^{-3.28} \rho_e \bar{Z}^{3.6} + \sigma_{KN}\left(\bar{E}_{\substack{\text{LOW} \\ \text{EFF}}}\right) \rho_e +$$

$$+ K_{coh} \rho_e \bar{E}_{\substack{\text{LOW} \\ \text{EFF}}}^{-2.0} \bar{Z}^{1.8} \qquad (1.3.1)$$

$$\bar{\mu}(\bar{E}_{\substack{HIGH \\ EFFECTIVE}}) = K_p \bar{E}_{\substack{HIGH \\ EFF}}^{-3.28} \rho_e \bar{Z}^{3.6} + \sigma_{KN}(\bar{E}_{\substack{HIGH \\ EFF}}) \rho_e +$$

$$+ K_{coh} \rho_e \bar{E}_{\substack{HIGH \\ EFF}}^{-2.0} \bar{Z}^{1.8} \qquad (1.3.2)$$

where:

$E_{\substack{LOW \\ EFF}}$, $E_{\substack{HIGH \\ EFF}}$ are the "effective energies" of the incident spectra - defined as those monochromatic energies which have the same attenuation coefficient for water as the spectrum-averaged attenuation coefficients measured experimentally.

The other parameters are the same as in Eq. (1.2.1).

By then dividing Eq. (1.3.1) by (1.3.2) Eq. (1.3.3) is obtained. This equation is satisfied for only one real value of $\bar{Z}$.

$$\frac{\bar{\mu}(\bar{E}_{\substack{LOW \\ EFF}})}{\bar{\mu}(\bar{E}_{\substack{HIGH \\ EFF}})} = \frac{K_p \bar{E}_{\substack{LOW \\ EFF}}^{-3.28} \bar{Z}^{3.6} + \sigma_{KN}(\bar{E}_{\substack{LOW \\ EFF}}) + K_{coh} \bar{E}_{\substack{LOW \\ EFF}}^{-2.0} \bar{Z}^{1.8}}{K_p \bar{E}_{\substack{HIGH \\ EFF}}^{-3.28} \bar{Z}^{3.6} + \sigma_{KN}(\bar{E}_{\substack{HIGH \\ EFF}}) + K_{coh} \bar{E}_{\substack{HIGH \\ EFF}}^{-2.0} \bar{Z}^{1.8}} \qquad (1.3.3)$$

$\bar{Z}$ can be solved in Eq. (1.3.3) by using an iterative numerical process. Determination of ρ_e can be made by substitution of the calculated value of $\bar{Z}$ into either Eqs. (1.3.1) or (1.3.2) and solving for ρ_e.

The results of an experimental clinical study (D.1) using the "effective energy" method is presented in Fig. 1.3.1. There are two main features to be noted from this figure. First, this preliminary clinical study indicates that the slight differences in soft tissue composition appear to be measurable. It is felt by this author that

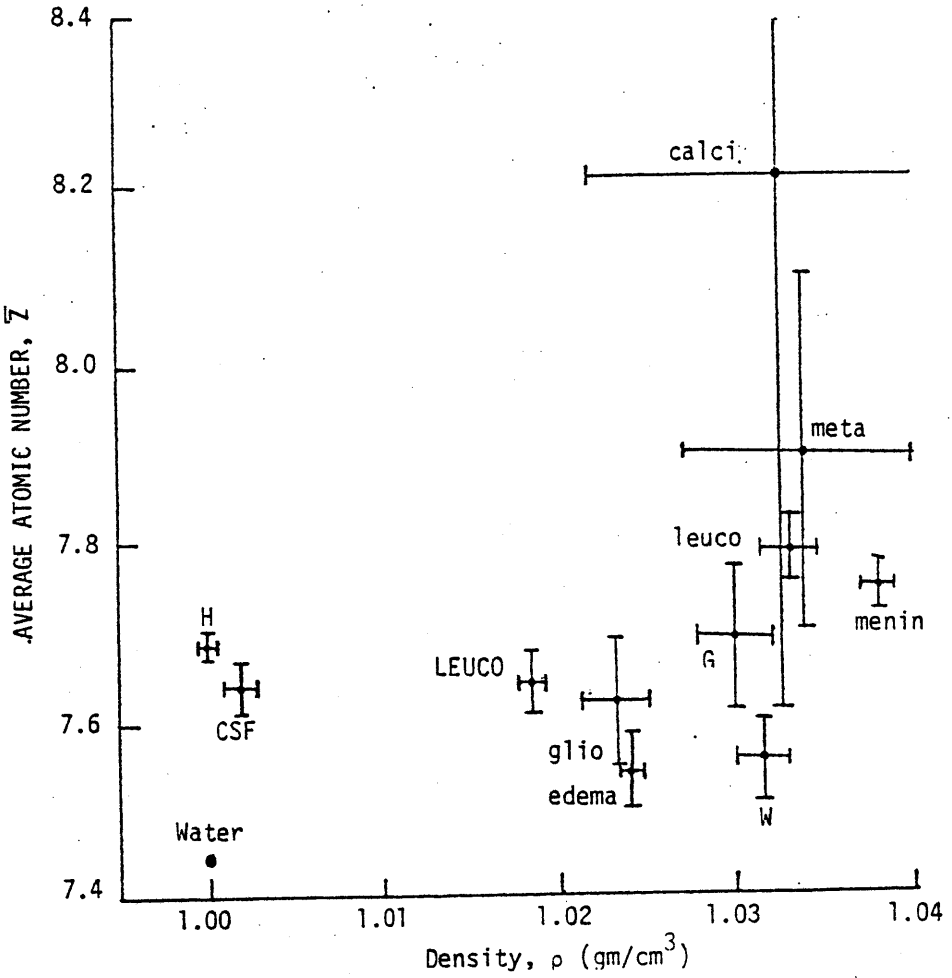

Figure 1.3.1 Measured estimates of atomic number versus density for abnormal brain tissue (D.1).

Key:

CSF Cerebral spinal fluid in a patient with metachromatic leukodystrophy and a patient with glioblastoma multiforme.

H Cerebral spinal fluid in a patient with hydrocephalus due to aqueductal stenosis.

LEUCO Cancerous brain tissue with recently discovered metachromatic leukodystrophy.

glio Cancerous brain tissue with blioblastoma multiforme.

edema Edema associated with meningioma.

G Grey matter in a patient with aqueductal stenosis.

W White matter in patients with aqueductal stenosis, meningioma, and metastasis due to bronchogenic carcinoma.

calci Calcified plexus tissue in a patient with blioblastoma multiforme.

leuco Cancerous brain tissue which has had metachromatic leukodystrophy for 3 years.

meta Cancerous brain tissue with metastasis.

menin Cancerous brain tissue with meningioma.

to infer more from this study - such as a pathological correlation - would be a premature effort. The second main feature of this figure are the large error bars in the composition estimates. The large statistical error of the $\overline{Z}$ determination is due to the relatively small size of the photoelectric effect in comparison to the Compton effect. Due to dose and signal size considerations (mentioned in Chapter 2) the lower practical bound to the low "effective energy" is about 63 keV. At this energy the ratio of photoelectric to Compton attenuation coefficients for water is about 0.075. Thus, the fractional statistical error in the $\overline{Z}$ determination is much larger than the fractional statistical error in the ρ_e determination.

The "effective energy" approach to tomochemical analysis is quite straightforward, however it is not rigorous. This method suffers from three major types of systematic error. First, since experimenters rely on the reconstructions from two separate scans, they implicitly assume that the patient doesn't move between scans. However, in reality this is not the case. Interscan movement of the patient can cause large errors in the determination of tomochemical parameters. The error is especially large in those regions where the tissue of interest is adjacent to a region with a very different attenuation coefficient from the tissue being studied. In these regions a slight mismatch in positioning can cause the $\overline{Z}$ determination to diverge.

The other two downfalls of the "effective energy" method is that the $\overline{Z}$ and "effective energy" parameterization methods are too simplistic. Parameterizing a polychromatic bremsstrahlung spectra by a single "effective energy" is a sensitive assumption for two reasons.

First, since the photoelectric and rayleigh cross sections are strongly dependent on energy, the "effective energy" required for this theory must be known with accuracy and precision. However, no rigorous method for the "effective energy" determination of a polychromatic spectrum exists. Second, as seen in Fig. 1.3.2 when x-ray bremsstrahlung spectra pass through the body, spectral hardening occurs; i.e., the "effective energy" of the spectrum increases due to selective absorption of low energy photons. Thus, to be truly rigorous one must determine an "effective energy" for every position within the scanned body slice.

The use of one parameter, $\overline{Z}$, as a quantitative measure of the average elemental composition is also a questionable assumption. This fact becomes clear by simply reviewing the literature. Different authors use different approximations to the $\overline{Z}$ dependence of the atomic cross sections. Figure 1.3.3 illustrates the discrepancy between four different authors in their parameterization of $\overline{Z}$. Note that one would calculate different values of the average atomic number for the same substance. White (W.1, W.2, W.3) has performed exhaustive studies on the validity of the average atomic number concept. In general he found that linear regression fits to cross section data using a single parameter, $\overline{Z}$, are poor in those energy regions where two Z-dependent processes are measureable. In the diagnostic energy range both Rayleigh scattering and photoelectric absorption are measureable for biological tissue; thus, White's work also puts a $\overline{Z}$ determination into question. Table 1.3.1 lists some other major findings of White pertinent to the accuracy of tomochemical analysis.

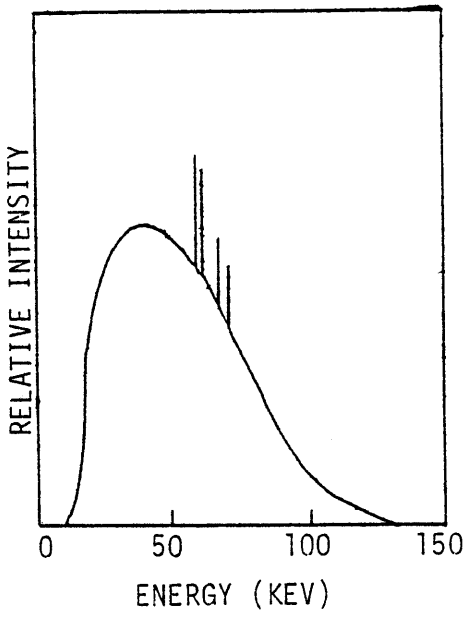

Bremsstrahlung Spectrum

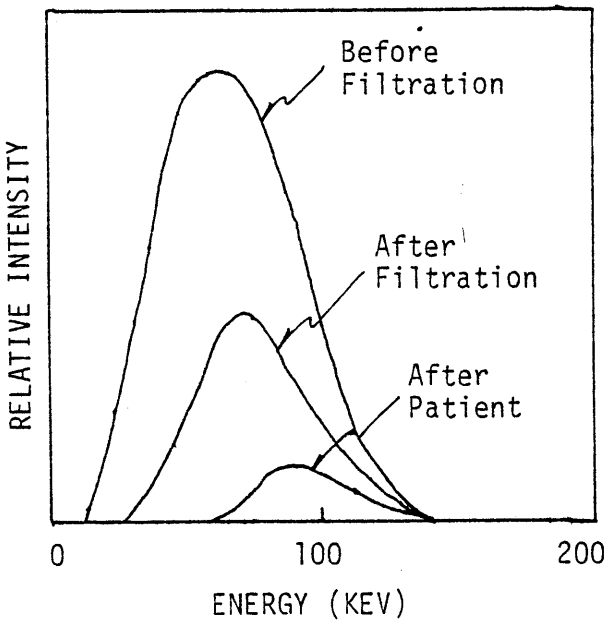

Figure 1.3.2 Illustration of Beam Hardening Phenomenon

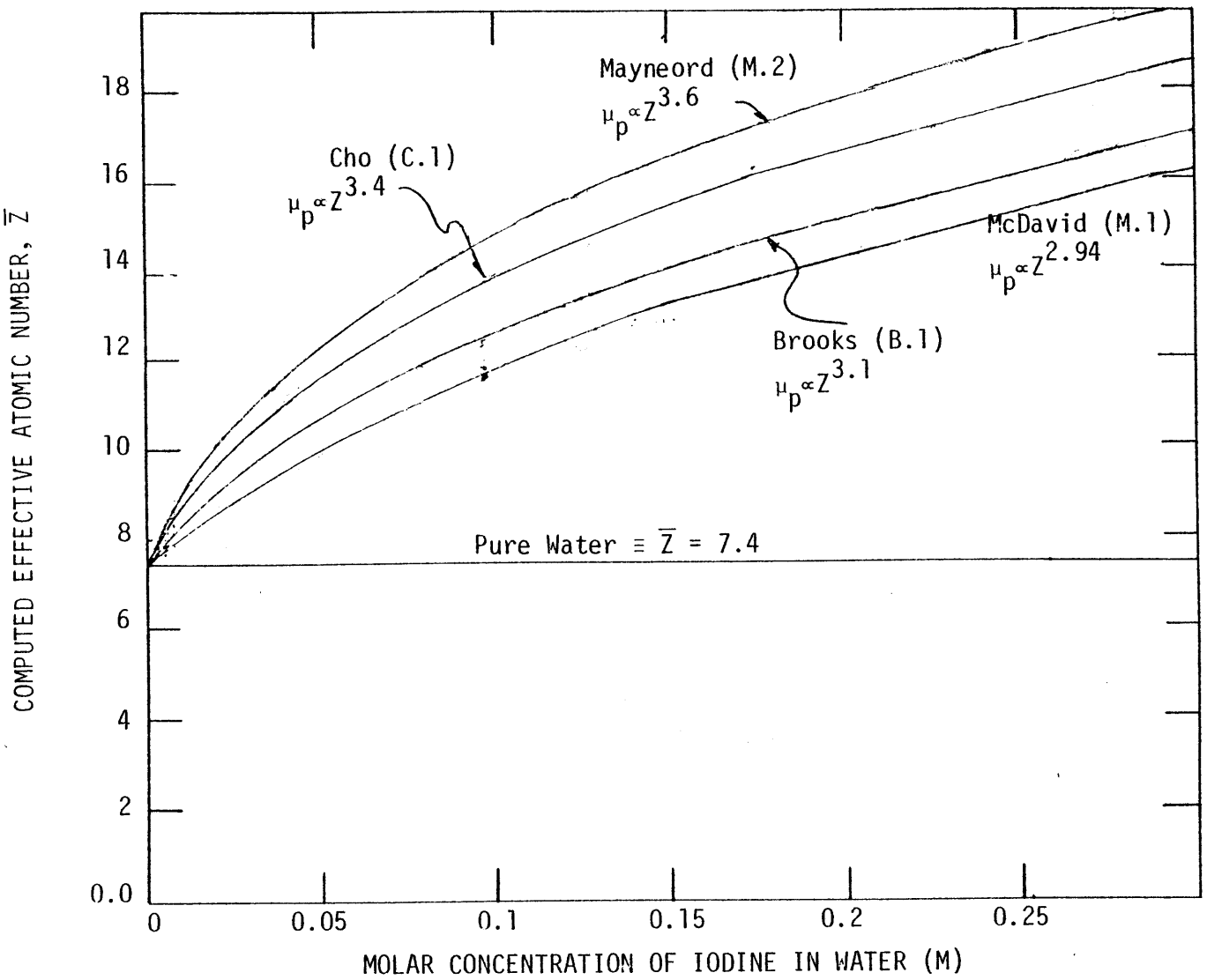

Figure 1.3.3 Computed effective atom number versus molar concentration of iodine in water for four different parameterizations of $\overline{Z}$.

1. For photons above 10 keV in energy, the addition rule of cross sections is very accurate.

2. The Z-dependence of total cross section data has been found to give poor linear regressions, except at energies where a single process dominates.

3. The few Z-exponents published in the literature are not adequate for precise clinical radiation studies.

4. Due to the strong energy dependence of many interactions, the concept of effective atomic number based upon a single Z-exponent is not acceptable in studies attempting to characterize interactions within extended energy ranges.

Table 1.3.1 Major findings of White (W.1, W.2, W.3) with respect to the determination of an effective atomic number, $\overline{Z}$.

The second method of data processing used for tomochemical composition analysis is based upon the theory of Alvarez and Macovski (A.1, A.2). As in the "effective energy" method, the required data set consists of low and high energy photon transmission measurements from a CT scanner; however, the method by which the data is processed is different. To illustrate the Alvarez and Macovski method assume for the moment that two monochromatic photon beams are used to measure photon transmissions along the same ray path in the body. As in Eq. (1.1.1) the photon transmission equations can be written:

$$-\ell n \frac{I(E_1)}{I_o(E_1)} = \int_A \mu(\bar{r},E_1)d\ell \qquad (1.3.4)$$

$$-\ell n \frac{I(E_2)}{I_o(E_2)} = \int_A \mu(\bar{r},E_2)d\ell \qquad (1.3.5)$$

where

E_1, E_2 are the energies of the low and high energy beams respectively.

Substituting the approximate functional form of the cross sections the line integrals can be written:

$$\int_A \mu(\bar{r},E_1)d\ell = \int_A (K_p\rho_e\bar{Z}(\bar{r})^{3.6}(\bar{r})E_1^{-3.28} + K_{coh}\rho_e\bar{Z}(\bar{r})^{1.8}(\bar{r})E_1^{-2.0} +$$

$$+ \rho_e(\bar{r})\sigma_{KN}(E_1))d\ell \qquad (1.3.6)$$

$$\int_A \mu(\bar{r},E_2)d\ell = \int_A (K_p\rho_e\bar{Z}(\bar{r})^{3.6}(\bar{r})E_2^{-3.28} + K_{coh}\rho_e(\bar{r})\bar{Z}(\bar{r})^{1.8}E_2^{-2.0} +$$

$$+ \rho_e(\bar{r})\sigma_{KN}(E_2))d\ell \qquad (1.3.7)$$

where the terms in these equations are the same as in Eqs. (1.3.1) and (1.3.2).

The key to the Alvarez and Macovski method is that at this point they assume separability of the spatial and energy terms in Eqs. (1.3.6) and (1.3.7), and they consolidate the photoelectric and Rayleigh dependences:

$$\int_A \mu(\bar{r},E_1)d\ell = \int_A a_{P+R}(\bar{r})f_{P+R}(E_1)d\ell + \int_A a_C(\bar{r})f_C(E_1)d\ell \qquad (1.3.8)$$

$$\int_A \mu(\bar{r},E_2)d\ell = \int_A a_{P+R}(\bar{r})f_{P+R}(E_2)d\ell + \int_A a_C(\bar{r})f_C(E_2)d\ell \qquad (1.3.9)$$

where:

$$a_{P+R}(\bar{r})f_{P+R}(E) = K_p\rho_e(\bar{r})\bar{Z}(\bar{r})^{3.6}E^{-3.28} + K_{coh}\rho_e(\bar{r})\bar{Z}(\bar{r})^{1.8}E^{-2.0}$$

$$= \text{photoelectric + Rayleigh cross sections}$$

$$a_C(\bar{r})f_C(E) = \rho_e(\bar{r})\sigma_{KN}(E)$$

$$= \text{Compton cross section}$$

Now due to separability the energy dependent terms can be taken outside of the spatial integral:

$$\int_A \mu(\bar{r},E_1)d\ell = f_{P+R}(E_1) \int_A a_{P+R}(\bar{r})d\ell + f_C(E_1) \int_A a_C(\bar{r})d\ell \qquad (1.3.10)$$

$$\int_A \mu(\bar{r},E_2)d\ell = f_{P+R}(E_2) \int_A a_{P+R}(\bar{r})d\ell + f_C(E_2) \int_A a_C(\bar{r})d\ell \qquad (1.3.11)$$

Hence, if the energy dependences of the photoelectric + Rayleigh and the Compton cross sections are known, Eqs. (1.3.10) and (1.3.11) can be solved for the photoelectric + Rayleigh line integral, $\int_A a_{P+R}(\bar{r})d\ell$, and Compton line integral, $\int_A a_C(\bar{r})d\ell$. Reconstructing the photoelectric + Rayleigh line integrals will produce an image of $(\rho_e K_P \bar{Z}^{3.6} + \rho_e K_{coh} \bar{Z}^{1.8})$ versus position while reconstructing the Compton line integrals will produce an image of (ρ_e) versus position.

In practice, transmission measurements are not made with monochromatic spectra. To get around the problems of spectral hardening Alvarez and Macovski considered the problem of transmission measurements using polychromatic source spectra. By defining:

$$A_{P+R} = \int_A a_{P+R}(\bar{r})d\ell$$

and

$$A_C = \int_A a_C(\bar{r})d\ell$$

the expression for the transmission ratios of two incident spectra can be written:

$$\frac{I_1(A_{P+R},A_c)}{I_{1o}} = \frac{\int S_1(E)\ \exp(-A_{P+R}f_{P+R}(E) - A_c f_c(E))dE}{\int S_1(E)dE} \qquad (1.3.12)$$

$$\frac{I_2(A_{P+R},A_c)}{I_{2o}} = \frac{\int S_2(E)\ \exp(-A_{P+R}f_{P+R}(E) - A_c f_c(E))dE}{\int S_2(E)dE} \qquad (1.3.13)$$

Where S_1 and S_2 are the low and high energy spectra used for the transmission measurements. To then determine A_{P+R} and A_c from these two measurements the following method was suggested: expand I_1/I_{1o} and I_2/I_{2o} into power series expansions:

$$\ln(I_1/I_{1o}) = b_o + b_1A_{P+R} + b_2A_c + b_3(A_{P+R})^2 + b_4A_c^2 + b_5A_{P+R}A_c$$

and

$$\ln(I_2/I_{2o}) = c_o + c_1A_{P+R} + c_2A_c + c_3(A_{P+R})^2 + c_4A_c^2 + c_5A_{P+R}A_c$$

or conversely:

$$A_{P+R} = B_o + B_1\ln(I_1/I_{1o}) + B_2\ln(I_2/I_{2o}) + B_3(\ln(I_1/I_{1o}))^2 +$$

$$+ B_4(\ln(I_2/I_{2o}))^2 + B_5\ln(I_1/I_{1o})\ln(I_2/I_{2o}) \qquad (1.3.14)$$

and

$$A_c = C_o + C_1 \ell n(I_1/I_{1o}) + C_2 \ell n(I_2/I_{2o}) + C_3(\ell n(I_1/I_{1o}))^2 +$$

$$+ C_4(\ell n(I_2/I_{2o}))^2 + C_5 \ell n(I_1/I_{1o}) \ell n(I_2/I_{2o}) \qquad (1.3.15)$$

The coefficients of these expansions are determined experimentally by determining the transmission ratios for materials with known values of A_{P+R} and A_c and then using a least squares curve fitting procedure. In practice, to determine A_{P+R} and A_c one would measure $\ell n(I_1/I_{1o})$ and $\ell n(I_2/I_{2o})$ and then compute A_{P+R} and A_c by direct substitution into expressions (1.3.14) and (1.3.15).

The major advantages of the Alvarez and Macovski calibration curve fitting procedure are that spectral hardening effects are implicitly included in the expansion coefficients of the polynomial fits, and no a priori assumptions about the cross section dependences are required.

The primary result of these advantages is that the low and high energy spectra used for tomochemical analysis can be formed in many ways. The incident bremsstrahlung energy spectrum of the two scans can be changed by changing the kilovoltage accelerating potential of the x-ray tube at fixed filtration, by changing the filtration of a bremsstrahlung spectrum at fixed kilovoltage, or by changing both filtration and tube kilovoltage simultaneously (A.1, A.2). Another method of determining the low and high energy transmission information is by the use of a simple two energy compartment spectrometer detector. Brownell and Weissberger (B.6) and Fenster (F.1) were the first researchers to describe and develop a practical "split ionization detector" which could be used for tomochemistry. This detector contained

two detectors. One of the detectors was sensitive to the low energy part of the incident x-ray spectrum while the other was sensitive to the high energy part of the incident x-ray spectrum. In all of the above methods calibration measurements would be made on targets of known composition and then measurements on unknown targets would be related to these calibrations through the polynomial expansions in Eqs. (1.3.14) and (1.3.15).

In this thesis the calibration comparison-prereconstruction data processing method of Alvarez and Macovski is used. It is felt that the rigor of this method far outweighed the complication of having to perform calibration measurements. Furthermore, it is also felt that any attempt to perform quantitative tomochemistry would have to use the Alvarez and Macovski method when the x-ray spectra used are polychromatic.

1.4 Plan of Work

The purpose of this thesis was to (1) study the engineering considerations which go into the development of a scanner which can perform tomochemistry in a single scan and (2) to determine the limitations and accuracy of such a scanner. In this experiment single-scan tomochemistry was performed by modulation of the filtration of the fan beam x-ray bremsstrahlung spectrum. As seen in Fig. 1.4.1, this was accomplished by rotating a beam analyser disk within the path of the fan beam during the rotation of the object being scanned. As indicated in the figure the analyser disk contained alternating filter materials. In this experiment the x-ray kilovoltage potential remained fixed during the filtration modulation. Hence, only the filtration change served to produce the low and high energy spectra required for the tomochemistry data processing. It was possible with this arrangement to alternate simultaneously the x-ray tube's kilovoltage potential and the spectra filtration; however, this was not attempted in this thesis due to the poor transient response characteristics of the x-ray tube system used in this experiment.

The work in this thesis can be categorized into three main areas:

1. Engineering design and construction of the experiment;
2. Calibration of the scanner and software development; and
3. Experimental measurements and reduction of the experimental data.

Figure 1.4.2 gives a more detailed breakdown of the development and analysis procedure used in this work.

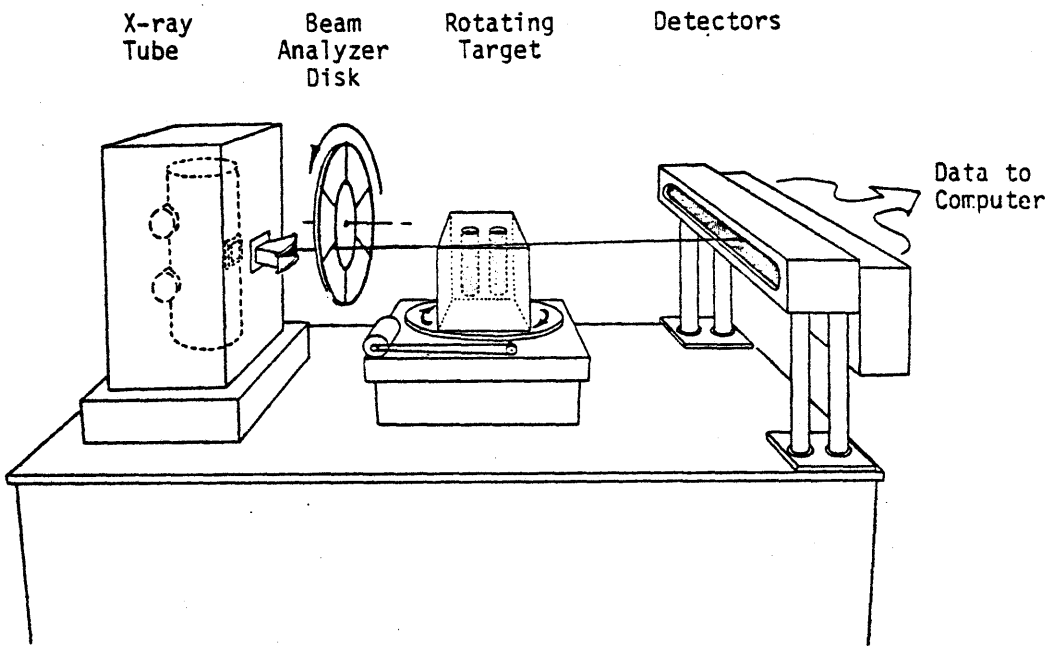

The two sets of transmission measurements for tomochemistry are obtained by modulation of the filtration of the x-ray fan beam.

Figure 1.4.1 Schematic representation of the modification of the MGH Benchtop scanner.

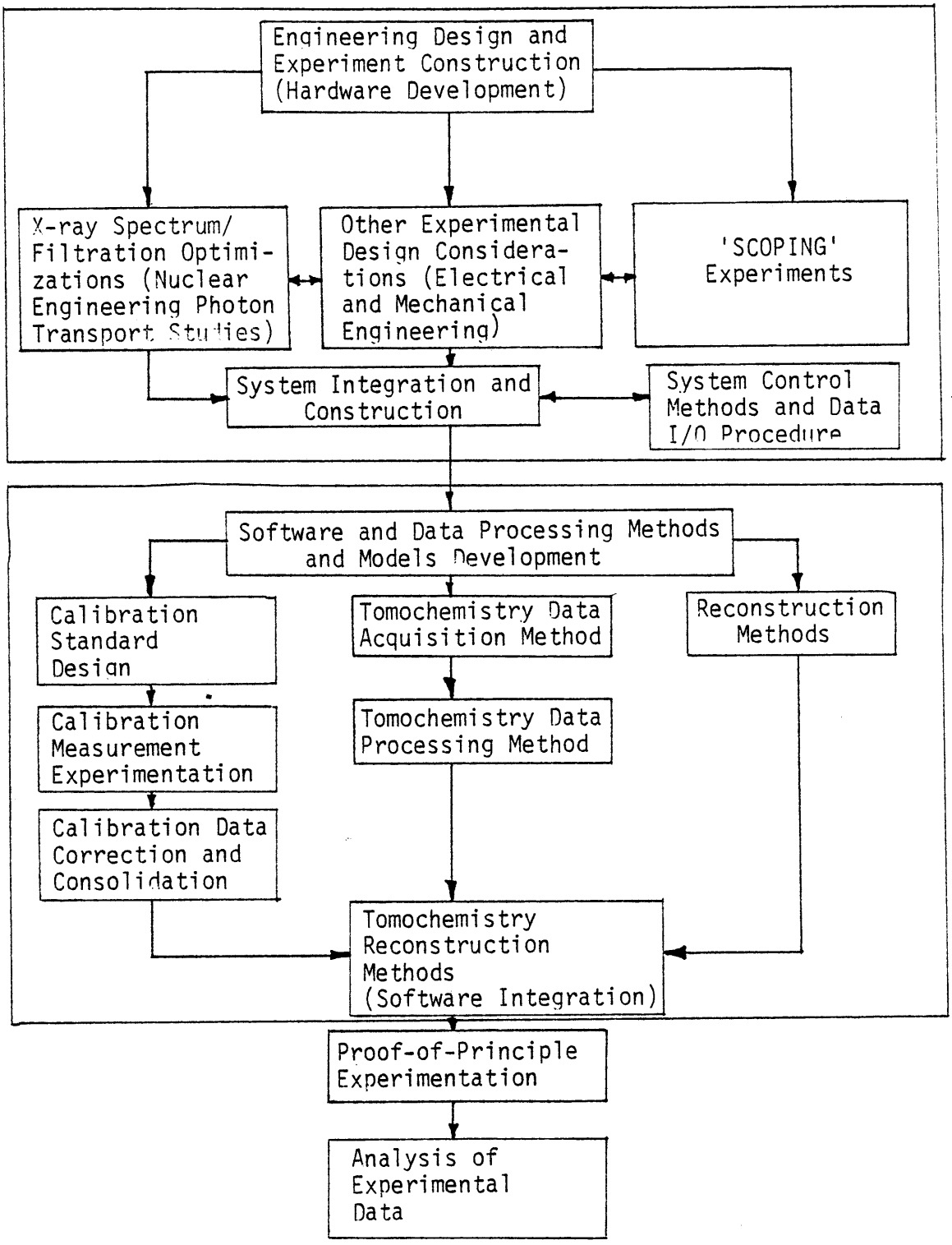

Figure 1.4.2 Block Diagram of the tomochemistry scanner system development.

The main considerations in the experiment design are the choice of the optimal spectra for tomochemistry, the transient response of the detection system, and the methods of data I/O and system control. The most important and most difficult consideration is the choice of the optimal spectra. This problem was addressed by calculational photon transport and experimental studies. The determination of those spectra which have the optimal (information/dose) and (information/photon) ratios is presented in the next chapter. Note that once the spectra are chosen a hardware design was then developed based upon the type of filtration required. The system control scheme was then developed after the disk RPM, and data I/O rate were determined from the hardware design.

With the basic experimental setup built a calibration standard was designed and constructed so that the reference data set required by the calibration comparison-prereconstruction method could be determined. In parallel with the standard's development, software was developed to handle the calibration data and to perform the polynomial fit procedure. Modification of the reconstruction software was also performed. This modification enabled the software to interpret the modulated spectrum data so that the photoelectric + Rayleigh and the Comption line integrals could be determined. A set of subprograms was also developed to merge the tomochemistry software into the original software so that reconstructions could be performed.

Experiments were performed to determine the linearity of the system and statistical error of the measurement process. A determination was made of the statistical accuracy limit of tomochemistry due

to electronic noise and Poisson error. The optimal kilovoltage potential for tomochemical analysis was determined experimentally in this thesis. Also, a determination of the sensitive aspects of the data processing and experimental measurement methods was made; i.e., those effects which cause large systematic errors in the tomochemical method were determined. A more complete description of the experimental methods and results are given in Chapter 4.

2.0 Engineering Design of a Single Scan Composition-Analysis CT Scanner

The major design goal of this research project is to develop a single scan composition-analysis CT scanner through the modification of a typical CT scanner. It was felt that this would be achieved most directly by the addition of a simple mechanical device to a CT scanner so that proof-of-principle experiments could be performed. Because tomochemical analysis requires twice as much x-ray transmission information as normal CT, a reasonable goal was felt to be a doubling of the normal scanning time and an approximate doubling of the absorbed patient dose during the tomochemistry scan. For the MGH scanner this meant increasing the scan time from 5 seconds to 10 seconds. A spatial resolution of 2-3 mm - compared to the normal 1-2 mm - was felt to be an acceptable target for tomochemical analysis. This poorer resolution would be commensurate with the envisioned applications of tomochemical analysis where quantitative information in a region is more pertinent than detailed information at a point in the scanned section. The slice section thickness was maintained at 1 cm, the same as that used in normal CT scanners. Finally, the aim of the quantitative accuracy of this method was +/- 0.5% for the electron density and +/- 6% for the atomic composition.

The design work of the experiment falls into three major areas:

(1) Nuclear Engineering

  (A) determination of the spectra to use for tomochemical analysis

  (B) determination of the degree of absorbed dose from CT scanning

(2) Mechanical Engineering

(A) design of the beam modulation device and integration of this device into the normal CT scanner

(B) design of the calibration standard used in the x-ray transmission calibration measurements

(3) Electrical Engineering

(A) development of the automatic experiment control system vis-a-vis computer control

(B) modification of the normal CT data I/O control system

(C) development of the system for simultaneous monitoring of the beam modulation device, rotating table, x-ray tube, and detector bank

These three areas are interrelated in the final system design. For example, the results of the photon transport studies serve as a basis for the mechanical engineering development of the beam modulation device. Furthermore, the automatic control aspects of the system are interrelated to the mechanical system which is being controlled. Hence, although the nuclear engineering, mechanical engineering, and electrical engineering work are presented below in separate sections, these three areas of work were coupled during the development process.

2.1 Support Work in Nuclear Engineering

This section presents the methods and results of the determination of the optimal spectra for tomochemical analysis. A detailed description of the MGH benchtop scanner is first presented. This is followed by a description of the photon transport models used to simulate the composition-analysis scan method. A presentation is then made of the findings of the transport studies and an explanation of these findings is given.

2.1A Physical Characteristics of the MGH Benchtop Scanner

The nuclear engineering modeling of the MGH CT scanner can be conceptually divided into three parts:

(1) the x-ray generation system

(2) the target scanned

(3) the x-ray detection system

A brief description of these parts and the models used to describe them in the photon transport calculations are presented below.

As in commercial CT scanners, the MGH benchtop scanner uses an x-ray tube as the photon source. X-ray tubes are used rather than isotopic sources because x-ray tubes can produce a large photon flux from a small focal spot. Furthermore, x-ray tubes are more convenient in the sense that the radiation source can be turned on and off -- thereby simplifying the radiation protection procedures. There are two major types of x-ray tubes, the rotating anode type and the fixed anode type. Figure 2.1A.1 contains line drawings of these two types of tubes. In both types of x-ray tubes electrons are accelerated onto the anode target where they are then de-accelerated. In diagnostic energy x-ray tubes the de-accelerating electrons deposit more than 99% of their kinetic energy in the anode while the remaining energy is radiated as x-rays (L.2, S.4). Rotating anode tubes usually have effective focal spot sizes of about 1 mm^2, whereas fixed anode tubes have focal spot sizes about 3 mm^2. Figure 2.1A.1 indicates that rotating anode tubes can achieve this smaller focal spot size - and hence higher power densities on the anode target - because the rotation of the anode distributes the energy dissipation over the entire

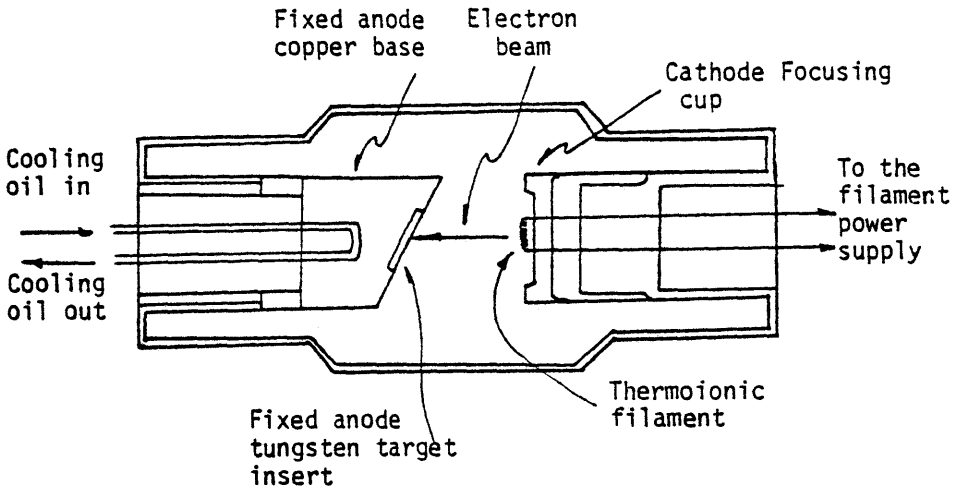

FIXED ANODE X-RAY TUBE

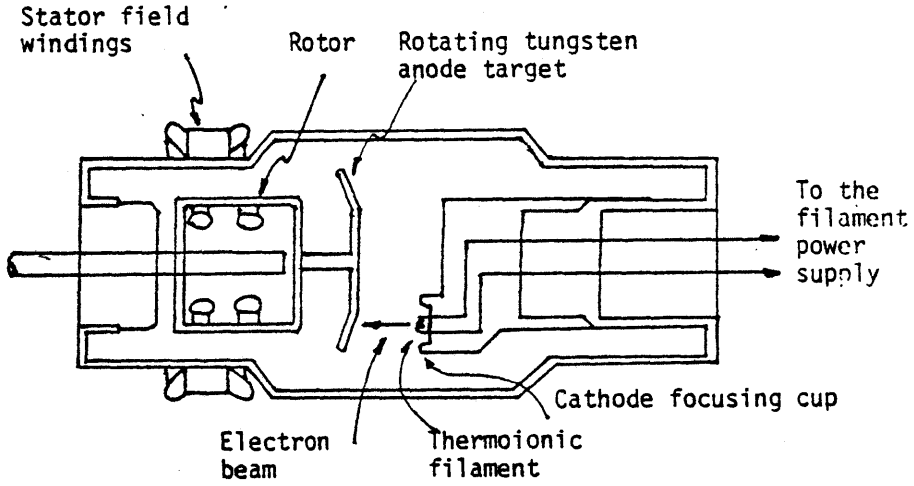

ROTATING ANODE X-RAY TUBE

Figure 2.1A.1 Schematic drawings of fixed and rotating anode x-ray tubes.

anode rather than at only one point in the anode. Rotating anode tubes have one major drawback compared to fixed anode tubes; the rotating anode has a much smaller mass than the fixed anode so that energy dissipation (heat) is poorer. Thus, at a given power level fixed anode tubes can be run continuously several times longer than rotating anode tubes. Because of the great number of 'scoping' measurements required in this experiment, it was felt that it was more desirable to have the higher duty cycle of fixed anode tubes than the smaller focal spot size of rotating anode tubes. Thus, a fixed anode tube was used in the experiment.

In the MGH scanner and in commercial scanners the x-ray tubes used operate at constant current and at constant kilovoltage. The power supply used in this experiment can drive an x-ray tube at 30 mA of electron current on the anode target at voltages from 0 to 150 kV. The power supply contains a high frequency oscillator. The signal from this oscillator is full-wave rectified and then highly regulated. The regulation is sufficient to reduce the AC ripple to +/- 15 V out of 150,000 V DC implying a percent ripple of only 0.01%. This high degree of regulation is required for CT scanner tubes because the instantaneous x-ray power generation of x-ray tubes at a fixed tube current is approximately proportional to the tube voltage squared, $(kV)^2$, (E.2, M.10). Hence, to keep the photon flux rate constant throughout the CT scan the voltage must be kept constant within a band half the magnitude of the allowable uncertainty in the photon flux rate.

The bremsstrahlung x-ray spectra generated by x-ray tubes depend upon the target angle, the type of target used, and the instantaneous

accelerating potential of the x-ray tube (S.4, S.5, T.3, E.3). Most x-ray tubes used in radiography are either half-wave or full-wave rectified. Hence, most experimental studies of x-ray tube spectra are for these rectifications. The MGH x-ray tube uses a 20° target angle, a tungsten target, and a high degree of voltage regulation. A complete review of the experimental literature was only able to unearth one accurate experimental study of bremsstrahlung spectra from such an x-ray tube (S.4). Figure 2.1A.2 illustrates the spectra measured for 100 kVp and 150 kVp spectra before the introduction of any inherent x-ray tube filtration. The investigators found that the photon flux at 1 m from the tube was about $2.2*10^8$ γ/cm^2-sec-ma at 100 kVp and $5.5*10^8$ γ/cm^2-sec-ma at 150 kVp. These two spectra in combination with the 1.7 mm Aℓ and 1.0 mm Be inherent filtration of the MGH x-ray tube were used in the photon transport model in this study.

Several general characteristics of these bremsstrahlung spectra should be noted. The characteristic broad spectral shape of the bremsstrahlung spectra is caused by the de-acceleration of the incident electrons as they are slowed down by the tungsten target. Classical and quantum mechanical theories of electromagnetic radiation both predict that charged particles radiate electromagnetic radiation when accelerated (L.3, J.2, H.5). The largest possible energy x-ray emitted from this de-acceleration process is equal to the energy of the incident electrons as predicted by the Duane-Hunt Rule (T.3). The characteristic peaks at 58.0, 59.3, 67.2, and 69.1 keV correspond to the fluorescent radiation emission of the tungsten target and account for

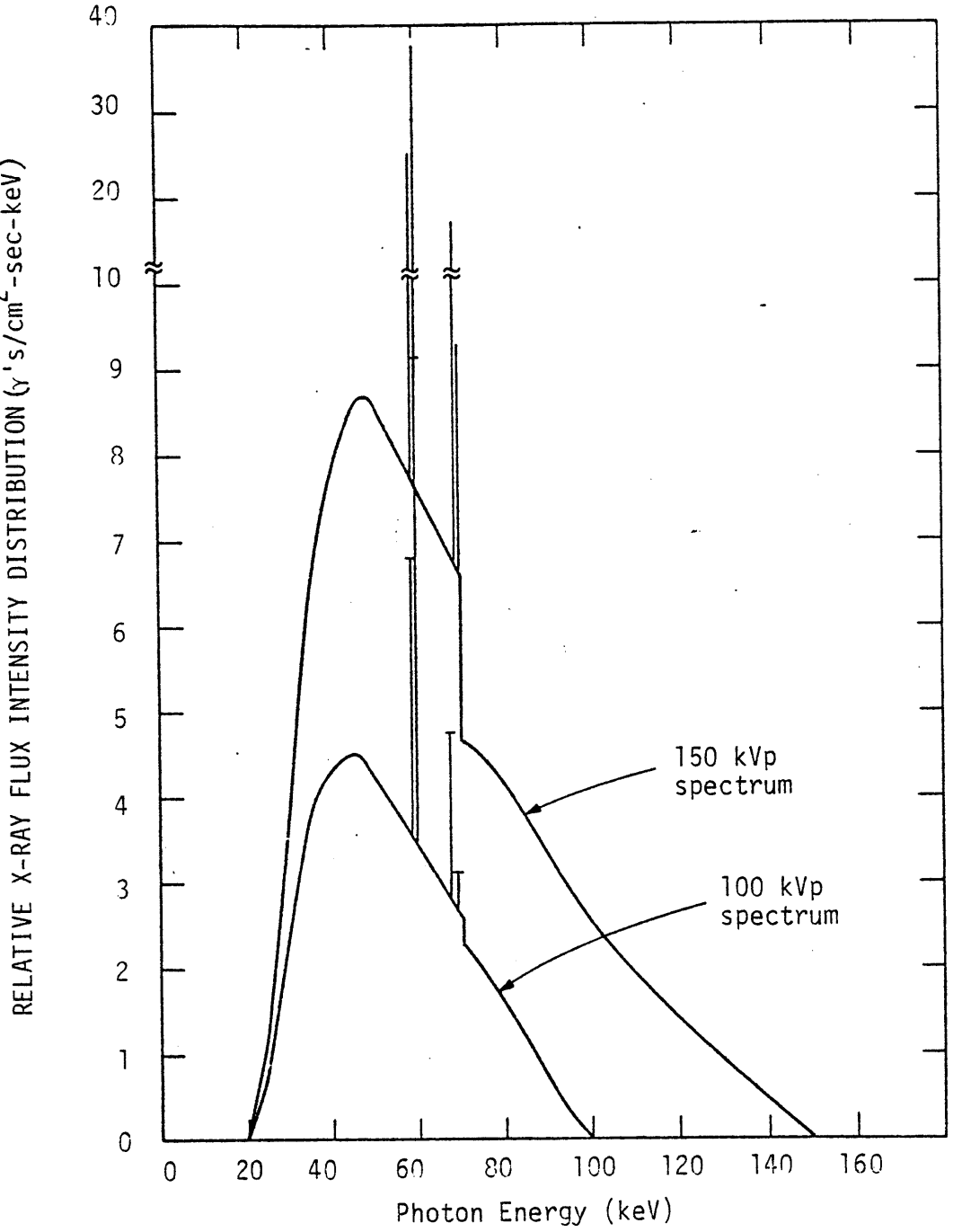

Figure 2.1A.2 Experimentally determined bremsstrahlung x-ray spectra from an x-ray tube run at constant voltage potential (S.4).

roughly 8% of the total radiation energy emitted from the tube (T.2, S.4). One subtle feature of bremsstrahlung spectra is that theory predicts that the emitted energy distribution, $\frac{EdN(E)}{dE}$, increases linearly with decreasing energy (a negative slope) (E.2). This is not observed here because the de-accelerating electrons penetrate to the interior of the tungsten target, the x-rays are emitted, and some are then reabsorbed within the tungsten (S.5, S.6). At the very low energy end of the spectrum the x-rays are reabsorbed completely. As the x-ray energy increases, more photons escape the tungsten target; thus the bremsstrahlung spectrum distribution increases. At 69.5 keV there is an abrupt decrease in intensity. This decrease corresponds to the absorption K-edge of tungsten where the photoelectric absorption cross section abruptly increases. The spectral distribution is then seen to monotonically decrease to zero, as predicted by theory.

In all CT scanners x-ray beam filtration is performed immediately after the x-ray tube. The purpose of filtration is to enhance the desired characteristics of the broad energy bremsstrahlung spectrum and to suppress the undesirable characteristics. In this research project, filtration was used to shape the incident bremsstrahlung spectrum to obtain optimal spectral characteristics for tomochemical measurements. Section 2.1B will present the methods and results of the filtration studies performed in this research.

After the filtration a fan beam is formed in the MGH scanner by twice collimating the x-rays from the tube. The first collimator is positioned immediately after the filters and before the patient to reduce the degree of extraneous dose and to reduce the amount of scattered

radiation from the patient to the detector. The second collimator is positioned behind the patient and in front of the detector to further reduce the scattered radiation detected. The collimation is such that the scan-slice thickness is about 1 cm at the rotation axis. In the analysis of the optimal spectra for tomochemistry, the scattered radiation was assumed to be at undetectably low levels. Monte Carlo transport and experimental studies (D.4, B.5) have shown that the level of detected scattered radiation is at worst 7% of the level of transmitted radiation for a 25 cm water cylinder target. Thus, this engineering assumption is justified for photon detection modeling purposes. However, scattered radiation was not ignored in the radiation absorbed dose aspect of the optimization. In fact, a significant fraction of the dose from CT scanners is due to scattered radiation (L.2). The description of the Monte Carlo transport models used to determine the radiation absorbed dose is presented in Section 2.1B and Appendix B.2.

For all of the design studies in this work a 20 cm diameter water cylinder was used as the reference target. Water is known to be a good soft tissue analogue when performing x-ray analyses (I.2). The presence of bone was not included in the transport modeling so as to keep the calculational analysis simple. The hypothetical target was also given axial symmetry (parallel to the rotation axis) to avoid partial volume effects in the axial direction. In the model the target was centered on the rotation axis of the rotating table. The scan was assumed to take 10 seconds. The other assumptions and models of the scanned target will be presented in the next section.

Those x-rays which get from the x-ray tube, are passed by the filtration, are transmitted through the scanned target, are assumed to then "enter" the detector; "enter" here does not mean detected. A schematic drawing of the MGH detector is presented in Fig. 2.1A.3. A set of 256 parallel-plate ionization detectors is enclosed within an aluminum pressure vessel containing a 95% Xe-5% CO_2 gas mixture at 213 psia. For an entering x-ray to be detected it must first pass through a 3.175 mm machined "window" in the aluminum pressure vessel. Then it must get through a 3.175 mm "dead space" region just prior to the active region of the ionization chamber. The "dead space" (referring to the inability of this region to collect any charge produced by an x-ray ionization of the gas mixture) is required so as to prevent electrical breakdown and current leakage between the ionization chamber high voltage plate and the grounded pressure vessel. If the entering x-ray doesn't strike the front edges or sides of the ionization chamber it may cause an ionization within the 10 cm region of the chamber or it may be transmitted through the chamber, thereby escaping detection. The MGH detector uses xenon gas as the detection medium because of xenon's large microscopic photoelectric cross section. The gas mixture is pressurized to increase the macroscopic cross section of the gas within the detector. If an incident x-ray is absorbed by the xenon within the "active" region (that region where x-ray detection is possible) the primary photoelectron ejected from the xenon produces secondary electron-ion pairs. About one electron-ion pair is produced for every 21.9 eV deposited in the gas media (Y.1). The electrons then either travel from low to high potential along the

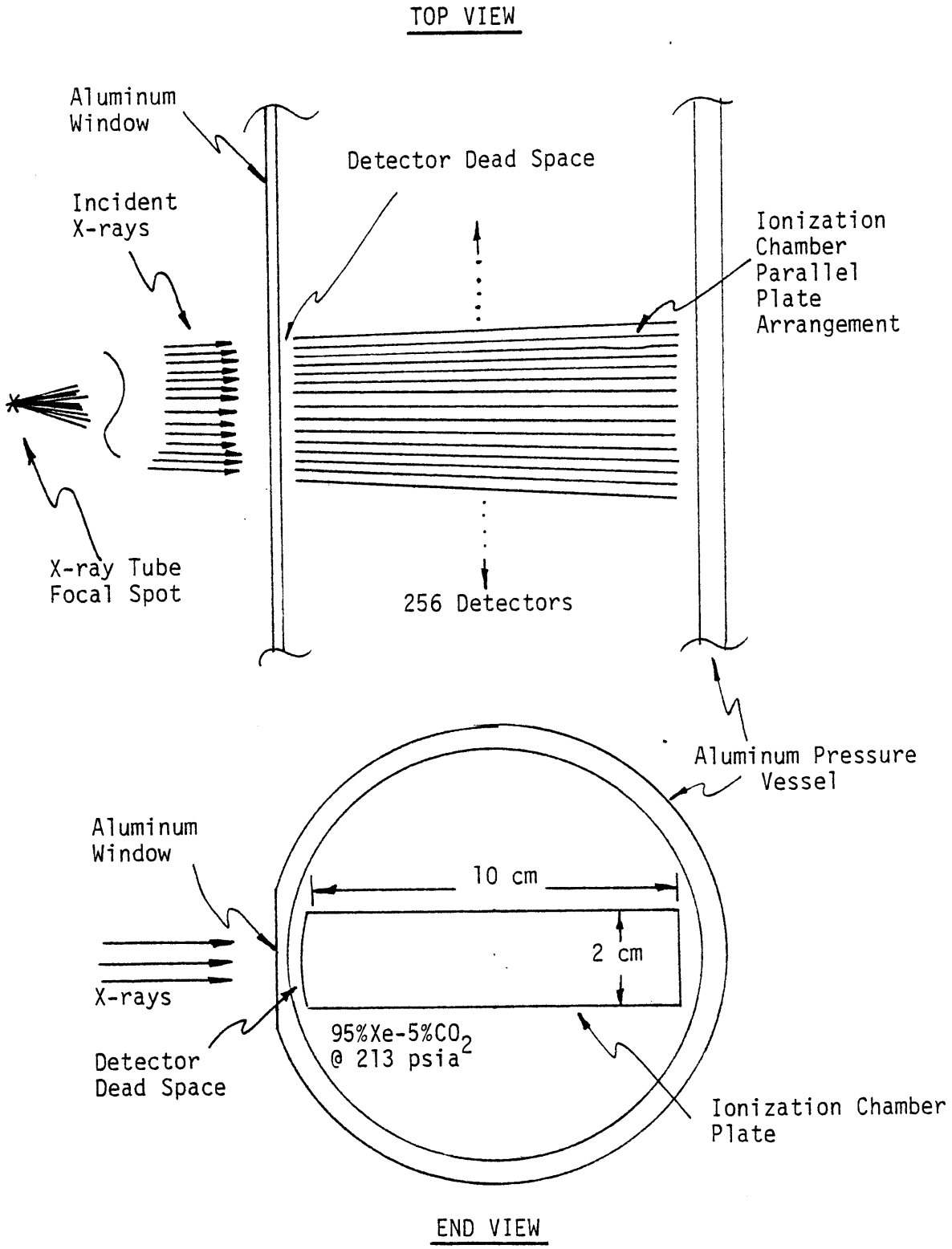

Figure 2.1A.3 Schematic Drawing of the Internals of the MGH Detector.

electric field lines within the chamber to then be collected, or they recombine with xenon ions in the gas. The ions also either travel along the electric field lines (from high to low potential) and are collected or they recombine with free electrons. Recombination of xenon ions and free electrons is kept to a practical minimum by running the detectors at a voltage potential that is sufficiently high to collect the charged particles before they have a chance to recombine; i.e., the detectors are run near to "saturation" (P.4, K.3). An experimentally-determined saturation curve is presented in Fig. 2.1A.4 for the centrally-located ionization chamber of this detector. Note that the ionization chamber never quite saturates with the Xe-CO_2 gas mixture. The operating point during the measurements in this research project was at 2500 V - well above the "knee" and in a comparatively flat region of the saturation curve. One final point about the detector is that if the incident x-ray has an energy greater than 34.56 keV there is about a 83.4% chance for a xenon K-shell electron to be ejected in the photoelectric process (D.3). The xenon ion, now lacking its K-shell electron, has about a 88.9% chance of emitting a 30.4 keV K-fluorescent x-ray (B.4, L.4). K-fluorescent x-rays are emitted isotropically from excited xenon atoms. These x-rays may do one of two things:

(1) interact with the gas media within the active region - forming electron-ion pairs which are then collected; or

(2) escape detection by either leaving the "active" region or getting absorbed within the charge collection plates.

Modeling of this process for parallel plate ionization chambers was considered by Yaffe (Y.1). An extension of his models was used in the transport calculations of this study.

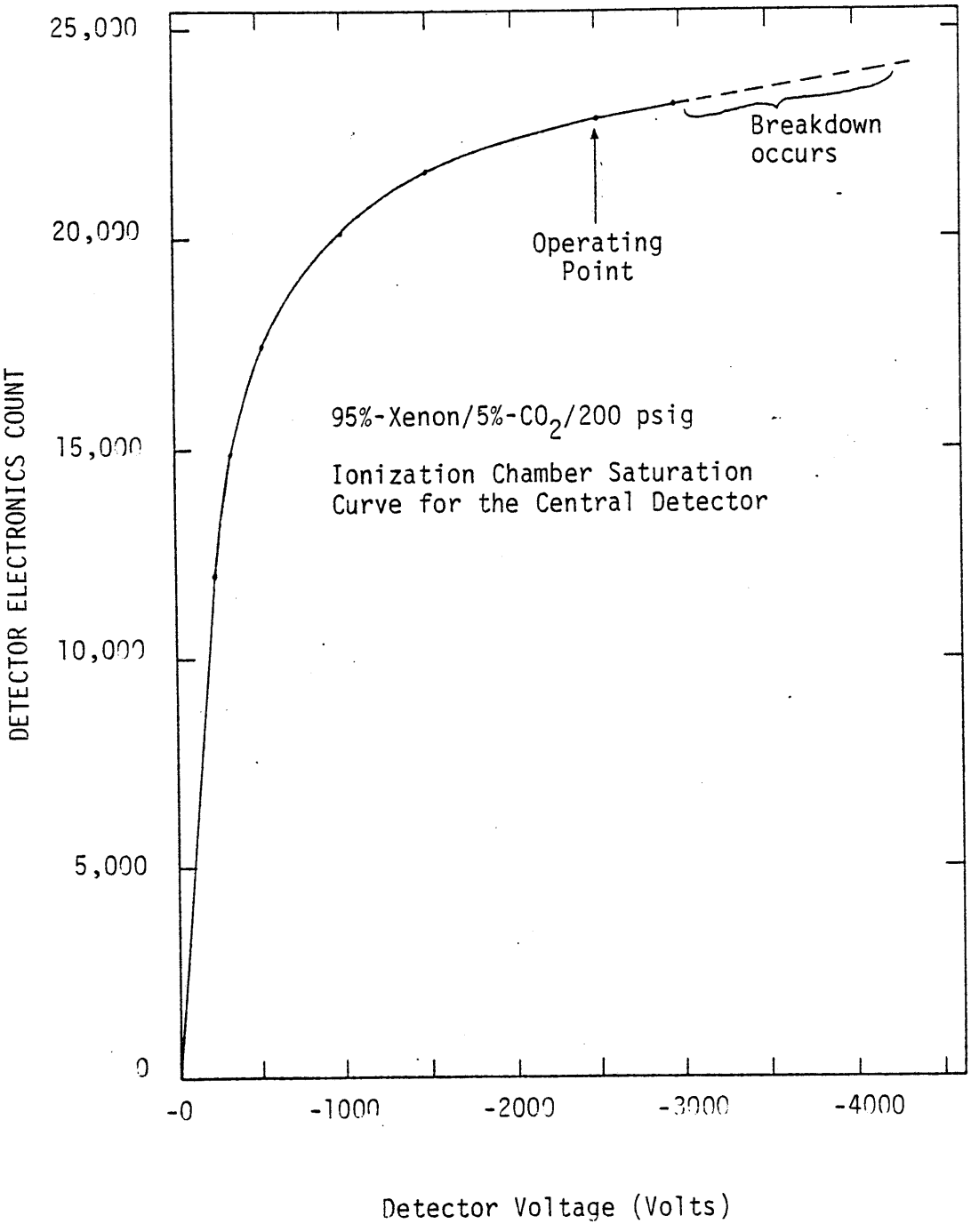

Figure 2.1A.4 Experimentally determined saturation curve for the detector's central ionization chamber (#129).

Due to the large photon fluxes used in CT scanning, the ionization chambers are run in the current mode and not the pulsed mode. The currents measured by each detector are very small. The currents range from 30 nA with no object in the path of the x-ray beam, down to 75 pA with 30 cm of water in the beam. In a typical scan, 300 measurements are performed on the rotating target; corresponding to one measurement every 30 msec. In the measurement process the current collected by the detectors is digitized by A/D (analog-to-digital) convertors. In the MGH scanner these convertors generate one pulse for a predetermined amount of charge collected. Thus, as the current increases the pulse rate increases. The average current measured during a 30 msec period can then be determined by summing the number of pulses produced by the A/D convertor during this period. This method of x-ray measurement and current digitization is very accurate. Figure 2.1A.5 shows the linearity of the detection system as a function of the incident photon flux (which is proportional to the electron current incident on the anode). Estimates of the degree of linearity (W.6) show that this detection system is linear to better than one part in a thousand.

One topic which is important to this experiment is transient response capability of the detectors. Since modulation of the incident x-ray beam is performed during the scan, the detectors must be able to quickly respond to the corresponding changes in the detected current. The transient response capability is discussed in Section 2.2B.

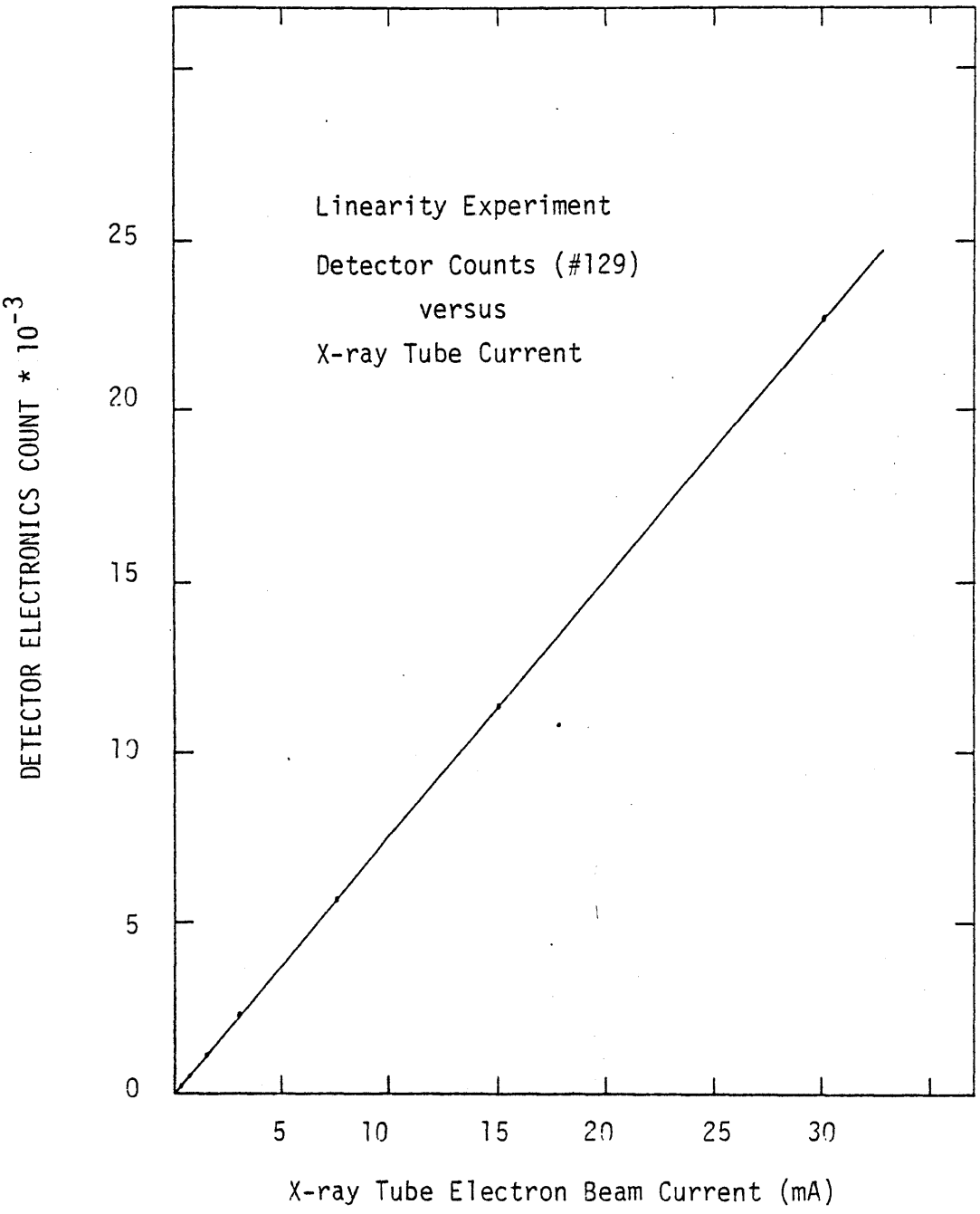

Figure 2.1A.5 Measurement of detector linearity for the central ionization detector (#129).

2.1B Physical Models and Figures-of-Merit Used in the Tomochemistry Spectra Study

The determination of the optimal pair of x-ray spectra to be used in tomochemistry involves a multiparameter study. Spectra filtration, x-ray tube voltage, patient dose, detected current, and statistical measurement accuracy are all interdependent variables in CT scanning. To aid in this study dimensionless figures-of-merit which uniquely characterize a spectrum were developed. It was shown that these figures-of-merit could be related to the statistical accuracy of the tomochemical composition measurement. In this section these figures-of-merit will be presented and their relationship to the physical models will be given.

As in most other medical x-ray imaging techniques CT scanning has been shown to be Poisson statistics limited (C.5). In this situation the primary tradeoff is between patient dose (photon fluence) and image quality (statistical noise). Since CT scanners use electronic detection systems, an additional consideration is the electronic signal to noise ratio. Furthermore, it has been shown that the statistical measurement accuracy of an attenuation coefficient within a picture element is related to the spatial resolution of the scanner (C.4); however, since the spatial resolution has been predetermined in this experiment, this parameter is not a free variable in this design.

Statistics Model - Normal CT

Chesler (C.5) has shown that if Poisson counting statistics error is the dominant error process in a CT system that the noise in

a reconstructed image due to statistical and reconstruction errors is given by the expression:

$$\sigma_\mu = \sqrt{\frac{4}{3}\frac{1}{N}}\left(\frac{1}{\mu_o \delta x}\right) \qquad (2.1B.1)$$

where:

δx (cm) is the size of the resolution element in the transverse element which is being reconstructed.

μ_o (cm^{-1}) is the water attenuation coefficient at the diagnostic energy of interest.

σ_μ is the standard deviation of the reconstructed resolution element attenuation coefficient.

N is the total number of photons counted which have pass through a resolution element.

It is assumed here that for this experiment that Poisson error is the dominant error process. Figure 2.1B.1 indicates the results of an experimental study to determine the validity of this assumption. It is seen that the electronic noise is not a negligible error process in comparison to Poisson statistics. It is believed that the additional error due to the electronics is not entirely noise, but rather that electronic drift due to temperature and line-voltage effects are also contributing to the error (B.7). Rather than developing a model for this electronic noise, it was assumed that the measurement error would still be proportional to $\sqrt{1/N}$ so that the results of this study would be valid for commercial CT scanners which presumably have less-noisy electronics.

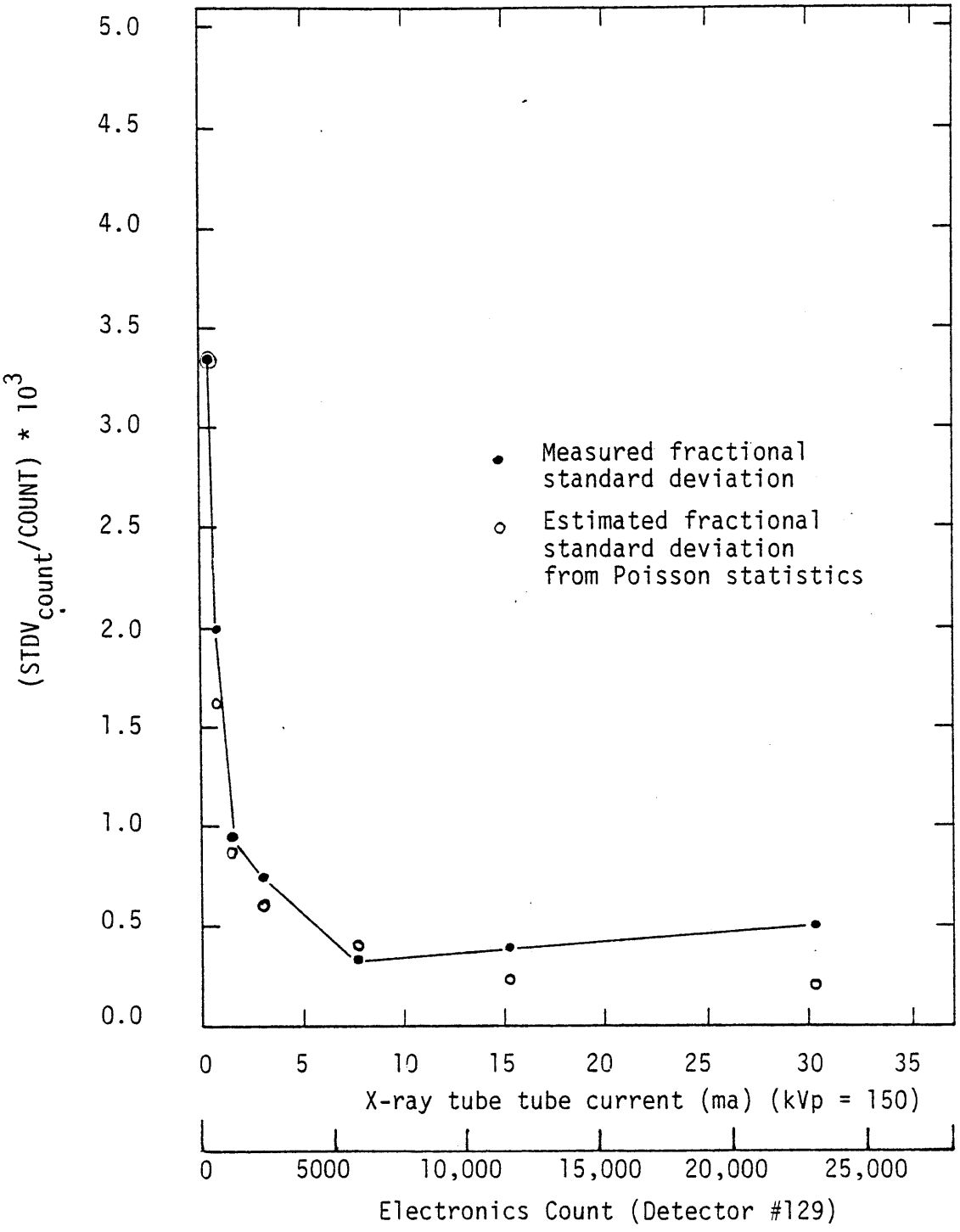

Figure 2.1B.1 Fractional standard deviation of the x-ray detector current versus the x-ray tube electron beam current (or electronics count) when the tube is operating at 150 kVp.

Surface Dose Model

Absorbed dose from CT scanning both in and out of the scanned slice of the body has been studied both with experimental and Monte Carlo methods (L.2). It was shown that over a wide range of incident spectra used in CT that

(1) the surface dose is the largest dose received from CT scanning

(2) scattered radiation contributes more than 10% to the surface dose and an even higher fraction to the internal dose

(3) for diagnostic energy x-rays the fraction of surface dose due to scattered radiation is approximately independent of the incident spectral shape.

The point dose kernel for surface dose (primary radiation) from CT scanning was solved approximately in the study. This derivation is presented in Appendix B.2. For a 20 cm water cylinder the primary surface dose is given by the expression:

$$\text{DOSE(primary)} = 0.68\ \Phi_R\ T \frac{\left(\int_0^{E_{max}} \phi(E)\ \exp(-\mu_F t_F)\ \frac{\mu_{en} E}{\rho}\ dE \right)}{\left(\int_0^{E_{max}} \phi(E)\ \exp(-\mu_F t_F)\ dE \right)} \frac{1\ \text{rad}}{6.25 * 10^{10}\ \frac{\text{keV}}{\text{gm}}} \qquad (2.1B.2)$$

where:

Φ_R is the photon flux in photons per cm^2-sec at the scanner rotation axis if no patient were present within the scanner.

T is the duration of the scan in seconds.

$\phi(E)$ (keV^{-1}) is the normalized bremsstrahlung spectral distribution of the x-ray tube operating at a given kVp.

$\mu_F(E)$, t_F are the beam-filtration attenuation coefficient at energy E and the thickness of the filter respectively.

$\frac{\mu_{en}}{\rho}\left(\frac{cm^2}{gm}\right)$ is the mass energy absorption coefficient of the tissue at the surface for photons of energy E.

Based on Eqs. (2.1B.1) and (2.1B.2) the calculational determination of an optimal experimental design concentrated on determining those spectra which would minimize the patient dose and maximize the statistical accuracy of a tomochemical composition measurement.

Development of Figures-of-Merit

To get a handle on the multiparameter analysis of possible spectra for tomochemistry a physical model was developed which could be related to three figures-of-merit. This model, presented in Fig. 2.1B.2, simulates the incident x-ray spectra from the x-ray tube, the beam filtration by the beam analyzer, the 20 cm water reference target, a 1 cm^2 centrally located resolution element within the water target, and the pressurized gas ionization detector. A more detailed description of the simulation model is given in Appendix B.3.

The three figures-of-merit developed which are related to the physical model are:

(1) the ratio of the surface dose to the energy detected, D/ϵ

(2) the average fraction of energy of a photon emitted by the x-ray tube which is detected, F

(3) the atomic composition sensitivity factor, S.

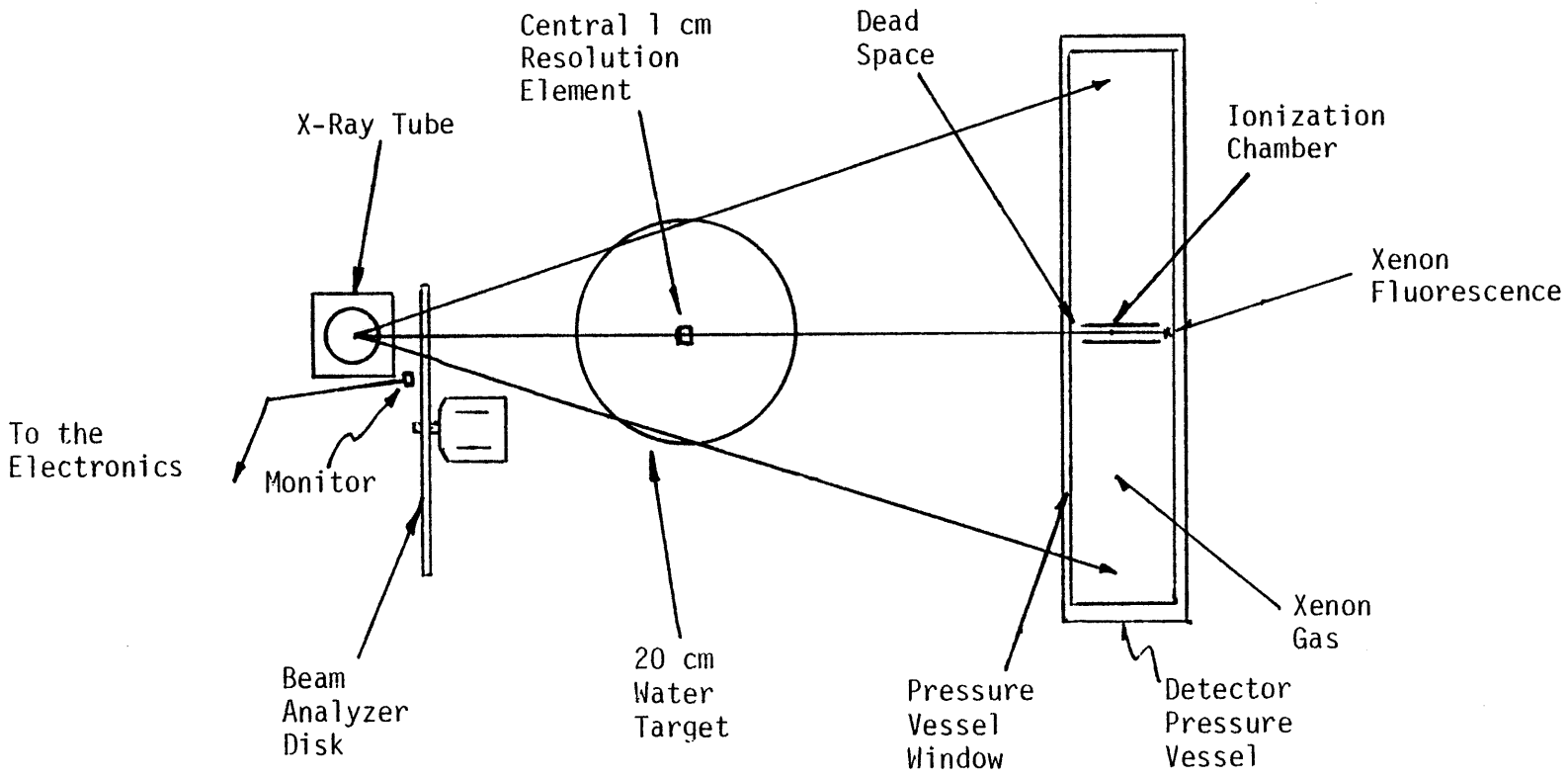

Figure 2.1B.2 Top view of the experiment simulation model.

All three of these figures-of-merit are dimensionless. They serve to characterize the quality of an incident spectrum for use in tomochemistry.

The first figure-of-merit is the ratio of the absorbed surface dose per photon to the energy detected per photon, D/ϵ:

$$D/\epsilon \equiv \frac{0.68 \int_0^{E_{max}} \phi(E)\, \exp(-\mu_F t_F) \left(\frac{\mu_{en} E}{\rho}\right) dE}{\int_0^{E_{max}} \phi(E)\, \exp(-\mu_F t_F)\, \exp(-\mu_W * 20)\, \varepsilon\, E\, dE} \qquad (2.1B.3)$$

where:

μ_W (cm^{-1}) is the water attenuation coefficient

$\varepsilon(E)$ is the detector efficiency at energy E

All other terms are the same as in Eq. (2.1B.2).

The two incident photon spectra used for tomochemistry must be chosen such that they are dose-efficient. This figure-of-merit quantifies this efficiency. For example, a very low energy ($\sim$ 40 keV) photon interacts primarily with water-like substances via the photoelectric effect. However, at this energy the surface dose per photon is high and the detected energy per photon is low so that the dose per energy detected ratio becomes large. This consideration thereby precludes the use of such low energy photons in tomochemistry. A more systematic treatment of optimal spectra choice is given in the next subsection.

The second figure-of-merit is the fraction, F, of the photon energy from the x-ray tube which is detected. F is given by the expression:

$$F \equiv \frac{\int_0^{E_{max}} \phi(E)\, \exp(-\mu_F t_F)\, \exp(-\mu_W * 20\ cm)\, \varepsilon(E)\, E\, dE}{\int_0^{E_{max}} \phi(E)\, E\, dE} \qquad (2.1B.4)$$

F, which is proportional to the current measured by the detector, is useful because it helps to determine an upper limit to the thickness of filtration which can be used in the beam analyzer disk. This upper thickness limit is determined by noting the detected current required to keep the Poisson error and the noise-to-signal ratio at acceptably low levels.

The third figure-of-merit used to characterize an x-ray spectrum is defined as the spectrum sensitivity factor, S. The sensitivity factor, described below, is an attempt to quantify the ability of a spectrum to accurately measure the photoelectric + Rayleigh cross section. The sensitivity factor is related to the tomochemistry measurement process by the definition:

$$S \equiv \left(\frac{I-I'}{I}\right) / \Delta Z = \frac{1}{I} (\Delta I / \Delta Z) \qquad (2.1B.5)$$

where the terms in this expression will be explained in the following discussion.

To motivate the definition of the sensitivity factor consider Fig. 2.1B.2. Imagine that a small 1 cm on a side test element has been postulated within the 20 cm water reference target. It is defined here that if the test element contains pure water, the detector measures a current, I. Now if the average atomic, $\bar{Z}$, within the test element is increased by a differential amount, $\Delta\bar{Z}$, the photoelectric and Rayleigh attenuation coefficients within the test element will also increase by a differential amount. Hence, in a transmission measurement of this new test element the detector will measure a differentially smaller current, defined here by the quantity I'. In general, as the energy of the incident x-rays decreases the Rayleigh and photoelectric attenuation coefficient increases much faster than the Compton attenuation coefficient. Thus the ratio $\Delta I/I$ (and hence the sensitivity) is larger when low energy x-rays rather than high energy x-rays are used to perform transmission measurements on the reference target. Therefore, in general one should use a spectrum with a large sensitivity to measure the photoelectric + Rayleigh cross section and another spectrum with a negligible sensitivity to only measure the Compton cross section.

Statistical Error Model

These three figures-of-merit were incorporated into the design procedure by relating them to the statistical error in a tomochemical composition measurement. It should be noted here that since the Rayleigh and photoelectric cross sections are much smaller than the Compton cross section in water-like tissue, the determination of the Rayleigh + photoelectric image is more difficult. Hence, the

corresponding noise level in the Rayleigh + photoelectric image will be larger than in the Compton image. Therefore, the effort in the design of this scanner concentrated on reducing the statistical noise level in the Rayleigh + photoelectric image.

As determined in Appendix B.3 the statistical error of measurement of the photoelectric + Rayleigh attenuation coefficient in the central resolution element is approximately given by the expression:

$$\frac{\delta\mu_{PR}}{\mu_{PR}} = \frac{\left[\frac{4}{3}\left(\frac{1}{N_{TH}} + \frac{1}{N_{TL}}\right)\right]^{1/2}}{\mu_{PR}} \frac{1}{X} \qquad (2.1B.6)$$

where

N_{TH}, N_{TL} is the number of detected photons using the high and low energy spectra respectively.

μ_{PR} is the photoelectric + Rayleigh attenuation coefficient of the central resolution element.

$\delta\mu_{PR}$ is the standard error of the measurement of μ_{PR}.

It is assumed in this expression that:

(1) The statistical error expression of Chesler (C.5) can be extended to describe tomochemistry statistical measurement error.

(2) The central resolution element corresponds to the worst case (largest fractional error) because compared to other positions within the target, transmission measurements of it must always be made through the full diameter of the water cylinder.

(3) Equal numbers of photons are detected at the 20 cm water thickness - corresponding to the optimal measurement efficiency as indicated in Appendix B.3.

It can be shown (Appendix B.3) that Eq. (2.1B.6) can be rewritten in terms of the three figures-of-merit in two unique ways.

The first alternative method of expressing Eq. (2.1B.6) has the x-ray tube energy-flux, Φ_E, as an explicit variable. This error formulation, derived in Appendix B.3, is given by the expression:

$$\frac{\delta\mu_{PR}}{\mu_{PR}} = \frac{\Delta\mu_{PR}}{\mu_{PR}} \frac{\left[\frac{4}{3}\left(\frac{\bar{E}_H}{F_H\Phi_E} + \frac{\bar{E}_L}{F_L\Phi_E}\right)\right]^{1/2}}{(S_L - S_H)\,\Delta Z} \qquad (2.1B.7)$$

where

subscripts H and L refer to the high and low energy x-ray beams respectively.

$\bar{E}$ refers to the average energy of the incident x-ray beam.

This expression can be used to determine the spectra combination which yields the minimum statistical error of a tomochemistry measurement for a fixed x-ray tube photon flux. Hence, through the use of Eq. (2.1B.7) one can determine those two x-ray spectra for use in tomochemistry which are photon-efficient.

The second alternative method of expressing Eq. (2.1B.6) has the x-ray surface dose, D, as an explicit variable. This error formulation, also derived in Appendix B.3, is given by the expression:

$$\frac{\delta\mu_{PR}}{\mu_{PR}} = \frac{\Delta\mu_{PR}}{\mu_{PR}} \frac{\left[\frac{4}{3}\left(\frac{\bar{E}_H\,[D/\epsilon]_H}{D_H\,A_D(D_D/D_R)^2} + \frac{\bar{E}_L\,[D/\epsilon]_L}{D_L\,A_D(D_D/D_R)^2}\right)\right]^{1/2}}{(S_L - S_H)\,\Delta Z} \qquad (2.1B.8)$$

where

D_D/D_R is the ratio of the source-detector to source-rotation axis distances.

All other terms are the same as those defined above. This expression can be used to determine the spectra combination which yields the minimum statistical error of a tomochemistry measurement for a fixed x-ray surface dose. Hence, through the use of Eq. (2.1B.8) one can determine those two x-ray spectra for use in tomochemistry which are dose-efficient.

In practice the choice of whether to use Eq. (2.1B.7) or Eq. (2.1B.8) is dependent upon whether the experimental situation is photon-fluence-limited or surface-dose-limited. A photon-fluence-limiting situation is one where, for a given pair of filters, the surface dose is less than the maximum acceptable dose when the x-ray tube photon fluence is at its physical maximum. Conversely, a dose-limiting situation is one where, for a given pair of filters, the maximum acceptable dose is reached at a photon fluence less than the maximum possible fluence. The next section uses the above models to determine whether the experimental setup is photon-fluence or surface-dose limited and then to determine which filters are optimal for tomochemistry.

2.1C Findings of the Photon Transport Studies

The purpose of this section is to present the calculational determination of the three figures-of-merit (F, S, and D/ϵ) for a wide range of experimental scenarios and to present the determination of the tomochemistry statistical measurement error using these figures-of-merit.

To begin the discussion consider the calculational determination of the sensitivity factor, S. As mentioned in the previous section and in Appendix B.3D, one wants to find the pair of filtered spectra which have the largest difference in their sensitivities so that the denominater in Eq. (B.3D.21) maximizes. Figures 2.1C.1 and 2.1C.2 illustrate the behavior of the $\Delta\overline{Z}$ sensitivity as a function of the filter atomic number for constant fractional transmission, F, for $\Delta\overline{Z} \simeq 0.148\ (0.02\ \overline{Z}_{H_2O})$. Note that the fractional transmission is kept constant and not the filter thickness because in general as the filter atomic number increases the fractional transmission of x-rays through the filter and target decreases - and hence the detected current decreases. To make a fair comparison between filters one should really compare them relative to one another at the same detected current (which corresponds to the same F). Thus, in general to have the same detected current at increasing filter Z the thickness must decrease. In the actual calculation of the figures-of-merit the fractional transmission, F, was chosen first, the computer program then iteratively determined the filter thickness required to give that fractional transmission.

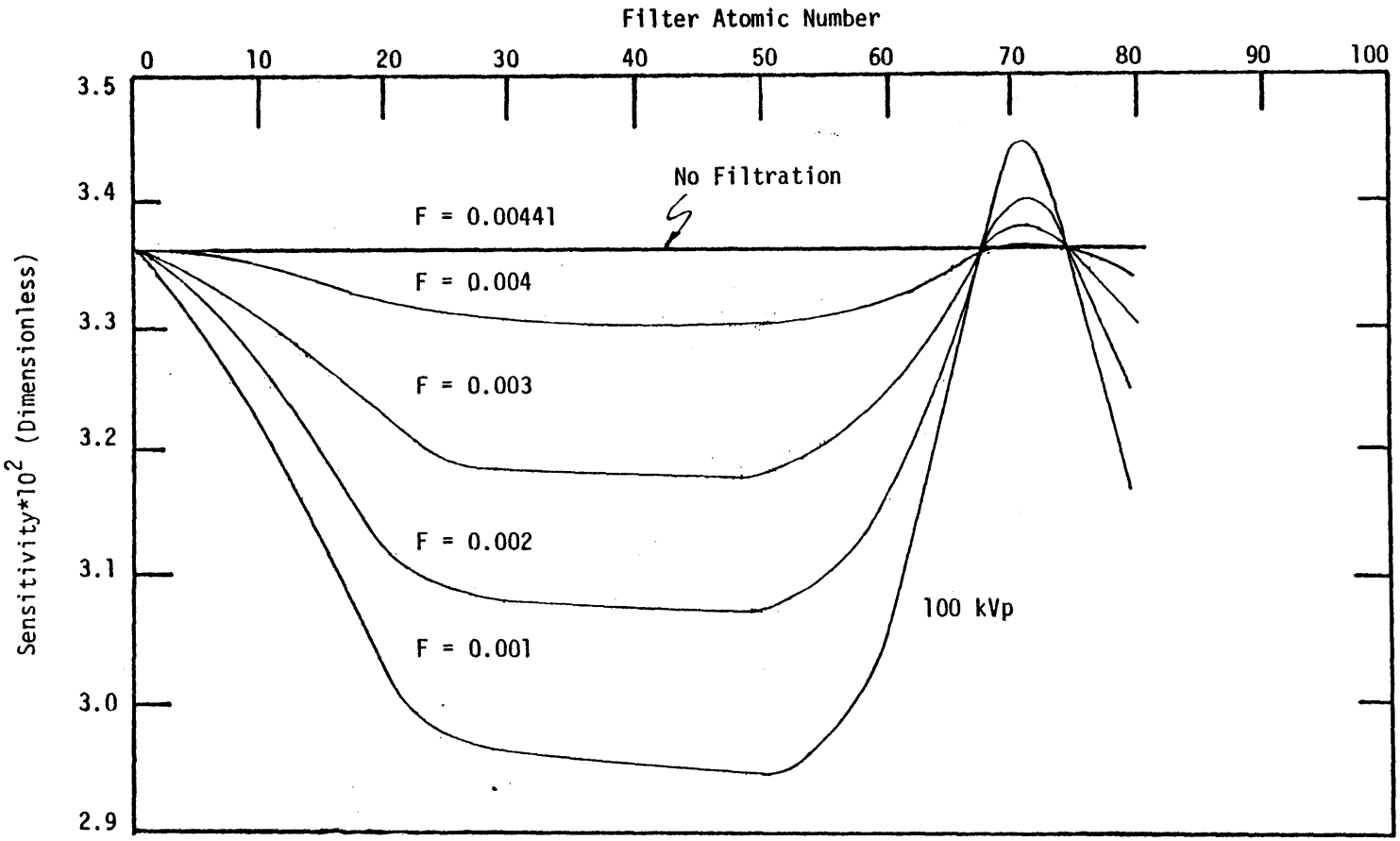

Figure 2.1C.1 Sensitivity factor versus filter atomic number for a 100 kVp x-ray spectrum for five different fractional transmissions, F.

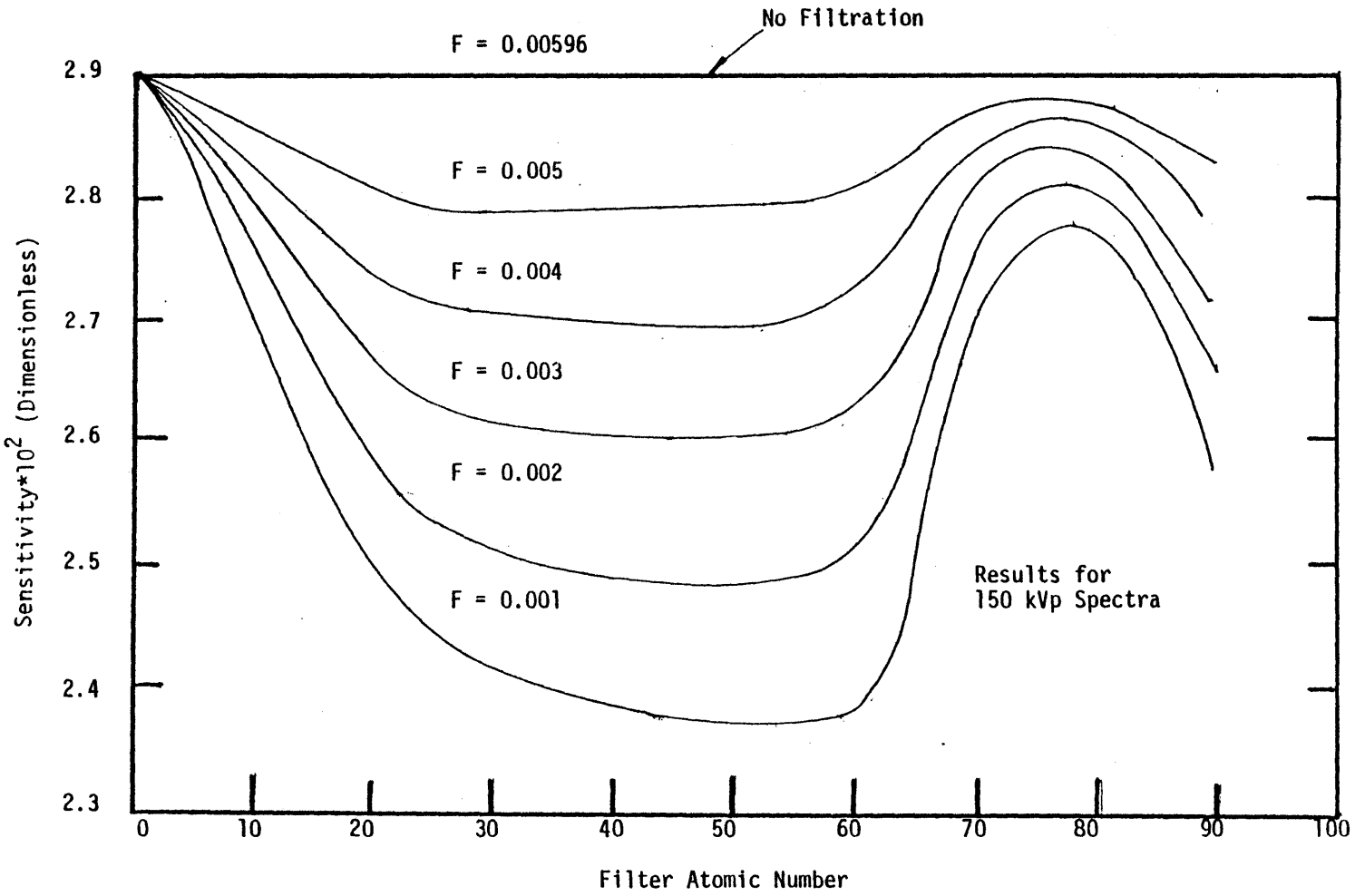

Figure 2.1C.2 Sensitivity factor versus filter atomic number for a 150 kVp x-ray spectrum for six different fractional transmissions, F.

In both Fig. 2.1C.1 and Fig. 2.1C.2 note that the straight line corresponds to the case of zero-thickness filtration. Hence, since the spectral shape doesn't change with changing filter atomic number the sensitivity is constant. For the 100 kVp spectrum $(\Delta I/I)/\Delta Z \cong 3.65*10^{-2}$ while for the 150 kVp spectrum $(\Delta I/I)/\Delta Z \cong 2.9*10^{-2}$. The larger sensitivity for a 100 kVp spectrum reflects the larger fraction of the photon population at the more $\bar{Z}$-sensitive lower energies.

At increasing filtration (decreasing F) with the same filter material, the sensitivity changes, reflecting the selective removal of different parts of the x-ray tube spectrum at increasing filtration. This is not unexpected. However, it is seen that a most interesting behavior occurs as the filter atomic number is increased while maintaining F constant. To understand this behavior it should be remembered that as the atomic number of an element increases the ratio $(\mu_{Compton}/\mu_{Photoelectric})$ decreases, and the K-edge energy increases.

To explain Figs. 2.1C.1 and 2.1C.2 consider first the behavior of the sensitivity for filtration with low-Z filters. With low-atomic-number filters Compton scattering dominates the attenuation. Since the Compton cross section is relatively flat at diagnostic energies, the filter only serves to depress the x-ray beam intensity while maintaining the original spectral profile. Hence the sensitivity changes very little.

At intermediate filter atomic numbers the ratio $(\mu_{Compton}/\mu_{Photoelectric})$ is small. Thus, filtration selectively removes the low energy Z-sensitive photons. As the filtration is increased (F decreased), the sensitivity is seen to decrease as the 'sensitive' photons get more totally removed from the spectrum.

As the filter atomic number is increased even further the effect of the K-edge becomes evident. Below the filter K-edge energy there is a sharp drop in the filter's attenuation coefficient. This sharp drop in the attenuation allows a 'window' of low energy x-rays to be transmitted through the filter. These low energy photons then contribute to the sensitivity of the resultant spectrum.

For both 100 kVp and 150 kVp the sensitivity factor peaks around Z = 75. For this atomic number the K-edge occurs at 71.68 keV. Further study into this phenomenon indicated that at about 65 keV (just below the Z = 75 K-edge energy) an optimum is struck. At this energy an incident photon's ability to pass through the water target and still be sensitive to $\Delta\bar{Z}$ changes is optimal. Beyond this optimum as the filter atomic number (and K-edge energy) is further increased, the 'window' photons are less sensitive to elemental composition ($\bar{Z}$) and the spectrum sensitivity decreases. Note that for 100 kVp the sensitivity at Z = 75 is greater than the original spectrum sensitivity. This signifies that the tantalum filtration was effective at producing a monochromatic low energy spectrum. A little thought should convince the reader that a low energy monochromatic spectrum has a greater sensitivity than a polychromatic spectrum. This is because a polychromatic spectrum contains both 'sensitive' and 'insensitive' photons while the monochromatic spectrum only contains 'sensitive' photons.

The possibility of using compound filters (a filter combination) was also investigated. It was found that no pair of filters would increase the sensitivity beyond the maximum sensitivity calculated above. This phenomenon can be quickly explained by the following

model of the photoelectric effect for a pair of filters. Let one filter have a K-edge and the other no K-edge. The total photoelectric cross section below the K-edge energy for this pair is given by:

$$\mu_{E<K} = C_{1<K} E^{-3.2} + C_2 E^{-3.2} \qquad E<K_{edge} \qquad (2.1C.1)$$

and above the K-edge energy

$$\mu_{E>K} = C_{1>K} E^{-3.2} + C_2 E^{-3.2} \qquad E>K_{edge} \qquad (2.1C.2)$$

Now the 'window' effect is most effective when the ratio of the attenuation coefficients just above and just below the K-edge, $(\mu_{E>K}/\mu_{E<K})$, is as large as possible. This is because as the ratio becomes larger the probability of transmission increases for a photon with an energy just less than the K-edge energy. To determine whether the compound filter is better than the simple filter compare the ratio of Eq. (2.1C.1) and Eq. (2.1C.2) with and without filter 2:

$$\frac{C_{1>K} + C_2}{C_{1<K} + C_2} \stackrel{?}{>} \frac{C_{1>K}}{C_{1<K}} \qquad (2.1C.3)$$

Since C_2 is a positive number, it is known that the left hand side of Eq. (2.1C.3) is less than the right hand side of Eq. (2.1C.3). Therefore, the simple filter is better than the compound filter to produce a low energy spectrum.

The next figure-of-merit to consider is the surface dose to energy detected ratio, D/ϵ. As seen in Fig. 2.1C.3 the surface dose per energy detected is minimum for a low sensitivity-high kVp spectrum (Fe, 150 kVp). This is because the photon transmission through the water is higher at higher x-ray energies while the dose per photon is lower at higher x-ray energies. At the other extreme a high sensitivity-low kVp spectrum, which has a larger fraction of low energy photons, has the highest D/ϵ ratio. One last feature to note is that at increased filtration the D/ϵ ratio decreases as more low energy photons are removed from the spectrum.

At this point, to simplify the further analysis, a choice was made of the filter materials to be used in the design. The choice of filters was narrowed significantly by keeping in mind the practical engineering criteria listed in Table 2.1C.1 as well as the behavior of the sensitivity factor. Iron was chosen as the leading candidate for use as the low sensitivity filter. Its strongest points are its availability, machinability and strength. For similar reasons, the prime candidate for the high sensitivity filter is tantalum ($Z = 73$). Other filters were eliminated as candidates for use as high sensitivity filters for various reasons. Beryllium ($Z = 4$), for example, was eliminated because of the bulky quantities required for filtration. Tungsten ($Z = 74$) was rejected because of its brittle nature and poor machinability.

With the filter materials chosen a determination must be made of the filtration thickness and the operating x-ray tube voltage. At this point recall Eqs. (2.1B.7) and (2.1B.8) where the statistical

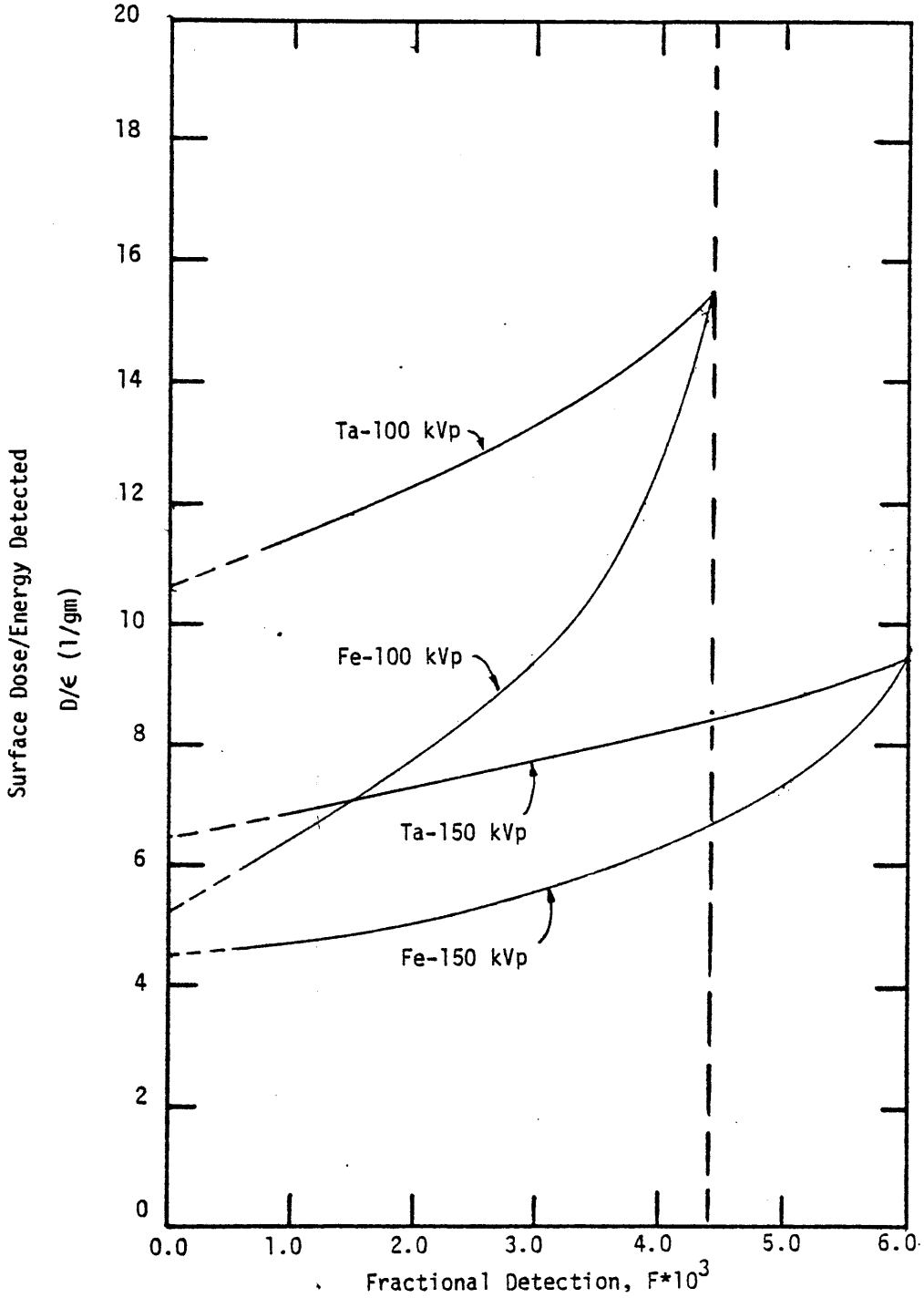

Figure 2.1C.3 Surface dose per energy detected versus fractional transmission, F, for the four different x-ray tube voltage-filtration combinations.

1. Mechanical strength

2. Machinability and workability and manufacturing methods required using these materials

3. Achievable tolerances of filter manufacture using these materials

4. Raw material availability and cost

5. Material toxicity

6. Normal physical state of the material, i.e., gas, liquid, or solid

Table 2.1C.1 Practical engineering considerations in the choice of filter materials for use in the beam analyzer disk.

error can be expressed in terms of the x-ray tube flux or the surface dose. Figures 2.1C.4, 2.1C.5, and 2.1C.6 present the measurement error, for a unit x-ray flux and for a unit surface dose, versus the fraction, F, of the incident x-ray tube spectrum which is detected for three different experimental scenarios. These scenarios represent experiments which use a fixed 100 kVp x-ray tube spectrum, a fixed 150 kVp x-ray tube spectrum and alternating 100 kVp-Ta/150 kVp-Fe spectra. The iron and tantalum thicknesses which correspond to the fractional detection are indicated in the figures.

The behavior of the statistical uncertainty as seen in these figures can be explained with three remarks:

(1) When no filtration is present, the input spectra are the same (at the same kVp). Therefore, the uncertainty of the photoelectric + Rayleigh cross section measurement using the 'two' spectra is infinite.

(2) As the filtration is increased (F decreased) while holding a constant incident photon flux, the difference in sensitivities between the two spectra increases, decreasing the measurement uncertainty. The uncertainty minimizes and then increases at heavier filtrations as the numerator in Eq. (2.1B.7) begins to dominate the error expression. In other words, at a fixed x-ray tube flux very heavy filtration eliminates such a large fraction of photons from the x-ray beam that the Poisson counting statistics dominate the tomochemical measurement uncertainty.

(3) In contrast to the fixed x-ray tube flux scenario, the constant dose scenario assumes that for any thickness of filtration used, the x-ray tube flux can be increased to any desired value such that the surface dose will remain constant. It is seen in the constant dose scenario that as the filtration is increased the denominator in Eq. (2.1B.8) once again dominates the error expression. As the filtration is made heavier (increasing the photon flux correspondingly) the error continues to decrease. This phenomenon is due to the more

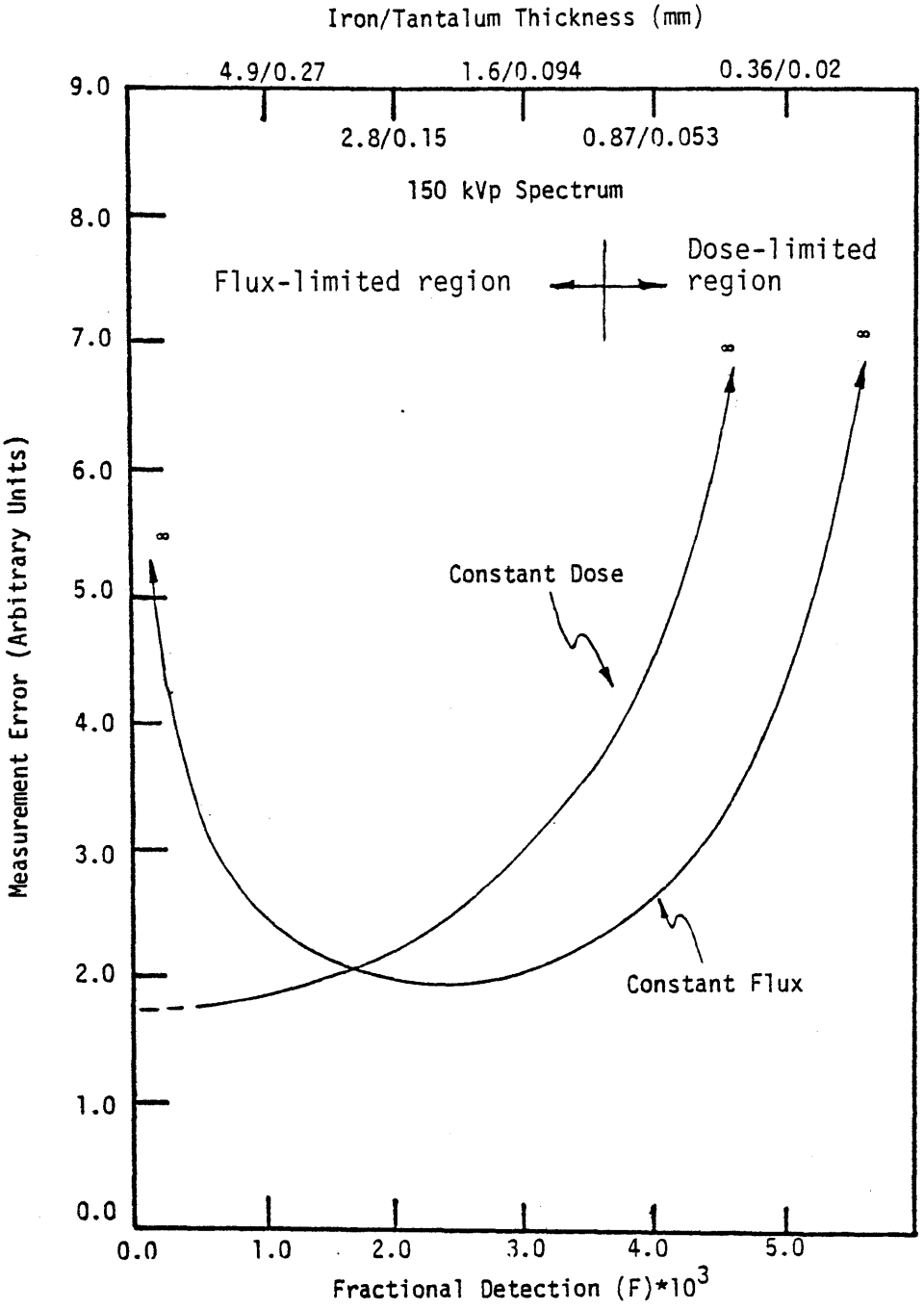

Figure 2.1C.4 Photoelectric + Rayleigh attenuation coefficient statistical measurement error versus fraction transmission, F, for a 150 kVp/Fe and 150 kVp/Ta incident spectra pair.

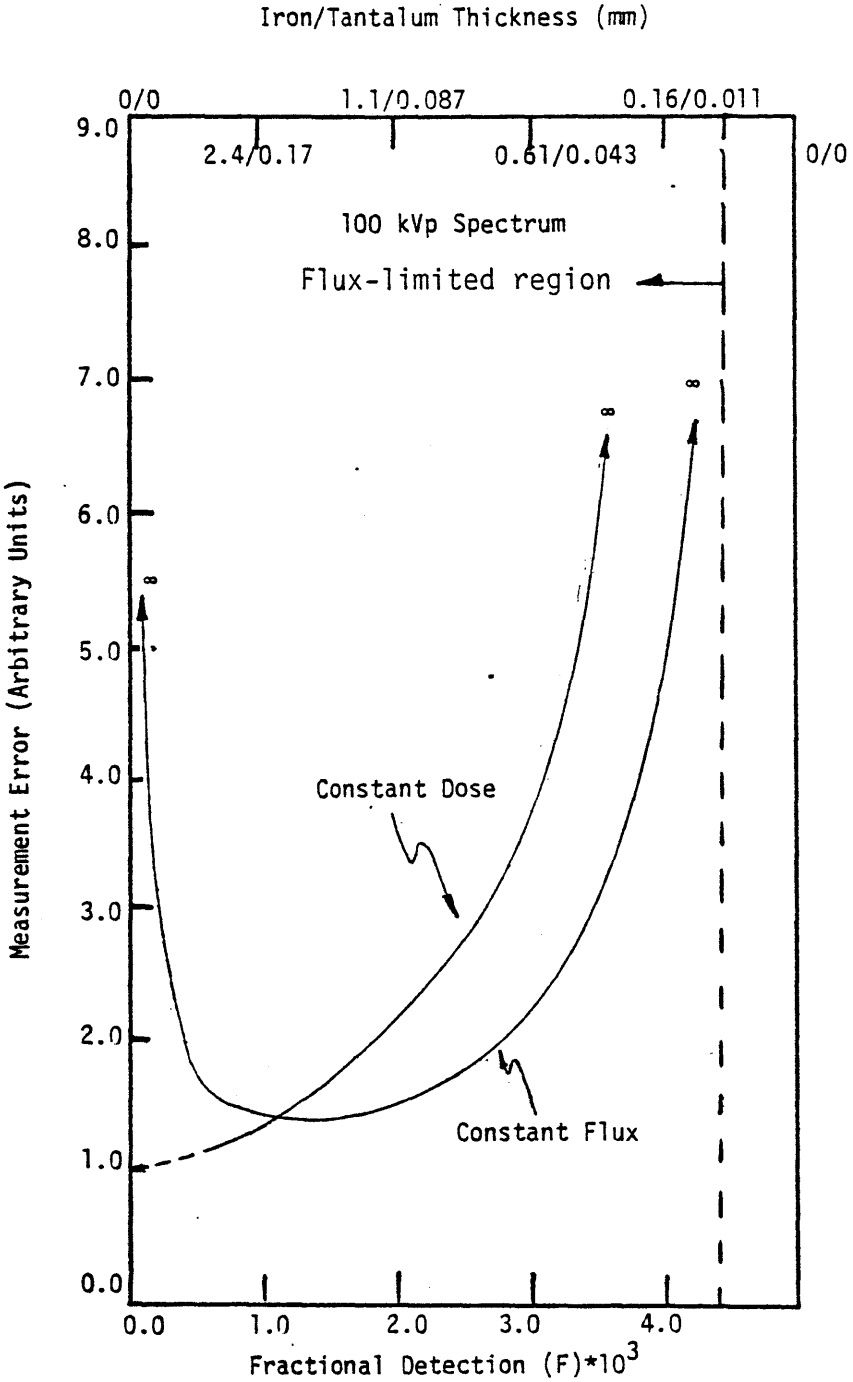

Figure 2.1C.5 Photoelectric + Rayleigh attenuation coefficient statistical measurement error versus fractional transmission, F.

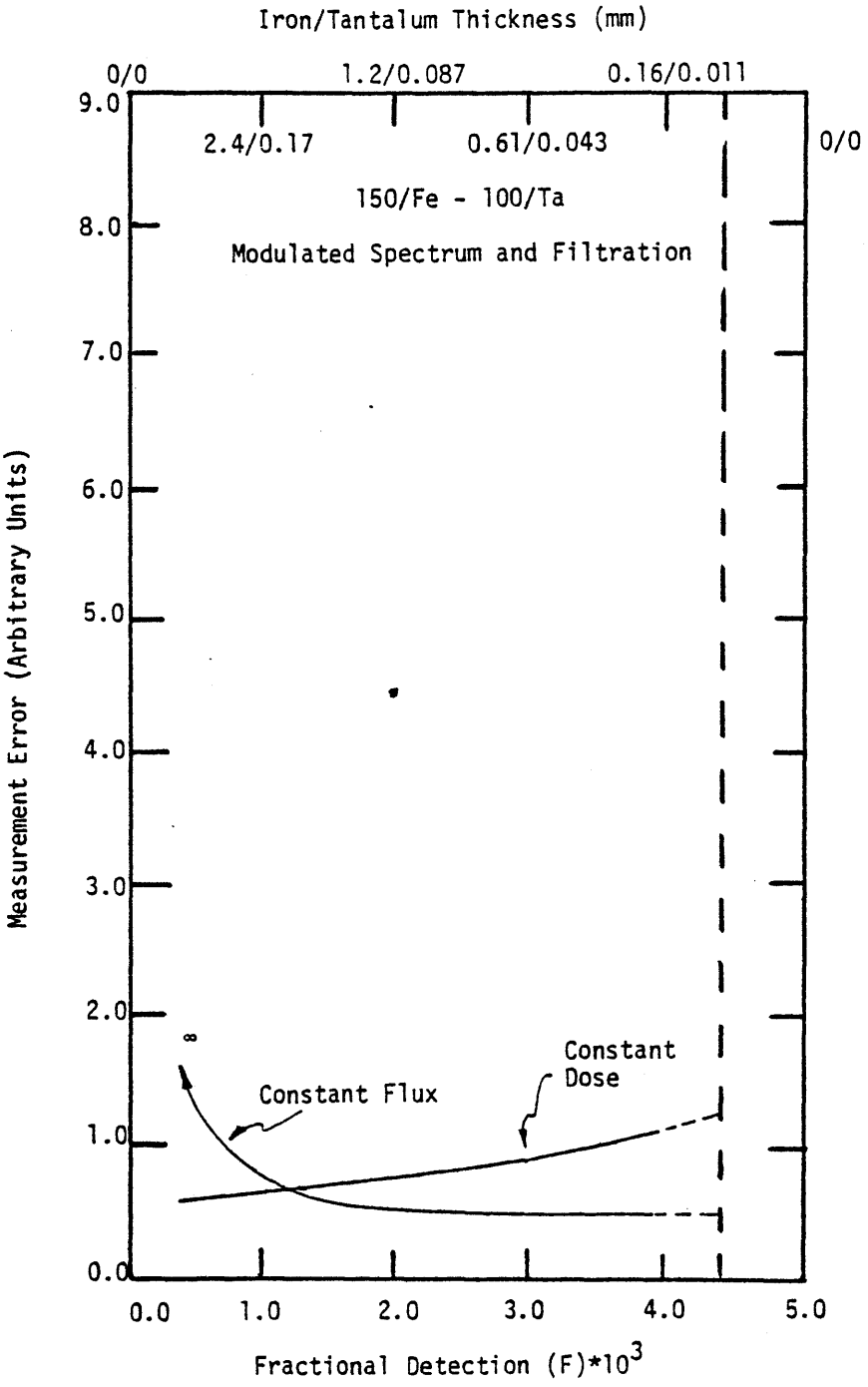

Figure 2.1C.6 Photoelectric + Rayleigh attenuation coefficient statistical measurement error versus fractional transmission, F, for a 150 kVp/Fe and 100 kVp/Ta incident spectra pair.

monochromatic nature of the resultant filtered spectra as the filter thickness is increased.

To determine how much filtration to use in the experiment, one must consider that in general there are photon flux limitations to all x-ray tubes. Indicated in Figs. 2.1C.4, 2.1C.5 and 2.1C.6 are the domains for a flux-limiting and dose-limiting situation (assuming that the maximum acceptable dose is 4 rads). It is seen that for all three experimental scenarios the minimal statistical error optima using constant dose or constant photon flux all occur in the flux limiting regime. Therefore, the choice of spectrum filtration was determined on the basis of a photon-flux-limiting situation. It should be noted here that there is fortuitously not much difference between the statistical error using the optimal constant dose filtration and the optimal constant flux filtration. With the above considerations in mind, the filters chosen for the experiment were a 2.16 mm thick iron filter and a 130 μm thick tantalum filter. Figure 2.1C.7 presents the resultant spectral distributions for 100 kVp and 150 kVp x-ray tube spectra when filtered with these filtrations. The specific design of these filters is described in Section 2.2.

Insight into the choice of which kVp to use in the experiment is obtained by observing once again the behavior of the statistical error curves in Figs. 2.1C.4, 2.1C.5, and 2.1C.6. Since the sensitivity terms in Eq. (2.1B.7) dominate the behavior of the statistical error, it is seen that at the same x-ray tube photon flux, successively smaller measurement errors are achieved as one goes from the 150 kVp to the 100 kVp to the alternating kVp 150-Fe/100-Ta scenario. Furthermore,

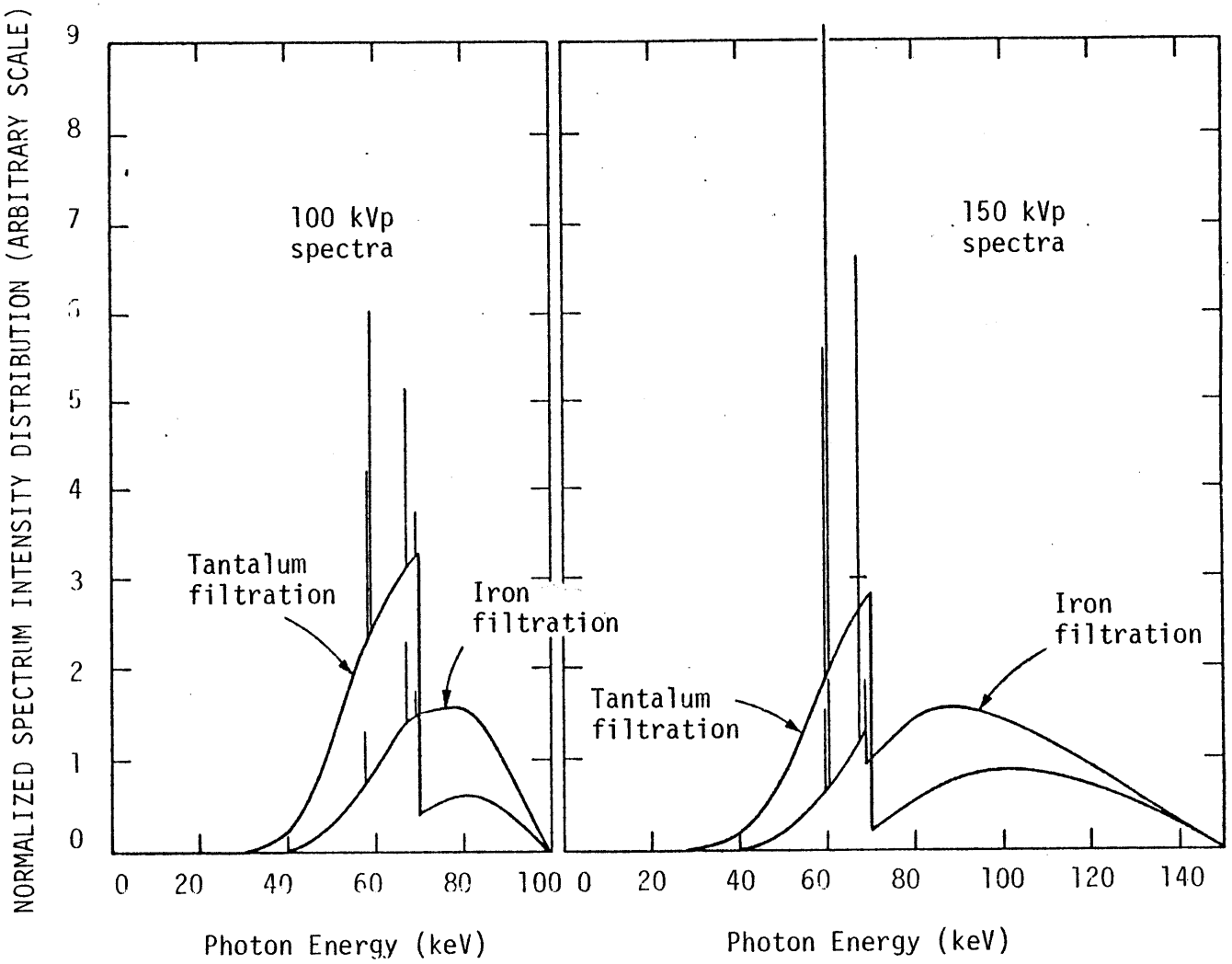

Figure 2.1C.7 X-ray spectrum distributions using x-ray voltage potentials of 100 kV and 150 kV with tantalum and iron filtrations.

it is also seen in these figures that at the same surface dose, successively smaller measurement errors are acheived as one goes from the 150 kVp to the 100 kVp to the alternating kVp 150-Fe/100-Ta scenario. Therefore, the information-to-dose ratio is better at 100 kVp than at 150 kVp and it is better yet if the x-ray tube voltage is alternated.

Experimentally, though, the surface dose or the x-ray tube photon flux are not kept constant as the kVp is changed. Usually it is the electron beam current on the target (ma) that is kept constant. At increasing kVp the bremsstrahlung x-ray production efficiency increases so that the photon flux also increases. Figure 2.1C.8 shows experimental measurements of the photon energy flux (detector current) versus x-ray tube kVp for the iron and tantalum filtrations. Since the photon energy flux is so much larger (the dose rate is also higher) at 150 kVp than at 100 kVp the statistical tomochemical measurement error is less at 150 kVp. More exactly:

$$\frac{(\delta\mu_{PR}/\mu_{PR})\big|_{150}}{(\delta\mu_{PR}/\mu_{PR})\big|_{100}} \simeq 0.89$$

Furthermore, by accounting for the different photon flux in the alternating kVp case it was found that:

$$\frac{(\delta\mu_{PR}/\mu_{PR})\big|_{150/100}}{(\delta\mu_{PR}/\mu_{PR})_{100}} \simeq 0.33$$

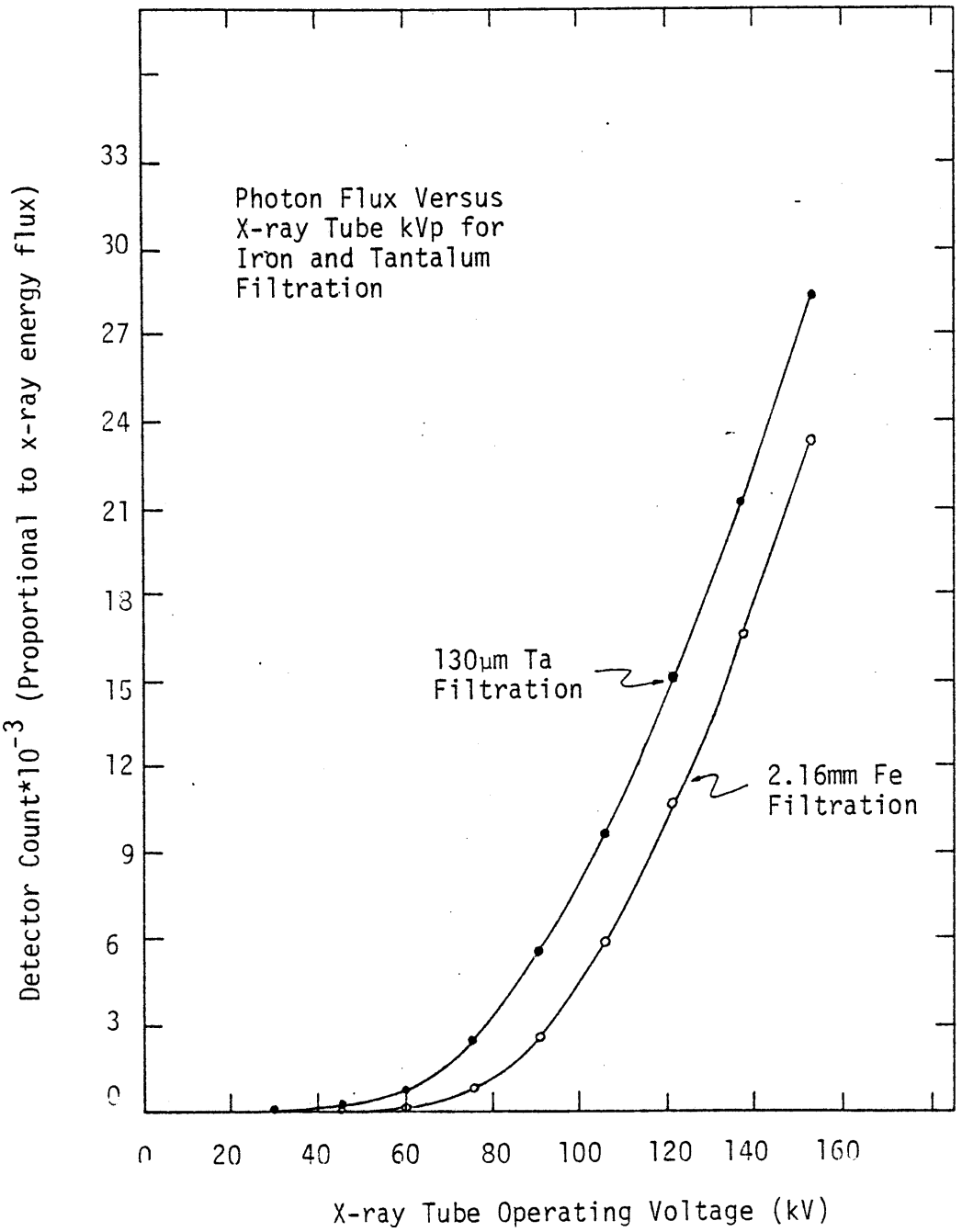

Figure 2.1C.8 X-ray tube flux versus x-ray tube operating voltage, kV.

Therefore, from a tomochemistry statistical error viewpoint,if a higher dose is acceptable then 150 kVp is better than 100 kVp and an alternating kVp/filter arrangement would be the best.

In the experiment an alternating kVp was not used in the proof-of-principle experiment so that any potential problems due to the transient response of the x-ray tube/power supply part of the experiment would be avoided. Furthermore, 100 kVp was used in the scanning experiments because it was felt that the better information-to-dose ratio made this kVp more worthy for investigation than 150 kVp.

It should be noted here that the above computations performed with 100 kVp and 150 kVp spectra do not necessarily infer that either of these spectra are the optimum for tomochemistry. The use of these spectra only reflect the availability of accurate experimental data. The optimum fixed kVp setup for tomochemistry was determined experimentally and is presented with the experimental results in Chapter 4.

Tomochemistry Scan Dose Estimate

With the filter materials chosen and the scan duration known, it is possible now to use Eq. (B.1.10) in Appendix B.1 to estimate the dose from a tomochemistry scan. Using a 100 kVp photon spectra with 30 mA of current on target the photon flux from the tube was estimated to be $6.6*10^{9}_{\gamma}/cm^{2}$-sec at 1 m from the focal spot. Hence, using the alternating 2.16 mm thick iron and 130 μm thick tantalum filtrations, the primary surface dose is about 820 mRad and the total surface dose is about 900 mRad for a single 10 second scan. As indicated in Appendix B the total surface dose from multiple contiguous scans will cause this

estimate to go up by as much as 50% (~1.35 R). Therefore, to get a valid estimate on the dose one must consider the clinical procedure used.

2.1D Conclusion - Findings of the Nuclear Engineering Studies

A model for the Poisson statistical error in average atomic number, $\bar{Z}$, or photoelectric + Rayleigh attenuation coefficient imaging in tomochemistry was developed. Through the use of this model figures-of-merit were developed which provided insight into the sources of error in a tomochemical analysis. By then using a one-dimensional transport code to simulate CT scanning in conjunction with the results from a three-dimensional Monte Carlo code which simulated photon dose from CT scanning, the full range of x-ray filtration possibilities and two x-ray tube spectra (100 kVp, 150 kVp) were examined. Given the engineering constraints of the experimental design it was determined that:

(1) Two possible optimization conditions exist: One optimization is the minimum measurement error for a specified patient surface dose, while the other optimization is the minimum measurement error for a fixed x-ray tube flux. Practical considerations dictate that one should design the experiment using the second optimization condition.

(2) For a fixed x-ray tube spectrum, 2.16 mm of iron and 130 μm of tantalum filtration are optimal for a tomochemical $\bar{Z}$ analysis.

(3) At the same x-ray tube photon flux or at the same surface dose for a fixed filtration combination, a 100 kVp spectrum is better than a 150 kVp spectrum.

(4) Simultaneous modulation of the peak kilovoltage and spectrum filtration using the 150 kVp/2.16 mm Fe and 100 kVp/130 μm Ta combination decreases the measurement error by more than a factor of 2 over filtration modulation alone.

(5) The total surface dose from a single 10 second 100 kVp-30 mA iron-tantalum tomochemistry scan is about 900 mRad. This estimate will increase with higher kVp due to the larger photon flux. The estimate will also increase as the number of contiguous scans performed increases.

2.2 Electrical and Mechanical Engineering Considerations in the Beam Analyser Design

With the filter materials chosen the problem remains as to how to mechanically modulate the x-ray fan beam filtration. This section presents the major electrical and mechanical problems to be considered in developing a filtration modulation device. This section also presents the filtration modulation method used in the proof-of-principle experiment of this research project.

Mechanical Engineering Considerations

A 14" diameter rotating steel disk with tantalum filter inserts was chosen to alternately filter the fan x-ray beam. This disk, shown in Fig. 2.2.1, was placed in the fan beam as close to the x-ray tube as possible ($\sim$10 cm from the focal spot) and in such a way so that the filtration change occurred simultaneously for all the detectors. The disk was driven by a 1/16 hp variable speed DC motor at the modest angular velocity of 166 RPM. It contained 12 different filter sections, 6 tantalum and 6 iron (steel), so that 300 different 30 msec transmission measurements were made in a 10 second scan.

A rotating disk was chosen as the primary candidate over alternative methods (such as a reciprocating filter arrangement) mainly because of the ease of manufacture. Low carbon steel (about 0.1 weight percent carbon) was used because of its availability and machinability. The carbon within the steel was determined to have a negligible effect upon the filtration process. The disk was manufactured as a solid plate and coupled to the drive shaft of the motor by a bushing specially manufactured for the disk. The uniform 2.14 mm thickness

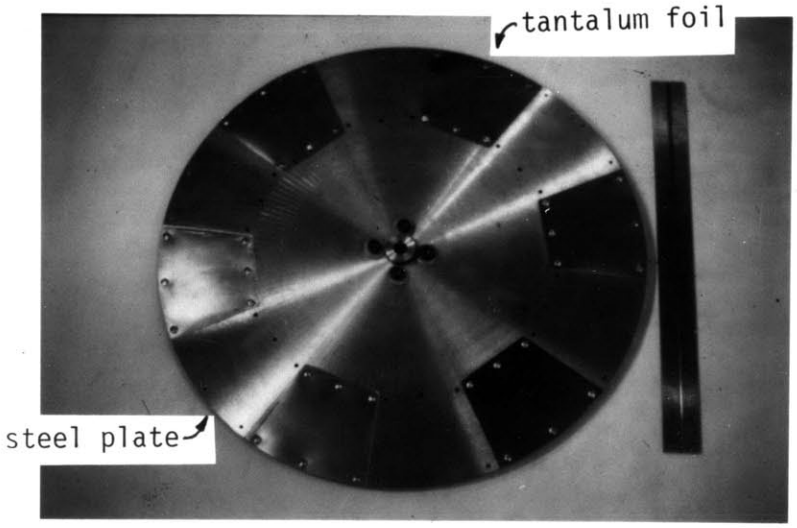

Figure 2.2.1 Photograph of the beam analyser disk used in the proof-of-principle experiment.

(+/- 13 μm) of the steel plate was achieved by grinding a slightly thicker plate on a blanchard grinder down to this desired thickness and uniformity. Note that the uniformity of the filter thickness was important to the performance of the filtration because it was important that the measured current fluctuations due to machining variations were negligible. After the grinding operation slots were machined out of the disk for the insertion of the tantalum foils.

The uniformity of the tantalum foil in the as-received condition was 130 μm +/- 1 μm. No attempt was made to better this uniformity. The machining of the tantalum foils for the insertion into the disk slots was accomplished through the use of an identical pair of steel templets. These steel templets were machined to match the dimensions of the machined slots of the steel disk. The tantalum foil to be machined was then clamped between these templets and the overhanging tantalum was removed, via milling, until the edge of the foil was flush with the steel. In this way the tantalum was accurately machined so that no 'light leaks' would be created when the foils were inserted within the disk.

Since the disk was flat and the fan beam subtended an angle, the x-rays from the x-ray tube did not all pass normally through the disk. Hence, the thickness of filtration as seen by the x-rays was not the same for every detector. In the extreme case of the end detector compared to the central detector the filtration thickness difference was 2.5%. This thickness change caused a negligible sensitivity change in the low (∿0.3% change) and high (∿1.7% change) energy spectra.

However, this slight difference was sufficient reason to perform independent detector calibrations with respect to the tomochemistry experiments.

For a variety of reasons it was desirable for the beam analyser disk diameter in the proof-of-principle experiment to be as large as possible. The 14" diameter was chosen here primarily because the blanchard grinder used in the manufacturing operation could not handle a disk with a diameter greater than 14". For geometry reasons the disk had to be large enough to avoid conflicts of the x-ray beam with the DC motor and to enable the scanning of reasonably large objects of interest ($\sim$25 cm diameter). Furthermore, from a control standpoint the stability of the angular velocity, ω, of the disk improves as the diameter and hence the moment of inertia of the disk increases (B.12).

The 166 RPM angular velocity of the disk was chosen because it was determined that 300 views were required in the CT scan. The requirement of 300 views was determined from the sampling criteria of CT scanning developed by Tretiak and others (T.5,R.7,S.3). The Tretiak condition states that the minimum number of views, N, in a CT scan required to faithfully reconstruct an image is related to the spatial resolution of the image, ΔX, and the radius of the target, R, by the relation

$$N \simeq \frac{2\pi R}{\Delta X}$$

Hence, for a 10 cm radius and a 2 mm resolution 300 views are required.

There were three advantages to using low angular velocities with the disk. First, at these low angular velocities static balancing was sufficient to prevent undesired vibrations. Furthermore, off-center point mass model calculations (B.12) indicated that dynamic balancing would not be required unless the disks were to be driven faster than 1500 RPM. Hence, the above disk design assured that at the angular velocities used, the rotation of the disk would not produce microphonic mechanical vibrations which would disturb the ionization chamber measurement process (V.1). Second, at these low velocities a small 1/16 hp motor was sufficient (V.2) to drive the disk and to overcome the air and bearing drag. Finally, from a safety consideration the task of constructing a safety shield was simplified (L.6,N.1) because of the low velocities used.

Detector Transient Response Considerations

An electrical schematic diagram of an ionization chamber and its current measuring circuit is given in Fig. 2.2.2. It is seen that the electronic equivalent of the chamber and its associated electronics was that of a resistor and capacitor in parallel (P.4,K.3,B.13,R.8). Therefore, the transient response of the detector to changes in the detected current due to the filtration modulation was limited by the detector's inherent RC time constant. The RC time constant for the MGH detectors was about 0.5 msec. From Kirchoff's laws the ionization chamber response can be modeled by the equation:

$$V + RC \frac{dV}{dt} = I(t)\ R \qquad (2.2.1)$$

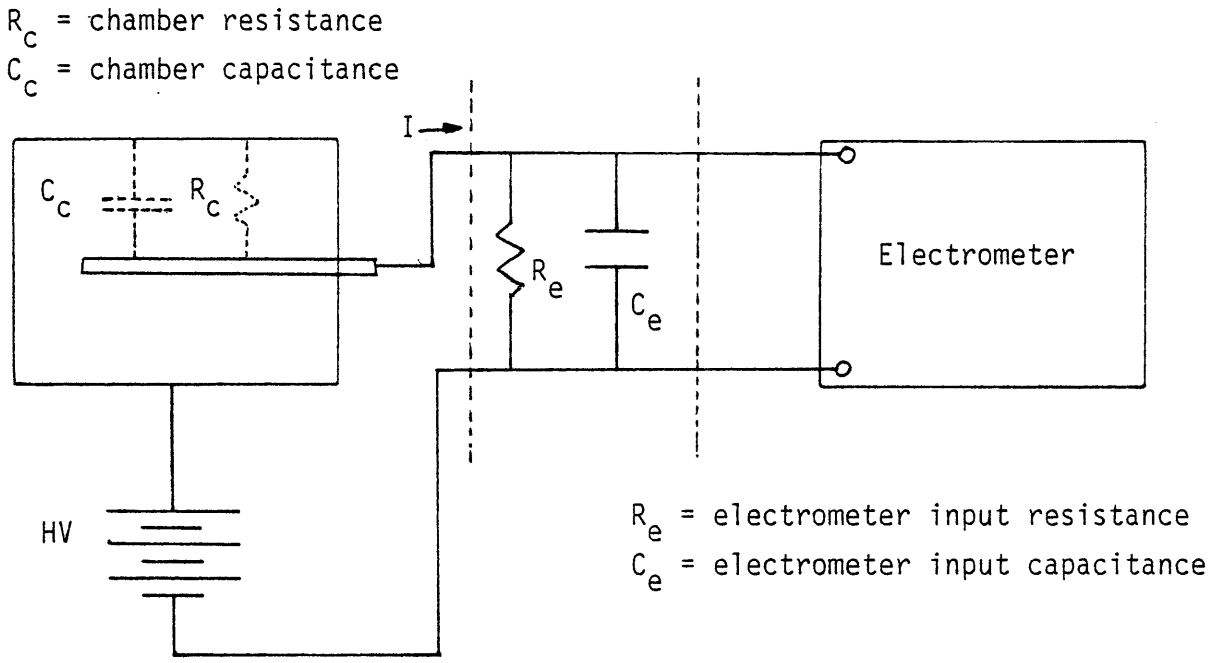

IONIZATION CHAMBER CIRCUIT

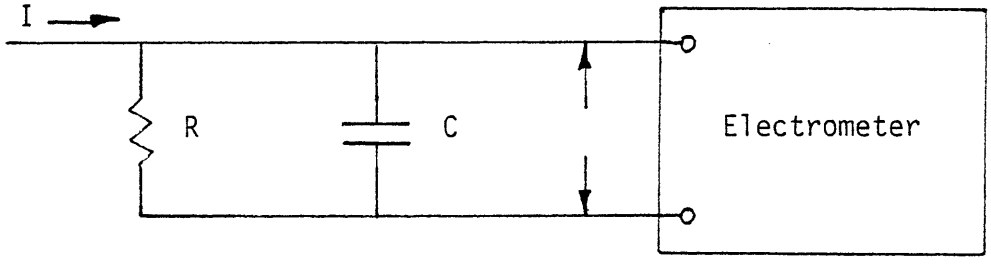

$R = R_e R_c/(R_e+R_c)$

$C = C_e+C_c$

EQUIVALENT CIRCUIT

Figure 2.2.2 Electrical schematic diagram of an ionization chamber and its current measuring circuit.

where

$I(t)$ is the current measured at the input of the current measuring electronics

R is the electronic input resistance

V is the voltage drop measured across the input resistance.

Equation (2.2.1) is readily solved for a stepwise change in the charge production rate within the ionization chamber.

$$I(t) = I_1 + (I_2-I_1)\ (1 - \exp(-t/RC)) \qquad (2.2.2)$$

where

I_1 is the ionization current produced when filter 1 is within the x-ray beam

I_2 is the ionization current produced when filter 2 is within the x-ray beam.

Equation (2.2.2) describes the current measured by the electronics if filtration changes occurred instantaneously. However, since the fan beam had a finite thickness it took a small amount of time for the tantalum-iron interface to 'cut' the fan beam. This time, referred to here as the transition time, t_{tr}, was about 1 msec for this experimental setup. With a finite transition time the photon flux change was modeled to occur in a rampwise fashion rather than a stepwise fashion as seen in Fig. 2.2.3. In this case the ionization chamber response equation, Eq. (2.2.1), was solved using an integral substitution technique (H.9) to give the measured current versus time:

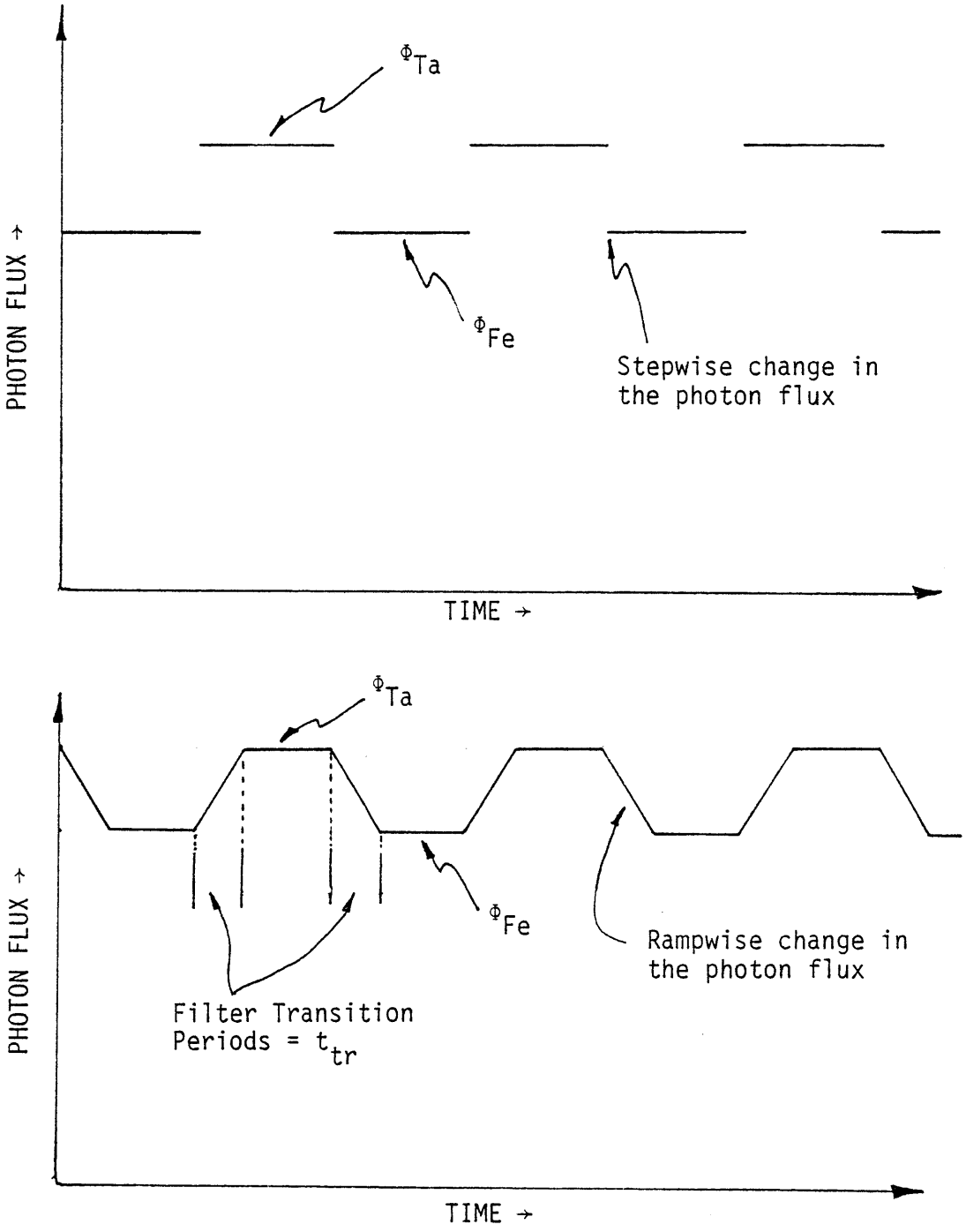

Figure 2.2.3 Ramp model of the photon flux change to account for the finite filter transition time.

$$I(t) = I_1 \qquad t \leq 0$$

$$I(t) = I_1 + \left(\frac{RC}{t_{tr}}\right)(I_2-I_1)\left[\frac{t}{RC} - (1-\exp(-t/RC))\right] \qquad 0 < t \leq t_{tr}$$

$$I(t) = I_1 + \left(\frac{RC}{t_{tr}}\right)(I_2-I_1)\left[\frac{t_{tr}}{RC} - (\exp(-t/RC+t_{tr}/RC) - \exp(-t/RC))\right] \qquad t > t_{tr}$$

(2.2.3)

Figure 2.2.4 presents the response of an ionization chamber for six different ratios of t_{tr}/RC. It is seen that as the t_{tr}/RC tends to zero the response curve approaches the step response case. Conversely, as t_{tr}/RC becomes large the measured current from the ionization chamber is seen to closely follow the ramp increase in the photon flux. For the MGH scanner the ratio t_{tr}/RC was about 2 so that with RC ≈ 0.5 msec the transient response effects died out in about 2.5 msec.

During a scan the instantaneous current from the detectors was not measured. Rather, the integral of the charge collected over a measurement time interval, T, was measured so that an estimate of the average current during that time interval could be determined. In a tomochemistry scan, to assure that the non-ideal transient response of the detector would not disrupt the estimate of the detected current, the time interval, T, was restricted to that period when it was known that the transient response effect was negligible. The method by which the transient response was eliminated will be presented below in Section 2.3.

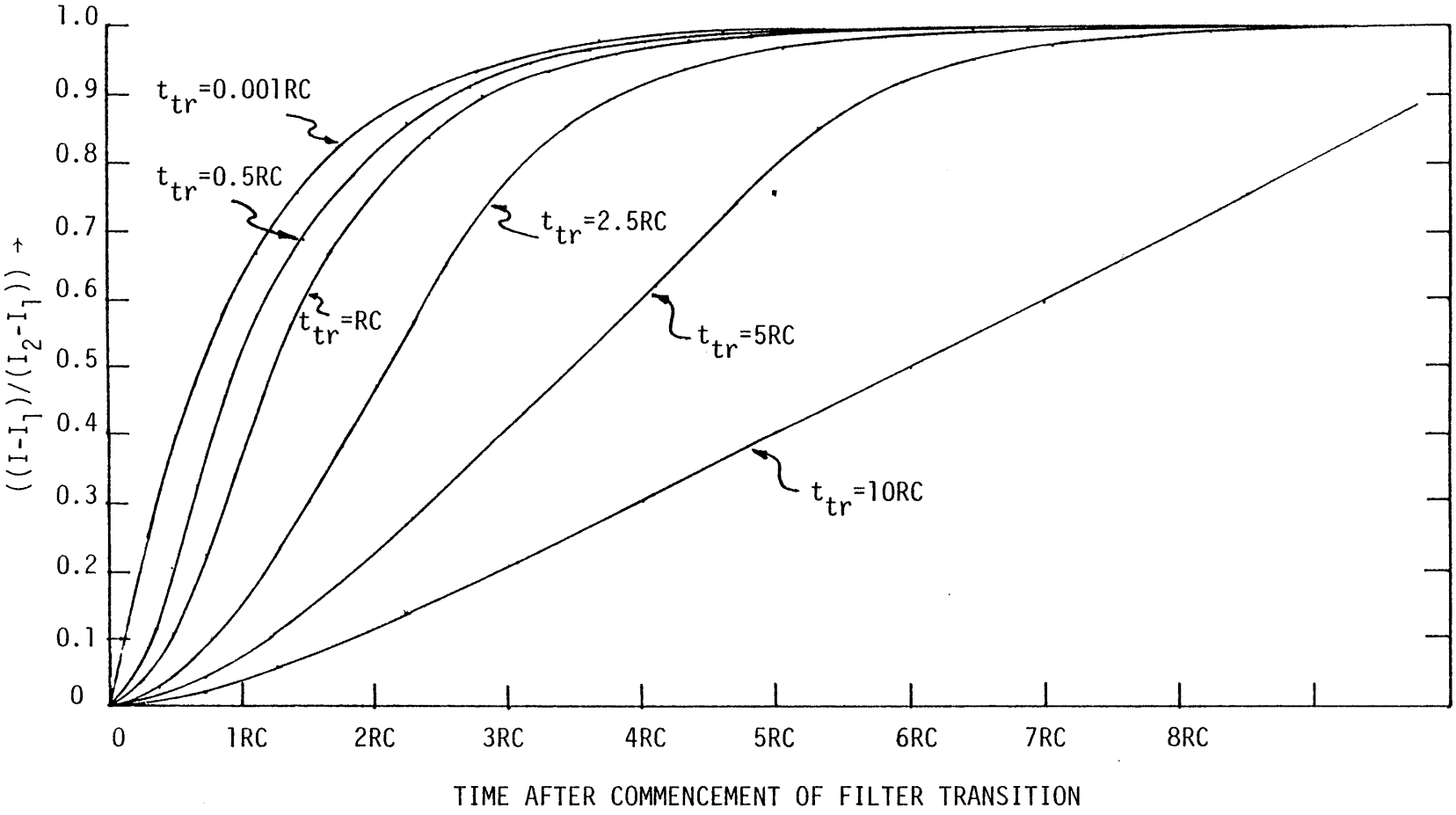

Figure 2.2.4 Response of an ionization chamber circuit for six different values of t_{tr}/RC.

2.3 System Integration and Control of the Tomochemistry Proof-of-Principle Scanner

In the previous sections the attention was centered on the design detail of the beam analyser disk. In this section the focus is on the integration and control of the scanner system with the addition of the beam analyser to the CT system.

To understand the integrated experimental setup, consider the view plan in Fig. 2.3.1. As seen in Fig. 2.3.2 the system was operated from a single control station. At this station the operator could control the x-ray tube, the beam analyser disk, the rotating table, and the detector (shown in Figs. 2.3.3a and 2.3.3b) as well as the scanner's computer (shown in Fig. 2.3.4). The scanner system itself (x-ray tube, rotating table, detector) was enclosed within a lead shielding box to avoid exposing the operator to radiation from the scanner.

The x-ray tube power supply and control system, located at the control station, drove a high voltage transformer. The high voltage transformer stepped up the voltage to the kilovoltage range required to drive the Machlett CL-150 x-ray tube shown in Fig. 2.3.5. At the control station the operator could control the kilovoltage (kVp) and electron beam (ma) current of the tube.

To prevent melting the anode the x-ray tube was forced flow cooled using oil as the working fluid. The oil coolant was pumped through the coolant channels within the anode and then through the coolant system's heat exchanger located in the corner of the laboratory. The heat exchanger used the water from the city water supply as the secondary coolant.

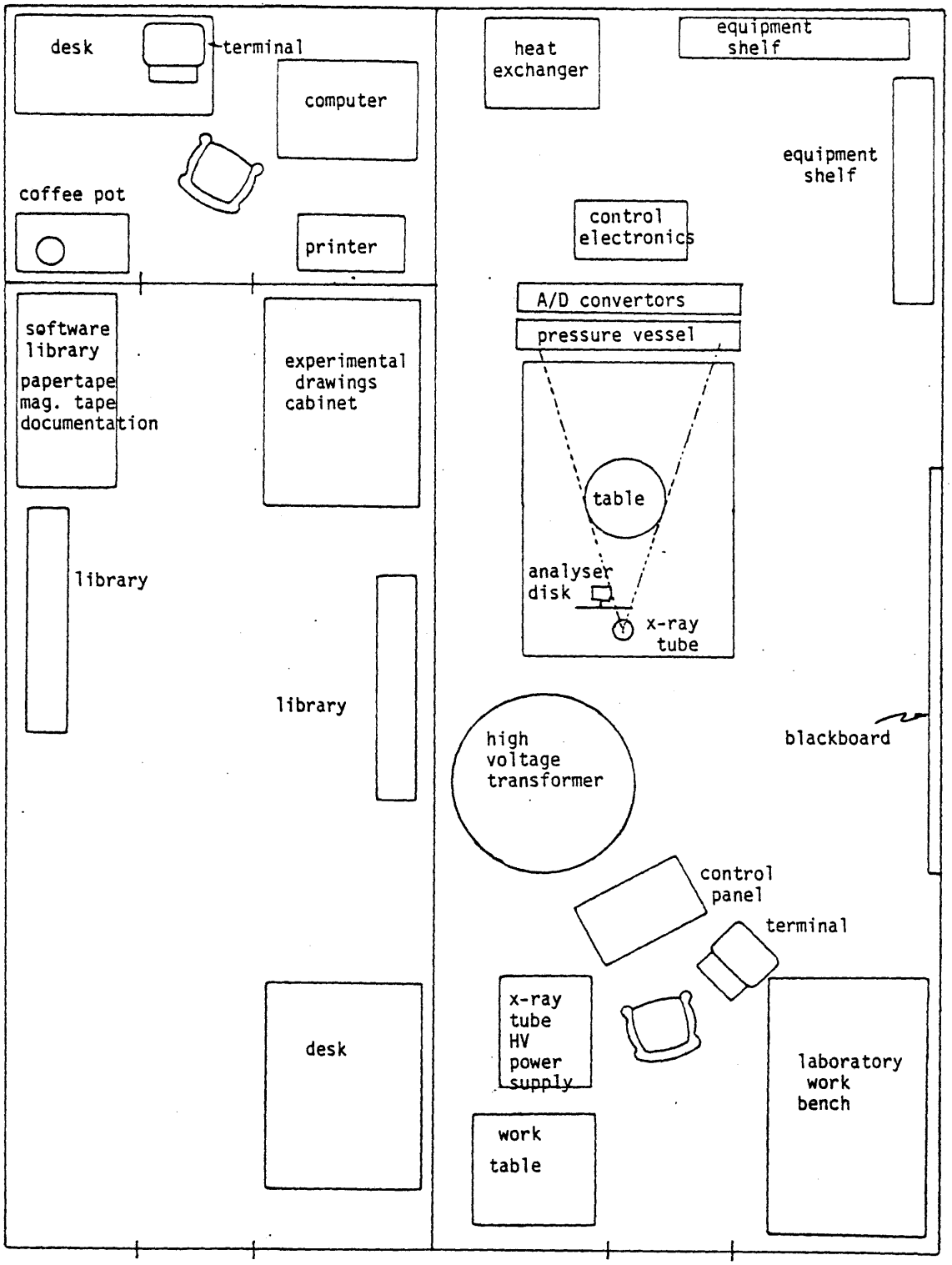

Figure 2.3.1 View plan of the experimental setup.

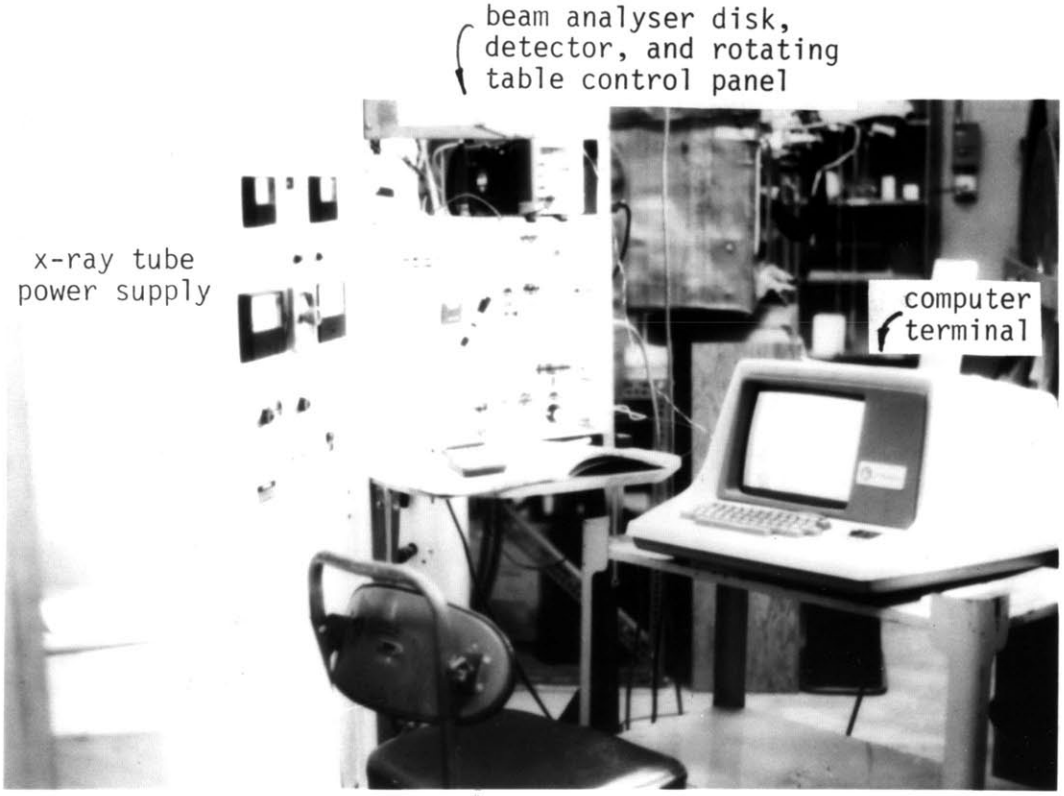

Figure 2.3.2 Photograph of the operation control station.

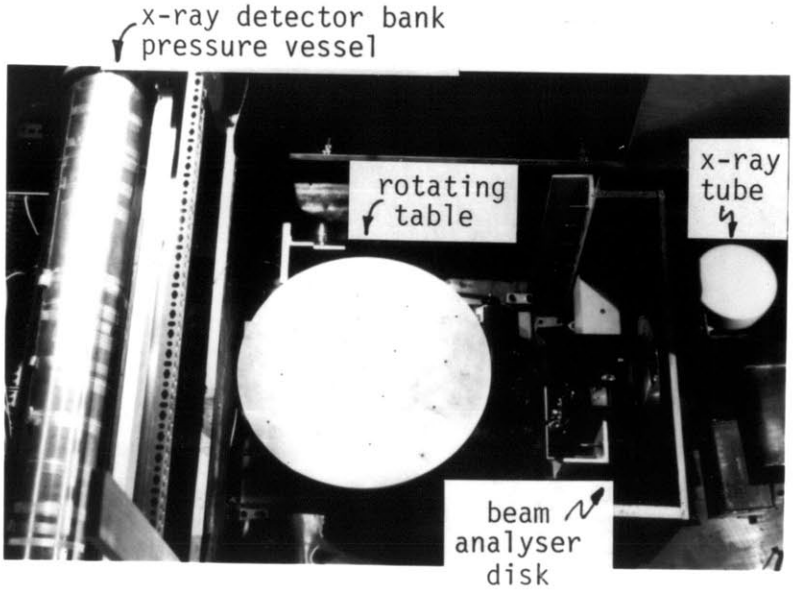

Figure 2.3.3a Top view of the MGH benchtop scanner.

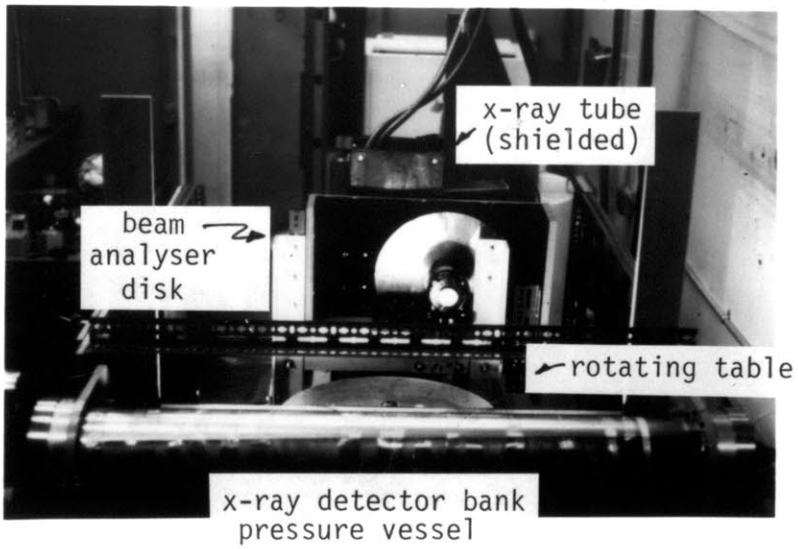

Figure 2.3.3b Rear view of the MGH benchtop scanner.

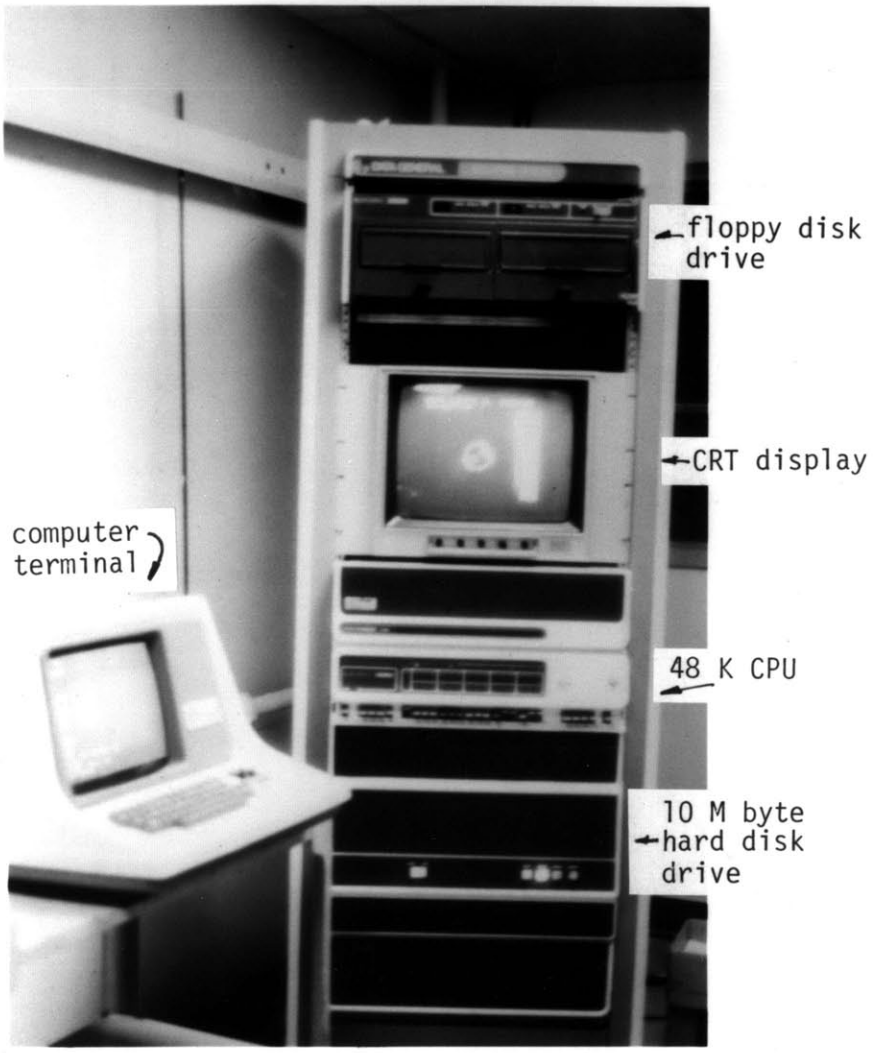

Figure 2.3.4 Photograph of the MGH scanner's Data General Ecllipse computer.

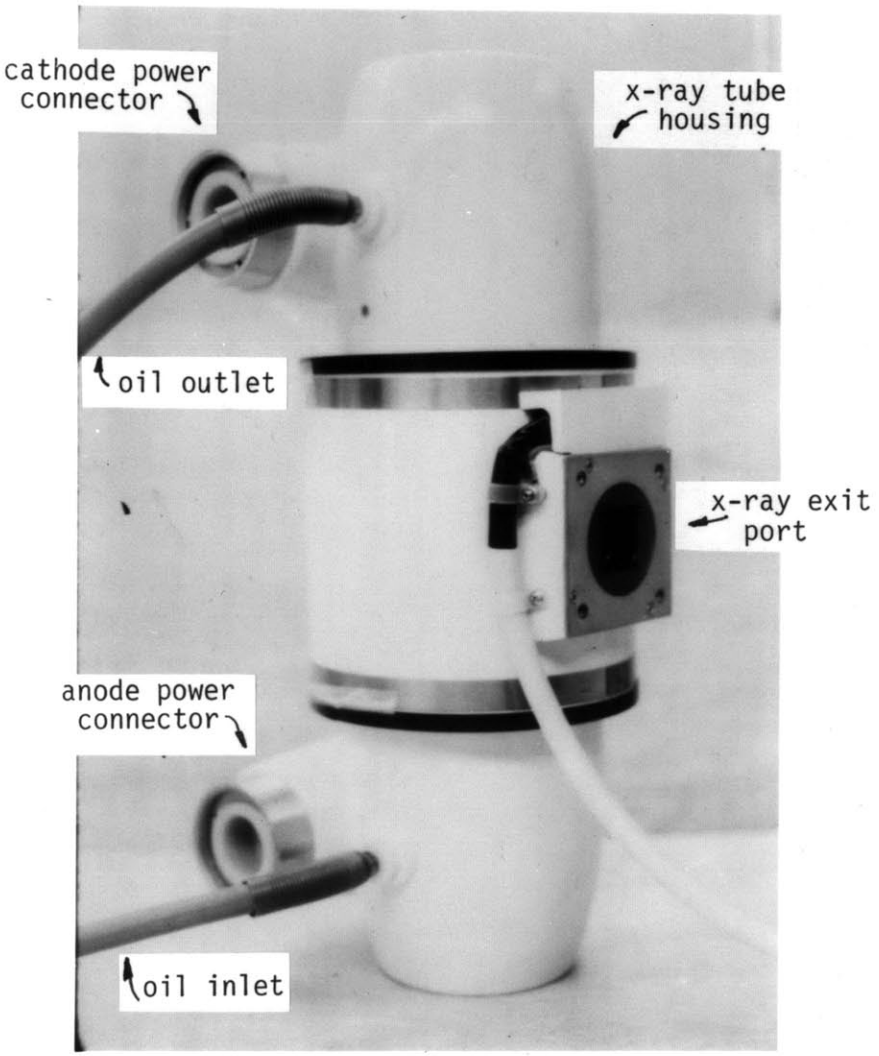

Figure 2.3.5 Photograph of the x-ray tube used in the experiment.

The beam analyser disk, shown in Fig. 2.3.6, was precisely aligned just in front of the x-ray tube (~10 cm from the focal spot). The beam analyser disk was also controlled by the operator at the control station. The disk speed was controlled using a commercially available DC variable speed motor controller. The disk speed was also monitored and displayed to the operator at the control panel as a double check on the motor controller.

The last two components of the scanner, the rotating table shown in Fig. 2.3.7 and the detector and its electronics shown in Fig. 2.3.8, were indirectly controlled by the operator via the computer terminal shown in Fig. 2.3.2. Direct control over the rotation of the table and I/O of the electronics was performed by the computer which was located in an adjacent climate-controlled room.

The rotating table, upon which the targets to be scanned were placed, was driven by a 1/2 hp synchronous motor. Its angular velocity was only approximately constant and hence the angular position was not determined by timing but by the shaft encoder indicated in Fig. 2.3.7. Angular positions were read out by the computer at the beginning and end of each transmission measurement so that the view angle would be known for every measurement.

As shown in Fig. 2.3.8 the detector's electronics was positioned immediately behind the x-ray detector pressure vessel to minimize the cable lengths between the detectors and the A/D convertors. The measurement process and data readout was automatically controlled by the computer. Communication between the detector electronics and the computer was performed via a computer interface located on the

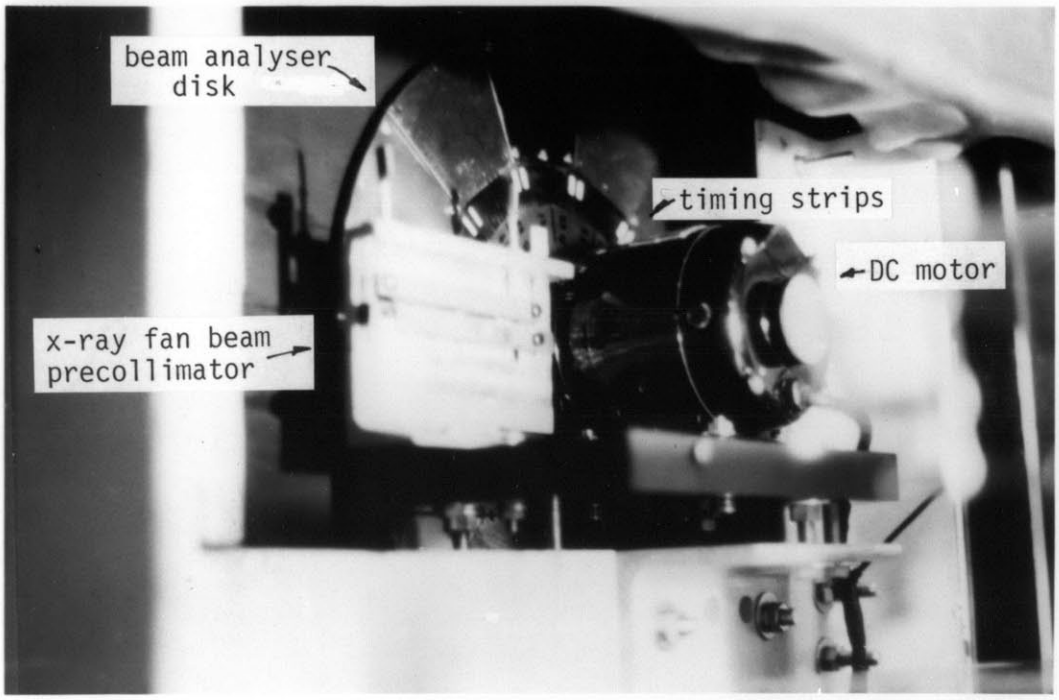

Figure 2.3.6 Photograph of the beam analyser disk and DC motor drive in position in front of the x-ray tube.

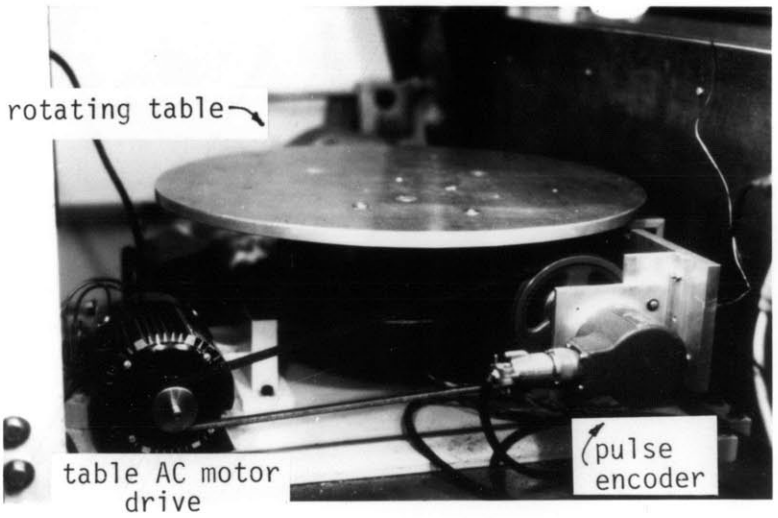

Figure 2.3.7 Photograph of the rotating table and the pulse encoder arrangement.

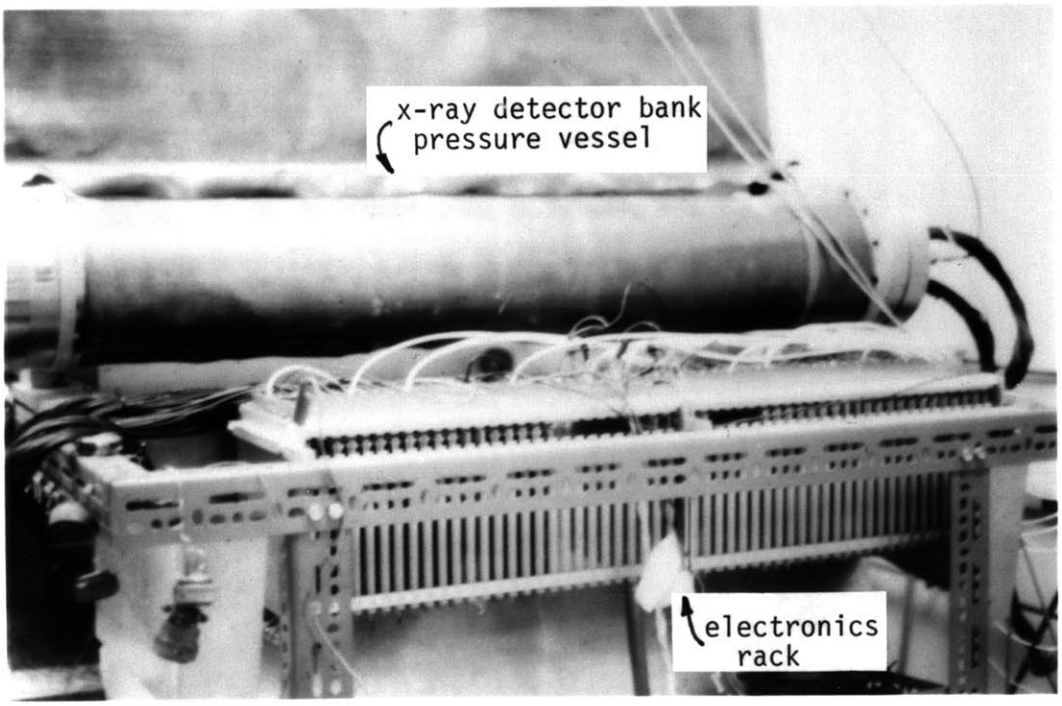

Figure 2.3.8 Photograph of the detector pressure vessel and the A/D convertor electronics rack.

electronics rack and an I/O bus which was merged to an I/O device control board of the computer. The software which was used to control the data I/O is described in the next chapter.

The computer which was used to orchestrate the automatic measurement process and to reconstruct the tomographic images was a Data General Ecllipse S-200 minicomputer with 48 K of random access memory. The computer system contained a Diablo disk drive which controlled the storage and retrieval of programs and data from two 10 M byte hard disks, and a Data General dual floppy disk drive for the storage of images on 0.6 M byte single density floppy disks. The computer CPU also controlled a Lexidata grey scale display, upon which the reconstructed images were displayed. The software which was used to reconstruct the images is described in the next chapter.

Scan Data I/O Control Method used in the Experiment

Although the computer controlled the data I/O it did not know a priori when a transmission measurement had been completed and when the data was ready to be retrieved from the scanner electronics. To inform the computer of the status of the measurement process I/O control pulses were generated by the scanner hardware when data was ready for retrieval. In normal CT scanning, the transmission measurements were made in equal angular intervals, $\Delta\theta$. This was accomplished by continually 'reading out' the angle of the table via the table's pulse encoder (shown in Fig. 2.3.7) and generating an I/O pulse each time the table had rotated by an angle $\Delta\theta$. Measurements were made in equal angles because the algorithms used for the image reconstruction required uniform angular sampling.

In the tomochemistry proof-of-principle experiment the angular position of the beam analyser disk served to determine the timing of the I/O control pulses. This was done so that the commencement and termination of transmission measurements coincided with the filtration modulation of the x-ray beam. As mentioned in the previous section, to assure that the non-ideal transient response of the detector would not disrupt the estimate of the average current within a measurement interval, the time interval, T, was restricted to time intervals where the transient effects were negligible.

As seen in Fig. 2.3.9 a measurement of the average current was commenced about 3 msec after the tantalum-iron edge had 'cut' the fan beam and completed about 1 msec before the next tantalum-iron edge would 'cut' the fan beam. As shown in Fig. 2.3.10 and Fig. 2.3.6 this transient rejection was achieved in the experiment by using an emitter-sensor array in conjunction with timing strips aligned on the disk. An I/O command pulse would be generated by the circuit shown in the figure each time a reflective strip would pass in front of the photo-optical device. In this scheme measurements were not made uniformly in angle because the table and the beam analyser disk were mechanically decoupled. Hence, the reconstruction algorithm had to be modified to correct for the nonuniform angular sampling. This software correction is presented in Chapter 3.

To experimentally verify that the above transients rejection method provided a sufficient rejection of the transient effects, experimental measurements were made of the average iron and tantalum currents for a range of disk angular velocities. The ratio of the

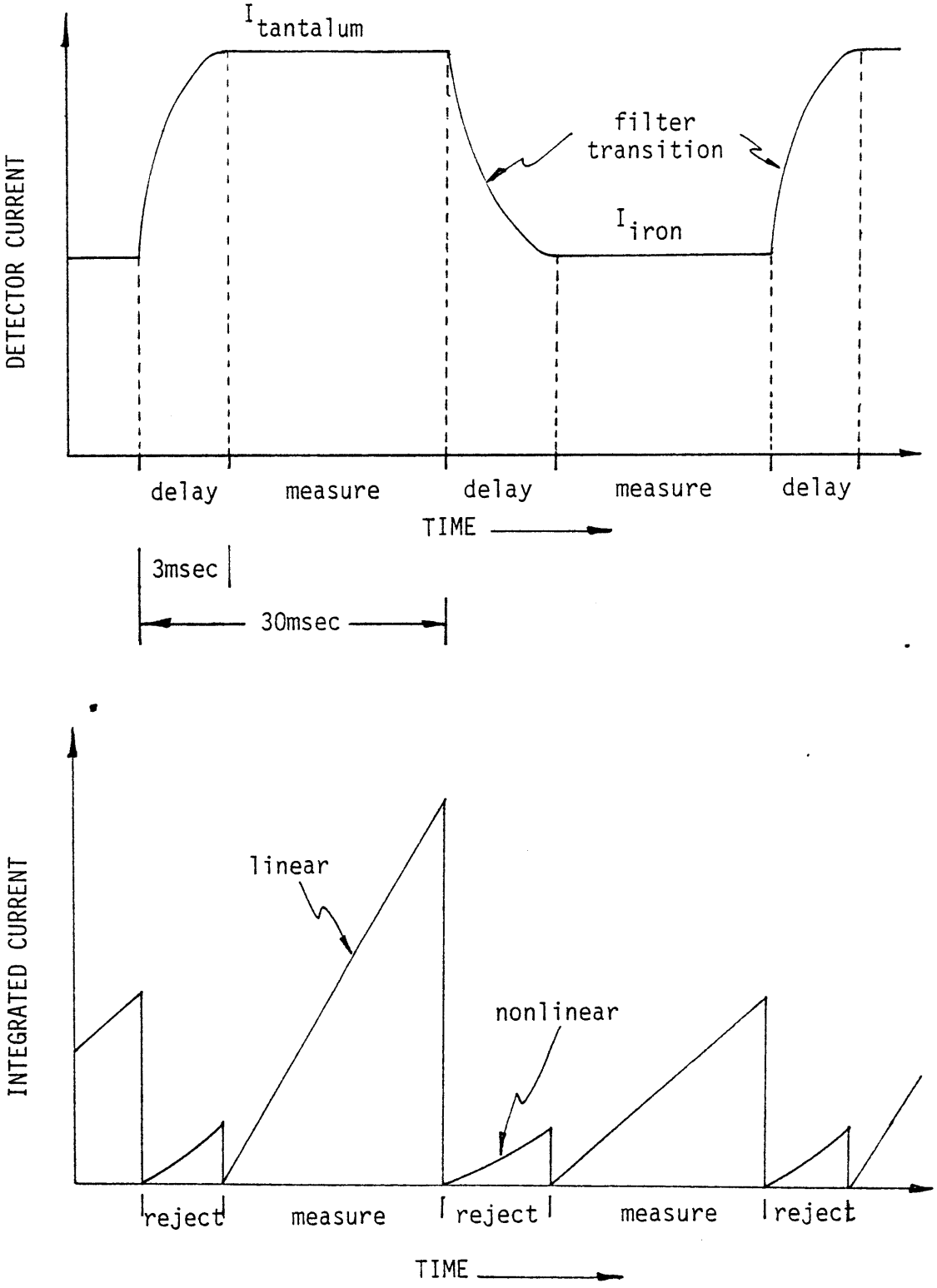

Figure 2.3.9 Method used to reject the effects of transients on the measured average current.

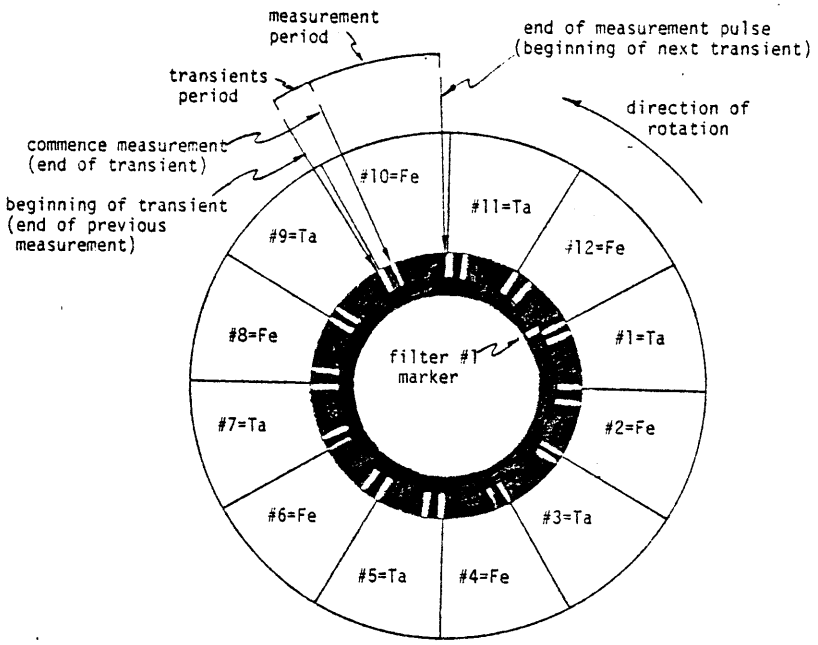

TIMING METHOD USED IN
THE PROOF-OF-PRINCIPLE EXPERIMENT

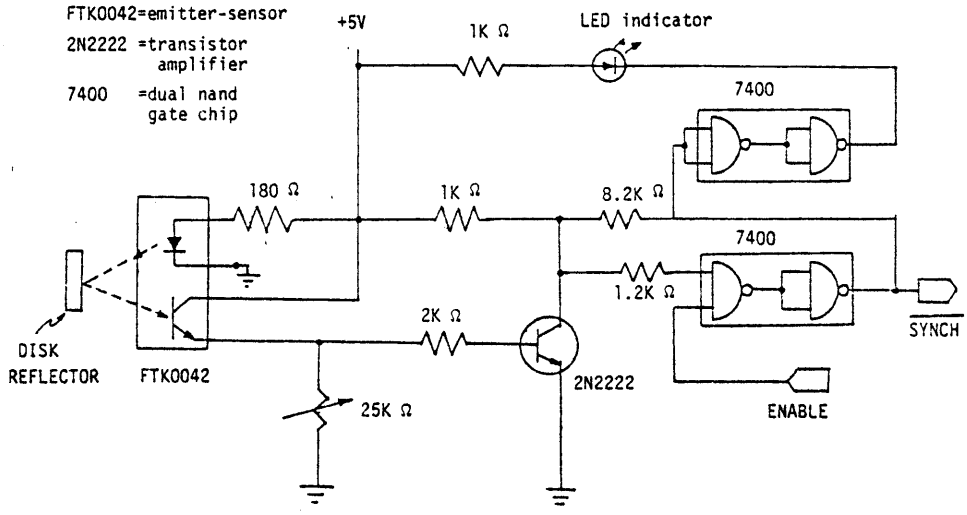

SCHEMATIC DIAGRAM OF THE EMITTER-SENSOR CIRCUIT

Figure 2.3.10 Beam analyser disk position determination and measurement timing method used in the proof-of-principle experiment.

measured currents is presented in Fig. 2.3.11. If the transient effects were sufficiently eliminated one would expect that the ratio of the two measured currents would be independent of the disk angular velocity. Conversely, if the transient effects were not completely eliminated one would expect the ratio of the estimated average currents to approach unity at increasing disk velocities. Figure 2.3.11 shows that in the operating range of interest the transient effects had been eliminated. For the reader's interest the author has also included in this figure an estimate of the ratio's behavior had it been possible to perform measurements at high disk angular velocities.

Automatic Control and Operation of the Scanner

For completeness a detailed explanation is given here of the scanning procedure used in this experiment. For a complete understanding of the process the automatic sequence of events within the hardware along with the operations the operator must perform during a measurement are presented.

Referring to Fig. 2.3.12 it is seen that a scan was performed in the following way.

(a) The operator first placed the target on which transmission measurements were to be made on the rotating table.

(b) Then the operator closed the lead shielding box seen in Fig. 2.3.1.

(c) With the lead box closed the operator then, (1), turned on the beam analyser disk and brought it up to speed, (1), turned on the detector HV, (1), turned on the power to the rotating table, and (1), turned on the x-ray tube and brought it up to the desired kilovoltage and current.

(d) Next the operator, (2), instructed the computer to begin a scan.

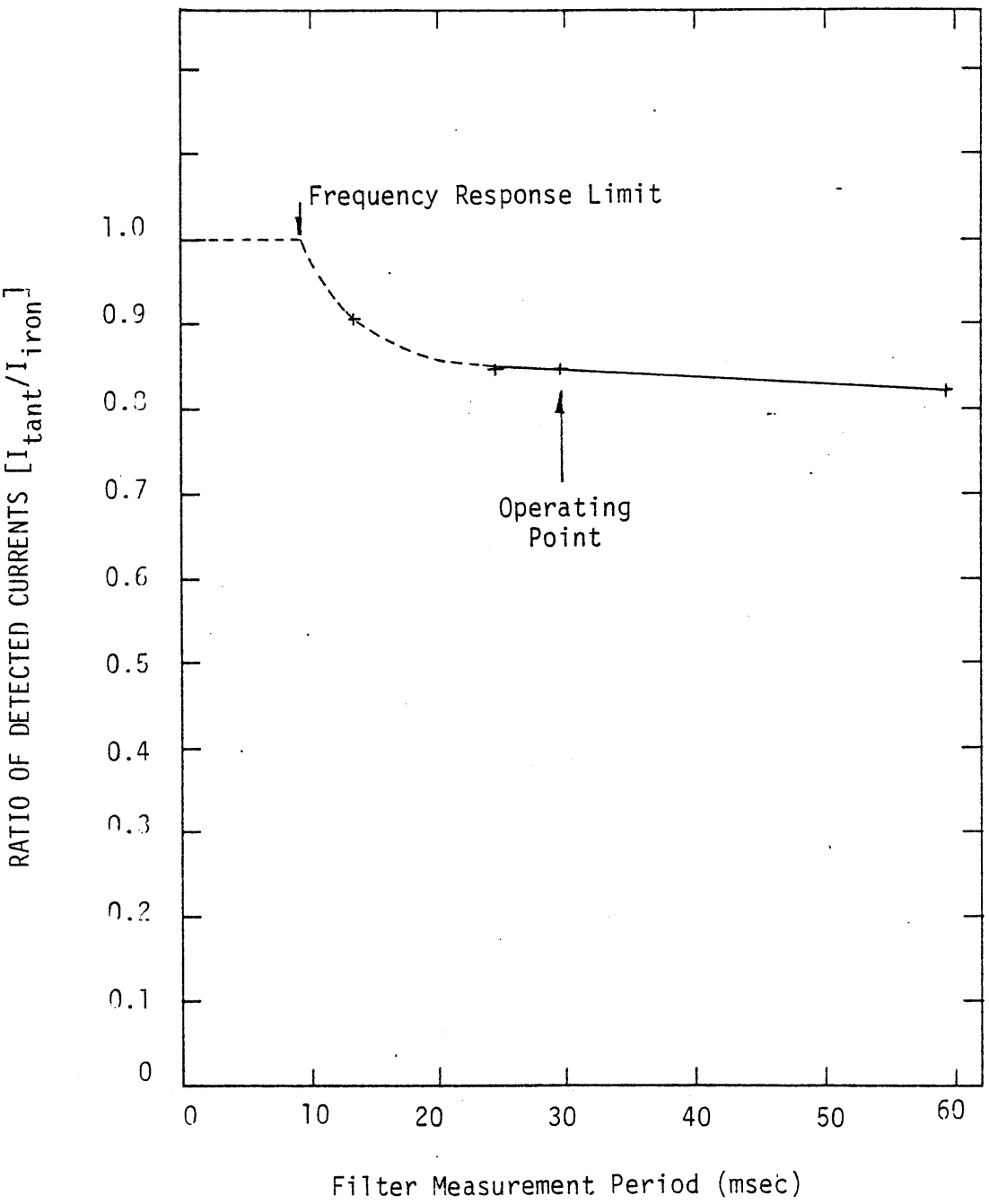

Figure 2.3.11 Ratio of the measured average iron and tantalum filter currents versus filter measurement period (inverse of the disk RPM).

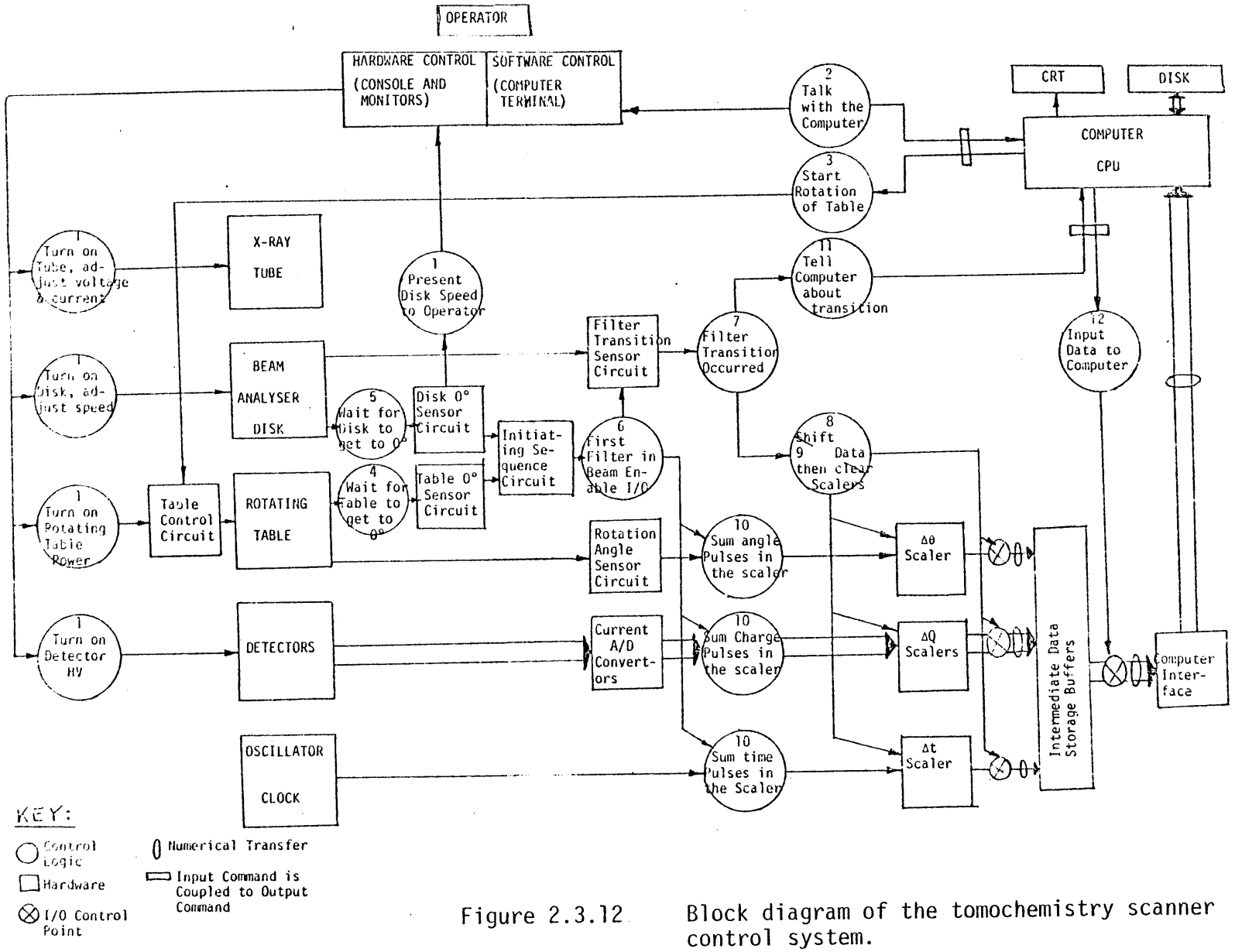

Figure 2.3.12 Block diagram of the tomochemistry scanner control system.

(e) At this command, (3), the computer sent a pulse to the table control circuit which started the rotation of the table.

(f) The electronics did not begin a measurement until the table, (4), got to 0° and then, (5), filter #1 got to the starting position.

(g) When filter #1 was at the starting position, the initiating sequence circuit sent out a pulse, (6), which turned on (enables) the filter transition sensor circuit. This circuit and sensor recognized when a transition had been made from one filter to the next. The pulse, (6), also turned on the scaler circuits which measured the charge, Q, from the detectors, the angle, $\Delta\theta$, of rotation of the table, and the time, Δt, which has transpired during the measurement process.

(h) When the filter transition sensor circuit had determined, (7), that a transition had occurred, a pulse was generated, (8), which shifted the accumulated data in the scalers (ΔQ, Δt, $\Delta\theta$) into a set of intermediate data storage buffers. Another pulse, (9), cleared the scalers (sets them to zero) and the next measurement operation began. The data from the previous measurement interval was still in the intermediate buffers waiting to be read out by the computer.

(i) In conjunction with the shift/clear pulses above, another pulse, (11), went to the computer's CPU indicating that a filter transition had occurred.

(j) The computer then fetched, (12), the data from the intermediate buffers via the computer interface and, (13), dumped the data onto the 10 M byte disk of the computer.

(k) While the computer was transferring data the next measurement of the, (10), table rotation, (10), collected detector charge, and (10), transpired time was simultaneously taking place.

(l) The next pulse produced by the filter transition sensor circuit was used to indicate that, (7), another transition had occurred. At this point the I/O process was repeated starting from step (h).

(m) The above process continued for 300 views, at which time the computer, (3), stopped the rotation of the table and the, (12), data transfer process.

(n) The operator then, (1), turned off the x-ray tube to remove the target from the rotating table.

(o) Then with the x-ray tube off the above sequence ((a) through (m)) was repeated so as to obtain measurements of the detector current with no x-ray flux (called here the leakage or 'dark' current).

(p) Finally, the x-ray tube was, (1), turned on again with no target on the rotating table. Sequence (a) through (m) was again repeated to obtain measurements of the detector current with no 'object' in the beam (called here the full flux or 'flood' current).

(q) The x-ray tube, (1), was again turned off and the data processing was begun so as to reconstruct an image of the scanned slice.

2.4 Summary

This chapter presented the major hardware design considerations in the development of a tomochemistry proof-of-principle experiment. It was found that a 10 second tomochemistry scan could be performed by modulating an incident diagnostic energy x-ray spectra (~100 to 150 kVp) with 2.16 mm iron and 130 μm tantalum filtration. The dose from such a scan was estimated to be about 900 mR. It was shown that these filter materials could be used to manufacture a beam analyser disk which satisfied the design criteria identified to be important in a tomochemistry scanner. Finally, it was shown that this device could be merged successfully into a normal CT scanner by the slight modification of a normal CT scanner's control system.

3.0 Software Development and Data Analysis Methods

The purpose of this chapter is to outline the particular methods used in this research project to reconstruct the photoelectric + Rayleigh and Compton images. The first section deals with a general overview of the data acquisition and data processing methods used in tomochemical scanning. The second section presents the experimental methods used to obtain the calibration data and the mathematical methods used to reduce the data to the desired polynomial functions. Finally, the third section presents the methods by which the raw and scan data was corrected and then processed to obtain the Compton and photoelectric + Rayleigh line integral data. This data was the base from which the photoelectric + Rayleigh and Compton line integrals were reconstructed.

Due to time and space limitations this chapter will not delve deeply into the detail of the software. In general, a complete understanding of the details of any particular data processing software is very difficult without actually having an opportunity to use or modify that software. In light of this difficulty the author will present below an overview of the software and reserve the detailed description to be determined by the reader. For completeness the software used to process the experimental data is given in Appendix C.

3.1 Overview of the Software Required for Tomochemistry

As indicated in Fig. 3.1.1 this research project used five blocks of software to perform the tomochemical analysis. The data acquisition software block consisted of those FORTRAN IV and ASSEMBLY language programs which controlled the data I/O process during the experimental measurements. The programs were modified slightly from the programs of normal CT to recognize that the beam analyser disk and not the rotating table generated the I/O command pulses.

The resultant data set obtained using the above data acquisition software is presented in Table 3.1.1. It should be noted here that, as indicated in the block diagram in Fig. 2.3.12, the first I/O command pulse was not generated by the hardware until the beam analyser disk reach the 0° reference position. In this way the CT scan process always began with the same filter (which was known by the experimenter). The filters used in successive transmission measurements were then known implicitly. Another important point to note from Table 3.1.1 is that the detected charge, q, measurement time, T, and table rotation, θ, corresponded to the transients-rejected measurement period. However, θ_T corresponded to the angle of the table rotation during the transients period. As mentioned in the previous chapter, the table rotation had to be measured throughout the scan so that the angles which corresponded to the transmission measurements were known by the computer in the reconstruction process.

There were three sets of measurements which were made in a CT scan procedure. They were:

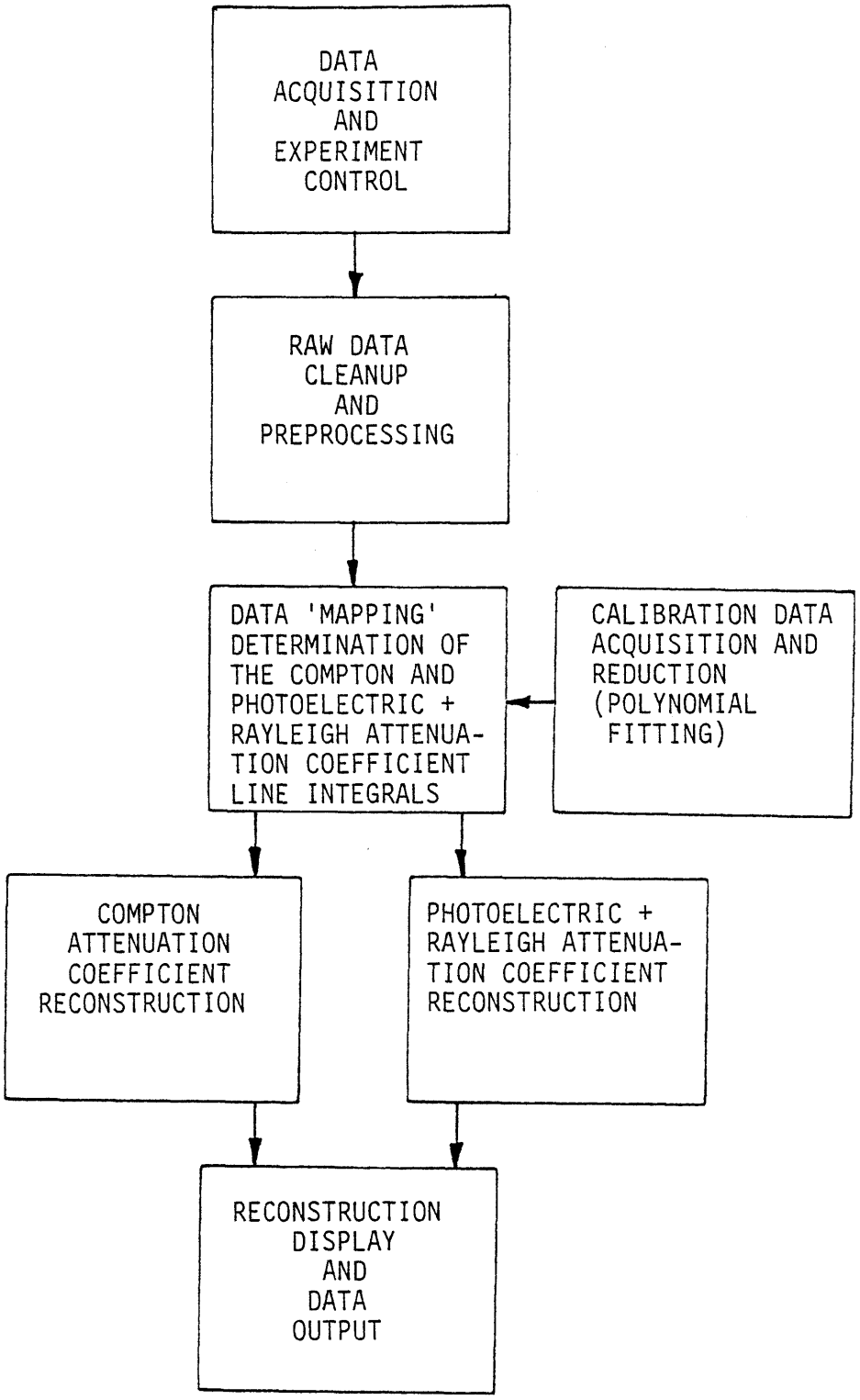

Figure 3.1.1 Block diagram of the tomochemistry data processing software.

Measurement Number	ΔTable Angle	ΔTime	Filter Number	Detected Charge				
				Det.#1	Det.#2	Det.#3	→	Det.#256
1 transient	$\Delta\theta_1$ $\Delta\theta_{1-2}$	Δt_1	1 1 → 2	$q_{1\ 1}$ -	$q_{2\ 1}$ -	$q_{3\ 1}$ -	→	$q_{256\ 1}$ -
2 transient	$\Delta\theta_2$ $\Delta\theta_{2-3}$	Δt_2	2 2 → 3	$q_{1\ 2}$ -	$q_{2\ 2}$ -	$q_{3\ 2}$ -	→	$q_{256\ 2}$ -
3 transient	$\Delta\theta_3$ $\Delta\theta_{3-4}$	Δt_3	3 3 → 4	$q_{1\ 3}$ -	$q_{2\ 3}$ -	$q_{3\ 3}$ -	→	$q_{256\ 3}$ -
4 transient	$\Delta\theta_4$ $\Delta\theta_{4-5}$	Δt_4	4 4 → 5	$q_{1\ 4}$ -	$q_{2\ 4}$ -	$q_{3\ 4}$ -	→	$q_{256\ 4}$ -
5 transient	$\Delta\theta_5$ $\Delta\theta_{5-6}$	Δt_5	5 5 → 6	$q_{1\ 5}$ -	$q_{2\ 5}$ -	$q_{3\ 5}$ -	→	$q_{256\ 5}$ -
6 transient	$\Delta\theta_6$ $\Delta\theta_{6-7}$	Δt_6	6 6 → 7	$q_{1\ 6}$ -	$q_{2\ 6}$ -	$q_{3\ 6}$ -	→	$q_{256\ 6}$ -
⋮ ↓	⋮ ↓	⋮ ↓	⋮ ↓	⋮ ↓	⋮ ↓	⋮ ↓	→ ⋯ ↓	⋮ ↓
300 transient	$\Delta\Theta_{300}$ STOP	Δt_{300}	12 12 → 1	$q_{1\ 300}$ -	$q_{2\ 300}$ -	$q_{3\ 300}$ -	→	$q_{256\ 300}$ -

Table 3.1.1 Data set obtained by the data acquisition software. (Projection measurement only)

(1) The projection measurement. This was the measurement of the detected charge when the x-ray tube was on and the target was within the scanner. Measurements were made of q_n, t_n, θ_n: the charge, time, and angle at view n.

(2) The flood measurement. This was the measurement of the detected charge when the x-ray tube was on and no target was within the scanner. Measurements were made of q_{on}, t_{on}: the charge and time at view n. The subscript o corresponds to the 'initial' measurement: that measurement with no target in the beam. θ was not measured because with no target within the scanner its value was inconsequential.

(3) The dark current measurement. This was the measurement of the leakage charge and zero offset of the electronics when the x-ray tube was off. Measurements were made of q_D, t_D: the charge accumulated during the elapsed time.

The above 'raw' data had to be obtained for every scan. It was desirable that the three sets of measurements be performed as close together in time as possible so that systematic measurement errors due to electronic drift were minimized.

The second block of software, called here the 'cleanup' software, served to process the above raw data so that it was acceptable for reconstruction. The first process performed was the determination of the ratio of the detected currents at each view. That is:

$$\ln\left(\frac{I}{I_o}\bigg|_{n,d}\right) = \ln\left(\frac{q_{nd}/t_n - q_{Dd}/t_D}{q_{ond}/t_{on} - q_{Dd}/t_D}\right) \qquad (3.1.1)$$

where

q_{nd} is the charge measured during a projection measurement by detector d in view n (corresponding to a particular filter and angle, θ_n).

t_n is the elapsed time of view n.

q_{Dd} is the charge measured during a dark current measurement by detector d.

t_D is the elapsed time of the dark current measurement.

q_{ond} is the charge measured during a flood measurement by detector d in measurement n (n corresponds to the same filter used in the above projection measurement).

t_{on} is the elapsed time of the flood measurement n.

With these ratios taken for every detector at each view n the resultant data set looks like that in Table 3.1.2.

The next process performed by this software block was to correct a transmission measurement of a particular detector if it was known that the detector was 'bad', i.e., if the detector was known to discharge frequently. A bad detector's reading was 'corrected' in the software by rejecting that detector's estimate of a transmission measurement in view n. A new estimate was obtained by assuming that the detector to detector transmission measurements at view n were continuous and that one could then interpolate between two good detectors to obtain an estimate of the measured transmission at the location of the bad detector. This interpolation process reduced the spatial resolution of the resultant image but it served to suppress very poor estimates of transmission measurements. It will be seen in the next chapter that if all the bad detectors were not found before the data reconstruction was performed the resultant tomochemical image contained many artifacts.

The third block of software, called the data 'mapping' software, was unique to tomochemistry. The purpose of this set of programs was

Measurement Number	ΔTable Angle	Filter Number	$\ell n(I/I_0)$ Det.#1	Det.#2	Det.#3	...	Det.#256
1	$\Delta\theta_1$	1	$\ell n(\frac{I}{I_0})_{1\ 1}$	$\ell n(\frac{I}{I_0})_{2\ 1}$	$\ell n(\frac{I}{I_0})_{3\ 1}$	→	$\ell n(\frac{I}{I_0})_{256\ 1}$
transient	$\Delta\theta_{1-2}$	1 → 2	-	-	-	.....	-
2	$\Delta\theta_2$	2	$\ell n(\frac{I}{I_0})_{1\ 2}$	$\ell n(\frac{I}{I_0})_{2\ 2}$	$\ell n(\frac{I}{I_0})_{3\ 2}$	→	$\ell n(\frac{I}{I_0})_{256\ 2}$
transient	$\Delta\theta_{2-3}$	2 → 3	-	-	-	.....	-
3	$\Delta\theta_3$	3	$\ell n(\frac{I}{I_0})_{1\ 3}$	$\ell n(\frac{I}{I_0})_{2\ 3}$	$\ell n(\frac{I}{I_0})_{3\ 3}$	→	$\ell n(\frac{I}{I_0})_{256\ 3}$
transient	$\Delta\theta_{3-4}$	3 → 4	-	-	-	.....	-
4	$\Delta\theta_4$	4	$\ell n(\frac{I}{I_0})_{1\ 4}$	$\ell n(\frac{I}{I_0})_{2\ 4}$	$\ell n(\frac{I}{I_0})_{3\ 4}$	→	$\ell n(\frac{I}{I_0})_{256\ 4}$
transient	$\Delta\theta_{4-5}$	4 → 5	-	-	-	.....	-
5	$\Delta\theta_5$	5	$\ell n(\frac{I}{I_0})_{1\ 5}$	$\ell n(\frac{I}{I_0})_{2\ 5}$	$\ell n(\frac{I}{I_0})_{3\ 5}$	→	$\ell n(\frac{I}{I_0})_{256\ 5}$
transient	$\Delta\theta_{5-6}$	5 → 6					
6	$\Delta\theta_6$	6	$\ell n(\frac{I}{I_0})_{1\ 6}$	$\ell n(\frac{I}{I_0})_{2\ 6}$	$\ell n(\frac{I}{I_0})_{3\ 6}$	→	$\ell n(\frac{I}{I_0})_{256\ 6}$
transient	$\Delta\theta_{6-7}$	6 → 7	-	-	-	.....	-
⋮ ↓	⋮ ↓	⋮ ↓	⋮ ↓	⋮ ↓	⋮ ↓	⋱ ↓	⋮ ↓
300	$\Delta\theta_{300}$	12	$\ell n(\frac{I}{I_0})_{1\ 300}$	$\ell n(\frac{I}{I_0})_{2\ 300}$	$\ell n(\frac{I}{I_0})_{3\ 300}$	→	$\ell n(\frac{I}{I_0})_{256\ 300}$
transient	STOP	12 → 1	-	-	-	.....	-

Table 3.1.2 Data set obtained after taking the proper ratios.

to map the data from the $(\ell n(I_1/I_{1o}),\ \ell n(I_2/I_{2o})$ coordinate space to the (A_{P+R},A_C) space as mentioned in Section 1.3. This mapping was done via Eqs. (1.3.14) and (1.3.15) where the coefficients in the polynomials were determined from calibration measurements of $\ell n(I_1/I_{1o})$ and $\ell n(I_2/I_{2o})$ on targets with known $A_{P+R}(=\int \mu_{P+R}(E_{REF})d\ell)$ and $A_C(=\int \mu_C(E_{REF})d\ell)$.

The whole concept of 'mapping' and line integral calibration was crucial to the data processing in tomochemistry. To understand this concept a brief pedagogic explanation is given here. Consider once again Eqs. (1.3.14) and (1.3.15). Remember that in essence in tomochemistry one is trying to solve two equations for two unknowns, A_{P+R} and A_C. In particular, with no spectral hardening artifacts the equations are:

$$\begin{aligned}\ell n(I_1/I_{1o}) &= b_1\ A_{P+R} + b_2\ A_C \\ &= b_1 \int \mu_{P+R}(E_{REF})d\ell + b_2 \int \mu_C(E_{REF})d\ell \\ \ell n(I_2/I_{2o}) &= c_1\ A_{P+R} + c_2\ A_C \\ &= c_1 \int \mu_{P+R}(E_{REF})d\ell + c_2 \int \mu_C(E_{REF})d\ell\end{aligned}$$

or conversely:

$$A_{P+R} = B_1\ \ell n(I_1/I_{1o}) + B_2\ \ell n(I_2/I_{2o}) \qquad (3.1.2)$$

$$A_C = C_1\ \ell n(I_1/I_{1o}) + C_2\ \ell n(I_2/I_{2o}) \qquad (3.1.3)$$

The higher order terms in Eq. (1.3.14) and Eq. (1.3.15) are there to correct for the nonlinear behavior of the measurement process. This nonlinear behavior is a small second-order process. Now Eqs. (3.1.2) and (3.1.3) define two surfaces - one surface in ($\ell n(I_1/I_{1o})$, $\ell n(I_2/I_{2o})$, A_{P+R}) space and the other in ($\ell n(I_1/I_{1o})$, $\ell n(I_2/I_{2o})$, A_C) space. If the higher order terms are zero, both of these surfaces are planes. Figure 3.1.2 presents perspective view drawings of these surfaces. The purpose of calibration measurements is to sample the coordinates of these two surfaces. Hence, if a sufficient number of transmission measurements are made on calibration standards with known A_{P+R} and A_C then the surfaces will be sufficiently sampled so that the functional form of those surfaces can be estimated (that is: B_1, B_2, C_1, C_2 can be determined). Similarly, if the higher order terms in Eq. (1.3.14) and Eq. (1.3.15) are retained so as to correct for the nonlinear processes, a multiple regression fit to the calibration data can be performed. In conclusion, if x-ray transmission measurements are made on an unknown target, as in a CT scan, then the line integrals A_{P+R} and A_C can be determined directly from Eq. (1.3.14) and Eq. (1.3.15). Table 3.1.3 presents the two data sets produced by this mapping.

The fourth block of software was the data reconstruction software. In this experiment the reconstruction software was the same as the normal CT reconstruction software. The Hanning-weighted-ramp filter backprojection technique was used. This method of image reconstruction is derived in Appendix A. The two resultant reconstructions were that of the photoelectric + Rayleigh cross section at reference

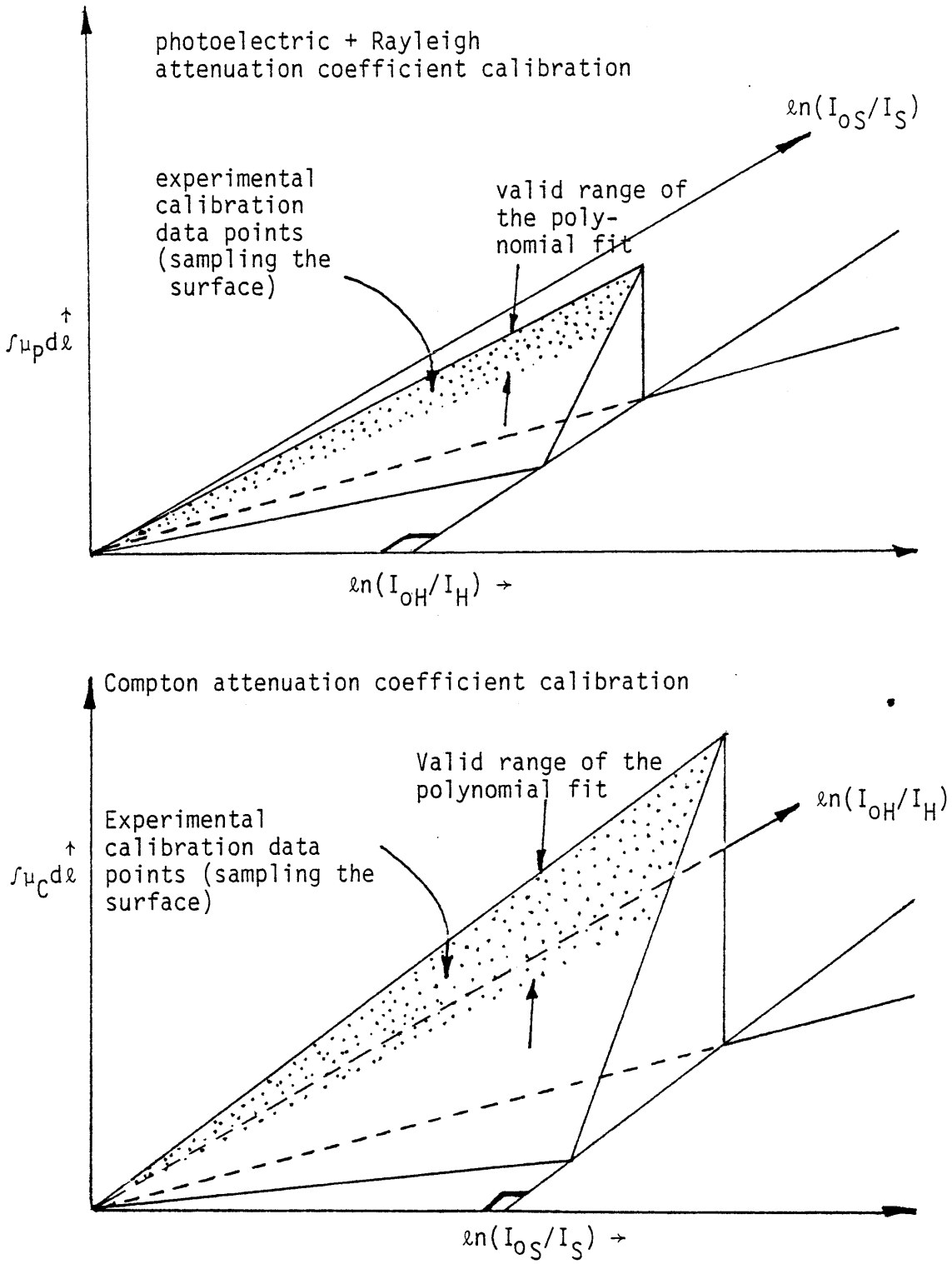

Figure 3.1.2 Schematic perspective view drawings of the calibration surfaces.

Measurement Number	ΔTable Angle	Compton and photoelectric + Rayleigh line integral		
		Det.#1	Det.#2	etc. →
1 transient	$\Delta\theta_1$ $\Delta\theta_{1-2}$	$\int_{-}\mu_C d\ell_{1\ 1}$	$\int_{-}\mu_P d\ell_{2\ 1}$	etc. → "
2 transient	$\Delta\theta_2$ $\Delta\theta_{2-3}$	$\int_{-}\mu_C d\ell_{1\ 2}$	$\int_{-}\mu_P d\ell_{2\ 2}$	" "
3 transient	$\Delta\theta_3$ $\Delta\theta_{3-4}$	$\int_{-}\mu_C d\ell_{1\ 3}$	$\int_{-}\mu_P d\ell_{2\ 3}$	" "
4 transient	$\Delta\theta_4$ $\Delta\theta_{4-5}$	$\int_{-}\mu_C d\ell_{1\ 4}$	$\int_{-}\mu_P d\ell_{2\ 4}$	" "
5 transient	$\Delta\theta_5$ $\Delta\theta_{5-6}$	$\int_{-}\mu_C d\ell_{1\ 5}$	$\int_{-}\mu_P d\ell_{2\ 5}$	" "
6 transient	$\Delta\theta_6$ $\Delta\theta_{6-7}$	$\int_{-}\mu_C d\ell_{1\ 6}$	$\int_{-}\mu_P d\ell_{2\ 6}$	" "
⋮ etc. ⋮ ↓	⋮ etc. ⋮ ↓	⋮ etc. ⋮ ↓	⋮ etc. ⋮ ↓	⋮ etc. ⋮ ↓
300 transient	$\Delta\theta_{300}$ STOP	$\int_{-}\mu_C d\ell_{1\ 300}$	$\int_{-}\mu_P d\ell_{2\ 300}$	" "

Table 3.1.3 Data sets obtained after the line integral data mapping process.

energy E_{REF} and the Compton cross section at reference energy E_{REF}.

After the reconstruction process one obtained a two-dimensional array of numbers, each of which corresponded to the reconstructed attenuation coefficient (μ_C or μ_{P+R}) within a particular picture element. The position of the picture element in the array corresponded to the position of the picture element within the reconstructed slice. It was the purpose of the fifth block of software to image this array in a grey scale format on the CRT.

In summary, the tomochemistry software performed the following tasks:

(1) control the hardware and the transmission data I/O process

(2) clean up the data

(3) map the data array into $\int \mu_{P+R} d\ell$ and $\int \mu_C d\ell$ space

(4) reconstruct $\int \mu_C d\ell$ to obtain $\mu_C(x,y)$ and reconstruct $\int \mu_{P+R} d\ell$ to obtain $\mu_{P+R}(x,y)$

(5) display the reconstructed values on the CRT.

3.2 Calibration Data Acquisition and Reduction

Description of the Calibration Standard

To obtain the calibration data set, which is a sampling of the two surfaces shown in Fig. 3.1.2, a calibration standard was designed and built specifically for this experiment. As seen in Figs. 3.2.1 and 3.2.2, the standard consisted of four interchangeable watertight containers which fit between an adjustable front and back aluminum faceplate arrangement. The containers were manufactured using 1/16" lucite for the front and back 'windows' and for the container itself. The windows and container were connected via flexible 1/32" neoprene rubber so that the whole arrangement would be flexible in the clamping dimension. The exact spacing between the front and back lucite windows was controlled by placing the waterbox arrangement between the flat front and back faceplates. Then, using matched spacer bars to determine the distance between the front and back faceplates, the faceplates were clamped together. The waterboxes were slightly wider than the length of the spacers so that the waterbox-windows were compressed flush with the faceplates upon clamping. The containers were then filled with various aqueous solutions with known atomic compositions, molar concentrations, and densities. In this way it was possible to easily and accurately vary the values of the Compton and photoelectric + Rayleigh line integrals, A_C and A_{P+R}, within the calibration standard. Table 3.2.1 gives the measured thickness dimensions of the four waterboxes and the molar concentrations of the saline solutions used in the calibration measurements.

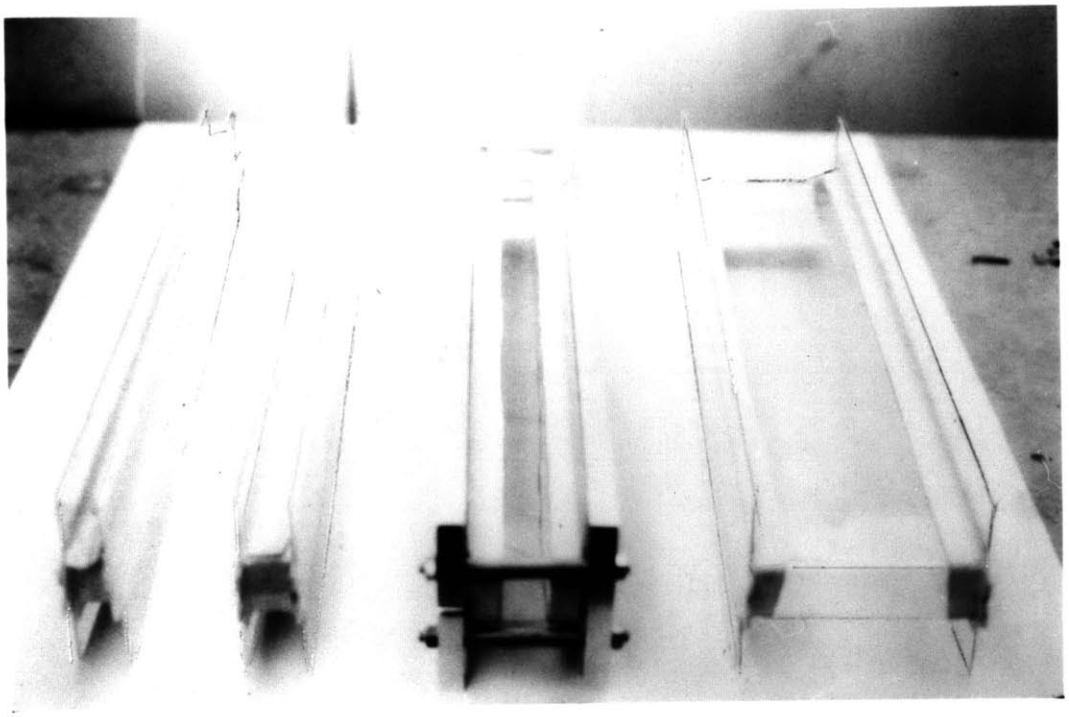

Figure 3.2.1 Photograph of the four interchangeable waterboxes used in the calibration experiment.

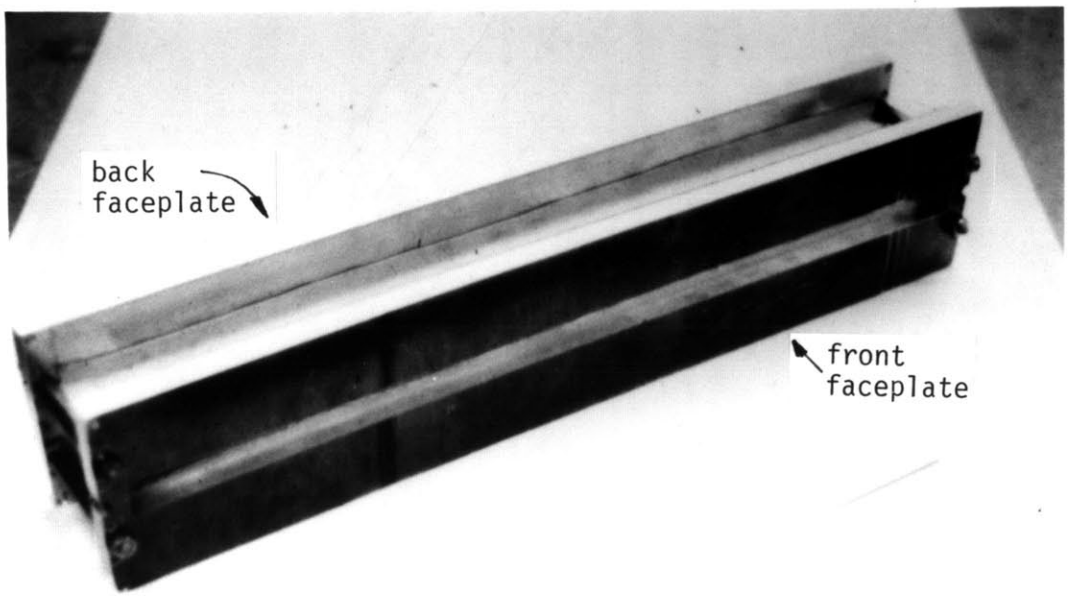

Figure 3.2.2 Photograph of the faceplate and waterbox arrangement of the calibration standard.

Thicknesses of the four waterboxes	
#1	1.410 cm
#2	2.834 cm
#3	5.704 cm
#4	11.413 cm

Molar concentrations of the five saline solutions	
A	0.0M NaCℓ
B	1.1665M NaCℓ
C	2.4300M NaCℓ
D	3.4546M NaCℓ
E	5.0510M NaCℓ

Table 3.2.1 Measured thickness dimensions of the waterboxes and measured molar concentrations of the saline solutions.

Design Considerations in the Calibration Standard

The philosophy in the design process of the standard was that the standard should be designed so that calibration measurements with the standard would be of comparable or better accuracy than measurements on unknown objects. In particular, the uncertainty in calibration measurements due to uncertainty in the thickness and atomic cross sections should be less than the uncertainty in the measurement on an unknown object due to Poisson statistical measurement error. Table 3.2.1a lists those errors which were identified to be of significance in the CT scan and calibration measurement processes. Those errors relevant to the standard design are mentioned immediately below while those errors relevant to the calibration measurement process are mentioned in the next subsection.

To minimize thickness errors the front and back faceplates were machined flat to 0.001". Also, the spacing bars were matched to better than 0.001" so that the constructed faceplate arrangement's thickness was uniform to about 0.0015". The major cause of variation in thickness was due to the clamping pressure of the faceplates on the waterbox. Estimates (D.6, T.7) indicated that with the 0.5" aluminum stock used and the dimensions of the faceplates the maximum deflection of both faceplates was a total of 0.010". Also, it was estimated (D.6) that the deflection of the lucite window due to hydrostatic pressure was about 0.001".

Rather than rely on the spacer bar dimensions for an indication of the standard's thickness, the thickness was measured versus position for each waterbox using the arrangement shown in Figs. 3.2.3

1. Poisson statistics.
2. Detector noise.
3. Calibration standard machining errors.
4. Calculation of the attenuation coefficients of the standard from published cross section tables due to errors in the published cross sections.
5. Saline solution manufacturing errors.
6. Interpolation errors in the reconstruction process.
7. Errors in the transmission measurement due to the continuous rotation of the scanner.
8. Variation in the filter thicknesses.
9. Problems with detector transient response.
10. Scattered radiation interferring with the measurement process.
11. Reproducibility of the x-ray tube kVp, mA.
12. X-ray detector discharges.
13. HV drift of the x-ray detector.
14. Non-saturation of the ionization detectors.

Table 3.2.1a Errors noted to be of significance in the CT scan and calibration measurement process.

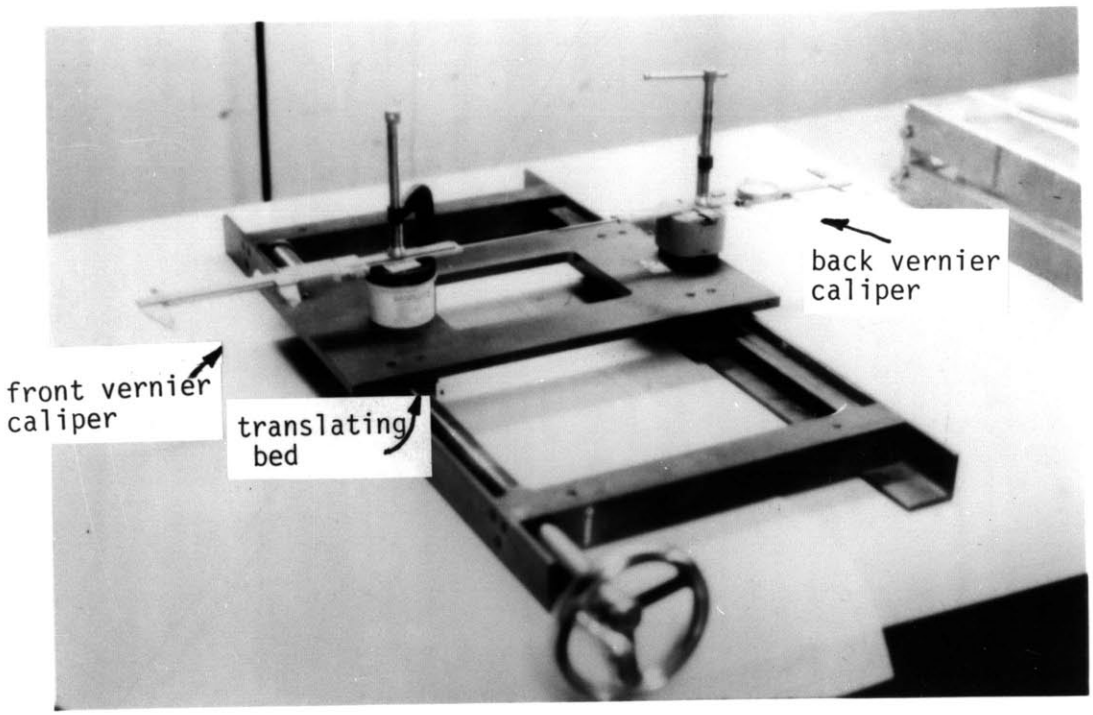

Figure 3.2.3 Null thickness measurement method.

and 3.2.4. It is seen in Fig. 3.2.3 that the null thickness reading on the calipers was measured first. Then with the standard placed between the calipers, the change from null was noted for both calipers so that the standard's thickness could be determined. This thickness measurement method was accurate to about 0.0015". Figure 3.2.5 presents the measured thickness versus position for the four standards.

The next consideration in the design of the standard was the development of the waterbox so that the uncertainty in the macroscopic cross sections of the window material and the aqueous solutions would be minimized. Lucite was chosen for the windows of the waterbox because of its:

(1) availability

(2) widespread use

(3) well known properties - mechanical and nuclear (G.5, B.12)

(4) low average atomic number.

Similarly, saline solutions were used because they were:

(1) easily available

(2) molar concentrations accurate to 0.02% were manufacturable

(3) aqueous solution properties of NaCℓ were well known

(4) NaCℓ is a low atomic number compound so that the cross section behavior was similar to biological tissue

(5) the high solubility of NaCℓ in water meant that relatively high cross sections were achievable.

Therefore, using the lucite waterbox and saline solution arrangement the atomic compositions and densities were accurately known. In this

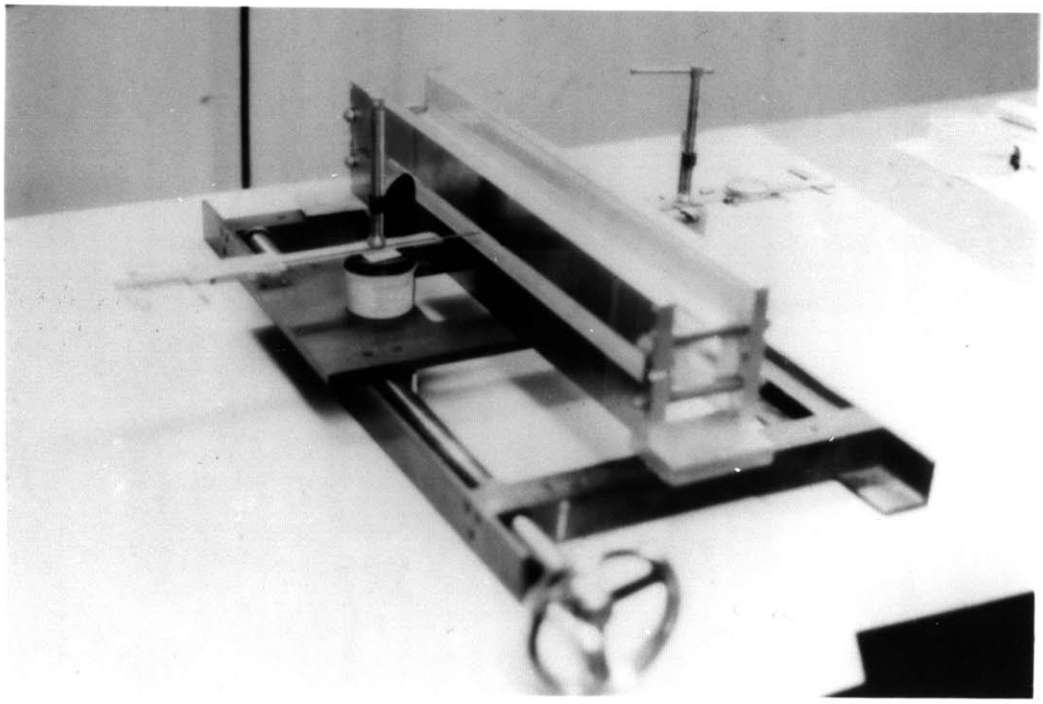

Figure 3.2.4 Calibration standard thickness measurement method.

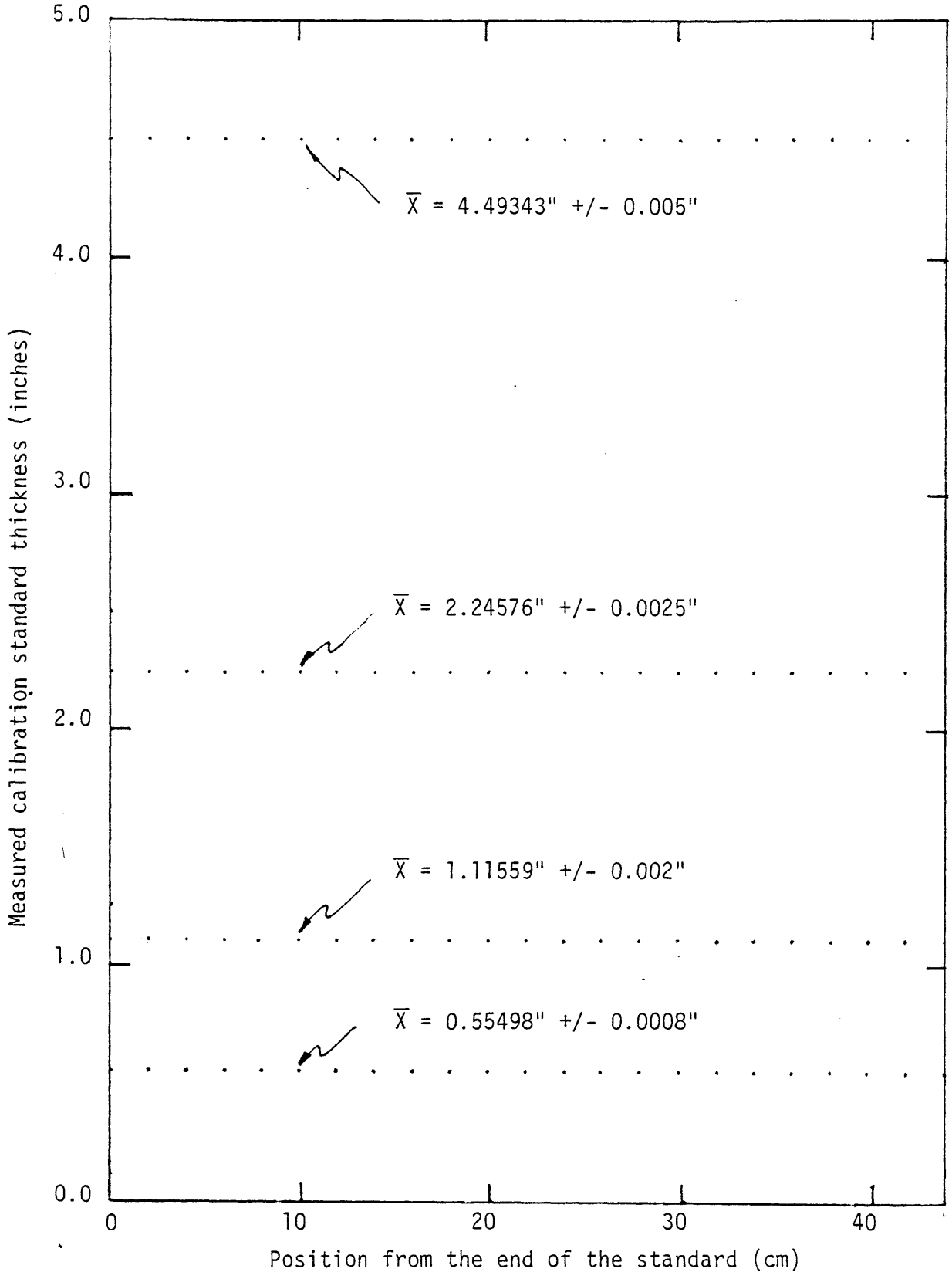

Figure 3.2.5 Measured thickness of the calibration standard waterboxes in situ versus position.

way the limit to the accuracy of the line integrals, A_C and A_{P+R}, was not due to the mechanical arrangement of the standard, but due to the accuracy of the microscopic cross sections used. The photoelectric, Rayleigh, and Compton cross sections were known to an accuracy of about 1%. Therefore, the ultimate limit to the accuracy of quantitative tomochemistry was determined by the accuracy of the available microscopic cross sections.

One final consideration in the design of the standard is that the front and back lucite windows had to be parallel because of the finite width of the x-ray beam. The possible use of a circular or triangular standard was precluded by the fact that calculations indicated that the geometric mean of the thickness, which varies with position along the beam, was not a sufficiently good estimate of the effective thickness of the target. Therefore, to avoid the uncertainty in the effective thickness, the standard was made square. As seen in Fig. 3.2.6 a parallel window arrangement was more flexible from an experimental viewpoint because the effective thickness of the standard was the same throughout the width of the beam. Furthermore, if the standard were to be rotated with respect to the x-ray beam the effective thickness was easy to determine from the base thickness t and the angle θ.

Method of Calibration Data Acquisition

As seen in Fig. 3.2.2 the standard was made long enough so that transmission measurements could be made simultaneously by all the detectors. As seen in Fig. 3.2.7 the standard was aligned on the rotating table so that the fan beam would pass through the

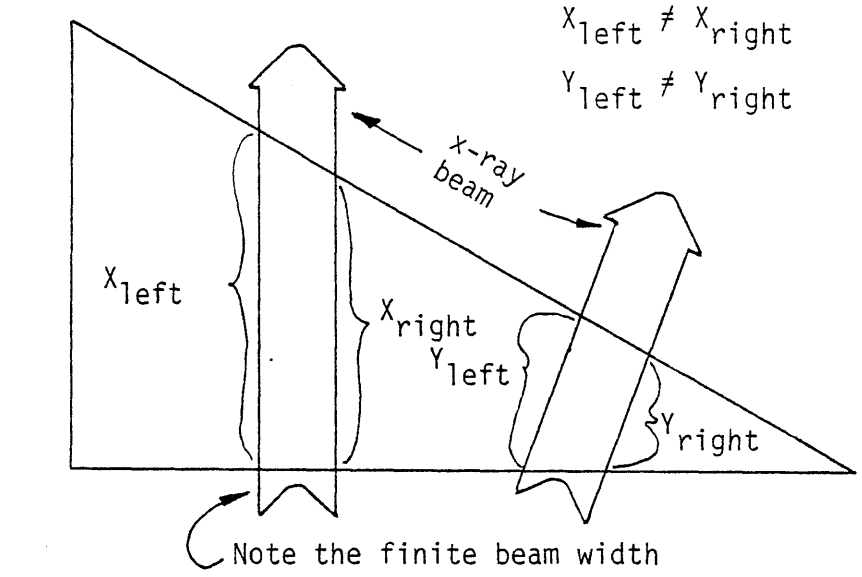

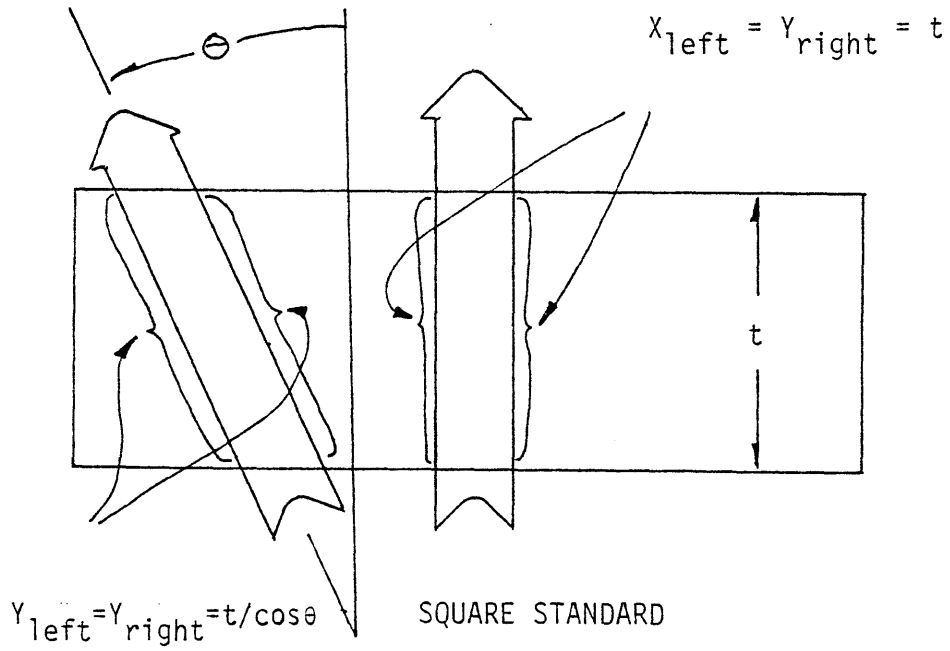

Figure 3.2.6 Illustration of the advantage of using a square calibration standard.

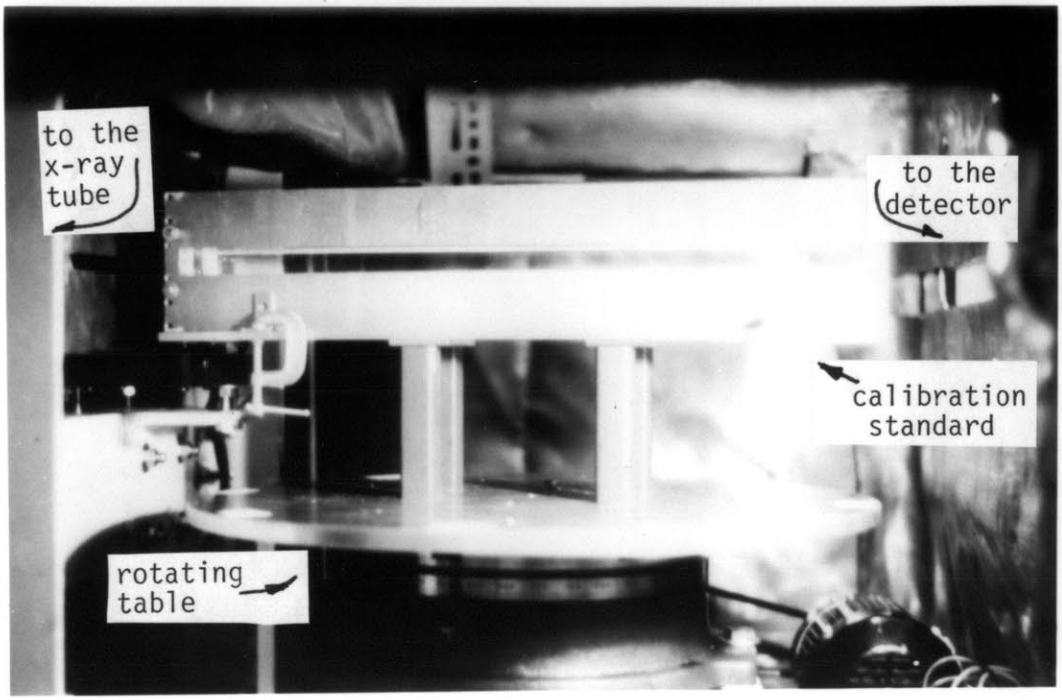

Figure 3.2.7 Position arrangement of the calibration standard on the rotating table.

standard without striking the top or bottom edges of the faceplates. The table was then rotated so that the standard was parallel to the detector pressure vessel (normal to the centerline of the scanner). Therefore, with the standard positioned at this 0° reference angle the effective thickness of the standard with respect to the detectors was known. In general, if the standard were then rotated by an angle θ the effective thickness was given by the formula (referring to Fig. 3.2.8):

$$T_D = t/\cos(\theta+\phi_D) \qquad (3.2.1)$$

where

T_D is the effective thickness of the standard as seen by detector D.

t is the base thickness of the standard.

θ is the angle of the table (and standard) with respect to the detector.

ϕ is the angle of the detector (ionization chamber) with respect to the centerline of the scanner.

In the calibration measurements the standard was rotated at angles of about 0°, 15°, -15°, 30°, -30°, 45°, -45°, 60° and -60° with respect to the detector so that the effective thickness of the standard could be varied by a factor of 2. The exact angle of the standard with respect to the 0° reference alignment position was measured using the pulse encoder of the table. In this way the relative angle between the standard and the detector was known to +/- 0.068°. Transmission measurements were not made beyond a relative

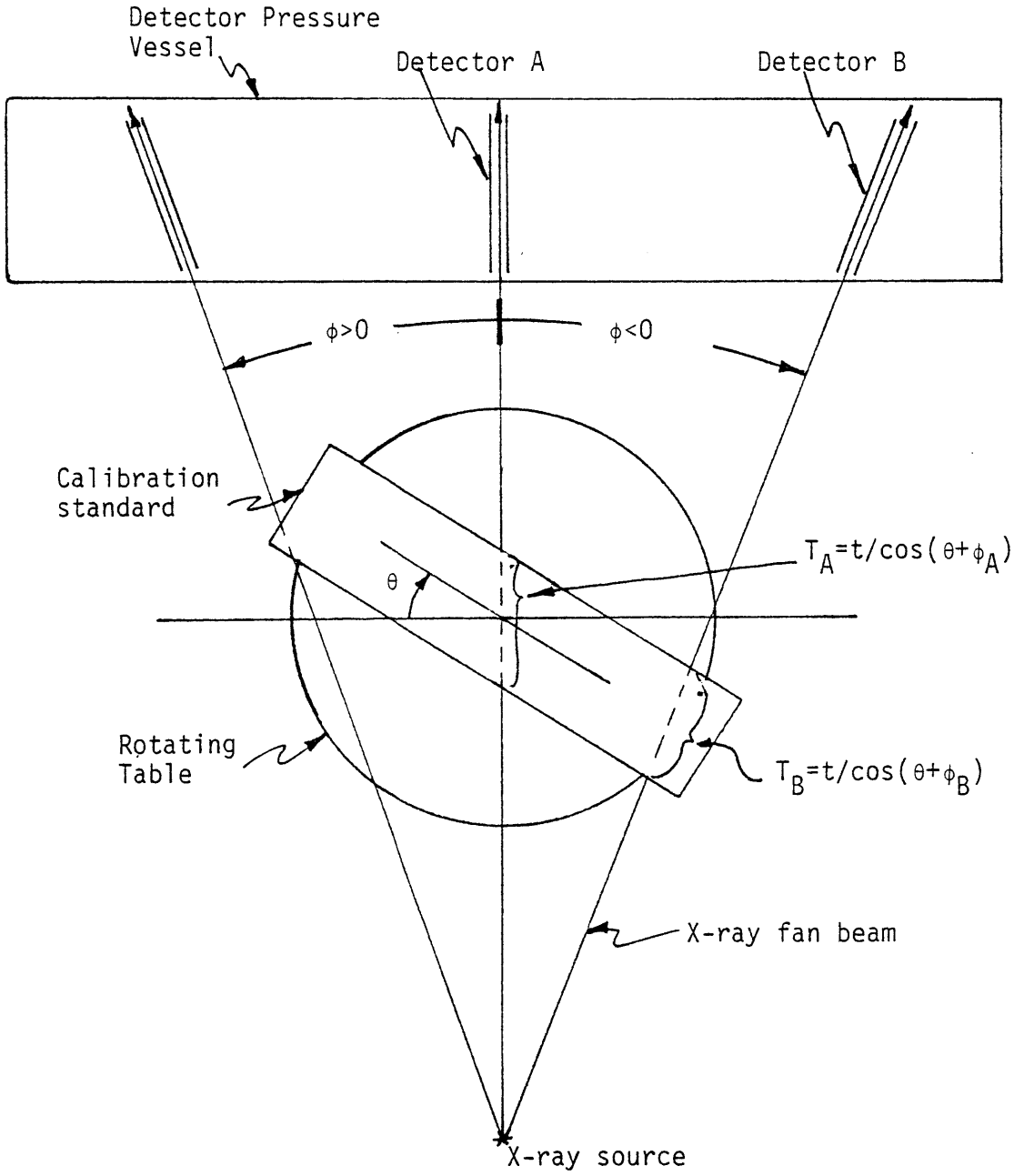

Figure 3.2.8 Definition of geometry in the calibration experiment.

angle of 60° because it was determined that the uncertainty in the thickness (given by the formula $\Delta X/X = (\tan\theta)\Delta\theta$) would be greater than 0.010" for a 10" thick standard.

In the calibration measurement process the disk RPM was the same as in the CT scan process. This was done so that the transient smoothing over the thickness variations of the filters would be the same as in the scan measurement process. One hundred transmission measurements were made per filter for a given position of the standard. This was done so that the uncertainty in the measurement due to Poisson error would be much smaller than that encountered in a CT scan transmission measurement.

During the calibration experiment the high voltage potential applied to the ionization chamber tended to drift by about 20 volts. This voltage change was sufficient to measureably change the current readings from the detectors because the change would cause the detector to operate in a different part of the saturation curve. Hence, in the experiment the voltage potential of the detectors was measured for every calibration measurement. The detector reading was then corrected to determine the detector current at HV = -2500V using the formula:

$$I_{2500} = I_{HV} \left(1 + (2500\text{-}HV) * 3.545 * 10^{-5}\right)$$

where

I_{2500} is the current measured on the detector when the high voltage is -2500V.

I_{HV} is the experimentally measured current with the high voltage equal to -HV.

HV is the magnitude of the high voltage at the time of the calibration measurement.

A final note about the calibration measurement process is that the saline concentration-standard thickness combinations were changed semi-randomly from one calibration point measurement to the next. This was done to avoid introducing extraneous systematic trends into the data set such as electronic drift. Table 3.2.2 presents the order in which the saline concentration-standard thickness combinations were changed. With 20 saline concentration-standard thickness combinations and 10 angular positions about 200 calibration measurements were made for every detector.

Reduction of the Calibration Data

After the calibration measurements were performed the above calibration data was then correlated to the cross section line integrals. As mentioned in Section 1.3 and Appendix B.3 the calibration transmission measurements were assumed to be highly linearly related to the photoelectric + Rayleigh and Compton cross section line integrals at a reference energy E_{REF}. The choice of the proper reference energy has been considered elsewhere by Alvarez and Seppi (A.4). In general it was found that the reference energy should be close to the average energies of the low and high energy spectra so that the relative magnitudes of the photon attenuation processes would be about the same. Figure 3.2.9 shows the behavior of the photoelectric, Rayleigh and Compton cross sections per electron versus atomic number at 60 and 80 keV. Note in particular that at $Z \sim 8$ the Rayleigh and photoelectric cross sections are about equal at these energies. Hence,

Calibration Measurement	Saline concentration - standard thickness combination
#1	0.0M NaCℓ - 5.704 cm
#2	5.0510M NaCℓ - 5.704 cm
#3	1.1665M NaCℓ - 5.704 cm
#4	2.4300M NaCℓ - 5.704 cm
#5	3.4546M NaCℓ - 5.704 cm
#6	3.4546M NaCℓ - 1.410 cm
#7	1.1665M NaCℓ - 1.410 cm
#8	5.0510M NaCℓ - 1.410 cm
#9	0.0M NaCℓ - 1.410 cm
#10	2.4300M NaCℓ - 1.410 cm
#11	2.4300M NaCℓ - 2.834 cm
#12	3.4546M NaCℓ - 2.834 cm
#13	0.0M NaCℓ - 2.834 cm
#14	1.1665M NaCℓ - 2.834 cm
#15	5.0510M NaCℓ - 2.834 cm
#16	5.0510M NaCℓ - 11.413 cm
#17	1.1665M NaCℓ - 11.413 cm
#18	2.4300M NaCℓ - 11.413 cm
#19	0.0M NaCℓ - 11.413 cm
#20	3.4546M NaCℓ - 11.413 cm

Table 3.2.2 Sequence of the saline concentration-standard thickness combination in the calibration measurements.

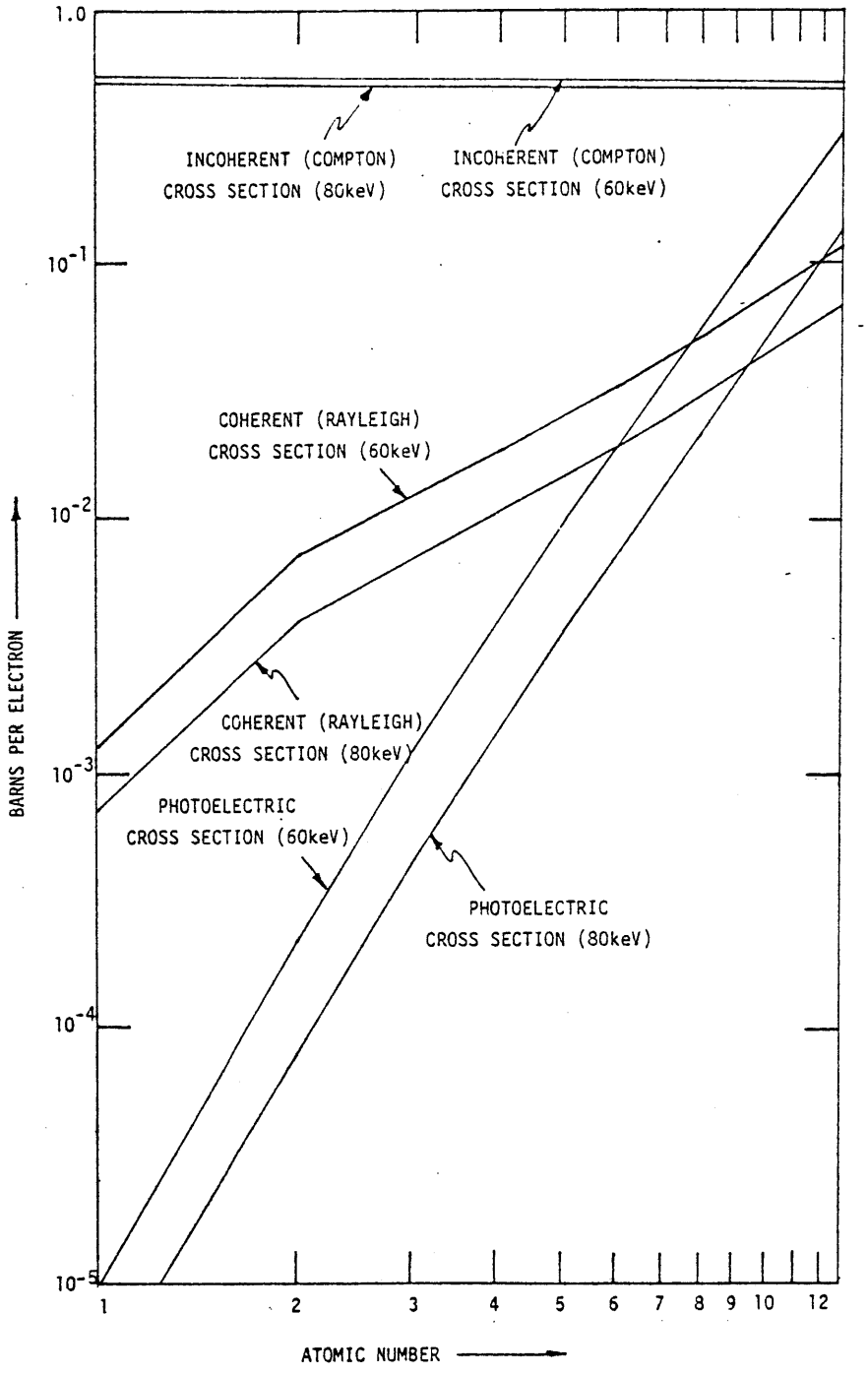

Figure 3.2.9 Behavior of the photoelectric, Rayleigh, and Compton cross sections per electron versus atomic number for 60 keV and 80 keV x-rays.

Rayleigh scattering is not a negligible effect. The reference energy used in this study was 60 keV. This energy was chosen because cross sections were readily available at this energy and also because 60 keV was close to the 58 keV average energy of the low energy tantalum filtration - 100 kVp spectrum. Using the cross sections at this reference energy and the equivalent thickness determined from Eq. (3.2.1) the line integrals are given by:

$$A_{P+R} = \int \mu_{P+R}(E_{REF})\, d\ell = \mu_{P+R}(E_{REF})\, t_{PLEX}/\cos(\theta+\phi) + \mu_{P+R}(E_{REF})\, t_{SALINE}/\cos(\theta+\phi) \quad (3.2.2)$$

$$A_C = \int \mu_C(E_{REF})\, d\ell = \mu_C(E_{REF})\, t_{PLEX}/\cos(\theta+\phi) + \mu_C(E_{REF})\, t_{SALINE}/\cos(\theta+\phi) \quad (3.2.3)$$

where

μ_{P+R}, μ_{P+R} PLEX SALINE	are the calculated photoelectric + Rayleigh attenuation coefficients at 60 keV for the lucite windows and the saline solution used.
μ_C, μ_C PLEX SALINE	are the calculated Compton attenuation coefficients at 60 keV for the lucite windows and the saline solution used.
t_{PLEX}, t_{SALINE}	are the base thicknesses of the lucite windows and the solution within the standard.

Systematic Search for and Removal of Outliers

It was known a priori that in the calibration data set some bad data would be present due to detector discharges or due to the rotated standard interfering with some of the detector transmission measurements. For this reason a program was developed which searched for outliers within the calibration data set. The program worked by investigating the data from one calibration standard setup at a time. The data from the five central detectors was assumed to be good. These five measurements served as an indication of the trend of the data as seen in Fig. 3.2.10. If the next adjacent detector's data was seen to fit the trend of the previous five data points to within 1% (3 standard deviations), that data point was kept. If the data did not fit the trend it was rejected. The author will not get into detail here on how the data trend was determined computationally. For explicit detail on the workings of the program the reader is referred to Appendix C.

Reduction of the Calibration Data

After the major outliers were removed from the data set, polynomial fits were performed on the remaining calibration data. The polynomial fitting was performed using a slightly modified version of a publicly available scientific software package from IBM Corporation (I.3). The functional fits assumed in the program are given by the expressions:

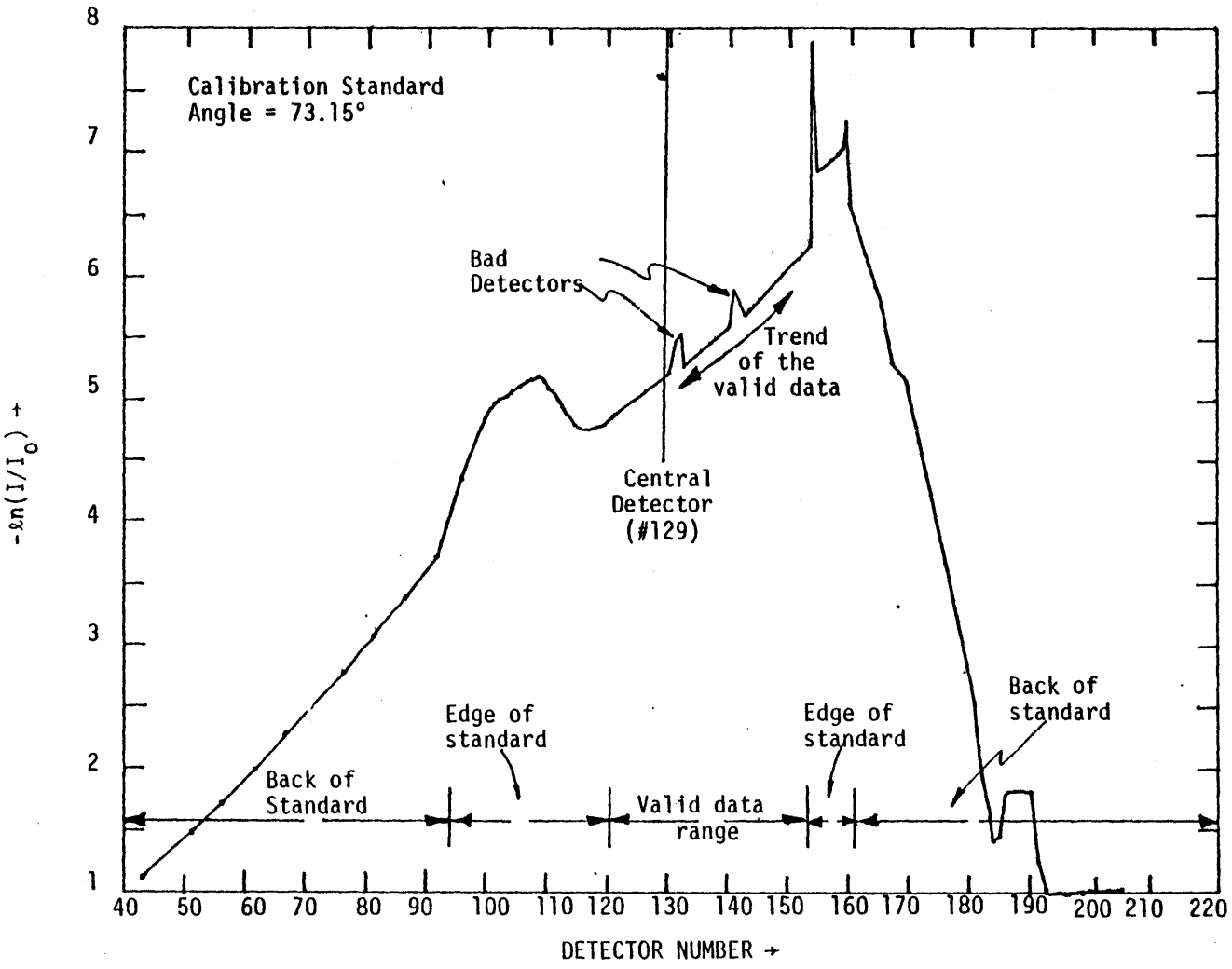

Figure 3.2.10 Typical calibration data set indicating the valid data range and the outliers in the data.

$$\frac{\int \mu_{P+R}(E_{REF})d\ell}{\ell n(I_2/I_{2o})} = B_1 \frac{\ell n(I_1/I_{1o})}{\ell n(I_2/I_{2o})} + B_2 + B_3 \frac{(\ell n(I_1/I_{1o}))^2}{\ell n(I_2/I_{2o})}$$

$$+ B_4\ \ell n(I_2/I_{2o}) + B_5\ \ell n(I_1/I_{1o}) \qquad (3.2.4)$$

$$\frac{\int \mu_{C}(E_{REF})d\ell}{\ell n(I_2/I_{2o})} = C_1 \frac{\ell n(I_1/I_{1o})}{\ell n(I_2/I_{2o})} + C_2 + C_3 \frac{(\ell n(I_1/I_{1o}))^2}{\ell n(I_2/I_{2o})}$$

$$+ C_4\ \ell n(I_2/I_{2o}) + C_5\ \ell n(I_1/I_{1o}) \qquad (3.2.5)$$

where the above terms are the same as in Eqs. (1.3.14) and (1.3.15). It should be noted here that B_o and C_o are equal to zero because it was known that the functional fits must pass through the origin. Equations (3.2.4) and (3.2.5) were chosen to be used as the functional fits because the least squares fitting program in itself did not assume that the data passed through the origin (B.14). Hence, to implicitly force B_o and C_o equal to zero the functions were modified so that B_2 and C_2 became the new intercept constants to be determined. It should also be noted here that normally in multiple regression analysis the independent variable (on the right hand side) is assumed to be known exactly while the dependent variable (on the left hand side) may contain statistical uncertainty. The opposite situation was true in this polynomial fitting procedure. After investigation of this dilemma in the literature (B.15,D.7) a rule of thumb was found:

> "Least squares analysis can be used safely if the variance of the independent variable is less than 1/10 of the average scatter of the independent variables from their mean" (D.7).

Therefore, multiple regression using Eq. (3.2.4) and Eq. (3.2.5) was justified.

Using the above methodologies unweighted polynomial fits were performed for every detector. Table 3.2.3 presents a sample output of the polynomial fit of the data for the central detector. The actual experimental data from the calibration of this detector is presented in Chapter 4 with the rest of the experimental results. For completeness the programs used to perform the polynomial fits are presented in Appendix C.

```
NO. OF OBSERVATIONS=      109
FIT TYPE=        1
TIME=       13        3       36
DATE=        2        2       80

VARIABLE      MEAN        STANDARD        CORRELATION     REGRESSION
  NO.                     DEVIATION         X VS Y        COEFFICIENT
   1        1.07582         0.02677         0.70858         3.13918
   2        1.59812         1.23527         0.20882       -20.92746
   3        1.45343         1.16522         0.18694        10.89892
   4        1.67132         1.31114         0.22997        10.02557
   5        3.46261         5.35167         0.16052         0.02168
   6        4.21386         6.27307         0.19078        -0.01038
VARIABLE NO.=        1
MEAN=          0.10758174051785600D  1
STANDARD DEVIATION=           0.26774869853860660D -1
CORRELATION X VS Y=           0.70858493921396140D  0
REGRESSION COEFF=             0.31391834465076560D  1
STD.ERROR OF REGR COEFF=              0.15396892291591440D  0
COMPUTED T VALUE=             0.20388422462512320D  2

VARIABLE NO.=        2
MEAN=          0.15981166737572440D  1
STANDARD DEVIATION=           0.12352681103022690D  1
CORRELATION X VS Y=           0.20881657196183260D  0
REGRESSION COEFF=            -0.20927460252965460D  2
STD.ERROR OF REGR COEFF=              0.57300923676742920D  0
COMPUTED T VALUE=            -0.36522603151138930D  2

VARIABLE NO.=        3
MEAN=          0.14534340304369370D  1
STANDARD DEVIATION=           0.11652156927515100D  1
CORRELATION X VS Y=           0.18694457625637750D  0
REGRESSION COEFF=             0.10898916769951580D  2
STD.ERROR OF REGR COEFF=              0.31051169660272490D  0
COMPUTED T VALUE=             0.35099858987880270D  2

VARIABLE NO.=        4
MEAN=          0.16713241375358410D  1
STANDARD DEVIATION=           0.13111421185152390D  1
CORRELATION X VS Y=           0.22996728621756270D  0
REGRESSION COEFF=             0.10025567106787480D  2
STD.ERROR OF REGR COEFF=              0.29115864625080200D  0
COMPUTED T VALUE=             0.34433048402614570D  2

VARIABLE NO.=        5
MEAN=          0.34626127684582550D  1
STANDARD DEVIATION=           0.53516653498307210D  1
CORRELATION X VS Y=           0.16051746010219290D  0
REGRESSION COEFF=             0.21679662855684360D -1
STD.ERROR OF REGR COEFF=              0.14739631567338280D -1
COMPUTED T VALUE=             0.14708415713541020D  1

VARIABLE NO.=        6
MEAN=          0.42138556082155450D  1
STANDARD DEVIATION=           0.62730629877800920D  1
CORRELATION X VS Y=           0.19078109194046380D  0
REGRESSION COEFF=            -0.10383816095038470D -1
STD.ERROR OF REGR COEFF=              0.12414574729695290D -1
COMPUTED T VALUE=            -0.83642140960399970D  0

DEPENDENT VARIABLE=        7
MEAN=          0.24786499861988D  0
STANDARD DEVIATION=           0.67454514810549980D -1
INTERCEPT=           -0.31504191780573100D  1

INTERCEPT                      -3.15042

MULTIPLE CORRELATION            0.97905

STD. ERROR OF ESTIMATE          0.01397

                    ANALYSIS OF VARIANCE FOR THE REGRESSION

    SOURCE OF VARIATION        DEGREES        SUM OF          MEAN
                               OF FREEDOM     SQUARES         SQUARES
ATTRIBUTABLE TO REGRESSION         6          0.77634         0.12939
DEVIATION FROM REGRESSION        172          0.03358         0.00020
     TOTAL                       178          0.80992
F VALUE=          0.66273585634086180D  3
```

Table 3.2.3 Sample output of the calibration data reduction (polynomial fitting) programs.

3.3 Tomochemistry Data Mapping and Data Correction

This section briefly describes the operation of the software programs which took the raw tomochemistry scan data and put it into the proper form for reconstruction. There were five major parts to the data processing:

(1) interpolate to determine the missing filter data

(2) map the data from $(\ell n(I_1/I_{10}), \ell n(I_2/I_{20}))$ space to (A_C, A_{P+R}) space

(3) correct the data to account for rejected transient periods

(4) correct the data so that the data set corresponded to scan measurements even in angle

(5) correct the data so that the data set corresponded to 300 views taken evenly in angle.

The meaning and operation of these five parts will be described in detail below. It should be noted here that in general all of the programs to be described assumed that the measurements at any one detector were continuous with angle and that the measurement after a 360° rotation of the table would match the 0° measurement. To convince the reader that these assumptions were reasonable, experimental transmission measurements of a rotating lucite cylinder with a particular detector are plotted in Fig. 3.3.1 versus the angle of the rotating table.

Missing Filter Interpolation and Data Mapping Methods

Probably the most sensitive assumption made in the tomochemistry software was that it was assumed valid to perform a straightforward linear interpolation between filter data to obtain missing filter measurements. Figure 3.3.2 and the discussion here will seek to

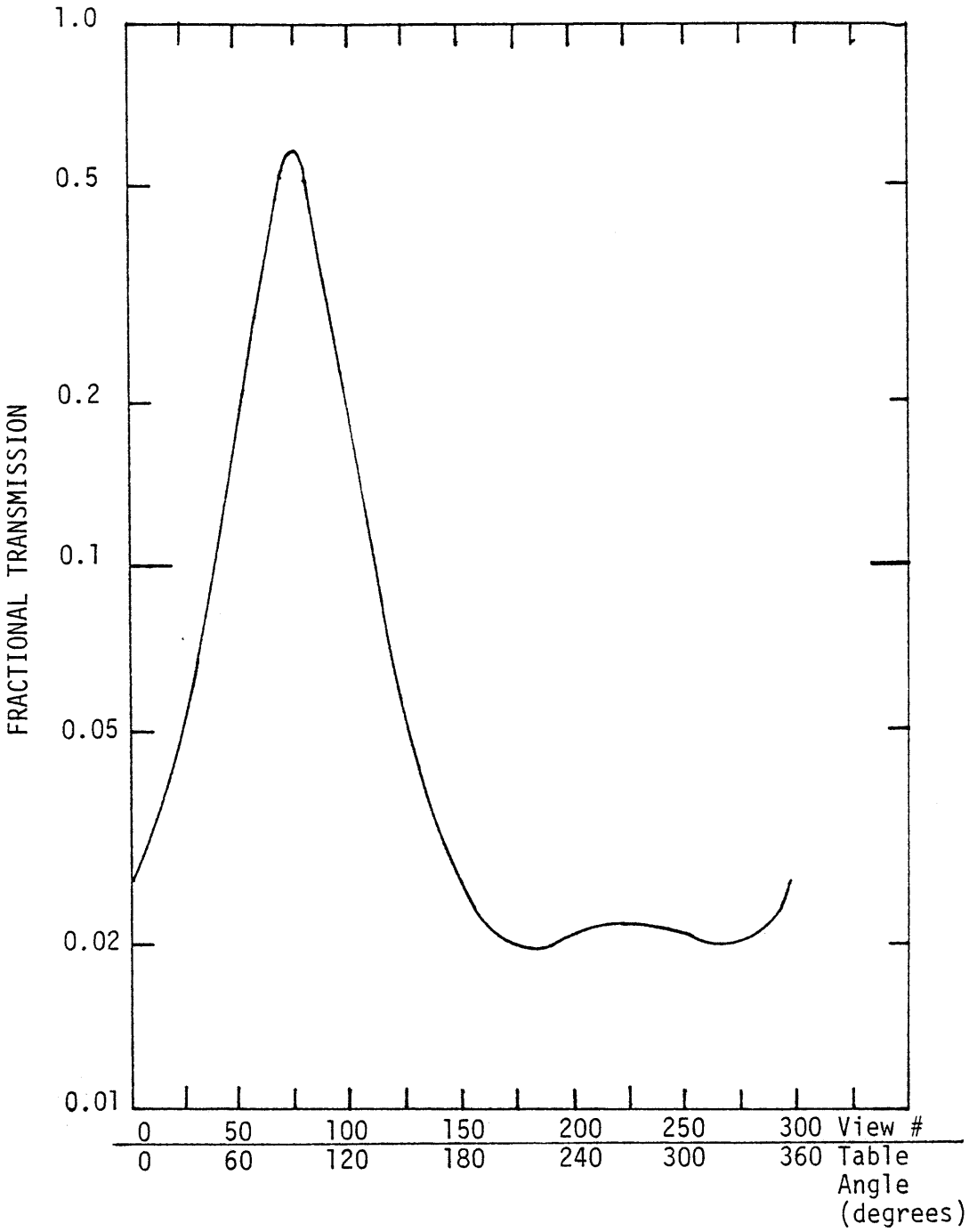

Figure 3.3.1 X-ray transmission through a 20 cm diameter lucite cylinder (not centered on the rotating table) versus view number.

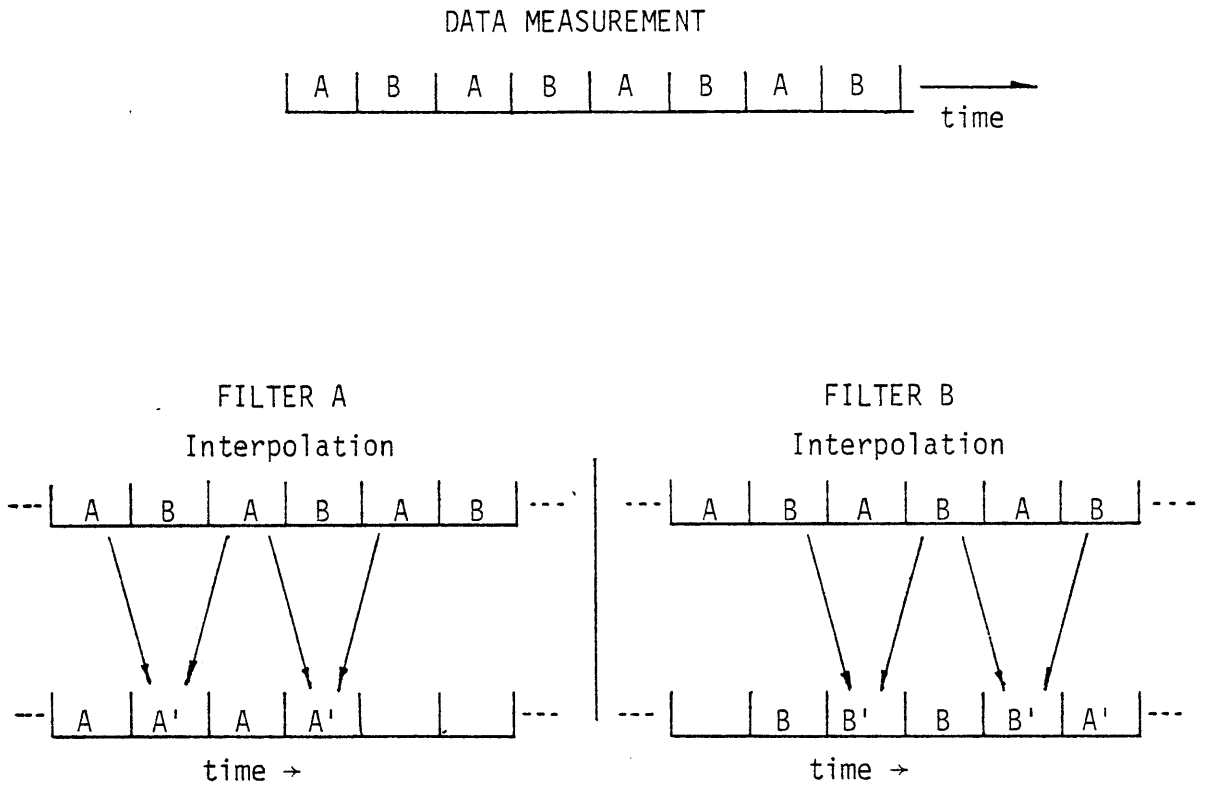

Figure 3.3.2 Method of interpolation between measurements to obtain the missing view data required for the data mapping.

clarify this statement. Note that in the tomochemistry scan the measurements alternated between transmission measurements with iron and tantalum filtration. To be able to perform the tomochemistry mapping, though, transmission measurements with the two filters had to be compared at the same angular position of the table. In this scanner dual measurements at each angular position were not possible because the scanner rotated continuously. Hence, it had to be assumed that the transmission measurements were sufficiently smooth so that it was valid to interpolate between two A filters to determine the equivalent A' measurement and to interpolate between two B filters to determine the equivalent B' measurement. In general, one would expect that this assumption broke down near discontinuities in in the scanned object, such as at the edges of tissue. The next chapter will present evidence to illustrate the sensitivity of this assumption.

The interpolation equation used in the software accounted for the fact that the average current measured during a measurement period corresponded to the instantaneous detected current in the middle of that period. The equation also accounted for the rotation of the table during the transient rejection period. With these features the interpolation formula is given by the expression:

$$\ell n(I/I_o)' = \frac{(\ell n(I/I_o)_{AFT} - \ell n(I/I_o)_{BEF})(\frac{1}{2}\Delta\theta_{BEF} + \Delta\theta_{TMID} + \frac{1}{2}\Delta\theta_{MID})}{(\frac{1}{2}\Delta\theta_{BEF} + \Delta\theta_{TMID} + \Delta\theta_{MID} + \Delta\theta_{TAFT} + \frac{1}{2}\Delta\theta_{AFT})} \quad (3.3.1)$$

where the terms in Eq. (3.3.1) are defined by the plot in Fig. 3.3.3. After all the interpolations on the filter transmission data were

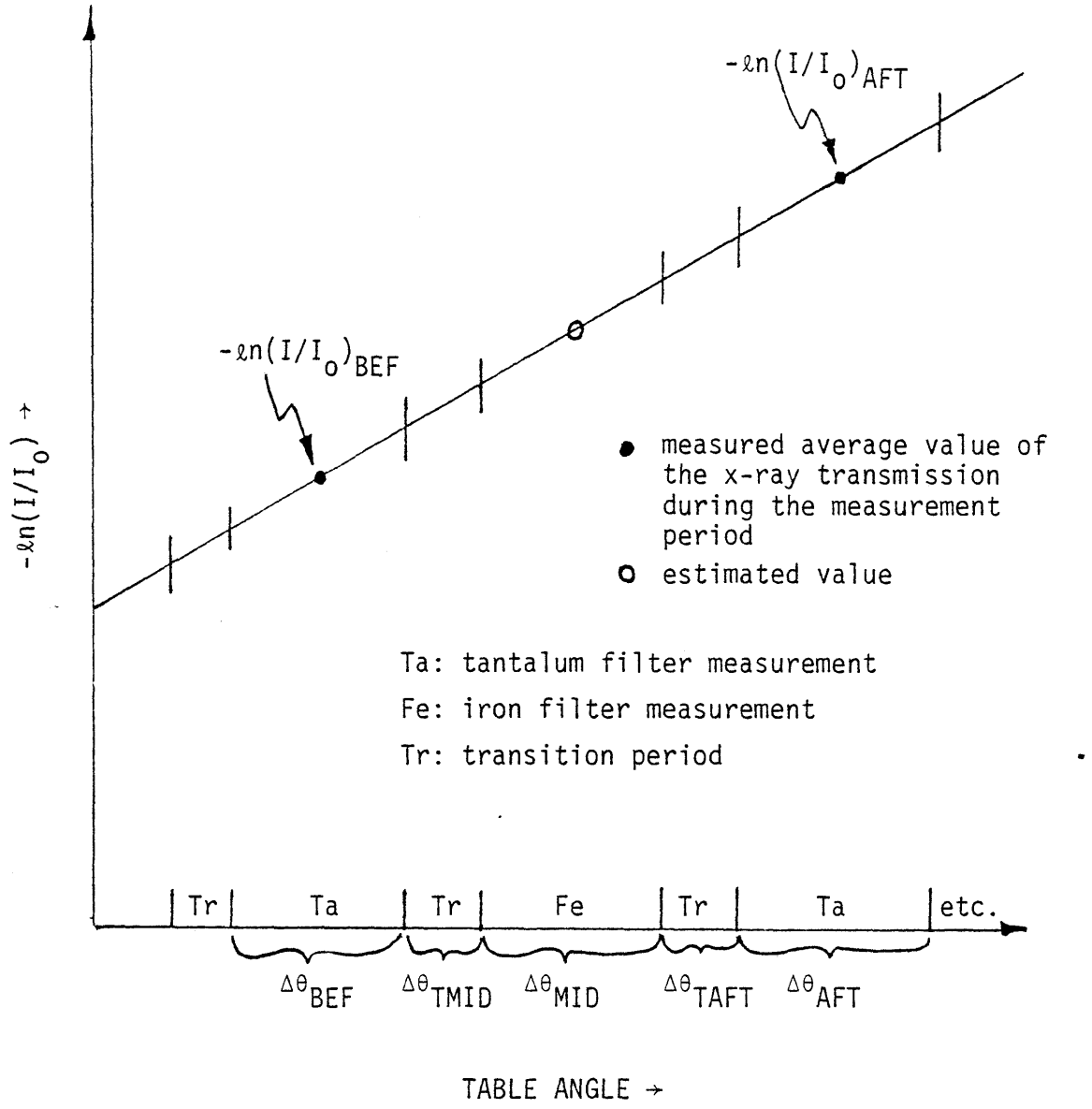

Figure 3.3.3 Illustration of the linear interpolation method used to obtain an estimate of the missing view data.

performed, the resultant data set was then mapped into (A_C, A_{P+R}) space using the polynomial fit equations of the calibration data (Eqs. (3.2.4) and (3.2.5)).

Methods used in the Rejected-Transient Data Correction, Even-Angle-Data Correction, and 300 Even-Angle-Data Correction

The purpose of the rejected-transient-data correction was to produce a data set which would approximately correspond to transmission measurements which were contiguous in time. This contiguous-view data set was needed so that the even-view data set could be determined. As seen in Fig. 3.3.4 the contiguous-view data set was produced by assuming that the data was continuous so that estimates of the sampled current within the rejected transient period could be found. Then from these estimates and the measurements themselves the contiguous data array was estimated.

The purpose of the even-view data correction was to create a data set of views even in angle which was then used by the 300-even-view-data subprogram. This correction had to be performed because the beam analyser disk was not coupled mechanically to the rotating table and neither of them rotated with a perfectly constant angular velocity. Hence, the contiguous-view data array did not correspond to measurements which were taken evenly in angle. As seen in Fig. 3.3.4 the correction was performed by again assuming that the measurement data was continuous. Then, by performing a linear interpolation the new estimate of the measured current versus time was obtained.

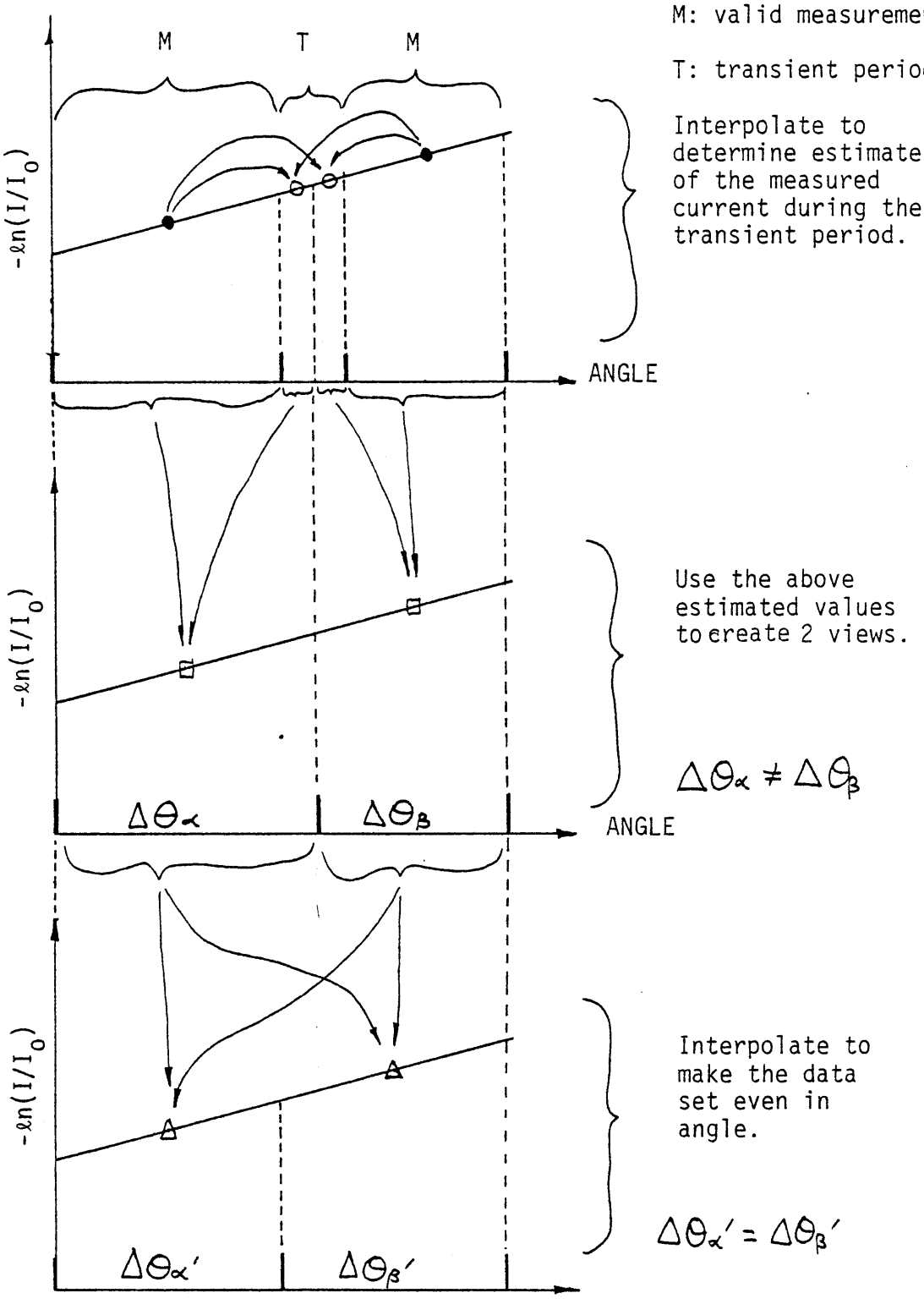

Figure 3.3.4 Method of determining an estimate of the contiguous measurement data sets. (Transients periods eliminated)

The purpose of the 300-even-view data correction subprogram was to create a data set of 300 views in 360° which were even in angle. This correction was performed because the particular reconstruction program used in this experiment required 300 views as an input. However, since the beam analyser disk was mechanically decoupled from the table, it was impossible to adjust the disk velocity so that a 360° rotation of the table would correspond to exactly 300 views. Instead, the disk velocity was set as close as possible to the above condition and software was used to perform the appropriate corrections. In this program it was assumed that the transmission data was continuous and that the 0° transmission measurement was exactly equal to the 360° transmission measurement. In this way the 0° and 360° measurements were merged so as to be continuous and the data was then divided evenly into 300 views. With the resultant 300-view data set the reconstructions were then performed using the normal CT reconstruction package which performed the Hanning-weighted ramp-filter backprojection reconstruction. It should be noted here that for completeness all of the above programs are listed with the rest of the tomochemistry software in Appendix C.

3.4 Summary

This chapter presented an outline of those methods used to process the scan data for the reconstruction of tomochemical scan images. Of the five blocks of software required for tomochemistry, only one was unique to computed tomography. This block - called the mapping software - served to map the data from the ($\ell n(I_1/I_{1o})$, $\ell n(I_2/I_{2o})$) measurement coordinate space to the ($\int \mu_{P+R} d\ell$, $\int \mu_C d\ell$) line integral space. The data mapping and correction methods mentioned above were used in all the tomochemical reconstructions performed in this research project.

4.0 Experimental Methods and Results

The purpose of this chapter is to present the major experimental results of this research project. The chapter is divided into three areas of discussion. The first area covers a brief review of the experimental setup of the scanner. The second area covers the transmission measurement characteristics of the scanner. The two major topics in this area are (1) the experimental determination of the optimal peak kilovoltage (kVp) for tomochemistry and (2) the description of the calibration results of a typical detector. The third area covers the results of the proof-of-principle experiments with the integrated tomochemistry scanner system. The three major topics in this area are (1) the accuracy of reconstruction, (2) the cause and elimination of artifacts within the images, and (3) the spatial resolution of the images. It is expected that the major findings presented here will illustrate the characteristics of all scanner systems which use the tomochemistry methodology.

4.1 Brief Review of the Experimental Setup

As seen in Figure 1.4.1 the basic tomochemistry scanner hardware used in the experiments consisted of an x-ray tube, beam analyser disk, rotating table, and detector bank. The entire arrangement was aligned as shown in the figure. The x-ray tube was aligned with respect to the 256 detectors so that the focal spot of the tube was along the line of sight of all the detectors. The rotating table was aligned with respect to the x-ray tube and the detector such that the table's rotation axis was less than 0.005" from the centerline of the detector bank. Finally, the beam analyser disk was aligned with respect to the rest of the scanner such that filtration changed simultaneously for all the ionization chambers.

The x-rays from the x-ray tube were twice collimated. The first collimation was performed just after the beam analyser disk so as to form a 1 cm thick fan x-ray beam incident upon the scanned target and to reduce the dose to the patient. The second collimation was performed immediately in front of the x-ray detector bank. This was done to eliminate the majority of scattered x-rays emanating from the target which would have otherwise entered the detector. It was found that this collimation arrangement reduced the scattered signal size to about $4*10^{-4}$ of the signal due to the original incident x-ray beam.

In the experiment the detection of x-rays was performed by 256 ionization detectors enclosed within a pressure vessel which contained a 95%-Xe/5%-CO_2 gas mixture at 200 psig pressure. As seen in Figure 2.1A.4 the detectors were operated at a voltage of -2500 V

which was well within the saturation region of the detectors. In the experiment the high voltage from the power supply was not perfectly constant. It was found that the voltage drifted by about 20V in about 30 minutes. This drift could not be neglected in the experiment because it caused the detectors to operate in a different part of the saturation curve. Hence, the exact operating voltage was recorded for each scan and a correction of the experimental data was performed. The correction formula, which is given in Eq. (3.2.1A), was based on a linear least squares fit for an approximation of the plateau region of the saturation curve.

In all of the reconstruction scans performed in this research project the x-ray tube was driven at a kilovoltage potential of 100 kV with an electron beam current on the target of 30 mA. The target to be scanned was centered on the rotating table and positioned at the proper height with respect to the x-ray fan beam.

The timing and duration of the measurement periods was determined by the rotation of the beam analyser disk. Measurements were commenced and terminated every time a filter transition occured. (However, transient response effects were rejected.) The angular velocity of the disk was adjusted so that each measurement lasted about 30 msec. Transmission measurements were made on the target in 360°. One rotation of the table took about 8.5 seconds so that at the above measurement rate the x-ray transmission through the target was measured at 300 views.

In this scanner the error in the transmission measurement process was due to two main processes: Poisson statistical error

and electronic noise. As seen in Figure 2.1B.1 Poisson error was the dominant error process at higher count rates. In this research project most of the transmission measurements were made at detector current levels where Poisson statistics was the dominant error process.

4.2 Experimental Determination of the Optimal kVp for Tomochemistry

The purpose of this section is to present the results of the experimental determination of the optimal kVp for use with the iron and tantalum filtration of the beam analyser disk. To accomplish this determination the model of the statistical measurement uncertainty of the photoelectric + Rayleigh attenuation coefficient (described in Derivation b of Appendix B.3D) was slightly extended. With the terminology defined in Appendix B.3D the fractional statistical uncertainty of μ_{PR} is given by the expression:

$$\frac{\delta\mu_{PR}}{\mu_{PR}} = \frac{\frac{4}{3}^{1/2}\frac{1}{X}\left[(A_{CL})^2\frac{1}{N_{TH}} + (A_{CH})^2\frac{1}{N_{TL}}\right]^{1/2}}{A_{CL}\mu_{TH} - A_{CH}\mu_{TL}} \qquad \text{(B.3D.14)}$$

where

μ_{TH}, μ_{TL}	are the total attenuation coefficients measured with the high and low energy x-ray beams respectively
H, L	subscripts correspond to the high and low energy x-ray beam respectively
P, C	subscripts correspond to the photoelectric + Rayleigh and Compton cross sections
X	is the spatial resolution
N_{TH}, N_{TL}	are the number of photons detected which passed through the central resolution element of the 20 cm reference water target.

Now if it is assumed that the dominant behavior of the polynomial fit functions, given by Eqs. (1.3.14) and (1.3.15), can be accounted for by the linear first order terms, then the total attenuation coefficients of a known target measured with the low and high energy spectra are given by the expressions:

$$\mu_{TL} = \mu_{CL} + \mu_{PL} \simeq A_{CL}\mu_{CR} + A_{PL}\mu_{PR} \tag{B.3D.7}$$

$$\mu_{TH} = \mu_{CH} + \mu_{PH} \simeq A_{CH}\mu_{CR} + A_{PH}\mu_{PR} \tag{B.3D.8}$$

where

R subscript refers to the reference energy cross section

A_{CL}, A_{PL}, A_{CH}, A_{PH} are all constants of proportionality.

In Eqs. (B.3D.7) and (B.3D.8) the reference energy attenuation coefficients, μ_{CR} and μ_{PR}, depend upon the target being measured while the proportionality constants depend upon the x-ray spectrum used for the transmission measurements. In general, the relative size of the proportionality constants is related to the relative contribution of the particular processes to the photon attenuation. Hence, one should expect that A_{PL} and A_{PH} will increase as the spectrum becomes softer and that A_{CH} and A_{CL} are relatively constant for all diagnostic energy spectra.

Now by substituting Eq. (B.3D.7) and Eq. (B.3D.8) into Eq. (B.3D.14) the statistical measurement uncertainty can be written:

$$\frac{\delta\mu_{PR}}{\mu_{PR}} = \frac{\frac{4}{3}^{1/2}\frac{1}{X}\left[(A_{CL})^2\frac{1}{N_{TH}} + (A_{CH})^2\frac{1}{N_{TL}}\right]^{1/2}}{\left(A_{CL}A_{PH} - A_{CH}A_{PL}\right)\mu_{PR}} \tag{4.2.1}$$

The advantage of formulating the statistical uncertainty expression in terms of the constants A_{PL}, A_{PH}, A_{CL}, and A_{CH} is that these constants can be determined experimentally. To show this

consider once again Eqs. (B.3D.7) and (B.3D.8) and imagine that measurements of x-ray transmission have been made on two targets of thickness x with both the low and high energy x-ray spectra. In this case the expressions for x-ray transmission can be written:

target 1 measurement using the low energy spectrum:

$$\mu_{TL1}x = A_{CL}\mu_{CR1}x + A_{PL}\mu_{PR1}x = \ell n(I_{L1}/I_{L1o}) \tag{4.2.2}$$

target 2 measurement using the low energy spectrum:

$$\mu_{TL2}x = A_{CL}\mu_{CR2}x + A_{PL}\mu_{PR2}x = \ell n(I_{L2}/I_{L2o}) \tag{4.2.3}$$

target 1 measurement using the high energy spectrum:

$$\mu_{TH1}x = A_{CH}\mu_{CR1}x + A_{PH}\mu_{PR1}x = \ell n(I_{H1}/I_{H1o}) \tag{4.2.4}$$

target 2 measurement using the high energy spectrum:

$$\mu_{TH2}x = A_{CH}\mu_{CR2}x + A_{PH}\mu_{PR2}x = \ell n(I_{H2}/I_{H2o}) \tag{4.2.5}$$

where

μ_{CR1}, μ_{CR2} are the Compton attenuation coefficients at the reference energy of targets 1 and 2.

μ_{PR1}, μ_{PR2} are the photoelectric + Rayleigh attenuation coefficients at the reference energy of targets 1 and 2.

μ_{TL1}, μ_{TL2}, μ_{TH1}, μ_{TH2} are the total measured attenuation coefficients of targets 1 and 2 using the low and high energy spectra.

Now if the $\mu_{CR1}x$, $\mu_{CR2}x$, $\mu_{PR1}x$, $\mu_{PR2}x$ of the targets are known then A_{PL}, A_{CL}, A_{PH}, A_{CH} can be determined by the expressions:

$$A_{PL} = \frac{\ell n(I_{L1}/I_{L1o})(\mu_{CR2}{}^{x}) - \ell n(I_{L2}/I_{L2o})(\mu_{CR1}{}^{x})}{(\mu_{PR1}{}^{x})(\mu_{CR2}{}^{x}) - (\mu_{PR2}{}^{x})(\mu_{CR1}{}^{x})} \tag{4.2.6}$$

$$A_{CL} = \frac{\ell n(I_{L1}/I_{L1o})(\mu_{PR2}{}^{x}) - \ell n(I_{L2}/I_{L2o})(\mu_{PR1}{}^{x})}{(\mu_{PR1}{}^{x})(\mu_{CR2}{}^{x}) - (\mu_{PR2}{}^{x})(\mu_{CR1}{}^{x})} \tag{4.2.7}$$

$$A_{PH} = \frac{\ell n(I_{H1}/I_{H1o})(\mu_{CR2}{}^{x}) - \ell n(I_{H2}/I_{H2o})(\mu_{CR1}{}^{x})}{(\mu_{PR1}{}^{x})(\mu_{CR2}{}^{x}) - (\mu_{PR2}{}^{x})(\mu_{CR1}{}^{x})} \tag{4.2.8}$$

$$A_{CH} = \frac{\ell n(I_{H1}/I_{H1o})(\mu_{PR2}{}^{x}) - \ell n(I_{H2}/I_{H2o})(\mu_{PR1}{}^{x})}{(\mu_{PR1}{}^{x})(\mu_{CR2}{}^{x}) - (\mu_{PR2}{}^{x})(\mu_{CR1}{}^{x})} \tag{4.2.9}$$

Hence, the relative behavior of the statistical measurement uncertainty as given by Eq. (4.2.1) can be determined experimentally.

In this research project the constants A_{PL}, A_{CL}, A_{PH}, and A_{CH} were determined by experimental measurements of x-ray transmission through the use of the calibration standard. Target 1 consisted of the 11.41 cm thick lucite box containing pure water while target 2 consisted of the 11.41 cm thick lucite box containing 5.051 M NaCl aqueous solution. In both cases measurements were made with the x-rays traversing normal to the standard and all measurements were performed with the central detector (#129). In this experiment measurements were made with constant filtration (the beam analyser disk fixed). The transmission measurement I/O control was performed through the use of a pulse generator. Transmission measurements were made on the targets using x-ray tube kilovoltages ranging from 60 kVp to 150 kVp.

transmission measurements were performed on each target using iron and tantalum filtration for each kVp studied. The experimentally determined values of A_{CL}, A_{CH}, A_{PL}, and A_{PH} versus kVp are tabulated in Table 4.2.1 while Figure 4.2.1 presents a plot of these coefficients versus kVp.

For both the iron and tantalum filtration, the values of A_{CH} and A_{CL} are about the same and relatively constant. This behavior is due to the fact that (1) the Compton cross section is relatively constant versus energy and (2) the Compton process is the dominant process for all diagnostic energy x-ray spectra. Hence, if one refers to Eqs. (4.2.2), (4.2.3), (4.2.4), and (4.2.5) it is seen that one would expect that the Compton term in the equations would be much larger than the photoelectric + Rayleigh term. Furthermore, since μ_{TL} and μ_{TH} are relatively constant for all kVp then that means that A_{CL} and A_{CH} should be relatively constant.

As seen in Figure 4.2.1, the photoelectric + Rayleigh coefficients, A_{PL} and A_{PH}, behave very differently than the Compton coefficients, A_{CL} and A_{CH}. In general, both photoelectric + Rayleigh coefficients decrease with increasing energy. This behavior reflects the lower relative contribution of the photoelectric + Rayleigh processes to the attenuation process as the spectrum becomes harder. The next behavior to note is that the coefficients approach the same values at very low and very high kVp. At very low kVp the two coefficients should tend toward one another because when the entire incident bremsstrahlung spectrum is below the tantalum K-edge energy the resultant iron and tantalum filtered spectra should be nearly

X-ray Tube kVp	photoelectric + Rayleigh coefficient		Compton coefficient	
	tantalum-filtered spectra: A_{PL}	iron-filtered spectra: A_{PH}	tantalum-filtered spectra: A_{CL}	iron-filtered spectra: A_{CH}
60	-1.5212	-1.541	-1.01	-0.955
75	-1.099	-0.896	-0.992	-0.960
90	-0.918	-0.637	-0.996	-0.964
105	-0.789	-0.486	-0.987	-0.959
120	-0.785	-0.428	-0.929	-0.944
135	-0.598	-0.373	-0.960	-0.934
150	-0.490	-0.333	-0.967	-0.925

Table 4.2.1 Experimentally determined values of the spectrum coefficients versus kVp.

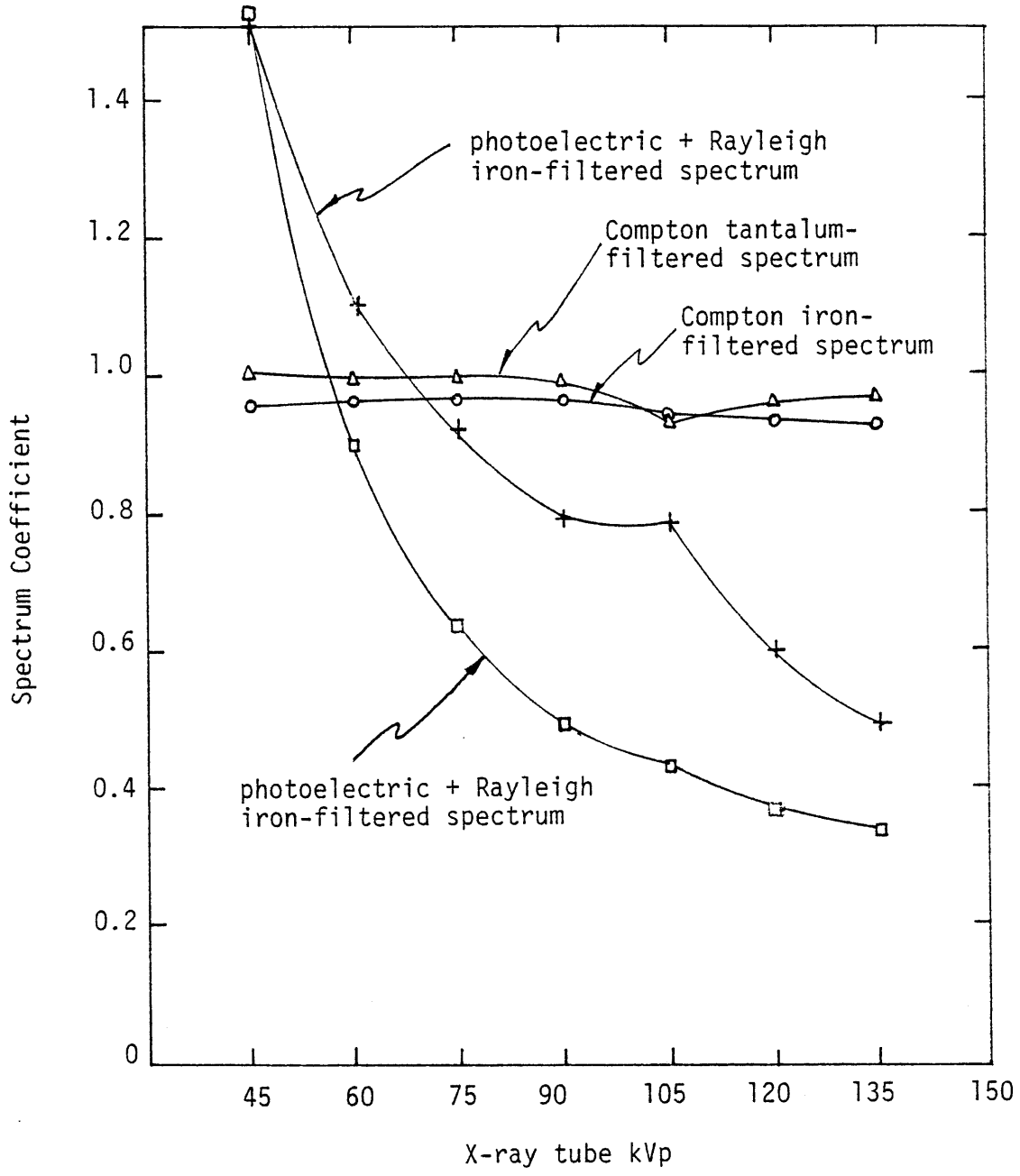

Figure 4.2.1 Plot of the experimentally determined values of the spectrum coefficients versus kVp.

the same. At very high kVp the two coefficients should approach each other because at peak kilovoltage energies much greater than the tantalum K-edge energy the differences in the attenuation properties of the resultant iron and tantalum filtered spectra become less significant. This is because at increasing kVp a larger fraction of the total spectrum is above the K-edge energy of tantalum.

In this research project all the interesting behavior of the photoelectric + Rayleigh coefficients occurs in the intermediate kVp range. As seen in Figure 4.2.1 the tantalum K-edge effect becomes more pronounced as the peak x-ray tube kilovoltage is increased from 60 kV. It is true that the tantalum coefficient decreases at increasing kVp, but what is important here is the <u>difference</u> between the iron and tantalum filtered spectra. The difference between the two spectra is seen to maximize at 120 kVp. At this kVp the overlap between the unfiltered spectrum and the tantalum K-edge window is optimal. Hence, the difference between the spectral shapes of the tantalum and iron filtered spectra is maximized.

As mentioned previously, it is now possible to determine the relative behavior of the statistical error as given by Eq. (4.2.1) since the values of the coefficients in Eqs. (B.3D.7) and (B.3D.8) are known. The result of an investigation of four different experiment scenarios will be described here.

The first two tests of interest involve the investigation of the statistical measurement uncertainty behavior when the kVp used is the same for both the iron and tantalum filtrations. In this situation one may investigate the behavior of the error when the number of

photons is held constant or investigate the behavior of the error when the electron beam current on the anode target is held constant. The later investigation is more realistic because since this experiment is photon-flux-limited it is important to have as many photons as possible for the analysis. This means that in practice one would drive the electron beam current at its maximum value (30mA) for all kVp. Recall that Figure 2.1C.8 in Chapter 2 presents the behavior of the photon flux versus x-ray tube kVp at a fixed electron beam current.

Figure 4.2.2 presents a plot of the relative statistical error versus kVp for both the fixed flux and varied flux (constant beam current) scenarios and Table 4.2.2 contains a tabulation of the computed values. Note that all curves in the figure are normalized to have the same photon flux at 150 kVp. It is seen in the figure that the relative error of the varied flux case is always greater than the fixed flux case. This is clearly true because as the kVp is decreased there are fewer photons produced by the x-ray tube (due to the lower x-ray generation efficiency) and hence the Poisson error is larger in the varied flux case. However, in spite of the difference in the relative behavior of the two curves, it is seen that for both cases the kVp of choice for fixed-kVp tomochemistry (using the iron and tantalum filters of this experiment) is 120 kVp.

The second two scenarios of interest involve the investigation of the statistical measurement uncertainty behavior when the kVp is allowed to alternate between a high and low energy kVp in coincidence with the iron and tantalum filtrations. In the alternating kVp scenario the high energy kVp can be determined immediately. Clearly, if

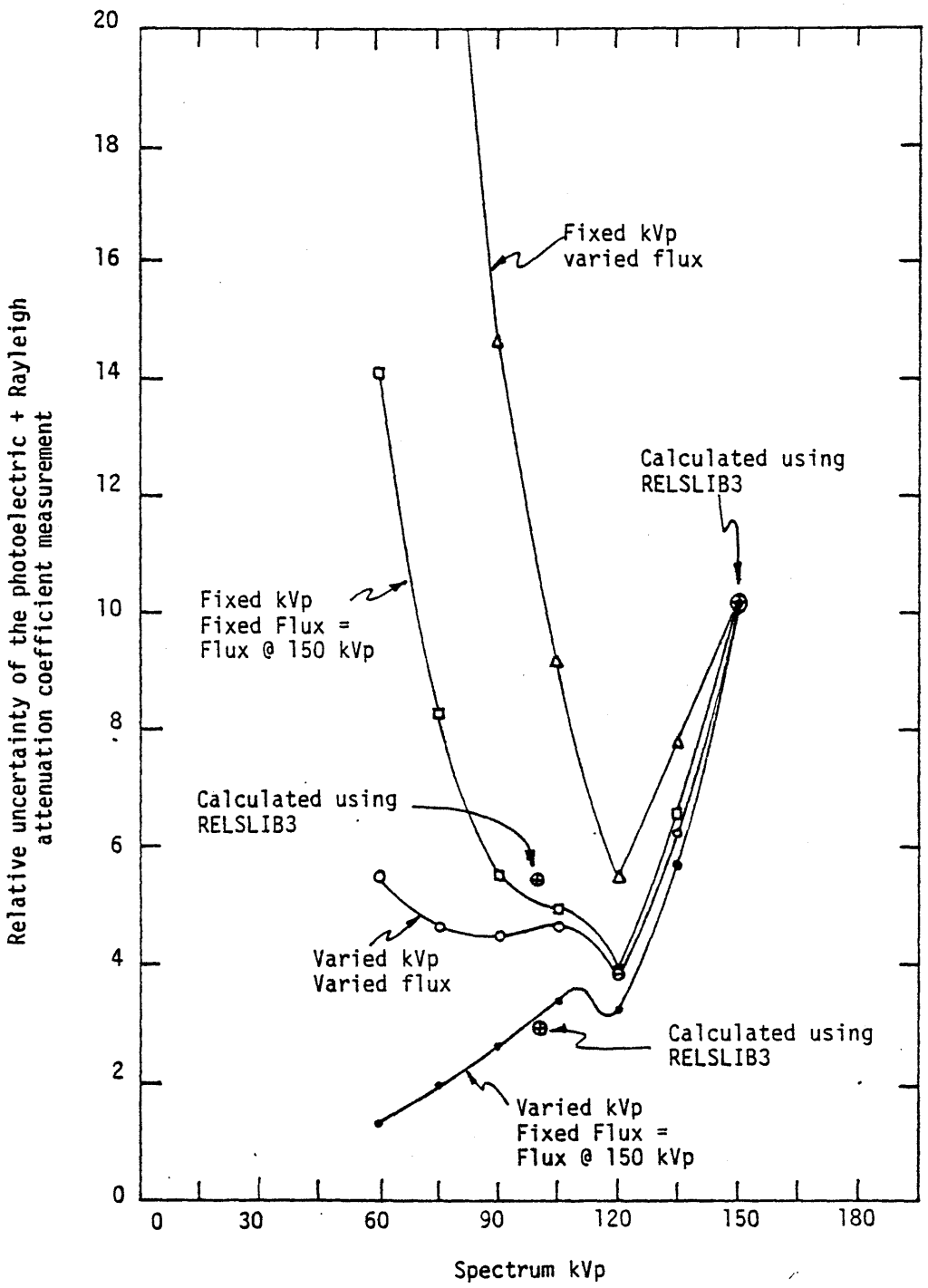

Figure 4.2.2 Calculated values of the relative uncertainty of the photoelectric + Rayleigh attenuation coefficient measurement versus the x-ray tube kVp. (Calculations are based on experimental measurements)

X-ray tube kVp	Fixed kVp Varied Flux	Fixed kVp Fixed Flux = Flux @ 150 kVp	Varied kVp Varied Flux	Varied kVp Fixed Flux = Flux @ 150 kVp
60	144.4	14.14	5.52	1.28
75	37.70	8.32	4.63	1.98
90	14.64	5.55	4.49	2.63
105	9.20	4.97	4.68	3.38
120	5.51	3.86	3.80	3.15
135	7.81	6.66	6.16	5.70
150	10.25	10.25	10.25	10.25

Table 4.2.2 Calculated values of the relative uncertainty of the photoelectric + Rayleigh attenuation coefficient measurement versus the x-ray tube kVp. (Calculations are based on experimental measurements)

one refers to Figure 4.2.1, it is seen that 150 kVp (or greater if that were possible) is the high energy spectrum of choice because A_{PH} has a local minimum at this point. To determine the corresponding low energy spectrum, one must refer to the behavior of the statistical uncertainty as a function of the low energy spectrum's kVp.

As in the fixed kVp case one has the choice in the analysis of allowing the photon flux of the low evergy spectrum to vary or to remain fixed (and equal to the flux at 150 kVp). Figure 4.2.2 presents the relative behavior of the statistical uncertainty for these two scenarios. In both cases it is seen that the simultaneous alternation of the kVp and the filtration is a more accurate method for measuring the photoelectric + Rayleigh cross sections than the fixed kVp method. It should also be noted that the fixed flux case is always more accurate than the varied flux case. However, the comparison of the varied flux case and the fixed flux case is really only an intellectual exercise because in practice it is not possible to maintain the photon flux at the 150 kVp photon flux level at lower kVps. However, on a per photon basis, the fixed photon case is a valid relative analysis. It is seen in the figure that the optimal kVp to use with the 150 kVp spectrum at a fixed photon flux is one where the kVp is as small as possible. The result is intuitively valid, however it does not account for the consideration of increased dose to the patient. Therefore, from a practical viewpoint this result is of limited value.

The alternated kVp-varied photon flux case is really the practical method of interest in tomochemistry. As it is seen in the figure, the low photon fluxes at low kVps has a tremendous effect on the behavior of

the statistical uncertainty versus kVp. For example, at 60 kVp the statistical error of the varied flux case is 4.4 times greater than the fixed flux case. Hence, it is truly not valid to ignore the behavior of the photon flux as a function of the kVp. It is seen in Figure 4.2.2 that once again the tantalum K-edge window effect dominates the choice of the kVp. Therefore, for the modulated kVp/filtration case the optimal spectra to use in the measurement process are the 120 kVp/Ta-filtered and the 150 kVp/Fe-filtered spectra.

One final point to note is that included in Figure 4.2.2 are the estimates of the relative uncertainty as calculated by the transport program RELSLIB3. It is seen that the agreement between the computed and measured behavior of the modulated and fixed kVp scenarios is excellent. Therefore, it appears that the models used for the incident x-ray spectra and the detector were sufficiently accurate for the design analyses performed in this research project.

4.3 Results of the Transmission Measurement Calibration Experiment

This section presents the major results of the calibration experiment as illustrated by measurements with the central ionization chamber detector (#129). These results are important in order to understand the behavior of the detector calibration measurements when observing the behavior of the proof-of-principle reconstructions in the next section.

It should be noted here that calibration measurements of x-ray transmission are unique to the particular pair of x-ray spectra used in the tomochemistry experiment as well as the particular detector used to detect these x-ray spectra. This is true because the measured values of x-ray transmission, $\ell n(I_1/I_{1o})$ and $\ell n(I_2/I_{2o})$, depend upon the x-ray spectra used and the detection efficiency of each particular detector. Hence, each detector was calibrated separately since it was known that (1) each detector had a slightly different efficiency, (2) the filter thickness varied slightly across the fan beam, and (3) the x-ray spectrum emitted from the x-ray tube varied slightly as a function of the angle from the tube. The slight detector to detector difference was noted by slight differences in the values of the coefficients of the polynomial functions used to perform the cross section mapping operation.

The calibration experiment transmission measurements presented below were performed on the calibration standard by using a 100 kVp x-ray spectrum at an electron beam current of 30 mA. The results at 100 kVp are representative of the results of calibration measurements at other x-ray tube kilovoltages.

The first experimental result that one should note is that, as seen in Figure 4.3.1, the attenuation of the tantalum-filtered spectrum is greater than the attenuation of the iron-filtered spectrum through a water absorber. Therefore, since the initial photon flux of the tantalum-filtered spectrum is greater than the photon flux of the iron-filtered spectrum, the photon fluxes of the two spectra will eventually be the same at some water thickness. For this experiment the fluxes are the same at about 20 cm of water. Hence, the determination of the appropriate filter thicknesses to be used in the experiment as determined by the photon transport program, RELSLIB3, was quite accurate.

The second result that one should note is that, as seen in Figure 4.3.2, the logarithm of the photon attenuation is a highly linear function of the solution thickness. This result thereby justifies the simplifying assumption used elsewhere in the thesis that the linear first order terms in the polynomial fit functions describe the dominant behavior of the photon attenuation process.

Also indicated in Figure 4.3.2 is the range of attenuations that were measured using the saline solutions. All of the experimental calibration data points of the tantalum-filtered and iron-filtered spectra fell within the transmission measurement ranges indicated. It is important to note that the calibration measurements on known targets must be made over a wide enough range of thicknesses, electron densities and atomic compositions so that any transmission measurement on an unknown will fall within the calibration range. Hence, in this research project calibration measurements were made over a range of

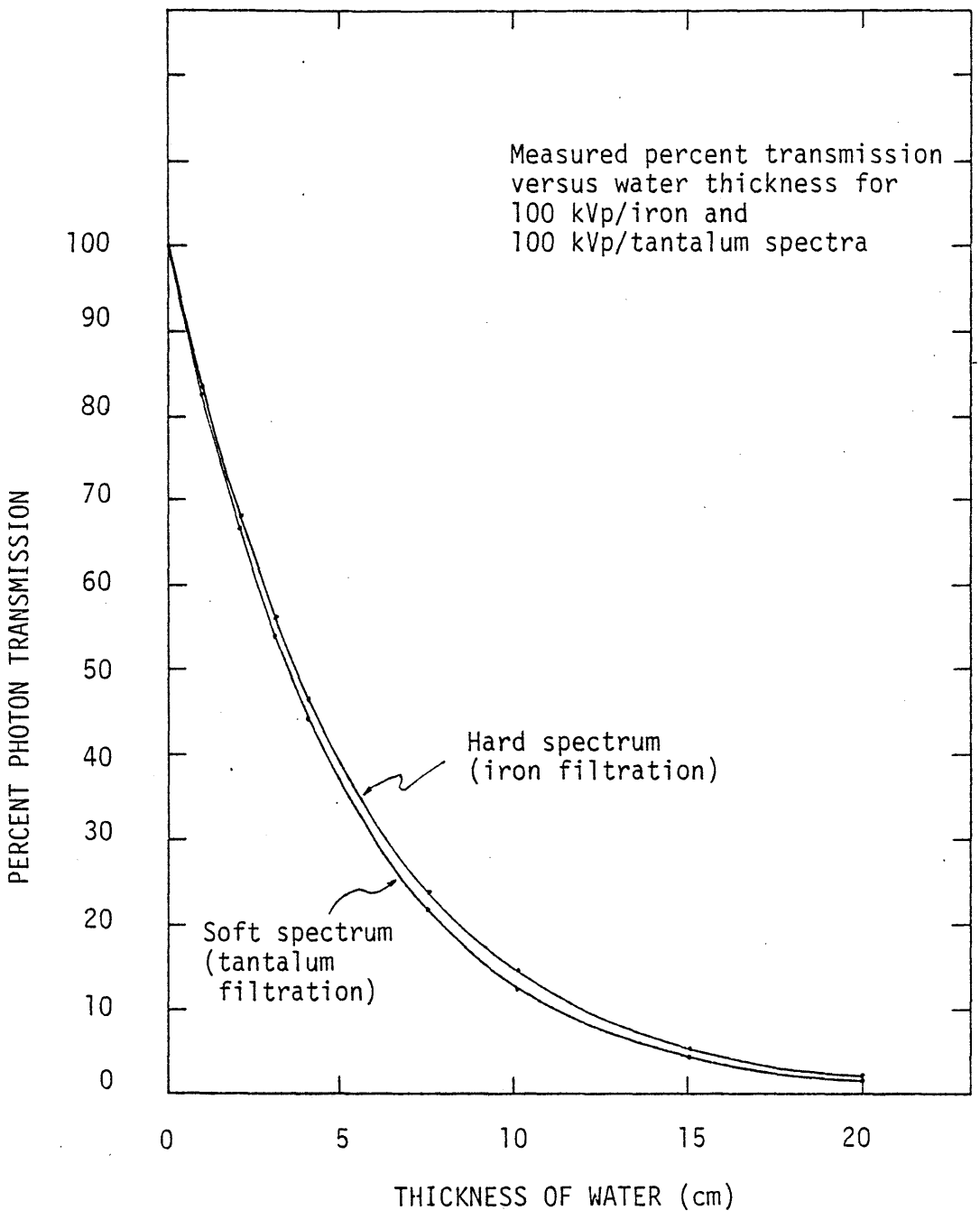

Figure 4.3.1 Percent photon transmission of the tantalum and iron filtered 100 kVp spectra versus water thickness.

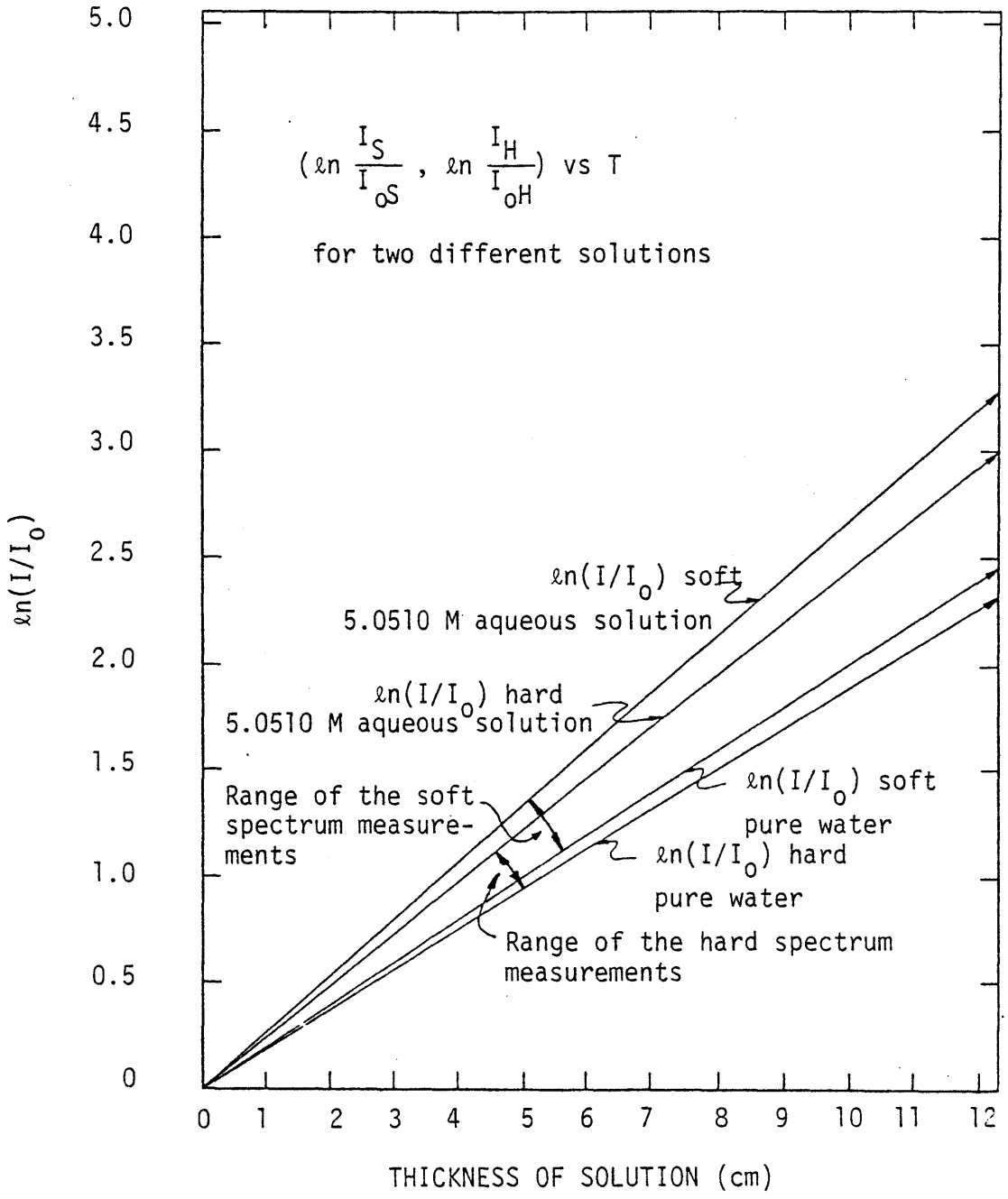

Figure 4.3.2 Experimental measurements of photon attenuation versus solution thickness for the hard and soft spectra incident upon two different solutions.

line integrals that were representative of biological tissue. The polynomial fit coefficients of the calibration data are only valid over this calibration range. If one wanted to use tomochemistry to scan other materials, such as iron-based materials, then the appropriate calibration measurements must be made over a range of line integrals that one would encounter in such a scan.

As mentioned in Section 3.2 the purpose of the calibration process is to sample the surfaces in $(\ell n(I_1/I_{1o}), \ell n(I_2/I_{2o}), \int \mu_{CR} d\ell)$ space and $(\ell n(I_1/I_{1o}), \ell n(I_2/I_{2o}), \int \mu_{PR} d\ell)$ space. To aid in the physical understanding of the calibration process, consider Figures 4.3.3, 4.3.3a, 4.3.4, and 4.3.4a where a schematic of these two surfaces are presented. Figures 4.3.3a and 4.3.4a are the same as plots 1 in Figures 4.3.3 and 4.3.4 except for the fact that they contain more detail. Experimentally one measures the x-ray transmission for a series of solutions and a range of thicknesses. Therefore, the contours in the drawings designated by 5M NaCl and pure H_2O correspond to measurements of $\int \mu_{PR} d\ell$ and $\int \mu_{CR} d\ell$ at fixed μ_{PR} and μ_{CR}.

Indicated in Figures 4.3.3 and 4.3.3a are the contours one would measure if it were possible to vary the photoelectric + Rayleigh line integral, $\int \mu_{PR} d\ell$ while maintaining the Compton line integral, $\int \mu_{CR} d\ell$, fixed. Also indicated in Figures 4.3.4 and 4.3.4a are the contours one would measure if it were possible to vary the Compton line integral while maintaining the photoelectric + Rayleigh line integral fixed. Hence, it is seen in Figures 4.3.3 and 4.3.4 that a measurement of the x-ray transmission on an unknown target with the tantalum-filtered and iron-filtered spectra corresponds to a point

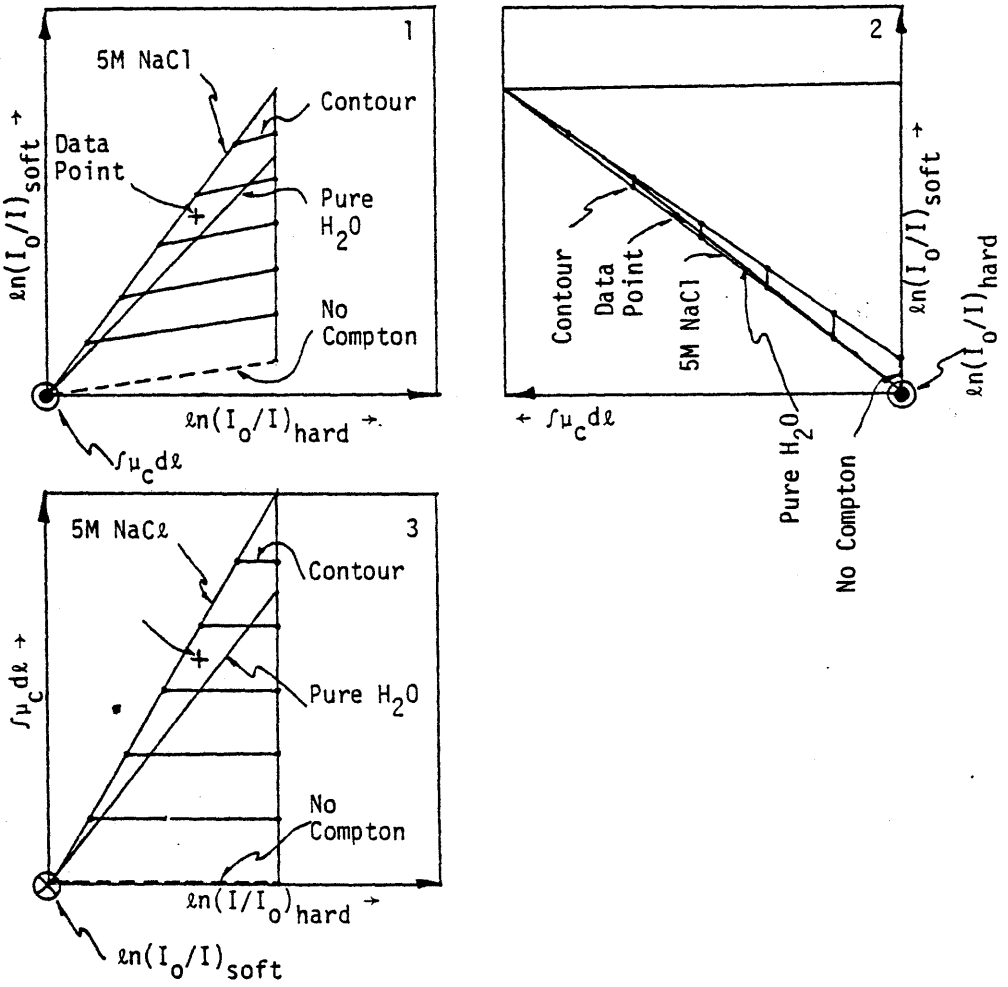

KEY:

NaCℓ	Calibration curve for a 5M NaCℓ solution (larger Compton cross section)
Pure H_2O	Calibration curve for a pure water solution (smaller Compton cross section)
No Compton	Calibration curve for a hypothetical water-like solution with the Compton cross section equal to zero
Contour	Constant Compton cross section contour line integral
Data Point	Representative data point measured in a scan. The cross represents the error bars for a hypothetical measurement. Note that the error bars in plot 1 appear differently when seen in plot 2 and plot 3

Figure 4.3.3 Orthogonal Projection Drawings of the Compton Contour Plot

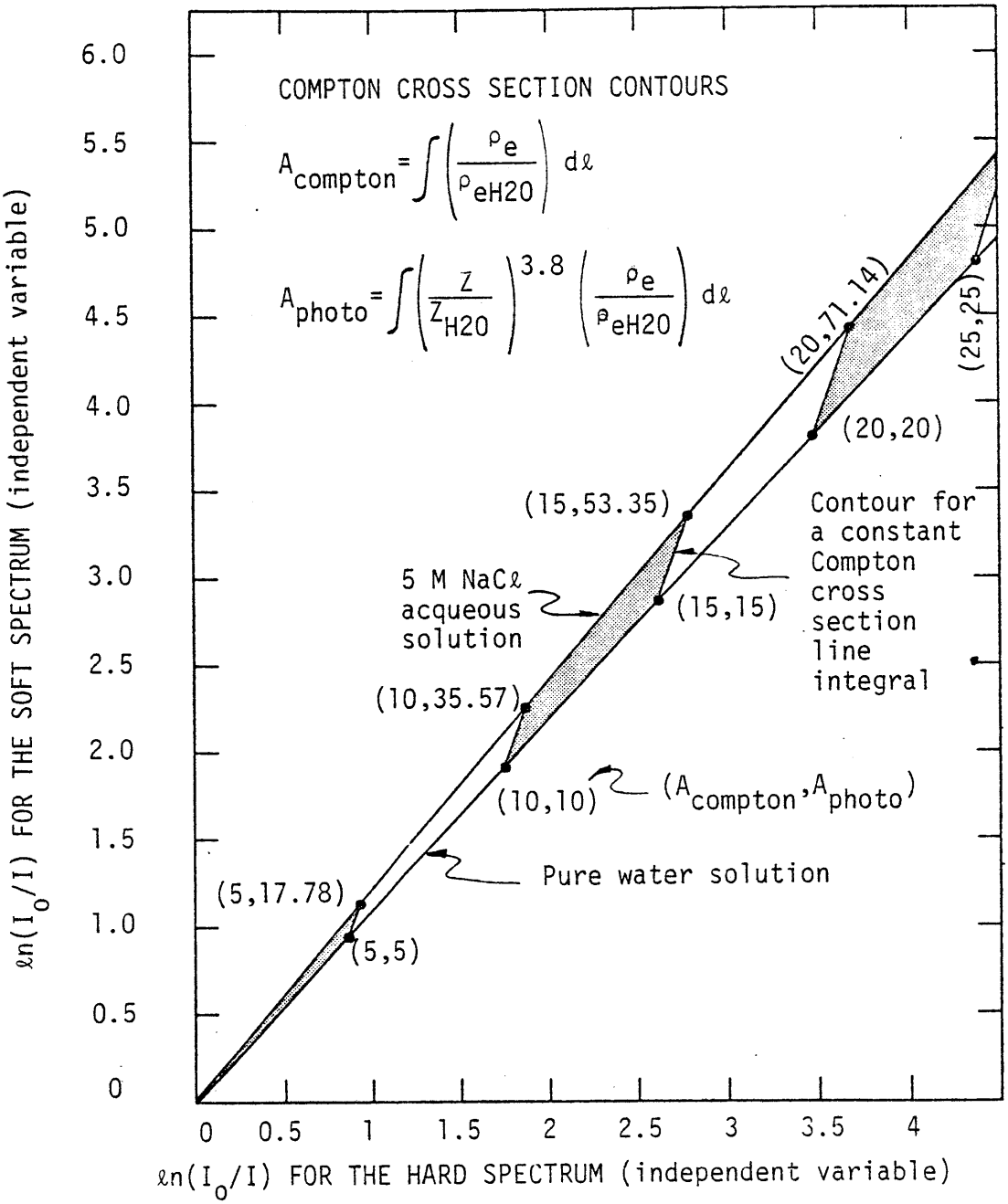

Figure 4.3.3a Detailed plot of the Compton attenuation coefficient contours.

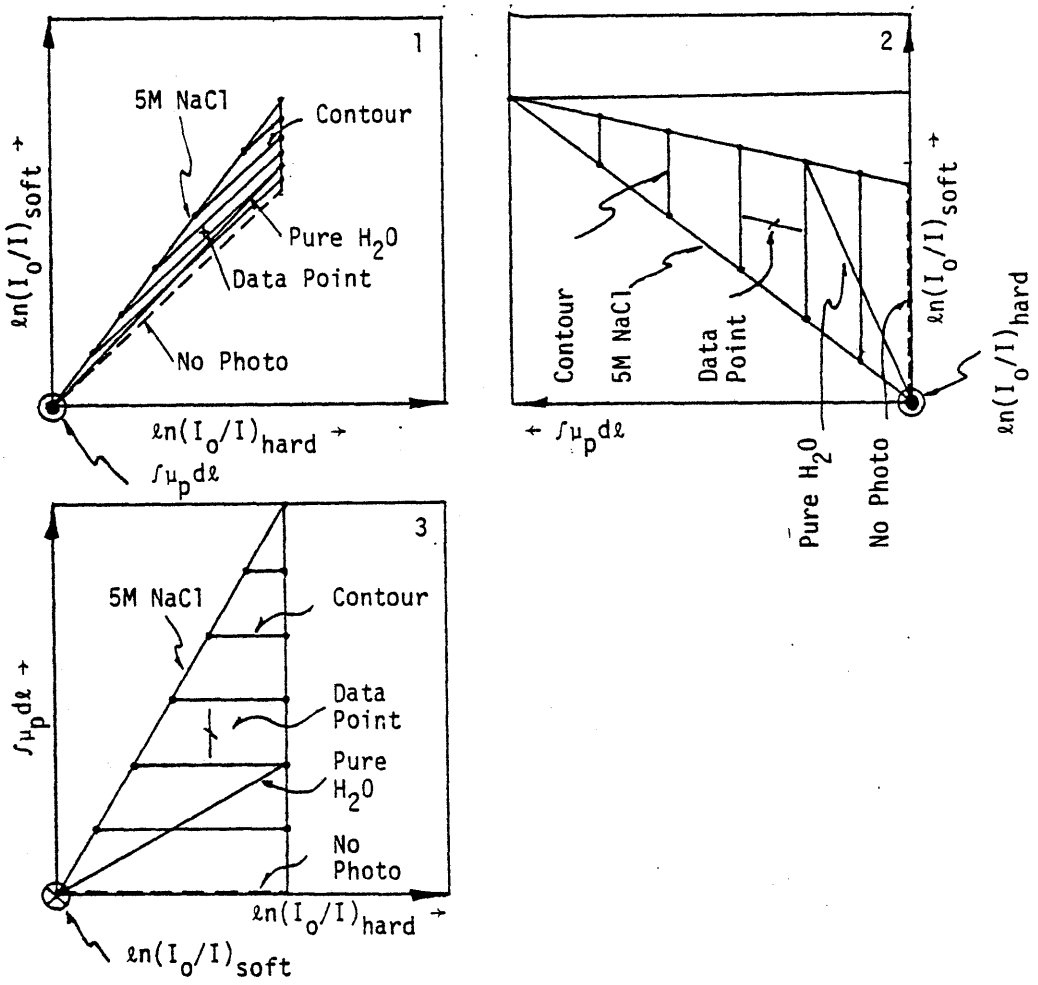

KEY:

5M NaCl	Calibration curve for a 5M Nacℓ solution (large photoelectric cross section)
Pure H_2O	Calibration curve for a pure water solution (small photoelectric cross section)
No Photo	Calibration curve for a hypothetical water-like solution with the photoelectric cross section equal to zero
Contour	Constant photoelectric cross section contour line integral
Data Point	Representative data point measured in a scan. The cross represents the error bars for a hypothetical measurement. Note that the error bars in plot 1 appear differently when seen in plot 2 and plot 3

Figure 4.3.4 Orthogonal projection drawings of the photoelectric contour plot

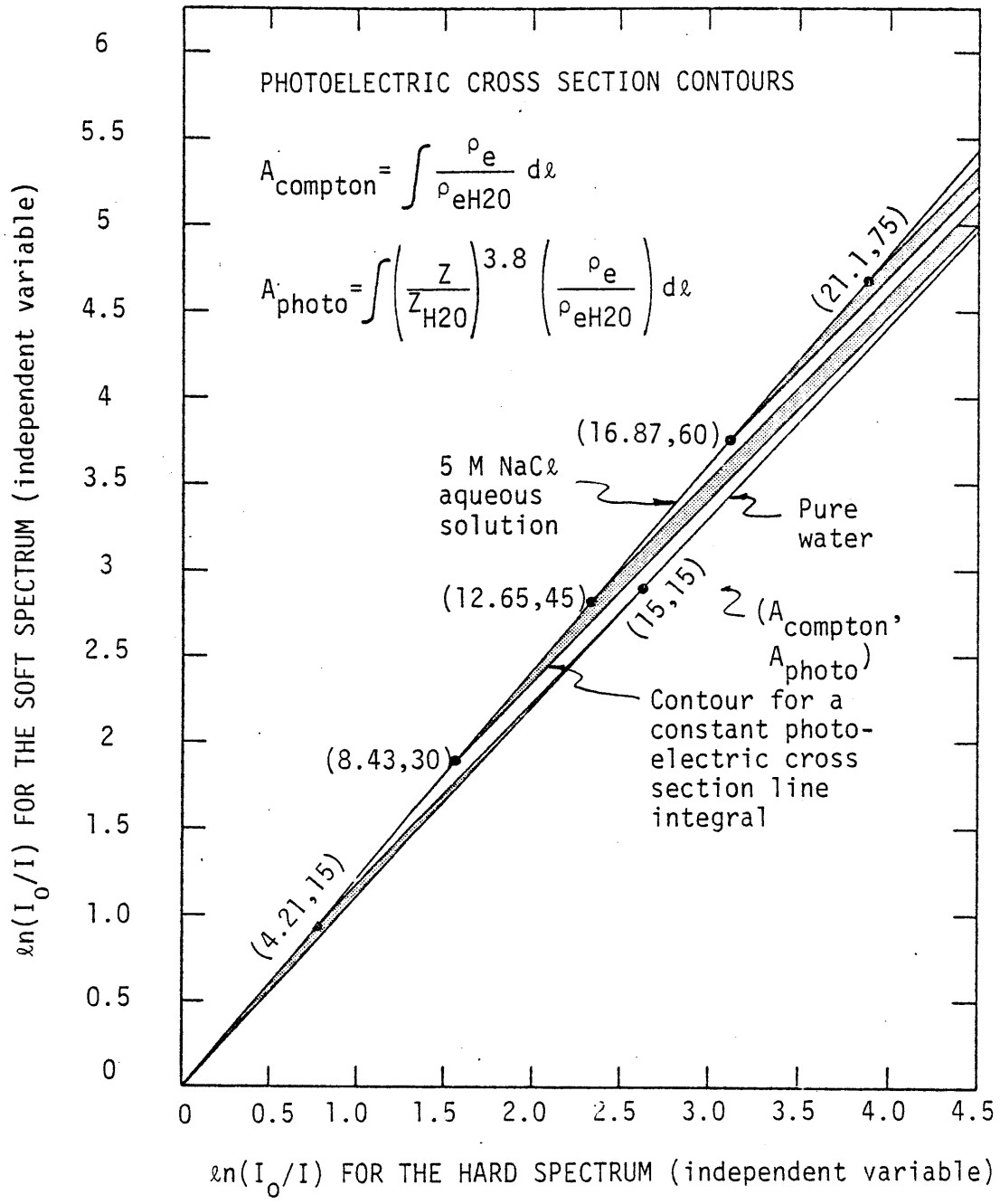

Figure 4.3.4a Detailed plot of the photoelectric + Rayleigh attenuation coefficient contours.

in the Compton line integral space and a point in the photoelectric + Rayleigh line integral space. These points then correspond to a value of $\int \mu_{CR} d\ell$ and a value of $\int \mu_{PR} d\ell$ as indicated by the figures.

It should be noted that in general there are statistical uncertainties in the transmission measurement process. These errors are schematically represented by the error bars in Figures 4.3.3 and 4.3.4. Note that since the contours are much closer in the photoelectric + Rayleigh calibration surface than in the Compton calibration surface, the fractional error of the line integral determination is greater for the photoelectric + Rayleigh case than for the Compton line integral case.

Experimental measurements of the 5.051 M NaCl solution contour and of the pure water contour are presented in Figure 4.3.5. It is seen that the actual range of $((\ell n I_{1o}/I_1)_{soft}, \ell n(I_{2o}/I_2)_{hard})$ is much narrower than that indicated schematically. Hence, statistical uncertainty in the measured values of transmission of the tantalum-filtered and iron-filtered spectra is a crucial limitation to the tomochemistry method. Furthermore, any small systematic errors in either the calibration measurement process or the transmission measurement process will cause the resultant reconstructions to have artifacts.

The results of the calibration of the central detector (#129) is typical of calibrations of the rest of the ionization chamber detectors. After elimination of the outliers (as best as possible using statistically acceptable methods) by the outlier data point removal program there were 178 valid calibration data points for the detector. Upon

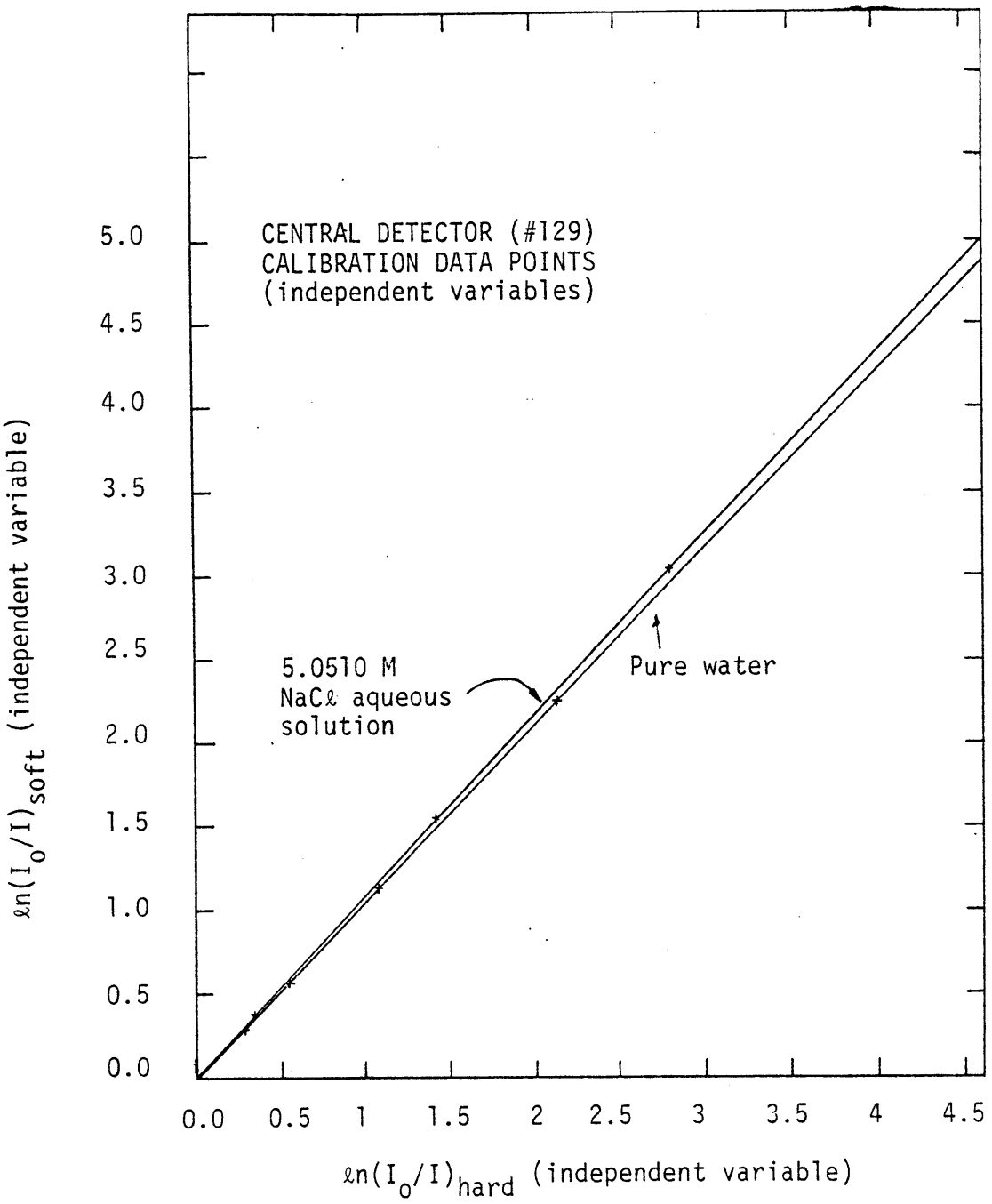

Figure 4.3.5 Experimental measurements of the 5.051 M NaCℓ solution contour and of the pure water contour.

performing the least squares polynomial regression analysis on the calibration data points the resultant fits were given by the expression:

Compton line integral fit:

$$\begin{aligned}\int \mu_{CR} d\ell = & -2.09558\ \ell n(I_{1o}/I_1) + 3.12915\ \ell n(I_{2o}/I_2) \\ & -15.28631\ (\ell n(I_{1o}/I_1))^2 - 17.37527\ (\ell n(I_{2o}/I_2))^2 \\ & +2.61161\ (\ell n(I_{1o}/I_1)\ell n(I_{2o}/I_2)) \\ & -0.01397\ (\ell n(I_{1o}/I_1))^3 + 0.01170\ (\ell n(I_{2o}/I_2))^3 \end{aligned} \tag{4.3.1}$$

and

photoelectric + Rayleigh line integral fit:

$$\begin{aligned}\int \mu_{PR} d\ell = & \ \ 3.13918\ \ell n(I_{1o}/I_1) - 3.15042\ \ell n(I_{2o}/I_2) \\ & +10.02557\ (\ell n(I_{1o}/I_1))^2 + 10.89892\ (\ell n(I_{2o}/I_2))^2 \\ & -20.92746\ (\ell n(I_{1o}/I_1)\ell n(I_{2o}/I_2)) \\ & -0.01038\ (\ell n(I_{1o}/I_1))^3 + 0.02168\ (\ell n(I_{2o}/I_2))^3 \end{aligned} \tag{4.3.2}$$

where

$\ell n(I_{1o}/I_1)$ corresponds to the tantalum-filtered spectrum transmission measurement and $\ell n(I_{2o}/I_2)$ corresponds to the iron-filtered spectrum transmission measurement.

The accuracy of the Compton line integral fit to the calibration data was good to 1.52% while the accuracy of the photoelectric + Rayleigh line integral fit was good to 5.65%.

Figure 4.3.6 presents a plot of a sample of measured and estimated values of the Compton and photoelectric + Rayleigh line integrals. It is seen here and it was found in general that the measured and estimated values were in good agreement at small ($\int \mu_{CR}\ d\ell$, $\int \mu_{PR} d\ell$) but that at large

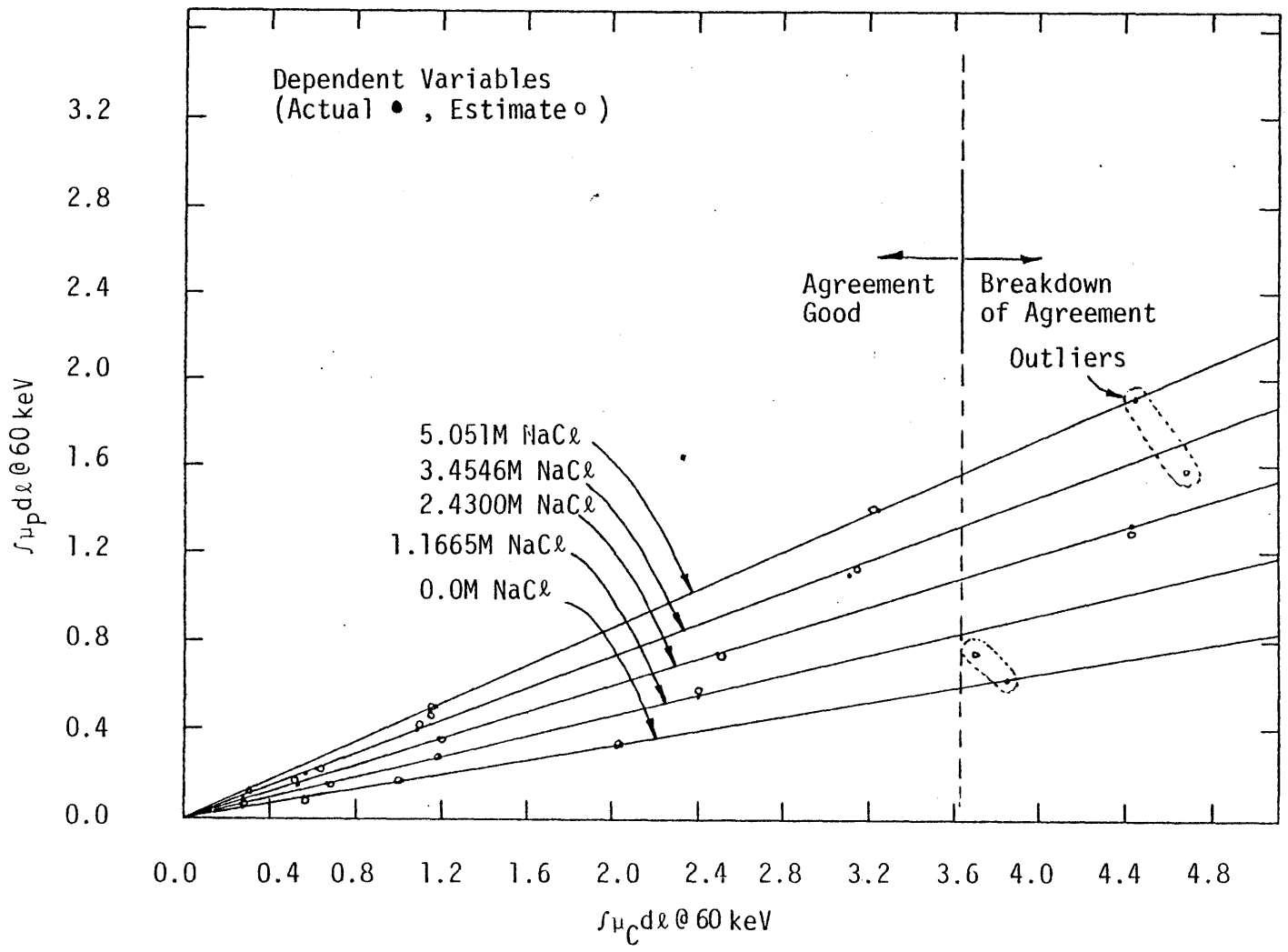

Figure 4.3.6 Plot of the measured values of the dependent variables and values of the dependent variables estimated from the polynomial fit functions.

($\int \mu_{CR}\, d\ell$, $\int \mu_{PR}\, d\ell$) there was poor agreement. It has not yet been determined as to why the estimates systematically break down. One plausible explanation is that the calibration data may be 'overfitted' by Eqs. (4.3.1) and (4.3.2). Thus, it would be expected that these expressions would break down near the 'edge' of the calibration data set. Another possible explanation for the breakdown of the fits is that most of the calibration measurements were performed at small thicknesses (small $\int \mu_{CR}\, d\ell$, $\int \mu_{PR}\, d\ell$). Hence, since the polynomial fitting was unweighted the least squares calculation would implicitly tend to overweight the small line integral measurements. These hypotheses require further study.

The implications of the breakdown of the polynomial fits is that one would expect that in the reconstructions the estimate of the attenuation coefficient in the center of the scanned target will be in error. Furthermore, depending upon the detector to detector polynomial fit variations, it would be expected that the reconstruction will contain ring and streak artifacts.

4.4 Results of the Proof-of-principle Experiment

To test out the performance of the integrated system a series of scans and reconstructions were performed on phantoms with known compositions and geometries. All scans were performed at 100 kVp and 30 mA on a 1 cm thick slice of the phantom. The phantoms were all axially symmetric so that partial volume effects in the axial direction would be minimized.

Reconstructions of Uniform Phantoms

The first series of phantoms scanned consisted of 0.125" walled lucite cylinders 15.14 cm in diameter which contained a range of saline solutions. The molar concentrations of these saline solutions was the same as those solutions used in the calibration experiment. These phantoms were used to perform a self-consistency check of both the measurement and the reconstruction process with the calibration process. In this way a study of the systematic errors encountered in tomochemistry scanning could be performed. Clearly, the system must be able to faithfully reconstruct the calibration solutions before it can be used to perform quantitative tomochemistry on unknown substances.

Reconstructions of these saline solution phantoms are shown in Figure 4.4.1 and the profiles of the reconstructed values across the diameter of the phantoms are shown in Figure 4.4.2. Note that in Figure 4.4.1 all Compton reconstructions are displayed with the grey scale extending from -999 to 3000. Similarly, all photoelectric + Rayleigh reconstructions are displayed with the grey scale extending from -999 to 2000. Furthermore, it should be noted that the grey

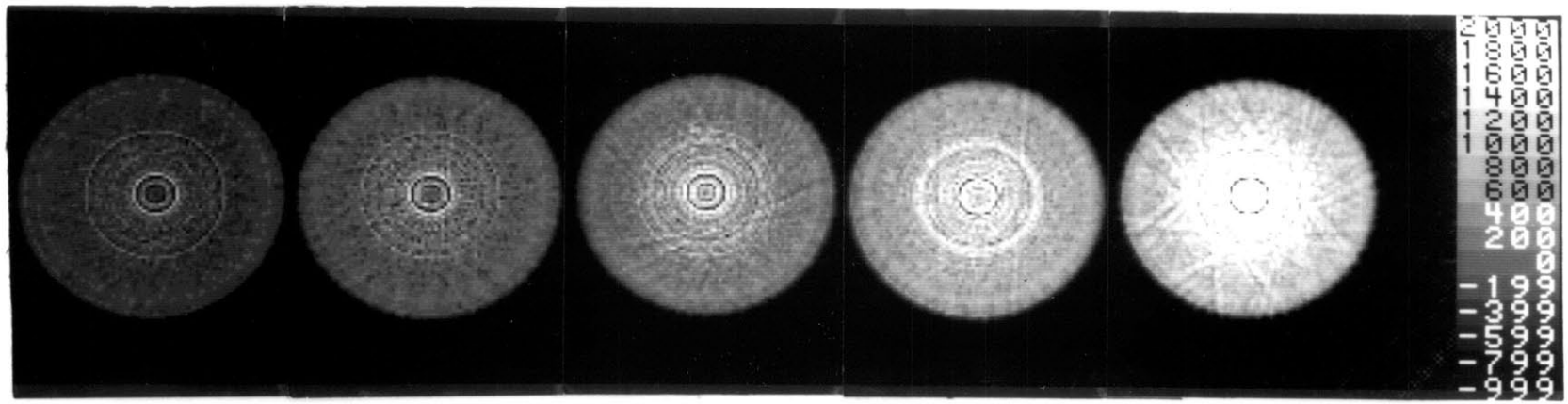

0.0M NaCl 1.1665M NaCl 2.4300M NaCl 3.4546M NaCl 5.0510M NaCl ::: Photoelectric + Rayleigh Reconstructions

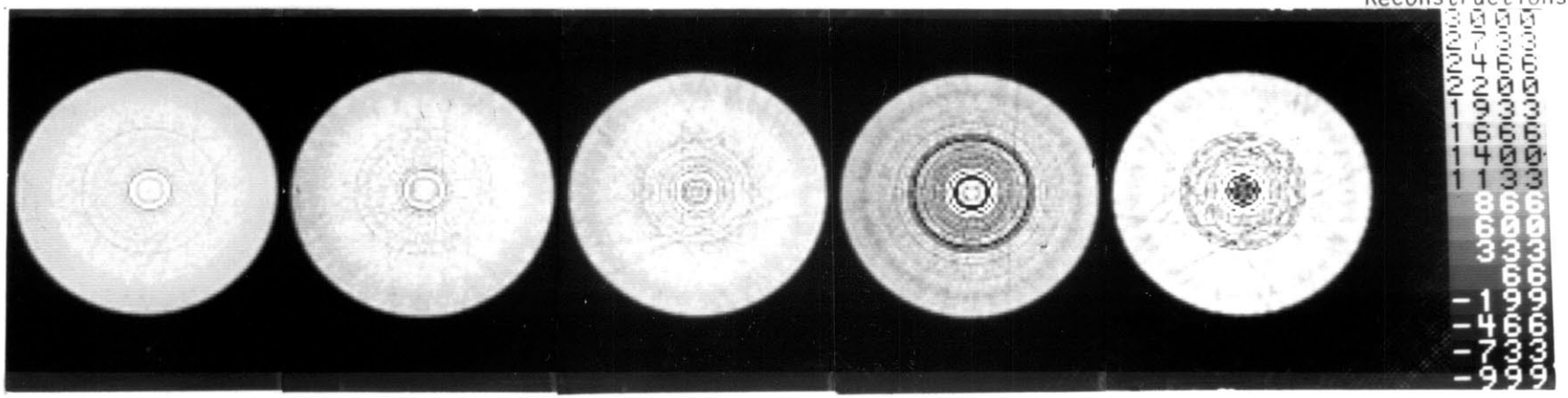

0.0M NaCl 1.1665M NaCl 2.4300M NaCl 3.4546M NaCl 5.0510M NaCl ::::: Compton Reconstructions

Figure 4.4.1 Reconstructions of the saline solution phantoms

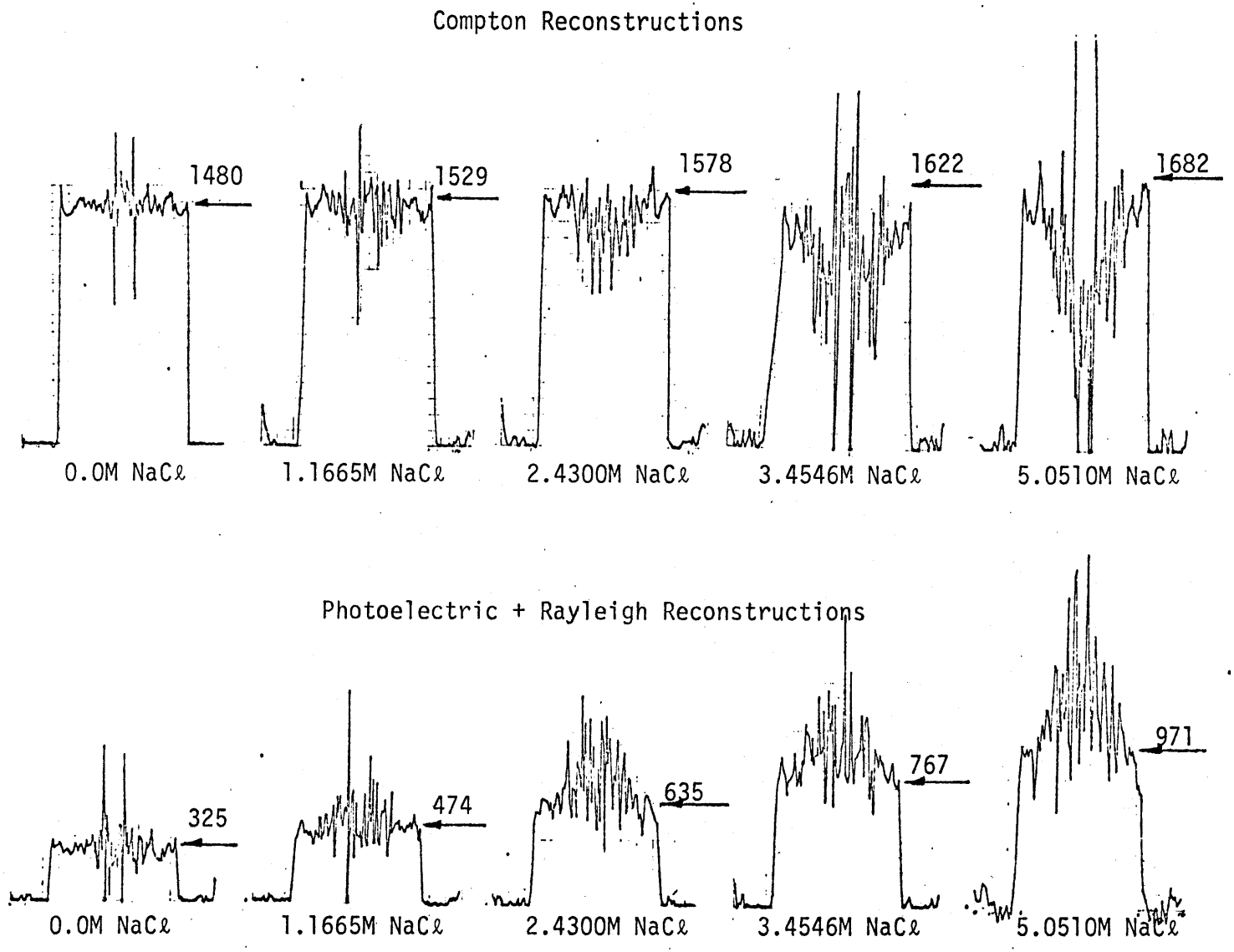

Figure 4.4.2 Profiles of the reconstructed values along the vertical diameter of the image.

scale numbers are shifted by 1000 from the actual reconstructed numbers; ie. -1000 in the grey scale corresponds to a reconstructed number of 0; 2000 in the grey scale corresponds to a reconstructed number of 3000; and so forth. The reconstructed numbers are at the moment only valid for relative comparisons of reconstructions. The reconstructed numbers are porportional to the attenuation coefficient reconstructed within each picture element. With the improvement of the tomochemistry methodology the proportionality constant could be determined exactly if the resultant reconstructions were artifact free and systematic-error free.

Several trends and characteristics of the reconstructions can be determined from Figures 4.4.1 and 4.4.2. In general it is seen that the reconstructed Compton attenuation coefficients are relatively constant as the saline solution molar concentration increases and that the reconstructed photoelectric + Rayleigh attenuation coefficients increase with increasing molar concentration. It is possible to compare the reconstructed attenuation coefficients to the known attenuation coefficients by using one reconstruction as a reference and then comparing the other reconstructions to this reference. For this purpose the pure water reconstructions were used as the reference reconstructions. Indicated in Figure 4.4.2 are the reconstructed profiles of the attenuation coefficients. It is seen that the estimates of the attenuation coefficients is most correct near the edge of the reconstruction while the accuracy of the reconstructed attenuation coefficient breaks down near the center of the reconstruction. The reconstructions are more accurate near the edge of the cylinder than in the center because

transmission measurements near the edge are generally through smaller thicknesses of solution than through the center of the cylinder. Hence, since it is known that the polynomial fits of the calibration data are more accurate when the values of the transmission line integrals are small, one would expect the reconstructions to be more accurate near the edge.

Another trend of the reconstructions is that the number of artifacts and the error of the reconstructions increases as the saline concentration increases. It is seen that the water photoelectric + Rayleigh and Compton reconstructions are relatively flat. However, as the saline concentration increases the Compton attenuation coefficient is increasingly underestimated in the center of the image while the photoelectric + Rayleigh attenuation coefficient is increasingly overestimated in the center of the image. The general cupping and bowing of the reconstruction profiles is due once again to the inaccuracy of the polynomial fits at large values of the solution thickness. It is seen here that this error becomes worse as the photoelectric + Rayleigh attenuation coefficient of the scanned phantom increases.

To investigate more closely the errors encountered in the reconstructions, the pure water and 5.051 M NaCl reconstructions are displayed with a narrower display window in Figure 4.4.3 and a more detailed plot of the profiles are given in Figures 4.4.4, 4.4.5, 4.4.6, 4.4.7. In the images one can clearly see that the pure water reconstructions are much more uniform than the 5.051 M NaCl reconstructions. Furthermore, although oscillations are present in all of the profiles, they are less prominent in the pure water reconstructions

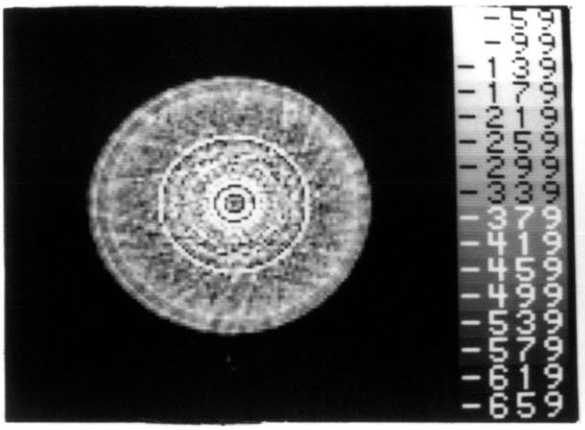

0.0M NaCl Photoelectric + Rayleigh reconstruction

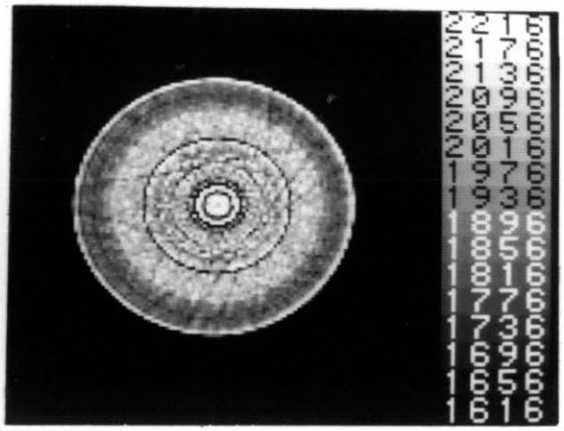

0.0M NaCl Compton reconstruction

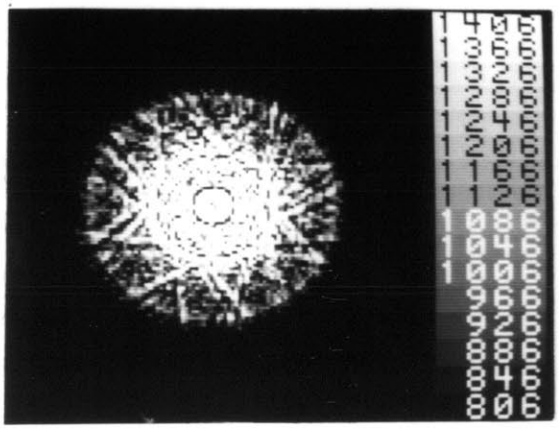

5.0510M NaCl Photoelectric + Rayleigh reconstruction

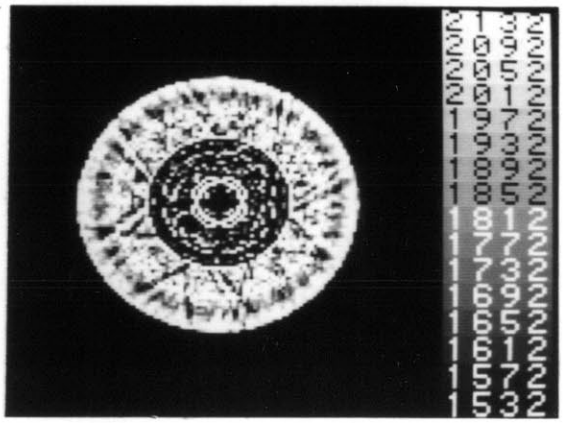

5.0510M NaCl Compton reconstruction

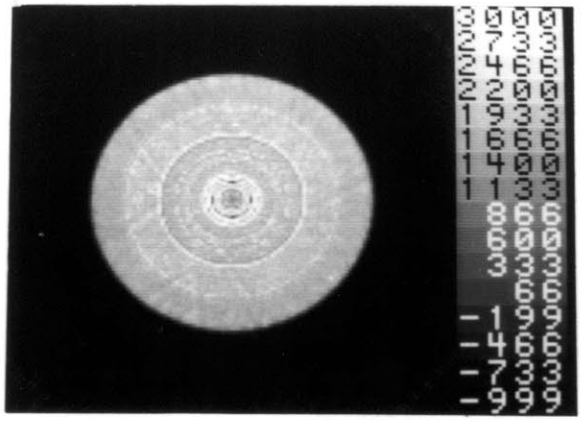

Summation of the reconstructions of the Compton and photoelectric + Rayleigh attenuation coefficients for the 5.0510M NaCl solution.

Figure 4.4.3 Display of the 0.0M NaCl and 5.0510M NaCl saline solution reconstructions at a smaller display window.

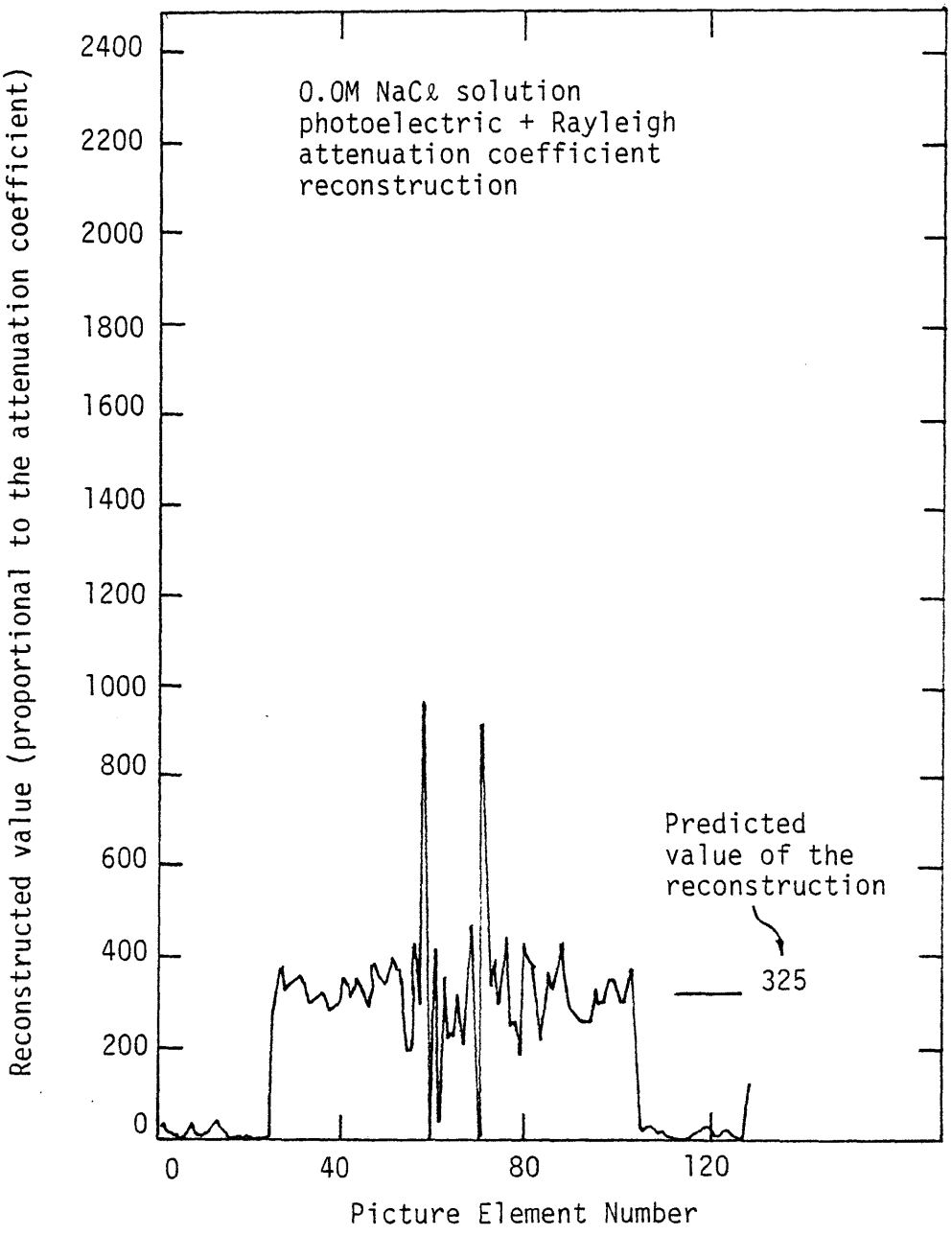

Figure 4.4.4 Detailed plot of the photoelectric + Rayleigh attenuation coefficient reconstruction of the pure water solution.

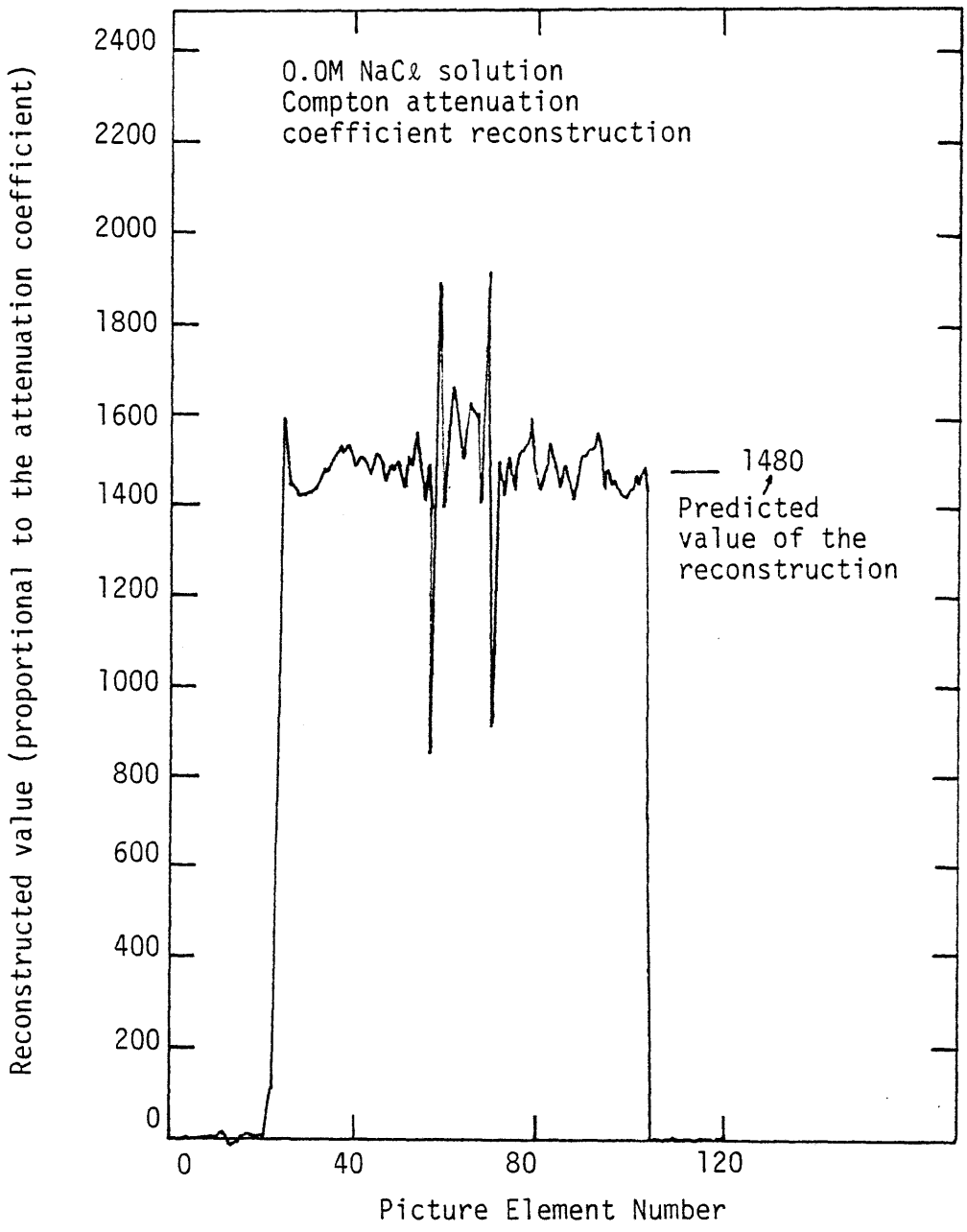

Figure 4.4.5 Detailed plot of the Compton attenuation coefficient reconstruction of the pure water solution.

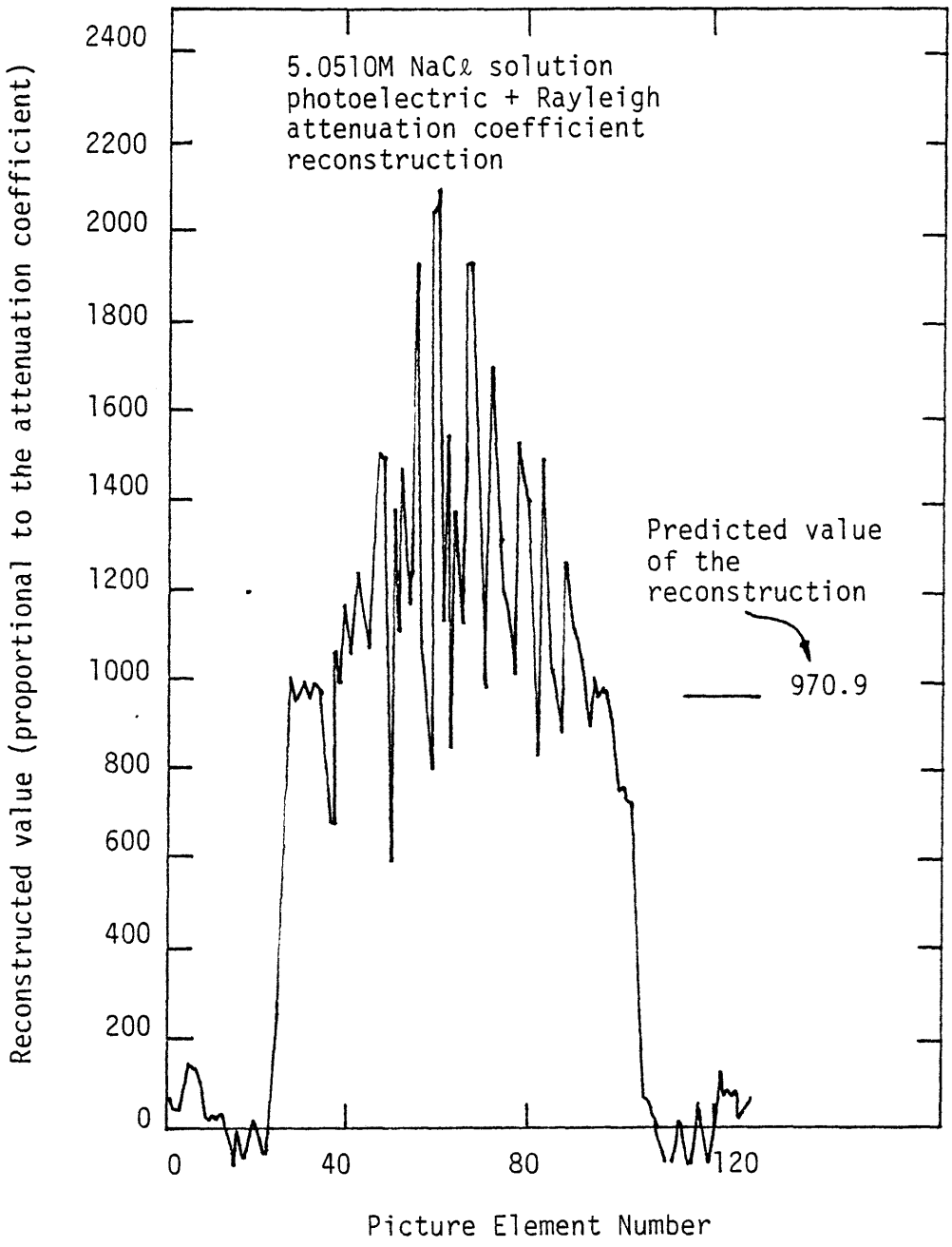

Figure 4.4.6 Detailed plot of the photoelectric + Rayleigh attenuation coefficient reconstruction of the 5.0510M NaCℓ solution.

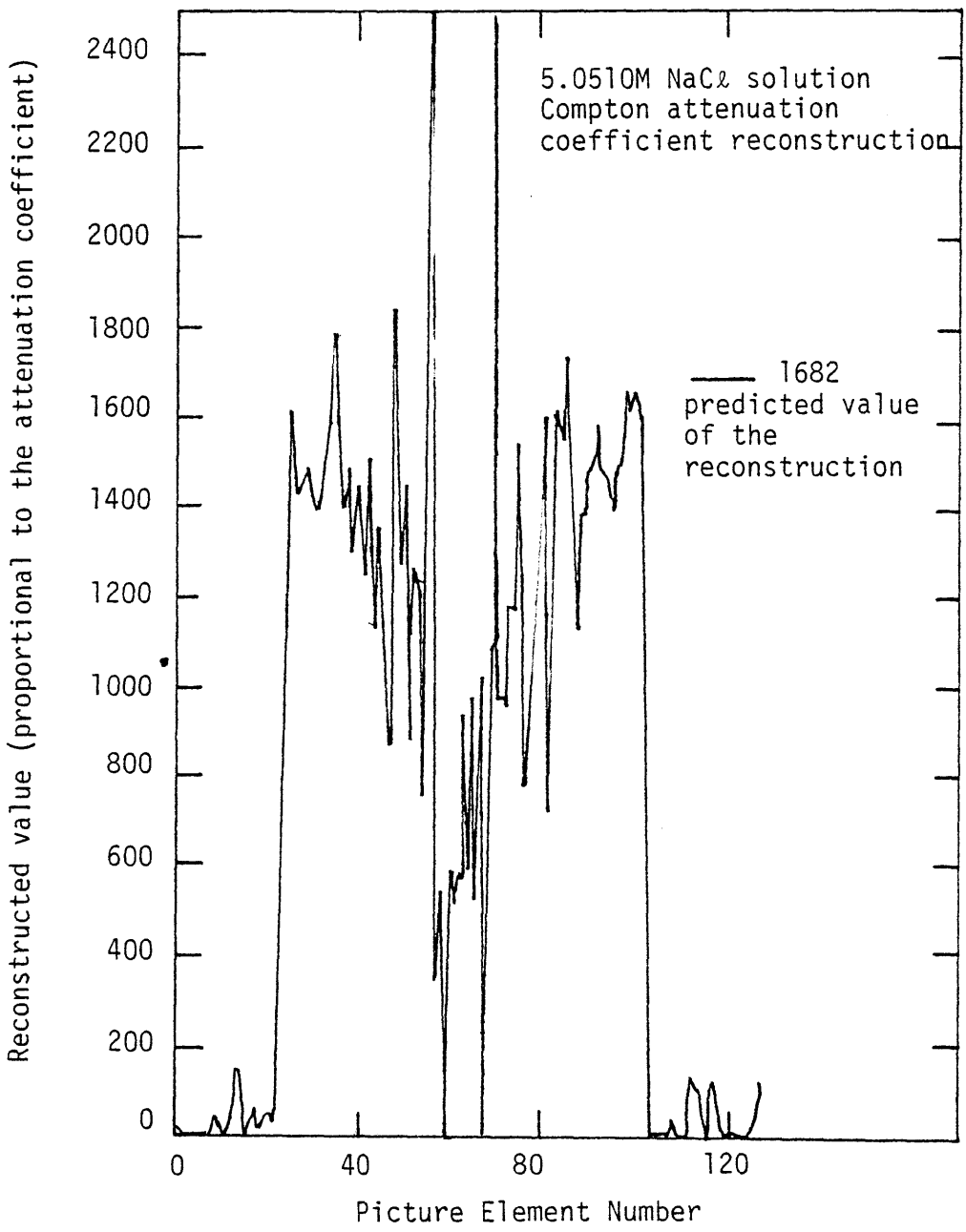

Figure 4.4.7 Detailed plot of the Compton attenuation coefficient reconstruction of the 5.0510M NaCℓ solution.

than in the 5.051 M NaCl reconstructions.

There are two major types of artifacts present in the images: ring artifacts and streak artifacts. Both the ring and streak artifacts are worse in the 5.051 M NaCl reconstructions than in the pure water reconstructions. The ring artifacts are due to detector variations in the tomochemistry calibration polynomial fit. Hence, it is seen that the detector-to-detector variations become more noticeable as the photoelectric + Rayleigh attenuation coefficients of the phantom increases. One other possible contributing factor to the rings within the image is that the images may have been undersampled, ie. too few view were taken in the scan. In hindsight it is felt by the author that due to the fact that so many interpolations have been performed to obtain these images that it may have been wiser to double the number of views in a scan. More exactly, 600 views should have been performed rather than the 300 views measured in these scans. If the transmission measurements are undersampled the Gibbs phenomenon and aliasing are known to occur. Increasing the number of views in a scan would help to alleviate this problem.

The streak artifacts present in the images are due to discharges within the ionization chambers. Discharges are relatively random events so that the measurement error is sporatic throughout the scan. It is seen in Figure 4.4.1 that streak artifacts are present in both the pure water and the 5.051 M NaCl solution reconstructions. However, since the polynomial fits perform more poorly for the 5.051 M NaCl solution than for the pure water solution, reconstructions of the former are more susceptible to streak artifacts.

One final point about the errors in these reconstructions is that the systematic errors are nearly equal and opposite for the photoelectric + Rayleigh reconstructions and the Compton reconstructions. To show that this is true, an image of the summation of the reconstructed Compton and photoelectric + Rayleigh attenuation coefficients for the 5.051 M NaCl solution is presented in Figure 4.4.3. The resultant image is remarkably uniform. This result substantiates the hypothesis that the transmission measurements themselves were good and that the error in the reconstructions is due to errors in the polynomial fitting process. Clearly, more work must be done on the calibration and polynomial fitting processes used in tomochemistry.

Determination of the Spacial Resolution

The next characteristic of tomochemistry that was investigated was the spacial resolution of the method. Figure 4.4.8 shows a sketch of the phantom used to estimate the spatial resolution. This phantom consisted of a lucite cylinder which contained decreasingly smaller air holes. The hole diameters were 2.54 cm, 1.91 cm, 1.27 cm, 9.525 mm, 6.35 mm, and 3.175 mm. The Compton and photoelectric + Rayleigh reconstructions of this phantom are presented in Figure 4.4.9. It is seen from the figure that the spatial resolution is not perfectly determinable because of the presence of streak and ring artifacts within the reconstructions. However, in spite of these difficulties it still can be determined from the image that the 5 mm holes can be seen within the image but that the 2.5 mm holes cannot be seen. Therefore, with the present noise level the spacial resolution is estimated to be about 4 mm as compared to the 2 mm resolution of normal

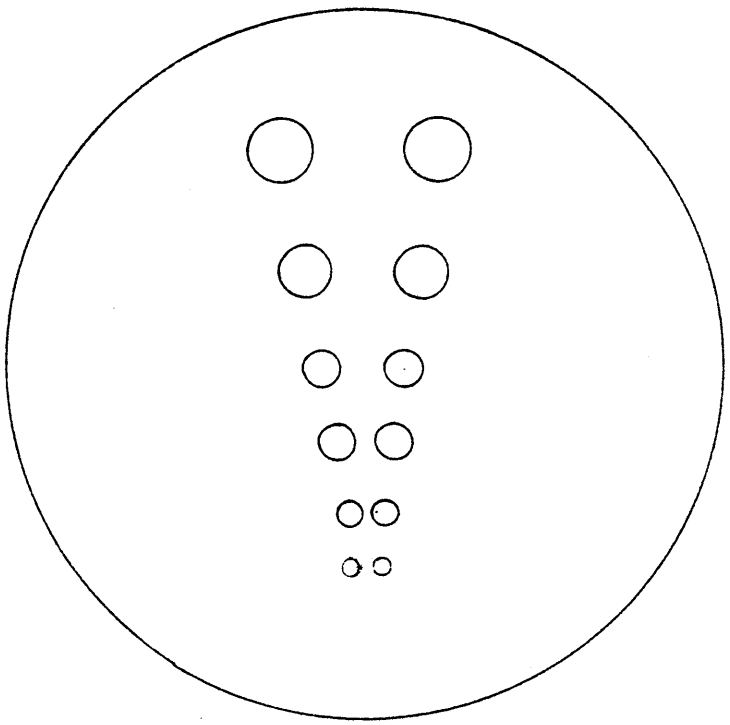

20 cm diameter lucite cylinder with air holes

Figure 4.4.8 Sketch of the internal structure of the lucite resolution phantom.

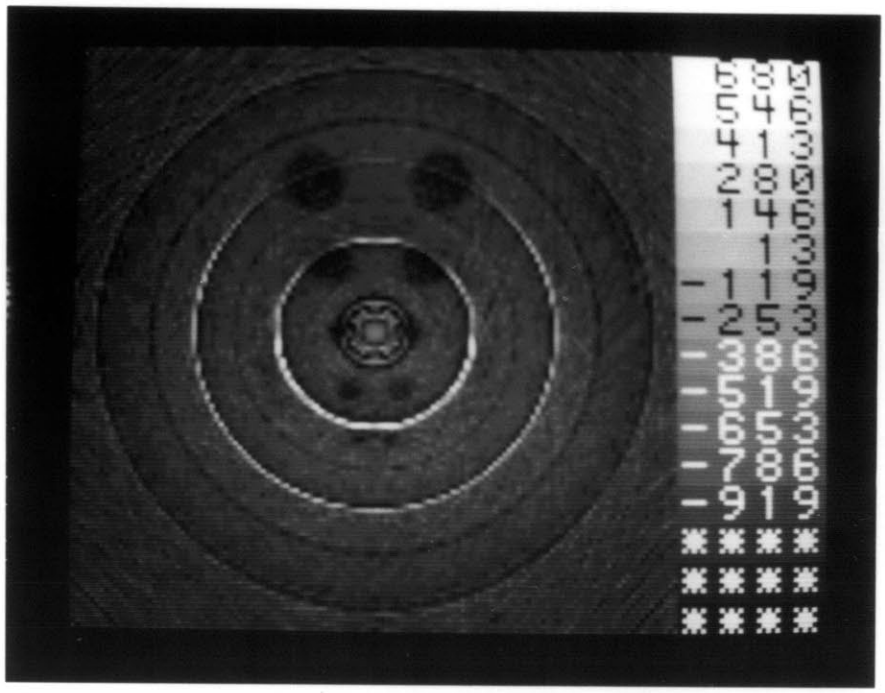

Compton attenuation coefficient reconstruction

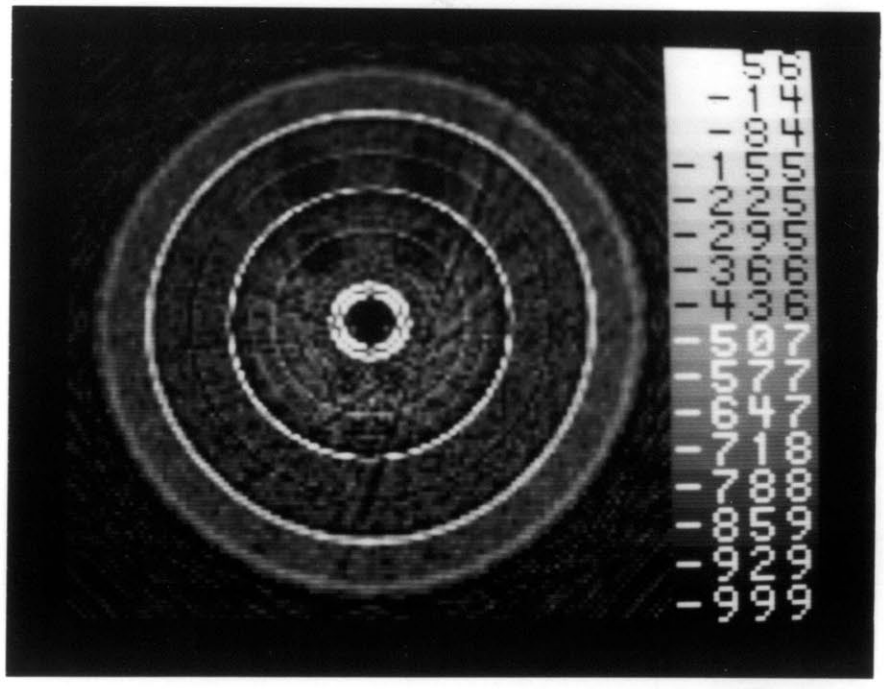

Photoelectric + Rayleigh attenuation coefficient reconstruction

Figure 4.4.9 Reconstructions of the spatial resolution phantom.

CT scanning with this scanner.

Intuitively, one would expect a poorer resolution when performing tomochemistry than with normal CT because of the interpolations performed in this method. In this particular scanner though it is believed by the author that the spacial resolution could have been made comparable to normal CT by doubling the angular sampling rate as mentioned previously.

A more rigorous approach could have been taken in the determination of the spatial resolution. In particular, Judy (J.4) and others (G.6) have determined rigorous methods of determining the modulation transfer function (MTF) and the line spread function (LSF) of CT scan images. These approaches were not taken here due to the present difficulties of noise and systematic error within the images.

Reconstructions of Nonuniform Phantoms

Scans and reconstructions of other phantoms were performed to glean how well the tomochemistry method performs when the phantom is geometrically nonuniform. Sketches of the internals of two of the scanned phantoms, a low contrast phantom and a high contrast phantom, are presented in Figure 4.4.10. The reconstructions of the low contrast phantom, presented in Figure 4.4.11, show that most of the detail within the image has been lost due to the streak artifacts within the image. It should be noted that most of the streaks appear to be caused by one detector. If the reconstruction would have been performed by removing the data of this detector from the reconstruction data set it may have been possible to perceive more detail within the images. Clearly, it is important that one remove all the data of those detectors

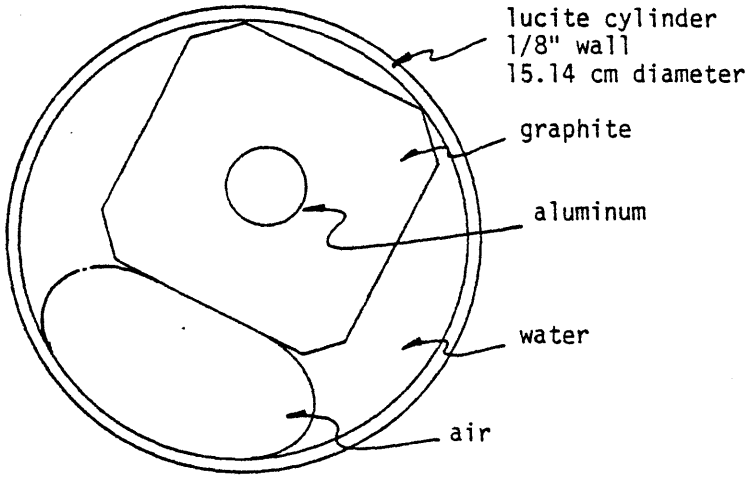

INTERNALS OF THE HIGH CONTRAST PHANTOM

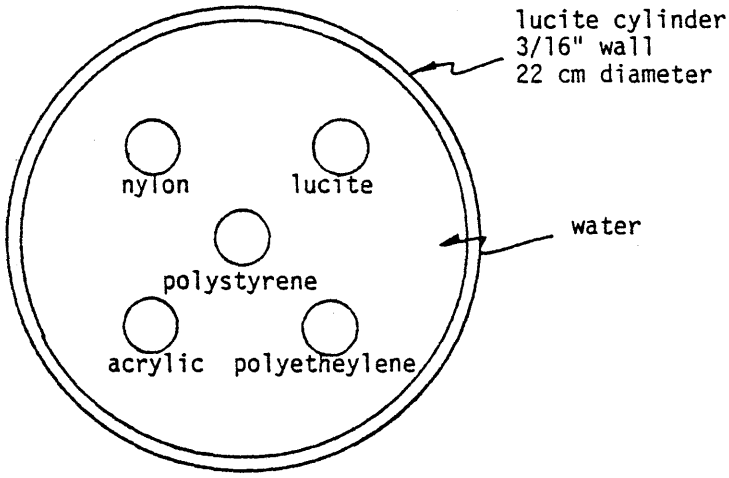

INTERNALS OF THE LOW CONTRAST PHANTOM

Figure 4.4.10 Internals of the low and high contrast phantoms.

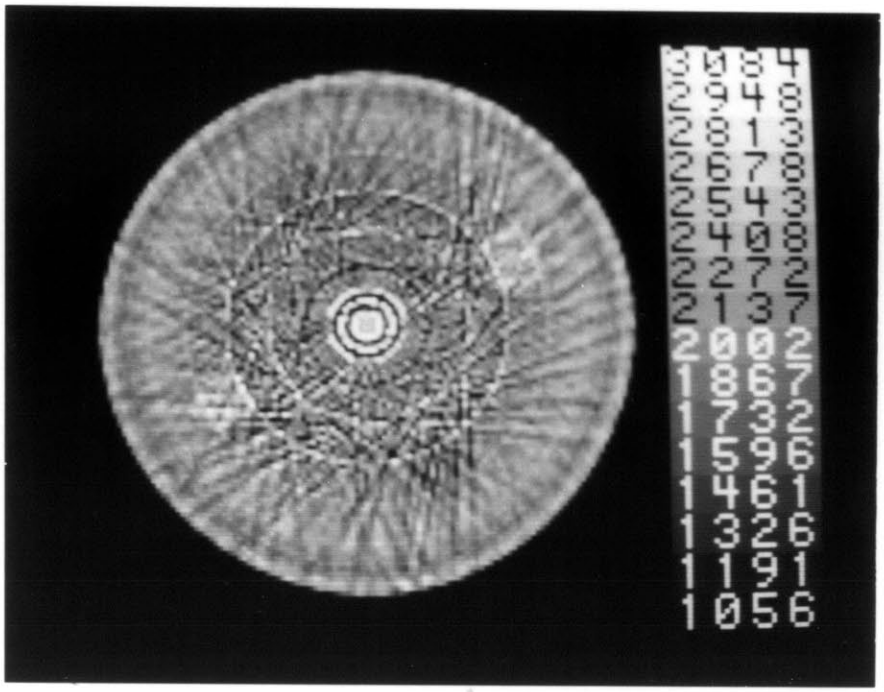

Compton attenuation coefficient reconstruction

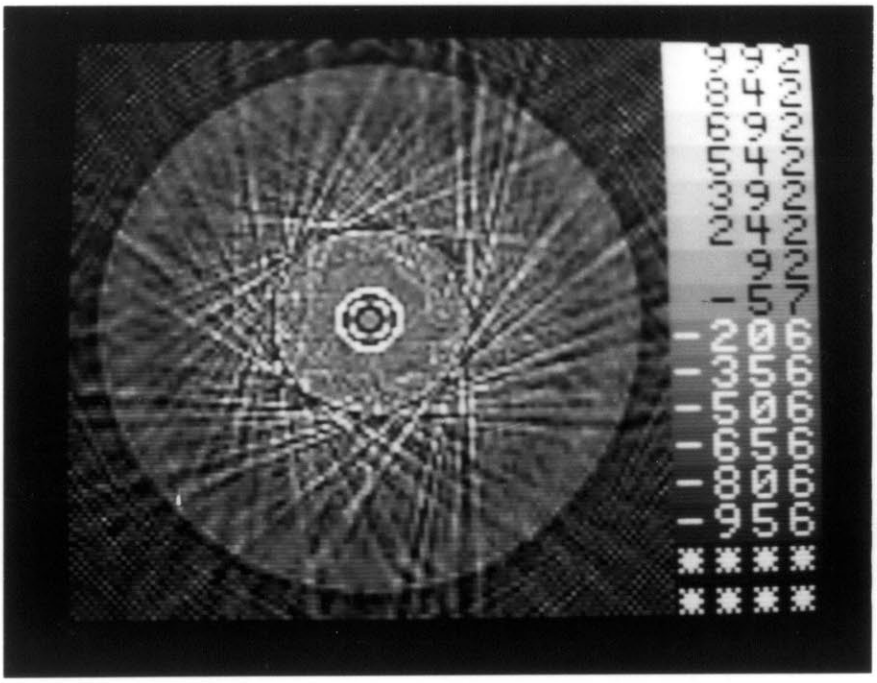

Photoelectric + Rayleigh attenuation coefficient reconstruction

Figure 4.4.11 Reconstructions of the low contrast phantom.

which are known to yield bad data from the basic data set which is going to be reconstructed. These bad data points add no information to the image. On the contrary these bad data points ruin the resultant reconstruction.

The reconstructions of the high contrast phantom are shown in Figure 4.4.12. The phantom consists of a graphite block, an aluminum rod, and an air hole surrounded by pure water. One striking detail to be noted from the reconstructions is that while the graphite block is the most prominent feature within the Compton reconstruction it is not even visible within the photoelectric + Rayleigh reconstruction. This is due to the fact that the electron density of graphite is about 45% greater than water while the photoelectric + Rayleigh cross section is about 14% less than water. Hence, in spite of the systematic errors mentioned previously, the tomochemistry method developed in this research project is seen to be able to distinguish between material properties that normal CT can not distinguish.

One other feature to note from the reconstructions are the streaks emanating from the aluminum rod. In this case the streaks are not caused by bad data from a single detector. Rather, these streaks are due once again to the inaccurate fitting of the detector calibration data for large line integral values. In this case the aluminum rod serves to put the measured line integrals beyond the valid range of the polynomial fits. It is seen in the figure that the reconstructed value of the aluminum photoelectric + Rayleigh attenuation coefficient is overestimated while the reconstructed value of the Compton attenuation coefficient is drastically underestimated. This result is consistent

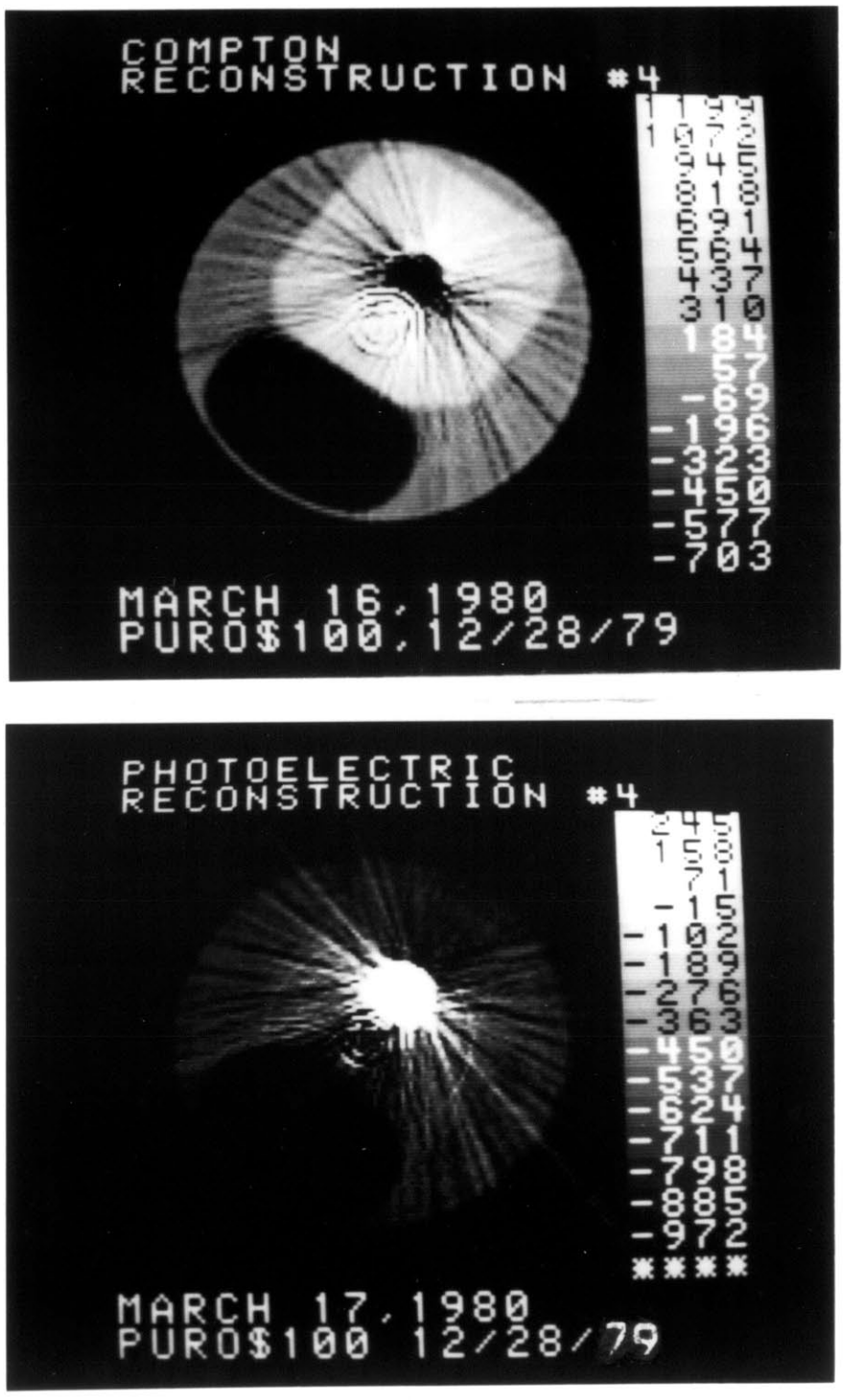

Figure 4.4.12 Reconstructions of the high contrast phantom.

with the results of the reconstructions of the uniform phantoms mentioned previously.

Determination of the Absolute Statistical Uncertainty of Tomochemistry Reconstructions

Due to the high degree of systematic error within the above reconstructions it is impossible to determine directly from the reconstructions the absolute values of the statistical uncertainties of the photoelectric + Rayleigh and Compton attenuation coefficients. It was found that this problem could be circumvented by slightly rewriting the error expression in Eq. (4.2.1) in terms of the standard deviation of the x-ray measurement process:

$$\frac{\delta\mu_{PR}}{\mu_{PR}} \simeq \frac{\left(\frac{4}{3}\right)^{1/2} \frac{1}{X}\left[(A_{CL})^2(STDV_{TH})^2 + (A_{CH})^2(STDV_{TL})^2\right]^{1/2}}{(A_{CL}A_{PH} - A_{CH}A_{PL})\mu_{PR}} \qquad (4.4.1)$$

where

$$STDV_{TH} = \frac{\text{standard deviation of high energy photon view measurement}}{\sqrt{\text{number of views}}}$$

and

$$STDV_{TL} = \frac{\text{standard deviation of low energy photon view measurement}}{\sqrt{\text{number of views}}}$$

The standard deviation of the photon measurement process versus photon flux has been determined experimentally and the results were presented previously in Section 2.1B. The statistical uncertainty of the photoelectric + Rayleigh reconstructions can be determined from Eq. (4.4.1) because all of the terms in the equation can be measured

experimentally. Furthermore, it can be shown that by working through the derivations of Section 4.2 the statistical uncertainty of the Compton attenuation coefficient reconstructions is given by the expression:

$$\frac{\delta\mu_{CR}}{\mu_{CR}} \simeq \frac{\left(\frac{4}{3}\right)^{1/2} \frac{1}{X} \left[(A_{PH})^2 (STDV_{TL})^2 + (A_{PL})^2 (STDV_{TH})^2\right]^{1/2}}{(A_{PH}A_{CL} - A_{PL}A_{CH})\mu_{CR}} \qquad (4.4.2)$$

Equations (4.4.1) and (4.4.2) can be used to determine a theoretical limit to the statistical accuracy of the Compton and photoelectric + Rayleigh reconstructions. The statistical accuracy is seen to depend upon the accuracy of the high and low energy photon measurement processes, the pixel size, and the spectrum coefficients. Using these equations it is found that for a 20 cm diameter water-like target using a 120 kVp spectrum with the alternating iron and tantalum filtration the statistical uncertainty of the reconstructed attenuation coefficients within a 5 mm X 5 mm pixel area is about 0.198 % for the conventional image, 7.5% for the photoelectric + Rayleigh image, and 0.6% for the Compton image.

These results compare favorably with those of Drost (D.8). Drost's estimates of the statistical uncertainty were higher than those presented here. This is most likely due to the fact that the two spectra used by Drost were not optimal for tomochemistry.

5.0 Summary

The purpose of this research project was to determine experimentally and theoretically the engineering considerations and limitations encountered in the development of a CT scanner which could perform tomochemistry in a single scan. The program of research can be classified into three areas: design and construction of the tomochemistry scanner, software and data processing methods development, and proof-of-principle experimentation. This chapter summarizes the major results in each of these areas and presents suggestions for future work based on these results.

5.1 Major Methods and Models Developed, and Major Theoretical and Experimental Results and Conclusions

Computational and Experimental Photon Transport Studies of the Optimal Pair of Incident Spectra to use in Tomochemistry - Nuclear Engineering Considerations

A series of photon transport studies were performed to determine the optimal pair of photon spectra to use for tomochemistry. More specifically, the goal of the transport studies was to determine those spectra which would yield the most accurate determination of the photoelectric + Rayleigh and Compton attenuation coefficients within a 20 cm head-like target at a minimal risk to the patient. To aid in the determination of the optimal spectra pair:

(1) A one-dimensional photon transport code was developed which simulated the CT scanning and image reconstruction process. By considering Fig. 2.1B.2 it is seen that models were developed to simulate the x-ray tube, beam filtration, scanned head-like target, and detector.

(2) A theoretical model was developed to quantify the expected uncertainty of the tomochemistry photoelectric + Rayleigh and Compton attenuation coefficient measurement process. From this model it was found that three optimization parameters or figures-of-merit could be defined. These figures-of-merit, which were found to be unique to the spectra used in the tomochemical analysis, provided a great deal of insight into the determination of those pair of spectra to use for tomochemistry.

(3) A three-dimensional Monte Carlo photon transport code and analytic transport programs were developed to determine the radiation absorbed dose received from CT scanning. As seen in Fig. B.2.1 the patient dose was computed using a series of water cylinders to simulate different parts of the human anatomy. Absorbed dose was tallied in concentric annular regions both in and out of the fan x-ray beam.

Using these photon transport and theoretical models it was determined that:

(1) In tomochemistry the photoelectric + Rayleigh attenuation coefficients are more difficult to measure in biological tissue than the Compton attenuation coefficients due to the relatively small contribution of the photoelectric and Rayleigh processes to the photon attenuation process.

(2) The fundamental limit to the accuracy of the tomochemistry measurement process is dictated by Poisson counting statistics.

(3) For all the x-ray spectra studied, the maximum radiation absorbed dose to the patient is at the surface of the patient. Furthermore, since the skin is the most sensitive 'organ' in head scanning, the surface dose is the limiting dose. It was also found in the transport studies that the absorbed dose from scattered radiation accounted for a significant fraction of the total dose to the patient.

(4) Two possible design optimization conditions exist. One possible optimum design corresponds to that pair of incident spectra to use such that the statistical error is minimized for a specified patient surface dose. The other possible optimum design corresponds to that pair of incident x-ray spectra to use for a fixed x-ray tube power (photon flux). Practical considerations dictated that one should design the experiment using the second optimization condition with due consideration toward minimizing the dose.

(5) If the x-ray tube kilovoltage were to remain fixed during a scan and only changes in filtration served to change the incident spectrum, then the optimal pair of filters to use in a tomochemistry scan are iron and tantalum. This choice is based on manufacturing considerations as well as photon transport considerations. For a 20 cm head-like target the iron filtration should be 2.15 mm thick and the tantalum filtration should be 130 μm thick. As seen in Fig. 2.1C.7 the tantalum-filtered spectrum is the low energy spectrum while the iron-filtered spectrum is the high energy spectrum.

(6) A comparison was performed between the use of a 150 kVp spectrum with alternated iron and tantalum filtration and the use of a 100 kVp spectrum with alternated iron and tantalum filtration in tomochemistry. As seen in Figs. 2.1C.4 and 2.1C.5, for the same x-ray tube photon flux or for the same surface dose, a 100 kVp spectrum is better than a 150 kVp spectrum for tomochemistry.

(7) A comparison was performed between the use of a fixed kVp/modulated filtration system to the use of a simultaneously modulated x-ray tube kilovoltage and spectrum filtration system. As seen in Fig. 2.1C.6, it was found that simultaneous modulation of the peak kilovoltage and spectrum filtration using a 150 kVp/2.16 mm Fe and 100 kVp/130 μm Ta combination decreases the statistical uncertainty of the measurement by more than a factor of 2 over filtration modulation alone.

(8) The total surface dose from a single 10 second 100 kVp-30 mA iron-tantalum tomochemistry scan is about 900 mRad. As seen in Fig. 2.1C.8 this estimate will increase with higher kVp due to the larger photon flux.

An experimental verification of the above photon transport results was performed. As seen in Fig. B.2.3 the estimated in-beam dose, as determined by Monte Carlo calculations, agreed very well with the experimental measurement of the in-beam dose profile. Also, as seen in Fig. 4.2.2, the computational estimates of the statistical uncertainty of the photoelectric + Rayleigh attenuation coefficient measurement agree well with experimental measurements.

An experimental study was performed to determine the optimal x-ray tube kilovoltages to use in conjunction with the iron and tantalum filtration. As seen in Fig. 4.2.2 it was found that:

(1) If comparisons are made between x-ray tube kilovoltages on the basis of the same incident photon flux then:

(a) for a fixed kVp system (filter modulation only), 120 kVp is the optimum spectrum

(b) for a modulated kVp/filtration system the low energy kVp should be as low as possible (ignoring dose considerations) while the high energy kVp should be as high as possible.

(2) If comparisons are made between x-ray tube kilovoltages on the basis of accounting for the fact that the x-ray tube photon production efficiency is dependent upon the kVp (as seen in Fig. 2.1C.8) then:

(a) for a fixed kVp system (filter modulation only), 120 kVp is the optimum kilovoltage

(b) for a modulated kVp/filtration system the low energy kVp should be 120 kVp and the high energy kVp should be as high as possible (150 kVp or more).

Design and Construction of the Proof-of-Principle Experiment - Electrical and Mechanical Engineering Considerations

The results of the photon transport studies served as the basis for the design of the proof-of-principle experiment. In this experiment single-scan tomochemistry was performed by modulation of the filtration of the fan beam x-ray bremsstrahlung spectrum. As seen in Fig. 1.4.1, this was accomplished by rotating a beam analyser disk within the path of the fan beam during the rotation of the object being scanned. In this experiment the x-ray potential remained fixed during the filtration modulation so that only filtration changes served to produce the low and high energy spectra required for the tomochemistry data processing.

As seen in Fig. 2.2.1 a 14" diameter 2.16 mm thick rotating steel disk with 130 μm thick tantalum foil inserts was used to modulate the incident x-ray beam. The disk was used to control the

measurement process; i.e., one x-ray transmission measurement was performed per filter and the disk was rotated at an angular velocity such that 300 different 30 msec transmission measurements were made in a 10 second scan.

There were two major considerations in the design of the filtration modulation system:

(1) disk manufacturing considerations

(2) detector transient response considerations.

In the development and manufacture of the beam analyser disk it was found that:

(1) filter materials must be chosen such that standard manufacturing methods could be used

(2) the rotating disk method was ideal for the proof-of-principle experiment because of the ease of manufacture

(3) the filters must have a highly uniform thickness so that fluctuations in the measured signal due to thickness fluctuations are negligible

(4) the angular velocity of the disk should be constant to better than 1% so that the x-ray transmission measurements are performed uniformly in angle.

The beam analyser disk was designed to conform to these requirements.

The transient response effects of the detector were not negligible. The transition from one filter to another filter took about 0.5 msec and the transient response effects did not die out until about 2.5 msec after the commencement of the filter transition process. Hence, measurements of the detected currents were limited to those periods where the transient effects were negligible. This was done by rejecting the detected current measurement at the beginning of the measurement period.

Tomochemistry - Scanner System Integration and Control

After the beam analyser disk was designed and manufactured it was then integrated into the normal CT system. A view plan of the experimental setup is shown in Fig. 2.3.1 and photographs of the experiment with the beam analyser disk in place are shown in Figs. 2.3.3a and 2.3.3b. The disk was positioned as close as possible to the x-ray tube and aligned in such a position so that the filtration changes occurred simultaneously for all the detectors. The control system was then modified to account for the addition of the disk to the system. In particular, the automatic control system was modified so that:

(1) timing indications from the rotation of the disk controlled the data I/O process

(2) transients were rejected from the measurements

(3) the type of filter used in the measurements was read out by the computer

(4) the angle of the rotating table was recorded during measurements so that the angle of the transmission measurement would be known by the reconstruction algorithm.

With these slight modifications it was then possible to obtain all the required information for the tomochemistry reconstruction.

Fundamental Concepts of the Data Processing Methods Used to Obtain the the Tomochemical Information

The tomochemistry data processing method used in this research project is based upon the theory of Alvarez and Macovski (A.1, A.2). In this method calibration transmission measurements are made on a series of targets. These targets have known compositions, geometries, as well as the Compton and photoelectric + Rayleigh attenuation

coefficients at a reference energy, E_{REF}. What one is doing in the calibration process is to sample the two surfaces shown in Fig. 3.1.2. Polynomial fits are then performed on the calibration data using expansions of the form:

$$\int \mu_C d\ell = C_1 \ell n(I_S/I_{oS}) + C_2 \ell n(I_H/I_{oH}) + C_3 (\ell n(I_S/I_{oS}))^2 + C_4 (\ell n(I_H/I_{oH}))^2 + C_5 \ell n(I_S/I_{oS}) \ell n(I_H/I_{oH}) \quad (5.4.1)$$

and

$$\int \mu_{P+R} d\ell = B_1 \ell n(I_S/I_{oS}) + B_2 \ell n(I_H/I_{oH}) + B_3 (\ell n(I_S/I_{oS}))^2 + B_4 (\ell n(I_H/I_{oH}))^2 + B_5 \ell n(I_S/I_{oS}) \ell n(I_H/I_{oH}) \quad (5.4.2)$$

where

$\int \mu_C d\ell$ is the line integral of the Compton attenuation coefficient at energy E_{REF} along the ray path measured.

$\int \mu_{P+R} d\ell$ is the line integral of the photoelectric + Rayleigh attenuation coefficient at energy E_{REF} along the ray path measured.

$\ell n(I_S/I_{oS}), \ell n(I_H/I_{oH})$	are the natural logs of the ratio of the measured currents of the hard and soft spectra; i.e., the negative of the spectrum-averaged attenuation coefficient line integrals of the soft and hard spectra respectively.
B_1, B_2, B_3, B_4, B_5 and C_1, C_2, C_3, C_4, C_5	are the coefficients to be determined from the multiple regression analysis.

With these polynomial fits the Compton and photoelectric + Rayleigh line integrals of unknown targets can be determined by measuring (I_{oS}/I_S) and (I_{oH}/I_H) using the soft and hard x-ray spectra and then directly substituting $\ell n(I_{oS}/I_S)$ and $\ell n(I_{oH}/I_H)$ into Eqs. (5.4.1) and (5.4.2). The resultant line integrals $\int \mu_C d\ell$ and $\int \mu_{P+R} d\ell$ are determined for all the views and detectors. These line integrals then serve as the basic data set for reconstruction. The resultant images one obtains is a two-dimensional profile of $\mu_P(E_{REF})$ versus position (the photoelectric + Rayleigh attenuation coefficient reconstruction) and a two-dimensional profile of $\mu_C(E_{REF})$ versus position (the Compton attenuation coefficient reconstruction).

The calibration-data-comparison method of Alvarez and Macovski was used in this research project because this method has the potential ability to eliminate the nonlinearities of the measured process such as spectral hardening and detector nonlinearities. It should be noted that the calibration measurements are unique to the kilovoltage of the x-ray tube, high voltage of the detector, spectral filtration, and ionization chamber. Hence, each of the 256 detectors must be calibrated spearately for a given x-ray tube kVp and special filtration.

Method of Scanner Calibration and Results of the Calibration Experiments

To obtain the calibration data set required for the sampling of the two surfaces shown in Fig. 3.1.2, a calibration standard was designed and built specifically for the experiment. The standard was designed so that the measurement uncertainty of the calibration process was less than the measurement uncertainty of the scanner measurement process. As seen in Figs. 3.2.1 and 3.2.2, the standard consisted of four interchangeable watertight containers which fit between an adjustable front and back aluminum faceplate arrangement. By then using a series of saline solutions within the waterboxes it was possible to sample the calibration surfaces from a target thickness of 1 cm up to 25 cm with attenuation coefficients spanning a range from soft tissue to bone. Calibrations were performed on the calibration standard using a 100 kVp x-ray spectrum at an electron beam current of 30 mA. The results of the calibration measurements at 100 kVp were found to be representative of calibration measurements at other kVps. About 200 calibration measurements were obtained for every detector so that about 50,000 data points were obtained altogether.

Before the polynomial fitting process:

(1) a systematic search for bad data points (outliers) was performed

(2) corrections were made for the voltage drift of the ionization chamber HV.

As seen in Fig. 4.3.5, it was found that the independent variables $(\ell n(I_o/I)_{soft}, \ell n(I_o/I)_{hard})$ spanned a narrow range. Hence, it was

found that small errors in the calibration or polynomial fitting process would cause large uncertainties in the determination of the dependent variables ($\int\mu_p d\ell, \int\mu_c d\ell$) shown in Fig. 4.3.6. Polynomial fits were performed to the corrected-calibration data of each detector. It was found that:

(1) The first order terms in Eqs. (5.4.1) and (5.4.2) described the dominant behavior of the calibration data

(2) The Compton attenuation coefficient line integral fits were good to about 1.5%

(3) The photoelectric + Rayleigh attenuation coefficient line integral fits were good to about 5.7%

(4) The polynomial fits were found to fit the calibration data well at small values of the line integrals but were found to break down at large values of the line integrals as seen in Fig. 4.3.6.

The results of the calibration process implied that:

(1) The calibration process was the weakest part of this tomochemistry method. Furthermore, the use of published cross sections to determine the line integrals of the Compton and photoelectric + Rayleigh attenuation coefficient was a weak point in the calibration method.

(2) Not all of the outliers may have been removed from the calibration data.

(3) The third order fits of Eqs. (5.4.1) and (5.4.2) were found to be valid only over a range which is smaller than the full range of the calibration measurements.

(4) Calibration of a CT scanner which contains 256 detectors must be done semiautomatically because of the large numbers of data points that must be processed.

Data Processing Methods Used to Obtain the Tomochemical Information

As seen in Fig. 3.1.1 the data processing software consisted of five major blocks. In the tomochemistry software only the data mapping and calibration data acquisition and reduction software blocks were unique to tomochemistry. Only slight modifications in the scan data acquisition and data preprocessing software blocks were required to allow for the integration of the beam analyser disk to the CT system. Furthermore, the standard Hanning-weighted ramp-filter back-projection method was used to reconstruct the Compton and photoelectric + Rayleigh attenuation coefficient line integrals and the resultant images were displayed in a manner similar to normal CT images.

The data 'mapping' software was programmed to perform three major tasks:

(1) To interpolate between filter data in order to obtain the missing filter measurements (see Fig. 3.3.2).

(2) To map the data from $(\ell n(I_S/I_{oS}), \ell n(I_H/I_{oH}))$ space to $(\int \mu_C d\ell, \int \mu_P d\ell)$ space (see Fig. 3.3.2).

(3) To 'even out' the data set so that the resultant data set for reconstruction would correspond to transmission measurements performed evenly in angle (see Fig. 3.3.4).

Tasks (1) and (3) assumed that the measured data was sufficiently continuous in angle so that straightforward linear interpolations could be performed. Figure 3.3.1 indicates that the angular sampling rate is sufficiently frequent (300 views in 360 degrees) so that performing linear interpolations is reasonable. However, this linear interpolation assumption is the most sensitive assumption in the data processing method and it breaks down near discontinuities in the scanned target (i.e., at bone-water interfaces, etc.).

Results of the Proof-of-Principle Experiments

To test out the performances of the integrated system a series of scans and reconstructions were performed on phantoms with known compositions and geometries. All scans were performed on a 1 cm thick slice of the phantom with the x-ray tube driven at 100 kVp and 30 mA. The phantoms were all axially symmetric so that partial volume effects in the axial direction would be minimized.

A series of 15.14 cm diameter uniform-composition cylindrical phantoms were scanned which contained a range of saline solutions. The saline solutions used were the same as the solutions used in the calibration experiment. In this way a self-consistency check between the measurement/reconstruction process with the calibration process could be performed.

Reconstructions of the saline solution phantoms are shown in Fig. 4.4.1 and profiles of the reconstructed values across the diameter of the phantoms are shown in Fig. 4.4.2. It was found that:

(1) Tomochemistry reconstructions could accurately predict the photoelectric + Rayleigh and Compton attenuation coefficients near the edge of the solution reconstruction.

(2) Systematic error is, at the moment, the dominant cause of measurement uncertainty within the images.

(3) At higher values of the photoelectric + Rayleigh attenuation coefficient (higher NaCℓ molar concentration) there is more noise within the image. It was also found that the Compton attenuation coefficient tends to be underestimated within the image while the photoelectric attenuation coefficient tends to be overestimated. The degree of underestimation and overestimation is approximately equal and opposite within the images.

These three findings reflect the fact that the polynomial fit functions perform well at small values of photon attenuation and more poorly at larger values. Hence, the reconstructed attenuation coefficients near the edge of the phantom are accurately predicted because transmission measurements there are generally through small solution thicknesses. Furthermore, the increased noise at higher molar concentrations is due to the detector-to-detector calibration variations becoming more noticeable as the photoelectric + Rayleigh attenuation coefficients of the phantom are increased.

Scans and reconstructions were also performed on a spatial resolution phantom and on nonuniform low and high contrast phantoms. The reconstructions of these phantoms are shown in Figs. 4.4.9, 4.4.11, and 4.4.12. It was found that:

(1) The spatial resolution of this scanner is about 4 mm as compared to 2 mm of normal CT scanners. This poorer resolution is due to the large number of interpolations performed within the 'raw' prereconstructed data set.

(2) As seen in Fig. 4.4.11, streak and ring artifacts, due to detector discharges and errors in the polynomial fit, can potentially reduce much of the information content within scanned targets. Hence, algorithms must be developed which can automatically search the 'raw' data set for bad data points and measurements.

(3) For reconstructions to be valid, measurements of x-ray transmission on unknown targets must be well within the range of the calibration transmission measurements.

Even with the above difficulties these experiments indicate that tomochemistry has the ability to distinguish between material properties that normal CT cannot distinguish. Its unique capabilities are

illustrated by the reconstructions in Fig. 4.4.12 where in the Compton reconstruction the graphite block is the most prominent feature while in the photoelectric + Rayleigh reconstruction it is not visible. This is due to the fact that the electron density of graphite is about 45% greater than water while the photoelectric + Rayleigh attenuation coefficient is about 14% less than water.

Finally, it was found in this research project that based upon experimental measurements, estimates of the theoretical limit to the statistical accuracy of the Compton and photoelectric + Rayleigh reconstructions could be determined. It was found that for a 20 cm diameter water-like target using a 120 kVp spectrum with the alternating iron and tantalum filtration the statistical uncertainty of the reconstructed attenuation coefficients within a 5 mm x 5 mm fixed area is about 0.198% for the conventional image, 7.5% for the photoelectric + Rayleigh image, and 0.6% for the Compton image.

5.2 Suggestions for Future Work

The results of this research project were quite successful and it is felt that several areas of development should be pursued more deeply. In particular it is suggested that:

(1) Experimental studies on improving the calibration method should be investigated. Some ideas worth pursuing are:

   (a) Develop better programs to more reliably find outliers within the calibration data set.

   (b) Use calibration standards which consist of slabs of interchangeable 'photoelectric + Rayleigh-dominant' and 'Compton-dominant' substances. For example, a 'Compton-dominant' substance would be a substance like beryllium where nearly 100% of the diagnostic energy photon interactions are via the Compton effect. Conversely, iron, copper, etc., could be used as a 'photo-electric + Rayleigh-dominant' substance.

   (c) Calibrate over a very wide range before performing polynomial fits.

   (d) Study more closely the required degree of the polynomial fits.

   (e) Develop methods to minimize the variations between the detector-to-detector calibrations.

(2) More development work should be performed to increase the speed of the software. At the present time a reconstruction of the tomochemical data takes about 3 hours. A significant amount of improvement can be realized in this area.

(3) Experimental studies should be performed to improve the spatial resolution of the scanner. The primary suggestion here is to double the number of views in the scan process. However, it should be noted that improvements as suggested by (2) must be realized before a doubling in the number of views is possible or practical.

(4) Experimental studies should be performed to investigate simultaneous kVp and filtration switching. It is felt by the author that the use of pulsed x-ray tubes would be more suitable for these experiments.

(5) Development should be performed on alternative filtration-switching methods. The most straightforward method to pursue would be a reciprocating filter arrangement which could potentially be attached to most commercial CT scanners as a retrofit.

(6) Investigations should be performed into the use of tomochemistry for the scanning of high-Z objects. This area of investigation is an open field at the moment. It is felt that the methods developed in this research project are sufficiently general so that they could be immediately extended into this area of investigation.

Appendix A Image Reconstruction Theorems of Tomography

The basis of computerized axial tomography lies in the ability to reconstruct a two-dimensional image through the measurement of one-dimensional line integrals. Given the method of 2-D reconstruction the extension to 3-D reconstruction is then possible. The treatment below is only a skeletal treatment of reconstruction theory. The reader is referred to the literature for a more complete treatment of reconstruction theory and methods (B.3, C.2, C.3, O.1, R.4, R.5, S.2, S.3, B.8, C.9, B.9, K.4, T.4, T.5, G.2, G.3, H.6, C.10, B.10).

To keep the treatment simple, four assumptions will be used in the following derivations. These assumptions are:

1. Perfect exponential attenuation (no spectral hardening);
2. An infinite number of views are measured in a scan;
3. Measurements are made uniformly in angle; and
4. In each view, parallel ray measurements are made.

The complications of performing a finite number of measurements will be touched on briefly at the end of this discussion.

Assume that a CT scanner has performed parallel ray measurements of photon attenuation in a plane of the body at a series of angles (as in Hounsfield's first scanner). There are methods to reconstruct an image from non-parallel ray measurements, however, the derivation for the parallel ray measurement case is the most straightforward. In CT one is trying to determine the two-dimensional attenuation coefficient profile within the scanned plane. Denote this profile as $\mu(x,y)$ in rectangular coordinates and $\mu(r,\theta')$ in polar coordinates. An illustration of the geometry is contained in Fig. A.1. Assume that $\mu(r,\theta')$

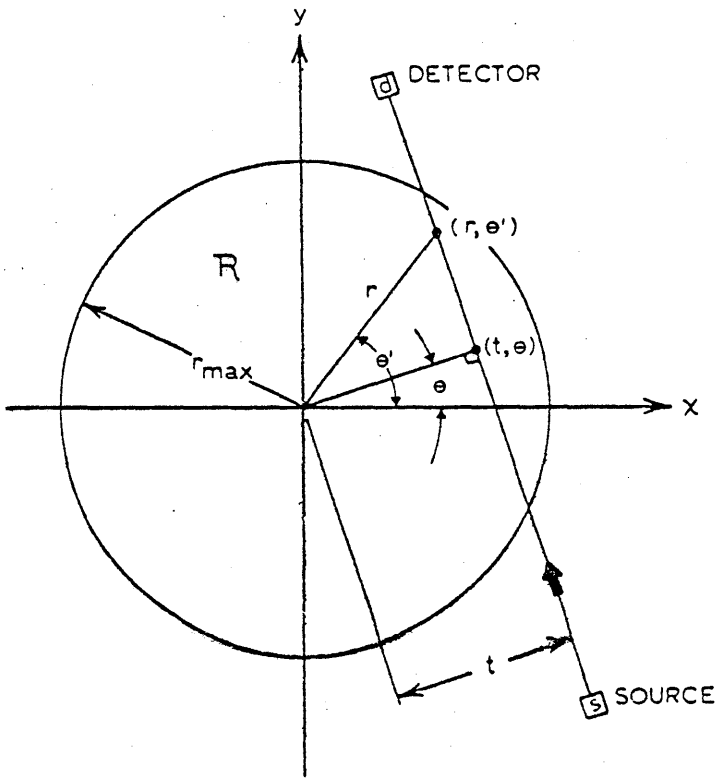

Figure A.1 Geometry used in the image reconstruction theorem derivations.

is restricted to a circular region, R, such that $\mu(r,\theta')$ is zero for all $|r| > r_{max}$.

The attenuation coefficient at a point, $\mu(r,\theta')$, cannot be measured directly because it is surrounded by other photon attenuating material. Hence, $\mu(r,\theta')$ must be inferred from the series of x-ray transmission measurements which were performed. To derive $\mu(r,\theta')$ from these measurements first define the ray path coordinates (t,θ). As seen in Fig. A.1, any relative position of the x-ray source and detector, s-d, defines a ray path as determined by the parametric relationship $t = r\cos(\theta-\theta')$. In this coordinate system let t take all positive and negative values and let θ take values between 0 and π. Using these coordinates the transmission measurement, $m(t,\theta)$, associated with a ray is given by the expression:

$$m(t,\theta) = -\ell n(\exp(-\int_s^d \mu(r,\theta')d\ell)) = -\ell n(\frac{I}{I_o})_{s-d} \qquad (A.1)$$

$$= \int_0^{2\pi}\int_0^{\infty} \mu(r,\theta')\,\delta[t-r\cos(\theta-\theta')]|r|dr\,d\theta' \qquad (A.2)$$

where

The integration in Eq. (A.1) is performed between the source, s, and the detector, d, and

I/I_o is the ratio of the detected currents in the transmission measurement along ray path s-d, with and without the patient in the x-ray beam.

Equation (A.2) is an equivalent and more formal mathematical representation of the transmission measurement. The Dirac delta function,

$\delta[t-r\cos(\theta-\theta')]$, indicates formally that only those points which lie on the ray s-d contribute to the two-dimensional surface integral. In the literature Eq. (A.2) is referred to as the projection equation.

The problem in reconstruction tomography is to invert the measurements taken for a sufficiently large number of x-rays so that the two-dimensional profile, $\mu(r,\theta')$, can be determined in the region R. The method of inversion to be derived here is the Fourier transform method. The one-dimensional Fourier transform, $M(\rho,\theta)$, of the measurements, $m(t,\theta)$, is given by the expression:

$$M(\rho,\theta) = \int_{-\infty}^{\infty} m(t,\theta)\, \exp[-j\,2\pi\rho t]\, dt \qquad (A.3)$$

Experimentally, the Fourier transform, $M(\rho,\theta)$, is determined from the parallel ray measurements over all t at the fixed view angle θ. By using the projection equation, Eq. (A.2), and integrating over all t, Eq. (A.3) becomes:

$$M(\rho,\theta) = \int_{0}^{2\pi} \int_{0}^{\infty} \mu(r,\theta')\, \exp[-j\,2\pi\rho r\cos(\theta-\theta')]|r|\, dr\, d\theta' \qquad (A.4)$$

Noting that the two-dimensional Fourier transform, $A(\rho,\theta)$, of the unknown profile $\mu(r,\theta')$ is given by the definition:

$$A(\rho,\theta) = \int_{-\infty}^{\infty} \int_{-\infty}^{\infty} \mu(x,y)\, \exp[-j2\pi\rho(x\cos\theta + y\sin\theta)]\, dx\, dy$$

$$= \int_{0}^{2\pi} \int_{0}^{\infty} \mu(r,\theta')\, \exp[-j2\pi\rho r\cos(\theta-\theta')]|r|\, dr\, d\theta' \qquad (A.5)$$

Equations (A.4) and (A.5) show that:

$$A(\rho,\theta) = M(\rho,\theta) \tag{A.6}$$

By now writing the inverse transform of $A(\rho,\theta)$using polar coordinates:

$$\mu(r,\theta') = \int_0^{\pi} \int_{-\infty}^{\infty} |\rho|\, A(\rho,\theta) \exp[j\, 2\pi\rho r \cos(\theta'-\theta)]\, d\rho\, d\theta$$

and using Eq. (A.6) it is found that:

$$\mu(r,\theta') = \int_0^{\pi} \int_{-\infty}^{\infty} |\rho|\, M(\rho,\theta) \exp[j\, 2\pi\rho r \cos(\theta'-\theta)]\, d\rho\, d\theta \tag{A.7}$$

In summary, to determine $\mu(r,\theta')$ from parallel ray projection measurements one must:

(1) determine the one-dimensional Fourier transform of the parallel ray measurements at each angle, θ:

$$m(t,\theta) \rightarrow M(\rho,\theta)$$

(2) determine the two-dimensional inverse Fourier transform of $M(\rho,\theta)$. Since parallel ray measurements were made at all angles, $M(\rho,\theta)$ is known for all θ.

$$M(\rho,\theta) \rightarrow \mu(r,\theta')$$

Performing forward and inverse Fourier transforming in practice is not practical for CT reconstructions. The above reconstruction method can be simplified by defining the function:

$$G(\rho,\theta) = |\rho|\, M(\rho,\theta) \tag{A.8}$$

and its one-dimensional inverse transform

$$g(t,\theta) = \int G(\rho,\theta) \exp(j\, 2\pi\rho t)\, d\rho \tag{A.9}$$

Now note the general form of Parseval's equation (P.5)

$$\int f_1(t)\, f_2(t)dt = \int F_1(\rho)\, F_2(\rho)^*\, d\rho \tag{A.10}$$

where

$f_1(t)$ and $f_2(t)$ are the Fourier transforms of
$F_1(\rho)$ and $F_2(\rho)$ respectively, and
$F_2^*(\rho)$ is the complex conjugate of $F_2(\rho)$.

Substituting Eq. (A.8) into Eq. (A.7) and using Parseval's equation results in the expression:

$$\mu(r,\theta') = \int_0^{\pi} \int_{-\infty}^{\infty} g(t,\theta)\, \delta[t-r\cos(\theta'-\theta)]\, dt\, d\theta$$

$$= \int_0^{\pi} g[r\cos(\theta'-\theta),\, \theta]\, d\theta \tag{A.11}$$

Using Eq. (A.11) it is seen that to obtain a reconstruction, one must

(1) determine the one-dimensional Fourier transform of the parallel ray measurements at all angles, $\theta = 0$ to $\theta = \pi$

$$m(t,\theta) \rightarrow M(\rho,\theta)$$

(2) determine the one-dimensional inverse Fourier transform of $M(\rho,\theta)$ weighted by the function $|\rho|$

$$|\rho|\ M(\rho,\theta) \rightarrow g(t,\theta) = g(r\ \cos(\theta'-\theta),\ \theta)$$

(3) integrate $g(r\ \cos(\theta'-\theta),\ \theta)$ from $\theta = 0$ to $\theta = \pi$ to determine $\mu(r,\theta')$

$$g(r\ \cos(\theta'-\theta),\ \theta) \rightarrow \mu(r,\theta')$$

The weighting of $M(\rho,\theta)$ by $|\rho|$ in step (2) is commonly interpreted as a frequency filtration of the projection transform, $M(\rho,\theta)$. This filtration is seen to suppress the low spatial frequency components and enhance the high spatial frequency components in the projection function, $m(r,\theta)$.

The reconstruction method can be simplified further by noting that the forward and inverse Fourier transforming in steps (1) and (2) are superfluous. These steps can be avoided through the use of the convolution theorem of Fourier transforms:

$$\int_{-\infty}^{\infty} f_1(\tau)\ f_2(t-\tau)d\tau = \int_{-\infty}^{\infty} F_1(\rho)\ F_2(\rho)\ \exp(j2\pi\rho t)dp \qquad (A.12)$$

where

τ is a dummy variable

$f_1(t)$ and $f_2(t)$ are the inverse Fourier transforms of $F_1(\rho)$ and $F_2(\rho)$ respectively.

Rewriting Eq. (A.11) and utilizing the convolution theorem the result is:

$$\mu(r,\theta') = \int_0^{\pi} \left[\int_{-\infty}^{\infty} \overline{F}(|\rho|)\, m(t-\tau,\, \theta)\, d\tau \right] d\theta \qquad (A.13)$$

where

$t = r \cos(\theta'-\theta)$

$\overline{F}(|\rho|)$ is the inverse Fourier transform of $|\rho|$.

Thus, to reconstruct an image from measurements of its projections one need only:

(1) convolve the projection function, $m(r,\theta)$, with the inverse Fourier transform of the function $|\rho|$.

(2) integrate the resultant convolution over the angles from $\theta = 0$ to $\theta = \pi$.

In practice one does not measure the projection function, $m(r,\theta)$, at an infinite number of angles; and at each angle, θ, one does not perform an infinite number of parallel ray measurements. Rather, in an experimental measurement one samples the distribution, $M(\rho,\theta)$, through a finite number of measurements. The highest spatial frequency that is sampled in a CT measurement is determined by the spatial separation between the parallel ray measurements and also the angular

separation between the projection measurements. If the characteristic spatial spearation of measurements is ΔX, sampling theory (0.2) states that the highest frequency sampled is given by:

$$\rho_n = \frac{1}{2\Delta X} \tag{A.14}$$

where

ρ_n is called the Nyquist frequency.

The Nyquist frequency has direct implications in the Fourier reconstruction method. In particular, frequency filtration cannot be performed with the ramp filter, $|\rho|$, beyond the Nyquist frequency. Frequency filtering past this frequency causes artifacts to occur in the reconstructed image. Regions in the image where sudden changes occur in the attenuation coefficient will have severe oscillations (G.4). These oscillations are similar to those produced at a discontinuity of a function when approximated by a Fourier series (L.5). This oscillation is sometimes called Gibb's phenomenon. Previous work (R.7) indicated that using the Nyquist-frequency-limited ramp filter:

$$R(\rho) = \begin{cases} |\rho| & |\rho| < \rho_n \\ 0 & \text{elsewhere} \end{cases}$$

and its corresponding inverse transform for the convolution:

$$r(t) = \frac{\rho_n \sin(2\pi\rho_n t)}{\pi t} - \frac{1-\cos(2\pi\rho_n t)}{2\pi^2 t^2}$$

in reconstructions introduced ripple into the image. An illustration of the ramp filter and its inverse transform is given in Fig. A.2. It was shown in the same work that the ripple could be adequately suppressed by Hanning-weighting the Nyquist-frequency-limited ramp filter. An illustration of the Hanning window function is given in Fig. A.3. The resultant frequency filter is then given by the expression:

$$H(\rho) = \begin{cases} |\rho| \left(\dfrac{1+\cos(\pi\rho/\rho_n)}{2} \right) & |\rho| < \rho_n \\ 0 & \text{elsewhere} \end{cases}$$

with the corresponding inverse transform given by the expression:

$$\begin{aligned} h(t) = & \left(\frac{\rho_n \sin(2\pi\rho_n t)}{2\pi t} - \frac{1-\cos(2\pi\rho_n t)}{4\pi^2 t^2} \right) + \\ & \left(\frac{\rho_n \sin(2\pi\rho_n (t - \frac{1}{2\rho_n}))}{4\pi(t - \frac{1}{2\rho_n})} - \frac{1-\cos(2\pi\rho_n (t - \frac{1}{2\rho_n}))}{8\pi^2 (t - \frac{1}{2\rho_n})^2} \right) + \\ & \left(\frac{\rho_n \sin(2\pi\rho_n (t + \frac{1}{2\rho_n}))}{4\pi(t + \frac{1}{2\rho_n})} - \frac{1-\cos(2\pi\rho_n (t + \frac{1}{2\rho_n}))}{8\pi^2 (t + \frac{1}{2\rho_n})^2} \right) \end{aligned} \qquad \text{(A.15)}$$

An illustration of the Hanning-weighted ramp filter and its inverse transform is given in Fig. A.4. By substitution of Eq. (A.15) into the convolution reconstruction equation, Eq. (A.13), the Hanning-weighted filtered-backprojection equation is obtained:

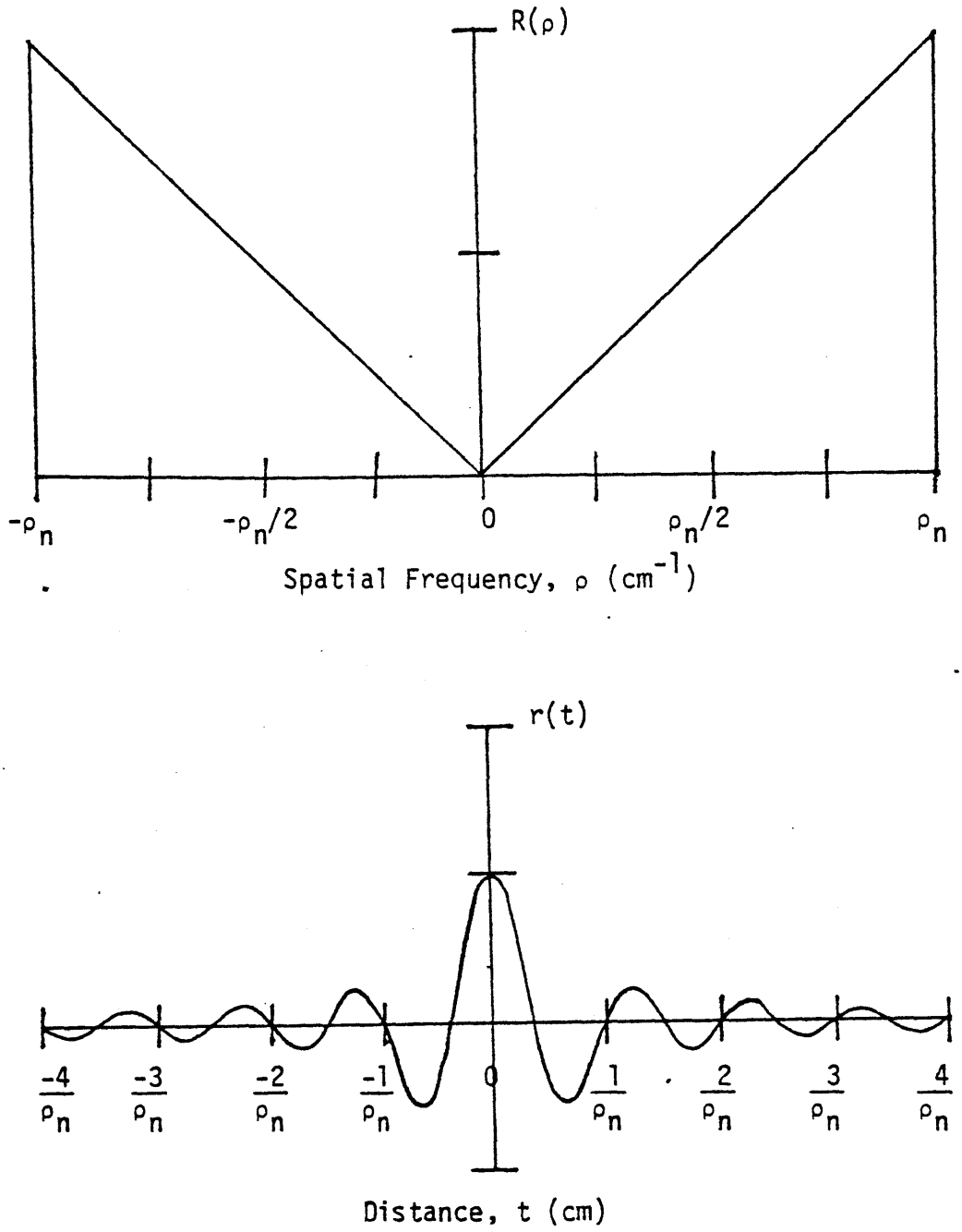

Figure A.2 Illustration of the Nyquist-frequency-limited ramp filter and its corresponding inverse Fourier transform.

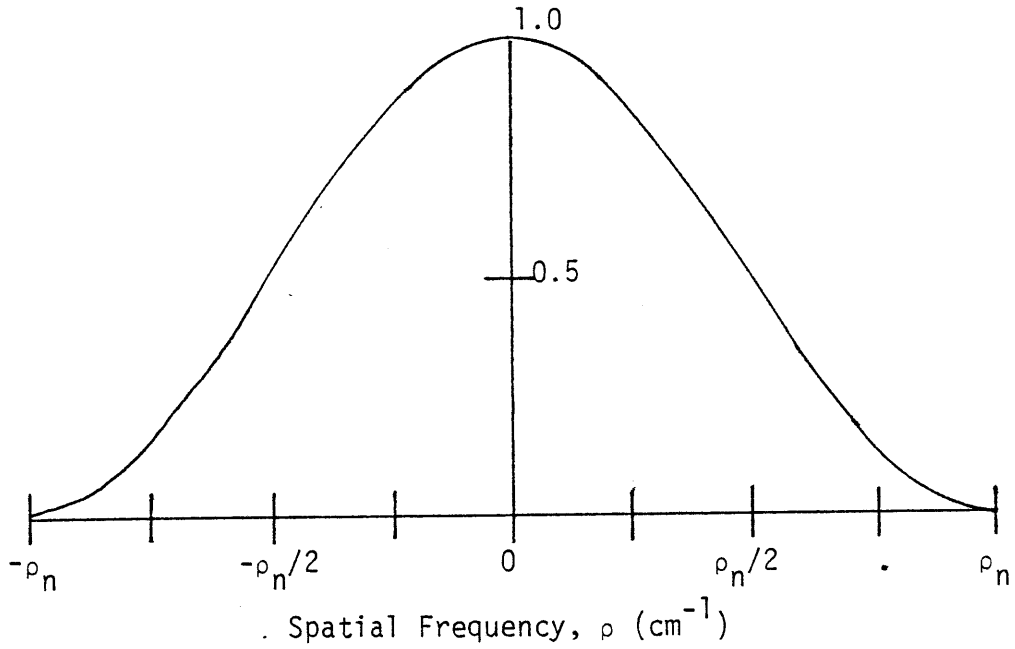

Figure A.3 Plot of the Hanning window function versus spatial frequency, ρ.

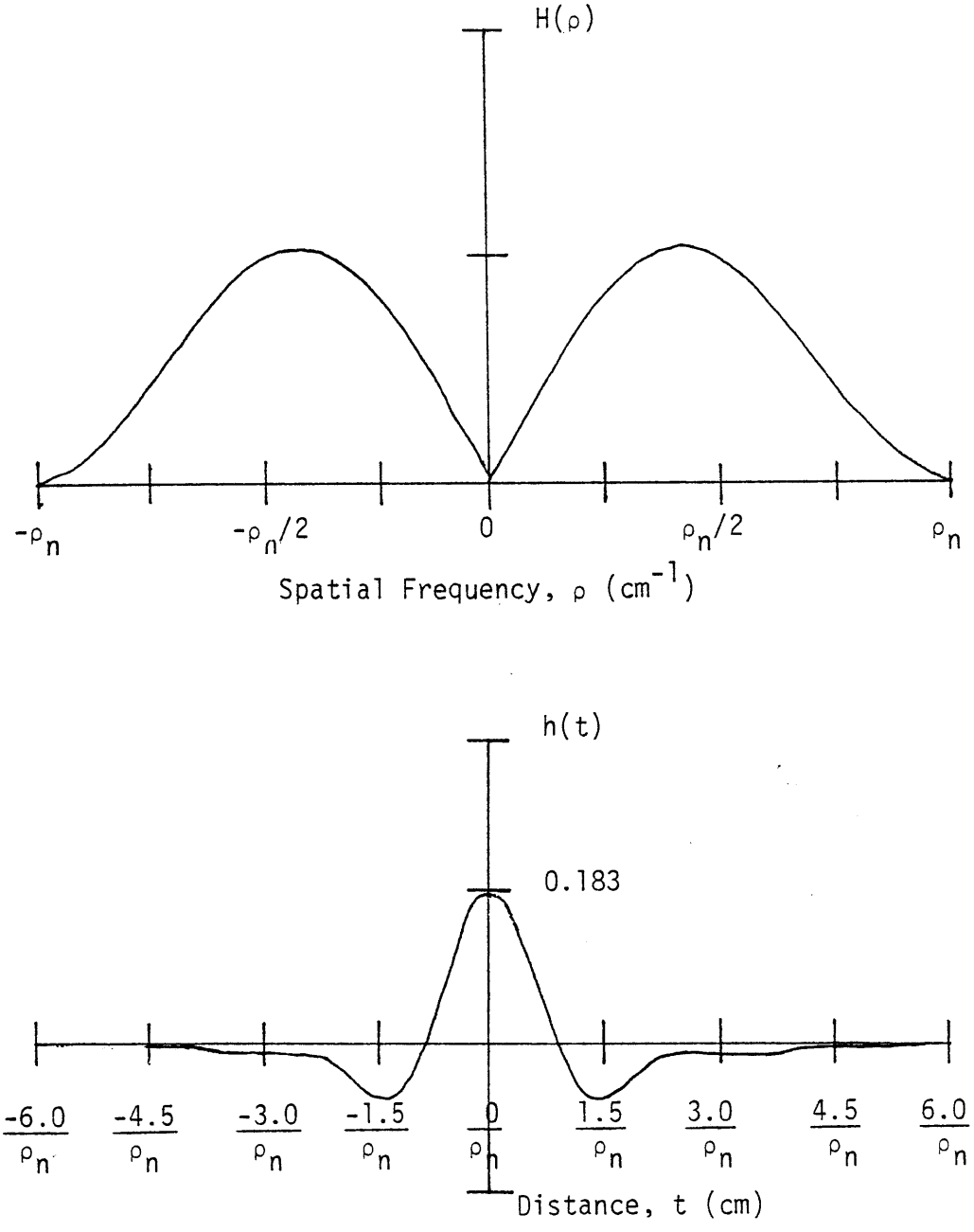

Figure A.4 Illustration of the Hanning-weighted ramp filter and its corresponding inverse transform.

$$\mu(r,\theta') = \int_0^{\pi} \left[\int_{-t_{max}}^{t_{max}} h(\tau)\, m(t-\tau,\, \theta)\, d\tau \right] d\theta \qquad \text{(A.16)}$$

where

$h(\tau)$ is defined by Eq. (A.15).

All the reconstructions performed in this thesis used the Hanning-weighted filtered-backprojection method of reconstruction.

Appendix B Transport Models and Calculations Used in the Nuclear Engineering Design

The purpose of this appendix is to present the important methods and models used in the photon transport work. There are two basic areas of transport work. These are the three-dimensional Monte Carlo transport calculations performed to estimate the absorbed dose and the one-dimensional transport simulations of the CT scanning process. The programs, derivations, calculations, and results of these transport studies will be presented below.

Appendix B.1 Solution of the Analytic Dose Kernel for Dose Received from CT Scanning

This section presents the analytic derivation of primary beam point dose received from CT scanning. The derivation assumes that the body can be modeled as a right circular cylinder, and that water can be used as the tissue analog. The derivation here is only for the dose due to primary x-rays. Monte Carlo dose calculations which determine the dose for both the primary and secondary radiation are presented in Appendix B.2.

Consider the primary dose calculation for a stationary fan x-ray beam incident upon a right circular cylinder which is centered on the rotation axis of the scanner. The geometry of the setup is shown in Fig. B.1.1. With this geometry the point dose kernel is given by the expression:

$$D(r,\theta) = \int_0^{E_{max}} S(E)\,\frac{\mu_{en}(E)\,E}{\rho}\,\Phi_R\,T\,\exp[-\mu_{at}(E)\,A]\,B\,dE$$

$$\cong \left(\frac{\overline{\mu_{en}E}}{\rho}\right)\Phi_R\,T\,\exp[-\bar{\mu}_{at}\,A]\,B \qquad (B.1.1)$$

where

$\frac{\overline{\mu_{en}E}}{\rho}$ is the spectrum-averaged mass energy absorption coefficient-energy product

Φ_R is the photon flux (γ/cm^2-sec) at the rotation axis of the scanner

T is the duration of the exposure in seconds

$\bar{\mu}_{at}$ is the spectrum-averaged x-ray attenuation coefficient

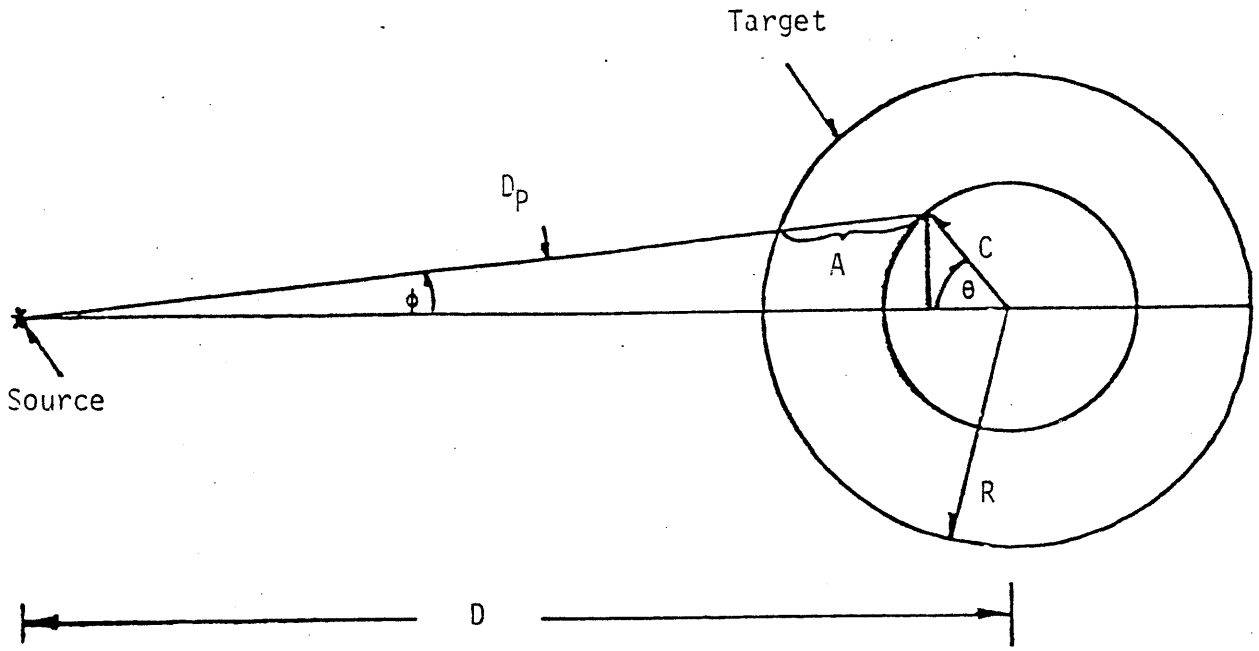

Figure B.1.1 Geometry used in the analytic dose calculation.

A is the thickness of water traversed by the x-rays to get to the point (r,θ)

B is the photon flux divergence factor; this factor corrects the reference photon flux for the inverse square relationship between flux and distance of (r,θ) from the source

$S(E)$ is the normalized x-ray source spectrum distribution

E_{max} is the maximum energy in the x-ray source spectrum distribution.

The spectrum-averaging approximation (averaging $\frac{\mu_{en}E}{\rho}$ and μ_{at} and then inserting them into the dose kernel) is not rigorously valid. However, for most diagnostic bremsstrahlung spectra of engineering interest this approximation is valid to within 5%. Furthermore, use of this approximation implicitly assumes that there is negligible spectral hardening as the x-rays traverse the water, implying that $\overline{\mu_{en}E}/\rho$ and $\bar{\mu}_{at}$ remain constant.

The water thickness traversed, A, can be determined from analytic geometry. It is given by the expression:

$$A = \sqrt{R^2 - D^2 \sin^2\phi} + \sqrt{C^2 - D^2 \sin^2\phi} \qquad \theta > \theta_{crit}$$

$$A = \sqrt{R^2 - D^2 \sin^2\phi} - \sqrt{C^2 - D^2 \sin^2\phi} \qquad \theta < \theta_{crit}$$

$$\theta_{crit_c} = \cos^{-1}(C/D) \qquad \text{(B.1.2)}$$

As seen in Fig. B.1.1, θ_{crit_c} refers to that angle at which x-rays pass tangent to the surface of a circle of radius C.

The photon divergence factor is given by the expression:

$$B = (D_p/D)^2$$

$$= \left[\frac{D^* \left[\cos(\tan^{-1}(C \sin\theta/(D-C \cos\theta)))\right]}{[D-C \cos\theta]}\right]^2 \qquad (B.1.3)$$

where

C is the radial position of interest

R is the outer radius

D is the distance from the source to the rotation axis

D_p is the distance from the source to the point of interest

$D_p = (D-C \cos\theta)/(\cos\phi)$

θ is the angular position with respect to the center of the cylinder

ϕ is the angular position with respect to the source

$\tan\phi = (C \sin\theta)/(D-C \cos\theta)$

To determine the dose from a CT scan using Eq. (B.1.1) assumes that the x-ray source rotates 360° around the patient at a constant rate. In this case one need only average the absorbed dose from the fixed source-target case by integrating over all θ at a fixed radius, r:

$$D(r) = \frac{\Phi_R \, T \, \overline{\frac{\mu_{en}}{\rho} E} \int_0^{2\pi} \exp[-\mu_{at} A] \, B \, d\theta}{\int_0^{2\pi} d\theta} \qquad (B.1.4)$$

where A and B are the same as in Eqs. (B.1.3) and (B.1.2).

Equation (B.1.4) is a simple expression to evaluate numerically but it is a very difficult expression to evaluate analytically. Before presenting the numerical analysis it is enlightening to consider the approximate solution of Eq. (B.1.4) for the surface and centerline positions of the cylinder.

Surface Dose, $\mu_{at} = \infty$

Consider the surface dose calculation assuming that no dose to the surface is contributed from those photons which are transmitted through the water. Physically this corresponds to the case where the water cylinder is opaque to photons. Geometrically this corresponds to the situation where no dose is given to the surface past the angle θ_{crit}. It has been found experimentally (L.2) that this is a reasonable approximation (error < 15%) for water cylinders with sizes of the order of the human body (20 - 40 cm diameter). With this approximation Eq. (B.1.4) becomes:

$$D(R) = \frac{\Phi_R T}{2\pi}\left(\frac{\overline{\mu_{en}E}}{\rho}\right)\int_{-\theta_{crit}}^{\theta_{crit}} B \, d\theta$$

$$= \left(\frac{\Phi_R T}{\pi}\right)\left(\frac{\overline{\mu_{en}E}}{\rho}\right)\int_{0}^{\theta_{crit}}\left[\frac{D^* \cos[\tan^{-1}(\tan\phi)]}{[D-R\cos\theta]}\right]^2 d\theta \quad \text{(B.1.5)}$$

Since ϕ is small for all θ ($\phi_{max} \sim 13°$) the integral can be further simplified:

$$D(R) \simeq \frac{\Phi_R T}{\pi}\left(\frac{\overline{\mu_{en}E}}{\rho}\right)\int_0^{\theta_{crit}}\left[\frac{\cos\phi}{1-\frac{R}{D}\cos\theta}\right]^2 d\theta$$

$$\cong \frac{\Phi_R T}{\pi}\left(\frac{\overline{\mu_{en}E}}{\rho}\right)\int_0^{\theta_{crit}}\left[\frac{1}{1-\frac{R}{D}\cos\theta}\right]^2 d\theta \qquad \text{(B.1.6)}$$

where $\theta_{crit} = \cos^{-1}(R/D)$.

Equation (B.1.6) can be solved and evaluated exactly giving the expression:

$$D(R) \cong \left(\Phi_R T\right)\left(\frac{\overline{\mu_{en}E}}{\rho}\right)\frac{1}{\pi}\left[\left[\frac{\alpha\sin(\cos^{-1}\alpha)}{(1-\alpha^2)^2}\right] + \left[\frac{2}{(1-\alpha^2)^{3/2}}\tan^{-1}\left(\sqrt{\frac{1+\alpha}{1-\alpha}}\tan\left(\frac{\cos^{-1}\alpha}{2}\right)\right)\right]\right] \qquad \text{(B.1.7)}$$

where $\alpha = R/D$.

Equation (B.1.7) shows that the dose equation can be broken up into a factor which depends on the x-ray beam characteristics and another factor which depends upon geometry

$$D = \left[\Phi_R T\left(\frac{\overline{\mu_{en}E}}{\rho}\right)\right] * [S]$$

where the term within the first set of brackets is the x-ray beam

characteristics factor and the term within the second set of brackets is defined as the surface dose factor, S.

The surface dose factor for $\mu_{at} = \infty$, plotted in Fig. B.1.2, is seen to slowly increase with increasing radius. This phenomenon is due to the source-to-surface distance decrease (corresponding to higher photon flux) as the cylinder radius increases. The $\mu_{at} = \infty$ case is the lower limit to the primary surface dose estimate because in this model photons have been considered to reach the surface from only one side. Note that in the limit of a 0 cm radius the surface dose factor is estimated to be 0.5. This is because the cylinder has been modeled to be perfectly self-shielding and thus the surface only 'sees' photons for half of the scan time.

Surface Dose, $\mu_{at} = 0$

The upper limit to the surface dose can be estimated by assuming that the water cylinder is transparent to x-rays ($\mu_{at} = 0$). Equation (B.1.6) can be used for this estimate by simply extending the upper limit of integration from θ_{crit} to π. The result of this integration yields the expression:

$$D(R) \cong (\Phi_R T)\left(\frac{\overline{\mu_{en}E}}{\rho}\right)\left(\frac{1}{(1 - (\frac{R}{D})^2)^{3/2}}\right) \qquad \text{(B.1.8)}$$

The surface does factor in this situation is then given by:

$$S\big|_{\mu_{at}=0} = \left(\frac{1}{(1 - (R/D)^2)^{3/2}}\right)$$

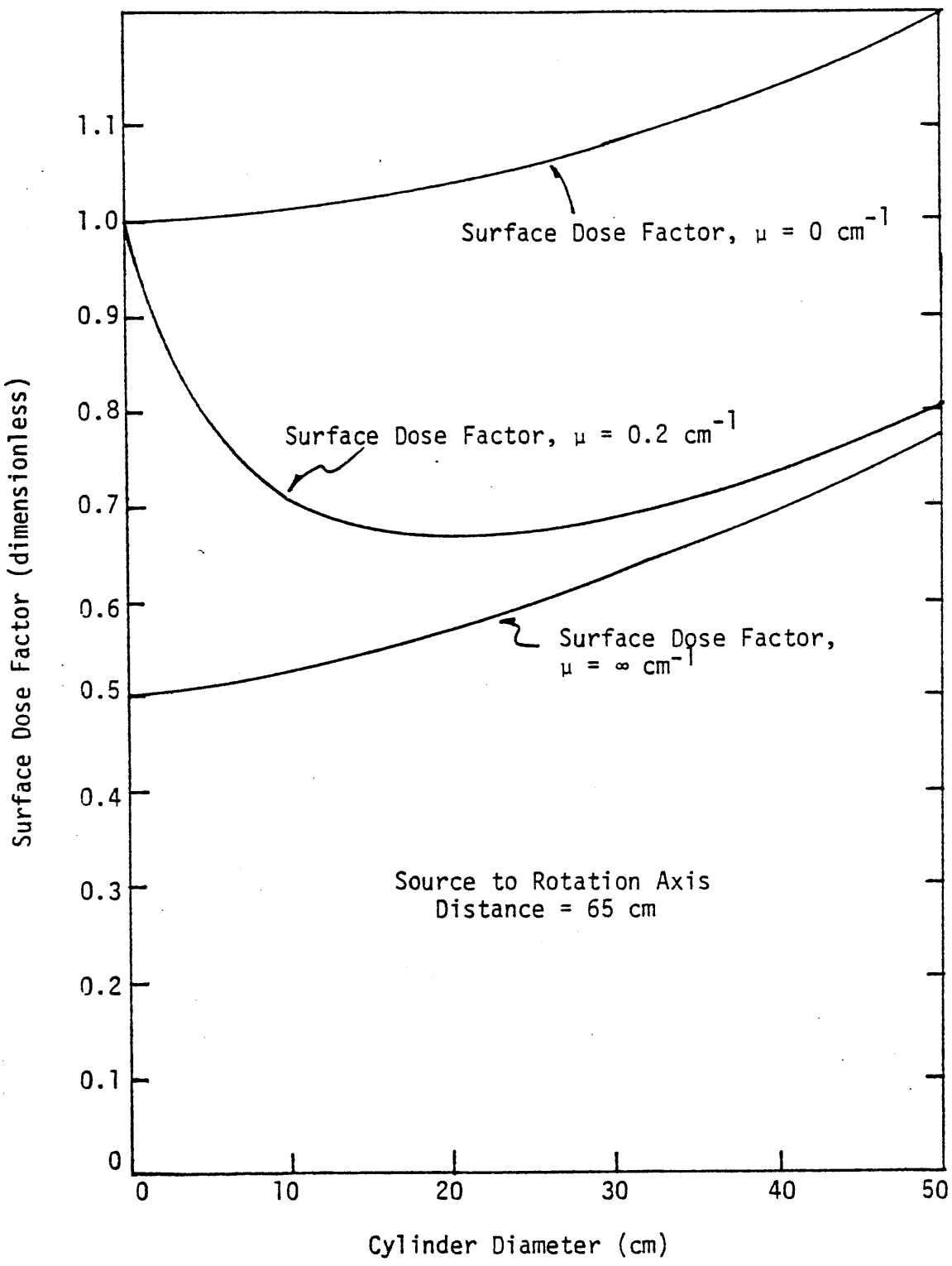

Figure B.1.2 The Surface Dose Factor versus cylinder diameter for three different attenuation coefficients, μ.

Figure B.1.2 shows that at a radius of 0 cm the surface factor has a value of 1. This is reasonable because in the transparent cylinder model the surface 'sees' the photons for the entire scan. As the radius increases the source-to-surface distance effect once again causes a steady rise in the surface dose factor.

Surface Dose, $\mu_{at} = 0.2\ cm^{-1}$

The true primary surface dose lies between the results of the transparent cylinder ($\mu_{at} = 0$) and the opaque cylinder ($\mu_{at} = \infty$) models. For water-like tissue the attenuation coefficient is approximately equal to 0.2 cm^{-1} in the diagnostic energy range. When using a finite nontrivial value for μ_{at}, Eq. (B.1.4) cannot be solved analytically. In this case the surface dose must be determined numerically. Figure B.1.2 illustrates the behavior of the surface dose factor as a function of the cylinder diameter. At the limit of very small cylinder diameter the water is relatively transparent because photons only have to traverse a few centimeters of water to reach the back side of the cylinder. As the radius increases the self-shielding is more effective and thus the calculated surface dose approaches the opaque cylinder case as the asymptotic limit.

In the diameter range between 10 cm and 35 cm the surface dose factor is relatively constant and approximately equal to 0.68. In the dose calculations in this research the primary surface dose was estimated by the expression:

$$D(\text{surface}) \simeq 0.68\ \Phi_R T \int_0^{E_{max}} S(E)\ \frac{\mu_{en}E}{\rho}\ dE$$

$$= 0.68\ \Phi_R T\ \frac{\displaystyle\int_0^{E_{max}} \phi(E)\ \exp(-\mu_F t_F)\ \frac{\mu_{en}E}{\rho}\ dE}{\displaystyle\int_0^{E_{max}} \phi(E)\ \exp(-\mu_F t_F)\ dE} \qquad \text{(B.1.9)}$$

$S(E)$ is the normalized bremsstrahlung spectrum distribution after filtration

$\phi(E)$ is the normalized bremsstrahlung spectrum distribution of the x-ray tube before filtration

$\mu_F t_F$ is the product of the beam filter attenuation coefficient at energy E and the thickness of the filter

T is the duration of the scan

Φ_R is the photon flux at the rotation axis after the inclusion of beam filtration.

In the experiment two filters alternatively filter the beam. If each filter is in the beam for the same amount of time during the scan, then Eq. (B.1.9) can be modified:

$$D(\text{surface}) = 0.68\ \frac{T}{2}\left[\Phi_{R1}\ \overline{\frac{\mu_{en}E_1}{\rho}} + \Phi_{R2}\ \overline{\frac{\mu_{en}E_2}{\rho}}\right] \qquad \text{(B.1.10)}$$

where

$$\overline{\frac{\mu_{en}E_1}{\rho}} = \frac{\int_0^{E_{max}} \phi(E)\, \exp(-\mu_{F1}t_{F1})\, \frac{\mu_{en}E}{\rho}\, dE}{\int_0^{E_{max}} \phi(E)\, \exp(-\mu_{F1}t_{F1})\, dE}$$

= the spectrum-1-averaged energy mass absorption coefficient-energy product (filter 1)

Φ_{R1} is the photon flux at the rotation axis after filtration with filter 1.

$$\overline{\frac{\mu_{en}E_2}{\rho}} = \frac{\int_0^{E_{max}} \cdot\ \phi(E)\, \exp(-\mu_{F2}t_{F2})\, \frac{\mu_{en}E}{\rho}\, dE}{\int_0^{E_{max}} \phi(E)\, \exp(-\mu_{F2}t_{F2})\, dE}$$

= the spectrum-2-averaged energy mass absorption coefficient-energy product (filter 2)

Φ_{R2} is the photon flux at the rotation axis after filtration with filter 2.

Equation (B.1.10) was used in this work to estimate dose from different filtration schemes of potential use in the experiment.

Centerline Dose, $\mu_{at} = 0.2\ cm^{-1}$

Another analytical dose estimate that is solvable in closed form is the centerline dose estimate. The dose kernel is given by the expression:

$$D(r=0) = \frac{\Phi_R T}{2\pi}\left(\frac{\overline{\mu_{en}E}}{\rho}\right)\int_0^{2\pi} \exp(-\bar{\mu}_{at}*R)\, d\theta$$

$$= \Phi_R T\left(\frac{\overline{\mu_{en}E}}{\rho}\right)\exp(-\bar{\mu}_{at}*R) \qquad \text{(B.1.11)}$$

The primary dose, therefore, is simply a function of the photon attenuation by the water and the spectrum-averaged energy absorption factor. Figure B.1.2 indicates the central geometry factor as a function of the water cylinder diameter assuming that $\bar{\mu}_{at}$ for the incident spectrum is equal to 0.2 cm^{-1}. It is seen that the primary photon dose at the center is always less than the primary dose at the surface. Because the surface dose is the largest dose given to the patient it is the limiting dose from a design standpoint. Therefore, the efforts at minimizing the dose received from CT scanning was aimed at reducing the surface dose.

Dose as a Function of Depth, $\mu_{at} = 0.2\ cm^{-1}$

To illustrate the behavior of the primary dose as a function of the radius within a water cylinder, numerical values of the surface dose factor were calculated for different geometries using μ_{at}=0.2 cm^{-1}. The numerical dose factor estimates are plotted in Fig. B.1.3 and tabulated in Table B.1.1. The contours shown correspond to the dose factor for a fixed radial position as a function of the cylinder radius (diameter). The contours all exhibit a similar exponential-like behavior. Therefore, interpolations for other radii would be easy and relatively accurate.

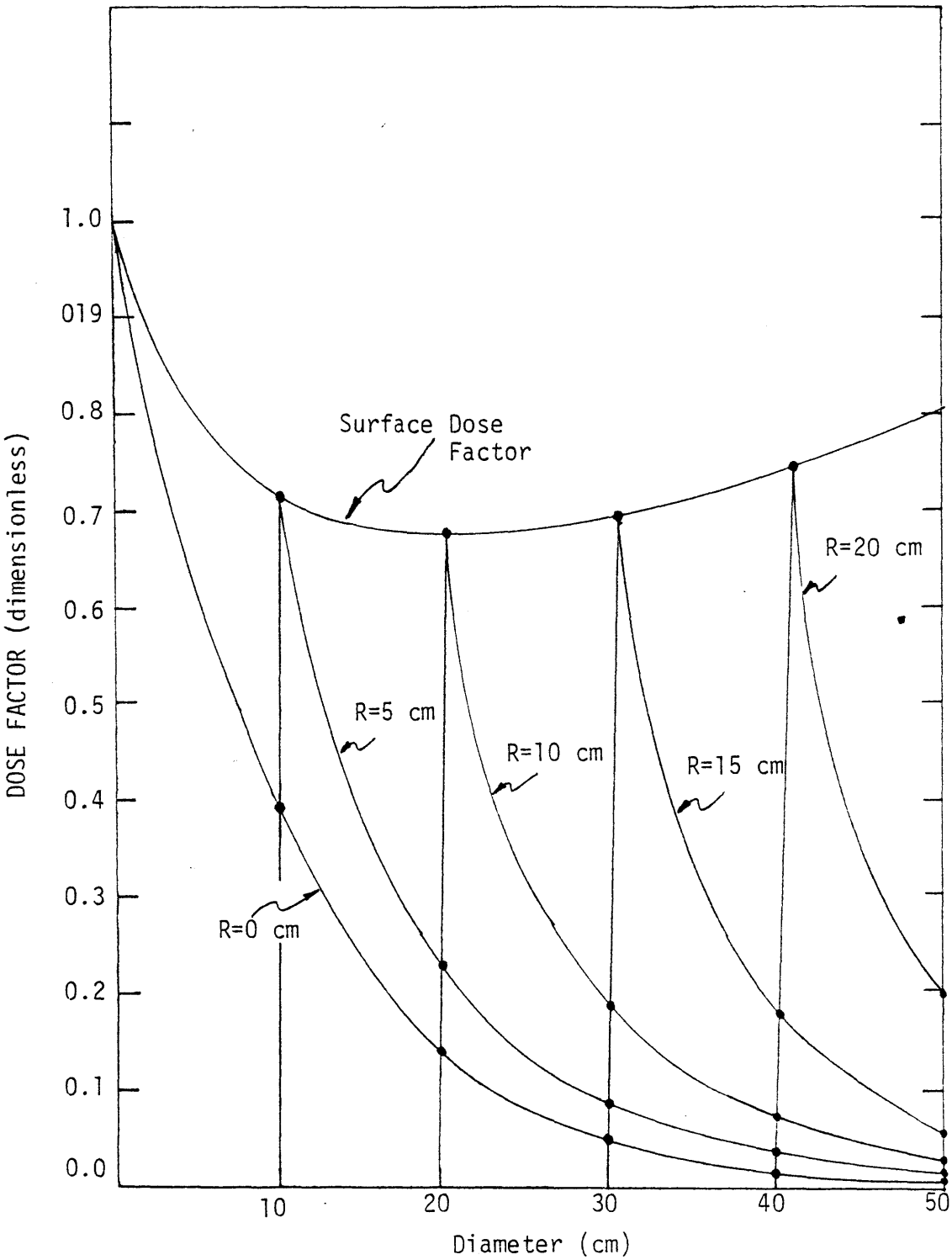

Figure B.1.3 Dose Factor versus cylinder diameter at different radial positions. μ_{at}=0.2 cm^{-1}.

Radial Position (cm)	Cylinder Radius (cm)					
	0	5	10	15	20	25
0	1.0	0.368	0.135	0.0498	0.0183	0.00673
5	x	0.706	0.2057	0.0725	0.02617	0.00952
10	x	x	0.663	0.1753	0.0595	0.02099
15	x	x	x	0.681	0.1731	0.0575
20	x	x	x	x	0.728	0.1817
25	x	x	x	x	x	0.7976

Table B.1.1 Dose factor estimates for different cylinder radii and radial positions assuming $\mu_{at} = 0.2\ cm^{-1}$.

Appendix B.2 Monte Carlo Photon Transport Determination of Dose Received from CT Scanning

Calculational Methods

This section presents the models and results of a previous Monte Carlo transport study (L.2) of photon dose received from CT scanning. Target geometries and x-ray beam spectra used in the simulations were chosen to approximately model the ICRU Reference Man (I.2) undergoing a CT scan. Diagnostic energy x-rays were modeled to interact with water-filled (as the tissue analog) right circular cylinders. The x-ray tube voltage-filtration combinations used in these transport studies are listed in Table B.2.1. Figure B.2.1 presents the geometry of the tally regions and Table B.2.2 gives the dimensions of the annular tally regions for the three radii studied. The size of the tally regions was chosen to vary inversely with the statistical accuracy in a region so as to keep the standard deviation of the estimated mean approximately constant throughout the phantom.

The Monte Carlo transport method models stochastic processes, such as photon-matter interactions, by simulation of the photon transmission process itself. Analytic means are not employed to determine the nature of interactions with a target, but rather individual photon "histories" are simulated. Typical computer simulations follow about 10,000 to 100,000 histories so that the investigator can get a statistically significant determination of the parameters of interest (dose, flux, attenuation, 'leakage', etc.). Rather than provide a full discussion of this method here, the reader is referred to the discussion by Carter and Cashwell in "Particle-Transport Simulation with the Monte Carlo Method" (C.6).

Harder Spectrum →

← Harder Spectrum — Kilovoltage used	Filtration used: 3 mm Aℓ	3 mm Aℓ/0.2 mm Cu	0.96 mm Cu
105 kVp	--- 15.16 cm = R ---	12.5 cm = R 15.16 cm = R 18.5 cm = R	--- 15.16 cm = R ---
20 kVp	--- --- ---	--- 15.16 cm = R ---	--- --- ---
140 kVp	--- --- ---	--- 15.16 cm = R ---	--- --- ---

Table B.2.1 X-ray tube voltage-filtration combinations studied in the Monte Carlo photon transport studies.

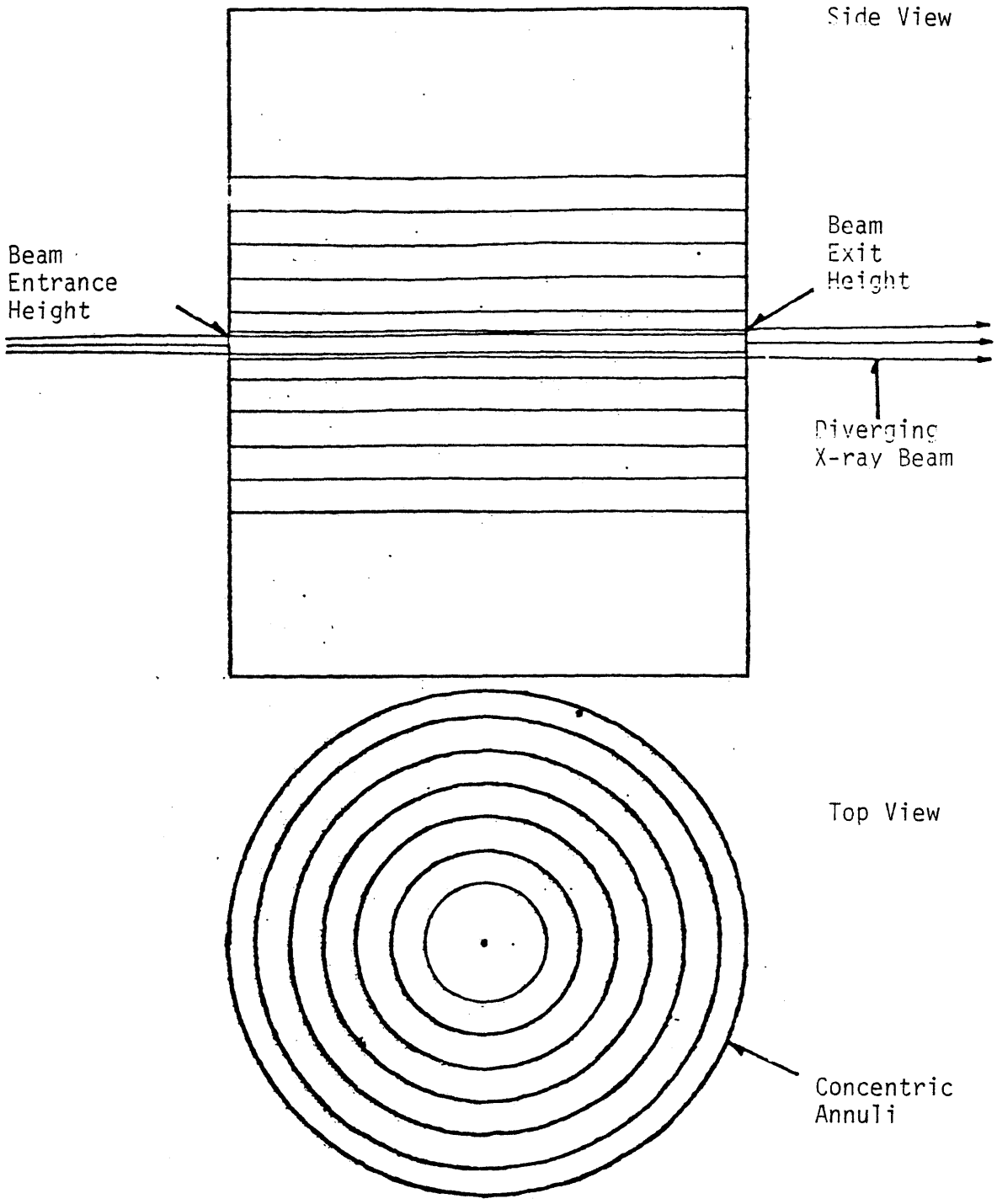

Figure B.2.1 Geometric tally regions used in the Monte Carlo program.

Cylinder Radius	Axial Dimensions (cm)			Radial Dimensions (cm)		
	(Z_1,Z_2)	ΔZ	$\bar{Z}$	(R_1,R_2)	Δr	$\bar{r}$
15.16	(-.4686,.4686)	.9372	0	(0,3.5)	3.5	2.333
	(.4686,.7476)	.279	.6081	(3.5,5.5)	2.0	4.574
	(.7476.2.0)	1.2524	1.3738	(5.5,7.5)	2.0	6.551
	(2.0,4.0)	2.000	3.000	(7.5,9.5)	2.0	8.539
	(4.0,6.0)	2.000	5.000	(9.5,11.5)	2.0	10.532
	(6.0,8.0)	2.000	7.000	(11.5,13.5)	2.0	12.527
	(8.0,10.0)	2.000	9.000	(13.5,15.16)	2.0	14.346
12.5						
	(-.493,.493)	.986	0	(0,3.5)	3.5	2.333
	(.493,.7232)	.2302	.6081	(3.5,5.5)	2.0	4.574
	(.7232,2.0)	1.2768	1.3616	(5.5,7.5)	2.0	6.551
	(2.0,4.0)	2.000	3.000	(7.5,9.5)	2.0	8.54
	(4.0,6.0)	2.000	5.000	(9.5,11.5)	2.0	10.532
	(6.0,8.0)	2.000	7.000	(11.5,12.5)	1.0	12.007
	(8.0,10.0)	2.000	9.000			
18.5	(-.4382,.4382)	.8764	0	(0,3.5)	3.5	2.333
	(.4382,.778)	.3338	.6081	(3.5,6.5)	3.0	5.15
	(.778, 2.00)	1.22	1.389	(6.5,8.5)	2.0	7.544
	(2.0,4.0)	2.000	3.000	(8.5,10.5)	2.0	9.535
	(4.0,6.0)	2.000	5.000	(10.5,12.5)	2.0	11.529
	(6.0,8.0)	2.000	7.000	(12.5,14.5)	2.0	13.529
	(8.0,10.0)	2.000	9.000	(14.5,16.5)	2.0	15.521
				(16.5,18.5)	2.0	17.520

Table B.2.2 Dimensions of the annular rings used for the different phantom sizes.

Figure B.2.2 presents a block diagram of the geometry condition and photon interaction tests used in the Monte Carlo study. During the simulation of photon histories there were three main 'tests' which occurred: geometry tests, interaction tests, and energy tests. The geometry tests in the simulation determined which tally region the photon was in and whether or not a photon escaped. The interaction tests chose the type of interaction a photon had with the target. If the photon was scattered, the code determined the energy deposited in the medium and also the angle of scatter. The Compton and Rayleigh scatter angle algorithm used in the simulation was based on a model developed by Everett, Cashwell and Turner at the Los Alamos Scientific Laboratory (E.4). The energy tests determined whether an incident or scattered photon had an energy of less than 20 keV. Photons with energy less than 20 keV were modeled to be perfectly absorbed within the water target.

In the study, 50,000 histories were simulated for the 15.16 cm radium cylinder simulations and 15,000 histories were simulated for the 12.5 cm and 18.5 cm radius cylinder simulations. In these studies the largest calculated standard deviation of the estimate of the mean was 5.4% for an in-beam tally region and 18.6% for an out-of-beam tally region.

To validate the photon transport code the Monte Carlo calculational results were compared to experimental measurements. Plotted in Fig. B.2.3 is the experimentally determined in-beam dose rate and the Monte Carlo estimate of the dose rate for a 105 kVp/0.96 mm Cu filter spectrum incident upon a 15.16 cm radius water cylinder. Because the

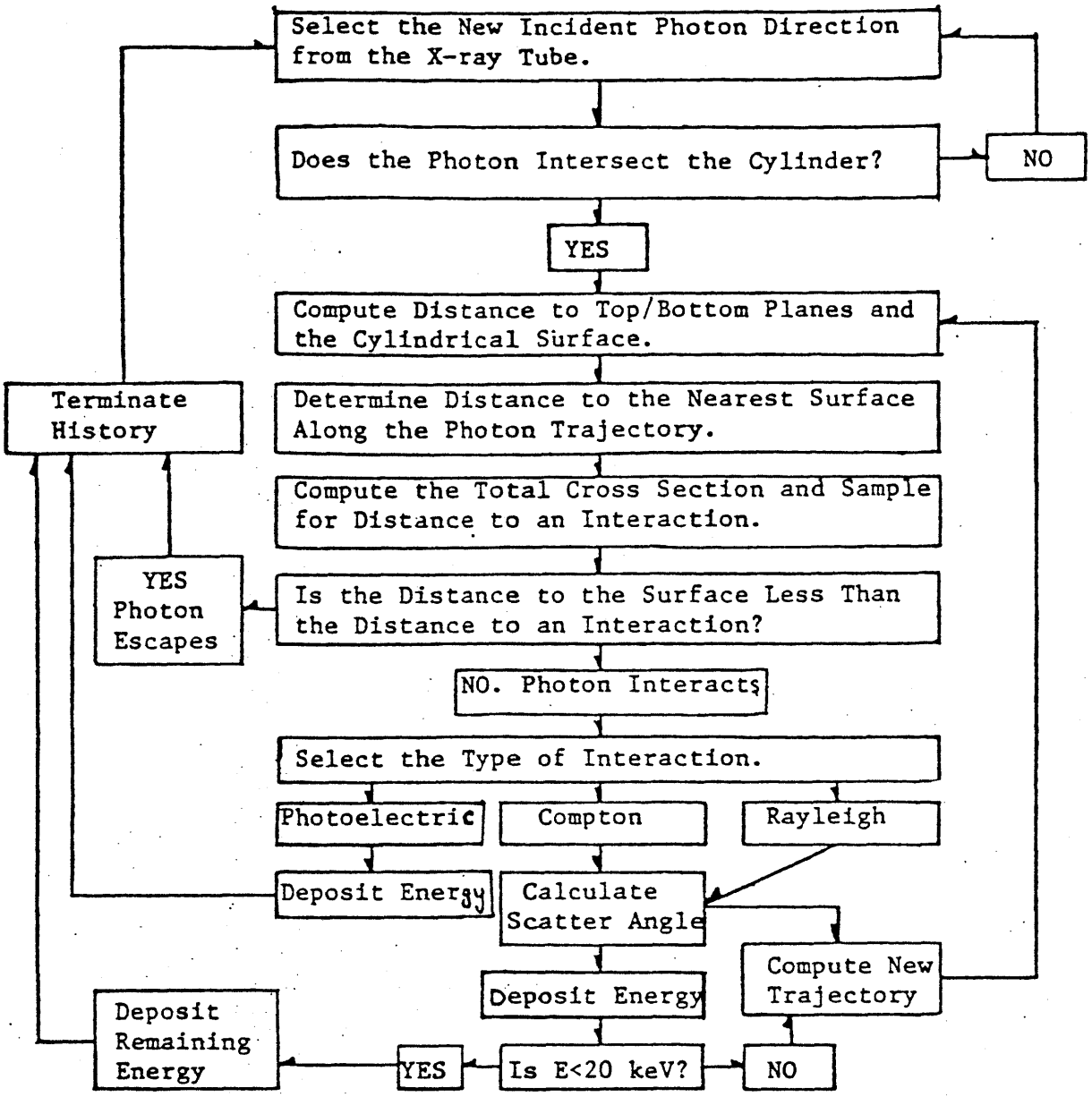

Figure B.2.2 Flow chart for geometry, photon interaction, and energy tests in the Monte Carlo transport program.

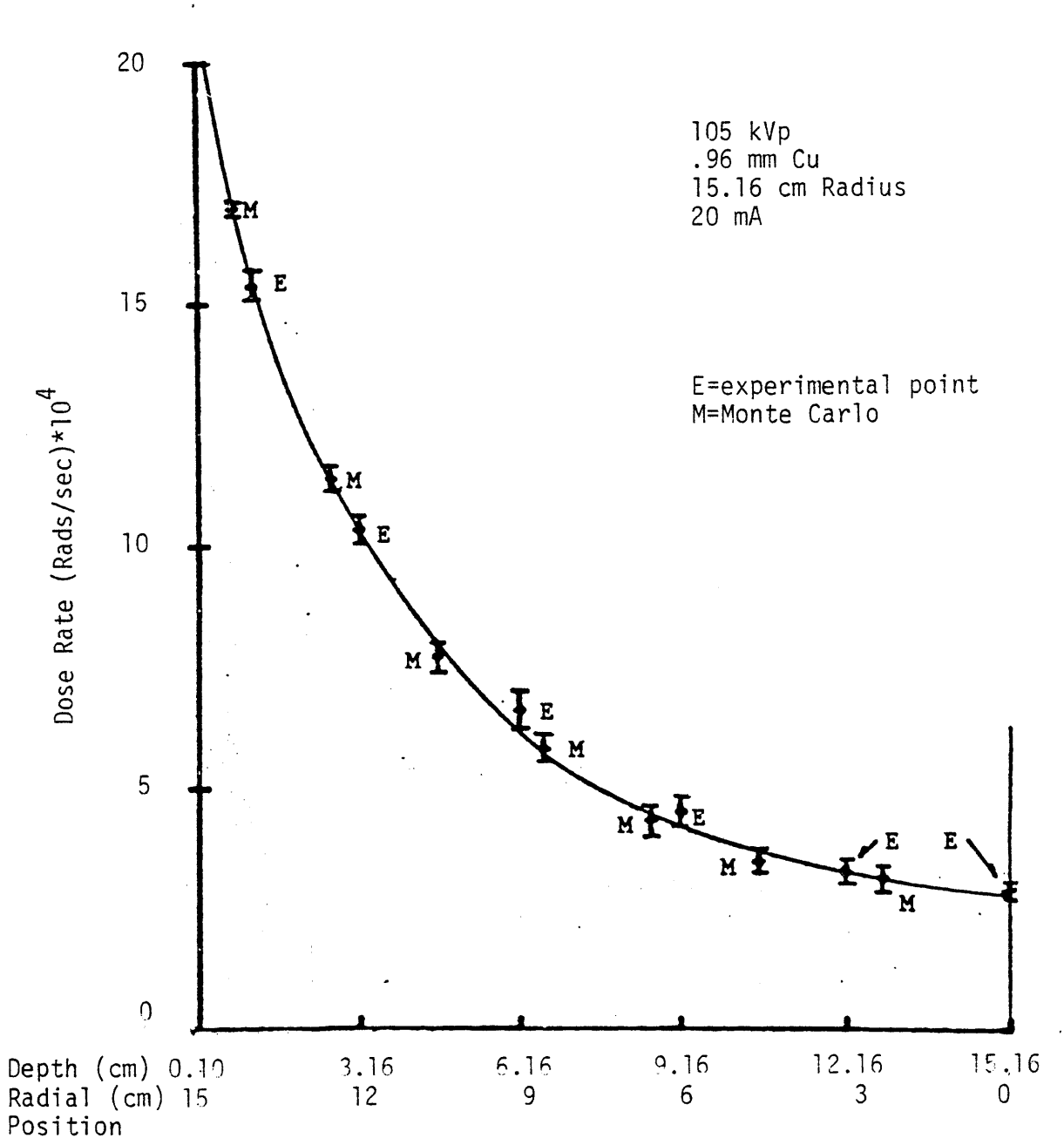

Figure B.2.3 Comparison of Experimental and Monte Carlo Results.

photon flux of the x-ray tube used in the experiment was only known approximately, the Monte Carlo simulation data had to be normalized. The Monte Carlo data indicated in Fig. B.2.3 was normalized to the experimental data at r = 14 cm. It is seen in the figure that the 2.9% standard deviation of the Monte Carlo result at the center of the cylinder is well within the 5.3% experimental error at the same position. Furthermore, there appear to be no apparent discrepancies between the Monte Carlo and experimental results.

It should be noted here that scanning procedures can vary quite significantly in the clinical environment. The clinician has the choice of the x-ray kVp, the x-ray tube electron current (ma) and the scan speed (seconds). The particular choice of the voltage, current, and speed of the scan depends upon the quality of the CT picture desired. For this reason it is important to present the computed dose relative to a clinically measureable quantity. A quantity that can be easily measured is the radiation exposure in Roentgens. Thus, the Monte Carlo results are presented in terms of rads per Roentgen where the exposure in Roentgens has been measured at the rotation axis of the scanner with no patient present within the scanner.

The Roentgen is defined as the amount of radiation required to produce 1 esu of charge in a cubic centimeter of dry air. To convert from Roentgens exposure to rads absorbed dose in water one can make use of the relation between exposure and absorbed dose for a monoenergetic x-ray source.

$$\text{Dose } (\text{Rads}_{H_2O}) = X(\text{Roentgens}_{air}) * 0.869 * \frac{(\mu_{en}/\rho)_{water}}{(\mu_{en}/\rho)_{air}}$$

$$= X * f \qquad \text{(B.2.1)}$$

where

0.869 is the exposure to absorbed dose in air conversion factor for diagnostic energy x-rays.

$\frac{(\mu_{en}/\rho)_{water}}{(\mu_{en}/\rho)_{air}}$ is the ratio of the mass energy absorption coefficients for water and air.

X is the measured exposure in Roentgens.

The variable, f, is the rad/Roentgen conversion factor. As seen in Fig. B.2.4, it is dependent upon the incident x-ray energy.

Since a monoenergetic x-ray source is not used experimentally, the rad/Roentgen conversion factor used to convert the experimental data must be a spectrally-weighted average. So in general Eq. (B.2.1) should read

$$\text{Dose}(\text{Rads}_{H_2O}) = X(\text{Roentgens}_{air}) * 0.869 \frac{\overline{\mu_{en}{}^{E/\rho}}_{water}}{\overline{\mu_{en}{}^{E/\rho}}_{air}} \qquad \text{(B.2.2)}$$

where

$\overline{\mu_{en}/\rho}$ is the spectrum-averaged energy absorption coefficient-energy product.

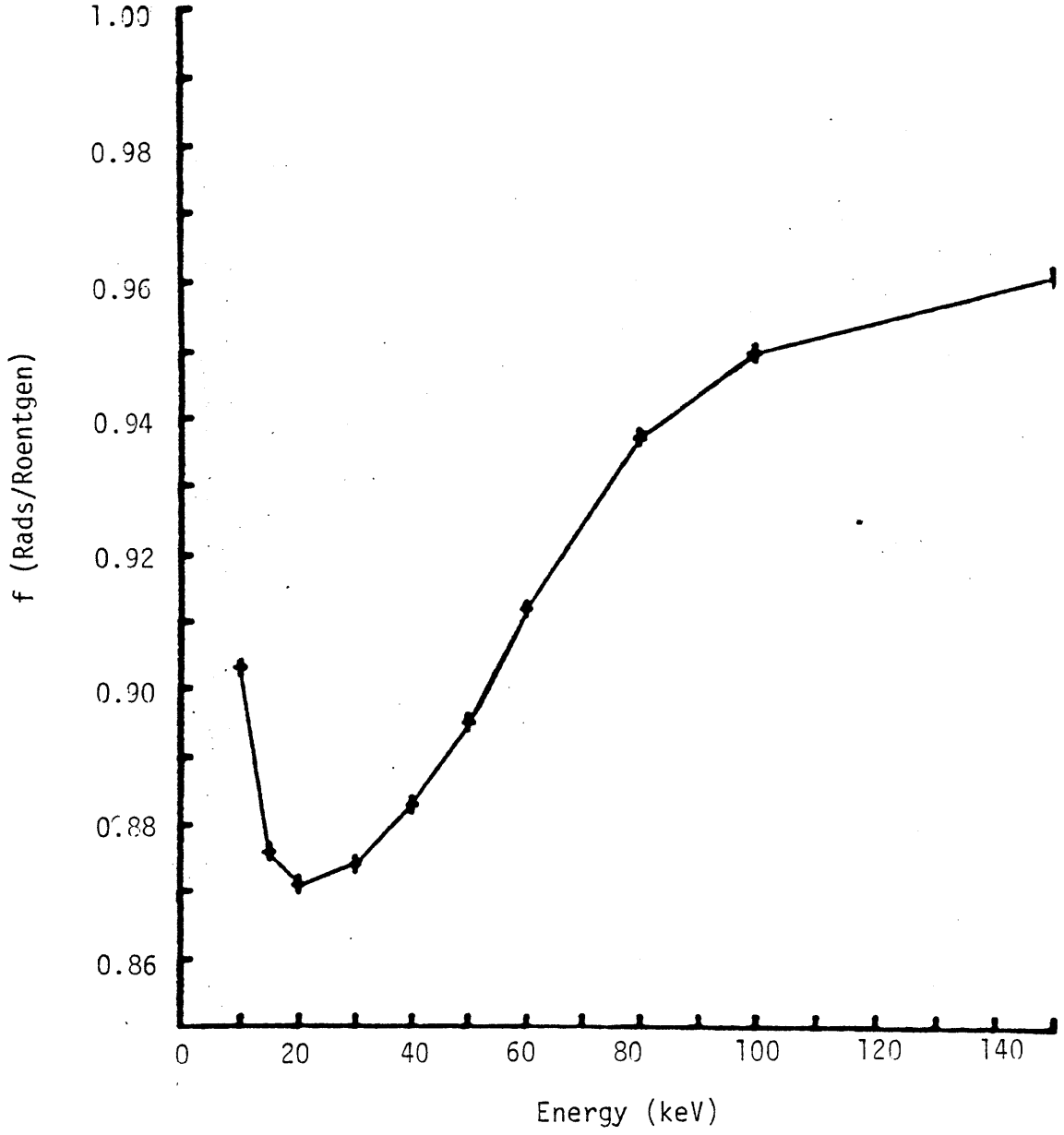

Figure B.2.4 Rad/Roentgen, f, Factor versus X-ray Energy.

$$\overline{\mu_{en}E/\rho} = \int_0^E S(E) * E * \mu_{en}(E)/\rho \, dE$$

S(E) is the normalized incident photon spectrum.

Table B.2.3 presents the spectrum-weighted quantities of interest of the spectra used in the Monte Carlo transport studies.

Calculational Results

Referring back to Fig. B.2.3 it is seen that the in-beam dose decreases monotonically however it does not decrease exponentially as a function of distance from the surface. This non-exponential behavior is due to the relative rotation of the photon source with respect to the patient. Hence, the dose at a point, $D(r,\theta)$, is due to contributions from photons entering the target from both the 'near' side and the 'far' side with respect to the position (r,θ). This phenomenon can be shown to occur in analytic calculations of primary doses from CT.

The out-of-beam dose can not be determined analytically; however, the Monte Carlo simulations can determine the out-of-beam dose. Figure B.2.5 presents the out-of-beam calculational results for a 105 kVp/0.96 mm Cu filtered x-ray spectrum incident upon a 15.16 cm radius cylinder. At the 0.608 cm axial position just above the in-beam slice, the dose is high at the surface and then decreases because at this position the diverging photon beam (as seen in Fig. B.2.1) is partly in and partly out of this tally region. In the other tally regions, which are completely out of the beam, a strikingly different

Spectrum \ Property	$\bar{\mu}_a$	$\bar{\mu}_e$	$\bar{E}$	Roentgen/flux $\frac{R\text{-}cm^2\text{-}sec}{\gamma}$
105 kVp 0.96 mmCu	0.1979	0.0305	66.57	$3.521 * 10^{-11}$
105 kVp 3 mmAl	0.2103	0.03852	60.21	$4.028 * 10^{-11}$
105 kVp 3 mmAl/.2 mmCu	0.2099	0.0379	60.24	$3.968 * 10^{-11}$
120 kVp 3 mmAl/.2 mmCu	0.2082	0.0369	61.01	$3.91 * 10^{-11}$
140 kVp 3 mmAl/.2 mmCu	0.2053	0.03597	62.88	$3.926 * 10^{-11}$

Table B.2.3 Spectrum-weighted quantities of interest for data conversion and interpolation.

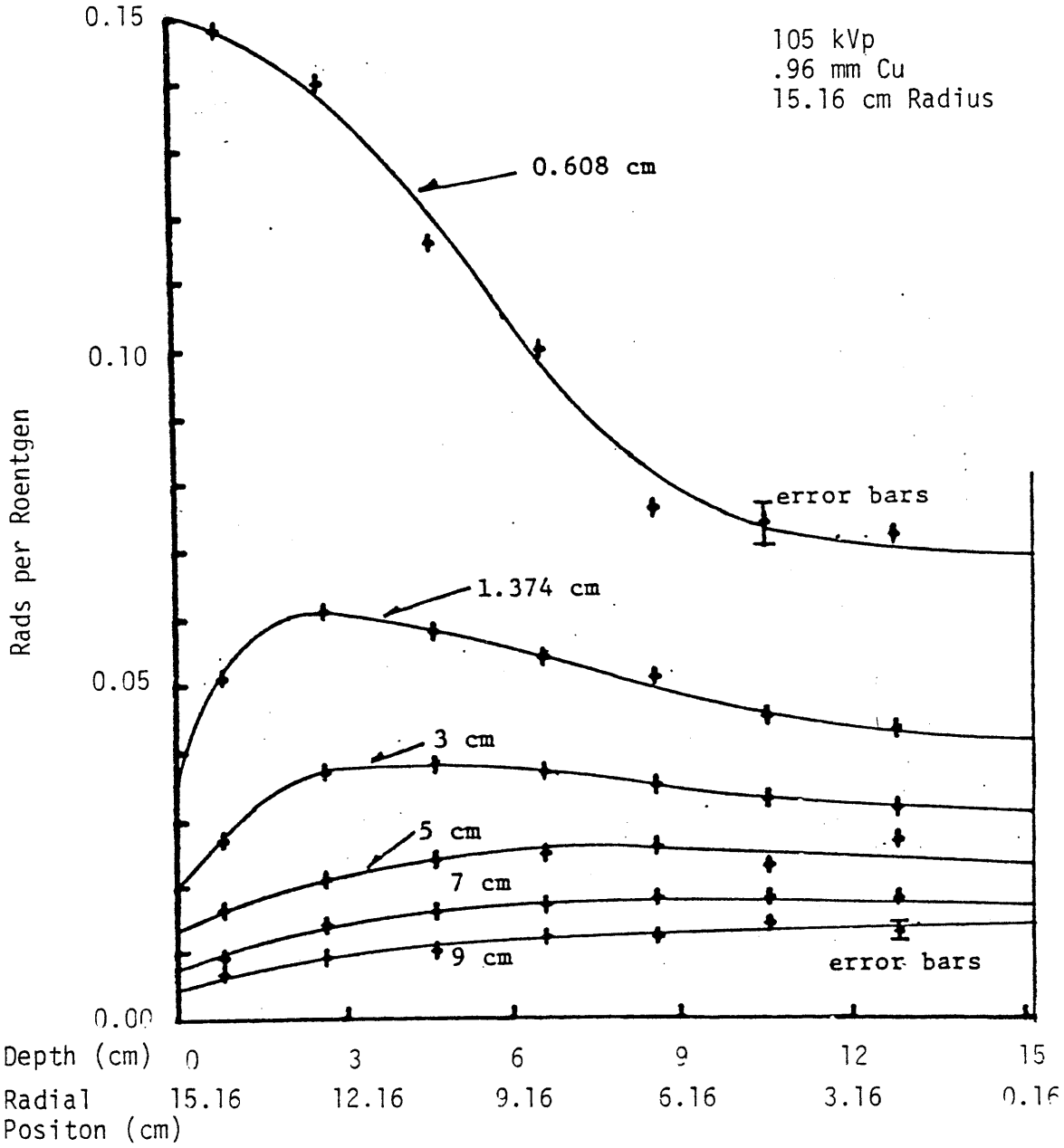

Figure B.2.5 Dose per Roentgen versus depth at various axial heights.

behavior is observed. The dose is seen to start at a value approximately half of the maximum value, maximize, and then slowly decrease. The low value near the surface is due to the flux leakage at the surface - a behavior similar to the neutron leakage in neutron diffusion theory (H.8). At the out-of-beam positions it is reasonable to consider the photon transport as a diffusion process because the photon scattering cross section is much larger than the photon absorption cross section. The flattening of the 'peak' near the surface, as the axial position increases, is due to the randomization of the radial intensity distribution as one gets further away from the in-beam slice "source".

The implication of the high degree of scattered radiation present in CT scanning is that one cannot ignore this radiation when estimating patient dose - especially when scanning several slices. Illustrated in Fig. B.2.6 is a comparison of dose estimates when ignoring and including the effect of scattered radiation. In this case 10 contiguous (not overlapping - but adjacent) scans were assumed to have been performed. It is seen that the dose estimate would have an error of more than 50% if one were to ignore scattered radiation. For a more complete treatment of the effect of scattered radiation on dose estimates the reader is referred to Reference (L.2).

For convenience the calculational results of the Monte Carlo studies are presented in Tables B.2.4 through B.2.10 in rads per Roentgen. Qualitatively there are no dramatic differences between the calculational results of the different spectra.

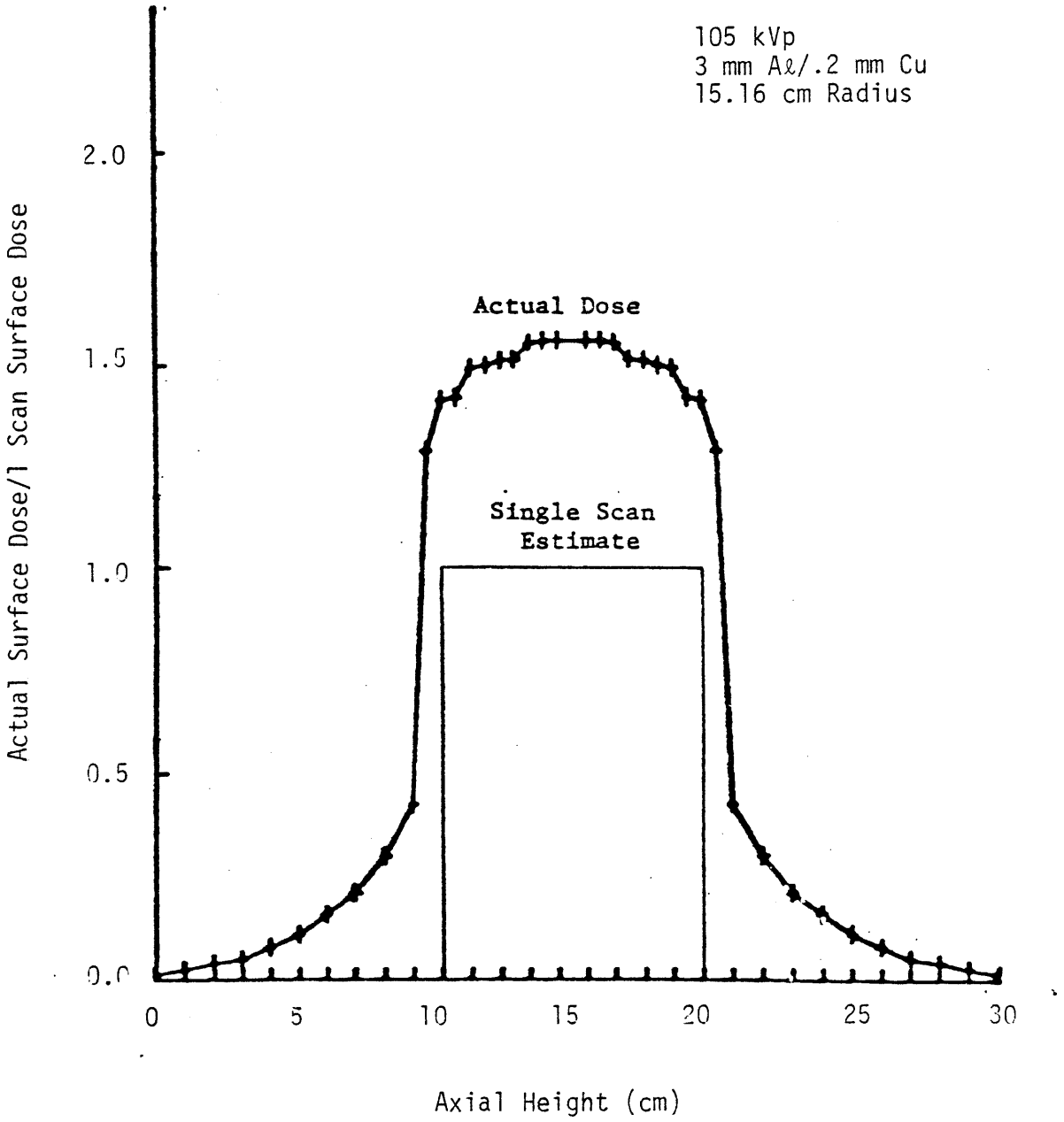

Figure B.2.6 Fraction of Actual Surface Dose to Single Scan Dose versus Axial Height. (10 scans at 1 cm scan separation).

<r> \ $\bar{Z}$	0.0	0.6081	1.3738	3	5	7	9
2.333	.0724	.0361	.0296	.0210	.0147	.0132	.0061
4.574	.089	.0487	.0258	.0237	.0151	.0110	.0068
6.551	.108	.0647	.0352	.0261	.018	.0112	.0061
8.539	.147	.0884	.0394	.0283	.0161	.0118	.0074
10.532	.204	.0973	.043	.029	.0172	.0094	.0069
12.527	.339	.125	.0507	.028	.0138	.0087	.0055
14.346	.537	.1353	.0491	.0223	.0113	.006	.0037

Table B.2.4 Rads per Roentgen versus average radial, <r>, and axial, $\bar{Z}$, position. 15.16 cm radius, 105 kVp, 3 mm Aℓ filtration.

<r> \ $\bar{Z}$	0	0.6081	1.3738	3	5	7	9
2.333	.062	.0566	.028	.0255	.0162	.0135	.0068
4.574	.096	.063	.0316	.0298	.0176	.013	.0094
6.551	.120	.061	.0366	.0272	.0192	.0137	.0083
8.539	.165	.084	.0459	.0298	.0194	.0139	.0086
10.532	.214	.0998	.0474	.0308	.0174	.0131	.0082
12.527	.338	.1248	.0512	.0314	.0162	.0096	.0064
14.346	.518	.1036	.0484	.0238	.0131	.0079	.0046

Table B.2.5 Rads per Roentgen versus average radial, <r>, and axial, $\bar{Z}$, position. 15.16 cm radius, 105 kVp, 3 mm Aℓ/0.2 mm Cu filtration.

<r> \ $\bar{Z}$	0	0.6081	1.3738	3	5	7	9
2.333	.104	.072	.043	.0317	.027	.018	.013
4.574	.116	.074	.045	.033	.023	.018	.014
6.551	.144	.076	.051	.035	.026	.018	.012
8.539	.191	.100	.054	.037	.025	.017	.012
10.532	.255	.116	.058	.038	.024	.016	.010
12.527	.376	.140	.061	.037	.021	.014	.009
14.346	.562	.148	.051	.0272	.0163	.00904	.0068

Table B.2.6 Rads per Roentgen versus average radial, <r>, and axial, $\bar{Z}$, position. 15.16 cm radius, 105 kVp, 0.96 mm Cu filtration.

<r> \ $\bar{Z}$	0	0.6081	1.3738	3	5	7	9
0.2333	.0807	.0422	.0359	.0268	.0194	.0154	.0133
0.4574	.0921	.0704	.0328	.0285	.0159	.0147	.0103
0.6551	.1179	.0741	.0422	.0253	.0216	.0316	.0085
0.8539	.1604	.0734	.0441	.0308	.0205	.0134	.0089
10.532	.2204	.1017	.0517	.0324	.0183	.0123	.0085
12.527	.3556	.1244	.0509	.0292	.0183	.0111	.0076
14.346	.5442	.144	.0453	.0241	.0137	.0077	.0045

Table B.2.7 Rads per Roentgen versus average radial, <r>, and axial, $\bar{Z}$, position. 15.16 cm radius, 120 kVp, 3 mm Aℓ/0.2 mm Cu filtration.

<r> \ $\bar{Z}$	0	0.6081	1.3738	3	5	7	9
0.233	.0879	.0557	.0348	.0266	.0209	.0155	.0150
4.574	.1079	.0674	.0319	.0284	.0173	.0156	.0093
6.551	.1268	.0771	.0414	.0272	.0221	.0132	.0094
8.539	.1601	.0777	.0443	.0323	.0200	.0132	.0108
10.532	.2236	.1003	.0542	.0332	.0193	.0133	.009
12.527	.3662	.1229	.0532	.0294	.0187	.0115	.0082
14.346	.5436	.1325	.0465	.0251	.0136	.008	.0052

Table B.2.8 Rads per Roentgen versus average radial, <r>, and axial, $\bar{Z}$, position. 15.16 cm radius, 140 kVp, 3 mm Aℓ/0.2 mm Cu filtration.

<r> \ $\bar{Z}$	0	0.6081	1.3616	3	5	7	9
2.333	.124	.0977	.0477	.0329	.0204	.0162	.0120
4.574	.1558	.0797	.0475	.0358	.0237	.0139	.0094
6.551	.1935	.1041	.054	.0326	.0206	.0129	.0097
8.54	.2629	.122	.0566	.0371	.0187	.0131	.0074
10.532	.3858	.1473	.0566	.0288	.0169	.0087	.0067
12.007	.565	.1424	.0441	.0242	.0133	.0071	.0042

Table B.2.9 Rads per Roentgen versus average radial, <r>, and axial, $\bar{Z}$, position. 12.5 cm radius, 105 kVp, 3 mm Aℓ/0.2 mm Cu filtration.

<r> \ $\bar{Z}$	0	0.6081	1.389	3	5	7	9
2.333	.051	.0385	.0188	.0153	.0136	.0106	.0084
5.14	.055	.0396	.0228	.019	.0153	.0101	.009
7.544	.062	.0481	.0267	.0208	.0146	.0113	.0056
9.535	.103	.0578	.0328	.0228	.0169	.010	.0071
11.529	.147	.0683	.0385	.0263	.0156	.0122	.0089
13.525	.206	.0814	.0481	.0282	.0176	.0100	.0076
15.521	.321	.0991	.0505	.0289	.0168	.0093	.0060
17.52	.519	.1282	.0462	.0249	.0127	.0074	.0047

Table B.2.10 Rads per Roentgen versus average radial, <r>, and axial, $\bar{Z}$, position. 18.5 cm radius, 105 kVp, 3 mm Aℓ/0.2 mm Cu filtration.

Appendix B.2A Listing of the Three-dimensional Monte Carlo Photon Transport Programs - TOMODOSE

Purpose

To compute the dose versus position within a patient undergoing a CT scan. Unweighted Monte Carlo photon transport methods are used to compute the radiation absorbed dose from primary and secondary x-rays in the scan procedure. The program computes in double precision.

Program Name	Function
Main Program:	
LMAIN	- to compute the dose from CT scanning using Monte Carlo methods.
Subroutines:	
GEOM	- to compute the three-dimensional coordinates and directions of the interacting photons.
ANGLIN	- to determine the initial direction of the incident photon.
EDIST	- to determine the energy of the incident photon.
CXDIST	- to determine the interaction cross sections of the target for a photon of a given energy.
RAND32	- to compute a 32 bit random number.
TALLY	- to tally the dose in a region when a photon deposits energy within that region.
FORT.LB	- FORTRAN IV mathematics library.

Main Program LMAIN:

```
      COMPILER DOUBLE PRECISION
C 10  MONTE CARLO CALCULATION OF X-RAY DOSE
C 20  IN COMPUTERIZED AXIAL TOMOGRAPHY
C30   ------------------------------------
C 203  THIS PROGRAM IS DESIGNED TO CALCULATE
C204  PATIENT DOSE (IN RADS) FROM CAT SCANNING.
C 205  HOMOGENEOUS AND INHOMOGENEOUS PHANTOM STUDIES
 C 206  WILL BE DONE. THIS PROGRAM IS A RESULT OF
C 207  PREVIOUS SIMPLER PROGRAMS WHICH HELPED THE
C 208  AUTHOR OF THIS PROGRAM TO LEARN THE MONTE
C 209  CARLO METHOD.
C
C
C 212  INITIALIZE THE VARIABLES:
C      -------------------------
C 257  ENERGY TALLY VARIABLE=TAL
C 258  SQRD TALLY VARIABLE=TALSQ
C 259  NUMBER EVENTS PER VOLUME=EVNTPV
CH     DIMENSION TAL(16,1,13),TALSQ(16,1,13),EVNTPV(16,1,13)
 CH     DIMENSION IMPTAL(16,1,13),RTAL(0:16),TLSQ2(5,1,13)
 CH12   DIMENSION TAL(13,1,13),TALSQ(13,1,13),EVNTPV(13,1,13)
 CH12   DIMENSION IMPTAL(13,1,13),RTAL(0:13),TLSQ2(5,1,13)
        DIMENSION TAL(19,1,13),TALSQ(19,1,13),EVNTPV(19,1,13)
        DIMENSION IMPTAL(19,1,13),RTAL(0:19),TLSQ2(5,1,13)
        COMMON/VAR/A,A1,A0,C8,C7,C6,C5,C9,C1,C0
       COMMON/VAR/D8,D3,D9,D,DN0,D7,D50,DL0,D1,D2,DL
        COMMON/VAR/EVNTPV,E1,E2,E,E0,G8,G2,G3,G4,G5,G6,G9,G7
        COMMON/VAR/HO,H,I,IA(2),II(2),IZTAL,IRTAL,IIRTAL,J
        COMMON/VAR/PI,P0,P,P1,R,S2,S9,S1,S3,S4,TAL,TALSQ
        COMMON/VAR/I,I8,I9,I1,J,J1,J2,V0,V1,V2,V0,I,=2,=0
        COMMON/VAR/X0,Y0,YEL,Y1,Z8,Z9,Z0,Z1
       COMMON/VAR/U3,UA,U5,U6,U7,V3,V4,V5,V6,V7
       COMMON/VAR/=3,=4,=5,=6,=7
      COMMON/VAR/IMPTAL,IIERM,RIIE,RDOJI,RTAL,RADIA,VTAL
        COMMON/VAR/SMPVAR,VARSE,STDV,TLSQ2
       DO 280 J=1,13
       DO 280 I=1,5
       TLSQ2(I,1,J)=0D0
280    CONTINUE
       RTAL(0)=0D0
CH     DO 290 I=1,16
CH12   DO 290 I=1,13
       DO 290 I=1,19
       RTAL(I)=RTAL(I-1)+1D0
       DO 290 J=1,13
       TAL(I,1,J)=0D0
       TALSQ(I,1,J)=0D0
       EVNTPV(I,1,J)=0D0
       IMPTAL(I,1,J)=0D0
C 285  THE ARRAYS ARE NOW INITIALIZED.
90     CONTINUE
       ACCEPT"NUMBER OF HISTORIES=",H
       DATA Z8/-20D0/Z9/20D0/R/1E.5D0/S2/0D0/HO/0D0/J3/0D0/
         DATA A0/-66.04D0/Y0/0D0/Z0/0D0/PI/3.1415926535897900/
         DATA D/0D0/IA(1)/1/IA(2)/13/
         IF(D.EQ.0D0) GOTO 615
C 605  THE PHANTOM,SOURCE,AND DETECTOR ARE NOW
C 606  READY FOR PHOTONS
C 607
C 608  NOW FROM STEPS 650 TO 1000 WE ARE CONTROLING
 C 609  THE PROGRAM TO CALCULATE THE "MONTE CARLO"
 C 610  HISTORIES OF THE PHOTONS. HOW MANY HISTORIES HAVE
 C      BEEN DONE?
       HCNT=0D0
       QPCNT=0D0
```

```
615     HO=HO+1DO
        HCNT=HCNT+1DO
        UPCNT=UPCNT+1DO
        IF(UPCNT.NE.2000)GOTO 614
        UPCNT=0DO
        CALL GETIM(IHR,IMIN,ISEC)
        TYPE IHR,IMIN,ISEC
614     CONTINUE
        TYPE "HO=",HO
        D3=D3+1DO
C       RESET(GET) THE TERMINATION VARIABLE (TERM=0)
         ITERM=0
        IF(HO.LE.H) GOTO 650
        IF(HO.GT.H) GOTO 990
C 642   SELECT THE INCIDENT ANGLE AND POSITION OF
C 643   THE PHOTON AND SOURCE IN SERIES 4000.
C 650   ANGLIN IS THE 4000 SERIES
650     CALL ANGLIN
C 655   NEXT WE SELECT THE INCIDENT PHOTON ENERGY
C 656   FROM THE X-RAY TUBE BY GOING TO THE
C 657   SERIES 5000
C 660   EDIST IS THE 5000 SERIES
        CALL EDIST
C 665   NOW, KNOWING THE INITIAL ENERGY(E2, WE
C 666   ARE GOING TO FOLLOW THE FLOW-CHART OF 10/16/77
 C 667   AND DETERMINE THE NEAREST SURFACE WE ARE
C 668   POINTING AT.
C 670   GEOM IS THE 1000 SERIES
670     CALL GEOM
C 675   WE NOW KNOW WHAT WE ARE POINTING AT AND THE DISTANCE.
 C 677   NOW CALCULATE THE PROBABILITY OF GETTING TO THAT
 C 679   SURFACE.(AND CALCULATE PHOTO- AND COMPTON C.S.'S)
 C 680   CXDIST IS THE 6000 SERIES
        CALL CXDIST
C 685   CHECK TO SEE IF THE EVENT MAKES IT TO THE NEXT SFC.
         IF(DNO.EQ.0DO) GOTO 715
        IF(DNO.EQ.1DO) GOTO 701
701     IF(PO.EQ.0DO) GOTO 615
C 710   IF WE GET TO THIS POINT, THAT MEANS THAT
C 711   EITHER (THE PHOTON IS GONE OR THE EVENT
C 712   DIDN'T MAKE IT TO THE NEXT SURFACE.
C 713   CHECK THIS FACT OUT FIRST!
715.    CONTINUE
        IF(PO.GE.2DO) GOTO 3000
        IF(PO.EQ.1DO) GOTO 670
       IF(PO.EQ.0DO) GOTO 615
C980    WE HAVE NOW CALCULATED ALL OF THE DESIRED
 C 981   PHOTON HISTORIES.
990     CONTINUE
800     ACCEPT"NORMALIZED?,1=YES,0=NO",IYES
        IF(IYES.EQ.1) GOTO 820
        ACCEPT "NORMALIZATION CONSTANT=",CNORM
        J=1
801     IF(J.EQ.1) RIE=2DO*((66.04DO-R)/108.6DO)
         IF(J.EQ.3) RIE=2DO*(2DO*R/108.6DO)
        IF(J.EQ.5) RIE=4DO-(2DO*(66.04DO+R)/108.6DO)
         IF(J.EQ.7) RIE=4.0DO
        IF(J.EQ.9) RIE=4.0DO
        IF(J.EQ.11) RIE=4.0DO
        IF(J.EQ.13) RIE=4.0DO
        IF(J.NE.1) GOTO 810
C       TALLIES FOR RADIUS=15.16CM WATER PHANTOM.
 CH      WRITE(12)"R=",R,Z=1"
CH      ZAP=(IAL(6,1,1)+IAL(15,1,1)+IAL(14,1,1)
CH     C         +IAL(13,1,1))*(CNORM)/(RIE*PI*12.25DO)
```

```
C H       WRITE(12)"R=12,Z=1"
CH        ZAP=(IAL(12,1,1)+IAL(11,1,1))*(CNORM)/(HITE*PI*18DO)
 CH        WRITE(12)ZAP
CH        WRITE(12)"R=10,Z=1"
CH        ZAP=(IAL(10,1,1)+IAL(9,1,1))*(CNORM)/(HITE*PI*26DO)
 CH        WRITE(12)ZAP
CH        WRITE(12)"R=8,Z=1"
CH        ZAP=(IAL(8,1,1)+IAL(7,1,1))*(CNORM)/(HITE*PI*34DO)
 CH        WRITE(12)ZAP
CH        WRITE(12)"R=6,Z=1"
CH        ZAP=(IAL(6,1,1)+IAL(5,1,1))*(CNORM)/(HITE*PI*42DO)
 CH        WRITE(12)ZAP
CH        WRITE(12)"R=4,Z=1"
CH        ZAP=(IAL(4,1,1)+IAL(3,1,1))*(CNORM)/(HITE*PI*50DO)
 CH        WRITE(12)ZAP
CH        WRITE(12)"R=2,Z=1"
CH        ZAP=(IAL(2,1,1)+IAL(1,1,1))*(CNORM)/(HITE*PI*47.5756DO)
 CH        WRITE(12)ZAP
C         TALLIES FOR RADIUS=18.5CM WATER CYLINDER
          WRITE(12)"R=19,Z=1"
          ZAP=(IAL(19,1,1)+IAL(18,1,1)+IAL(17,1,1)+IAL(16,1,1))*
      C  (CNORM)/(HITE*PI*12.25DO)
          WRITE(12)ZAP
          WRITE(12)"R=15,Z=1"
          ZAP=(IAL(15,1,1)+IAL(14,1,1)+IAL(13,1,1))*(CNORM)/(HITE*PI*30DO)
         WRITE(12)ZAP
          WRITE(12)"R=12,Z=1"
          ZAP=(IAL(12,1,1)+IAL(11,1,1))*CNORM/(HITE*PI*30DO)
          WRITE(12)ZAP
          WRITE(12)"R=10,Z=1"
          ZAP=(IAL(10,1,1)+IAL(9,1,1))*(CNORM)/(HITE*PI*38DO)
          WRITE(12)ZAP
          WRITE(12)"R=8,Z=1"
          ZAP=(IAL(8,1,1)+IAL(7,1,1))*(CNORM)/(HITE*PI*46DO)
          WRITE(12)ZAP
          WRITE(12)"R=6,Z=1"
          ZAP=(IAL(6,1,1)+IAL(5,1,1))*(CNORM)/(HITE*PI*54DO)
         WRITE(12)ZAP
          WRITE(12)"R=4,Z=1"
          ZAP=(IAL(4,1,1)+IAL(3,1,1))*(CNORM)/(HITE*PI*62DO)
          WRITE(12)ZAP
          WRITE(12)"R=2,Z=1"
          ZAP=(IAL(2,1,1)+IAL(1,1,1))*(CNORM)/(HITE*PI*70DO)
          WRITE(12)ZAP
C         TALLIES RADIUS=12.5CM WATER CYLINDER
CH12      WRITE(12)"R=13,Z=1"
CH12      ZAP=(IAL(13,1,1)+IAL(12,1,1)+IAL(11,1,1)+IAL(10,1,1))
 CH12       C       *(CNORM)/(HITE*PI*12.25DO)
CH12      WRITE(12)ZAP
CH12      WRITE(12)"R=9,Z=1"
CH12      ZAP=(IAL(9,1,1)+IAL(8,1,1))*CNORM/(HITE*PI*18DO)
 CH12      WRITE(12)ZAP
CH12      WRITE(12)"R=7,Z=1"
CH12      ZAP=(IAL(7,1,1)+IAL(6,1,1))*CNORM/(HITE*PI*26DO)
 CH12      WRITE(12)ZAP
CH12      WRITE(12)"R=5,Z=1"
CH12      ZAP=(IAL(5,1,1)+IAL(4,1,1))*CNORM/(HITE*PI*34DO)
 CH12      WRITE(12)ZAP
CH12      WRITE(12)"R=3,Z=1"
CH12      ZAP=(IAL(3,1,1)+IAL(2,1,1))*CNORM/(HITE*PI*42DO)
 CH12      WRITE(12)ZAP
CH12      WRITE(12)"R=1,Z=1"
CH12      ZAP=(IAL(1,1,1))*CNORM/(HITE*PI*24DO)
CH12      WRITE(12)ZAP
          GOTO 815
```

```
 810     CONTINUE
C        TALLIES RADIUS=15.16 WATER CYLINDER
CH       WRITE(12)"R=16",J
CH       ZAP=(TAL(16,1,J)+TAL(16,1,J-1)+TAL(15,1,J)+TAL(15,1,J-1)
 CH      C          +TAL(14,1,J)+TAL(14,1,J-1)+TAL(13,1,J)+TAL(13,1,J-1))
  CH     C          *(CNORM)/(PIE*PI*12.25D0)
CH       WRITE(12)ZAP
CH       WRITE(12)"R=12",J
CH       ZAP=(TAL(12,1,J)+TAL(12,1,J-1)+TAL(11,1,J)+
CH      C          TAL(11,1,J-1))*(CNORM)/(PIE*PI*18D0)
 C H      WRITE(12)ZAP
C H      WRITE(12)"R=10",J
CH       ZAP=(TAL(10,1,J)+TAL(10,1,J-1)+TAL(9,1,J)+
 C H     C          TAL(9,1,J-1))*(CNORM)/(PIE*PI*26D0)
 C H      WRITE(12)ZAP
CH       WRITE(12)"R=8",J
CH       ZAP=(TAL(8,1,J)+TAL(8,1,J-1)+TAL(7,1,J)+TAL(7,1,J-1))
 C H     C          *(CNORM)/(PIE*PI*34D0)
C H      WRITE(12)ZAP
CH       WRITE(12)"R=6",J
CH       ZAP=(TAL(6,1,J)+TAL(6,1,J-1)+TAL(5,1,J)+TAL(5,1,J-1))
 C H     C          *CNORM/(PIE*PI*42D0)
CH       WRITE(12)ZAP
CH       WRITE(12)"R=4",J
CH       ZAP=(TAL(4,1,J)+TAL(4,1,J-1)+TAL(3,1,J)+TAL(3,1,J-1))
  CH     C          *CNORM/(PIE*PI*50D0)
CH       WRITE(12)ZAP
CH       WRITE(12)"R=2",J
CH       ZAP=(TAL(2,1,J)+TAL(2,1,J-1)+TAL(1,1,J)+TAL(1,1,J-1))
  CH     C          *CNORM/(PIE*PI*47.5756D0)
CH       WRITE(12)ZAP
C        TALLIES FOR RADIUS=18.5CM WATER CYLINDER
         WRITE(12)"R=19,Z=",J
         ZAP=(TAL(19,1,J)+TAL(19,1,J-1)+TAL(18,1,J)+TAL(18,1,J-1)
       C  +TAL(17,1,J)+TAL(17,1,J-1)+TAL(16,1,J)+TAL(16,1,J-1))*(CNORM)
       C  /(PIE*PI*12.25D0)
         WRITE(12)ZAP
         WRITE(12)"R=15,Z=",J
         ZAP=(TAL(15,1,J)+TAL(15,1,J-1)+TAL(14,1,J)+TAL(14,1,J-1)
       C  +TAL(13,1,J)+TAL(13,1,J-1))*(CNORM)/(PIE*PI*30D0)
         WRITE(12)ZAP
         WRITE(12)"R=12,Z=",J
        ZAP=(TAL(12,1,J)+TAL(12,1,J-1)+TAL(11,1,J)+TAL(11,1,J-1))
       C  *(CNORM)/(PIE*PI*30D0)
        WRITE(12)ZAP
        WRITE(12)"R=10,Z=",J
         ZAP=(TAL(10,1,J)+TAL(10,1,J-1)+TAL(9,1,J)+TAL(9,1,J-1))
     C  *(CNORM)/(PIE*PI*38D0)
        WRITE(12)ZAP
         WRITE(12)"R=8,Z=",J
         ZAP=(TAL(8,1,J)+TAL(8,1,J-1)+TAL(7,1,J)+TAL(7,1,J-1))
       C  *(CNORM)/(PIE*PI*46D0)
         WRITE(12)ZAP
         WRITE(12)"R=6,Z=",J
         ZAP=(TAL(6,1,J)+TAL(6,1,J-1)+TAL(5,1,J)+TAL(5,1,J-1))*
      C  (CNORM)/(PIE*PI*54D0)
         WRITE(12)ZAP
         WRITE(12)"R=4,Z=",J
         ZAP=(TAL(4,1,J)+TAL(4,1,J-1)+TAL(3,1,J)+TAL(3,1,J-1))
       C  *(CNORM)/(PIE*PI*62D0)
         WRITE(12)ZAP
         WRITE(12)"R=2,Z=",J
         ZAP=(TAL(2,1,J)+TAL(2,1,J-1)+TAL(1,1,J)+TAL(1,1,J-1))
       C  *(CNORM)/(PIE*PI*70D0)
         WRITE(12)ZAP
```

```
C        TALLIES RADIUS=12.5CM WATER CYLINDER
CH12     WRITE(12)"R=13,Z=",J
CH12     ZAP=(TAL(13,1,J)+TAL(13,1,J-1)+TAL(12,1,J)+TAL(12,1,J-1)+
 CH12      C       TAL(11,1,J)+TAL(11,1,J-1)+TAL(10,1,J)+TAL(10,1,J-1))*CN
HC2      C       (HITE*PI*12.25D0)
CH12     WRITE(12)ZAP
CH12     WRITE(12)"R=9,Z=",J
CH12     ZAP=(TAL(9,1,J)+TAL(8,1,J)+TAL(9,1,J-1)+TAL(8,1,J-1))*CNORM
 CH12      C       /(HITE*PI*16D0)
CH12     WRITE(12)ZAP
CH12     WRITE(12)"R=7,Z=",J
CH12     ZAP=(TAL(7,1,J)+TAL(7,1,J-1)+TAL(6,1,J)+
CH12       C       TAL(6,1,J-1))*CNORM/(HITE*PI*20D0)
CH12     WRITE(12)ZAP
CH12     WRITE(12)"R=5,Z=",J
CH12     ZAP=(TAL(5,1,J)+TAL(5,1,J-1)+TAL(4,1,J)+TAL(4,1,J-1))*CNORM/
 CH12      C       (HITE*PI*34D0)
CH12     WRITE(12)ZAP
CH12     WRITE(12)"R=3,Z=",J
CH12     ZAP=(TAL(3,1,J)+TAL(2,1,J)+TAL(3,1,J-1)+TAL(2,1,J-1))*CNORM/
 CH12      C       (HITE*PI*42D0)
CH12     WRITE(12)ZAP
CH12     WRITE(12)"R=1,Z=",J
CH12     ZAP=(TAL(1,1,J)+TAL(1,1,J-1))*CNORM/(HITE*PI*24D0)
HC2      WRITE(12)ZAP
815      J=J+2
         IF(J.LT.14) GOTO 801
         GOTO 900
820      CONTINUE
         ITHTAL=1
CH       DO 995 IRTAL=1,16
CH12     DO 995 IRTAL=1,13
         DO 995 IRTAL=1,19
         DO 995 IZTAL=1,13
         IF(IZTAL.EQ.1) HITE=2D0*((66.04D0-R)/108.6D0)
        IF(IZTAL.EQ.1) GOTO 992
         IF(IZTAL.GT.1.AND.IZTAL.LT.4) HITE=(2D0*R/108.6D0)
          IF(IZTAL.GT.1.AND.IZTAL.LT.4) GOTO 992
         IF(IZTAL.GT.3.AND.IZTAL.LT.6) HITE=2D0-((66.04D0+R)/108.6D0)
          IF(IZTAL.GT.3.AND.IZTAL.LT.6) GOTO 992
         IF(IZTAL.GT.5.AND.IZTAL.LT.14) HITE=2.000D0
         IF(IZTAL.GT.5.AND.IZTAL.LT.14) GOTO 992
CH992    IF(IRTAL.EQ.1) RDOUT=15.16D0
992      RDOUT=19.5D0-RTAL(IRTAL)
CH12992  RDOUT=13.5D0-RTAL(IRTAL)
CH       IF(IRTAL.EQ.1) GOTO 993
CH       RDOUT=16.5D0-RTAL(IRTAL)
CH993    IF(IRTAL.EQ.16) RADIN=0D0
         IF(IRTAL.EQ.19) RADIN=0D0
CH12     IF(IRTAL.EQ.13) RADIN=0D0
CH       IF(IRTAL.EQ.16) GOTO 994
         IF(IRTAL.EQ.19) GOTO 994
CH12     IF(IRTAL.EQ.13) GOTO 994
CH       RADIN=15.5D0-RTAL(IRTAL)
         RADIN=18.5D0-RTAL(IRTAL)
CH12     RADIN=12.5D0-RTAL(IRTAL)
994      VTAL=PI*HITE*(RDOUT**2D0-RADIN**2D0)
         TALSU(IRTAL,ITHTAL,IZTAL)=(TALSU(IRTAL,ITHTAL,IZTAL)/
     C  VTAL)*(1.60219D-11**2)
         TAL(IRTAL,ITHTAL,IZTAL)=(TAL(IRTAL,ITHTAL,IZTAL)/
       C  VTAL)*1.60219D-11
         IF(EVNTPV(IRTAL,1,IZTAL).EQ.0D0) GOTO 991
         SRPVAR=(TALSU(IRTAL,ITHTAL,IZTAL)/EVNTPV(IRTAL,1,IZTAL))
     C  -((TAL(IRTAL,ITHTAL,IZTAL)/EVNTPV(IRTAL,1,IZTAL))**2D0)
          GOTO 9910
```

```
991     SMPVAR=0D0
9910    CONTINUE
        VARSM=SMPVAR/(H-1D0)
        IF(IAL(IRIAL,IIHIAL,IZIAL).EQ.0D0) GOTO 997
         STDV=DSQRT(VARSM)/IAL(IRIAL,IIHIAL,IZIAL)
997     CONTINUE
        WRITE(12)ZAP
        WRITE(12)"RADIAL POSITION=",IRIAL
        WRITE(12)"AZIMUTHAL POS=",IZIAL
       WRITE(12)"ENERGY TALLY=",TAL(IRIAL,1,IZIAL)
         WRITE(12)"TALSQ=",TALSQ(IRIAL,1,IZIAL)
        WRITE(12)"SAMPLE VARIANCE=",SMPVAR
        WRITE(12)"VAR. SMPL. MEAN=",VARSM
       WRITE(12)"STANDARD DEV.=",STDV
       WRITE(12)"EVENTS=",EVNTPV(IRIAL,1,IZIAL)
995     CONTINUE
        WRITE(12) "THE NUMBER OF HIST=",H
        WRITE(12)"YPL=",YPL
        WRITE(12)"IX(1)=",IX(1)
        WRITE(12)"IX(2)=",IX(2)
        WRITE(12)"IY(1)=",IY(1)
        WRITE(12)"IY(2)=",IY(2)
        STOP
```

```
3000    CONTINUE
C       THE GAMMA SCATTER AND PHOTOELECTRIC SERIES
C       ------------------------------------------
C 3005  THIS SERIES DETERMINES THE TYPE OF
C 3006  EVENT WHICH OCCURS AND HOW MUCH
C 3007  ENERGY IS DEPOSITED IN THE EVENT
C 3008
C 3009
C 3010  SELECT THE TYPE OF EVENT
        C2=P/1
        CALL RAND32(IX,IY,YFL)
        IX(1)=IY(1)
        IX(2)=IY(2)
        IF(YFL.LE.C2) GOTO 3100
        IF(YFL.GT.C2) GOTO 3200
C 3050  SINCE THE EVENT IS PHOTO, WE MUST DEPOSIT
C 3060  ALL THE ENERGY. SO THEREFORE THE FINAL GAMMA
C 3070  ENERGY E1=0. FOR THE PHOTO EVENT
3100    E1=0D0
        GOTO 3400
C 3190  SINCE THE EVENT IS A SCATTER, DETERMINE THE
C 3192  SCATTER ANGLE, THETA. FROM THIS THEN COMPUTE THE
C 3194  FINAL GAMMA ENERGY,E1. FOR SCATTERING:
3200    BETA=1D0+2D0*A
        TZE=1D0/BETA
        EN=DLOG(BETA)
        BETA=1D0/A
        PHI=.25D0
        EX0=TZE+PHI*(1D0-TZE)
        EM=DLOG(EX0)
        RKAY1=(.5D0)*(1D0-DABS(EX0)**2)-EM
        RKAY2=2D0*(EM+1D0-EX0)
        RKAY3=1D0/EX0-EX0+2D0*EM
        EF=RKAY1+BETA*(RKAY2+BETA*RKAY3)
       GE=2D0*A*(A+1D0)/(DABS(BETA)**2)+4D0+BETA
     C  +(1D0-2D0*BETA*(1D0+BETA))*EN
        RJ=EF/GE
        CALL RAND32(IX,IY,YFL)
        IX(1)=IY(1)
        IX(2)=IY(2)
        IF(YFL.GT.RJ) GOTO 3300
        ARE=YFL/RJ
        EN1=EX0+1D0/EX0
        EN2=2D0*(1D0-1D0/EX0)
        EN3=DABS(1D0-1D0/EX0)**2
        SMLEF=EN1+BETA*(EN2+BETA*EN3)
        SMLA=-1D0*EF/2D0
        SMLB=EF*EF/SMLEF-3D0*(1D0-EX0)
       SMLC=EF/(-2D0)-EF/SMLEF+2D0*(1D0-EX0)
        EX=1D0+ARE*(SMLA+ARE*(SMLB+ARE*SMLC))
        GOTO 3310
3300    LAMBDA=(EF+EN)/(1D0-RJ)
        EX=EX0*DEXP((-1D0)*LAMBDA*(YFL-RJ))
3310    A1=EX*A
C 3314  NEW GAMMA ENERGY:
        E1=511.006D0*A1
C 3335  NOW TEST THE NEW ENERGY TO SEE IF
C 3336  IT IS WORTHWHILE TO CONTINUE.
3400    IF(E1.LE.20D0) GOTO 3450
        IF(E1.GT.20D0) GOTO 3500
C 3420  THE ENERGY IS TOO LOW TO CONTINUE. THEREFORE
C 3430  TALLY THE ENERGY AND TERMINATE THIS HISTORY:
3 450     E=E2
C 3460  SPECIFY THAT WE ARE TERMINATING(IERR=1)
        IERR=1D0
        CALL TALLY
```

```
      GOTO 615
C 3480  THE ENERGY IS STILL ENOUGH TO CONTINUE.THEREFORE
C 3490  TALLY THE ENERGY AND CONTINUE:
300   E=E2-E1
      E2=E1
      CALL TALLY
C 3530  CALCULATE THE NEW SCATTERING ANGLES AND THE NEW
C 3540  DIRECTION COSINES. THE NEW COSINE(THETA):
        U=1D0+1D0/A-1D0/A1
C 3555  NEW THETA:
        IF(U.GE.0D0) GOTO 3556
        T8=PI-DATAN(DSQRT((DABS(U)**(-2D0))-1D0))
        GOTO 3560
3556    T8=DATAN(DSQRT((DABS(U)**(-2D0))-1D0))
3560    CONTINUE
        CALL RAND32(IX,IY,YFL)
        IX(1)=IY(1)
        IX(2)=IY(2)
C 3570  THE NEW PHI:
        T9=YFL*2D0*PI
C 3585  THE NEW DIRECTION COSINES
        IF(C7.EQ.1D0) GOTO 3450
        IF(C9.EQ.0D0) GOTO 3450
C       THE NEW DIRECTION COSINES ALGORITHM
      D8=DATAN2(C8,C7)
       D9=DATAN(C9/(DSQRT(1D0-DABS(C9)**2)))
       C7=(DCOS(D8)*(DCOS(D6)*DCOS(T8)-DSIN(D9)*DCOS(T9)*DSIN(T8))
     C  +DSIN(D8)*DSIN(T9)*DSIN(T8))
      C8=DSIN(D8)*(DCOS(D6)*DCOS(T8)-DSIN(D9)*DCOS(T9)*DSIN(T8))
     C  -DSIN(T9)*DSIN(T8)*DCOS(D8)
      C9=DSIN(D9)*DCOS(T8)+DCOS(D9)*DCOS(T9)*DSIN(T8)
C 3620  WE NOW HAVE THE NEEDED INFORMATION TO CONTINUE
        GOTO 670
        END
```

Subroutine GEOM:

```
C+++++++++++++++++++++++++++++++++++++++++++++++++++++++++++++++
+6++++++++++++++++++++++++++++++++++++++++++++++++++++++++++++++

C 1000  THE SFC GEOMETRY TESTING SERIES
C1001  ----------------------------
C1002  WHAT WE DO HERE IS TO CALCUATE THE COORDINATE
 C  1003  OF THE NEAREST POSITIVE SFC AND TO DETERMINE
 C  1004  WHAT THE NEXT SUBSTANCE IS THAT WE MAY BE
 C  1005  ENTERING. SOLVE FOR THE INTERSECTION COORDINATE
 C  1006  VALUE. DETERMINE IF DIRECTION COSINES=0:
         COMPILER DOUBLE PRECISION
       SUBROUTINE GEOM
C       ---------------
C
CH       DIMENSION TAL(16,1,13),TALSQ(16,1,13),EVNTPV(16,1,13)
HC      DIMENSION IMPTAL(16,1,13),RTAL(0:16),TLSQ2(5,1,13)
         DIMENSION TAL(19,1,13),TALSQ(19,1,13),EVNTPV(19,1,13)
         DIMENSION IMPTAL(19,1,13),RTAL(0:19),TLSQ2(5,1,13)
 CH12    DIMENSION TAL(13,1,13),TALSQ(13,1,13),EVNTPV(13,1,13)
 CH12    DIMENSION IMPTAL(13,1,13),RTAL(0:13),TLSQ2(5,1,13)
         COMMON/VAR/A,A1,A0,C2,C7,C8,C6,C5,C9,C1,C0
         COMMON/VAR/D8,D3,D9,D,DNO,D7,DSO,DLO,D1,D2,DL
         COMMON/VAR/EVNTPV,E1,E2,E,E0,G8,G2,G3,G4,G5,G6,G9,G7
         COMMON/VAR/HO,H,I,IX(2),IY(2),IZTAL,IRTAL,ITHAL,J
         COMMON/VAR/PI,PO,P,P1,R,S2,S9,S1,S3,S4,TAL,TALSQ
         COMMON/VAR/T,TS,T9,T1,U,U1,U2,U0,V1,V2,V0,W1,W2,W0
         COMMON/VAR/XO,YO,YFL,Y1,Z8,Z9,Z0,Z1
        COMMON/VAR/U3,U4,U5,U6,U7,V3,V4,V5,V6,V7
        COMMON/VAR/W3,W4,W5,W6,W7
        COMMON/VAR/IMPTAL,ITERM,HITE,RDOUT,RTAL,RADIN,VTAL
         COMMON/VAR/SMPVAR,VARSM,STDV,TLSQ2
        IF(C7.NE.0D0) GOTO 1020
        GOTO 1155
1020    IF(C8.NE.0D0) GOTO 1030
        GOTO 1110
C 1029  CALCULATE INTERSECTION POINTS FROM A GENERAL EQN.
 1030    CONTINUE
        C6=C8/C7
        C5=(DABS(C6))**2
        S9=DABS(XO*C5-YO*C6)**2-(1D0+C5)*(C5*(DABS(XO)**2)
      C  +DABS(YO)**2-R**2-2*YO*XO*C6)
        IF(DABS(S9).GT.1D-10) GOTO 1070
       P0=0D0
        DNO=1D0
        GOTO 1995
1070    CONTINUE
C 1070  WE HAVE TESTED HOW CLOSE THE INTERSECTION IS
 C  1071  TO BEING A TANGENT TO THE SFC. NOW TEST TO
 C  1072  SEE IF THERE IS AN INTERSECTION:
       IF(S9.LT.1D-10)GOTO 1900
C1074  DETERMINE THE TWO POSSIBLE ROOTS,X'S AND Y'S
        U1=((XO*C5-YO*C6)+DSQRT(S9))/(1D0+C5)
        U2=((XO*C5-YO*C6)-DSQRT(S9))/(1D0+C5)
        V1=C6*(U1-XO)+YO
        V2=C6*(U2-XO)+YO
        GOTO 1300
C 1100  COSINE(BETA) WAS EQUAL TO ZERO. THEREFORE USE
 C  1101  THE NEXT POSSIBLE EQUATION HERE.
1110    V1=YO
        V2=YO
        IF(DABS(R**2D0-DABS(YO)**2D0).GT.1D-10) GOTO 1125
         P0=0D0
        DNO=1D0
        GOTO 1995
C       WE TESTED CLOSENESS TO SFC. NOW TEST IF WE MISS.
```

```
 1125     CONTINUE
         IF(R**2D0-DABS(Y0)**2D0.LE.0D0) GOTO 1900
C 1135   DETERMINE THE 2 POSSIBLE ROOTS, X'S AND Y'S
          U1=DSQRT(R**2D0-DABS(Y0)**2D0)
         U2=-1D0*DSQRT(R**2D0-DABS(Y0)**2D0)
         GOTO 1300
C 1154   COSINE(ALPHA) WAS EQUAL TO ZERO THEREFORE USE
 C        THE FINAL POSSIBLE EQUATION HERE.
 1155    CONTINUE
         U1=X0
         U2=X0
         IF(DABS(R**2D0-DABS(X0)**2D0).GT.1D-10)GOTO 1185
          P0=0D0
         DN0=1D0
         GOTO 1995
C 1184   WE TESTED CLOSENESS TO THE SURFACE NO. SEE IF WE MISS.
 1185     CONTINUE
         IF(R**2D0-DABS(X0)**2D0.LE.0D0) GOTO 1900
C 1195   DETERMINE THE TWO POSSIBLE ROOTS, X'S AND Y'S
          V1=DSQRT(R**2D0-DABS(X0)**2D0)
         V2=-1D0*DSQRT(R**2D0-DABS(X0)**2D0)
         GOTO 1220
 1220    IF(C9.EQ.0D0) GOTO 1450
         W1=(C9/C8)*(V1-Y0)+Z0
         W2=(C9/C8)*(V2-Y0)+Z0
         IF(W1.GT.20D0) GOTO 1240
         GOTO 1246
 1240    W1=20D0
         U1=X0
         V1=(C8/C9)*(20D0-Z0)+Y0
         GOTO 1256
 1246    IF(W1.LT.-20D0) GOTO 1250
         GOTO 1256
 1250    W1=-20D0
         U1=X0
         V1=(C8/C9)*(-20D0-Z0)+Y0
 1256    IF(W2.GT.20D0) GOTO 1260
         GOTO 1266
 1260    W2=20D0
         U2=X0
         V2=(C8/C9)*(20D0-Z0)+Y0
         GOTO 1276
 1266     IF(W2.LT.-20D0) GOTO 1270

          GOTO 1276
 1270    W2=-20D0
         U2=X0
         V2=(C8/C9)*(-20D0-Z0)+Y0
 1276    GOTO 1500
C 1276   THE ABOVE CALCULATION ADJUSTED THE POSITION IF WE
 C  1279  HAD PASSED THRU THE UPPER SURFACES.

C 1299   CHECK IF COSINE(GAMMA)=0
 800     CONTINUE
         IF(C9.EQ.0D0) GOTO 1450
          W1=(C9/C7)*(U1-X0)+Z0
          W2=(C9/C7)*(U2-X0)+Z0
          IF(W1.GT.20D0) GOTO 1324
         GOTO 1330
 1324     W1=20D0
         V1=Y0
         U1=(C7/C9)*(20D0-Z0)+X0
          GOTO 1340
 1330     IF(W1.LT.-20D0)GOTO 1334
          GOTO 1340
```

```
1334    W1=-20D0
        V1=Y0
        U1=(C7/C9)*(-20D0-Z0)+X0
1340    IF(W2.GT.20D0) GOTO 1344
        GOTO 1350
1344    W2=20D0
        V2=Y0
        U2=(C7/C9)*(20D0-Z0)+X0
        GOTO 1360
1350    IF(W2.LT.(-20D0)) GOTO 1354
        GOTO 1360
1354    W2=-20D0
       V2=Y0
        U2=(C7/C9)*(-20D0-Z0)+X0
1360    GOTO 1500
C 1370  WE WANT TO TEST IF THE PHOTON IS CONTAINED
C 1372   IN THE Z DIRECTION AGAIN.

C 1379  CHECK IF COS(GAMMA)=0
1380    CONTINUE
        IF(C9.EQ.0D0) GOTO 1450
        W1=(C9/C7)*(U1-X0)+Z0
        W2=(C9/C7)*(U2-X0)+Z0
        IF(W1.GT.20D0) GOTO 1392
        GOTO 1398
1392    W1=20D0
        V1=(C8/C9)*(20D0-Z0)+Y0
        U1=(C7/C9)*(20D0-Z0)+X0
        GOTO 1408
1398    IF(W1.LT.-20D0) GOTO 1402
        GOTO 1408
1402    W1=-20D0
        V1=(C8/C9)*(-20D0-Z0)+Y0
        U1=(C7/C9)*(-20D0-Z0)+X0
1408    IF(W2.GT.20D0) GOTO 1412
        GOTO 1418
1412    W2=20D0
        V2=(C8/C9)*(20D0-Z0)+Y0
        U2=(C7/C9)*(20D0-Z0)+X0
        GOTO 1428
1418    IF(W2.LT.-20D0) GOTO 1422
        GOTO 1428
1422    W2=-20D0
        V2=(C8/C9)*(-20D0-Z0)+Y0
        U2=(C7/C9)*(-20D0-Z0)+X0
1428    GOTO 1500
1450    W1=Z0
        W2=Z0
C 1490  NOW CHECK ALL THE TEMPORARY VARIABLES AND
C 1491   DETERMINE IF THE DIRECTION IS CORRECT.
C 1492  IN THIS GENERAL TESTING SCHEME WE WILL
C 1493  ASSIGN AN ARBITRARY LARGE VALUES TO THE
C 1494  U1,U2,U3... IF WE MISS A SEC. THIS WILL
C 1495  THEN BE SEPARATED OUT IN THE DISTANCE TO
C 1496   A SURFACE LOGIC.
1500    IF(C7.EQ.0D0) GOTO 1570
       IF(((U1-X0)/C7).LE.0D0) GOTO 1520
       D50=DSQRT(DABS(U1-X0)**2D0+DABS(V1-Y0)**2D0+DABS(W1-Z0)**2D0)
         GOTO 1525
1520    D50=50000
1525    IF(((U2-X0)/C7).LE.0D0) GOTO 1540
        E0=DSQRT(DABS(U2-X0)**2D0+DABS(V2-Y0)**2D0+DABS(W2-Z0)**2D0)
         GOTO 1545
1540    E0=100000
1545    IF(E0.LT.D50) D50=E0
```

```
C 1546  IF THERE IS NO POSITIVE INTERSECTION OR THE
C 1547  HOMO. CYLINDER THEN ESCAPE.
        IF(DSO.EQ.500D0) GOTO 1910
C 1555  DEFINE THE SUBSTANCE IN THE NEXT VOLUME.
        PI=0D0
C 1563  WE HAVE A SHORTEST DISTANCE ,NOW RETURN TO THE
C 1564  MAIN PROGRAM.
        GOTO 1995
C 1568  DO AS ABOVE EXCEPT IN THE CASE WHERE THE
C 1569  COS(BETA) DOES NOT EQUAL 0
1570    IF(C8.EQ.0D0) GOTO 1635
        IF((V1-Y0)/C8.LT.0D0) GOTO 1590
        DSO=DSQRT(DABS(U1-X0)**2D0+DABS(V1-Y0)**2D0+DABS(W1-Z0)**2D0)
          GOTO 1595
1590    DSO=500D0
1595    IF((V2-Y0)/C8.LT.0D0) GOTO 1610
        E0=DSQRT(DABS(U2-X0)**2D0+DABS(V2-Y0)**2D0+DABS(W2-Z0)**2D0)
          GOTO 1615
1610    E0=1000D0
1615    IF(E0.LT.DSO) DSO=E0
C 1616  IF THERE IS NO POSITIVE INTERSECTION FOR THE
C 1617  HOMO. CYLINDER , THEN ESCAPE.
        IF(DSO.EQ.500D0) GOTO 1910
C 1625  DEFINE THE SUBSTANCE IN THE NEXT VOLUME
        PI=0D0
C 1633  WE HAVE A SHORTEST DISTANCE. NOW RETURN TO THE
C 1634  MAIN PROGRAM
1635    GOTO 1995
        IF((W1-Z0)/C9.LT.0D0) GOTO 1650
        DSO=DSQRT(DABS(U1-X0)**2D0+DABS(V1-Y0)**2D0+DABS(W1-Z0)**2D0)
          GOTO 1655
1650    DSO=500D0
1655    IF((W2-Z0)/C9.LT.0D0) GOTO 1670
        E0=DSQRT(DABS(U2-X0)**2D0+DABS(V2-Y0)**2D0+DABS(W2-Z0)**2D0)
        GOTO 1675
1670    E0=1000D0
1675    IF(E0.LT.DSO) DSO=E0
        IF(DSO.EQ.500D0) GOTO 1910
C 1685  DEFINE THE SUBSTANCE IN THE NEXT VOLUME
        PI=0D0
        GOTO 1995
1900    CONTINUE
C 1901  WE MISSED THE TARGET. IN THIS CASE THE SFC WAS
1905  JUST THE HOMO. PHANTOM. SO TRY AGAIN.
1910    P0=0D0
        DN0=1D0
        GOTO 1995
1995    RETURN
        END
```

Subroutine ANGLIN:

```
C*************************************************************
 C*************************************************************


C 4000  INCIDENT PHOTON DIRECTION FROM X-RAY TUBE
C 4001  ----------------------------------------
C 4002  THIS SUBROUTINE SAMPLES PHOTONS FROM A
C 4003  UNIFORM DISTRIBUTION OF PHOTONS INCIDENT ON A
 C 4004  RECTANGULAR "DETECTOR" LOCATED AT THE POSITION
 C 4005  OF THE REAL DETECTOR. SINCE THERE IS ABOUT
C 4006  A 5% LINEAR FALLOFF OF THE PHOTON INTENSITY
 C 4007  AS ONE MOVES OFF THE AXIS OF THE DETECTOR,
C 4008  A POSITION DISTRIBUTION FUNCTION IS
C 4009  INVERTED WHICH HAS A LINEAR FALLOFF.
C 4010  I.E., IN THIS SITUATION WE SAMPLED UNIFORMLY IN
 C 4011  THE Z DIRECTION. BUT WE SAMPLED FROM AN
C 4012  INTENSITY DISTRIBUTION IN THE Y DIRECTION.
 C 4013  (SAMPLE FROM -26.5 TO 26.5 CM)
C 4014  PHYSICAL DATA USED:
C 4015  XD-XS=108.6 CM (SOURCE-DETECTOR DISTANCE)
C 4016  XD=42.56 CM (DETECTOR POSITION)
C 4017  XS=-66.04 CM (SOURCE POSITION)
C 4018  R=15.16 CM (PHANTOM RADIUS)
C 4019  SELECT Y OF INCIDENT PHOTON(YI) AND SIGN(SI):
        COMPILER DOUBLE PRECISION
      SUBROUTINE ANGLIN
CH      DIMENSION TAL(16,1,13),TALSQ(16,1,13),EVNTPV(16,1,13)
 CH      DIMENSION IMPTAL(16,1,13),RTAL(0:16),TLSQ2(5,1,13)
        DIMENSION TAL(19,1,13),TALSQ(19,1,13),EVNTPV(19,1,13)
        DIMENSION IMPTAL(19,1,13),RTAL(0:19),TLSQ2(5,1,13)
 CH12   DIMENSION TAL(13,1,13),TALSQ(13,1,13),EVNTPV(13,1,13)
 CH12   DIMENSION IMPTAL(13,1,13),RTAL(0:13),TLSQ2(13,1,13)
        COMMON/VAR/A,A1,A0,C2,C7,C8,C6,C5,C9,C1,C0
        COMMON/VAR/DR,D3,D9,D,DNO,D7,D50,DLO,D1,D2,DL
        COMMON/VAR/EVNTPV,E1,E2,E,E0,G8,G2,G3,G4,G5,G6,G9,G7
        COMMON/VAR/HO,H,I,IX(2),IY(2),IZTAL,IRTAL,IIRTAL,J
        COMMON/VAR/PI,PO,P,P1,R,S2,S9,S1,S3,S4,TAL,TALSQ
        COMMON/VAR/T,TM,I9,I1,U,U1,U2,U0,V1,V2,V0,W1,W2,W0
        COMMON/VAR/XO,YO,YFL,Y1,Z6,Z9,ZO,Z1
        COMMON/VAR/U3,U4,U5,U6,U7,V3,V4,V5,V6,V7
        COMMON/VAR/W3,W4,W5,W6,W7
        COMMON/VAR/IMPTAL,ITERB,HITE,RDOUT,RTAL,RADIN,VTAL
        COMMON/VAR/SMPVAR,VARSM,STDV,TLSQ2
4010    CALL RAND32(IX,IY,YFL)
        IX(1)=IY(1)
        IX(2)=IY(2)
        Y1=(1D0-DSQRT(1D0-2D0*(0.096982D0/23.58D0)*29.89419915D0*YFL))/
      C  (0.096982D0/23.58D0)
CH      Y1=(1D0-DSQRT(1D0-2D0*(0.096982D0/23.58D0)*25.0558607D0*YFL))/
 CH     C         (0.096982D0/23.58D0)
CH12    Y1=(1D0-DSQRT(1D0-2D0*(0.096982D0/23.58D0)*20.54940777D0)*YFL))/
 CH12     C              (0.096982D0/23.58D0)
        CALL RAND32(IX,IY,YFL)
        IX(1)=IY(1)
        IX(2)=IY(2)
        SI=YFL
        IF(SI.LT.0.5D0) GOTO 4050
        GOTO 4055
4050    Y1=-1D0*Y1
C       TEST WHETHER THE PHOTON HITS THE PHANTOM(TI)
 4 055   SLOPE=DABS(Y1)/108.6D0
        TI=(((2D0)*(66.04D0))**2D0-4D0*(1+SLOPE**2)*(66.04D0**2-R**2))
         IF(TI.LT.1D-19) GOTO 4010
C 4054  SELECT Z OF THE INCIDENT PHOTON(Z1)
```

```
      CALL RAND32(IX,IY,YFL)
      IX(1)=IY(1)
      IX(2)=IY(2)
      Z1=2D0*YFL-1D0
C 4085  FIND  PHANTOM INTERSECTION POINT (U0--X,V0--Y,W0--Z)
       U0=((2D0)*(66.04D0)-DSQRT(T1))/(2D0*(1+SLOPE**2))-66.04D0
       V0=((66.04+U0)/106.6)*Y1
      W0=((66.04+U0)/106.6)*Z1
      DLO=DSQRT(DABS(Z1)**2D0+DABS(Y1)**2D0+11793.96D0)
C 4125  CALCULATE PHOTON DIRECTION COSINES; C7=COS(ALPHA)
C 4126  C8=COS(BETA),C9=COS(GAMMA)
      C7=106.6D0/DLO
      C8=Y1/DLO
      C9=Z1/DLO
C 4160  WE HAVE NOW CALCULATED THE INCIDENT ANGLE AND
C 4170  DIRECTION. NOW LETS ROTATE THE SOURCE (INHOMO CASE)
C 4180  THE ROTATION ANGLE WILL BE 2*PI RADIANS
C 4190  DIVIDED BY THE NUMBER OF HISTORIES.
C 4200  CALL THE ANGLE OF ROTATION S2.
C4201  IN THE HOMO. CASE BYPASS THIS STEP (PHANTOM ROT.)
       GOTO 4370
      IF(NO.EQ.1D0) GOTO 4300
      S2=S2+(2D0*PI/N)
      S3=DCOS(S2)
      S4=DSIN(S2)
C 4215  THE NEW DIRECTION COSINES:
      C7=C7*S3-C8*S4
      C8=C8*S3+C7*S4
C 4240  THE NEW INCIDENT GAMMA INTERSECTION POINT
       U0=U0*S3-V0*S4
      V0=V0*S3+U0*S4
C 4265  NOW CALCULATE THE NEW SOURCE POSITION
C 4266  IF D3.LT.D .
      IF(D3.GT.D) GOTO 4370
4300    IF(D3.GT.D) GOTO 4370
4370    CONTINUE
C 4371  NOW THE DIRECTION SELECTION HAS BEEN
C 4380  GENERALIZED FOR THE INHOMO. PHANTOM.
C 4381  BEFORE WE RETURN, WE MUST IDENTIFY THE
C 4382  SURFACE WE ARE ENTERING AS BEING WATER.
C 4383  CALL PO=PHANTOM SUBSTANCE. IN MY NOTATION
C 4384  0=GONE, 1=AIR, 2=H20, 3=BONE
C 4385
C 4386  WE ARE ENTERING WATER!
      PO=2D0
      XO=UO
      YO=VO
      ZO=WO
      RETURN
      END
```

Subroutine EDIST:

```
C*************************************************************
 C*************************************************************


        COMPILER DOUBLE PRECISION
        SUBROUTINE EDIST
C       ----------------

C       ENERGY DISTRIBUTION SUBROUTINE
C 5001  ------------------------------
C 5002  THIS SUBROUTINE SAMPLES FROM A 105 KVP
C 5003  BREMSSTRAHLUNG X-RAY DISTRIBUTION WHICH
C 5004  HAS BEEN FILTERED BY 0.96MM OF COPPER.
C 5005  IN(4010-4030) WE SELECT THE ENERGY REGION THE
C 5006  AREA IS IN. IN(4150-4235) WE CALCULATE THE UNIQUE
C  5007  ENERGY THAT THIS AREA CORRESPONDS TO.
C 5008  WE HAVE NOW INVERTED THE DISTRIBUTION AND
C  5009  DETERMINED THE PHOTON ENERGY.
CH      DIMENSION TAL(16,1,13),TALSQ(16,1,13),EVNIPV(16,1,13)
 CH      DIMENSION IMPIAL(16,1,13),RIAL(0:16),ILSQ2(5,1,13)
         DIMENSION TAL(19,1,13),TALSQ(19,1,13),EVNIPV(19,1,13)
         DIMENSION IMPIAL(19,1,13),RIAL(0:19),ILSQ2(5,1,13)
 CH12    DIMENSION TAL(13,1,13),TALSQ(13,1,13),EVNIPV(13,1,13)
 CH12    DIMENSION IMPIAL(13,1,13),RIAL(0:13),ILSQ2(5,1,13)
         COMMON/VAR/A,A1,A0,C2,C7,C4,C6,C5,C9,C1,C0
         COMMON/VAR/D8,D3,D9,D,DN0,D7,D50,DL0,D1,D2,DL
         COMMON/VAR/EVNIPV,E1,E2,E,E0,G6,G2,G3,G4,G5,G6,G9,G7
         COMMON/VAR/H0,H,I,IX(2),IY(2),IZIAL,IRIAL,ITHIAL,J
         COMMON/VAR/PI,P0,P,P1,R,S2,S9,S1,S3,S4,TAL,TALSQ
         COMMON/VAR/I,I8,I9,I1,U,U1,J2,J0,V1,V2,V0,W1,W2,W0
         COMMON/VAR/X0,Y0,YFL,Y1,Z8,Z9,Z0,Z1
        COMMON/VAR/U3,U4,U5,U6,U7,V3,V4,V5,V6,V7
        COMMON/VAR/W3,W4,W5,W6,W7
        COMMON/VAR/IMPIAL,ITERM,HITE,RDOUT,RIAL,RADIN,VIAL
         COMMON/VAR/SMPVAR,VARSE,STDV,ILSQ2
5010    CALL RAND32(IX,IY,YFL)
        IX(1)=IY(1)
        IX(2)=IY(2)
CC      SPECTRUM 120KVP 3MM AL, CALCULATED FROM KRAMER'S FORMULA
 C       A0=YFL*6.1137D4
C       IF(A0.LE.0D0) GOTO 5010
C       IF(A0.LT.7.343D3) GOTO 5150
C       IF(A0.LT.1.8403D4) GOTO 5160
C       IF(A0.LT.2.9194D4) GOTO 5170
C       IF(A0.LT.3.72215D4) GOTO 5180
C      IF(A0.LT.4.17795D4) GOTO 5190
C       IF(A0.LT.4.59045D4) GOTO 5200
C      IF(A0.LT.4.80905D4) GOTO 5210
C       IF(A0.LT.5.3607D4) GOTO 5220
C       IF(A0.LT.5.9437D4) GOTO 5230
C       IF(A0.LE.6.1137D4) GOTO 5240
C       IF(A0.GT.6.1137D4) GOTO 5010
C5150   E2=1.5891578D1*DSQRT((1.1755346D-2)*(2.71055180D-2)*(A0))
 C       GOTO 5300
C5160   E2=-5.807698D1*DSQRT((6.4123136D3)*(1.5384615D-1)*(A0-7.343D3))
 C       GOTO 5300
C5170   E2=1.0398907D2-DSQRT((4.0946012D3)*(-1.0926962D-1)*(A0-1.8403D4)
 C       GOTO 5300
C5180   E2=9.4072539D1-DSQRT((2.1226788D3)*(-9.3264249D-2)*(A0-2.919ED4)
 C       GOTO 5300
C5190   E2=5900*((A0-3.72215D4)/2279D0)
C       GOTO 5300
C5200   E2=9.7D1-DSQRT((1.296D3)*(-9.6D-2)*(A0-4.17795D4))
 C       GOTO 5300
C5210   E2=6700*((A0-4.59045D4)/1093D0)
```

```
C       GOTO 5300
C5220   E2=1.0566667D2-DSQRT((1.3444444D3)*(-1.2429379D-1)*(A0-4.8090508
 C       GOTO 5300
C5230   E2=1.1399177D2-DSQRT((1.1554404D3)*(-1.6460905D-1)*(A0-5.3607D4)
 C       GOTO 5300
C5240   E2=1.2D2-DSQRT((4000D0)*(-2.3529412D-1)*(A0-5.9437D4))
 C       GOTO 5300
CC      ENERGY SPECTRUM 120KVP 3MMAL.+2MMCU:CORRECTED KRAMER'S
 C       A0=3.44210505
C        IF(A0.LE.0D0) GOTO 5010
C        IF(A0.LT.6.035D3) GOTO 5150
C       IF(A0.LT.3.37D4) GOTO 5160
C       IF(A0.LT.8.8365D4) GOTO 5170
C       IF(A0.LT.1.473465D5) GOTO 5180
C        IF(A0.LT.1.857125D5) GOTO 5190
C       IF(A0.LT.2.202125D5) GOTO 5200
C        IF(A0.LT.2.407745D5) GOTO 5210
C       IF(A0.LT.3.220655D5) GOTO 5220
C       IF(A0.LT.3.354205D5) GOTO 5230
C       IF(A0.LE.3.442105D5) GOTO 5240
C       IF(A0.GT.3.442105D5) GOTO 5010
C5150   E2=2D1+DSQRT(1.6570008D-2*A0)
C       GOTO 5300
C5160   E2=2.613017D1+DSQRT(1.4975585D1+6.4123116D-3*(A0-6.035D3))
 C       GOTO 5300
C5170   E2=2.1034634D1+DSQRT(3.5968511D2+8.7680842D-3*(A0-3.37D4))
 C       GOTO 5300
C5180   E2=6.0572897D2-DSQRT(3.0883469D5-1.682243D-1*(A0-8.8365D4))
 C       GOTO 5300
C5190   E2=59D0+((A0-1.473465D5)/1.9183D4)
C       GOTO 5300
C5200   E2=9.85D1-DSQRT(1.40625D3-1.2D-2*(A0-1.857125D5))
 C       GOTO 5300
C5210   E2=67D0+((A0-2.202125D5)/1.0281D4)
C       GOTO 5300
C5220   E2=9.9050505D1-DSQRT(9.0303285D2-1.010101D-2*(A0-2.407745D5))
 C       GOTO 5300
C5230   E2=1.0962764D2-DSQRT(3.852429302-2.1905805D-2*(A0-3.220655D5))
 C       GOTO 5300
C5240   E2=1.2D2-DSQRT(4D2-4.5506257D-2*(A0-3.354205D5))
 C       GOTO 5300
C       ENERGY SPECTRUM FOR 140KVP 3MMAL.+2MMCU:CORRECTED KRAMER'S
 C       A0=4.6969905 + A
C        IF(A0.LE.0D0) GOTO 5010
C        IF(A0.LT.7.38D3) GOTO 5150
C        IF(A0.LT.4.1795D4) GOTO 5160
C        IF(A0.LT.1.1130505) GOTO 5170
C        IF(A0.LT.1.48246D5) GOTO 5180
C        IF(A0.LT.2.39404D5) GOTO 5190
C        IF(A0.LT.2.86504D5) GOTO 5200
C       IF(A0.LT.3.1529D5) GOTO 5210
C        IF(A0.LT.4.19114D5) GOTO 5220
C        IF(A0.LT.4.42849D5) GOTO 5230
C        IF(A0.LT.4.650699D5) GOTO 5240
C        IF(A0.LE.4.69699D5) GOTO 5250
C       IF(A0.GT.4.69699D5) GOTO 5010
C5150   E2=20D0+DSQRT(1.3550136D-2*A0)
C       GOTO 5300
C5160   E2=8.624523D1+DSQRT(1.4098296D1+5.0877639D-3*(A0-7.38D3))
 C       GOTO 5300
C5170   E2=2.2490285D1+DSQRT(3.0659012D2+6.4766839D-3*(A0-4.1795D4))
 C       GOTO 5300
C5180   E2=-4.5791667D2+DSQRT(5.0114601D5+1.6666667D-1*(A0-1.1130505))
 C       GOTO 5300
C5190   E2=59D0+((A0-1.48246D5)/2.5579D4)
```

```
C       GOTO 5300
C5200    E2=1.0641818D2-DSQRT(2.0993058D3-1.0909091D-2*(A0-2.39404D5))
 C        GOTO 5300
C5210    E2=67D0*((A0-2.8650405)/1.4393D4)
C       GOTO 5300
C5220    E2=1.0+03988D2-DSQRT(1.3719325DJ-1.0736196D-2*(A0-3.1529D5))
 C      GOTO 5300
C5230    E2=1.1431245D2-DSQRT(5.9109518D2-1.6273393D-2*(A0-4.19114D5))
 C        GOTO 5300
C5240    E2=1.2714506D2-DSQRT(7.3685438D2-3.0864198D-2*(A0-4.42849D5))
 C        GOTO 5300
C5250    E2=140D0-DSQRT(400D0-8.6393089D-2*(A0-4.65069D5))
 C        GOTO 5300
C        SPECTRUM SAMPLING FOR 105KVP 3MM AL .2MMCU:

          A0=YFL*1.96488D5
         IF(A0.LE.0D0) GOTO 5010
        IF(A0.LT.1.68285D4) GOTO 5150
        IF(A0.LT.5.10435D4) GOTO 5160
        IF(A0.LT.8.95365D4) GOTO 5170
        IF(A0.LT.1.141905D5) GOTO 5180
        IF(A0.LT.1.366155D5) GOTO 5190
        IF(A0.LT.1.489955D5) GOTO 5200
        IF(A0.LT.1.76193D5) GOTO 5210
        IF(A0.LE.1.96488D5) GOTO 5220
        IF(A0.GT.1.96488D5) GOTO 5010
5150    E2=27D0+DSQRT(1.0042487D-2*A0)
         GOTO 5300
5160     E2=2.445045D1+DSQRT(2.4178849D2+1.2012012D-2*
      C  (A0-1.68285D4))
         GOTO 5300
5170     E2=-7.4230435D2+DSQRT(6.9273053D5+3.9130435D-1*
      C  (A0-5.10435D4))
         GOTO 5300
5180     E2=59D0+((A0-8.95365D4)/1.2327D4)
         GOTO 5300
5190     E2=9.4931034D1-DSQRT(1.1513151D3+(-1.4551724D-2)*
      C  (A0-1.141905D5))
       GOTO 5300
5200     E2=67D0+((A0-1.366155D5)/6.19D3)
         GOTO 5300
5210     E2=9.6171315D1-DSQRT(7.3828034D2+(-1.752988D-2)*
      C  (A0-1.489955D5))
         GOTO 5300
5220     E2=102D0-DSQRT(4.84D2+(-2.3848238D-2)*
      C  (A0-1.76193D5))
         GOTO 5300
C        ENERGY SPECTRUM FOR 105KVP 3MM AL FILTRATION:
 C        A0=YFL*3.1581785D5
C       IF(A0.LE.0D0) GOTO 5010
C       IF(A0.LT.1.325485D4) GOTO 5150
C        IF(A0.LT.6.284535D4) GOTO 5160
C        IF(A0.LT.1.2726035D5) GOTO 5170
C       IF(A0.LT.1.835193D5) GOTO 5180
C        IF(A0  1.2.1622535D5) GOTO 5190
C        IF(A0.LT.2.447285D5) GOTO 5200
C       IF(A0.LT.2.6020735D5) GOTO 5210
C        IF(A0.LT.2.925858D5) GOTO 5220
C        IF(A0.LE.3.158178D5) GOTO 5230
C        IF(A0.GT.3.158178D5) GOTO 5010
6150    E2=23D0+DSQRT(3.6967601D-3*A0)
C        GOTO 5300
C5160    E2=1.4642741D1+DSQRT(2.5105703D2+8.5327872D-3*
 C      C (A0-1.325485D4))
C        GOTO 5300
```

```
C 5170   E2=-5.672785&D1+DSQRT(9.7471903+3.2206119D-2*
 C      C (A0-6.2845350D4))
C        GOTO 5300
C 5180   E2=1.1064671D2-DSQRT(3.6736023D3+(-1.7964072D-2)*
 C      C (A0-1.2726035D5))
C        GOTO 5300
C 5190   E2=59D0+((A0-1.8351935D5)/1.6353D4)
C        GOTO 5300
C 5200   E2=8.9909091D1-DSQRT((8.3573554D2+(-1.0909091D-2)*
 C      C (A0-2.1622535D5))
C        GOTO 5300
C 5210   E2=67D0+DSQRT((A0-2.4472535D5)/7.741D3)
C        GOTO 5300
C 5220   E2=9.3969934D1-DSQRT(6.234976D2+(-1.3229104D-2)*
 C      C (A0-2.6020735D5))
C        GOTO 5300
C 5230   E2=1.02D2-DSQRT(4.84D2+(-2.0833333D-2)*(A0-2.9256585D5))
 C         GOTO 5300
C        ENERGY SPECTRUM 105KVP .9MM CU&
C 5015  SELECT A AND DETERMINE E REGION ITS IN
C        A0=YPL*1D6
C        IF(A0.LE.0D0) GOTO 5010
C       IF(A0.LT.3.4402812D4) GOTO 5150
C       IF(A0.LT.8.0107085D4) GOTO 5160
C       IF(A0.LT.2.5898585D5) GOTO 5170
C       IF(A0.LT.3.6156622D5) GOTO 5180
C       IF(A0.LT.5.1411518D5) GOTO 5190
C       IF(A0.LT.5.8500262D5) GOTO 5200
C       IF(A0.LT.8.1711744D5) GOTO 5210
C       IF(A0.LE.1.000000D6)   GOTO 5220
C 5120 &E HAVE JUST SAMPLED THE AREA
C       IF(A0.GT.1.000000D6)   GOTO 5010
C 5135
CC 5140 A0= FIND THE ENERGY LOCATION OF THE SAMPLED AREA
 C C 5145
C5150   E2=DSQRT((2D0*A0)/849.44AD0)+37D0
C       GOTO 5300
C5160   E2=41.955027D0+DSQRT(16.361811D0+1.0579212D-3*
 C      C (A0-3.4402812D4))
C        GOTO 5300
C5170   E2=35.341551D0+DSQRT(214.67013D0+1.9278554D-3*
 C      C (A0-8.0107085D4))
C        GOTO 5300
C5180   E2=59D0+((A0-2.5898585D5)/5.12902D4)
C        GOTO 5300
C5190   E2=164.99895D0-DSQRT(10815.782D0-(7.9449163D-3)*
 C      C (A0-3.6156622D5))
C        GOTO 5300
C5200   E2=67D0+((A0-5.1411518D5)/3.54437D4)
C        GOTO 5300
C5210   E2=115.75596D0-DSQRT(2186.1201D0-3.9102769D-3*
 C      C (A0-5.8500262D0))
C        GOTO 5300
C5220   E2=100D0-DSQRT(400D0-2.1671900D-3*(A0-8.1711744D5))
 C        GOTO 5300
C 5240  FINISHED!
C 5250
C 5260
C 5270  NOW RETURN TO THE MAIN PROGRAM AND
C 5280  COMPUTE DISTANCE TO A TYPE OF NEXT SURFACE
5300     RETURN
         END
```

Subroutine CXDIST:

```
C+++++++++++++++++++++++++++++++++++++++++++++++++++++++++++++++++++++++
 C+++++++++++++++++++++++++++++++++++++++++++++++++++++++++++++++++++++++


       COMPILER DOUBLE PRECISION
        SUBROUTINE CXDIST
C       ----------------
C 6001  CROSS SECTION CALC. AND DISTANCE SAMPLING
C 6002  ----------------------------------------
C 6003  IN THIS SUBROUTINE I WILL DETERMINE THE CROSS SECTION
 C 6004  FOR THE GIVEN ENERGY IN THE SUBSTANCE WE ARE ENTERING
 6005  STEPS 6000 TO 6299 WILL BE FOR THE WATER CROSS SECT.
 C 6006  6000-6099:PHOTO H2O
C6007  6100-6199:COMPTON H2O
C 6008  6200-6299:RAYLEIGH H2O
C6009
C 6010  6400-6499:PHOTO BONE
C 6011  6500-6599:COMPTON BONE
C 6012  6600-6699:RAYLEIGH BONE
C 6013
C 6014  6700-6799:SAMPLE FOR DISTNCE
C6015  6800-6999:CONTROL FOLLOWING HISTORY:GOTO 3000 OR
 C 6016  PUT GAMMA ON SEC. AND GOSUB 1000 AND 2000 AGAIN
 C 6017
C 6020  DETERMINE WHERE TO GO
@       DIMENSION TAL(16,1,13),TALSQ(16,1,13),EVNTPV(16,1,13)
 CH       DIMENSION TMPTAL(16,1,13),RTAL(0:16),TLSQ2(5,1,13)
          DIMENSION TAL(19,1,13),TALSQ(19,1,13),EVNTPV(19,1,13)
         DIMENSION TMPTAL(19,1,13),RTAL(0:19),TLSQ2(5,1,13)
 C H12     DIMENSION TAL(13,1,13),TALSQ(13,1,13),EVNTPV(13,1,13)
  CH12     DIMENSION TMPTAL(13,1,13),RTAL(0:13),TLSQ2(5,1,13)
          COMMON/VAR/A,A1,A0,C2,C7,C8,C6,C5,C9,C1,C0
          COMMON/VAR/D8,D3,D9,D,DN0,D7,DS0,DL0,D1,D2,DL
          COMMON/VAR/EVNTPV,E1,E2,E,E0,G8,G2,G3,G4,G5,G6,G9,G7
          COMMON/VAR/H0,H,I,IX(2),IY(2),IZTAL,IRTAL,IITAL,J
          COMMON/VAR/P1,P0,P,P1,R,S2,S9,S1,S3,S4,TAL,TALSQ
          COMMON/VAR/T,I8,I9,T1,J,U1,U2,U0,V1,V2,V0,W1,W2,W0
          COMMON/VAR/X0,Y0,YEL,Y1,Z8,Z9,Z0,Z1
         COMMON/VAR/U3,U4,U5,U6,U7,V3,V4,V5,V6,V7
         COMMON/VAR/W3,W4,W5,W6,W7
         COMMON/VAR/TMPTAL,ITERM,HITE,RDOUT,RTAL,RADIN,VTAL
          COMMON/VAR/SEPVAR,VARSM,STDV,TLSQ2
         IF(P0.EQ.0D0) GOTO 6740
         IF(P0.EQ.1D0) GOTO 6400
         IF(P0.EQ.2D0) GOTO 6050
         IF(P0.EQ.3D0) GOTO 6400
C 6040  PHOTOELECTRIC CROSS SECTION FOR H2O(P):
6050     P=10D0**(-3.2004634D0*DLOG10(E2)+3.4663D0)
C        PHOTOELECTRIC CROSS SECTION FOR TISSUE EQUIV.
 C 6050   P=10D0**(-3.1969753D0*DLOG10(E2)+3.4808012D0)
 C 6055
         GOTO 6100
C 6070  COMPTON SCAT. CROSS SECTION FOR H2O (C1):
6100     A=E2/511.006D0
C 6105  DLOG MEANS NATURAL LOG
         D1=((1D0+A)/(A**2D0))*(2D0*(1D0+A)/(1D0+2D0*A)-(DLOG
       C   (1D0+2D0*A)/A))
         D2=((1D0/(2D0*A))*DLOG(1D0+2D0*A))-((1D0+3D0*A)/((
       C   1D0+2D0*A)**2D0))
C        COMPTON CROSS SECTION FOR H2O:
        C1=0.16729D0*(D1+D2)
C       COMPTON CROSS SECTION FOR TISSUE EQUIV.
C        C1=0.16729D0*(D1+D2)*0.9898477157D0
C 6140
```

```
      GOTO 6200
C 6160  RAYLEIGH (COHERENT) SCAT. CROSS SECTION FOR H20(CO):
 6200    CO=10D0**(-1.891**82D0+DLOG10(E2)+1.30086*3D0)
C        RAYLEIGH(COHERENT) SCAT. CROSS SECTION FOR TISS.EQUIV.:
 C6200   CO=10D0**(-1.741348000D0*DLOG10(E2)+1.04935277D0)
C 6205
C 6210  NOW THE CROSS SECTIONS FOR H20 HAVE BEEN CALCULATED.
 C 6220  NOW SAMPLE FOR DISTANCE:
C 6230
      GOTO 6700
C 6250
6400    CONTINUE
C 6401  IN THE NEXT 300 STEPS WE WILL CALCULATE THE PHOTO.
 C 6402  COMPTON,AND RAYLEIGH CROSS SECTIONS FOR BONE.
 C 6410
C 6420 PHOTOELECTRIC CROSS SECTION FOR BONE (P):
      P=10D0**1D0
C 6440
      GOTO 6500
C 6460 COMPTON SCATTER CROSS SECTION FOR BONE (C1):
6 500    A=E2/511.006D0
      D1=((1D0+A)/(A**2D0))*(2D0*(1D0+A)/(1D0+2D0*A)-(DLOG
     C   (1D0+2D0*A)/A))
      D2=((1D0/(2D0*A))*DLOG(1D0+2D0*A))-((1D0+3D0*A)/
     C   ((1D0+2D0*A)**2D0))
      C1=100D0*(D1+D2)
C 6540
      GOTO 6600
C 6560  RAYLEIGH(COHERENT) SCAT. CROSS SECTION FOR BONE (C1):
 6600    CO=10D0**(100D0)
C 6605
C 6610  NOW THE CROSS SECTIONS FOR BONE HAVE BEEN CALCULATED.
 C 6620  NOW SAMPLE FOR DISTANCE.
C 6630
6700    T=P+C0+C1
      CALL RAND32(IX,IY,YFL)
      IX(1)=IY(1)
      IX(2)=IY(2)
      CONTINUE
      DL=-DLOG(YFL)/T
      DN0=0D0
      IF(DL-G1.D50) GOTO 6800
C6735  WE DIDN'T MAKE IT TO THE SFC SO WE'D BETTER
C 6736  CALCULATE THE NEW POSITION AT THE EVENT.
       X0=X0+DL*C7
      Y0=Y0+DL*C8
      Z0=Z0+DL*C9
      IF(D3.GT.D) GOTO 6770
C 6769  THE NEW POSITION IS DETERMINED
6770    CONTINUE
C 6776  SINCE WE DON'T MAKE IT TO THE SFC(L<D0),THEN CONTINUE
 C   TO THE NEXT SUBROUTINE SERIES WHICH DETERMINES
C 6777    THE TYPE OF EVENT AND THE SCATTERING ANGLE.
 C 6779
6780    RETU !
C 6790  SINCE WE MADE IT TO THE NEXT SURFACE, CHANGE THE
 C 6795    COORDINATES TO THOSE OF THE NEW SURFACE.
 C 6799  PUT THE GAMMA ON THE NEW SURFACE:
6800    CONTINUE
      DN0=1D0
      ITERR=1
      P0=P1
      X0=X0+D50*C7
       Y0=Y0+D50*C8
       Z0=Z0+D50*C9
```

```
      DO 6884 J=1,13
      ILSQ2(1,1,J)=(IMPIAL(1,1,J)+IMPIAL(2,1,J)+IMPIAL(3,1,J))**2
       ILSQ2(2,1,J)=(IMPIAL(4,1,J)+IMPIAL(5,1,J)+IMPIAL(6,1,J))**2
       ILSQ2(3,1,J)=(IMPIAL(7,1,J)+IMPIAL(8,1,J)+IMPIAL(9,1,J))**2
       ILSQ2(4,1,J)=(IMPIAL(10,1,J)+IMPIAL(11,1,J)+IMPIAL(12,1,J))**2
       ILSQ2(5,1,J)=(IMPIAL(13,1,J)+IMPIAL(14,1,J)+IMPIAL(15,1,J)
     C  +IMPIAL(16,1,J))**2
6884    CONTINUE
CH      DO 6885 I=1,16
       DO 6885 I=1,19
CH12    DO 6885 I=1,13
        DO 6885 J=1,13
        IF (IMPIAL(I,1,J).EQ.0D0) GOTO 6885
        TALSQ(I,1,J)=TALSQ(I,1,J)+IMPIAL(I,1,J)**200
         IMPIAL(I,1,J)=0D0
6885    CONTINUE
        IF(D3.GT.D) GOTO 6990
C6880  WE HAVE MOVED TO THE NEXT SURFACE
6990    RETURN
        END
```

Subroutine TALLY:

```
C+++++++++++++++++++++++++++++++++++++++++++++++++++++++++++++++++++++++++
*C+++++++++++++++++++++++++++++++++++++++++++++++++++++++++++++++++++++++++


      COMPILER DOUBLE PRECISION
      SUBROUTINE TALLY
C     ----------------
C 7002  THIS SUBROUTINE TALLYS THE ENERGY
C7004  DEPOSITED IN THE PHANTOM. WE USE A
C 7006  COMPUTED GOTO TO TRANSFER OUR ENERGY
C 7008  TALLY TO THE CORRECT MATRIX POSITION
C 7010  THE TALLY GEOMETRY IS GIVEN ON PAGE 4
C 7012  OF THE FORMATING AND THE 7000 SERIES (11/5/77)
 C 7014  FIRST, DETERMINE IF THE PHOTON LIES NEAR THE
 C 7016  Z=ZERO PLANE
CH      DIMENSION TAL(16,1,13),TALSQ(16,1,13),EVNTPV(16,1,13)
 CH      DIMENSION INPTAL(16,1,13),RTAL(0:16),TLSQ2(5,1,13)
         DIMENSION TAL(19,1,13),TALSQ(19,1,13),EVNTPV(19,1,13)
        DIMENSION INPTAL(19,1,13),RTAL(0:19),TLSQ2(5,1,13)
 CH12    DIMENSION TAL(13,1,13),TALSQ(13,1,13),EVNTPV(13,1,13)
 CH12    DIMENSION INPTAL(13,1,13),RTAL(0:13),TLSQ2(5,1,13)
         COMMON/VAR/A,A1,A0,C2,C7,C8,C6,C5,C9,C1,C0
         COMMON/VAR/D8,D3,D9,D,DNO,D7,D50,DLO,D1,D2,DL
         COMMON/VAR/EVNTPV,E1,E2,E,E0,G8,G2,G3,G4,G5,G6,G9,G7
         COMMON/VAR/NO,R,I,IX(2),IY(2),IZTAL,IRTAL,ITHTAL,J
         COMMON/VAR/PI,P0,P,P1,R,S2,S9,S1,S3,S4,TAL,TALSQ
         COMMON/VAR/T,T8,T9,TI,U,U1,U2,U0,V1,V2,V0,W1,W2,W0
         COMMON/VAR/X0,Y0,YPL,Y1,Z8,Z9,Z0,Z1
        COMMON/VAR/U3,U4,U5,U6,U7,V3,V4,V5,V6,V7
        COMMON/VAR/W3,W4,W5,W6,W7
        COMMON/VAR/INPTAL,ITERM,HITE,RDOUT,RTAL,RADIN,VTAL
         COMMON/VAR/SEEVAR,VARSM,STDV,TLSQ2
        IF(DABS(Z0)-((66.04D0-R)/108.6D0)) 7030,7030,7029
 C 7022  NOT IN THE ZERO PLANE. IS Z POS. OR NEG.?
7029    GOTO 7035
7030    IZTAL=1
        GOTO 7200
C 7034  IS Z NEGATIVE?
7035    IF(Z0.LT.0D0) GOTO 7100
C 7036  IS Z IN THE FIRST PLANE ABOVE ZERO?
        IF(DABS(Z0)-((66.04D0+R)/108.6D0)) 7050,7050,7049
 C 7042  WHICH PLANE ABOVE Z=0 IS IT IN?
7049    GOTO 7060
7050    IZTAL=2
        GOTO 7200
7060    IZTAL=(IDINT(Z0/2D0)+2D0)+2D0
       IF(IZTAL.GE.14) GOTO 7500
C 7062  NOW DETERMINE THE RADIAL POSITION
        GOTO 7200
7100    IF(DABS(Z0)-((66.04D0+R)/108.6D0)) 7110,7110,7109
 7109    GOTO 7130
7110    IZTAL=3
        GOTO 7200
C 7120  CALCULATE FOR Z PLANE
7130     IZTAL=(IDINT(DABS(Z0)/2D0)+2D0)+2D0+1D0
        IF(IZTAL.GE.15) GOTO 7500
        GOTO 7200
C 7190  NOW WHAT IS THE RADIAL POSITION?
CH7200  IRTAL=IDINT(16.5D0-DSQRT(DABS(X0)**2D0+DABS(Y0)**2D0))
 7200    IRTAL=IDINT(19.5D0-DSQRT(DABS(X0)**2D0+DABS(Y0)**2D0))
 CH127200        IRTAL=IDINT(13.5D0-DSQRT(DABS(X0)**2D0+DABS(Y0)**2D0))
 C 7210  NOW WHAT IS THETA?
        GOTO 7300
C 7290  THETA'S VALUE IS:
```

```
7300     ITHTAL=1
C 7310   NOW TALLY
         TAL(IRTAL,ITHTAL,IZTAL)=TAL(IRTAL,ITHTAL,IZTAL)+E
          TMPTAL(IRTAL,ITHTAL,IZTAL)=TMPTAL(IRTAL,ITHTAL,IZTAL)
       C  +E
         EVNTPV(IRTAL,ITHTAL,IZTAL)=EVNTPV(IRTAL,ITHTAL,IZTAL)
       C  +1D0
C 7410   WE HAVE NOW TALLIED THE ENERGY.
         IF(ITERM.EQ.0) GOTO 7500
         DO 7498 J=1,13
         TLSQ2(1,1,J)=TMPTAL(1,1,J)+TMPTAL(2,1,J)+TMPTAL(3,1,J)
          TLSQ2(2,1,J)=TMPTAL(4,1,J)+TMPTAL(5,1,J)+TMPTAL(6,1,J)
          TLSQ2(3,1,J)=TMPTAL(7,1,J)+TMPTAL(8,1,J)+TMPTAL(9,1,J)
          TLSQ2(4,1,J)=TMPTAL(10,1,J)+TMPTAL(11,1,J)+TMPTAL(12,1,J)
          TLSQ2(5,1,J)=TMPTAL(13,1,J)+TMPTAL(14,1,J)+TMPTAL(15,1,J)
       C  +TMPTAL(16,1,J)
7498     CONTINUE
CH       DO 7499 I=1,16
         DO 7499 I=1,19
CH12     DO 7499 I=1,13
         DO 7499 J=1,13
         IF (TMPTAL(I,1,J).EQ.0D0) GOTO 7499
         TALSQ(I,1,J)=TALSQ(I,1,J)+TMPTAL(I,1,J)**2D0
          TMPTAL(I,1,J)=0D0
7499     CONTINUE
7500     RETURN
         END
         SUBROUTINE RAND32(IX,IY,YFL)
         DIMENSION IX(2),IY(2)
         DOUBLE PRECISION YFL
C        INITIAL IY(1)=1
C        INITIAL IY(2)=3
C        SECOND IY(1)=29513/AFTER 22.5K HISTORIES
C        SECOND IY(2)=9597/AFTER 22.5K HISTORIES
C        THIRD IY(1)=27107/AFTER 37.5K HISTORIES
C        THIRD IY(2)=-2031/AFTER 37.5K HISTORIES
C        FOURTH IY(1)=500
C        FOURTH IY(2)=27309
         IY(1)=2478                 I65536
        IY(2)=-4201                I+3=65539
        NCHK=0
         CALL DUMPY(IX,IY,NCHK)
         IF(IY(1).GE.0) GO TO 200
         IY(1)=IY(1).AND.77777K
20       CONTINUE
         CALL DUFL(IY,YFL)
         YFL=YFL*.4656613D-9
         RETURN
         END
```

Appendix B.3 Models Used in the Spectrum - Design Code - RELSLIB3

The purpose of this appendix is to present the models and methods used to simulate the operation of a hypothetical tomochemistry CT scanner. The aim of the simulation was to determine the pair of x-ray spectra which would be optimal for the proof-of-principle tomochemistry experiment. This appendix section is divided into four subsections each of which describes one of the four major parts of the scanner - the x-ray tube, the beam filtration, the x-ray detector, and the hypothetical scanned target. The results of the simulations using these models are presented in Section 2.1.3.

Appendix B.3A X-ray Tube Model

As mentioned in Section 2.1.1 the x-ray tube used in the experiment was a fixed anode x-ray tube a line drawing of which is given in Fig. 2.1A.1. In the scanner simulation program x-ray kilovoltages of 100 and 150 kVp were simulated. The spectra used for the simulation were those determined experimentally by Storm, Israel, and Lier (S.4) at the Los Alamos Scientific Laboratory. These spectra are illustrated in Fig. 2.1A.2. The x-ray tube used in the experiment was a Machlett CL-150 tube. This tube had 1.7 mm Aℓ and 1.0 mm Be inherent filtration. With this filtration the extant spectrum from the tube is given by the expression (ignoring scattered radiation):

$$\Phi(E) = \Phi^{(E)}_{EXPT} \exp(-\mu_{A\ell}(E) * 1.7 \text{ mm} - \mu_{Be}(E) * 1.0 \text{ mm}) \quad (B.3A.1)$$

where

$\Phi^{(E)}_{EXPT}$ is the experimentally determined flux from the x-ray tube at energy E in γ/cm^2-sec-ma-keV at 1 m from the x-ray tube.

$\mu_{A\ell}$, μ_{Be} is the attenuation coefficient of aluminum and beryllium respectively.

The aluminum and beryllium attenuation coefficients at energy E were determined from the expression (V.1):

$$\mu(cm^{-1}) = \frac{\rho(\frac{gm}{cm^3})}{A(\frac{gm}{mole})} N_A(\frac{atoms}{mole}) * 10^{-24} \frac{cm^2}{barn} * [\sigma_p + Z\sigma_{KN}] \frac{barns}{atom} \quad (B.3A.2)$$

$$\sigma_p = \exp\left(\sum_{i=0}^{n} a_i (\ell n\ E)^i\right) \frac{barns}{atom} \quad (B.3A.3)$$

$$\sigma_{KN} = 2\pi r_o^2 \left\{ \frac{1+\alpha}{\alpha^2} \left[\frac{2(1+\alpha)}{1+2\alpha} - \frac{1}{\alpha} \ell n(1+2\alpha) \right] + \frac{1}{2\alpha} \ell n(1+2\alpha) - \frac{1+3\alpha}{(1+2\alpha)^2} \right\} \frac{barns}{electron} \quad (B.3A.4)$$

where

ρ is the density of the material m gm/cm^3.

A is the atomic weight in gm/mole.

N_A is avogadro's number = $6.0225*10^{23} \frac{atoms}{mole}$

σ_p is the photoelectric cross section in barns/atom.

Z is the atomic number.

σ_{KN} is the Klein-Nishina cross Section (E.2) in barns/electron.

a_i is the ith polynomial fit coefficient in the polynomial expansion representation of the photoelectric cross section (V.1).

E is the photon energy in keV.

r_o is the classical radius of the electron - $2.818*10^{-13}$cm.

The functional fit was chosen for use rather than a look-up table to facilitate computation. The photon flux of the x-ray tube given by the expression:

$$\Phi_{EXPT} = \int_{0}^{E_{max}} \Phi_{EXPT}^{(E)} \, dE$$

is dependent upon the peak kilovoltage of the x-ray tube. It is about $2.2*10^{8}$ γ/cm^{2}-sec-ma at 100 kVp and $5.5*10^{8}$ γ/cm^{2}-sec-ma at 150 kVp at a distance of 1 m from the tube.

Appendix B.3B Filter Model

The x-ray beam filtration with the beam analyzer disk was modeled assuming that scattered radiation and possible K-fluorescence radiation from the filters were not detectable. In the simulation the filter being investigated could be either a simple or compound filter (2 filters in series). The thickness could be varied in the simple filter and in both filters of the compound filter. As in the x-ray tube inherent filtration, the attenuation coefficient was described by Eq. (B.3A.2). The fit coefficients and densities of the filter materials were also taken from Ref. (V.1). Thus, the resultant normalized bremsstrahlung spectrum distribution after filtration is given by the expression:

$$S(E) = \frac{\Phi(E)\ \exp(-\mu_{FA}t_{FA} - \mu_{FB}t_{FB})}{\int_0^{E_{max}} \Phi(E)\ \exp(-\mu_{FA}t_{FA} - \mu_{FB}t_{FB})\ dE} \qquad (B.3B.1)$$

where

$\Phi(E)$ is the unnormalized bremsstrahlung spectrum distribution exetant from the inherently filtered x-ray tube.

μ_{FA}, μ_{FB} is the attenuation coefficient (cm^{-1}) of filter A and B in the compound filter respectively. If the filter is a simple filter, μ_{FB} is set to zero.

t_{FA}, t_{FB} is the thickness (cm) of filter A and B respectively. If the filter is a simple filter, t_{FB} is set to zero.

It is important to note that the filter which is being studied may have a K-edge and L-edge within the diagnostic energy range. In this

case more than one expression similar to Eq. (B.3A.3) was used to describe the photoelectric attenuation coefficient of the filter. More exactly, a different set of coefficients was used for energies less than the L-edge, between the L-edge and K-edge, and greater than the K-edge.

Appendix B.3C Detector Model

The x-ray detector as described in Section 2.1.1 and illustrated in Fig. 2.1A.3 has an energy-dependent detection efficiency. To model this efficiency, $\varepsilon(E)$, it was assumed that the geometry was sufficiently 'good' so that scattered radiation from the scanned target was not detectable. The total detection efficiency of the detector is given by the product of the efficiencies of each process of the detector.

The efficiency at energy E of photon transmission through the 3.175 Aℓ window is given by the expression:

$$\varepsilon_W(E) = \exp(-\mu_{A\ell}(E)\ T_{wind}) \qquad (B.3C.1)$$

where

T_{wind} is the 'window' thickness. The window is actually not flat but slightly curved, with the thickness varying with the axial position. In the calculation the 'window' was assumed to be flat with a mean thickness of 3.175 mm.

The efficiency at energy E of photon transmission through the 'dead space' (the region between the aluminum window and the active region of the ionization detector) is given by the expression:

$$\varepsilon_d(E) = \exp(-\mu_{Xe}(E)\ T_d) \qquad (B.3C.2)$$

where

T_d is the thickness (cm) of the 'dead space'. This 'dead space' is about 3.175 mm long.

$\mu_{Xe}(E)$ is the attenuation coefficient of the xenon gas within the pressure vessel for the 95% Xe-5% CO_2/213 psia mixture. It was assumed that the CO_2 attenuation coefficient was negligible.

The probability that an incident photon entering the active region will interact with the 95% Xe-5% CO_2 gas is defined as the interaction efficiency. The interaction efficiency is given by the expression:

$$\varepsilon_I(E) = (1 - \exp(-\mu_{Xe}(E)\ X_{det})) \qquad \text{(B.3C.3)}$$

where

$\mu_{Xe}(E)$ is the same as in Eq. (B.3C.2)

X_{det} is the length of the active region ($\sim$10 cm).

It was assumed in Eq. (B.3C.3) that there was no Compton scattering within the gas, that the incident x-ray doesn't strike the sides or edge of the ionization chamber, and that the CO_2 gas attenuation coefficient is negligible.

Once an incident x-ray of energy E has interacted with a xenon atom within the active region the resultant xenon ion may or may not fluoresce. A fluorescence can occur only if the incident x-ray energy is greater than 34.56 keV and if that x-ray interacts with the K-shell electron of the xenon. The model of Davidson (D.3) was used to determine the probability of an interaction of a photon with a K-shell electron. The probability of interaction is given by the ratio of the photoelectric cross section contribution due only to the K-shell to the total photoelectric cross section:

$$P_K = \frac{\mu_{PTOT} - \mu_{PNON-K}}{\mu_{PTOT}} \qquad \text{(B.3C.4)}$$

where

μ_{PTOT} is the total photoelectric cross section

μ_{PNON-K} is the non K-shell contribution to the photoelectric cross section. It is approximately determined by extrapolation of the cross section at energies less than the K-edge to those energies greater than the K-edge.

After a K-shell electron interaction has occurred the probability of a fluorescence of the xenon atom is (B.4,L.4,F.2):

$$\omega_K = 0.889$$

Therefore, the probability of a fluorescence event to occur is given by the expression:

$$\varepsilon_F = \omega_K \left(\frac{\mu_{PTOT} - \mu_{PNON-K}}{\mu_{PTOT}} \right) \qquad \text{(B.3C.5)}$$

Furthermore, the probability of a non-fluorescence event to occur is given by the expression:

$$\varepsilon_{NON-F} = 1 - \omega_K \left(\frac{\mu_{PTOT} - \mu_{PNON-K}}{\mu_{PTOT}} \right) \qquad \text{(B.3C.6)}$$

If a non-fluorescence event occurs all of the x-ray energy is assumed to be absorbed within the gas of the ionization chamber. If a fluorescence event occurs all but 30.4 keV of the incident x-ray energy is assumed to be absorbed within the gas. The 30.4 keV fluorescent x-rays are emitted from the excited xenon atoms isotropically. These

x-rays may either strike one of the parallel plates of the ionization chamber - thereby not depositing its energy within the gas - or interact with the gas producing electron-ion pairs within the active region.

The probability of a K-fluorescent photon reabsorption is given by the expression:

$$\varepsilon_{F.REABS.} = (1 - \exp(-\mu_{Xe}(30.4\ keV) * \delta)) \qquad (B.3C.7)$$

where

$\mu_{Xe}(30.4\ keV)$ is the Xenon gas attenuation coefficient for a 30.4 keV fluorescent photon

δ is the distance from the site of K-fluorescence photon emission to the boundary of the active region in the direction of the x-ray fluorescence emission. The boundary is determined by the parallel plates and also the ends of the chamber.

Yaffe, Fenster, and Johns (Y.1) studied in detail the reabsorption of fluorescent x-rays within xenon parallel plate ionization chambers. In general it was found that for the geometries typical of CT scanner detectors that the majority of the x-ray fluorescence energy is not reabsorbed within the active region. Based on Yaffe's work it was estimated that for the MGH scanner about 25% of the fluorescent x-rays are reabsorbed ($\varepsilon_{F.REABS.} = 0.25$).

The final efficiency consideration for the detector is the charge collection efficiency, ε_q. It was experimentally determined that at the -2500 V operating potential that about 96% of the charge formed within the detector is collected ($\varepsilon_q = 0.96$).

Combining all the above efficiencies the total energy-dependent x-ray detection efficiency is given by the expression:

$$\varepsilon = \varepsilon_q \, \varepsilon_d \, \varepsilon_W \, [\varepsilon_I(\varepsilon_{NON\text{-}F} + \varepsilon_F * \varepsilon_{F.REABS.})] \qquad (B.3C.8)$$

For xenon the amount of energy per ion-pair, w, is about 21.9 eV. Therefore, the current production efficiency of the detector is given by:

$$I(amps) = \int_0^{E_{max}} \Phi^{(E)}_{E.DET.} \, \frac{A_D \, \varepsilon \, q_o}{w} \, dE \qquad (B.3C.9)$$

where

$\Phi^{(E)}_{E.DET.}$	is the energy flux at the detector in keV/sec-cm^2-keV at energy E
A_D	is the area of the detector
ε	is the x-ray detection efficiency at energy E
q_o	is the fundamental charge of the electron = $1.6*10^{-19}$coul
w	is the energy required to form one electron-ion pair.

Appendix B.3D Water Cylinder Target and Resolution Element Model

The goal of this subsection is to develop models to determine the accuracy of reconstruction of a reference target in a tomochemistry scan. A 20 cm water cylinder was chosen to represent a reference head-like target scanned in a scanner which was assumed to have 'good' geometry. The detected x-ray signal in the scanning process was determined from analytic attenuation calculations which used water attenuation and absorption (for dose) coefficients from Hubbell (H.4). To model a reconstructed resolution element a 1 cm^2 test element was placed in the center of the water cylinder. Of all the resolution elements within the scanned target the central resolution element's attenuation coefficient is the most difficult to determine. This is because transmission measurements on this element must always be made through the full diameter of the water target. Therefore, the results of the statistical error calculations represent a worst case from a statistical measurement accuracy viewpoint.

The following derivations represent the heart of the optimal design approach taken by this author. Other authors have considered and modeled the error of tomochemistry measurements (A.2,A.4,A.6,K.1). However, their works (which were all published after this author's design work had already been completed) all fall short of presenting any systematic design method of a tomochemistry CT scanner. Generally it was found that the results of this work agreed with their work except that since they all assumed that the x-ray detection efficiency was perfect at low energies (< 50 keV this is a very poor assumption) their estimate of the optimal x-ray energies were lower than this author's estimate.

Derivation a: If a total of N photons are used to perform two transmission measurements the minimum total error of those two measurements occurs if an equal number of photons, N/2, are used for each measurement. To show that this is true let:

$$N = \epsilon N + (N-\epsilon N)$$

$$N_1 = \epsilon N$$

$$N_2 = (N-\epsilon N)$$

where

ϵ is a parameter to be determined

N_1 is the number of photons used in the first photon transmission measurement

N_2 is the number of photons used in the second photon transmission measurement.

From Poisson statistics the error of measurements 1 and 2 are given by:

$$\delta N_1 = \sqrt{\epsilon N}$$

$$\delta N_2 = \sqrt{N-\epsilon N}$$

The total error per photon of the two measurements is given by:

$$\frac{\sum_i \delta N_i}{N} = \frac{\sqrt{\epsilon N} + \sqrt{N-\epsilon N}}{N} \qquad \text{(B.3D.1)}$$

To find the minimum of the total error take the derivative of Eq. (B.3D.1) with respect to ϵ:

$$\frac{\partial\left(\sum_i \delta N_i/N\right)}{\partial \epsilon} = \frac{1}{2\sqrt{\epsilon N}} - \frac{1}{2\sqrt{N-\epsilon N}} = 0$$

therefore:

$$\epsilon N = N - \epsilon N$$

$$\epsilon = 1/2$$

hence

$$N_1 = N_2 = N/2 \qquad \text{(B.3D.2)}$$

Therefore, in a tomochemistry measurement where two transmission measurements are performed on an unknown target, the tomochemistry measurement is most accurate if an equal number of photons are detected in each transmission measurement.

Derivation b: The statistical error of a tomochemical determination of $(\mu_p+\mu_R)$, the photoelectric + Rayleight cross sections. In this derivation assume that a reference energy, R, is used to present the data and that the two incident x-ray beams can be considered monochromatic for this derivation. As seen in Fig. B.3D.1 the reference energy photoelectric + Rayleigh and Compton cross sections can be related to the photoelectric + Rayleigh and Compton cross sections of the two x-ray beams by four constants:

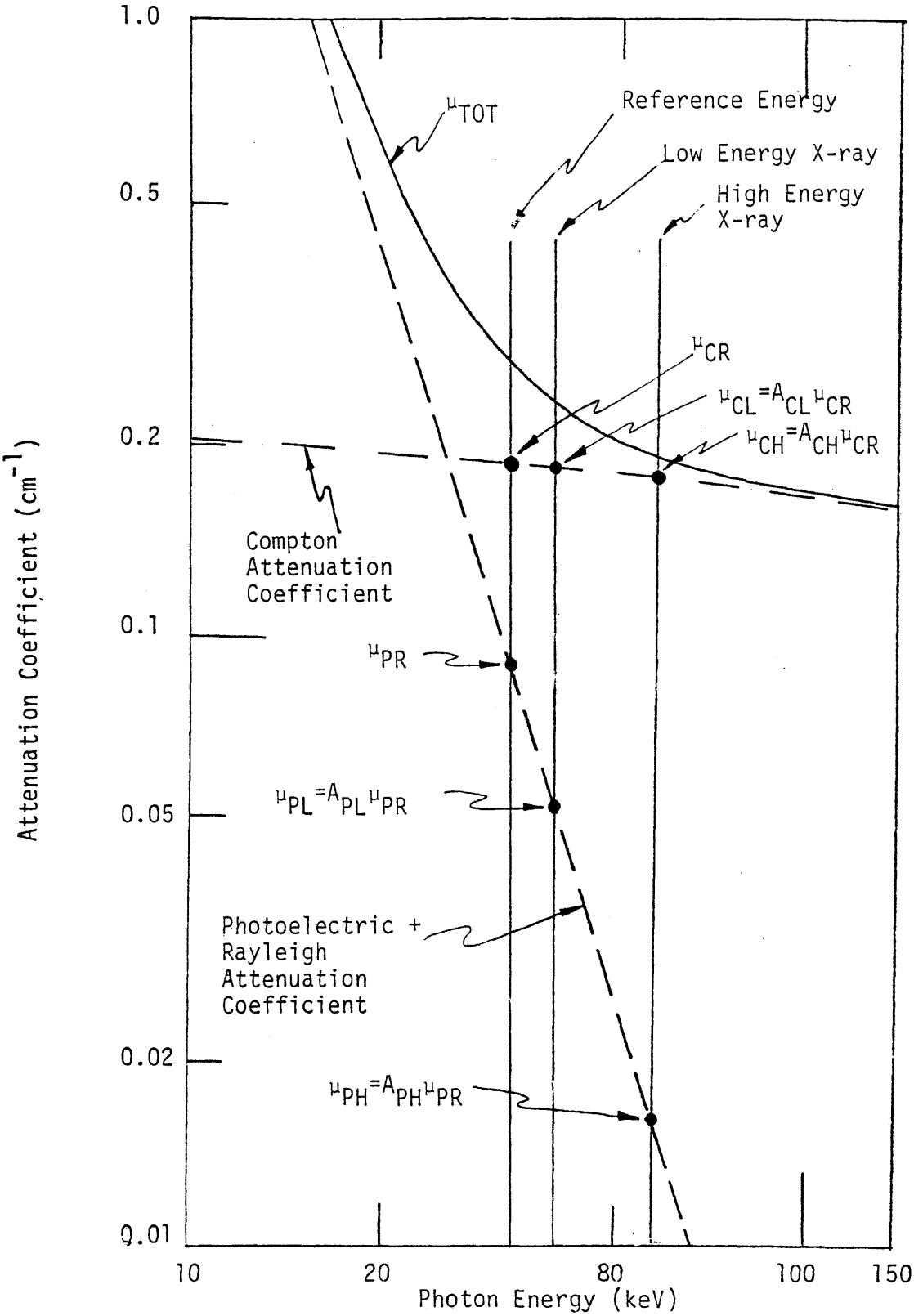

Figure B.3D.1 Relation between the reference energy and high and low energy attenuation coefficients.

$$\mu_{CL} = A_{CL}\ \mu_{CR} \tag{B.3D.3}$$

$$\mu_{PL} = A_{PL}\ \mu_{PR} \tag{B.3D.4}$$

$$\mu_{CH} = A_{CH}\ \mu_{CR} \tag{B.3D.5}$$

$$\mu_{PH} = A_{PH}\ \mu_{CR} \tag{B.3D.6}$$

where

H,L subscripts correspond to the high and low energy x-ray beam respectively

P,C subscripts correspond to the photoelectric + Rayleigh and Compton cross sections

R subscript refers to the reference energy cross section

A_{CL}, A_{PL}, A_{CH}, A_{PH} are all constants of proportionality.

Using Eqs. (B.3D.3) through (B.3D.6) μ_{CR}, and μ_{PR} can be determined by noting that:

$$\begin{aligned}\mu_{TL} &= \mu_{CL} + \mu_{PL} \\ &= A_{CL}\ \mu_{CR} + A_{PL}\ \mu_{PR}\end{aligned} \tag{B.3D.7}$$

$$\begin{aligned}\mu_{TH} &= \mu_{CH} + \mu_{PH} \\ &= A_{CH}\ \mu_{CR} + A_{PH}\ \mu_{PR}\end{aligned} \tag{B.3D.8}$$

where

μ_{TL},μ_{TH} are the total attenuation coefficients measured with the low and high energy x-ray beams.

Solving Eq. (B.3D.7) and Eq. (B.3D.8) it is found that

$$\mu_{CR} = \frac{A_{PH}\ \mu_{TL} - A_{PL}\ \mu_{TH}}{A_{CL}\ A_{PH} - A_{CH}\ A_{PL}} = \frac{A_{PH}\ \mu_{TL} - A_{PL}\ \mu_{TH}}{|D|} \qquad \text{(B.3D.9)}$$

$$\mu_{PR} = \frac{A_{CL}\ \mu_{TH} - A_{CH}\ \mu_{TL}}{A_{CL}\ A_{PH} - A_{CH}\ A_{PL}} = \frac{A_{CL}\ \mu_{TH} - A_{CH}\ \mu_{TL}}{|D|} \qquad \text{(B.3D.10)}$$

where

$|D|$ is the determinant of the coefficient matrix of the simultaneous equations.

Since μ_{PR} is much smaller than μ_{CR} the fractional error of the determination of μ_{PR} is larger than that of μ_{CR}. Hence, minimization of the statistical error should concentrate on μ_{PR}. μ_{PR} is then given by:

$$\mu_{PR} \pm \delta\mu_{PR} = \frac{A_{CL}}{|D|}\ \mu_{TH} - \frac{A_{CH}}{|D|}\ \mu_{TL} \pm \left[\left(\frac{A_{CL}}{|D|}\ \delta\mu_{TH}\right)^2 + \left(\frac{A_{CH}}{|D|}\ \delta\mu_{TL}\right)^2\right]^{1/2} \qquad \text{(B.3D.11)}$$

Using Chesler's theory (C.5) $\delta\mu_{TH}$ and $\delta\mu_{TL}$ are given by:

$$\delta\mu_{TH} = \left(\frac{4}{3}\ \frac{1}{N_{TH}}\right)^{1/2}\ \frac{1}{X} \qquad \text{(B.3D.12)}$$

$$\delta\mu_{TL} = \left(\frac{4}{3}\ \frac{1}{N_{TL}}\right)^{1/2}\ \frac{1}{X} \qquad \text{(B.3D.13)}$$

where

N_{TH}, N_{TL} are the number of photons detected which passed through the central resolution element.

X is the size of the picture element (spatial resolution).

Using Eq. (B.3D.12) and Eq. (B.3D.13) the fractional statistical error of μ_{PR} is given by:

$$\frac{\delta\mu_{PR}}{\mu_{PR}} = \frac{\left(\frac{4}{3}\right)^{1/2}\left(\frac{1}{X}\right)\left[(A_{CL})^2\,\frac{1}{N_{TH}} + (A_{CH})^2\,\frac{1}{N_{TL}}\right]^{1/2}}{A_{CL}\,\mu_{TH} - A_{CH}\,\mu_{TL}} \qquad \text{(B.3D.14)}$$

Derivation c: Extension of the μ_{PR} statistical error expression and its relationship to the figures-of-merit. Equation (B.3D.14) as it stands can be used to estimate the fractional statistical measurement error of μ_{PR}, however to use this expression to aid in the design process it must be slightly modified. Imagine that wihtin the central resolution element of the pure water target the average atomic number has been increased by an incremental amount $\Delta\bar{Z}$ but that the number of atoms per cubic centimeter is kept constant. In this situation the attenuation coefficients change by an amount given by:

$$\Delta\mu_{PR} = N\,k_{PR}\,Z^{4.6}\left[\left(1 + \frac{\Delta Z}{\bar{Z}}\right)^{4.6} - 1\right] \quad \text{(photoelectric change)}$$

$$\Delta\mu_{CR} = N\,\sigma_{KN}\,Z\left[\left(1 + \frac{\Delta Z}{\bar{Z}}\right) - 1\right] \quad \text{(Compton change)}$$

$$\Delta\mu_{RR} = N\,k_{R}\,Z^{2.9}\left[\left(1 + \frac{\Delta Z}{\bar{Z}}\right)^{2.9} - 1\right] \quad \text{(Rayleigh change)}$$

and

$$\Delta\mu_{(P+R)R} = \Delta\mu_{PR} + \Delta\mu_{CR} = \Delta\mu_{PL}/A_{PL} = \Delta\mu_{PH}/A_{PH}$$

$$\Delta\mu_{CR} = \Delta\mu_{CL}/A_{CL} = \Delta\mu_{CH}/A_{CH}$$

where

subscripts C, P, L, H, R and variables A_{PL}, A_{PH}, A_{CL}, A_{CH} are the same as in Eqs. (B.3D.3) through (B.3D.6).

Now imagine that one wants to measure the change in the photoelectric + Rayleigh cross section due to the change in $\bar{Z}$. This measurement process can be modeled by considering the measurement of this added attenuation as a transmission measurement of an excised picture element. This approach, illustrated in Fig. B.3D.2, is justified because of:

(1) The linear behavior of transmission measurements, i.e., the x-ray transmission fraction of one resolution element with an attenuation coefficient of $\mu_T = \mu_1 + \mu_2$ is the same as the transmission fraction of two resolution elements - one with an attenuation coefficient μ_1 and the other with an attenuation coefficient μ_2; and

(2) Chesler's principle - which states that in CT the measurement statistics of the attenuation coefficient of an element embedded within a target is the same to within a constant as the measurement statistics for an element which has been excised from the target.

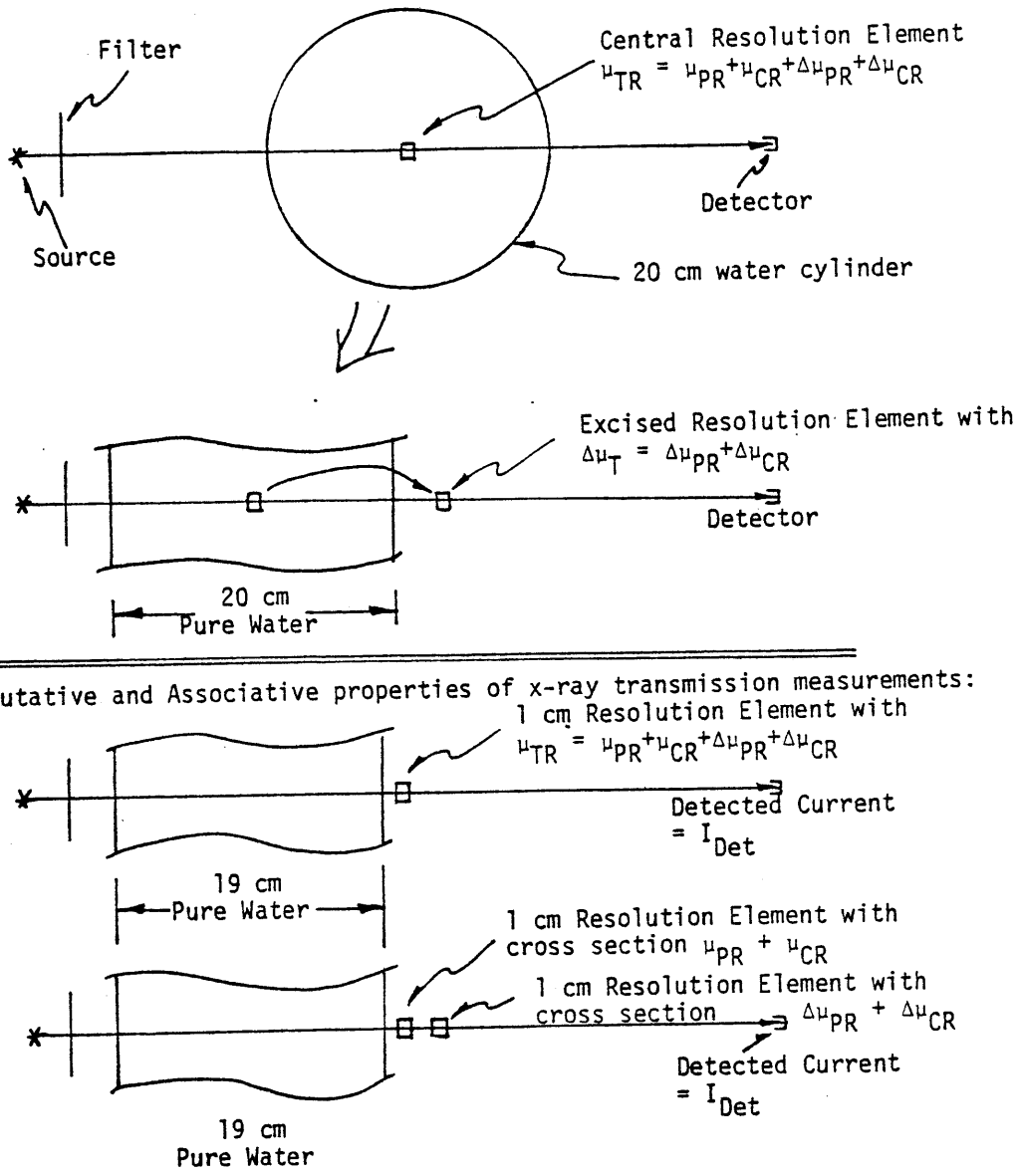

Figure B.3D.2 Picture element model used in the statistical measurement uncertainty derivations.

By using Eq. (B.3D.14) the statistical error of the measurement of $\Delta\mu_{PR}$ is given by:

$$\frac{\delta\Delta\mu_{PR}}{\Delta\mu_{PR}} = \frac{\left(\frac{4}{3}\right)^{1/2}\left(\frac{1}{X}\right)\left[(A_{CL})^2\,\frac{1}{N_{TH}} + (A_{CH})^2\,\frac{1}{N_{TL}}\right]^{1/2}}{A_{CL}\,\Delta\mu_{TH} - A_{CH}\,\Delta\mu_{TL}} \qquad \text{(B.3D.15)}$$

Equation (B.3D.15) can be simplified by considering the measurement process on an excised element. In the measurement process assume that in the high and low energy transmission measurements equal numbers of photons are used in the transmission measurements of the excised element shown in Fig. B.3D.2 ($N_L = N_H = N_o$). The high and low energy total attenuation coefficients are determined from the expression:

$$\ell n\,(\exp(-\Delta\mu_{TL}\,X)) = \ell n\,\frac{N_{\Delta TL}}{N_o} = -\,\Delta\mu_{TL}\,X \qquad \text{(B.3D.16)}$$

$$\ell n\,(\exp(-\Delta\mu_{TH}\,X)) = \ell n\,\frac{N_{\Delta TH}}{N_o} = -\,\Delta\mu_{TH}\,X \qquad \text{(B.3D.17)}$$

Now at $\frac{N_\Delta}{N_o}$ close to 1 ($\Delta\mu X$ small) the natural logarithm can be approximated by the expression:

$$-\ell n\,\frac{N_{\Delta TL}}{N_o} \simeq 1 - \frac{N_{TL}}{N_o} = \Delta\mu_{TL}\,X = \frac{N_o - N_{TL}}{N_o} \qquad \text{(B.3D.18)}$$

$$-\ell n\,\frac{N_{\Delta TH}}{N_o} \simeq 1 - \frac{N_{TH}}{N_o} = \Delta\mu_{TH}\,X = \frac{N_o - N_{TH}}{N_o} \qquad \text{(B.3D.19)}$$

Furthermore, since the Compton cross section is relatively constant with energy then $A_{CL} \sim A_{CH}$. Hence, with these approximations Eq. (B.3D.15) can be rewritten:

$$\frac{\delta\Delta\mu_{PR}}{\Delta\mu_{PR}} \cong \frac{\left[\frac{4}{3}\left(\frac{1}{N_{TH}} + \frac{1}{N_{TL}}\right)\right]^{1/2}}{\frac{N_o - N_{TL}}{N_o} - \frac{N_o - N_{TH}}{N_o}} \qquad \text{(B.3D.20)}$$

Now it is known that:

$$\frac{N_o - N_{TL}}{N_o} = \frac{I_o - I_{TL}}{I_o} = \left(\frac{I_o - I_{TL}}{I_o}/\Delta\bar{Z}\right) * \Delta\bar{Z} \equiv S_L * \Delta\bar{Z}$$

and

$$\frac{N_o - N_{TH}}{N_o} = \frac{I_o - I_{TH}}{I_o} = \left(\frac{I_o - I_{TH}}{I_o}/\Delta\bar{Z}\right) * \Delta\bar{Z} \equiv S_H * \Delta\bar{Z}$$

where

I_o is the detected current with no excised element within the x-ray beam

I_{TL} is the low energy x-ray detected current with the excised element within the beam

I_{TH} is the high energy x-ray detected current with the excised element within the beam

S_L defined as the low energy x-ray sensitivity factor

S_H defined as the high energy x-ray sensitivity factor

$\Delta\bar{Z}$ is the small change in the average atomic number which caused the change in the cross sections within the original resolution element.

Therefore Eq. (B.3D.20) can be rewritten:

$$\frac{\delta\Delta\mu_{PR}}{\Delta\mu_{PR}} = \frac{\left[\frac{4}{3}\left(\frac{1}{N_{TH}} + \frac{1}{N_{TL}}\right)\right]^{1/2}}{(S_L - S_H)\ \Delta Z} \qquad \text{(B.3D.21)}$$

It is seen here that S_H and S_L are characteristic of the two incident x-ray beams. Also it is seen that the fractional error of the determination of $\Delta\mu_{PR}$ can be minimized by maximizing the difference between the two spectrum sensitivities. Equation (B.3D.21) can be further modified by expressing N_{TH} and N_{TL} in terms of other spectrum-related characteristics. The approach taken here is analogous to the four-factor formula derivation of Fermi (H.8) in reactor physics where the ratio of two unmeasureable integrals were expressed in terms of the product of four measureable integral ratios.

To begin the derivation first consider the expression for the average number of photons detected, $\bar{N}$, after their transmission through the beam filter and the water target:

$$\bar{N} = A_D\left(\frac{D_D}{D_R}\right)^2 \Phi_R\ T\ \frac{\int_0^E \phi(E)\ \exp(-\mu_F t_F)\ \exp(-\mu_W{}^*20)\varepsilon\ dE}{\int_0^E \phi(E)\ \exp(-\mu_F t_F)\ dE} \qquad \text{(B.3D.22)}$$

where

A_D is the area of the detector

D_D/D_R is the ratio of the source-to-detector distance to the source-to-rotation axis distance

Φ_R is the photon flux (γ/cm^2-sec) at the rotation axis of the scanner

T is the duration of the scan in seconds

$\phi(E)$ is the normalized bremsstrahlung spectrum distribution before the spectrum shaping filtration and after the inherent x-ray tube filtration

The other terms are the same as in the previous subsection.

Now to express Eq. (B.3D.22) in terms of other physical quantities note that:

(1) the average energy of the detected photons is given by the expression:

$$\overline{E}\left(\frac{keV}{\gamma_{DET}}\right) = \frac{\int_0^{E_{max}} \phi(E)\, \exp(-\mu_F t_F)\, \exp(-\mu_W 20)\varepsilon\, E\, dE}{\int_0^{E_{max}} \phi(E)\, \exp(-\mu_F t_F)\, \exp(-\mu_W 20)\varepsilon\, dE} \qquad \text{(B.3D.23)}$$

(2) the average amount of energy detected per photon incident, ϵ/γ_{IN} upon the water target is given by the expression:

$$\epsilon/\gamma\left(\frac{keV}{gm\text{-}\gamma_{IN}}\right) = \frac{\int_0^{E_{max}} \phi(E)\, \exp(-\mu_F t_F)\, \exp(-\mu_W * 20)\varepsilon\, E\, dE}{\int_0^{E_{max}} \phi(E)\, \exp(-\mu_F t_F)\, dE} \qquad \text{(B.3D.24)}$$

(3) the average surface dose absorbed per photon incident upon the water target is given by the expression:

$$D/\gamma\left(\frac{keV}{gm\text{-}\gamma_{IN}}\right) = \frac{0.68\int_{o}^{E_{max}} \phi(E)\ \exp(-\mu_F t_F)\ \left(\frac{\mu_{en}E}{p}\right)\ dE}{\int_{o}^{E_{max}} \phi(E)\ \exp(-\mu_F t_F)\ dE} \qquad \text{(B.3D.25)}$$

(4) the surface dose is given by the expression:

$$D\left(\frac{keV}{gm}\right) = \frac{\Phi_R\ T\ 0.68\int_{o}^{E_{max}} \phi(E)\ \exp(-\mu_F t_F)\ \left(\frac{\mu_{en}E}{p}\right)\ dE}{\int_{o}^{E_{max}} \phi(E)\ \exp(-\mu_F t_F)\ dE} \qquad \text{(B.3D.26)}$$

(5) the ratio of the amount of energy detected by the detector (the detected fraction of energy) is given by the expression:

$$F\left(\frac{keV}{keV}\right) = \frac{\int_{o}^{E_{max}} \phi(E)\ \exp(-\mu_F t_F)\ \exp(-\mu_W 20)\ \varepsilon\ E\ dE}{\int_{o}^{E_{max}} \phi(E)\ E\ dE} \qquad \text{(B.3D.27)}$$

(6) the energy fluence of the x-ray tube measured at the detector if no spectrum shaping filtration or water target were present in the x-ray beam:

$$\Phi_E(\text{keV}) = \left(\int_0^{E_{max}} \phi(E)\, E\, dE \right) \left[\frac{\Phi_R \left(\frac{D_D}{D_R} \right)^2}{\int_0^{E_{max}} \phi(E) \exp(-\mu_F t_F)\, dE} \right] * A_D * T \qquad \text{(B.3D.28)}$$

With these expressions it is seen that by combining Eq. (B.3D.23), Eq. (B.3D.27) and Eq. (B.3D.28) that:

$$\frac{1}{N} = \frac{\overline{E}}{F\Phi_E} \qquad \text{(B.3D.29)}$$

and combining Eq. (B.3D.23), Eq. (B.3D.24), Eq. (B.3D.25) and Eq. (B.3D.26) that:

$$\frac{1}{N} = \frac{\overline{E}[(D/\gamma)/(\epsilon/\gamma)]}{D\, A_D \left(\frac{D_D}{D_R} \right)^2} \qquad \text{(B.3D.30)}$$

Therefore, the number of detected photons can be expressed in terms of the energy fluence, of the x-ray tube, Φ_E, or in terms of the surface dose, D. These two parameters are the choice of the experimenter and are independent of the spectrum shape. The three quantities, $\overline{E}$, F, and $[(D/\gamma)/(\epsilon/\gamma)]$ are not arbitrarily variable but rather they are fixed by the experiment design. The third term, $[(D/\gamma)/(\epsilon/\gamma)]$, (considered in the analyses as one spectrum quality) is the surface dose per energy detected ratio.

Using Eq. (B.3D.29), Eq. (B.3D.30) and Eq. (B.3D.21) it is seen that Eq. (B.3D.14) can be written in two independent ways:

$$\frac{\delta\mu_{PR}}{\mu_{PR}} = \left(\frac{\Delta\mu_{PR}}{\mu_{PR}}\right) \frac{\left[\frac{4}{3}\left(\frac{\bar{E}_H}{F_H\,\Phi_E} + \frac{\bar{E}_L}{F_L\,\Phi_E}\right)\right]^{1/2}}{(S_L - S_H)\,\Delta Z} \tag{B.3D.31}$$

and

$$\frac{\delta\mu_{PR}}{\mu_{PR}} = \left(\frac{\Delta\mu_{PR}}{\mu_{PR}}\right) \frac{\left[\frac{4}{3}\left(\frac{\bar{E}_H\,[D/\epsilon]_H}{D_H\,A_D(D_D/D_R)^2} + \frac{\bar{E}_L\,[D/\epsilon]_L}{D_L\,A_D\,(D_D/D_R)^2}\right)\right]^{1/2}}{(S_L - S_H)\,\Delta Z} \tag{B.3D.32}$$

where

L,H subscripts refer to the low and high energy x-ray beam respectively.

D/ϵ is equal to $[(D/\gamma)/(\epsilon/\gamma)]$.

Therefore, it is seen that two independent optimum operating conditions may be determined - minimum error at a fixed photon flux from the x-ray tube and minimum error at a fixed surface dose. As mentioned in Section 2.1B the choice of which experimental design to use depends upon whether the experiment is dose limited or flux limited.

Section 2.1C presents the behavior of these figures-of-merit and also the behavior of the statistical error in the optimization process. A listing of the spectral characteristics and figures-of-

merit for the chosen filters are presented below in Tables B.3D.1 and B.3D.2. The computer program, RELSLIB4 which simulated the tomochemistry measurement process and also determined the values of the figures of merit for the different kVp and filtration schemes is also presented below.

Fractional Transmission F*10^2	Thickness		Sensitivity*10^2		Dose/Energy*10^2 (gm^{-1})Detected		Average Energy (keV)	
	Ta	Fe	Ta	Fe	Ta	Fe	Ta	Fe
0.4413	0μm	0mm	3.363	3.363	15.5	15.5	55.34	55.34
0.40	11.1μm	0.16mm	3.365	3.303	14.7	12.7	56.01	58.20
0.35	26.8μm	0.34mm	3.368	3.246	14.0	11.0	56.68	60.72
0.30	42.6μm	0.61mm	3.375	3.189	13.3	9.4	57.35	63.25
0.25	63.2μm	0.87mm	3.382	3.138	12.8	8.6	57.91	65.37
0.20	87.6μm	1.26mm	3.394	3.086	12.3	7.7	58.47	67.49
0.15	120.1μm	1.75mm	3.406	3.025	11.9	7.1	59.01	69.93
0.10	171.4μm	2.47mm	3.429	2.964	11.5	6.5	59.55	72.36
0.05			3.447	2.904	11.0	5.8	60.09	74.79

Table B.3D.1 Spectral characteristics of the filtered 100 kVp spectrum for a range of filtration thicknesses of iron and tantalum.

Fractional Transmission*10^2,F	Thickness		Sensitivity*10^2		Dose/Energy*10^2(gm^{-1}) Detected		Average Energy (keV)	
	Ta	Fe	Ta	Fe	Ta	Fe	Ta	Fe
0.5956	0μm	0mm	2.900	2.900	9.45	9.45	66.76	66.76
0.50	21.6μm	0.36mm	2.883	2.811	8.83	7.40	68.42	73.28
0.40	53.1μm	0.88mm	2.860	2.720	8.26	6.31	70.28	79.34
0.30	94.7μm	1.61mm	2.835	2.629	7.81	5.63	72.16	85.50
0.25	123.8μm	2.12mm	2.819	2.581	7.60	5.37	73.22	88.90
0.20	155.4μm	2.83mm	2.803	2.528	7.42	5.12	74.28	93.07
0.15	210.3μm	3.76mm	2.778	2.477	7.19	4.93	75.82	97.25
0.10	269.3μm	4.87mm	2.750	2.425	6.99	4.79	77.36	101.43
0.05	422.0μm	7.85mm	2.694	2.356	6.68	4.68	78.9	105.61

Table B.3D.2 Spectral characteristics of the filtered 150 kVp spectrum for a range of filtration thicknesses of iron and tantalum.

Appendix B.3E Listing of the One-Dimensional Photon Transport Program - RELSLIB3

Purpose

To compute the photon transport behavior of a variety of incident spectra to determine their relative viability for use in tomochemistry. The values of the three figures-of-merit, the average spectrum energy, the surface dose, and an estimate of the relative statistical error are computed for two chosen incident spectra. Other parameters of interest which are pertinent to the design process are described within the text of the program.

Program Name	Function
Main Program:	
RELSLIB3	- to simulate CT scanning for a wide range of potential incident x-ray spectra to aid in the design process.
Subprograms:	
FORT.LB	- FORTRAN IV mathematics library.

Main Program RELSLIB3:

```
      COMPILER NOSTACK
      DIMENSION SPEC(150),WMUA(150),WMUE(150),IAR(3)
C     INSERT THE REAL SPECTRA HERE  120,140,100 ETC. KVP
C
C     100 KVP SPECTRUM FROM LA-4624 BY STORM AND ISRAEL

      KVP=100

      DATA SPEC/20*0.0,1.3E2,5.0E2,9.0E2,1.1E3,1.66E3,
     C  2.3E3,3.0E3,3.6E3,4.25E3,5.0E3,5.7E3,6.3E3,6.7E3,7.25E3,7.6E
     C  ,7.9E3,8.0E3,8.3E3,8.6E3,8.7E3,8.75E3,8.8E3,8.9E3,8.95E3,
     C  9.0E3,8.95E3,8.85E3,8.75E3,8.65E3,8.45E3,8.33E3,8.1E3,7.9E3,
     C  7.66E3,7.45E3,7.25E3,7.1E3,1.3558E4,1.823E4,
     C  6.66E3,6.5E3,6.33E3,
     C  6.25E3,6.1E3,6.0E3,5.8E3,9.508E3,
     C  5.5E3,6.2791E3,5.1E3,4.45E3,
     C  4.3E3,4.15E3,4.0E3,3.85E3,3.66E3,3.55E3,3.45E3,3.3E3,3.15E3,
     C  3.0E3,2.8E3,2.66E3,2.5E3,2.25E3,2.0E3,1.9E3,1.7E3,1.5E3,
     C  1.35E3,1.3E3,1.15E3,9.3E2,7.8E2,6.0E2,4.6E2,4.0E2,2.5E2,2.0E
     C  ,0.0E0,50*0.0E0/
C
C     150 KVP SPECTRUM FROM LA-4624 BY STORM AND ISRAEL

C     KVP=150

C     DATA SPEC/20*0.0,3.00E2,7.5E2,1.5E3,1.8E3,2.75E3,
C    C 3.4E3,4.3E3,5.66E3,6.6E3,7.6E3,9.5E3,1.05E4,1.1E4,1.15E4,
C    C 1.25E4,1.35E4,1.45E4,1.50E4,1.55E4,1.6E4,1.62E4,1.64E4,
C    C 1.66E4,1.68E4,1.70E4,1.73E4,1.75E4,1.73E4,1.72E4,1.7E4,
C    C 1.68E4,1.66E4,1.64E4,1.62E4,1.60E4,1.58E4,1.56E4,
C    C 5.071E4,
C    C 7.65E4,
C    C 1.5E4,1.48E4,1.46E4,1.44E4,1.42E4,1.41E4,1.39E4,
C    C 3.442E4,
C    C 1.35E4,1.8572E4,9.33E3,9.25E3,9.0E3,8.9E3,8.9E3,
C    C 8.75E3,8.66E3,8.5E3,8.4E3,8.30E3,8.25E3,8.0E3,7.85E3,
C    C 7.66E3,7.60E3,7.4E3,7.25E3,7.1E3,6.9E3,6.7E3,6.65E3,
C    C 6.55E3,6.4E3,6.15E3,5.9E3,5.8E3,5.75E3,5.5E3,5.3E3,
C    C 5.2E3,5.1E3,
C    C 5.0E3,4.9E3,4.8E3,4.66E3,4.5E3,4.45E3,4.35E3,4.25E3,
C    C 4.10E3,3.95E3,3.85E3,3.70E3,3.60E3,3.50E3,3.33E3,3.25E3,
C    C 3.15E3,3.00E3,2.9?E3,2.9E3,2.80E3,2.70E3,2.65E3,2.60E3,
C    C 2.50E3,2.33E3,2.20E3,2.00E3,1.90E3,1.8E3,1.74E3,1.68E3,
C    C 1.62E3,1.56E3,1.50E3,1.37E3,1.25E3,1.12E3,1.0E3,9.6E2,
C    C 8.64E2,7.68E2,6.72E2,5.76E2,4.8E2,3.84E2,2.88E2,1.92E2,
C    C 0.96E2,0.0E2/
C
C
C
C
C
C     RAMP SPECTRUM
C     -------------
C     THIS IS A RAMP SPECTRUM AND NOT A SPECTRUM THAT WAS
C     PUBLISHED.
C     THIS SPECTRUM RAMPS UP TO 30 KEV AND RAMPS DOWN TO 120 KEV.
C     DATA SPEC/4*0.0,0.0146,4*0.0,0.0292,4*0.0,0.0438,4*0.0,
C    C 0.058,4*0.0,
C    C 0.0731,4*0.0,0.0822,4*0.0,0.0776,4*0.0,0.0731,4*0.0,
C    C 0.0685,4*0.0,
C    C 0.0639,4*0.0,0.0594,4*0.0,0.0548,4*0.0,0.0502,4*0.0,
C    C 0.0457,4*0.0,
C    C 0.0410,4*0.0,0.0365,4*0.0,0.0320,4*0.0,0.0274,4*0.0,
C    C 0.0228,4*0.0,
C   1C 0.0183,4*0.0,0.0137,4*0.0,0.00913,4*0.0,0.00456,4*0.0
```

```
C      C ,0.0,4*0.0,
C      C 0.0,4*0.0,0.0,4*0.0,0.0,4*0.0,0.0,4*0.0,0.0,4*0.0,
C      C 0.0/

C        FLAT SPECTRUM
C        -------------
C        DATA SPEC/150*6.66666E-3/

         DATA WMUA/5*41.96,5*5.223,3.977,3.10,2.47,1.99,1.638,
     C   1.393,1.196,1.036,0.905,7.956E-1,
     C   .726,.665,.612,.565,5.233E-1,
     C   4.861E-1,4.53E-1,4.230E-1,3.96E-1,3.716E-1,
     C   3.578E-1,3.449E-1,3.329E-1,3.217E-1,3.111E-1,
     C   3.011E-1,2.918E-1,2.830E-1,2.747E-1,2.668E-1,
     C   2.619E-1,2.573E-1,2.528E-1,2.486E-1,2.445E-1,
     C   2.406E-1,2.367E-1,2.331E-1,2.296E-1,2.262E-1,
     C   2.238E-1,2.216E-1,2.193E-1,2.172E-1,2.151E-1,
     C   2.13E-1,2.11E-1,2.092E-1,2.073E-1,2.055E-1,
     C   2.042E-1,2.028E-1,2.016E-1,2.003E-1,1.991E-1,
     C   1.979E-1,1.967E-1,1.956E-1,1.945E-1,1.934E-1,
     C   1.923E-1,1.912E-1,1.902E-1,1.892E-1,1.882E-1,
     C   1.872E-1,1.862E-1,1.853E-1,1.844E-1,1.835E-1,
     C   1.827E-1,1.820E-1,1.813E-1,1.806E-1,1.799E-1,
     C   1.792E-1,1.785E-1,1.779E-1,1.772E-1,1.766E-1,
     C   1.759E-1,1.754E-1,1.748E-1,1.742E-1,1.736E-1,
     C   1.730E-1,1.724E-1,1.718E-1,1.713E-1,1.707E-1,
     C   1.701E-1,1.696E-1,1.691E-1,1.686E-1,1.681E-1,
     C   1.676E-1,1.671E-1,1.666E-1,1.662E-1,1.657E-1,
     C   1.652E-1,1.648E-1,1.643E-1,1.638E-1,1.634E-1,
     C   1.630E-1,1.625E-1,1.621E-1,1.617E-1,1.613E-1,
     C   1.609E-1,1.605E-1,1.601E-1,1.597E-1,1.593E-1,
     C   1.598E-1,1.585E-1,1.581E-1,1.577E-1,1.573E-1,
     C   1.569E-1,1.566E-1,1.562E-1,1.558E-1,1.555E-1,
     C   1.551E-1,1.548E-1,1.545E-1,1.541E-1,1.538E-1,
     C   1.534E-1,1.531E-1,1.528E-1,1.524E-1,1.521E-1,
     C   1.518E-1,1.514E-1,1.511E-1,1.508E-1,1.505E-1/

         DATA WMUE/5*21.0,5*4.9,
     C   3.58,2.72,2.11,1.667,1.340,
     C   1.091E0,8.997E-1,7.501E-1,6.315E-1,5.364E-1,
     C   4.608E-1,3.987E-1,3.472E-1,3.042E-1,2.679E-1,
     C   2.371E-1,2.108E-1,1.883E-1,1.688E-1,1.519E-1,
     C   1.386E-1,1.268E-1,1.164E-1,1.071E-1,9.874E-2,
     C   9.127E-2,8.455E-2,7.848E-2,7.298E-2,6.800E-2,
     C   6.439E-2,6.105E-2,5.796E-2,5.509E-2,5.242E-2,
     C   4.993E-2,4.761E-2,4.545E-2,4.34E-2,4.153E-2.
     C   4.030E-2,3.913E-2,3.802E-2,3.696E-2,3.595E-2,
     C   3.498E-2,3.405E-2,3.317E-2,3.232E-2,3.151E-2,
     C   3.115E-2,3.080E-2,3.046E-2,3.013E-2,2.981E-2,
     C   2.949E-2,2.919E-2,2.889E-2,2.860E-2,2.832E-2,
     C   2.804E-2,2.777E-2,2.751E-2,2.725E-2,2.699E-2,
     C   2.675E-2,2.651E-2,2.627E-2,2.604E-2,2.582E-2,
     C   2.579E-2,2.577E-2,2.575E-2,2.572E-2,2.570E-2,
     C   2.568E-2,2.566E-2,2.563E-2,2.561E-2,2.559E-2,
     C   2.557E-2,2.555E-2,2.553E-2,2.551E-2,2.549E-2,
     C   2.547E-2,2.545E-2,2.543E-2,2.541E-2,2.539E-2,
     C   2.544E-2,2.549E-2,2.555E-2,2.559E-2,2.565E-2,
     C   2.570E-2,2.575E-2,2.579E-2,2.585E-2,2.590E-2,
     C   2.595E-2,2.599E-2,2.604E-2,2.609E-2,2.614E-2,
     C   2.618E-2,2.623E-2,2.628E-2,2.632E-2,2.637E-2,
     C   2.614E-2,2.646E-2,2.650E-2,2.655E-2,2.659E-2,
     C   2.664E-2,2.668E-2,2.672E-2,2.677E-2,2.681E-2,
     C   2.685E-2,2.689E-2,2.694E-2,2.698E-2,2.702E-2,
     C   2.706E-2,2.710E-2,2.714E-2,2.719E-2,2.723E-2,
     C   2.727E-2,2.731E-2,2.735E-2,2.739E-2,2.743E-2,
     C   2.746E-2,2.750E-2,2.754E-2,2.758E-2,2.762E-2/
```

```
C       DATA WMUE/5*21.0,5*.839,5*1.34,5*5.364E-1,
C      C 5*
C      C 2.679E-1,5*1.519E-1,5*9.874E-2,5*6.8E-2,5*
C      C 5.242E-2,5*4.153E-2,5*3.595E-2,5*3.151E-2,5*
C      C 2.981E-2,5*2.832E-2,5*2.699E-2,5*2.582E-2,5*
C      C 2.570E-2,5*2.559E-2,5*2.549E-2,5*2.539E-2,5*
C      C 2.565E-2,5*2.590E-2,5*2.614E-2,5*2.637E-2,5*
C      C 2.695E-2,5*2.698E-2,5*2.702E-2,5*2.723E-2,5*
C      C 2.743E-2,5*2.762E-2/

C ACCEPT DATA ACCEPT DATA ACCEPT DATA ACCEPT DATA ACCEPT DATA


        ACCEPT "DO YOU WANT TO READ ABOUT THE PROGRAM?",IDOCU
        IF(IDOCU.EQ.0)GOTO 90
        CALL DOCURELSENS
90      CONTINUE

C       REFERENCE Z FOR PHOTOELECTRIC EFFECT:
        Z=7.66

C       REFERENCE Z FOR RAYLEIGH SCATTERING:
        ZR=6.98

        EMAX=150

100     ACCEPT "ARE WE DONE?",IDONE
        IF(IDONE.EQ.1)GOTO 2000
        TYPE"INSERT THE NEW VARIABLES"

        ACCEPT "NEW PERCENT INCREASE IN Z??",IPIIZ
        IF(IPIIZ.EQ.0) GOTO 210
        ACCEPT "PIIZ=",PIIZ
        DELZ=(PIIZ/100)*Z
        DELZR=(PIIZ/100)*ZR

210     ACCEPT "NEW PERCENT INCREASE IN ELECTRON DENSITY?",IPIIED
        IF(IPIIED.EQ.0) GOTO 215
        ACCEPT "PIIED=",PIIED

215     ACCEPT"DO YOU WANT TO STORE(1) OR INPUT(2) VALUES FOR A
     C  TRANSMISSION INTERPOLATION?",ISTOR
        ISTOR=ISTOR+1
        GOTO(217,2161,2162),ISTOR
2161    ACCEPT"STORE UPPER(1) OR LOWER(2) BOUND THICKNESS?",ITCK
        GOTO(2171,2172),ITCK
C       STORE UPPER BOUND THICKNESS VALUES
2171    CUBT=FIL1
        PUBT=PCTTBE
        GOTO 217
C       STORE LOWER BOUND THICKNESS VALUES
2172    CLBT=FIL1
        PLBT=PCTTBE
        GOTO 217
2162    ACCEPT"NEW THICKNESS AND TRANSMISSION BOUNDS?",IBOUND
        IF(IBOUND.EQ.0) GOTO 217
        ACCEPT"LOWER BOUND THICKNESS,AND TRANSMISSION",CLBT,PLBT
        ACCEPT"UPPER BOUND THICKNESS,AND TRANSMISSION=",CUBT,PUBT
217     ACCEPT"DO YOU WANT TO DO A PERCENT TRANSMISSION
     C  INTERPOLATION?",INTERP
        IF(INTERP.EQ.0)GOTO 220
        ACCEPT"DESIRED PERCENT TRANSMISSION=",PCT
        FIL1=(((ALOG(PLBT)-ALOG(PCT))/(ALOG(PLBT)-ALOG(PUBT)))*
     C  (CUBT-CLBT))+CLBT
```

```
220     ACCEPT "NEW FILTER-1 THICKNESS?",IFIL1
        IF(IFIL1.EQ.0) GOTO 230
        ACCEPT "FIL1=",FIL1

230     ACCEPT "NEW FILTER-1?",NFIL1
        IF(NFIL1.EQ.0)GOTO 290
        ACCEPT"ATOMIC NUMBER:1=",ATN81
        ATN=ATN81
        FILNBR=1
        ACCEPT"FROM TABLE(1) OR ENTER(2)",CXINPUT
        IF(CXINPUT.EQ.1) GOTO 1000

        ACCEPT "COEFFICIENT M-L0=",C1ML0
        ACCEPT "COEFFICIENT M-L1=",C1ML1
        ACCEPT "LEDGE ENERGY=",E1LEG
        ACCEPT "COEFFICIENT L-K0=",C1LK0
        ACCEPT "COEFFICIENT L-K1=",C1LK1
        ACCEPT "KEDGE ENERGY=",E1KEG
        ACCEPT "COEFFICIENT K0=",C1K0
        ACCEPT "COEFFICIENT K1=",C1K1
        ACCEPT "COEFFICIENT K2=",C1K2
        ACCEPT "COEFFICIENT K3=",C1K3
        ACCEPT "FILTER 1 CMSQ/GM FACTOR=",CMSQ1
        ACCEPT "FILTER 1 DENSITY=",DENS1

290     ACCEPT "NEW FILTER-2 THICKNESS ?",IFIL2
        IF(IFIL2.EQ.0)GOTO 300
        ACCEPT "FIL2=",FIL2

300     ACCEPT "NEW FILTER-2?",NFIL2
        IF(NFIL2.EQ.0)GOTO 400
        ACCEPT"ATOMIC NUMBER:2=",ATN82
        ATN=ATN82
        FILNBR=2
        ACCEPT"FROM TABLE(1) OR ENTER(2)",CXINPUT
        IF(CXINPUT.EQ.1) GOTO 1000

        ACCEPT "COEFFICIENT M-L0=",C2ML0
        ACCEPT "COEFFICIENT M-L1=",C2ML1
        ACCEPT "LEDGE ENERGY=",E2LEG
        ACCEPT "COEFFICIENT L-K0=",C2LK0
        ACCEPT "COEFFICIENT L-K1=",C2LK1
        ACCEPT "KEDGE ENERGY =",E2KEG
        ACCEPT "COEFFICIENT K0=",C2K0
        ACCEPT "COEFFICIENT K1=",C2K1
        ACCEPT "COEFFICIENT K2=",C2K2
        ACCEPT "COEFFICIENT K3=",C2K3

        ACCEPT "FILTER 2 CMSQ/GM FACTOR=",CMSQ2

        ACCEPT"FILTER 2 DENSITY=",DENS2

400     ACCEPT "NEW WATER PHANTOM THICKNESS?",IBODSZ
        IF(IBODSZ.EQ.0) GOTO 410
        ACCEPT "BODSZ=",BODSZ

410     ACCEPT "NEW DETECTOR SIZE?",IDTKSZ
        IF(IDTKSZ.EQ.0)GOTO 420
        TYPE "CENTRAL DETECTOR AREA = 2.388 CM2/CM"
        ACCEPT "DTKSZ=",DTKSZ

420     ACCEPT "NEW GAMMA FLUX?", IGAMFX
        IF(IGAMFX.EQ.0)GOTO 430
        TYPE"PHOTONS/SEC-MA-SR"
        TYPE"     100KVP--2.214*E12"
        TYPE"     150KVP--5.515*E12"
```

```
      TYPE""
      TYPE"PHOTONS/CM2-SEC @ 108.77CM"
      TYPE"     100KVP--1.895E8"
      TYPE"     150KVP--4.722E8"
      ACCEPT "GAMFX=",GAMFX

430   ACCEPT"NEW MEASUREMENT TIME?",ITIM
      IF(ITIM.EQ.0) GOTO 435
      ACCEPT"TIMEN=",TIMEN

435   ACCEPT "NEW PIXEL SIZE?",IPIX
      IF(IPIX.EQ.0) GOTO 440
      ACCEPT "PIXEL=",PIXEL

440   CONTINUE

C     INSERT THE IONIZATION-EXCITATION ENERGY OF THE XENON GAS.
C     THE VALUE GIVEN HERE IS REVISED FROM OUR PREVIOUS VALUE.
C     THIS VALUE IS TAKEN FROM YAFFE'S PAPER ON IONIZATION
C     CHAMBERS FOR COMPUTED TOMOGRAPHY.
      W=21.9E-3

C     INSERT THE PRESSURE VESSEL ALUMINUM WINDOW THICKNESS.
C     THIS THICKNESS REDUCES OUR DETECTOR EFFICIENCY. IT IS
C     KNOWN TO HAVE A MARKED EFFECT ON THE TOMOCHEMISTRY
C     OPTIMIZATION CALCULATION. IN THE PROCESS OF THIS PROGRAM WE
C     ARE CHANGING NAMES FROM WINTK TO TWIND. TWIND=0.3175 CM
      TWIND=0.3175

C     INSERT THE REAL EFFICIENCY OF THE DETECTORS HERE.

C     EFFICIENCY OF CHARGE COLLECTION IS EFCHCO. THIS QUANTITY WAS
C     EXPERIMENTALLY DETERMINED.
      EFCHCO=0.96

C     INSERT THE K FLUORESCENCE YIELD: WK WHICH WE CALL OMEGAK
C     HERE.
C     THE FLUORESCENCE YIELD IS THE FRACTION OF THE ATOMS WHICH
C     K FLUORESCE WHEN THE K SHELL ELECTRON HAS BEEN REMOVED.
      OMEGAK=0.889

C     INSERT THE XENON GAS DETECTOR DEAD SPACE GAP: THE DISTANCE
C     BETWEEN THE INSIDE OF THE PRESSURE VESSEL AND THE ACTIVE
C     REGION OF THE DETECTOR.
      TDEAD=0.3175

C     INSERT THE LENGTH OF THE DETECTOR. THIS IS THE TOTAL LENGTH
C     OF THE DETECTOR AND IS EXPRESSED IN CM.
      XDET=10.0

C     INSERT THE LENGTH OF THE FRONT FINGER IF THE EXPERIMENT
C     WERE TO WORK IN THE SPLIT FINGER MODE. THIS LENGTH IS
C     EXPRESSED IN CM.
      XDETFR=2.5

C     DECIDE HERE WHETHER YOU WANT TO WORK IN THE SPLIT FINGER
C     MODE:

      ACCEPT "SPLIT FINGER CALCULATION?",ISPLIT
      IF(ISPLIT.EQ.          IF(ISPLIT.EQ.0) GOTO 450
      ACCEPT "FRONT(1) OR BACK(2) OF DETECTOR?",IDET
      IF(IDET.EQ.2) GOTO 445

C     FRONT DETECTOR SETUP:

C     SET THE DETECTOR LENGTH EQUAL TO THE FRONT PART OF THE
```

```
C       FINGER. THE DEAD SPACE REMAINS THE SAME.
        XDET=XDETFR
        GOTO 450

445     CONTINUE

C       BACK DETECTOR SETUP:

C       SET THE DETECTOR LENGTH EQUAL TO THE BACK PART OF THE
C       FINGER:
C       NEW   OLD   FRONT OF FINGER
C        !     !      !
        XDET=(XDET-XDETFR)

C       AND THE DEAD SPACE INCREASES TO:
C       NEW   OLD   FRONT OF FINGER
C        !     !      !
        TDEAD=TDEAD+XDETFR

450     CONTINUE

C       INSERT THE NUMBER OF ATMOSPHERES OF XENON GAS WITHIN THE
C       DETECTOR CHAMBER. THIS CORRESPONDS TO 95% XE AT 15 ATM
C       PRESSURE.
        ATMXE=14.25

C       NOTE THAT WE WILL COMPUTE THE EFFICIENCY OF THE DETECTOR
C       JUST BEFORE THE COMPUTATION OF THE CURRENT MEASURED
C       ON THE DETECTOR.

C NORMALIZE  NORMALIZE  NORMALIZE  NORMALIZE  NORMALIZE  NORMALIZE

C       HERE WE ARE NORMALIZING THE INCIDENT SPECTRUM. WE MUST NOTE
C       THAT THE BELOW CALCULATIONS NEED A NORMALIZED SPECTRUM
C       INCIDENT UPON THE PHANTOM TO MAKE SENSE.  NORMALIZE
C       SPECTUBE HERE.

C       INITIALIZE THE VARIABLES HERE:
        ENERGY=10.0
        IENERGY=10.0
        DELTE=1.0
        SPECNORM=0.0E0

C       DO LOOP BEGINS HERE

        DO 499 I=10,150,1


C       X-RAY TUBE INHERENT FILTRATION NORMALIZATION:

C       HERE WE WILL ADD THE INHERENT FILTRATION OF THE X-RAY
C       TUBE. THE INHERENT FILTRATION CONSISTS OF BERYLLIUM AND
C       ALUMINUM. THE ALUMINUM FILTRATION IS 0.17 CM THICK AND THE
C       BERYLLIUM FILTRATION IS 0.1 CM THICK.
C       USE THE CROSS SECTION FITS FOR DETERMINING THE ALUMINUM
C       AND THE BERYLLIUM CROSS SECTIONS.

C       FIRST COMPUTE THE ALUMINUM ATTENUATION COEFFICIENT.

C       THE FIT COEFFICIENTS ARE:

        CAL0=1.3177E1
        CAL1=-2.1458E0
        CAL2=-2.8944E-1
        CAL3=2.7907E-2
        DENSAL=2.694E0
```

```
      CMSQAL=2.232E-2

      ALMUPHOT=EXP(CAL0+CAL1*ALOG(ENERGY)+
     C CAL2*((ALOG(ENERGY))**2)+CAL3*((ALOG(ENERGY))**3))*
     C CMSQAL*DENSAL

      ALMUA=ALMUPHOT+
     C (0.50028*(((1+ENERGY/511.006)/((ENERGY/511.006)**2))
     C *(2*(1+ENERGY/511.006)/(1+2*ENERGY/511.006)
     C -(ALOG(1+2*ENERGY/511.006)/(ENERGY/511.006)))
     C +((1/(2*ENERGY/511.006))*ALOG(1+2*ENERGY/511.006))
     C -((1+3*ENERGY/511.006)/((1+2*ENERGY/511.006)**2)))
     C *(CMSQAL*DENSAL*13))

C     FRACTION OF TRANSMISSION AFTER THE ALUMINUM WINDOW:

      TRAL=EXP(-ALMUA*0.17)

C     SIMILARLY:

C     COMPUTE THE BERYLLIUM ATTENUATION COEFFICIENT

C     THE FIT COEFFICIENTS ARE:

      CBE0=9.1061E0
      CBE1=-2.9314E0
      CBE2=-7.3572E-2
      CBE3=7.2012E-3
      DENSBE=1.845E0
      CMSQBE=6.683E-2
      BEMUPHOT=EXP(CBE0+CBE1*ALOG(ENERGY)+
     C CBE2*((ALOG(ENERGY))**2)+CBE3*((ALOG(ENERGY))**3))*
     C CMSQBE*DENSBE

      BEMUA=BEMUPHOT+
     C (0.50028*(((1+ENERGY/511.006)/((ENERGY/511.006)**2))
     C *(2*(1+ENERGY/511.006)/(1+2*ENERGY/511.006)
     C -(ALOG(1+2*ENERGY/511.006)/(ENERGY/511.006)))
     C +((1/(2*ENERGY/511.006))*ALOG(1+2*ENERGY/511.006))
     C -((1+3*ENERGY/511.006)/((1+2*ENERGY/511.006)**2)))
     C *(CMSQBE*DENSBE*4))

C     FRACTION OF TRANSMISSION AFTER THE BERYLLIUM WINDOW:

      TRBE=EXP(-BEMUA*0.1)

C     NOW THE NORMALIZATION TERM IS GIVEN BY:

      SPECNORM=SPECNORM+SPEC(IENERGY)*TRAL*TRBE*DELTE

C     INCREMENT THE VARIABLES:
      ENE
C     ----------------------------------------


C     INITIALIZE HERE THE VALUES OF THOSE QUANTITIES WHICH WILL
C     BE SUMMED OVER THE SPECTRA. THESE QUANTITIES INCLUDE THE
C     POST-FILTER ENERGY,THE PREFILTER ENERGY, THE CURRENT, THE
C     DIDZ, THE SENSITIVITY, THE DOSE, THE ENERGY TRANSMITTED,
C     AND SO FORTH.

      PREFE=0.0
      POSFE=0.0
      POSSUM=0.0
      CURRENT=0.0
      DIDZ=0.0
```

```
      AICF=0.0
      DELTE=1.0
      IENERGY=10
      ENERGY=10.0
      ETRANS=0.0
      DOSE=0.0

C     ----------------------------------------

C DO LOOP DO LOOP DO LOOP DO LOOP DO LOOP DO LOOP DO LOOP DO LOOP

C     NOW DETERMINE THE PROPER COEFFICIENTS FOR THE FILTER
C     CROSS SECTIONS.

500   IF(ENERGY.GT.E1LEG)GOTO 510
      C10=C1ML0
      C11=C1ML1
      C12=0.0
      C13=0.0
      GOTO 525
510   IF(ENERGY.GT.E1KEG) GOTO 520
      C10=C1LK0
      C11=C1LK1
      C12=0.0
      C13=0.0
      GOTO 525
520   IF(ENERGY.GT.EMAX) GOTO 600
      C10=C1K0
      C11=C1K1
      C12=C1K2
      C13=C1K3
      GOTO 525
525   IF(ENERGY.GT.E2LEG) GOTO 530
      C20=C2ML0
      C21=C2ML1
      C22=0.0
      C23=0.0
      GOTO 545
530   IF(ENERGY.GT.E2KEG) GOTO 540
      C20=C2LK0
      C21=C2LK1
      C22=0.0
      C23=0.0
      GOTO 545
540   IF(ENERGY.GT.EMAX) GOTO 600
      C20=C2K0
      C21=C2K1
      C22=C2K2
      C23=C2K3
      GOTO 545
545   CONTINUE

C     ----------------------------------------

C     X-RAY TUBE INHERENT FILTRATION

C     HERE WE WILL ADD THE INHERENT FILTRATION OF THE X-RAY
C     TUBE. THE INHERENT FILTRATION CONSISTS OF BERYLLIUM AND
C     ALUMINUM. THE ALUMINUM FILTRATION IS 0.17 CM THICK AND THE
C     BERYLLIUM FILTRATION IS 0.1 CM THICK.
C     USE THE CROSS SECTION FITS FOR DETERMINING THE ALUMINUM
C     AND THE BERYLLIUM CROSS SECTIONS.

C     FIRST COMPUTE THE ALUMINUM ATTENUATION COEFFICIENT.
```

```
C       THE FIT COEFFICIENTS ARE:

        CAL0=1.3177E1
        CAL1=-2.1458E0
        CAL2=-2.8944E-1
        CAL3=2.7907E-2
        DENSAL=2.694E0
        CMSQAL=2.232E-2

        ALMUPHOT=EXP(CAL0+CAL1*ALOG(ENERGY)+
     C  CAL2*((ALOG(ENERGY))**2)+CAL3*((ALOG(ENERGY))**3))*
     C  CMSQAL*DENSAL

        ALMUA=ALMUPHOT+
     C  (0.50028*(((1+ENERGY/511.006)/((ENERGY/511.006)**2))
     C  *(2*(1+ENERGY/511.006)/(1+2*ENERGY/511.006)
     C  -(ALOG(1+2*ENERGY/511.006)/(ENERGY/511.006)))
     C  +((1/(2*ENERGY/511.006))*ALOG(1+2*ENERGY/511.006))
     C  -((1+3*ENERGY/511.006)/((1+2*ENERGY/511.006)**2)))
     C  *(CMSQAL*DENSAL*13))

C       FRACTION OF TRANSMISSION AFTER THE ALUMINUM WINDOW:

        TRAL=EXP(-ALMUA*0.17)

C       SIMILARLY:

C       COMPUTE THE BERYLLIUM ATTENUATION COEFFICIENT

C       THE FIT COEFFICIENTS ARE:

        CBE0=9.1061E0
        CBE1=-2.9314E0
        CBE2=-7.3572E-2
        CBE3=7.2012E-3
        DENSBE=1.845E0
        CMSQBE=6.683E-2
        BEMUPHOT=EXP(CBE0+CBE1*ALOG(ENERGY)+
     C  CBE2*((ALOG(ENERGY))**2)+CBE3*((ALOG(ENERGY))**3))*
     C  CMSQBE*DENSBE

        BEMUA=BEMUPHOT+
     C  (0.50028*(((1+ENERGY/511.006)/((ENERGY/511.006)**2))
     C  *(2*(1+ENERGY/511.006)/(1+2*ENERGY/511.006)
     C  -(ALOG(1+2*ENERGY/511.006)/(ENERGY/511.006)))
     C  +((1/(2*ENERGY/511.006))*ALOG(1+2*ENERGY/511.006))
     C  -((1+3*ENERGY/511.006)/((1+2*ENERGY/511.006)**2)))
     C  *(CMSQBE*DENSBE*4))

C       FRACTION OF TRANSMISSION AFTER THE BERYLLIUM WINDOW:

        TRBE=EXP(-BEMUA*0.1)

C       NOW THE SPECTRUM EMANATING FROM THE TUBE IS:

        SPECTUBE=SPEC(IENERGY)*TRAL*TRBE/SPECNORM

C       ------------------------------------

C       DETECTOR EFFICIENCY

C       THIS SEGMENT OF THE PROGRAM COMPUTES THE DETECTOR
C       EFFICIENCY. WE WILL FIRST COMPUTE EACH COMPONENT OF THE
C       OVERALL EFFICIENCY AND THEN COMPUTE THE RESULTANT
C       TOTAL EFFICIENCY.
```

```
C       XENON DETECTOR TOTAL CROSS SECTION DETERMINATION.

C       COMPUTE HERE THE XENON GAS DETECTOR PHOTOELECTRIC ATTEN-
C       UATION COEFFICIENTS USING THE POWER FITS OF THE CROSS
C       SECTIONS.

C       THE FIT COEFFICIENTS FOR THE TOTAL PHOTOELECTRIC CROSS
C       SECTION FOR XENON: (1ATM)

        IF(ENERGY.GT.5.1) GOTO 5452
        CXE0HI=1.469E1
        CXE1HI=-2.3511E0
        CXE2HI=0.0E0
        CXE3HI=0.0E0
        GOTO 5458
5452    IF(ENERGY.GT.34.566) GOTO 5454
        CXE0HI=1.6774E1
        CXE1HI=-2.7149E0
        CXE2HI=0.0E0
        CXE3HI=0.0E0
        GOTO 5458
5454    IF(ENERGY.GT.EMAX) GOTO 600
        CXE0HI=2.2771E1
        CXE1HI=-4.8359E0
        CXE2HI=3.4466E-1
        CXE3HI=-1.8996E-2
5458    CONTINUE
        DENSXE=5.458E-3
        CMSQXE=4.587E-3


C       NOW COMPUTE THE TOTAL PHOTOELECTRIC CROSS SECTION FOR XENON
C       XEMUTOTP (1 ATM)

        XEMUTOTP=EXP(CXE0HI+CXE1HI*ALOG(ENERGY) +
     C  CXE2HI*((ALOG(ENERGY))**2)+CXE3HI*((ALOG(ENERGY))**3))*
     C  CMSQXE*DENSXE


C       THE NON-KSHELL PHOTOELECTRIC CROSS SECTIONS. THIS CROSS
C       SECTION IS DEFINED AS MUPHOTOLOW. HERE WE GIVE THE
C       COEFFICIENT FIT FOR THIS CROSS SECTION. WE ASSUME THAT THE
C       TERMS BELOW 10 KEV DO NOT CONTRIBUTE TO THE CALCULATION.
C       HENCE WE DO NOT MENTION THIS LOW ENERGY FIT.
        CXE0LOW=1.6774E1
        CXE1LOW=-2.7149E0
        CXE2LOW=0.0E0
        CXE3LOW=0.0E0

C       NOW COMPUTE THE NON-KSHELL PHOTOELECTRIC CROSS SECTION:
C       XEMULOW (1 ATM)

        XEMULOW= EXP(CXE0LOW+CXE1LOW*ALOG(ENERGY)+
     C  CXE2LOW*((ALOG(ENERGY))**2)+CXE3LOW*((ALOG(ENERGY))**3))*
     C  CMSQXE*DENSXE

C       WITH THE ABOVE INFORMATION WE CAN NOW COMPUTE THE TOTAL
C       ATTENUATION COEFFICIENT FOR XENON AT 1 ATM PRESSURE:
C       XEMUA.

        XEMUA= XEMUTOTP+
     C  (0.50028*(((1+ENERGY/511.006)/((ENERGY/511.006)**2))
     C  *(2*(1+ENERGY/511.006)/(1+2*ENERGY/511.006)
     C  -(ALOG(1+2*ENERGY/511.006)/(ENERGY/511.006)))
```

```
     C  +((1/(2*ENERGY/511.006))*ALOG(1+2*ENERGY/511.006))
     C  -((1+3*ENERGY/511.006)/((1+2*ENERGY/511.006)**2)))
     C  *(CMSQXE*DENSXE*54))

C       NOW COMPUTE THE COMPONENTS OF THE EFFICIENCY

C       THE FIRST LOSS OF PHOTONS OCCURS IN THE PRESSURE VESSEL
C       ALUMINUM WINDOW. COMPUTE EFWIND(OW)
C       BEFORE WE COMPUTE THE TERM EFWIND WE MUST COMPUTE THE OVER-
C       FLOW FLAG : EFWFLG
        EFWFLG=-ALMUA*TWIND
        IF(EFWFLG.LT.-20) GOTO 5410
        EFWIND=EXP(-ALMUA*TWIND)
        GOTO 5415
5410    EFWIND=0.0E0
5415    CONTINUE

C       THE NEXT LOSS OCCURS IN THE DEAD SPACE BETWEEN THE WINDOW
C       AND THE ACTIVE REGION OF THE DETECTOR. COMPUTE:EFDEAD
C       FIRST COMPUTE THE UNDERFLOW FLAG
        EFDFLG=-XEMUA*ATMXE*TDEAD
        IF(EFDFLG.LT.-20) GOTO 5420
        EFDEAD=EXP(-XEMUA*ATMXE*TDEAD)
        GOTO 5425
5420    EFDFLG=0.0E0
5425    CONTINUE

C       THE DETECTOR GAS NOW INTERACTS WITH THE XRAYS AT SOME
C       EFFICIENCY. WE CALL THE INTERACTION EFFICIENCY:EFINT
C       FIRST COMPUTE THE UNDERFLOW FLAG
        EFIFLG=-XEMUA*ATMXE*XDET
        IF(EFIFLG.LT.-20) GOTO 5430
        EFINT=(1-EXP(-XEMUA*ATMXE*XDET))
        GOTO 5435
5430    EFINT=1.0E0
5435    CONTINUE

C       NOW COMPUTE THE PROBABILITY OF A FLUORESCENCE EVENT TO
C       OCCUR:EFFLUOR
        EFFLUOR=((XEMUTOTP-XEMULOW)/XEMUTOTP)*OMEGAK

C       FURTHERMORE, THE PROBABILITY OF A NON-FLUORESCENCE TYPE OF
C       EVENT TO OCCUR IS GIVEN BY:
C       EFNONFL
        EFNONFL=((XEMULOW/XEMUTOTP)+
     C  (1-OMEGAK)*((XEMUTOTP-XEMULOW)/XEMUTOTP))

C       NOW WE WILL ASSUME HERE THAT THE PROBABILITY OF THE FLUORE-
C       SCENCE RADIATION TO BE ABSORBED BEFORE IT HITS THE DETEC-
C       TOR (EFFLREABS) IS 25%.
        EFFLREABS=0.25

C       FINALLY, WE CAN COMPUTE THE TOTAL EFFICIENCY OF THE
C       DETECTOR (EFF) TO BE:
        EFF=EFCHCO*EFDEAD*EFWIND*(EFINT*(EFNONFL+EFFLUOR*EFFLREABS))

C       SPLIT FINGER DETECTION EFFICIENCY

C       NOTE THAT FROM OUR COMMENTS IN LOG BOOK 4 PAGE 47, THAT
C       IT IS EASIEST TO CONSIDER THE SPLIT FINGER CALCULATION
C       AS TWO CALCULATIONS WHERE THE FILTRATION (XENON DEAD SPACE)
C       AND THE DETECTOR LENGTH CHANGE. THEREFORE WE WILL
C       TEMPORARILY ABORT THIS APPROACH TO THE SPLIT FINGER
C       CALCULATION.
C       NOW IF WE WERE TO WORK IN THE SPLIT FINGER MODE WE HAVE TO
```

```
C       COMPUTE THE FRONT AND BACK EFFICIENCIES.(EFFRONT,EFBACK)
C       DERIVATIONS ARE ON PAGES 46&47 LOG BOOK 4.
C       TO COMPUTE THE EFFICIENCIES, ALL WE NEED IS THE FRONT
C       INTERACTION EFFICIENCY,EFFRINT.
C       EFFRINT=(1-EXP(-XEMUA*ATMXE*XDETFR))

C       THE FINGER FRONT EFFICIENCY IS GIVEN BY:
C       EFFRONT=EFCHCO*EFDEAD*EFWIND*
C     C           (EFFRINT*(EFNONFL+EFFLUOR*EFFLREABS))

C       SIMILARLY, THE FINGER BACK EFFICIENCY IS GIVEN BY:
C       EFBACK=EFCHCO*EFDEAD*EFWIND*(1-EFFRINT)*
C     C (((EFINT-EFFRINT)/(1-EFFRINT))*(EFNONFL+EFFLUOR*EFFLREABS))

C       WE NOW HAVE ALL THE DETECTOR EFFICIENCY PARAMETERS NEEDED
C       FOR A SIMULATION CALCULATION.

C       ----------------------------------------

C       THIS IS THE CURRENT MEASURED ON THE DETECTOR

C       SETUP EXPONENTIAL UNDERFLOW FLAG: CURFLG
        CURFLG=(-EXP(C10+C11*ALOG(ENERGY)+C12*((ALOG(ENERGY))**2)+
     C  C13*((ALOG(ENERGY))**3))*FIL1*CMSQ1*DENS1

     C  -EXP(C20+C21*ALOG(ENERGY)+C22*((ALOG(ENERGY))**2)+
     C  C23*((ALOG(ENERGY))**3))*FIL2*CMSQ2*DENS2

     C  -WMUA(IENERGY)*BODSZ

     C  -((10.0**(-3.20086*ALOG10(ENERGY)+3.8663))*
     C  ((((Z+DELZ)/Z)**3.2)-1))*PIXEL

     C  -(0.167295*(((1+ENERGY/511.006)/((ENERGY/511.006)**2))
     C  *(2*(1+ENERGY/511.006)/(1+2*ENERGY/511.006)
     C  -(ALOG(1+2*ENERGY/511.006)/(ENERGY/511.006)))
     C  +((1/(2*ENERGY/511.006))*ALOG(1+2*ENERGY/511.006))
     C  -((1+3*ENERGY/511.006)/((1+2*ENERGY/511.006)**2)))
     C  *(PIIED/100)*PIXEL))


C       TYPE"CURFLG=",CURFLG
        IF(CURFLG.LT.-20.0) GOTO 546
C       TYPE"CURFLG.GT.-20...CONTINUE"
C       TYPE"CURRENT=",CURRENT


C       INSERT MORE REFINED Z DEPENDENCES AND ADD RAYLEIGH SCATTER
C       INTO THE CALCULATION OF THE CURRENT AND THE SENSITIVITY.
C       DONT FORGET TO ADD THE DETECTOR EFFICIENCY INTO THE CALCU
C       LATION OF THE CURRENT AND THE OTHER CALCULATED QUANTITIES.
C
C

        CURRENT=CURRENT+((SPECTUBE*DELTE)*ENERGY*

     C  EXP(-EXP(C10+C11*ALOG(ENERGY)+C12*((ALOG(ENERGY))**2)+
     C  C13*((ALOG(ENERGY))**3))*FIL1*CMSQ1*DENS1

     C  -EXP(C20+C21*ALOG(ENERGY)+C22*((ALOG(ENERGY))**2)+
     C  C23*((ALOG(ENERGY))**3))*FIL2*CMSQ2*DENS2

     C  -(0.50028*(((1+ENERGY/511.006)/((ENERGY/511.006)**2))
     C  *(2*(1+ENERGY/511.006)/(1+2*ENERGY/511.006)
     C  -(ALOG(1+2*ENERGY/511.006)/(ENERGY/511.006)))
```

```
C   +((1/(2*ENERGY/511.006))*ALOG(1+2*ENERGY/511.006))
C   -((1+3*ENERGY/511.006)/((1+2*ENERGY/511.006)**2)))
C   *(CMSQ1*FIL1*DENS1*ATNB1+CMSQ2*FIL2*DENS2*ATNB2))

C   -WMUA(IENERGY)*BODSZ

C   -((10.0**(-3.20086*ALOG10(ENERGY)+3.8663))*
C   ((1+PIIED/100)*((1+DELZ/Z)**4.6)-1))*PIXEL

C   -((10.0**(-1.89167*ALOG10(ENERGY)+1.30089))*
C   ((1+PIIED/100)*((1+DELZR/ZR)**2.705)-1))*PIXEL

C   -(0.167295*(((1+ENERGY/511.006)/((ENERGY/511.006)**2))
C   *(2*(1+ENERGY/511.006)/(1+2*ENERGY/511.006)
C   -(ALOG(1+2*ENERGY/511.006)/(ENERGY/511.006)))
C   +((1/(2*ENERGY/511.006))*ALOG(1+2*ENERGY/511.006))
C   -((1+3*ENERGY/511.006)/((1+2*ENERGY/511.006)**2)))
C   *((1+PIIED/100)*(1+DELZ/Z)-1)*PIXEL))*

C   (GAMFX*DTKSZ*EFF/W)*1.6E-19)
C       TYPE"CURRENT=",CURRENT

546     CONTINUE
C       ----------------------------------------

C       THIS IS THE RATE CHANGE OF CURRENT WITH RESPECT TO THE
C       CHANGE IN Z IN A PIXEL:DIDZ

C       SETUP EXPONENTIAL UNDERFLOW FLAG: DIDZFLG

        DIDZFLG=(-EXP(C10+C11*ALOG(ENERGY)+C12*((ALOG(ENERGY))**2)+
C   C13*((ALOG(ENERGY))**3))*FIL1*CMSQ1*DENS1

C   -EXP(C20+C21*ALOG(ENERGY)+C22*((ALOG(ENERGY))**2)+
C   C23*((ALOG(ENERGY))**3))*FIL2*CMSQ2*DENS2

C   -WMUA(IENERGY)*BODSZ

C   -(0.167295*(((1+ENERGY/511.006)/((ENERGY/511.006)**2))
C   *(2*(1+ENERGY/511.006)/(1+2*ENERGY/511.006)
C   -(ALOG(1+2*ENERGY/511.006)/(ENERGY/511.006)))
C   +((1/(2*ENERGY/511.006))*ALOG(1+2*ENERGY/511.006))
C   -((1+3*ENERGY/511.006)/((1+2*ENERGY/511.006)**2)))
C   *(PIIED/100)*PIXEL))


C       TYPE"DIDZFLG=",DIDZFLG
        IF(DIDZFLG.LT.-20.0) GOTO 550
C       TYPE"DIDZFLG.GT.-20....CONTINUE"
C       TYPE"DIDZ=",DIDZ

        DIDZ=DIDZ+((SPECTUBE*DELTE)*ENERGY*

C   EXP(-EXP(C10+C11*ALOG(ENERGY)+C12*((ALOG(ENERGY))**2)+
C   C13*((ALOG(ENERGY))**3))*FIL1*CMSQ1*DENS1

C   -EXP(C20+C21*ALOG(ENERGY)+C22*((ALOG(ENERGY))**2)+
C   C23*((ALOG(ENERGY))**3))*FIL2*CMSQ2*DENS2

C   -(0.50028*(((1+ENERGY/511.006)/((ENERGY/511.006)**2))
C   *(2*(1+ENERGY/511.006)/(1+2*ENERGY/511.006)
C   -(ALOG(1+2*ENERGY/511.006)/(ENERGY/511.006)))
C   +((1/(2*ENERGY/511.006))*ALOG(1+2*ENERGY/511.006))
C   -((1+3*ENERGY/511.006)/((1+2*ENERGY/511.006)**2)))
C   *(CMSQ1*FIL1*DENS1*ATNB1+CMSQ2*FIL2*DENS2*ATNB2))
```

```
C   -WMUA(IENERGY)*BODSZ

C   -(0.167295*(((1+ENERGY/511.006)/((ENERGY/511.006)**2))
C   *(2*(1+ENERGY/511.006)/(1+2*ENERGY/511.006)
C   -(ALOG(1+2*ENERGY/511.006)/(ENERGY/511.006)))
C   +((1/(2*ENERGY/511.006))*ALOG(1+2*ENERGY/511.006))
C   -((1+3*ENERGY/511.006)/((1+2*ENERGY/511.006)**2)))
C   *((1+PIIED/100)*(1+DELZ/Z)-1)*PIXEL))

C   *(1-EXP(
C   -((10.0**(-3.20086*ALOG10(ENERGY)+3.8663))*
C   ((1+PIIED/100)*((1+DELZ/Z)**4.6)-1))*PIXEL

C   -((10.0**(-1.89167*ALOG10(ENERGY)+1.30089))*
C   ((1+PIIED/100)*((1+DELZR/ZR)**2.705)-1))*PIXEL

C   -(0.167295*(((1+ENERGY/511.006)/((ENERGY/511.006)**2))
C   *(2*(1+ENERGY/511.006)/(1+2*ENERGY/511.006)
C   -(ALOG(1+2*ENERGY/511.006)/(ENERGY/511.006)))
C   +((1/(2*ENERGY/511.006))*ALOG(1+2*ENERGY/511.006))
C   -((1+3*ENERGY/511.006)/((1+2*ENERGY/511.006)**2)))
C   *((1+PIIED/100)*(1+DELZ/Z)-1)*PIXEL)))

C   *(GAMFX*DTKSZ*EFF/W)*1.6E-19)/DELZ

C       TYPE"DIDZ=",DIDZ
550     CONTINUE


C       ----------------------------------------

C       ETRANS IS THE ENERGY TRANSMITTED INTO THE DETECTOR PER
C       PHOTON EMITTED FROM THE XRAY SOURCE

C       SETUP EXPONENTIAL UNDERFLOW FLAG: ETRFLG

        ETRFLG=(-EXP(C10+C11*ALOG(ENERGY)+C12*((ALOG(ENERGY))**2)+
C   C13*((ALOG(ENERGY))**3))*FIL1*CMSQ1*DENS1

C   -EXP(C20+C21*ALOG(ENERGY)+C22*((ALOG(ENERGY))**2)+
C   C23*((ALOG(ENERGY))**3))*FIL2*CMSQ2*DENS2

C   -WMUA(IENERGY)*BODSZ)


C       TYPE"ETRFLG=",ETRFLG
        IF(ETRFLG.LT.-20.0) GOTO 560
C       TYPE"ETRFLG.GT.-20...CONTINUE"
C       TYPE"ETRANS=",ETRANS

        ETRANS=ETRANS+((SPECTUBE*DELTE)*ENERGY*

C   EXP(-EXP(C10+C11*ALOG(ENERGY)+C12*((ALOG(ENERGY))**2)+
C   C13*((ALOG(ENERGY))**3))*FIL1*CMSQ1*DENS1

C   -EXP(C20+C21*ALOG(ENERGY)+C22*((ALOG(ENERGY))**2)+
C   C23*((ALOG(ENERGY))**3))*FIL2*CMSQ2*DENS2

C   -(0.50028*(((1+ENERGY/511.006)/((ENERGY/511.006)**2))
C   *(2*(1+ENERGY/511.006)/(1+2*ENERGY/511.006)
C   -(ALOG(1+2*ENERGY/511.006)/(ENERGY/511.006)))
C   +((1/(2*ENERGY/511.006))*ALOG(1+2*ENERGY/511.006))
C   -((1+3*ENERGY/511.006)/((1+2*ENERGY/511.006)**2)))
C   *(CMSQ1*FIL1*DENS1*ATNB1+CMSQ2*FIL2*DENS2*ATNB2))
```

```
C   -WMUA(IENERGY)*BODSZ))

C   *EFF


C       ETRNOPHAN IS THE ENERGY TRANSMITTED INTO THE DETECTOR
C       PER PHOTON EMITTED FROM THE X-RAY SOURCE HAD THERE
C       BEEN NO PHANTOM.

        ETRNOPHAN=ETRNOPHAN+((SPECTUBE*DELTE)*ENERGY*

C   EXP(-EXP(C10+C11*ALOG(ENERGY)+C12*((ALOG(ENERGY))**2)+
C   C13*((ALOG(ENERGY))**3))*FIL1*CMSQ1*DENS1

C   -EXP(C20+C21*ALOG(ENERGY)+C22*((ALOG(ENERGY))**2)+
C   C23*((ALOG(ENERGY))**3))*FIL2*CMSQ2*DENS2

C   -(0.50028*(((1+ENERGY/511.006)/((ENERGY/511.006)**2))
C   *(2*(1+ENERGY/511.006)/(1+2*ENERGY/511.006)
C   -(ALOG(1+2*ENERGY/511.006)/(ENERGY/511.006)))
C   +((1/(2*ENERGY/511.006))*ALOG(1+2*ENERGY/511.006))
C   -((1+3*ENERGY/511.006)/((1+2*ENERGY/511.006)**2)))
C   *(CMSQ1*FIL1*DENS1*ATNB1+CMSQ2*FIL2*DENS2*ATNB2))

C   ))

C   *EFF


C       TYPE"ETRANS=",ETRANS
560     CONTINUE

C       ----------------------------------------

C       DOSE IS THE DOSE IN KEV PER GRAM DEPOSITED AT THE
C       SURFACE. THE EQUATION IS TAKEN FROM MY MASTERS THESIS.

C       SETUP EXPONENTIAL UNDERFLOW FLAG: DOSEFLG

        DOSEFLG=(-EXP(C10+C11*ALOG(ENERGY)+C12*((ALOG(ENERGY))**2)+
C   C13*((ALOG(ENERGY))**3))*FIL1*CMSQ1*DENS1

C   -EXP(C20+C21*ALOG(ENERGY)+C22*((ALOG(ENERGY))**2)+
C   C23*((ALOG(ENERGY))**3))*FIL2*CMSQ2*DENS2)
C       TYPE"DOSEFLG=",DOSEFLG

        IF(DOSEFLG.LT.-20.0) GOTO 565
C       TYPE"DOSEFLG.GT.-20...CONTINUE"
C       TYPE"DOSE=",DOSE

        DOSE=DOSE+1.566*((SPECTUBE*DELTE)*ENERGY*

C   EXP(-EXP(C10+C11*ALOG(ENERGY)+C12*((ALOG(ENERGY))**2)+
C   C13*((ALOG(ENERGY))**3))*FIL1*CMSQ1*DENS1

C   -(0.50028*(((1+ENERGY/511.006)/((ENERGY/511.006)**2))
C   *(2*(1+ENERGY/511.006)/(1+2*ENERGY/511.006)
C   -(ALOG(1+2*ENERGY/511.006)/(ENERGY/511.006)))
C   +((1/(2*ENERGY/511.006))*ALOG(1+2*ENERGY/511.006))
C   -((1+3*ENERGY/511.006)/((1+2*ENERGY/511.006)**2)))
C   *(CMSQ1*FIL1*DENS1*ATNB1+CMSQ2*FIL2*DENS2*ATNB2))

C   -EXP(C20+C21*ALOG(ENERGY)+C22*((ALOG(ENERGY))**2)+
C   C23*((ALOG(ENERGY))**3))*FIL2*CMSQ2*DENS2)*WMUE(IENERGY))
C       TYPE"DOSE=",DOSE
```

```
565     CONTINUE
C       ----------------------------------------
C       PREFE IS THE PREFILTER ENERGY OF THE SPECTRUM IN KEV.
        PREFE=PREFE+((SPECTUBE*DELTE)*ENERGY)
C       TYPE"PREFE=",PREFE
C       ----------------------------------------
C       POSFE IS THE POST FILTER ENERGY OF THE SPECTRUM IN KEV.
C       SETUP EXPONENTIAL UNDERFLOW FLAG: POSFLG
        POSFLG=(-EXP(C10+C11*ALOG(ENERGY)+C12*((ALOG(ENERGY))**2)+
     C  C13*((ALOG(ENERGY))**3))*FIL1*CMSQ1*DENS1
     C  -EXP(C20+C21*ALOG(ENERGY)+C22*((ALOG(ENERGY))**2)+
     C  C23*((ALOG(ENERGY))**3))*FIL2*CMSQ2*DENS2)
C       TYPE"POSFLG=",POSFLG
        IF(POSFLG.LT.-20.0) GOTO 570
C       TYPE"POSFLG.GT.-20...CONTINUE"
C       TYPE"POSFE=",POSFE
        POSFE=POSFE+((SPECTUBE*DELTE)*ENERGY*
     C  EXP(-EXP(C10+C11*ALOG(ENERGY)+C12*((ALOG(ENERGY))**2)+
     C  C13*((ALOG(ENERGY))**3))*FIL1*CMSQ1*DENS1
     C  -(0.50028*(((1+ENERGY/511.006)/((ENERGY/511.006)**2))
     C  *(2*(1+ENERGY/511.006)/(1+2*ENERGY/511.006)
     C  -(ALOG(1+2*ENERGY/511.006)/(ENERGY/511.006)))
     C  +((1/(2*ENERGY/511.006))*ALOG(1+2*ENERGY/511.006))
     C  -((1+3*ENERGY/511.006)/((1+2*ENERGY/511.006)**2)))
     C  *(CMSQ1*FIL1*DENS1*ATNB1+CMSQ2*FIL2*DENS2*ATNB2))
     C  -EXP(C20+C21*ALOG(ENERGY)+C22*((ALOG(ENERGY))**2)+
     C  C23*((ALOG(ENERGY))**3))*FIL2*CMSQ2*DENS2))
C       TYPE"POSFE=",POSFE
C       THIS THE ATTENUATION FACTOR OF POSFE WHICH IS IN THE
C       DENOMINATOR OF THE POSFE EXPRESSION:POSSUM
        POSSUM=POSSUM+((SPECTUBE*DELTE)*
     C  EXP(-EXP(C10+C11*ALOG(ENERGY)+C12*((ALOG(ENERGY))**2)+
     C  C13*((ALOG(ENERGY))**3))*FIL1*CMSQ1*DENS1
     C  -(0.50028*(((1+ENERGY/511.006)/((ENERGY/511.006)**2))
     C  *(2*(1+ENERGY/511.006)/(1+2*ENERGY/511.006)
     C  -(ALOG(1+2*ENERGY/511.006)/(ENERGY/511.006)))
     C  +((1/(2*ENERGY/511.006))*ALOG(1+2*ENERGY/511.006))
     C  -((1+3*ENERGY/511.006)/((1+2*ENERGY/511.006)**2)))
     C  *(CMSQ1*FIL1*DENS1*ATNB1+CMSQ2*FIL2*DENS2*ATNB2))
     C  -EXP(C20+C21*ALOG(ENERGY)+C22*((ALOG(ENERGY))**2)+
     C  C23*((ALOG(ENERGY))**3))*FIL2*CMSQ2*DENS2))
570     CONTINUE
C       ----------------------------------------
        TYPE"INCREMENT ENERGY HERE:OLD ENERGY",ENERGY-
```

```
C       INCREMENT THE ENERGY HERE.
        ENERGY=ENERGY+1.0
        IENERGY=IENERGY+1
        TYPE"NEW ENERGY=",ENERGY
        GOTO 500
600     CONTINUE
        TYPE"ENERGY.GT.EMAX"
        TYPE"DIDZ=",DIDZ

C       ----------------------------------------

C       SNSTVTY IS THE DIMENSIONLESS FRACTIONAL CHANGE IN THE
C       CURRENT PER UNIT CHANGE IN THE ATOMIC NUMBER.

        SNSTVTY=DIDZ/CURRENT
        TYPE"SNSTVTY=",SNSTVTY

C       ----------------------------------------

C       DOPED IS THE DOSE PER ENERGY DEPOSITED IN THE DETECTOR.
C       WE USE DOPED AS A FIGURE OF MERIT OF THE INPUT SPECTRUM.

        DOPED =DOSE/ETRANS
        TYPE"DOPED=",DOPED

C       ----------------------------------------

C       FILTRAN IS THE FRACTION OF THE BEAM ENERGY FROM
C       THE X-RAY TUBE (AFTER INHERENT FILTRATION) THAT
C       IS TRANS BY THE FILTERS. NOTE THAT THE POSFE USED
C       IS THE NON-NORMALIZED POSFE. THIS IS BECAUSE THIS
C       THE CORRECT INTEGRAL NEEDED FOR THE CALCULATION.


        FILTRAN=POSFE/PREFE

C       ----------------------------------------

C       STUDYOFLOOD IS THE RATIO OF THE MEASURED SIGNALS WITH
C       AND WITHOUT A PHANTOM. (OR ALSO THE RATIO OF
C       THE MEASURED X-RAYS DETECTED WITH AND WITHOUT
C       A PHANTOM)

        STUDYOFLOOD=ETRANS/ETRNOPHAN

C       ----------------------------------------

C       POSFE IS THE POSTFILTER SPECTRUM ENERGY.

        POSFE=POSFE/POSSUM
        TYPE "POSFE=",POSFE
        TYPE "PREFE=",PREFE
C       ----------------------------------------

C       PCTTBE IS THE PERCENT TRANSMISSION OF THE PREFILTER SPECTRUM
C       WE USE PCTTBE TO GIVE US AN IDEA OF THE FRACTION OF ENERGY
C       WHICH IS ABSORBED IN THE FILTER AND THE WATER PHANTOM.

        PCTTBE=ETRANS/PREFE
        TYPE""
        TYPE"PCTTBE=",PCTTBE
        TYPE""


C       ----------------------------------------
```

```
C       PCTTAF IS THE PERCENT TRANSMISSION OF THE POSTFILTER
C       SPECTRUM. WE USE PCTTAF TO GIVE US AN IDEA OF THE
C       FRACTION OF ENERGY WHICH IS ABSORBED IN THE WATER PHANTOM.

        PCTTAF=ETRANS/(POSFE*POSSUM)
        TYPE"PCTTAF=",PCTTAF

C       ---------------------------------------

C       INSERT THE PERCENT ERROR OF THE MEASUREMENT BY USING THE
C       FORMULA FOR PERCENT ERROR WHICH USES THE TRANSMISSION
C       AND THE SENSITIVITY FACTOR.
```

```
      ACCEPT"IS PCTTBE OKAY?",IPCTCHK
      IF(IPCTCHK.EQ.0)GOTO 100

      ACCEPT"SAVE DATA FOR OPTIMIZATION?",ISAVE
      IF(ISAVE.EQ.0)GOTO 602
      ACCEPT"1ST OR 2ND DATA?",IDATA
      GOTO(6001,6002),IDATA
6001  CONTINUE
      PCT1=PCTTBE
      SNS1=SNSTVTY
      DOPD1=DOPED
      GOTO 602
6002  CONTINUE
      PCT2=PCTTBE
      SNS2=SNSTVTY
      DOPD2=DOPED

602   CONTINUE

      TYPE"EXPERIMENTAL SETUP"

      TYPE"  SPECTRUM KVP=",KVP
      TYPE""
      TYPE"  FILTER1=",ATNB1
      TYPE"  THICKNESS1=",FIL1
      TYPE"  CMSQ1/GM=",CMSQ1
      TYPE"  DENSITY1=",DENS1
      TYPE""
      TYPE"  FILTER2=",ATNB2
      TYPE"  THICKNESS2=",FIL2
      TYPE"  CMSQ2/GM=",CMSQ2
      TYPE"  DENSITY2=",DENS2
      TYPE""
      TYPE"  PATIENT SIZE=",BODSZ
      TYPE"  PIXEL SIZE=",PIXEL
      TYPE"  DETECTOR SIZE=",DTKSZ
      TYPE"  GAMMA FLUX=",GAMFX
      IF(ISPLIT.EQ.0) GOTO 603
      TYPE"SPLIT FINGER CALCULATION"," IDET=",IDET
603   CONTINUE
      ACCEPT"DO YOU WANT TO OUTPUT EXPT. SETUP?",IEXPS
      IF(IEXPS.EQ.0) GOTO 605
      WRITE(12)""
      WRITE(12)""
      CALL FGTIM(IHR,IMIN,ISEC)
      CALL DATE(IAR,IER)
      WRITE(12)"TIME=",IHR,":",IMIN,":",ISEC
      WRITE(12)"DATE=",IAR(1),"/",IAR(2),"/",IAR(3)
      WRITE(12)""
      WRITE(12)"EXPERIMENTAL SETUP"
      WRITE(12)"  SPECTRUM KVP=",KVP
      WRITE(12)""
      WRITE(12)"  FILTER1=",ATNB1
      WRITE(12)"  THICKNESS1=",FIL1
      WRITE(12)"  CMSQ1/GM=",CMSQ1
      WRITE(12)"  DENSITY1=",DENS1
      WRITE(12)""
      WRITE(12)"  FILTER2=",ATNB2
      WRITE(12)"  THICKNESS2=",FIL2
      WRITE(12)"  CMSQ2/GM=",CMSQ2
      WRITE(12)"  DENSITY2=",DENS2
      WRITE(12)""
```

```
      WRITE(12)"  PATIENT SIZE=",BODSZ
      WRITE(12)"  PIXEL SIZE=",PIXEL
      WRITE(12)"  DETECTOR SIZE=",DTKSZ
      WRITE(12)"  GAMMA FLUX=",GAMFX
      IF(ISPLIT.EQ.0) GOTO 604
      WRITE(12)"  SPLIT FINGER CALCULATION"," IDET=",IDET
604   CONTINUE
605   TYPE "DESIGN CRITERION"
      TYPE"  SNSTVTY: SENSITIVITY=DIDZ/CURRENT"
      TYPE"  FILTRAN: FRACTION OF ENERGY TRANS BY FILTERS"
      TYPE"  STUDYOFLOOD: FRACTION OF TRANS THRU PHANTOM"
      TYPE"  PCTTBE: PERCENT TRANSMISSION: XRAY TUBE-DETECTOR"
      TYPE"  DOPED: DOSE PER ENERGY DEPOSITED"
      ACCEPT"DO YOU WANT TO OUTPUT THE DESIGN CRIT VALS",IDES
      IF(IDES.EQ.0) GOTO 610
      WRITE(12)"DESIGN CRITERION"
      WRITE(12)"  SNSTVTY:DIDZ/CURRENT=",SNSTVTY
      WRITE(12)"  FILTRAN:FRAC TRANS IN FILTERS=",FILTRAN
      WRITE(12)"  STUDYOFLOOD:FRAC TRNS IN PHANTOM=",STUDYOFLOOD
      WRITE(12)"  PCTTBE:TRANS:XRAY TUBE-DETECTOR=",PCTTBE
      WRITE(12)"  DOPED: DOSE PER ENERGY DEPOSITED=",DOPED
      TYPE "DESIGN CRITERION"
      TYPE"  SNSTVTY: DIDZ/CURRENT=",SNSTVTY
      TYPE"  FILTRAN:FRAC TRAN IN FILTERS=",FILTRAN
      TYPE"  STUDYOFLOOD:FRAC TRNS IN PHANTOM=",STUDYOFLOOD
      TYPE "  PCTTBE: TRANS: TUBE-DETECTOR=",PCTTBE
      TYPE "  DOPED: DOSE PER ENERGY DEPOSITED=",DOPED
610   TYPE"MEASURED QUANTITIES"
      TYPE"  CURRENT: DETECTOR CURRENT"
      TYPE"  DIDZ:"
      TYPE"  ETRANS: TRANSMITTED ENERGY"
      TYPE"  DOSE: SURFACE DOSE"
      TYPE"  PCTTAF: PERCENT TRANSMISSION THRU THE PHANTOM"
      ACCEPT "DO YOU WANT TO OUTPUT MEASURED QUANTITIES?",IQUAN
      IF(IQUAN.EQ.0) GOTO 620
      WRITE(12)"MEASURED QUANTITIES"
      WRITE(12)"  CURRENT: DETECTOR CURRENT=",CURRENT
      WRITE(12)  "  DIDZ=",DIDZ
      WRITE(12)  "  ETRANS:TRANSMITTED ENERGY=",ETRANS
      WRITE(12)  "  DOSE:SURFACE DOSE=",DOSE
      WRITE(12)  "  PCTTAF: PCT PHANTOM TRANSMISSION=",PCTTAF
      TYPE"MEASURED QUANTITIES"
      TYPE"  CURRENT: DETECTOR CURRENT=",CURRENT
      TYPE"  DIDZ=",DIDZ
      TYPE"  ETRANS:TRANSMITTED ENERGY=",ETRANS
      TYPE"  DOSE:SURFACE DOSE=",DOSE
      TYPE"  PCTTAF: PCT PHANTOM TRANSMISSION=",PCTTAF
620   ACCEPT"OUTPUT OPT. QUANTITIES?",IOPT
      IF(IOPT.EQ.0)GOTO 6005

C     ERROR: THIS THE ERROR OF MEASUREMENT WITH OUR DETECTOR.
C     THE FORMULA FOR THIS EXPRESSION IS DERIVED ON PAGES
C     75 THRU 80 IN THE LOG BOOK 3.

      ERROR=(SQRT((2*W)/(DTKSZ*GAMFX*PREFE*TIMEN*PCTTBE)))
     C/(DELZ*(SNS1-SNS2))

C     ERFLX: IS THE ERROR FROM A MEASUREMENT WHEN THERE
C     IS A UNIT FLUX, UNIT DETECTOR SIZE, 1MSEC TIME,
C     AND THE FLUX IS THEREFORE HELD CONSTANT.

      ERFLX=(SQRT((2*W)/(1.0*1.0*PREFE*0.001*PCTTBE)))
     C/(DELZ*(SNS1-SNS2))

C     ERDOS: THIS IS THE ERROR FROM A MEASUREMENT WHEN THE
C     DOSE IS HELD FIXED. WE CALCULATE THIS FOR DIFFERENT
```

```
C       FILTER THICKNESSES.

        ERDOS=(SQRT(((2*W)*(DOPD1)/DTKSZ)*
     C  (108.66*108.66/((63.0-BODSZ/2)*(63.0-BODSZ/2)))))/
     C  (DELZ/(SNS1-SNS2))

        WRITE(12)"OPTIMIZATION QUANTITIES"
        WRITE(12)"  ERROR=",ERROR
        WRITE(12)"ERFLX=",ERFLX
        WRITE(12)"ERDOS=",ERDOS
        TYPE"OPTIMIZATION QUANTITIES"
        TYPE"  ERROR=",ERROR
        TYPE"  ERFLX=",ERFLX
        TYPE"  ERDOS=",ERDOS

6005    TYPE "THEORETICAL QUANTITIES"
        TYPE"  SNSTVTY: DIDZ/CURRENT"
        ACCEPT "DO YOU WANT TO OUTPUT THEORETICAL QUANT.?",ITHEO
        IF(ITHEO.EQ.0) GOTO 630
        WRITE(12) "THEORETICAL QUANTITIES"
        WRITE(12)  "  SNSTVTY: DIDZ/CURRENT=",SNSTVTY
        TYPE "THEORTICAL QUANTITIES"
        TYPE  "  SNSTVTY: DIDZ/CURRENT=",SNSTVTY

630     TYPE"MISCELLANEOUS QUANTITIES"
        TYPE"  PREFE: PREFILTER SPECTRUM ENERGY"
        TYPE"  POSFE: POSTFILTER SPECTRUM ENERGY"
        ACCEPT "DO YOU WANT TO OUTPUT MISC. QUANTITIES?",IMISC
        IF(IMISC.EQ.0) GOTO 640
        WRITE(12)"MISCELLANEOUS QUANTITIES"
        WRITE(12)"  PREFE: PREFILTER SPECTRUM ENERGY=",PREFE
        WRITE(12)"  POSFE: POSTFILTER SPEDTRUM ENERGY=",POSFE
        TYPE"MISCELLANEOUS QUANTITIES"
        TYPE"  PREFE: PREFILTER SPECTRUM ENERGY=",PREFE
        TYPE  "  POSFE: POSFILTER SPECTRUM ENERGY=",POSFE

640     CONTINUE
        GOTO 100
C       ----------------------------------------
C       LIBRARY OF PHOTON CROSS SECTIONS. IN THIS LIBRARY THE COEFF-
C       ICIENTS OF THE CROSS SECTION FITS ARE GIVEN. ALSO GIVEN
C       ARE THE BARNS TO CMSQ/GM AND DENSITY FACTORS.

1000    GOTO 1003
1001    ACCEPT "ERROR-TRY AGAIN. ATOMIC NUMBER=?",ATN
        ACCEPT "WAS THAT FILTER 1 OR 2?",FIL12
        IF(FIL12.EQ.2) GOTO 1002
        ATNB1=ATN
        GOTO 1003
1002    ATNB2=ATN
1003    IATN=ATN
        GOTO(1001,1001,1001,1004,1001,1001,1001,1001,1001,
     C  1001,1001,1001,1001,1001,1001,1001,1001,1001,1001,
     C  1001,1001,1001,1001,1001,1001,1026,1001,1028,1029,
     C  1001,1001,1001,1001,1001,1001,1001,1001,1001,1001,
     C  1001,1001,1001,1001,1001,1001,1001,1001,1001,1001,
     C  1050,1001,1001,1053,1001,1001,1001,1001,1001,1001,
     C  1060,1001,1001,1001,1001,1065,1001,1001,1001,1001,
     C  1070,1001,1001,1073,1074,1075,1001,1001,1001,1001,
     C  1080,1001,1001,1001,1001,1001,1001,1001,1001,1001,
     C  1001,1001,1001,1001,1001,1001,1001,1001,1001,1001),IATN
C       FORMAT FOR THE CROSS SECTION LIBRARY SETUP
C       CONTINUE
C       CML0=
C       CML1=
C       ELEG=
```

```
C       CLK0=
C       CLK1=
C       EKEG=
C       CK0=
C       CK1=
C       CK2=
C       CK3=
C       DENS=
C       CMSQ=
C       GOTO 1200
1004    CONTINUE
        CML0=0.0
        CML1=0.0
        ELEG=0.0
        CLK0=5.5508E0
        CLK1=-2.9314E0
        EKEG=1.11E-1
        CK0=9.1061E0
        CK1=-2.9314E0
        CK2=-7.3572E-2
        CK3=7.2012E-3
        DENS=1.845
        CMSQ=6.683E-2
        GOTO 1200
1026    CONTINUE
        CML0=1.236E1
        CML1=-2.8459E0
        ELEG=1.0
        CLK0=1.4047E1
        CLK1=-2.8459E0
        EKEG=7.112E0
        CK0=1.462E1
        CK1=-1.4284E0
        CK2=-3.8376E-1
        CK3=3.1286E-2
        DENS=7.86
        CMSQ=1.078E-2
        GOTO 1200
1028    CONTINUE
C       CML0=1.2462E1
C       CML1=
C       ELEG=
C       CLK0=
C       CLK1=
C       EKEG=
C       CK0=
C       CK1=
C       CK2=
C       CK3=
C       DENS=
C       CMSQ=
C       GOTO 1200
C       CONTINUE
C       CML0=
C       CML1=
C       ELEG=
C       CLK0=
C       CLK1=
C       EKEG=
C       CK0=
C       CK1=
C       CK2=
C       CK3=
C       DENS=
C       CMSQ=
C       GOTO 1200
```

```
C       CONTINUE
C       CML0=
C       CML1=
C       ELEG=
C       CLK0=
C       CLK1=
C       EKEG=
C       CK0=
C       CK1=
C       CK2=
C       CK3=
C       DENS=
C       CMSQ=
C       GOTO 1200

1029    CONTINUE
        CML0=1.204E1
        CML1=-2.3152E0
        ELEG=1.0
        CLK0=1.4280E1
        CLK1=-2.7311E0
        EKEG=8.979
        CK0=1.4995E1
        CK1=-1.4602E0
        CK2=-3.6065E-1
        CK3=2.865E-2
        DENS=8.94
        CMSQ=9.478E-3
        GOTO 1200

1050    CONTINUE
        CML0=1.4531E1
        CML1=-2.4953E0
        ELEG=4.0
        CLK0=1.6476E1
        CLK1=-2.7325E0
        EKEG=2.92E1
        CK0=1.396E1
        CK1=1.8787E-1
        CK2=-6.2938E-1
        CK3=4.2822E-2
        DENS=7.29
        CMSQ=5.074E-3
        GOTO 1200

1053    CONTINUE
        CML0=1.4844E1
        CML1=-2.5987E0
        ELEG=2
        CLK0=1.6714E1
        CLK1=-2.7204E0
        EKEG=3.317E1
        CK0=1.9349E1
        CK1=-2.9618E0
        CK2=8.4674E-4
        CK3=1.6966E-3
        DENS=4.92E0
        CMSQ=4.746E-3
        GOTO 1200

1060    CONTINUE
        CML0=1.5487E1
        CML1=-2.7124E0
        ELEG=7.0
        CLK0=1.7494E1
        CLK1=-2.8131E0
```

```
      EKEG=43.57
      CK0=2.3415E1
      CK1=-5.0766E0
      CK2=4.1182E-1
      CK3=-2.4502E-2
      DENS=7.0
      CMSQ=4.174E-3
      GOTO 1200

1065  CONTINUE
      CML0=1.581E1
      CML1=-2.669E0
      ELEG=7.0
      CLK0=1.7852E1
      CLK1=-2.8184E0
      EKEG=52.0
      CK0=2.5153E1
      CK1=-5.8494E0
      CK2=5.5475E-1
      CK3=-3.3427E-2
      DENS=8.27E0
      CMSQ=3.790E-3
      GOTO 1200

1070  CONTINUE
      CML0=1.6098E1
      CML1=-2.6378E0
      ELEG=9.0
      CLK0=1.8043E1
      CLK1=-2.7859E0
      EKEG=61.33
      CK0=1.7877E1
      CK1=-1.9444E0
      CK2=-1.0537E-1
      CK3=3.1465E-3
      DENS=7.0
      CMSQ=3.480E-3
      GOTO 1200

1073  CONTINUE
      CML0=1.6304E1
      CML1=-2.6605E0
      ELEG=10.0
      CLK0=1.7906E1
      CLK1=-2.7074E0
      EKEG=67.42
      CK0=2.404E1
      CK1=-5.4397E0
      CK2=5.5020E-1
      CK3=-3.655E-2
      DENS=1.660E1
      CMSQ=3.328E-3
      GOTO 1200

1074  CONTINUE
      CML0=1.6339E1
      CML1=-2.6379E0
      ELEG=10.0
      CLK0=1.8138E1
      CLK1=-2.7537E0
      EKEG=69.53
      CK0=1.694E1
      CK1=-1.5494E0
      CK2=-1.4264E-1
      CK3=3.9831E-3
      DENS=19.3
```

```
        CMSQ=3.276E-3
        GOTO 1200

1075    CONTINUE
        CML0=1.6385E1
        CML1=-2.6273E0
        ELEG=10.0
        CLK0=1.8194E1
        CLK1=-2.7511E0
        EKEG=71.68E1
        CK0=2.7190E1
        CK1=-6.7485E0
        CK2=7.3957E-1
        CK3=-4.6056E-2
        DENS=20.53
        CMSQ=3.234E-3
        GOTO 1200

1080    CONTINUE
        CML0=1.6544E1
        CML1=-2.6034E0
        ELEG=10.0
        CLK0=1.8291E1
        CLK1=-2.7015E0
        EKEG=83.1
        CK0=6.7857E1
        CK1=-2.8402E1
        CK2=4.5527E0
        CK3=-2.6691E-1
        DENS=13.52
        CMSQ=3.002E-3
        GOTO 1200

1200    IF(FILNBR.EQ.2) GOTO 1210
        C1ML0=CML0
        C1ML1=CML1
        E1LEG=ELEG
        C1LK0=CLK0
        C1LK1=CLK1
        E1KEG=EKEG
        C1K0=CK0
        C1K1=CK1
        C1K2=CK2
        C1K3=CK3
        CMSQ1=CMSQ
        DENS1=DENS
        GOTO 1220
1210    C2ML0=CML0
        C2ML1=CML1
        E2LEG=ELEG
        C2LK0=CLK0
        C2LK1=CLK1
        E2KEG=EKEG
        C2K0=CK0
        C2K1=CK1
        C2K2=CK2
        C2K3=CK3
        CMSQ2=CMSQ
        DENS2=DENS
        GOTO 1220
1220    IFILNBR=FILNBR
        GOTO(290,400),IFILNBR
2000    TYPE"ENDING PROGRAM"
        STOP
        END
```

Appendix C Complete Listing of the Software Used in the Experimental Data Acquisition, Reconstruction, and Display

The purpose of this appendix is to list those programs used in the tomochemistry proof-of-principle experiments. Listed below are the main programs used and their respective subroutines. A short description of the purpose and structure of the programs is provided prior to the listing.

Appendix C.1 Listing of the Programs Used to Setup the Data Files Prior to the Scan - TCSETUP

Purpose

To setup the name of the reconstruction file, the number of detectors used and other parameters pertinent to a scan.

Program Name	Function
Main Program:	
TCSETUP	- to setup a CT scan.
Subprograms:	
NAMMAK	- to create a new ASCII name.
FILNAM	- to open a new name file.
TCFACC	- to check the name format.
CLEAR	- to clear a buffer to zero.
FORT.LB	- FORTRAN IV mathematics library.

Main Program TCSETUP:

```
C       THIS ROUTINE SETS UP THE INPUT PARAMETERS OF FILE --.AL
        DIMENSION IBUF(256),ILINE(60)
        DIMENSION IFNAME(20)
        CALL CLEAR(IBUF,256)
        CALL FILNAM(IFNAME)
        CALL NAMMAK(IFNAME,"AL")
        CALL OPEN(1,IFNAME,3,IER,512)
        IF(IER.NE.1) GO TO 900
        CALL TCFACC("FIRST FINGER",IFIRST,"I")
        CALL TCFACC("NUMBER OF FINGERS",NF,"I")
        CALL TCFACC("VIEWS PER BUFFER",NVIEW,"I")
        CALL TCFACC("BUFFERS",NBUF,"I")
        NFETH=0
        CALL TCFACC("REFERENCE FINGER",NREF,"I")
        CALL TCFACC("CLOCK FINGER",NCLOCK,"I")
        TYPE "PRECEDE CHARACTER WITH <136> FOR LOWER CASE"
"       TYPE "----------------------     ENTER FOUR 20 CHARACTER TITLE
        CALL CLEAR(IBUF(11),40)
        DO 100 J=1,4
        CALL CLEAR (ILINE,60)
        J2=J*10+1
        READ(11,1101) ILINE
1101    FORMAT(60A1)
        JB=0
        DO 80 JCHAR=1,20
        IUP=0
60      JB=JB+1
        IC=ISHFT(ILINE(JB),-8).OR.200K
        IF(IC.GE.340K.OR.IC.LT.240K) IC=240K
        IF(IC.EQ.200K)IC=240K
        IF(IC.NE.336K) GO TO 70
        IUP=1
        GO TO 60
70      IF(IUP.EQ.1) IC=IC.OR.40K
        JC1=(JCHAR-1)/2
        JC2=MOD(JCHAR,2)
        JC3=J2+JC1
        IF(JC2.EQ.1)IBUF(JC3)=ISHFT(IC,8)
        IF(JC2.EQ.0)IBUF(JC3)=IBUF(JC3).OR.IC
80      CONTINUE
100     CONTINUE
        IBUF(8)=IFIRST
        IBUF(9)=NF
        IBUF(10)=NVIEW
        IBUF(3)=NFETH
        IBUF(4)=NREF
        IBUF(5)=NCLOCK
        IBUF(7)=NBUF
        CALL WRBLK(1,1,IBUF,1,IER)
        IF(IER.NE.1) GO TO 900
        CALL FCLOS(1)
        STOP SETUP DONE
900     TYPE "<07>I/O ERROR FORTRAN CODE = ",IER
        STOP ERROR
        END
```

Subroutine NAMMAK:

```
        .TITL   NAMMA
        .ENT    NAMMA
        .EXTD   .CPYL,.FRET
        .NREL
;MAKE A NEW ASCII NAME FROM THAT PASSED IN PARAMETERS
FNAME=-167
SUF=-166
        2
NAMMA:  JSR     @.CPYL
        LDA     2,FNAME,3       ;GET ADDRESS OF OLD NAME
        MOVZL   2,2     ;SHIFT FOR BYTE ADDRESS
        NEG     2,0     ;STORE NEGATIVE IN AC0@
LOOP:   LDB     2,1             ;LOAD AC1 W/ BYTE
        MOV     1,1,SNR
        JMP     STORE   ;ZERO VALUE: IT'S A NULL
        XORI    56,1    ;CHECK FOR PERIOD
        MOV     1,1,SNR
        JMP     STORE   ;IT'S A .
        INC     2,2
        JMP     LOOP    ;NOT DONE--LOOP
STORE:  ADD     2,0     ;COMPUTE NUMER OF CHARACTERS - 1
        CLM     0,0
        0
        15.             ;NO MORE THAN 15 WITH DIRECTORY PREFIX
        JMP     ERR     ;SIGNAL ERROR IF APPROPRIATE
        ELEF    1,56,0  ;LOAD A PERIOD
        STB     2,1
        INC     2,2
        LDA     1,@SUF,3        ;LOAD THE NEW SUFFIX INTO AC1
        MOVS    1,1
        STB     2,1
        INC     2,2
        MOVS    1,1
        STB     2,1
        INC     2,2
        SUB     1,1
        STB     2,1
        JSR     @.FRET
ERFNM=1
ERR:    ELEF    2,ERFNM,0
        .SYSTM
        .ERTN
        .END
```

Subroutine FILNAM:

```
      SUBROUTINE FILNAM(I)
      DIMENSION I(1)
      CALL OPEN(8,"TOMO.FN",1,IER)
      IF(IER.NE.1) GO TO 900
      IER=9
      READ(8,1101,END=900,ERR=900) I(1)
1101  FORMAT(S20)
      CALL CLOSE(8,IER)
      WRITE(10,1001) I(1)
1001  FORMAT(1X,S20)
      RETURN
900   TYPE "I/O ERROR",IER
      STOP ERROR
      END
```

Subroutine TCFACC:

```
      COMPILER NOSTACK
      SUBROUTINE TCFACC(S,I,ITYPE)
      INTEGER S(30),I(30)
      INTEGER S2(30)
      COMMON/CFACC/ IX(2)
      EQUIVALENCE (IX(1),X)
      DATA ICALLED/0/
      IBYTE(K,L)=377K.AND.ISHFT(K,-8*MOD(L,2))
      IF(ICALLED.EQ.0)CALL OPEN(9,"TOMO.TC",1,IER)
      IF(IER.NE.1) GO TO 900
      ICALLED=1
      REWIND 9
      LUN=9
100   CONTINUE
      READ(9,101,END=200,ERR=200) S2(1)
101   FORMAT(S30)
      DO 110 J=1,30
      IW=(J+1)/2
      JB1=IBYTE(S(IW),J)
      JB2=IBYTE(S2(IW),J)
      IF(JB1.NE.JB2) GO TO 120
      IF(JB1.EQ.0) GO TO 150
110   CONTINUE
      GO TO 150
120   CONTINUE
      READ(9,101,END=200,ERR=200) S2(1)
      GO TO 100
150   IF(ITYPE.NE."I") GO TO 160
      READ(LUN,END=200,ERR=200) I(1)
      GO TO 300
160   IF(ITYPE.NE."F")GO TO 170
      READ(LUN,END=200,ERR=200) X
      I(1)=IX(1)
      I(2)=IX(2)
      GO TO 300
170   IF(ITYPE.NE."S") GO TO 400
      READ(LUN,101,END=200,ERR=200) I(1)
      GO TO 300
200   CONTINUE
      WRITE(10,102) S(1)
      LUN=11
102   FORMAT(1X,S30,2X,Z)
      GO TO 150
300   CONTINUE
      RETURN
400   CONTINUE
      TYPE "***BAD FORMAT***"
      RETURN
900   TYPE "I/O ERROR",IER
      GO TO 200
      END
```

Subroutine CLEAR:

```
        .TITL CLEAR
;       CLEAR BUFFER TO ZERO
        .ENT CLEAR
        .EXTD   .FRET,.CPYL
BUF=-167
N=BUF+1
.FS=N+167+1
        .NREL
        .FS
CLEAR:  JSR     @.CPYL
        LDA     1,@N,3          ;LOAD COUNT
        SBI     1,1             ;DECREMENT
        SUB     0,0             ;CLEAR ZERO
        LDA     2,BUF,3         ;LOAD ADDRESS
        STA     0,0,2           ;CLEAR FIRST
        INC     2,3             ;(2)+1->3
        BLM                     ;MOVE THE ZERO
        JSR     @.FRET
        .END
```

Appendix C.2 Listing of the Programs Used to Spool in the Experimental Data TSPOOL

Purpose

To control the data acquisition sequence. This program is the software which is central to the data I/O control.

Program Name	Function
Main Program:	
TSPOOL	- to coordinate the data I/O process during a scan.
Subprograms:	
FMABILD	- to build a detector finger map.
FINMOVE/U	- to reorder a collected set of data according to the map JFMAP.
DWACQ	- routine to acquire data in a double word format.
BLMOVE	- to move the zero in a buffer block.
FILNAM	- to open a new name file.
NOPEN	- to open a new name file.
SPDISK	- to spool raw data to disk from a circular buffer.
SPFILL	- to spool raw data into a circular buffer.
REBLOCK	- to reblock the spooled raw data on the disk.
BLKIO	- to perform a fast binary read/write of a block of data.
IERCH	- to note an error in the data blocks.
CLEAR	- to clear a buffer to zero.
DWFL	- to convert data from double word to floating point format.
DWCHS	- to change the sign of the double word data.
NAMMAK	- to create a new ASCII name.
FACC	- to check the name format.

SUMWD	- to add N words from single precision IB1 to double precision IB2.
TACQ/U	- to control the automatic data acquisition.
FMT.LB	- FORTRAN IV multitasking library.
FSYS.LB	- FORTRAN IV system library.
FORT.LB	- FORTRAN IV mathematics library.

Main Program TSPOOL:

```
      CHANTASK 10,4
C     PROGRAM TO SPOOL A SERIES OF READINGS OUT TO A NAMED FILE
C     DATA COLLECTION IS DONE BY SPFILL
C     DISK WRITING IS DONE BY TASK SPDISK
      DIMENSION IB(60))
      DIMENSION INAME(30)
      EXTERNAL SPDISK,SPFILL
      COMMON/ACBUF/ICBUF(300)
      COMMON/SPBUF/IFIRST,ILAST,NMAX,NVIEW,IMESS,IBUF(6400)
      COMMON/SPMAP/NFCOLL,JFMAP(300)
      DATA NMAX/6400/
      NMAX=NMAX-MOD(NMAX,256)          ;NMAX MUST BE MULTIPLE OF 256
      IMESS=0
      IFIRST=1
      ILAST=1
      NFCOLL=300
      NTMAX=300                  ;MAXIMUM NUMBER OF VIEWS
      IFMAP=0
      CALL FMABILD(JFMAP,IFMAP)
      CALL OPEN(5,"DPOF:RAWDATA",2,IER)
      IF(IER.NE.1) GO TO 910
      CALL FILNAM(INAME)
      CALL NOPEN(INAME,"AL",1,$900)
      CALL RDBLK(1,1,IB,1,IER)
      IF(IER.NE.1) GO TO 900
      CALL FCLOS(1)
      IFIRSTF=IB(8)
      NF=IB(9)
      ILASTF=IFIRSTF+NF-1
      NREAD=IB(10)
      NPASS=IB(7)
      NCLOCK=IABS(IB(5))
      CALL FACC("CLOCK ON ELECTRONICS CHANNEL",NCLEL,"I")
      NSWITCH=NCLOCK+1
      NVIEW=NREAD*NPASS
      IF(NREAD.LE.0.OR.NVIEW.GT.NTMAX) GO TO 900
C
C     SET CLOCK SIGNAL BOARD TO START AT NCLOCK
      DO 50 JCL=1,6
      JNCL=NCLOCK+JCL-1
      JFOLD=JFMAP(JNCL)
      JFNEW=NCLEL+JCL-1
      JFMAP(JNCL)=JFNEW
50    CONTINUE
      CALL NOPEN(INAME,"PR",1,$910)
      CALL NOPEN(INAME,"DK",2,$910)
      CALL NOPEN(INAME,"FL",3,$910)
      READ BINARY(1,END=60,ERR=60) IB
UE    PAUSE FILE ALREADY EXISTS, CTRL A TO ABORT, ANY KEY TO CONTI
60    CONTINUE
      REWIND 1
      TYPE "<07>"
      PAUSE STRIKE KEY FOR STUDY
      CALL ITASK(SPFILL,1,1,IER)
      CALL ITASK(SPDISK,2,2,IER)
      IF(IER.NE.1) GO TO 920
      CALL REC(IMESS,IDONE)
      TYPE "<07>"
      PAUSE STRIKE KEY FOR DARK CURRENT
      CALL TACQ(ICBUF,IDONE)  ;DUMMY
      CALL DWACQ(IB,NVIEW,JFMAP)
      WRITE BINARY(2) IB
```

```
        CALL FCLOS(2)
        TYPE "<07>"
        PAUSE STRIKE KEY FOR FLOOD
        CALL TACQ(ICBUF,IDONE)
        CALL DWACQ(IB,NVIEW,JFMAP)
        WRITE BINARY(3) IB
        CALL FCLOS(3)
        CALL MTROF
        TYPE " <07>FLOOD DONE"
C       COPY DPOF:RAWDATA TO FILE 1 AND RE-BLOCK DATA
        CALL REBLOCK(IFIRSTF,ILASTF)
        CALL RESET
        STOP DONE
900     CONTINUE
        TYPE "ERROR",IER,". CANNOT USE PARAMETERS ON .AL FILE"
        STOP ERROR
910     CONTINUE
        TYPE "ERROR",IER,". ON DATA FILE"
        STOP ERROR
920     TYPE "TASKING ERROR ",IER
        STOP ERROR
        END
```

Subroutine FMABILD:

```
      COMPILER NOSTACK
      SUBROUTINE FMABILD(JFMAP,IMAPF)
      DIMENSION JFMAP(300)
      DIMENSION JFMTAB(2,12),JFM2(300)
57,   DATA NFSEQ,JFMTAB/11,1,259,7,265,13,121,139,251,265,127,269,
     X          271,271,277,277,283,283,289,289,295,295,301,301/
      IF(IMAPF.NE.0) ACCEPT
PF    X "FINGER NUMBERS -- BY DETECTOR (0,STANDARD) OR BOARD (1)",IM
C     USE BOUNDARY SEQUENCING TABLE JFMTAB TO RETURN A
C     CHANNEL NUMBER->DETECTOR MAP.
C     TABLE IS FIRST CHANNEL OF CHAIN, FIRST DETECTOR OF CHAIN.
C     CHANNELS AND DETECTORS INCREMENT BY SIX, THEN TE BASE ADDRES
BS    OF THE CHANNELS INCREMENTS BY 6 WHILE THE BASE OF THE DETECT
NEL OF DECREMENTS BY 6. A NEW CHANNEL NUMBER EQUAL TO THE FIRST CHA
C     THE NEXT CHAIN TERMINATES THE SEQUENCE AT ANY TIME.
      DO 10 JFSEQ=1,NFSEQ
      JST=JFMTAB(1,JFSEQ)
      JTO=JFMTAB(2,JFSEQ)
      JEND=JFMTAB(1,JFSEQ+1)
11    DO 12 JFS2=1,6
      JFS3=JFS2-1
      IF(JST+JFS3.GE.JEND) GO TO 10
      JFM2(JST+JFS3)=JTO+JFS3
      IF(IMAPF.EQ.1) JFM2(JST+JFS3)=JST+JFS3
12    CONTINUE
      JST=JST+6
      JTO=JTO-6
      GO TO 11
10    CONTINUE
C     DETECTOR->OP-AMP TABLE COMPUTED. NOW INVERT IT
      DO 100 J=1,300
      JVAL=JFM2(J)
      JFMAP(JVAL)=J
100   CONTINUE
      RETURN
      END
```

Subroutine FINMOVE/U:

```
        .TITL FINMOVE
;       TWO FORTRAN ROUTINES TO REORDER A COLLECTED SET OF DATA
%GER)   INTO IB ACCORDING TO MAP JFMAP (A LIST OF INDICES FOR EACH F
%G      ENTRY FINMOVE MOVES INTO TEMPORARY BUFFER HBUF BEFORE SHUFFL
;       ENTRY FINM2 ASSUMES DATA IS ALREADY IN IBTEMP
        .NREL
        .ENT FINMOVE,FINM2
        .EXTD .CPYL,.FRET
IB=-167
JFMAP=IB+1
N=JFMAP+1
.FS=N+167+1
IBTEMP=N+1
.FS2=IBTEMP+167+1
        .FS
FINMOVE: JSR    @.CPYL
        ELEF    0,HBUF,0        ;STORE INDEX TO INTERNAL BUFFER
        STA     0,HBUFA
        MOV     3,2             ;STORE INDEX
        JSR     PCOPY
;FIRST MOVE THE DATA TO A TEMP BUFFER
        LDA     1,NWDS
        LDA     2,BUFAD
        ELEF    3,HBUF,0
        BLM
        JMP     FMAIN           ;CONTINUE TO MAIN BODY OF CODE
        .FS2
FINM2:  JSR     @.CPYL
        LDA     0,IBTEMP,3
        STA     0,HBUFA
        MOV     3,2
        JSR     PCOPY
;NOW MOVE THE INDEXED WORDS FROM THE BUFFER
FMAIN:  LDA     2,BUFAD
        STA     2,BPTR
        LDA     2,MAPAD
        STA     2,MPTR
        LDA     0,NWDS
        STA     0,NCNT
LOOP:   LDA     0,@MPTR
        LDA     3,HBUFA
        ADD     0,3
        SBI     1,3
        LDA     0,0,3
        STA     0,@BPTR
        ISZ     BPTR
        ISZ     MPTR
        DSZ     NCNT
        JMP     LOOP
        JSR     @.FRET
;
PCOPY:  LDA     0,IB,2
        STA     0,BUFAD
        LDA     0,JFMAP,2
        STA     0,MAPAD
        LDA     0,@N,2
        STA     0,NWDS
        JMP     0,3             ;RETURN
BUFAD:  0
BPTR:   0
MAPAD:  0
MPTR:   0
```

```
NWDS:   0
NCNT:   0
HBUFA:  0
HBUF:   .BLK 350.
        .END
```

Subroutine DWACQ:

```
        COMPILER NOSTACK
        SUBROUTINE DWACQ(IB,NTIMES,JFMAP)
        DOUBLE PRECISION DPWORD
        DIMENSION IB(600)
        DIMENSION IBTEMP(300),IWORD(4)
        COMMON/ACBUF/ICBUF(300)
C       ROUTINE TO ACQUIRE DATA IN DOUBLE WORD FORMAT INTO IB,
C       AND THEN CONVERT TO REAL IN PLACE
        TYPE NTIMES," VIEWS"
        CALL CLEAR(IB,600)
        CALL CLEAR(ICBUF,300)
        CALL ACQ(ICBUF,IDONE)
        IDONE=0
        DO 100 JTIME=1,NTIMES
        CALL ACQ(ICBUF,IDONE)
        IF(IDONE.NE.1) TYPE "MISSED VIEW, IDONE=",IDONE
        IDONE=0
        CALL FINM2(IBTEMP,JFMAP,300,ICBUF)
C90     IF(IDONE.NE.1) GO TO 90
        CALL SUMWD(IBTEMP,IB,300)
100     CONTINUE
        DO 200 JF=1,300
        JF2=JF+JF-1
        JF3=JF2+1
        CALL DWFL(IB(JF2),IWORD)
        IB(JF2)=IWORD(1)
        IB(JF3)=IWORD(2)
200     CONTINUE
        RETURN
        END
```

Subroutine BLMOVE:

```
        .TITL BLMOV
;       BLMOV BUFFER TO ZERO
        .ENT BLMOV
        .EXTD   .FRET,.CPYL
BUF=-167
BUF2=BUF+1
N=BUF2+1
.FS=N+167+1
        .NREL
        .FS
BLMOV:  JSR     @.CPYL
        LDA     1,@N,3          ;LOAD COUNT
        LDA     2,BUF,3         ;LOAD ADDRESS
        LDA     3,BUF2,3        ;ADR->3
        BLM                     ;MOVE THE ZERO
        JSR     @.FRET
        .END
```

Subroutine FILNAM:

See Appendix C.1.

Subroutine NOPEN:

```
SUBROUTINE NOPEN(INAME,ISUF,LUN,ISNO)
CALL NAMFAK(INAME,ISUF)
CALL OPEN(LUN,INAME,0,IER)
IF(IER.NE.1) RETURN ISNO
RETURN
END
```

Subroutine SPDISK:

```
        COMPILER NOSTACK
        TASK SPDISK
C       SPOOLING TASK FOR TSPOOL
C       TASK ID 2, PRIORITY 2
        COMMON/SPBUF/IFIRST,ILAST,NMAX,NVIEW,IMESS,IBUF(6400)
        TYPE "SPDISK TASK ACTIVATED"
        JBLOCK=0
100     CONTINUE
TION    CALL FDELY(1) IF BUFFER IS EMPTY -- REACTIVATED ON I/O COMPL
        IF(IFIRST.NE.ILAST) GO TO 110
        TYPE "LAST BLOCK=",JBLOCK
        CALL FDELY(1)
        GO TO 100
110     CONTINUE
C       SOME DATA IN BUFFER -- COMPUTE HOW MUCH
        IHIGH=IFIRST    ;HIGH END OF BUFFER
ROUND   IF(IFIRST.LT.ILAST) IHIGH=NMAX+1 ;UNLESS BUFFER HAS WRAPPED
        NSECT=(IHIGH-ILAST)/256          ;NUMBER OF SECTORS
        CALL WRBLK(5,JBLOCK,IBUF(ILAST),NSECT,IER)
        IF(IER.NE.1) GO TO 900
        ILAST=IHIGH
        IF(ILAST.GT.NMAX) ILAST=1
        JBLOCK=JBLOCK+NSECT
        GO TO 100
900     TYPE "<07>WRITE ERROR ",IER
        CALL EXIT
        END
```

Subroutine SPFILL:

```
      COMPILER NOSTACK
      TASK SPFILL
C     TASK TO COLLECT INTO CIRCULAR BUFFER IBUF
C     TASK 1, PRIORITY 1
      COMMON/ACBUF/ICBUF(300)
      COMMON/SPBUF/IFIRST,ILAST,NMAX,NVIEW,IMESS,IBUF(6400)
      COMMON/SPMAP/NFCOLL,JFMAP(300)
      TYPE "FILL COLLECTION TASK ENTERED"
      CALL TACQ(ICBUF,IDONE)  ;DUMMY
      DO 100 JVIEW=1,NVIEW
C     FIRST CHECK BUFFER NOT FULL
      IFIRST2=IFIRST+256
      IF(IFIRST2.GT.NMAX) IFIRST2=1
      IF(IFIRST2.EQ.ILAST) GO TO 900
C     OK, NOW COLLECT
      IDONE=0
      CALL TACQ(ICBUF,IDONE)
      IF(IDONE.NE.1) GO TO 910
      CALL FINM2(IBUF(IFIRST),JFMAP,256,ICBUF)
      IFIRST=IFIRST2
      CALL RELSE(2,IER)
      IF(IER.NE.1) TYPE "SPFILL RELSE TASK ERROR ",IER
100   CONTINUE
110   CONTINUE
      CALL FDELY(5)
      IF(IFIRST.NE.ILAST) GO TO 110
      TYPE "I/O DONE"
      IMVAL=1
      CALL XMT(IMESS,IMVAL,$920)
      CALL ABORT(2,IER)       ;KILL I/O TASK
      CALL KILL
900   TYPE "<07>BUFFER FULL ON VIEW ",JVIEW
      CALL EXIT
910   TYPE "<07>MISSED VIEW ",JVIEW,IDONE
      GO TO 100
920   TYPE "TRANSMIT ERROR ",IER
      END
```

Subroutine REBLOCK:

```
      SUBROUTINE REBLOCK(IFIRSTF,ILASTF)
      DIMENSION IUBUF(256)
      COMMON/SPBUF/IFIRST,ILAST,NMAX,NVIEW,IMESS,IBUF(6400)
      NMAX2=NMAX/2
      LENU=256
      NF=ILASTF-IFIRSTF+1
      LUNIN=5
      LUNOUT=1
      IREAD=1
      IWRITE=2
      INIT=0
      IFLUSH=-1
      CALL BLKIO(LUNIN,IBUF(1),NMAX2,IFIN,ILIN,JBIN,
     X           IUBUF,LENU,INIT)
      CALL BLKIO(LUNOUT,IBUF(NMAX2+1),NMAX2,IFOUT,ILOUT,JBOUT,
     X           IUBUF(IFIRSTF),NF,INIT)
      DO 200 JVIEW=1,NVIEW
      CALL BLKIO(LUNIN,IBUF(1),NMAX2,IFIN,ILIN,JBIN,
     X           IUBUF,LENU,IREAD)
      CALL BLKIO(LUNOUT,IBUF(NMAX2+1),NMAX2,IFOUT,ILOUT,JBOUT,
     X           IUBUF(IFIRSTF),NF,IWRITE)
200   CONTINUE
      CALL BLKIO(LUNOUT,IBUF(NMAX2+1),NMAX2,IFOUT,ILOUT,JBOUT,
     X           IUBUF(IFIRST),NF,IFLUSH)
      RETURN
      END
```

Subroutine BLKIO:

```
      SUBROUTINE BLKIO(LUN,IOBUF,LEN,IFIRST,ILAST,JBLOCK,
     X           IUBUF,LENU,IACT)
      DIMENSION IOBUF(LEN),IUBUF(LENU)
C     SUBROUTINE TO DO BLOCK TRANSFER I/O AS A REPLACEMENT FOR
C     BINARY READ/WRITE
C
C     CODES--
C     IACT=-1          FLUSH OUTPUT BUFFER
C     IACT=0           INITIALIZE POINTERS (SHOULD BE FIRST CALL)
C     IACT=1           READ FROM CURRENT FILE POSITION TO IUBUF
C     IACT=2           WRITE "     "
C
C     SCRATCH BUFFER IOBUF IS USED TO HOLD BLOCKS FOR RDBLK/WRBLK
C
      IF(IACT.NE.-1) GO TO 200
C     FLUSH OUTPUT BUFFER
      IF(ILAST.LE.1) GO TO 100
      NBLK=1+(ILAST-2)/256
      CALL WRBLK(LUN,JBLOCK,IOBUF,NBLK,IER)
      CALL IERCH(IER,"ON BLOCK FLUSH")
      JBLOCK=JBLOCK+NBLK
100   ILAST=1
      RETURN
200   IF(IACT.NE.0) GO TO 300
C     INITIALIZE
      ILAST=1
      IFIRST=1
      JBLOCK=0
      RETURN
300   IF(IACT.NE.1) GO TO 400
C     READ
      JSTART=1
      JLEFT=LENU
C     COMPUTE AVAILABLE WORDS IN BUFFER
310   IF(IFIRST.LT.ILAST) GO TO 320
C     NONE, MUST READ SOME IN
      NBLK=LEN/256
      IF(NBLK.LE.0) GO TO 910
      CALL RDBLK(LUN,JBLOCK,IOBUF,NBLK,IER,IBLK)
      IF(IER.EQ.9) NBLK=IBLK
      IF(IER.NE.9)CALL IERCH(IER,"ON BLOCK READ")
      IF(IER.EQ.9.AND.IBLK.EQ.0) GO TO 920
      JBLOCK=JBLOCK+NBLK
      ILAST=NBLK*256+1
      IFIRST=1
320   NAVAIL=ILAST-IFIRST
      NTRAN=MINO(NAVAIL,JLEFT)
      CALL BLMOVE(IOBUF(IFIRST),IUBUF(JSTART),NTRAN)
      JSTART=JSTART+NTRAN
      IFIRST=IFIRST+NTRAN
      JLEFT=JLEFT-NTRAN
      IF(JLEFT.NE.0) GO TO 310
      RETURN
400   IF(IACT.NE.2) GO TO 900
C     WRITE BUFFER
      JSTART=1
      JLEFT=LENU
C     COMPUTE AVAILABLE SPACE TO FILL
      NBLK=LEN/256
      LEN2=256*NBLK
410   NAVAIL=LEN2+1-ILAST
      IF(NAVAIL.GT.0) GO TO 420
```

```
C       WRITE OUT BUFFER
        CALL WRBLK(LUN,JBLOCK,IOBUF,NBLK,IER)
        CALL IERCH(IER,"ON BLOCK WRITE")
        JBLOCK=JBLOCK+NBLK
        ILAST=1
420     NTRAN=MIN0(NAVAIL,JLEFT)
        CALL BLMOVE(IUBUF(JSTART),IOBUF(ILAST),NTRAN)
        JSTART=JSTART+NTRAN
        ILAST=ILAST+NTRAN
        JLEFT=JLEFT-NTRAN
        IF(JLEFT.GT.0) GO TO 410
        RETURN
900     STOP BAD BLKIO ACTION CODE
910     STOP BAD BLOCK SIZE COMPUTED
920     STOP ATTEMPT TO READ PAST END OF FILE
        END
```

Subroutine IERCH:

```
      SUBROUTINE IERCH(IER,ISTR)
      DIMENSION ISTR(10)
      IF(IER.NE.1) WRITE(10,1001) IER,ISTR(1)
1001  FORMAT(" I/O ERROR ",I3,1X,S40)
      RETURN
      END
```

Subroutine CLEAR:

See Appendix C.1.

Subroutine NAMMAK:

See Appendix C.1.

Subroutine FACC:

See Appendix C.1.

Subroutine SUMWD:

```
        .TITL SUMWD
;ADD N WORDS FROM SINGLE PRECISION IB1 TO DOUBLE PRECISION IB2
        .NREL
        .EXTD   .FRET,.CPYL
        .ENT    SUMWD
IB1=-167
IB2=IB1+1
NWD=IB2+1
.FS=NWD+167+1
        .FS
SUMWD:  JSR     @.CPYL
        LDA     0,@NWD,3
        STA     0,NFING
        LDA     2,IB1,3
        LDA     3,IB2,3
LOOP:   LDA     1,1,3
        LDA     0,0,2
        ADDZ    0,1,SZC
        ISZ     0,3
        JMP     .+1
        STA     1,1,3
        INC     2,2
        ADI     2,3
        DSZ     NFING
        JMP     LOOP
            ;RESTORE STACK PTR
        LDA     1,BUFAD,3
        .SYSTM
        .STMAP                  ;SET HARDWARE MAP
        JMP     ERCALL
        STA     1,MAPBUF        ;STORE MAPPED ADR
        LDA     3,HOLD3         ;RESTORE POINTER
        LDA     1,IDONE,3       ;LOAD ADDRESS OF DONE FLAG
        STA     1,ACINT         ;STORE MESSAGE ADDRESS
        LDA     0,@ACINT        ;LOAD OLD CONTENTS
        STA     0,NINT          ;TO BE INCREMENTED
        SKPBZ   AQDEV
        JMP     DTEST
        JSR     ACCALL
        NIOS    AQDEV
DTEST:  LDA     0,ACINT ;LOAD DONE FLAG ADDR
        .REC
        STA     1,@ACINT        ;STORE RESULT
        JSR     @.FRET
NBLK:   2               ;RESERVE 2 (1?) BLOCKS
ACCALL: SUB     0,0             ;ZERO
        STA     0,@ACINT
        SKPBZ   AQDEV
        JMP     0,3
        LDA     0,MAPBUF
        DOAP    0,AQDEV
        LDA     0,WDCNT
        DOB     0,AQDEV
        JMP     0,3
ISERV:  STA     3,IACST
        JSR     ACCALL
        ISZ     NINT
        JMP     .+2
        ISZ     NINT    ;SKIP OVER ZERO AS COUNT
        LDA     0,ACINT ;LOAD MES ADR
        LDA     1,NINT
        .IXMT
```

```
        JMP     .+1
        SUBZL   1,1     ;ENSURE RESCHEDULING
        NIOS    AQDEV
        LDA     3,IACST         ;RESTORE AC3
        .UIEX
ERCALL: .SYSTM
        .ERTN
AQDEV=25
IACST:  0
HOLD3:  0
DEVADR: AQDEV
DCTAD:  .+1+100000
        0               ;RTOS
        10              ;MASK
        ISERV           ;SERVICE ROUTINE
SETUP:  0               ;FLAG INDICATING SERVICE SET UP
MAPBUF: 0               ;MAPPED BUF LOCN
WDCNT:  -276.
D1:     2.
ACINT:  0
ACHOLD: 0
NINT:   0
        .END
```

Subroutine TACQ/U:

```
        .TITL   TACQ
        .EXTD   .CPYL,.FRET
        .EXTN   .UIEX,.IXMT,.REC
        .ENT    TACQ,ACQ,MTRON,MTROF
        .NREL
        2
MTRON:  JSR     @.CPYL
        JSR     @.FRET
        2
MTROF:  JSR     @.CPYL
        NIOC    AQDEV
        JSR     @.FRET
BUFAD=-167
IDONE=BUFAD+1
FS.=IDONE+167+1
        .NREL
        FS.
TACQ:
ACQ:    JSR     @.CPYL
        STA     3,HOLD3
        LDA     0,SETUP
        MOV#    0,0,SZR
        JMP     NOSET
        SUBZL   0,0
        STA     0,SETUP         ;RESET FLAG
        LDA     0,DEVADR
        LDA     1,DCTADR
        LDA     2,NBLK          ;NUMBER OF BLOCKS IN 2
        .SYSTM
        .IDEF
        JMP     ERCALL
NOSET:  LDA     0,DEVADR
        LDA     3,HOLD3         ;RESTORE STACK PTR
        LDA     1,BUFAD,3
        .SYSTM
        .STMAP                  ;SET HARDWARE MAP
        JMP     ERCALL
        STA     1,MAPBUF        ;STORE MAPPED ADR
        LDA     3,HOLD3         ;RESTORE POINTER
        LDA     1,IDONE,3       ;LOAD ADDRESS OF DONE FLAG
        STA     1,ACINT         ;STORE MESSAGE ADDRESS
        LDA     0,@ACINT        ;LOAD OLD CONTENTS
        STA     0,NINT          ;TO BE INCREMENTED
        SKPBZ   AQDEV
        JMP     DTEST
        JSR     ACCALL
        NIOS    AQDEV
DTEST:  LDA     0,ACINT ;LOAD DONE FLAG ADDR
        .REC
        STA     1,@ACINT        ;STORE RESULT
        JSR     @.FRET
NBLK:   2               ;RESERVE 2 (1?) BLOCKS
ACCALL: SUB     0,0             ;ZERO
        STA     0,@ACINT
        SKPBZ   AQDEV
        JMP     0,3
        LDA     0,MAPBUF
        DOAP    0,AQDEV
        LDA     0,WDCNT
        DOB     0,AQDEV
        JMP     0,3
ISERV:  STA     3,IACST
```

```
        JSR     ACCALL
        ISZ     NINT
        JMP     .+2
        ISZ     NINT    ;SKIP OVER ZERO AS COUNT
        LDA     0,ACINT ;LOAD MES ADR
        LDA     1,NINT
        .IXMT
        JMP     .+1
        SUBZL   1,1     ;ENSURE RESCHEDULING
        NIOS    AQDEV
        LDA     3,IACST         ;RESTORE AC3
        .UIEX
ERCALL: .SYSTM
        .ERTN
AQDEV=25
IACST:  0
HOLD3:  0
DEVADR: AQDEV
DCTAD:  .+1+100000
        0               ;RTOS
        10              ;MASK
        ISERV           ;SERVICE ROUTINE
SETUP:  0               ;FLAG INDICATING SERVICE SET UP
MAPBUF: 0               ;MAPPED BUF LOCN
WDCNT:  -276.
D1:     2.
ACINT:  0
ACHOLD: 0
NINT:   0
        .END
```

Appendix C.3 Listing of the Data Cleanup and Preprocessing Programs - TCNORMAL

Purpose

This set of programs reads in the data from the data files and then computes the ratio I/IO. The data is correct for bad detector measurements and takes the natural log of the data.

Program Name	Function
Main Program:	
TCNORMAL	- to coordinate the raw experimental data preprocessing.
Subprograms:	
CLEAR	- to clear a buffer to zero.
FLODCMP	- to compress the flood measurement data.
NAMMAK	- to create a new ASCII name.
TCFACC	- to check the name format.
FILNAM	- to open a new name file.
FORT.LB	- FORTRAN IV mathematics library.

Main Program TCNORMAL:

```
C          ::::::  TCNORMAL  ::::::

C THIS PROGRAM READS IN THE DATA FROM THE DATA FILES AND
C THEN COMPUTES THE RATIO I/IO.  THE DATA IS CORRECTED FOR
C DETECTOR NONLINEARITIES AND BEAM HARDENING AND THEN THE
C LOG OF THE CORRECTED DATA IS THEN TAKEN.
C PROGRAM TO NORMALIZE INPUT DATA AND OUTPUT STANDARD FILE -.IN

        DIMENSION IFLOOD(256),FLOOD(256),DARK(256)
        DIMENSION BUF(256),IBUF(256),IDBUF(256),IFNAME(20)
        DIMENSION IBADFIN(256),IBADVIEW(360)
        DIMENSION XBUF(256)
1102    FORMAT(5E13.4)
        CLKMIN=15000.

C CLEAR THE BUFFER IBADFIN BEFORE READING IN THE NAME
C OF THE BAD FINGERS.
        CALL CLEAR(IBADFIN,256)

C INPUT THE SCAN DATA FROM TOMO.TC
        CALL TCFACC("TYPE OUT OF RANGE",ITYPE,"I")
        CALL TCFACC("ELIMINATE NEGATIVES",IOTYPE,"I")
        CALL TCFACC("USE REFERENCE",IUSEREF,"I")
        CALL TCFACC("USE HARDENING",IHARD,"I")
        CALL TCFACC("USE K-EDGE",IKEDGE,"I")
        CALL TCFACC("CLOCK OVERFLOW LEVEL",CLKADD,"F")

C INSERT THE VALUES OF THE BAD DETECTORS:
        TYPE "ENTER BAD FINGER NUMBERS, ZERO TO END LIST"
20      CONTINUE
        ACCEPT "BAD FINGER-- ",IBAD
        IF(IBAD.EQ.0) GO TO 30
        IBADFIN(IBAD)=1
        GO TO 20
C WRITE THE BADFINGER LIST TO DISK
30      CALL FILNAM(IFNAME)
        CALL NAMMAK(IFNAME,"BF")
        CALL FOPEN(1,IFNAME)
        WRITE BINARY(1) IBADFIN
        CALL FCLOS(1)

C INSERT THE VALUES OF THE BAD VIEWS:
        CONTINUE
        CALL CLEAR(IBADVIEW,360)
        TYPE "ENTER BAD VIEWS, ZERO TO STOP"
35      CONTINUE
        ACCEPT "BAD VIEW--",IBAD
        IF(IBAD.EQ.0) GO TO 37
        IBADVIEW(IBAD)=1
        GO TO 35

37      CONTINUE
C READ IN THE VALUES OF THE SCAN PARAMETERS FROM THE .AL FILE
        CALL FILNAM(IFNAME)
        CALL NAMMAK(IFNAME,"AL")
        CALL FOPEN(1,IFNAME,512)
        CALL ROBLK(1,1,IBUF,1,IER)
        IF(IER.NE.1) GO TO 900
        TYPE "PARAMETERS ARE ",(IBUF(J),J=1,10)

C FIRST FINGER IS NUMBER:
        IFIRST=IBUF(8)
```

```
C NUMBER OF FINGERS ARE:
        NF=IBUF(9)

C NUMBER OF VIEWS PER BUFFER
        NVIEW=IBUF(10)

C WHAT IS NFETH?
        NFETH=IBUF(3)

C REFERENCE FINGER IS NUMBER:
        NREF=IBUF(4)

C PULSE ENCODER LONG ON CHANNEL NCLOCK+2, PULSE ENCODER SHORT
C ON CHANNEL NCLOCK+4.

C CLOCK FINGER IS NUMBER:
        NCLOCK=IBUF(5)

C CHOOSE WHETHER OR NOT TO USE REFERENCE FINGER.
C THIS IS DONE INDIRECTLY BY HAVING NCLOCK BE POSITIVE
C (NO REFERENCE) OR NEGATIVE(REFERENCE USED).
        IDARKTYPE=NCLOCK
        NCLOCK=IABS(NCLOCK)
        IF(IDARKTYPE.LT.0) TYPE "FIVE SECOND DARK CURRENT"
        IF(IDARKTYPE.GT.0) TYPE "SHORT DARK CURRENT"

C THE FOLLOWING STATEMENTS ARE HERE TO ASSURE THAT WE DONT
C ACCIDENTALLY DESTROY THE DATA ON THE FIRST ELECTRONICS BOARD.
        IBADFIN(NCLOCK)=1          ;1-CLOCK FINGER
        IBADFIN(NCLOCK+1)=1        ;2-DIAGNOSTIC
        IBADFIN(NCLOCK+2)=1        ;3-PULSE ENCODER LONG
        IBADFIN(NCLOCK+3)=1        ;4-CLOCK OVERFLOW
        IBADFIN(NCLOCK+4)=1        ;5-PULSE ENCODER SHORT
        IBADFIN(NCLOCK+5)=1        ;6-FILTER NUMBER
        IBADFIN(NCLOCK+6)=1        ;7-FILTER TYPE(FE=1,TA=2)

C NUMBER OF BUFFERS USED IN THE SCAN.
        NBUF=IBUF(7)

C FIGURE NUMBER OF VALID FINGERS AND VIEWS, AND WRITE TO FILE
C THIS MAY BE THE PLACE WHERE ONLY A SYMMETRIC AMOUNT OF DATA
C IS SELECTED TO BE USED IN THE RECONSTRUCTION PROGRAM.
C STUDY THE FOLLOWING STATEMENTS AND SEE IF THIS IS TRUE.

C DETERMINE THE CENTER FINGER NUMBER
        CALL TCFACC( "CENTER+.75",NCENT,"I")

C WIDTH OF THE DETECTOR DATA FIELD TO BE USED IN THE RE-
C CONSTRUCTION?
        CALL TCFACC("MAXIMUM WIDTH OF DATA",MAXWID,"I")

C NUMBER OF FINGERS LEFT OF CENTER:
        NLEFT=NCENT-IFIRST

C NUMBER OF FINGERS RIGHT OF CENTER:
        NRIGHT=IFIRST+NF-NCENT

C NUMBER OF SAMPLES=MINIMUM OF (NLEFT,NRIGHT)*2
        NSAMP=MINO(NLEFT,NRIGHT)*2
C CHOOSE THE SMALLER OF MAX DATA WIDTH AND NSAMPLES:
        NSAMP=MINO(NSAMP,MAXWID)

C NOW THAT WE KNOW THAT THE DATA IS SYMMETRIC DETERIMINE
C THE VALUES OF THE LEFT AND RIGHT FINGER NUMBERS.
        ILEFT=NCENT-NSAMP/2
```

```
        IRIGHT=ILEFT+NSAMP-1
        TYPE "USING LEFT,RIGHT OF ",ILEFT,IRIGHT

C MAKE SURE THAT THE REFERENCE FINGER IS LOCATED WITHIN THE
C DATA SET THAT IS VALID?
        ILEFT1=MINO(NREF,ILEFT)
        IRIT1=MAXO(IRIGHT,NREF)

C COMPUTE THE TOTAL NUMBER OF VIEWS TAKEN IN THE SCAN
        NTVIEW=NBUF*NVIEW

C INSERT THE VALUES OF THE TOTAL NUMBER OF VIEWS AND
C THE WIDTH OF THE VALID DATA SET INTO THE BUFFER.
        IBUF(1)=NSAMP
        IBUF(2)=NTVIEW
C COMPUTE THE NUMBER OF WORDS IN THE BLOCK OF PROJECTION
C DATA WHICH IS PROCESSED
        NWDS=NF*NVIEW

C WRITE THE PARAMETERS OF THE SCAN INTO CHANNEL 1
        CALL WRBLK(1,1,IBUF,1,IER)
        IF(IER.NE.1) GO TO 900
        CALL FCLOS(1)
C READ IN THE DATA FILE NAMES:
1101    FORMAT(S20)
        TYPE"ENTER THE PROJECTION DATA FILENAME"
        READ(11,1101)IFNAME(1)
        CALL FOPEN(1,IFNAME)
        ACCEPT"DETECTOR HV DURING THE PROJECTION WAS=",HVPROJ
        TYPE"ENTER THE FLOOD DATA FILENAME"
        READ(11,1101) IFNAME(1)
        CALL FOPEN(2,IFNAME)
        ACCEPT"DETECTOR HV DURING THE FLOOD WAS=",HVFLOD
        TYPE"ENTER THE DARK DATA FILENAME"
        READ(11,1101) IFNAME(1)
        CALL FOPEN(3,IFNAME)
        ACCEPT"DETECTOR HV DURING THE DARK WAS=",HVDARK
C OPEN UP THE COMPRESSED FLOOD DATA FILE:
        CALL FOPEN(4,"FCOMP")
C CLEAR THE DATA ARRAYS BEFORE READING IN THE DATA:
        CALL CLEAR(FLOOD,512)
        CALL CLEAR(DARK,512)
        CALL CLEAR(IFLOOD,256)
        CALL CLEAR(XBUF,512)
        CALL CLEAR(BUF,512)
C READ IN THE DARK CURRENT DATA:
        READ BINARY(3) DARK
C CORRECT FOR FLOATING POINT CLOCK OVERFLOWS
        DARK(NCLOCK)=DARK(NCLOCK)+65536.*DARK(NCLOCK+3)
        TYPE"DARK CLOCK=",DARK(NCLOCK)
C CALL THE FLOOD-DATA COMPRESSION SUBPROGRAM:
        CALL FLODCMP(NCLOCK,NF,NTVIEW,IFIRST,HVFLOD)
        REWIND 4
C CLOSE THE RAW FLOOD DATA FILE:
        CALL FCLOS(2)
C CLOSE THE DARK DATA FILE
        CALL FCLOS(3)
C ***NOTE THAT AT THIS POINT BOTH THE DARK AND FLOOD DATA SHOULD
C BE IN 'ABSOLUTE NUMBERING SPACE'.
C OPEN UP THE TCNORMAL OUTPUT FILE
        CALL FILNAM(IFNAME)
        CALL NAMMAK(IFNAME,"IN")
        CALL FOPEN(2,IFNAME)
        TYPE"BEFORE PROJECTION I/O"
C NOW READ IN THE PROJECTION DATA:
        JFIL=1
```

```
        REWIND 1
        DO 200 JVIEW=1,NTVIEW
        TYPE"VIEW#",JVIEW
        TYPE"NF=",NF
        TYPE"IFIRST=",IFIRST
        READ BINARY(1) (IDBUF(KDET),KDET=1,NF)
        IF(IBADVIEW(JVIEW).NE.0) GOTO 190
C TRANSLATE THE DATA INTO 'ABSOLUTE' DETECTOR # SPACE
        DO 145 JF=1,NF
        BUF(JF+IFIRST-1)=IDBUF(JF)
C TEST FOR OVERFLOWS AND ZEROS
        IF(IDBUF(JF)) 80,90,90
C NEGATIVE: IMPLIES OVERFLOW
80      BUF(JF+IFIRST-1)=BUF(JF+IFIRST-1)+65536.
        GOTO 100
90      CONTINUE
C CORRECT FOR DETECTOR HV:
        IF(21-JF) 100,95,95
95      BUF(JF+IFIRST-1)=BUF(JF+IFIRST-1)*(1.0+(2500.0-HVPROJ)*
     X    3.54523E-5)
        DARK(JF+IFIRST-1)=DARK(JF+IFIRST-1)*(1.0+(2500.0-HVDARK)*
     X    3.54523E-5)
100     CONTINUE
145     CONTINUE
C ADD 16 BIT OVERFLOW TO THE CLOCK VALUE
        BUF(NCLOCK)=BUF(NCLOCK)+BUF(NCLOCK+3)*65536.
        REWIND 4
147     READ BINARY(4) FLOOD
        IFILTE=FLOOD(NCLOCK+5)
        IF(IFILTE-JFIL) 147,148,147
148     CONTINUE
        TYPE"IFILTE=",IFILTE
C WRITE THE FILE SPECIFIERS ONTO XBUF:
        DO 149 JXFER=0,4
149     XBUF(NCLOCK+JXFER)=BUF(NCLOCK+JXFER)
        XBUF(NCLOCK+5)=JFIL
        XBUF(NCLOCK+6)=AINT((AINT(JFIL/2.)/(JFIL/2.)))+1.
C NOW TAKE THE RATIO I/IO FOR EACH DETECTOR.
C FIND OUT IF WE USE A REFERENCE DETECTOR OR NOT:
        IF(IUSEREF) 155,155,150
C USE A REFERENCE DETECTOR
150     CONTINUE
C COMPUTE REFERENCE CURRENT DURING THE PROJECTION MEASUREMENT:
        CPREF=(BUF(NREF)/BUF(NCLOCK)-DARK(NREF)/DARK(NCLOCK))
C COMPUTE REFERENCE CURRENT DURING THE FLOOD MEASUREMENT:
        CFREF=(FLOOD(NREF)/FLOOD(NCLOCK)-DARK(NREF)/DARK(NCLOCK))
        GOTO 160
C DON'T USE THE REFERENCE: DUMMY CPREF AND CFREF
155     CPREF=1
        CFREF=1
160     CONTINUE
C ENTER THE RATIO CALCULATION DO LOOP:
        DO 170 JF=ILEFT1,IRIT1
C CHECK FOR A BAD FINGER
        IF(IBADFIN(JF).NE.0) GOTO 170
        XBUF(JF)=((((BUF(JF)/BUF(NCLOCK))-(DARK(JF)/DARK(NCLOCK)))
     X    /CPREF)/
     X    (((FLOOD(JF)/FLOOD(NCLOCK))-(DARK(JF)/DARK(NCLOCK)))
     X    /CFREF))
C TAKE THE NEGATIVE OF THE NATURAL LOG TO OBTAIN THE PROJECTION
C VALUE:
        XBUF(JF)=(-1.0)*ALOG(XBUF(JF))
C CHECK FOR NEGATIVE PROJECTION VALUES (FLOOD VALUE WAS LESS THAN
C THE PROJECTION: WHICH MAY IMPLY A DISCHARGE)
        IF(XBUF(JF)) 165,165,170
165     XBUF(JF)=0
```

```
170     CONTINUE
C LINEARLY INTERPOLATE ANY BAD FINGERS IN THE TCTRANSL1 PROGRAM
C INCREMENT THE FILTER NUMBER
        JFIL=JFIL+1
C CHECK FOR FILTER 'OVERFLOWS'
        IF(JFIL-12) 185,185,180
180     JFIL=1
185     CONTINUE
190     CONTINUE
C NOW WRITE THE DATA TO DISK
        IF(IBADVIEW(JVIEW).NE.0) STOP BAD VIEW
        WRITE BINARY(2) (XBUF(JOUTPT),JOUTPT=1,256)
        TYPE"VIEW ",JVIEW," OUTPUT"
        IF(JVIEW.LE.1) WRITE(10,1102) (XBUF(JOUTPT),JOUTPT=1,256)
200     CONTINUE
        CALL RESET
        STOP TCNORMAL DONE
900     TYPE"FORTRAN I/O ERROR",IER
        STOP ERROR
        END
```

Subroutine CLEAR:

See Appendix C.1.

Subroutine FLODCMP:

```
      SUBROUTINE FLODCMP(NCLOCK,NF,NTVIEW,IFIRST,HVFLOD)
C     PURPOSE
C     TO COMPRESS THE FLOOD DATA FROM THE TOMOCHEMISTRY EXPERIMENT
C     INTO ONE FLOOD READING FOR EACH FILTER:
      DIMENSION IFLOOD(256),FLOOD(256,12)
      CALL CLEAR(FLOOD,6144)
      CALL CLEAR(IFLOOD,256)
      TYPE"ENTERING THE FLOOD COMPRESSION SUBROUTINE"
C     READ IN THE FLOOD DATA FROM THE DISK:
      REWIND 2
      REWIND 4
      JFIL=1
      DO 200 JCOMPR=1,NTVIEW
      TYPE"VIEW #:",JCOMPR
      READ BINARY(2) (IFLOOD(KFIN),KFIN=1,NF)
      DO 90 KFIN=1,NF
C     DETERMINE THE CORRECTION FACTOR:
      IF(KFIN-20) 75,75,85
75    CORRECT=1.0
      GOTO 87
85    CORRECT=(1.0+(2500.-HVFLOD)*3.54523E-5)
87    CONTINUE
C     TEST FOR OVERFLOWS
C     PUT THE FLOOD DATA INTO 'ABSOLUTE' DETECTOR # POSITIONS
      FLOOD(KFIN+IFIRST-1,JFIL)=IFLOOD(KFIN)*CORRECT+
     X FLOOD(KFIN+IFIRST-1,JFIL)
      IF(IFLOOD(KFIN)) 80,90,90
80    FLOOD(KFIN+IFIRST-1,JFIL)=FLOOD(KFIN+IFIRST-1,JFIL)+
     X 65536.*CORRECT
90    CONTINUE
C     CORRECT FOR 16 BIT OVERFLOW OF THE CLOCK
      FLOOD(NCLOCK,JFIL)=FLOOD(NCLOCK,JFIL)+
     X IFLOOD(4)*65536.
C     SET UP THE FILTER SPECIFIERS IN THE COMPRESSED FILE:
      FLOOD(NCLOCK+5,JFIL)=JFIL
      FLOOD(NCLOCK+6,JFIL)=AINT((AINT(JFIL/2.)/
     X (JFIL/2.)))+1.
C     INCREMENT THE FILTER COUNT
      JFIL=JFIL+1
C     CHECK FOR OVERFLOW
      IF(JFIL-12) 200,200,100
100   JFIL=1
200   CONTINUE
C     COMPRESSION COMPLETED:WRITE TO DISK
C1102 FORMAT(5E13.4)
C     TYPE"FLOOD FILE::::::::::::::::::::::::::::::::::<12>"
C     WRITE(10,1102) FLOOD
      WRITE BINARY(4) FLOOD
      TYPE"FLOOD COMPRESSION COMPLETED"
      RETURN
      END
```

Subroutine NAMMAK:

See Appendix C.1.

Subroutine TCFACC:

See Appendix C.1.

Subroutine FILNAM:

See Appendix C.1.

Appendix C.4 Listing of the Data Mapping and Tomochemistry Data Processing Programs - TCTRANSL1

Purpose

This set of programs takes the preprocessed line integral data and performs the required interpolations and data mapping to obtain the tomochemistry data sets for reconstruction. This set of programs is unique to tomochemistry.

Program Name	Function
Main Program:	
TCTRANSL1	- to coordinate the mapping of the 'raw' tantalum filter and iron filter data into Compton and photoelectric + Rayleigh line integral space.
Subprograms:	
MAPDATA	- to map the data from $\ell n(I_{oS}/I_S)$, $\ell n(I_{oH}/I_H)$ space to $\int \mu_C d\ell$, $\int \mu_{P+R} d\ell$ space.
CLEAR	- to clear a buffer to zero.
FILNAM	- to open a new name file.
NAMMAK	- to create a new ASCII name.
VWPAR	- to determine the view parameters of the experiment such as the number of views in 360 degrees.
PINTRPDAT	- to get the data required for the subroutine PREINTERP.
PREINTERP	- to preinterpolate the views before entering the even-view subroutine.
DATARA	- to setup the data array "ATRIX" from which the interpolations are performed.
TRNSLT	- to translate measurements from hard and soft spectra space to Compton and photoelectric line integral space.
TCINTERP	- to perform a weighted interpolation of the data points between filters.
TCENDINT	- to perform a weighted interpolation of the end-views.

EVENVW	- to create a set of even-view data.
EVENDAT	- to obtain the scan data required for EVENVW.
EVENTVW	- to create a file of NTVIEWS starting with a file containing NEVVWS.
TCFCORR	- to correct for bad data from bad detectors.

Main Program TCTRANSL1:

```
C TCTRANSL1
C
C PURPOSE
C TO TRANSLATE DATA FROM "RAW" DATA TO PHOTOELECTRIC AND COMPTON
C LINE INTEGRAL DATA.
C CALL THE FILENAME
        DIMENSION LINE(256),IFNAME(20),
     X  MAPRIX(256,-1:1),MACRIX(256,-1:1),SAV(-1:1),ALAV(-1:1)
     X  ,MATEMP(256),IBADFIN(256)
C READ IN THE BADFINGER NUMBERS
        CALL FILNAM(IFNAME)
        CALL NAMMAK(IFNAME,"BF")
        CALL FOPEN(1,IFNAME)
        READ BINARY(1) IBADFIN
        CALL FCLOS(1)
C OPEN THE PARAMETER FILE AND OBTAIN THE REQUIRED PARAMETERS
        CALL NAMMAK(IFNAME,"AL")
        CALL FOPEN(5,IFNAME,512)
        CALL RDBLK(5,1,LINE,1,IER)
        IF(IER.NE.1) GOTO 900
        NSAMP=LINE(1)
        NTVIEW=LINE(2)
        NCLOCK=LINE(5)
        NCLOCK=IABS(NCLOCK)
        IFIRST=LINE(8)
        NF=LINE(9)
        CALL FCLOS(5)
C OPEN THE SCAN DATA FILE
        CALL NAMMAK(IFNAME,"IN")
        CALL FOPEN(1,IFNAME,512)
C DETERMINE THE EXPERIMENTS VIEW PARAMETERS. IE THE NUMBER OF VIEWS
C IN 360 DEGREES.
        TYPE"ENTERING VWPAR"
        CALL VWPAR(N360VW,NTVIEW,ITYPEL,NCLOCK,FANGOVFL,
     X  IFTYPE)
        TYPE"JUST LEFT VWPAR"
C OPEN THE INTERMEDIATE FILTER INTERPOLATION FILES
C ** IRON ** AND ** TANTALUM **
        CALL NAMMAK(IFNAME,"PE")
        CALL FOPEN(2,IFNAME)
        CALL NAMMAK(IFNAME,"CO")
        CALL FOPEN(5,IFNAME)
C OPEN THE PHOTOELECTRIC FIT FILE:
        CALL FOPEN(3,"PFIT7V")
C OPEN THE COMPTON POLYNOMIAL FIT FILE:
        CALL FOPEN(4,"CFIT7V")
C ** START DO START DO START DO START DO **
        REWIND 2
        REWIND 5
        REWIND 1
        TYPE"ENTERING THE VIEW MAPPING ROUTINE"
        DO 100 IVIEW=1,N360VW
        TYPE"MAPPING VIEW #",IVIEW
C  NOW MAP THE DATA TO PHOTOELECTRIC AND COMPTON LINE INTEGRAL
C  SPACE.
        CALL MAPDATA(IVIEW,N360VW,ITYPEL,NCLOCK,IFTYPE,
     X    FANGOVFL,IBADFIN)
100     CONTINUE
        CALL FCLOS(1)
        CALL NAMMAK(IFNAME,"IN")
        CALL DELETE(IFNAME)
C CLOSE THE POLYNOMIAL COEFFICIENTS FILES.
```

```
        CALL FCLOS(3)
        CALL FCLOS(4)
C OPEN THE INTERMEDIATE DESTINATION FILES.
        CALL NAMMAK(IFNAME,"P")
        CALL FOPEN(3,IFNAME)
        CALL NAMMAK(IFNAME,"C")
        CALL FOPEN(4,IFNAME)
C NOW PREINTERPOLATE THE MAPPED DATA(PHOTOELECTRIC AND COMPTON)
C BEFORE CREATING AN EVENVW DATA SET.
        TYPE"ENTERING THE PREINTERPOLATE ROUTINE"
        DO 200 IVIEW=1,N360VW
        TYPE"PREINTERPOLATING VIEW #",IVIEW
C FIRST GET THE DATA
        CALL PINTRPDAT(MAPRIX,MACRIX,SAV,ALAV,IVIEW,NCLOCK,N360VW)
C NOW PREINTERPOLATE THE PHOTOELECTRIC DATA:
        CALL PREINTERP(MAPRIX,SAV,ALAV,NCLOCK,MATEMP)
C WRITE THE RESULT TO DISK (INSERT IN THE .P FILE):
        REWIND 3
        REWIND 4
        CALL WRBLK(3,IVIEW,MATEMP,1,IER)
        IF(IER.NE.1) GOTO 900
C NOW PREINTERPOLATE THE COMPTON DATA:
        CALL PREINTERP(MACRIX,SAV,ALAV,NCLOCK,MATEMP)
C NOW WRITE THE RESULT TO DISK(INSERT IN THE .C FILE)
        CALL WRBLK(4,IVIEW,MATEMP,1,IER)
        IF(IER.NE.1) GOTO 900
C FINISHED WITH THIS VIEW THEREFORE:
200     CONTINUE
C NOW CONTINUE ON TO THE EVEN-VIEW ROUTINE:
C NOTE THAT WHEN ONE LOOKS AT THE LOGIC OF PRODUCING EVEN VIEWS
C WE SEE THAT WE CAN ONLY PRODUCE A DATA SET WITH(N360VW-1) VIEWS.
        NEVVW=N360VW-1
        BEGA=0
        ENDA=0
        EVBEGA=0
        EVENDA=0
        TYPE"ENTERING THE EVEN VIEW ROUTINE"
        DO 300 IVIEW=1,NEVVW
        TYPE"EVENING OUT VIEW #",IVIEW
C GO GET THE DATA NEEDED:
        CALL EVENDAT(MAPRIX,MACRIX,BEGA,ENDA,EVBEGA,EVENDA,IVIEW,
     X  NEVVW,NCLOCK)
C EVEN OUT THE PHOTOELECTRIC VIEW DATA SET
        CALL EVENVW(MAPRIX,MATEMP,BEGA,ENDA,EVBEGA,EVENDA,NEVVW,
     X  NCLOCK)
        REWIND 2
C WRITE THE RESULT TO DISK
        MATEMP(204)=1
        CALL WRBLK(2,IVIEW,MATEMP(54),1,IER)
        IF(IER.NE.1) GOTO 900
C EVEN OUT THE COMPTON VIEW DATA SET
        CALL EVENVW(MACRIX,MATEMP,BEGA,ENDA,EVBEGA,EVENDA,NEVVW,
     X  NCLOCK)
        REWIND 5
C WRITE THE RESULT TO DISK
        MATEMP(204)=2
        CALL WRBLK(5,IVIEW,MATEMP(54),1,IER)
        IF(IER.NE.1) GOTO 900
300     CONTINUE
        TYPE"ENTERING THE NEVVWS TO NTVIEWS PROGRAM"
        CALL EVNTVW(NEVVW,NTVIEW,NSAMP)
C CLOSE THE FILES
        CALL RESET
        CALL NAMMAK(IFNAME,"PE")
        CALL DELETE(IFNAME)
        CALL NAMMAK(IFNAME,"CO")
```

```
        CALL DELETE(IFNAME)
        STOP TRANSLATION COMPLETED
900     TYPE"I/O ERROR IN TCTRANSL1"
        STOP
        END
```

Subroutine MAPDATA:

```
      SUBROUTINE MAPDATA(IVIEW,N360VW,ITYPEL,NCLOCK,
     X  IFTYPE,FANGOVFL,IBADFIN)
C
C PURPOSE
C TO MAP THE DATA FROM LN(IS),LN(IH) SPACE TO PEX AND ZX SPACE.
      DIMENSION ATRIX(256,-2:2),AIRON(256),TANT(256),MATCOM(256),
     X  MATPHO(256),IBADFIN(256)
C CLEAR THE DATA ARRAYS BEFORE READING IN THE DATA
      CALL CLEAR(TANT,512)
      CALL CLEAR(AIRON,512)
      CALL CLEAR(MATCOM,256)
      CALL CLEAR(MATPHO,256)
C INCREASED ACCURACY CONSTANTS: USED TO TAKE ADVANTAGE OF THE FIXED
C POINT SIZE OF THE WORDS.
C MARCH 9,1980 SEE THE LAB BOOK 9.103 FOR COMMENTARY ON THE
C BELOW CHANGES:
C ** COMPTON ACCURACY CONSTANT **
      IACCC=1000   ;CHANGED FROM 4000 3/16/80
C ** PHOTOELECTRIC ACCURACY CONSTANT **
      IACCP=1000   ;CHANGED FROM 4000 3/16/80
C ENTER THE MAPPING ROUTINE
C GO GET THE DATA TO BE INTERRPOLATED
      TYPE"ENTERING DATARA"
      CALL DATARA(IVIEW,N360VW,ATRIX)
C FIRST DETERMINE IF WE ARE INTERPOLATING AN END OR MIDDLE VIEW:
      IF(IVIEW.EQ.1.OR.IVIEW.EQ.N360VW) GOTO 100
C MIDDLE VIEW INTERPOLATION
      TYPE"ENTERING TCINTERP"
      CALL TCINTERP(ATRIX,AIRON,TANT,NCLOCK)
      GOTO 200
C END VIEW INTERPOLATION
100   CALL TCENDINT(ATRIX,AIRON,TANT,IFTYPE,ITYPEL,N360VW,
     X   IVIEW,NCLOCK,FANGOVFL)
      TYPE"LEFT TCENDINT"
200   CONTINUE
C NOW THAT WE HAVE THE DATA FOR THE TRANSLATION GO DO IT:
      TYPE"ENTERING TRNSLT"
      CALL TRNSLT(AIRON,TANT,MATCOM,MATPHO,IACCC,IACCP,NCLOCK)
C NOW INTERPOLATE OVER THE BAD FINGERS
      CALL TCFCORR(MATPHO,IBADFIN,54,203,203)
      CALL TCFCORR(MATCOM,IBADFIN,54,203,203)
C NOW WRITE THE TRANSLATED DATA TO DISK
      CALL WRBLK(2,IVIEW,MATPHO(1),1,IER)
      IF(IER.NE.1) GOTO 900
      CALL WRBLK(5,IVIEW,MATCOM(1),1,IER)
      IF(IER.NE.1) GOTO 900
C WE ARE DONE TRANSLATING HENCE:
      RETURN
900   TYPE "I/O ERROR IN MAPDATA"
      STOP
      END
```

Subroutine CLEAR:

See Appendix C.1.

Subroutine FILNAM:

See Appendix C.1.

Subroutine NAMMAK:

See Appendix C.1.

Subroutine VWPAR:

```
      SUBROUTINE VWPAR(N360VW,NTVIEW,ITYPEL,NCLOCK,FANGOVFL,
     X   IFTYPE)
C  PURPOSE
C    TO DETERMINE THE VIEW PARAMETERS OF THE EXPERIMENT. WE
C    COMPUTE THE NUMBER OF VIEWS IN 360 DEGREES AND THE OVERFLOW
C    FRACTION OF THE LAST VIEW.
C    COMPUTE THE ((NUMBER OF FULL VIEWS)+1) IN 360 DEGREES.
C  500 PULSE ENCODER PULSES EQUALS ONE DEGREE. THUS 180,000
C  PULSES EQUALS ONE REVOLUTION. IN THE CONTROL I/O WE READ IN
C  THE SHORT ANGLE FIRST, THEN THE LONG ANGLE.
C  INITIALIZE THE PARAMETERS:
      DIMENSION XBUF(256)
      N360VW=0
      TANG=000000.
C  REWIND THE DATA FILE
      REWIND 1
      DO 80 J=1,NTVIEW
      READ BINARY(1) XBUF
      IF(J.NE.1) GOTO 40
      IFTYPE=XBUF(NCLOCK+6)-1
40    CONTINUE
      SNGVL=XBUF(NCLOCK+4)
      ANGLVL=XBUF(NCLOCK+2)
      IF(J-1) 50,50,60
50    SNGVL=0
60    CONTINUE
C CHECK FOR 360DEG OVERFLOW
      IF(180000.-TANG) 80,80,70
70    TANG=TANG+SNGVL+ANGLVL
      SVL=SNGVL
      ALVL=ANGLVL
      N360VW=J
      ITYPEL=XBUF(NCLOCK+6)-1
80    CONTINUE
C  OVERFLOW FRACTION OF THE LAST VIEW:
      FANGOVFL=((TANG-180000.)/(SVL+ALVL))
      TYPE"THE NUMBER OF VIEWS IN 360DEG=",N360VW
C  WE NOW HAVE DETERMINED THE AVERAGE SCAN PARAMETERS. HENCE:
      RETURN
      END
```

Subroutine PINTRPDAT:

```
      SUBROUTINE PINTRPDAT(MAPRIX,MACRIX,SAV,ALAV,IVIEW,NCLOCK,
     X  N360VW)
C PURPOSE
C  TO GET THE DATA REQUIRED FOR THE SUBPROGRAM PREINTERP
      DIMENSION MAPRIX(256,-1:1),MACRIX(256,-1:1),SAV(-1:1),
     X  ALAV(-1:1)
C SEE LAB NOTEBOOK PAGES 8.019 THRU 8.022.
      IVWM1=IVIEW-1
      IVWP1=IVIEW+1
      IF(IVIEW.EQ.1.OR.IVIEW.EQ.N360VW) GOTO 150
C MIDDLE VIEW INTERPOLATION DATA:
      REWIND 2       ;PHOTOELECTRIC FILE
      REWIND 5       ;COMPTON FILE
C READ IN THE DATA
      CALL RDBLK(2,IVWM1,MAPRIX(1,-1),3,IER)
      IF(IER.NE.1) GOTO 900
      CALL RDBLK(5,IVWM1,MACRIX(1,-1),3,IER)
      IF(IER.NE.1) GOTO 900
C SETUP THE ANGLE FILE
      DO 140 NV=IVWM1,IVWP1
      SAV(NV-IVIEW)=MAPRIX(NCLOCK+4,NV-IVIEW)
140   ALAV(NV-IVIEW)=MAPRIX(NCLOCK+2,NV-IVIEW)
      GOTO 180
150   CONTINUE
C END VIEW INTERPOLATION
C DETERMINE WHICH END: FIRST OR LAST
      IF(IVIEW-1) 900,160,170
C FIRST VIEW INTERPOLATION
C INPUT DUMMY DATA TO THE -1 COORDINATE
160   DO 164 K=1,256
      MAPRIX(K,-1)=0
164   MACRIX(K,-1)=0
C INPUT THE REST OF THE DATA:
      REWIND 2       ;PHOTOELECTRIC FILE
      REWIND 5       ;COMPTON FILE
      CALL RDBLK(2,1,MAPRIX(1,0),2,IER)
      IF(IER.NE.1) GOTO 900
      CALL RDBLK(5,1,MACRIX(1,0),2,IER)
      IF(IER.NE.1) GOTO 900
C SETUP THE ANGLE FILE
      SAV(-1)=0
      SAV(0)=0
      SAV(1)=MAPRIX(NCLOCK+4,1)
      ALAV(-1)=0
      ALAV(0)=MAPRIX(NCLOCK+2,0)
      ALAV(1)=MAPRIX(NCLOCK+2,1)
      GOTO 180
170   CONTINUE
C LAST VIEW INTERPOLATION
C GET THE -1 AND 0 VIEWS:
      REWIND 2       ;PHOTOELECTRIC FILE
      REWIND 5       ;COMPTON FILE
      CALL RDBLK(2,IVWM1,MAPRIX(1,-1),2,IER)
      IF(IER.NE.1) GOTO 900
      CALL RDBLK(5,IVWM1,MACRIX(1,-1),2,IER)
      IF(IER.NE.1) GOTO 900
C INPUT DUMMY DATA TO THE +1 VIEW.
      DO 174 K=1,256
      MAPRIX(K,+1)=0
174   MACRIX(K,1)=0
C SETUP THE ANGLE FILE:
      SAV(-1)=MAPRIX(NCLOCK+4,-1)
```

```
        SAV(0)=MAPRIX(NCLOCK+4,0)
        SAV(1)=0
        ALAV(-1)=MAPRIX(NCLOCK+2,-1)
        ALAV(0)=MAPRIX(NCLOCK+2,0)
        ALAV(1)=0
80      CONTINUE
C WE NOW HAVE THE SCAN DATA. THEREFORE:
        RETURN
900     TYPE"I/O ERROR IN PINTRPDAT"
        STOP
        END
```

Subroutine PREINTERP:

```
      SUBROUTINE PREINTERP (MATRIX,SAV,ALAV,NCLOCK,MATEMP)
C
C  PREINTERP
C
C PURPOSE
C  TO PREINTERPOLATE VIEWS BEFORE ENTERING INTO THE EVEN-VIEW
C  SUBROUTINE.  PREINTERPOLATION IS REQUIRED TO PRODUCE APPARENTLY
C  CONTIGUOUS VIEWS SO THAT IT WILL BE IN THE PROPER FORMAT
C  RECOGNIZED BY THE EVEN-VIEW SUBROUTINE.
C METHOD
C  BASED ON A METHOD DEVELOPED ON NOV. 6, 1979.  PRESENTED IN
C  LAB NOTEBOOK PAGES 8.019 THRU 8.022.  THE ESSENCE OF THE METHOD
C  IS TO HYPOTHETICALLY SPLIT THE SHORT VIEWS INTO TWO EQUAL
C  HALVES.  THEN, INTERPOLATING BETWEEN THE TWO SHORT VIEWS
C  STRADDLING THE LONG VIEW OBTAIN VALUES FOR EACH HALF. NEXT,
C  COMPUTE A WEIGHTED AVERAGE OF THE INTERPOLATED VIEWS AND THE
C  MEASURED VIEW TO CREATE AN INTERPOLATED FULL VIEW.  (THAT
C  WHICH WOULD BE MEASURED IF NO DEAD TIME WERE PRESENT IN THE
C  MEASUREMENT PROCESS).
      DIMENSION MATRIX(256,-1:1),SAV(-1:1),ALAV(-1:1),MATEMP(256)
C  ENTER THE INTERPOLATION DO LOOP
C CLEAR THE TEMPORARY DATA ARRAY:
      CALL CLEAR(MATEMP,256)
C COPY THE SCAN PARAMETERS
      DO 50 J=1,53
50    MATEMP(J)=MATRIX(J,0)
      DO 100 J=54,203
C  COMPUTE THE (RIGHT-HALF-OF-0:SHORT) INTERPOLATED CENTROID
C  VIEW:
      SHRT0=(((ALAV(-1)/2+3*SAV(0)/4)/(ALAV(-1)/2+SAV(0)+
     X    ALAV(0)/2))*(MATRIX(J,0)-MATRIX(J,-1)))+MATRIX(J,-1)
C  COMPUTE THE (LEFT-HALF-OF ONE:SHORT) INTERPOLATED CENTROID
C  VIEW:
      SHLT1=(((ALAV(0)/2+SAV(1)/4)/(ALAV(0)/2+SAV(1)+
     X    ALAV(1)/2))*(MATRIX(J,1)-MATRIX(J,0)))+MATRIX(J,0)
C  COMPUTE THE LONG CENTROID VIEW:
      CLONG=MATRIX(J,0)
C  COMPUTE THE WEIGHTED AVERAGE OF THESE VIEWS:
      MATEMP(J)=((SHRT0*(SAV(0)/2)+CLONG*ALAV(0)+SHLT1*
     X    (SAV(1)/2))/(SAV(0)/2+ALAV(0)+SAV(1)/2))
100   CONTINUE
C  INTERPOLATIONS COMPLETED, THUS:
      RETURN
      END
```

Subroutine DATARA:

```
      SUBROUTINE DATARA(IVIEW,N360VW,ATRIX)
C PURPOSE
C  TO SETUP THE DATA ARRAY 'ATRIX' FROM WHICH THE INTERPOLATIONS
C  ARE PERFORMED.
      DIMENSION ATRIX(256,-2:2),ATEMP(256)
C METHOD
C  WE NEED FIVE CONTIGUOUS VIEWS SO THAT WE ARE SURE TO HAVE ENOUGH
C  DATA FOR EITHER THE MIDDLE OR END VIEW INTERPOLATIONS.
      N258VW=N360VW-2
      N259VW=N360VW-1
      IF(IVIEW.NE.1) GOTO 100
C  FIRST VIEW READING
      REWIND 1
      DO 50 JV=1,N258VW
C     TYPE"JV =",JV
50    READ BINARY(1) ATEMP
C -2 VIEW
      READ BINARY(1) (ATRIX(JNF,-2),JNF=1,256)
C -1 VIEW
      READ BINARY(1) (ATRIX(JNF,-1),JNF=1,256)
      REWIND 1
C  0 VIEW
      READ BINARY(1) (ATRIX(JNF,0),JNF=1,256)
C +1 VIEW
      READ BINARY(1) (ATRIX(JNF,1),JNF=1,256)
C +2 VIEW
      READ BINARY(1) (ATRIX(JNF,2),JNF=1,256)
      GOTO 1000
C  CHECK IF WE ARE READING THE LAST 2 VIEWS:
100   IF(IVIEW-N259VW) 120,110,120
C  2ND LAST VIEW DATA, REWIND THE DATA FILE
110   REWIND 1
C  UPDATE THE ARRAY VALUES, SHIFTING FROM BACK TO FRONT
120   DO 150 NF=1,256
      ATRIX(NF,-2)=ATRIX(NF,-1)
      ATRIX(NF,-1)=ATRIX(NF,0)
      ATRIX(NF,0)=ATRIX(NF,1)
      ATRIX(NF,1)=ATRIX(NF,2)
150   READ BINARY(1) ATRIX(NF,2)
C  FINISHED WITH THIS I/O FROM THE DATA FILE
1000  RETURN
      END
```

Subroutine TRNSLT:

```
      SUBROUTINE TRNSLT(AIRON,TANT,MATCOM,MATPHO,IACCC,IACCP,
     X    NCLOCK)
C
C PURPOSE
C  TO TRANSLATE MEASUREMENTS FROM HARD AND SOFT SPECTRA SPACE
C  TO COMPTON AND PHOTOELECTRIC LINE INTEGRAL SPACE.
C METHOD
C  USE POLYNOMIAL FITS OF THE MAPPING TO PRODUCE THE NEW LINE
C  INTEGRALS.
C
      DIMENSION TANT(256),AIRON(256),MATCOM(256),MATPHO(256),
     X  P(7),C(7)
      DOUBLE PRECISION P,C
      NCKP19=NCLOCK+19
C TRANSFER THE PERTINANT SCAN PARAMETERS
      DO 50 J=1,NCKP19
      TANT(NCLOCK)=0
      AIRON(NCLOCK)=0
      MATPHO(J)=TANT(J)
50    MATCOM(J)=AIRON(J)
C NOW ENTER THE MAPPING DO LOOP:
      REWIND 3
      REWIND 4
      IDET=0
      JDET=0
      DO 500 J=54,203
C     TYPE"MAPPING DETECTOR #",J
C COMPUTE THE COMPTON LINE INTEGRAL
100   IF(IDET.NE.206) GOTO 110
      REWIND 3
C SEARCH FOR THE PHOTOELECTRIC FIT COEFFICIENTS:
110   READ BINARY(3) DETNBR,TYPEP,P
      IDET=DETNBR
C     TYPE"IDET=",IDET
      IF(IDET.NE.J) GOTO 100
C SEARCH FOR THE COMPTON COEFFICIENTS:
200   IF(JDET.NE.206) GOTO 210
      REWIND 4
210   READ BINARY(4) DETNBR,TYPEC,C
      JDET=DETNBR
C     TYPE"JDET=",JDET
      IF(JDET.NE.J) GOTO 200
C NOW COMPUTE THE LINE INTEGRALS WHICH ARE WEIGHTED BY AN AMP-
C LIFICATION FACTOR. USE AN AMPLIFICATION FACTOR OF 4000(IACCC,
C IACCP). THE LARGEST LINE INTEGRAL WE EXPECT TO SEE IS ABOUT
C 4.5. RENORMALIZE THE DATA TO 300 VIEWS LATER IN THE TCINTERP
C PROGRAM.
      ATPHO=IACCP*1.0*(P(1)*TANT(J)+P(2)*TANT(J)*AIRON(J)+
     X  P(3)*AIRON(J)*AIRON(J)+P(4)*TANT(J)*TANT(J)+P(5)*
     X  AIRON(J)*AIRON(J)*AIRON(J)+P(6)*TANT(J)*TANT(J)*TANT(J)+
     X  P(7)*AIRON(J))+0.5
      IF(ATPHO-32448) 250,230,230
230   ATPHO=IACCP*3
250   MATPHO(J)=ATPHO
      ATCOM=IACCC*1.0*(C(1)*TANT(J)+C(2)*TANT(J)*AIRON(J)+
     X  C(3)*AIRON(J)*AIRON(J)+C(4)*TANT(J)*TANT(J)+C(5)*
     X  AIRON(J)*AIRON(J)*AIRON(J)+C(6)*TANT(J)*TANT(J)*TANT(J)+
     X  C(7)*AIRON(J))+0.5
      IF(ATCOM-32448) 350,330,330
330   ATCOM=IACCC*3.0
350   MATCOM(J)=ATCOM
500   CONTINUE
```

Subroutine TCINTERP:

```
      SUBROUTINE TCINTERP(ATRIX,AIRON,TANT,NCLOCK)
C
C  PURPOSE
C     TO PERFORM A WEIGHTED INTERPOLATION OF THE DATA POINTS BE-
C     TWEEN FILTERS.
C  METHOD
C     BASED ON A WEIGHTED SCHEME DEVELOPED ON AUG 12,1979.
C     PRESENTED IN LAB NOTEBOOK PAGES 7.011 THRU 7.014.  THE
C     ESSENCE OF THE METHOD INVOLVES A TIME-CENTROID-WEIGHTED
C     INTERPOLATION.
      DIMENSION ATRIX(256,-2:2),SAV(-2:2),ALAV(-2:2),AIRON(256),
     X  TANT(256)
      NCLKP20=NCLOCK+20
      NCKP19=NCLOCK+19
C DETERMINE THE TYPE OF FILTER USED IN THIS VIEW
C ITYP=0 IMPLIES IRON
C ITYP=1 IMPLIES TANTALUM
      ITYP=ATRIX(NCLOCK+6,0)-1
C SETUP THE ANGLE VALUE ARRAYS:
      DO 50 NBR=-2,2
      SAV(NBR)=ATRIX(NCLOCK+4,NBR)
50    ALAV(NBR)=ATRIX(NCLOCK+2,NBR)
      DO 100 J=1,NCKP19
      AIRON(J)=ATRIX(J,0)
100   TANT(J)=ATRIX(J,0)
C  **NOW PERFORM THE DATA INTERPOLATION**
C  COMPUTE THE ANGLE BETWEEN THE -1 AND +1 MEASUREMENT CENTROIDS
      ANGNP=ALAV(-1)/2+SAV(0)+ALAV(0)+SAV(1)+ALAV(1)/2
C  COMPUTE THE ANGLE BETWEEN THE -1 AND 0 MEASUREMENT CENTROIDS.
      ANGNZ=ALAV(-1)/2+SAV(0)+ALAV(0)/2
C  COMPUTE THE SLOPE OF THE DATA.
      DO 90 J=NCLKP20,256
      DSLOPE=(ATRIX(J,1)-ATRIX(J,-1))/ANGNP
C  COMPUTE INTERPOLATED VALUES
      TEMP=DSLOPE*ANGNZ+ATRIX(J,-1)
      IF(ITYP) 150,200,150
C IRON EQUIVALENT INTERPOLATION,(WE ALREADY HAVE TA), HENCE:
150   AIRON(J)=TEMP
      TANT(J)=ATRIX(J,0)
      GOTO 90
C TANTALUM EQUIVALENT INTERPOLATION,(WE ALREADY HAVE FE), HENCE:
200   TANT(J)=TEMP
      AIRON(J)=ATRIX(J,0)
90    CONTINUE
C  INTERPOLATION AND BINNING COMPLETED THIS VIEW.
      RETURN
      END
```

Subroutine TCENDINT:

```
      SUBROUTINE TCENDINT(ATRIX,AIRON,TANT,IFTYPE,ITYPEL,N360VW,
     X  IVIEW,NCLOCK,FANGOVFL)
C
C  PURPOSE
C    TO PERFORM A WEIGHTED INTERPOLATION OF THE END VIEWS.
C  METHOD
C    BASED ON A WEIGHTED SCHEME DEVELOPED ON FEB 6,1980.
C    PRESENTED IN LAB NOTEBOOK PAGES 9.082 AND 9.083.  THE
C    ESSENCE OF THE METHOD INVOLVES A TIME-CENTROID-WEIGHTED
C    INTERPOLATION.
      DIMENSION ATRIX(256,-2:2),SAV(-2:2),ALAV(-2:2),AIRON(256),
     X  TANT(256)
      NCKP19=NCLOCK+19
      NCLKP20=NCLOCK+20
C DETERMINE THE TYPE OF FILTER USED IN THIS VIEW.
C ITYP=0 IMPLIES IRON
C ITYP=1 IMPLIES TANTALUM
      ITYP=ATRIX(NCLOCK+6,0)-1
C SETUP THE ANGLE VALUE ARRAYS:
      DO 50 NBR=-2,2
      SAV(NBR)=ATRIX(NCLOCK+4,NBR)
50    ALAV(NBR)=ATRIX(NCLOCK+2,NBR)
C INSERT THE FILE SPECIFIERS AND VIEW DATA INTO THE ARRAYS:
      DO 100 J=1,NCKP19
      AIRON(J)=ATRIX(J,0)
100   TANT(J)=ATRIX(J,0)
C  **NOW PERFORM THE DATA INTERPOLATION**
      IF(IVIEW.EQ.N360VW) GOTO 300
C FIRST VIEW INTERPOLATION
      IF(ITYPEL.EQ.IFTYPE) GOTO 200
C FIRST AND LAST VIEWS USE DIFFERENT FILTERS
C  COMPUTE THE ANGLE BETWEEN THE -1 AND +1 MEASUREMENT CENTROIDS
      ANGNP=((SAV(-1)+ALAV(-1))/2)*(1-FANGOVFL)+ALAV(0)+
     X    SAV(1)+ALAV(1)/2
C  COMPUTE THE ANGLE BETWEEN THE -1 AND 0 MEASUREMENT CENTROIDS.
      ANGNZ=((SAV(-1)+ALAV(-1))/2)*(1-FANGOVFL)+ALAV(0)/2
C  COMPUTE THE SLOPE OF THE DATA.
      DO 90 J=NCLKP20,256
      DSLOPE=(ATRIX(J,1)-ATRIX(J,-1))/ANGNP
C  COMPUTE INTERPOLATED VALUES
      TEMP=DSLOPE*ANGNZ+ATRIX(J,-1)
      IF(ITYP) 130,150,130
C IRON EQUIVALENT INTERPOLATION,(WE ALREADY HAVE TA), HENCE:
130   AIRON(J)=TEMP
      TANT(J)=ATRIX(J,0)
      GOTO 90
C TANTALUM EQUIVALENT INTERPOLATION,(WE ALREADY HAVE FE), HENCE:
150   TANT(J)=TEMP
      AIRON(J)=ATRIX(J,0)
90    CONTINUE
      GOTO 1000
200   CONTINUE
C FIRST AND LAST VIEWS USE THE SAME FILTERS:
C  COMPUTE THE ANGLE BETWEEN THE -2 AND +1 MEASUREMENT CENTROIDS
      ANGNP=ALAV(-2)/2+(SAV(-1)+ALAV(-1))*(1-FANGOVFL)
     X    +ALAV(0)+SAV(1)+ALAV(1)/2
C  COMPUTE THE ANGLE BETWEEN THE -2 AND 0 MEASUREMENT CENTROIDS.
      ANGNZ=ALAV(-2)/2+(SAV(-1)+ALAV(-1))*(1-FANGOVFL)+ALAV(0)/2
C  COMPUTE THE SLOPE OF THE DATA.
      DO 290 J=NCLKP20,256
      DSLOPE=(ATRIX(J,1)-ATRIX(J,-2))/ANGNP
C  COMPUTE INTERPOLATED VALUES
```

```
        TEMP=DSLOPE*ANGNZ+ATRIX(J,-2)
        IF(ITYP) 230,250,230
C IRON EQUIVALENT INTERPOLATION,(WE ALREADY HAVE TA), HENCE:
230     AIRON(J)=TEMP
        TANT(J)=ATRIX(J,0)
        GOTO 290
C TANTALUM EQUIVALENT INTERPOLATION,(WE ALREADY HAVE FE), HENCE:
250     TANT(J)=TEMP
        AIRON(J)=ATRIX(J,0)
290     CONTINUE
        GOTO 1000
C LAST VIEW INTERPOLATION
300     CONTINUE
        IF(ITYPEL.EQ.IFTYPE) GOTO 400
C FIRST AND LAST VIEWS USE DIFFERENT FILTERS
C  COMPUTE THE ANGLE BETWEEN THE -1 AND +1 MEASUREMENT CENTROIDS
        ANGNP=ALAV(-1)/2+(SAV(0)+ALAV(0))*(1-FANGOVFL)+ALAV(1)/2
C  COMPUTE THE ANGLE BETWEEN THE -1 AND 0 MEASUREMENT CENTROIDS.
        ANGNZ=ALAV(-1)/2+((SAV(0)+ALAV(0))/2)*(1-FANGOVFL)
C  COMPUTE THE SLOPE OF THE DATA.
        DO 390 J=NCLKP20,256
        DSLOPE=(ATRIX(J,1)-ATRIX(J,-1))/ANGNP
C  COMPUTE INTERPOLATED VALUES
        TEMP=DSLOPE*ANGNZ+ATRIX(J,-1)
        IF(ITYP) 330,350,330
C IRON EQUIVALENT INTERPOLATION,(WE ALREADY HAVE TA), HENCE:
330     AIRON(J)=TEMP
        TANT(J)=ATRIX(J,0)
        GOTO 390
C TANTALUM EQUIVALENT INTERPOLATION,(WE ALREADY HAVE FE), HENCE:
350     TANT(J)=TEMP
        AIRON(J)=ATRIX(J,0)
390     CONTINUE
        GOTO 1000
400     CONTINUE
C FIRST AND LAST VIEWS USE THE SAME FILTERS:
C  COMPUTE THE ANGLE BETWEEN THE -1 AND +2 MEASUREMENT CENTROIDS
        ANGNP=ALAV(-1)/2+(SAV(0)+ALAV(0))*(1-FANGOVFL)+ALAV(1)
     X     +SAV(2)+ALAV(2)/2
C  COMPUTE THE ANGLE BETWEEN THE -1 AND 0 MEASUREMENT CENTROIDS.
        ANGNZ=ALAV(-1)/2+(SAV(0)+ALAV(0))*(1-FANGOVFL)/2
C  COMPUTE THE SLOPE OF THE DATA.
        DO 490 J=NCLKP20,256
        DSLOPE=(ATRIX(J,2)-ATRIX(J,-1))/ANGNP
C  COMPUTE INTERPOLATED VALUES
        TEMP=DSLOPE*ANGNZ+ATRIX(J,-1)
        IF(ITYP) 430,450,430
C IRON EQUIVALENT INTERPOLATION,(WE ALREADY HAVE TA), HENCE:
430     AIRON(J)=TEMP
        TANT(J)=ATRIX(J,0)
        GOTO 490
C TANTALUM EQUIVALENT INTERPOLATION,(WE ALREADY HAVE FE), HENCE:
450     TANT(J)=TEMP
        AIRON(J)=ATRIX(J,0)
490     CONTINUE
C  INTERPOLATION AND BINNING COMPLETED THIS VIEW. HENCE:
1000    RETURN
        END
```

Subroutine EVENVW:

```
G
C  SUBROUTINE EVENVW
C
C PURPOSE
C  TO CREATE A SET OF EVEN-VIEW DATA. THIS DATA MUST BE EVEN IN
C  ANGLE TO BE RECOGNIZED BY THE ROUTINE TCNDEFAN.
C METHOD
C  BASED ON AN EVEN VIEW INTERPOLATION METHOD DEVELOPED ON OCT
C  13, 1979.  PRESENTED ON LAB NOTEBOOK PAGES 7.117 AND 7.118.
      SUBROUTINE EVENVW (MATRIX,MATEMP,BEGA,ENDA,EVBEGA,
     X  EVENDA,NEVVW,NCLOCK)
      DIMENSION MATRIX(256,-1:1), MATEMP(256)
      CALL CLEAR(MATEMP,256)
C  COMPUTE DELTA THETA BEGINNING
      BDT=BEGA-EVBEGA
C  COMPUTE DELTA THETA CENTER
      DT=ENDA-BEGA
C  COMPUTE DELTA THETA ENDING
      EDT=EVENDA-ENDA
C  COMPUTE THE EVEN VIEW: NORMALIZED TO 300 VIEWS
      DO 100 K=54,203
      MATEMP(K)=((BDT*MATRIX(K,-1)+DT*MATRIX(K,0)+EDT*
     X    MATRIX(K,1))/(BDT+DT+EDT))*(300.0/NEVVW)+0.5
100   CONTINUE
C  WEIGHTED CORRECTION COMPLETED.  THEREFORE:
      RETURN
      END
```

Subroutine EVENDAT:

```
      SUBROUTINE EVENDAT(MAPRIX,MACRIX,BEGA,ENDA,EVBEGA,EVENDA,
     X  IVIEW,NEVVW,NCLOCK)
C PURPOSE
C  TO OBTAIN THE SCANDATA REQUIRED FOR EVENVW.
      DIMENSION MAPRIX(256,-1:1),MACRIX(256,-1:1)
      REWIND 3
      REWIND 4
      IVWM1=IVIEW-1
      IVW2=IVIEW+(NEVVW+1)
      IV2M1=(IVIEW-1)+(NEVVW+1)
      IF(IVIEW.NE.1) GOTO 215
C FIRST VIEW DATA
      DO 212 J=1,256
      MAPRIX(J,-1)=0
212   MACRIX(J,-1)=0
C PHOTOELECTRIC DATA
      CALL RDBLK(3,IVIEW,MAPRIX(1,0),2,IER)
      IF(IER.NE.1) GOTO 900
C SET THE FIRST SHORT VIEW EQUAL TO ZERO:
      MAPRIX(NCLOCK+4,0)=0
C COMPTON DATA
      CALL RDBLK(4,IVIEW,MACRIX(1,0),2,IER)
      IF(IER.NE.1) GOTO 900
      GOTO 280
215   CONTINUE
C MIDDLE VIEW DATA
C PHOTOELECTRIC DATA
      CALL RDBLK(3,IVWM1,MAPRIX(1,-1),3,IER)
      IF(IER.NE.1) GOTO 900
C COMPTON DATA
      CALL RDBLK(4,IVWM1,MACRIX(1,-1),3,IER)
      IF(IER.NE.1) GOTO 900
280   CONTINUE
C COMPUTE THE ANGLE INFORMATION
C BEGINNING EVEN ANGLE=
      EVBEGA=(IVIEW-1)*(180000./NEVVW)
C END EVEN ANGLE=
      EVENDA=IVIEW*(180000./NEVVW)
C BEGINNING ANGLE OF PREINTERPOLATION DATA SET:
      BEGA=ENDA
C END ANGLE OF THE PREINTERPOLATION DATA SET
      ENDA=BEGA+MAPRIX(NCLOCK+4,0)/2.0+MAPRIX(NCLOCK+2,0)+
     X  MAPRIX(NCLOCK+4,1)/2.0
C WE NOW HAVE THE DATA. THEREFORE:
      RETURN
900   TYPE"I/O ERROR IN EVENDATA"
      STOP
      END
```

Subroutine EVNTVW:

```
      SUBROUTINE EVNTVW(NEVVW,NTVIEW,NSAMP)
C PURPOSE:
C       TO CREATE A FILE OF NTVIEWS STARTING WITH A FILE
C       CONTAINING NEVVWS.
      DIMENSION MATRIX(256,2),MPTEMP(256),MCTEMP(256)
C METHOD:
C       WE FIRST DETERMINE THE VIEWS WHICH ARE REQUIRED FOR
C       THE DATA INTERPOLATION. THEN WE INTERPOLATE THE VALUE
C       OF THE NEW VIEW WRT THE CENTROIDS OF THE TWO ORIGINAL
C       VIEWS.
        CALL CLEAR(MPTEMP,256)
        CALL CLEAR(MCTEMP,256)
        DO 500 NVIEW=1,NTVIEW
        TYPE"DETERMINING VIEW#",NVIEW
C       FIRST DETERMINE WHICH VIEWS WE NEED:FOR THE INTERPOLATION
C       TO DETERMINE NVIEW.
        IVIEW=INT((((NEVVW*1.0)/(NTVIEW*1.0))*(NVIEW-1))+1)
        ALPHA=(NVIEW-0.5)*(360./NTVIEW)
        ACENT=(IVIEW-0.5)*(360./NEVVW)
        BCENT=(IVIEW+0.5)*(360./NEVVW)
        REWIND 2      ;PHOTOELECTRIC FILE .PE
        REWIND 5      ;COMPTON       FILE .CO
C       COMPUTE THE PHOTOELECTRIC VIEW
        CALL RDBLK(2,IVIEW,MATRIX,2,IER)
        IF(IER.NE.1) GOTO 900
C NOTE:CHECK THE FILE STRUCTURE (IE FINGER 54 CORRESPONDS TO JFIN=1
        DO 100 JFIN=1,150
100     MPTEMP(JFIN)=MATRIX(JFIN,1)+(((ALPHA-ACENT)/(BCENT-ACENT))
     X    *(MATRIX(JFIN,2)-MATRIX(JFIN,1)))
        DO 125 JFIN=151,160
125     MPTEMP(JFIN)=MATRIX(JFIN,1)
C       NOW COMPUTE THE COMPTON VIEW:
        CALL RDBLK(5,IVIEW,MATRIX,2,IER)
        IF(IER.NE.1) GOTO 900
        DO 200 JFIN=1,150
200     MCTEMP(JFIN)=MATRIX(JFIN,1)+(((ALPHA-ACENT)/(BCENT-ACENT))*
     X    (MATRIX(JFIN,2)-MATRIX(JFIN,1)))
        DO 225 JFIN=151,160
225     MCTEMP(JFIN)=MATRIX(JFIN,1)
        REWIND 3
        REWIND 4
C OKAY NOW WRITE THE RESULT TO DISK:
        CALL WRBLK(3,NVIEW,MPTEMP,1,IER) ;PHOTOELECTRIC VIEW
        IF(IER.NE.1) GOTO 900
        CALL WRBLK(4,NVIEW,MCTEMP,1,IER) ;COMPTON VIEW
        IF(IER.NE.1) GOTO 900
500     CONTINUE
        RETURN
900     TYPE "I/O ERROR IN EVNTVWS"
        STOP
        END
```

Subroutine TCFCORR:

```
      SUBROUTINE TCFCORR(IX,IBADFIN,ILEFT,IRIGHT,NREF)
      DIMENSION IX(256),IBADFIN(256)
      DO 100 JF=ILEFT,IRIGHT
C     ASSUME NO 100 CONSECUTIVE BAD FINGERS
      IF(IBADFIN(JF).EQ.0) GO TO 100
      IF(JF.EQ.IRIGHT) GO TO 57
      IF(JF.EQ.ILEFT) GO TO 58
      DO 52 JF2=1,100
      IF(JF+JF2.GT.IRIGHT .OR. JF-JF2.LT.ILEFT) GO TO 58
      IF(IBADFIN(JF-JF2).EQ.0.AND.IBADFIN(JF+JF2).EQ.0) GO TO 55
52    CONTINUE
55    CONTINUE
      IX(JF)=(IX(JF-JF2)/2.+IX(JF+JF2)/2.)+0.5
      GO TO 100
57    CONTINUE
58    CONTINUE
      IX(JF)=IX(NREF)
100   CONTINUE
      RETURN
      END
```

Appendix C.5 Listing of the Calibration Data Reduction Programs - REGCHVAR

Purpose

To take the calibration data from the detectors and input it into a multiple regression analysis where polynomial fits of the calibration data are then performed.

Program Name	Function
Main Program:	
REGCHVAR	- to coordinate the multiple regression analysis of the calibration data of the detectors.
Subprograms:	
CORRE	- to compute means, standard deviations, sums of cross-products of deviations, and correlation coefficients.
DATAM	- to read in experimental data from the calibration data file.
EXPTPTS	- to read in data from the calibration data file and to compute the line integral values needed for the polynomial fit.
PHI1ANG	- to determine the relative angle between the detector in question and the centerline of the scanner.
ORDER	- to construct from a larger matrix of correlation coefficients a subset matrix of intercorrelations among independent variables and a vector of intercorrelations of independent variables with dependent variable.
MINV	- to invert a matrix.
MULTR	- to perform a multiple linear regression analysis for a dependent variable and a set of independent variables.
FORT.LB	- FORTRAN IV mathematics library.

Main Program REGCHVAR:

```
C
C     ..................................................
C
C     SAMPLE MAIN PROGRAM FOR MULTIPLE REGRESSION- REGRE
C           P407 IN THE IBM SCIENTIFIC SOFTWARE DOCUMENT
C     PURPOSE
C        (1) READ THE PROBLEM PARAMETER CARD FOR A MULTIPLE
C        REGRESSION, (2) READ SUBSET SELECTION CARDS, (3)
C        CALL THE SUBROUTINES TO CALCULATE MEANS, STANDARD DEVIA-
C        TIONS, SIMPLE AND MULTIPLE CORRELATION COEFFICIENTS,
C        REGRESSION COEFFICIENTS, T-VALUES, AND ANALYSIS OF VAR-
C        IANCE FOR MULTIPLE REGRESSION, AND (4) PRINT THE RESULTS.
C
C     REMARKS
C        THE NUMBER OF OBSERVATIONS,N, MUST BE GREATER THAN M+1,
C        WHERE M IS THE NUMBER OF VARIABLES. IF SUBSET SELECTION
C        CARDS ARE NOT PRESENT, THE PROGRAM CAN NOT PERFORM MULTI-
C        PLE REGRESSION.
C        AFTER RETURNING FROM SUBROUTINE MINV, THE VALUE OF DETER
C        MINANT (DET) IS TESTED TO CHECK WHETHER THE CORRELATION
C        MATRIX IS SINGULAR.  IF DET IS COMPARED AGAINST A SMALL
C        CONSTANT, THIS TEST MAY ALSO BE USED TO CHECK NEAR-SING-
C        ULARITY.
C
C     SUBROUTINES AND FUNCTION SUBPROGRAMS REQUIRED
C        CORRE (WHICH, IN TURN, CALLS THE SUBROUTINE NAMED DATA)
C        ORDER
C        MINV
C        MULTR
C
C     METHOD
C        REFER TO B. OSTLE, "STATISTICS IN RESEARCH",THE IOWA
C        STATE COLLEGE PRESS, 1954, CHAPTER 8.
C
C        ..................................................
C
C        THE FOLLOWING DIMENSIONS MUST BE GREATER THAN OR EQUAL TO
C        THE NUMBER OF VARIABLES, M..
C
      DIMENSION XBAR(10),STD(10),D(10),RY(10),ISAVE(10),B(10),
     X          SB(10),T(10),W(10)
C
C        THE FOLLOWING DIMENSION MUST BE GREATER THAN OR EQUAL TO
C        THE PRODUCT OF M*M..
C
      DIMENSION RX(100)
C
C        THE FOLLOWING DIMENSION MUST BE GREATER THAN OR EQUAL TO
C        (M+1)*M/2..(SEE CORRE ALSO)
C
      DIMENSION R(55)
C        THE FOLLOWING DIMENSION MUST BE GREATER THAN OR EQUAL TO
C        10...
C
      DIMENSION ANS(10)
C        THE FOLLOWING ARRAYS ARE ADDED BY ME:
      DIMENSION NAME(20),NAMCNT(20),JCNT(210),NAMFILE(20)
     X ,IDAY(3)
C
C        ..................................................
C
C        IF A DOUBLE PRECISION VERSION OF THIS ROUTINE IS DESIRED,
```

```
C       THE C IN COLUMN 1 SHOULD BE REMOVED FROM THE DOUBLE PRE-
C       CISION STATEMENT WHICH FOLLOWS.
C
        DOUBLE PRECISION XBAR,STD,RX,R,D,B,T,RY,DET,SB,ANS,SUM
C
C       THE C MUST ALSO BE REMOVED FROM DOUBLE PRECISION STATE-
C       MENTS APPEARING IN OTHER ROUTINES USED IN CONJUNCTION
C       WITH THIS ROUTINE.
C
C       ..................................................
C
C2      FORMAT(20X,S20)
3       FORMAT(9HOVARIABLE,5X,4HMEAN,6X,8HSTANDARD,6X,
     X  11HCORRELATION,4X,10HREGRESSION,/,
     X  6H   NO.,18X,9HDEVIATION,7X,6HX VS Y,7X,11HCOEFFICIENT)
4       FORMAT(1H ,I4,4F14.5)
C3      FORMAT(9HOVARIABLE,5X,4HMEAN,6X,8HSTANDARD,6X,
C      X 11HCORRELATION,4X,/,10HREGRESSION,4X,10HSTD. ERROR,5X,
C      X 8HCOMPUTED/
C      X 6H   NO.,18X,9HDEVIATION,7X,6HX VS Y,7X,/,11HCOEFFICIENT,
C      X 3X,12HOF REG.COEF.,3X,7HT VALUE)
C4      FORMAT(1H ,I4,3F14.5,/,3F14.5)
5       FORMAT(10H DEPENDENT)
6       FORMAT(1HO/10H INTERCEPT,10X,F16.5//
     X  23H MULTIPLE CORRELATION  ,F13.5/
     X  /23H STD. ERROR OF ESTIMATE,F13.5//)
7       FORMAT(1HO,21X,39HANALYSIS OF VARIANCE FOR THE REGRESSION/
     X  /5X,19HSOURCE OF VARIATION,7X,7HDEGREES,7X,6HSUM OF,
     X  10X,4HMEAN,/,30X,10HOF FREEDOM,4X,7HSQUARES,
     X  9X,7HSQUARES)
8       FORMAT(30H ATTRIBUTABLE TO REGRESSION   ,I6,2F16.5/,
     X  30H DEVIATION FROM REGRESSION    ,I6,2F16.5).
9       FORMAT(1H ,5X,5HTOTAL,19X,I6,F16.5)
11      FORMAT(1H ,15X,18HTABLE OF RESIDUALS//9H CASE NO.,5X,
     X  7HY VALUE,5X,10HY ESTIMATE,6X,8HRESIDUAL)
12      FORMAT(1H ,I6,F15.5,2F14.5)
13      FORMAT(36H1NUMBER OF SELECTIONS NOT SPECIFIED.,
     X  17H  JOB TERMINATED.)
14      FORMAT(24HOTHE MATRIX IS SINGULAR.,
     X  28H  THIS SELECTION IS SKIPPED.)
C       ENTER THE FILENAME INPUT/OUTPUT FORMATS
1101    FORMAT(S20)
C
C       ..................................................
C
C       FIRST READ IN THE PARAMETERS REQUIRED FOR THIS POLYNOMIAL
C       FIT:
C
C       N............NUMBER OF OBSERVATIONS(READ IN AUTOMATICALLY)
C       M............NUMBER OF VARIABLES(INCLUDING DEP. VARIABLES)
CHANGE M TO CORRESPOND TO THE PARTICULAR CASE
CNOTE THAT M MEANS: NUMBER OF **POTENTIAL VARIABLES**
        M=7
C       NS...........NUMBER OF SELECTIONS=1
        NS=1
C
100     TYPE"WELCOME TO THE POLNOMIAL FIT SOFTWARE"
        CALL RESET
        TYPE"ENTER THE NAME OF THE POLYNOMIAL"
        TYPE"FIT COEFFICIENT FILE:(OUTPUT FILE)"
        READ(11,1101) NAME(1)
C       OPEN UP THE FIT FILE WHICH HOLDS THE REGRESSION
C       COEFFICIENTS.
        CALL FOPEN(2,NAME)
        TYPE"ENTER THE NAME OF THE FILE WHICH CONTAINS THE"
        TYPE"OBSERVATION COUNT FOR EACH DETECTOR:(INPUT FILE)"
```

```
      READ(11,1101) NAMCNT(1)
C     OPEN UP THIS DATA FILE
      CALL FOPEN(3,NAMCNT)
C     READ IN THIS DATA FROM THE DISK
      READ BINARY(3) JCNT
C    LOGICAL TAPE 13 IS USED AS INTERMEDIATE STORAGE TO HOLD IN-
C    PUT DATA. THE INPUT DATA ARE WRITTEN ON LOGICAL TAPE 13 BY
C    THE SPECIAL INPUT SUBROUTINE NAMED DATA. THE STORED DATA MAY
C    BE USED FOR RESIDUAL ANALYSIS.
C
      TYPE"THE INTERMEDIATE INPUT DATA IS HELD IN 'DFILE'"
      CALL FOPEN(13,"DFILE")
      TYPE"ENTER THE NAME OF THE FILE HOLDING THE EXPT.DATA"
      READ(11,1101) NAMFILE(1)
      CALL FOPEN(1,NAMFILE)
      TYPE"WHAT KIND OF FIT ARE WE DOING?"
      ACCEPT"PHOTO(1),COMPTON(2):",ITYPEFIT
C     ENTER THE POLYNOMIAL FIT DO LOOP.
      TYPE"WHICH DETECTORS DO YOU WANT TO FIT?"
      ACCEPT"1STDET,LASTDET:",JD1ST,JDLAST
C     REWIND THE FIT COEFFICIENT FILE:
      REWIND 2
      DO 200 JDET=JD1ST,JDLAST
      TYPE"COMPUTING FIT COEFFICIENTS FOR DETECTOR #",JDET
      TYPE"WHICH HAS",JCNT(JDET)," OBSERVATIONS"
C     SET THE NUMBER OF OBSERVATIONS:N
      N=JCNT(JDET)
CTEMP N=30
      IF(N.LE.5) GOTO 200
      TYPE"WE ASSUME",M," VARIABLES DESCRIBE THE FIT."
C     REWIND THE CHANNELS
      REWIND 1
      REWIND 13
C
      IO=0
      X=0.0
C
C     COMPUTE THE MEANS,STANDARD DEVIATIONS, SUMS OF CROSS-
C     PRODUCTS OF DEVIATIONS, AND CORRELATION COEFFICIENTS:
C     (AND CALL THE SUBROUTINE DATAM)
C     HERE D CONTAINS THE DIAGONAL AND B IS A WORKING VECTOR
CTEMP CALL CORRE(N,M,IO,X,XBAR,STD,RX,R,D,B,T)
      CALL CORRE(N,M,IO,X,XBAR,STD,RX,R,D,B,T,JDET,ITYPEFIT)
C
      REWIND 13
C
C     TEST NUMBER OF SELECTIONS
C
      IF(NS) 108,108,109
108   WRITE(12,13)
      GOTO 300
C
109   DO 200 I=1,NS
      CALL FGTIM(IHOUR,IMIN,ISEC)
      CALL DATE(IDAY,IER)
      WRITE(12) "DETECTOR(RELATIVE)=",JDET
      WRITE(12) "FITTYPE=",ITYPEFIT
      WRITE(12) "TIME=",IHOUR,IMIN,ISEC
      WRITE(12) "DATE=",IDAY
C     WRITE(12,2) NAME
C
C     READ SUBSET SELECTION CARD
C
CDL   HARD WIRE THE BELOW PARAMETERS
C         NRESI.....OPTION CODE FOR TABLE OF RESIDUALS
C                   0 IF IT IS NOT DESIRED.
```

```
C                        1 IF IT IS DESIRED.
CHANGE NRESI TO CORRESPOND TO THE PARTICULAR CASE
       NRESI=1
C           NDEP.....**DEPENDENT** VARIABLE SUBSCRIPT=
CHANGE NDEP TO CORRESPOND TO TTHE PARTICULAR CASE
       NDEP=7
C           K.........NUMBER OF INDEPENDENT VARIABLES *INCLUDED*
CHANGE K TO CORRESPOND TO THE PARTICULAR CASE:
       K=6
C           ISAVE.....A VECTOR CONTAINING THE **INDEPENDENT**
C                     VARIABLES INCLUDED. (THEIR SUBSCRIPTS)
C       THE ASSUMED FORMAT IS DESCRIBED IN THE SUBPROGRAM MULTR.
CHANGE ISAVES TO CORRESPOND TO THE PARTICULAR CASE
       ISAVE(1)=1
       ISAVE(2)=2
       ISAVE(3)=3
       ISAVE(4)=4
       ISAVE(5)=5
       ISAVE(6)=6
C
C      CONSTRUCT FROM A LARGER MATRIX OF CORRELATION COEFFICIENTS
C      A SUBSET MATRIX OF INTERCORRELATIONS AMONG INDEPENDENT
C      VARIABLES AND A VECTOR OF INTERCORRELATIONS OF INDEPEN-
C      DENT VARIABLES WITH DEPENDENT VARIABLE.
       CALL ORDER (M,R,NDEP,K,ISAVE,RX,RY)
C
C      INVERT THE MATRIX (NOTE THAT HERE B IS A WORKING VECTOR)
       CALL MINV (RX,K,DET,B,T)
C
C      TEST SINGULARITY OF THE MATRIX INVERTED
C
       IF(DET) 112,110,112
110    WRITE(12,14)
       GOTO 200
C
C      PERFORM A MULTIPLE LINEAR REGRESSION ANALYSIS FOR A DEP-
C      ENDENT VARIABLE AND A SET OF INDEPENDENT VARIABLES.
C      HERE: D=DIAGONAL VECTOR,B=WORKING VECTOR
112    CALL MULTR(N,K,XBAR,STD,D,RX,RY,ISAVE,B,SB,T,ANS)
C
C      PRINT MEANS, STANDARD DEVIATIONS, INTERCORRELATIONS
C      BETWEEN X AND Y, REGRESSION COEFFICIENTS, STANDARD
C      DEVIATIONS OF REGRESSION COEFFICIENTS, AND COMPUTED T-
C      VALUES
C
       MM=K+1
C      WRITE(12,3)
       WRITE(12,3)
       DO 114 J=1,K
       L=ISAVE(J)
114    WRITE(12,4) L,XBAR(L),STD(L),RY(L),B(J)
       DO 115 J=1,K
       L=ISAVE(J)
       WRITE(12)"VARIABLE NO.=",L
       WRITE(12)"MEAN=",XBAR(L)
       WRITE(12)"STANDARD DEVIATION=",STD(L)
       WRITE(12)"CORRELATION X VS Y=",RY(J)
       WRITE(12)"REGRESSION COEFF=",B(J)
       WRITE(12)"STD.ERROR OF REGR COEFF=",SB(J)
115    WRITE(12)"COMPUTED T VALUE=",T(J),"<12>"
C115   WRITE(12,4) L,XBAR(L),STD(L),RY(J),B(J),SB(J),T(J)
       WRITE(12,5)
       L=ISAVE(MM)
       WRITE(12)"DEPENDENT VARIABLE=",L
       WRITE(12)"MEAN=",XBAR(L)
       WRITE(12)"STANDARD DEVIATION=",STD(L)
```

```
C       WRITE(12,4) L,XBARTLT,STD(L)
C
C       PRINT INTERCEPT, MULTIPLE CORRELATION COEFFICIENT,AND
C       STANDARD ERROR OF ESTIMATE.
C
        WRITE(12) "INTERCEPT=",ANS(1)
        WRITE(12,6) ANS(1),ANS(2),ANS(3)
C
C       PRINT ANALYSIS OF VARIANCE FOR THE REGRESSION
C
        WRITE(12,7)
        L=ANS(8)
        WRITE(12,8) K,ANS(4),ANS(6),L,ANS(7),ANS(9)
        L=N-1
        SUM=ANS(4)+ANS(7)
        WRITE(12,9) L,SUM
        WRITE(12)"F VALUE=",ANS(10)
        IF(NRESI) 200,200,120
C
C       PRINT TABLE OF RESIDUALS
C
120     REWIND 1
        REWIND 13
        WRITE(12,11)
        MM=ISAVE(K+1)
        DO 140 II=1,N
        CALL DATAM(M,W,JDET,ITYPEFIT)
C       INSERT W(3) IN APPROPRIATE PLACES TO YIELD LINE
C       INTEGRAL VALUES RATHER THAN MUX/LN(IH)
CDAVE   SUM=ANS(1)
        SUM=ANS(1)*W(3)
        DO 130 J=1,K
        L=ISAVE(J)
CDAVE130        SUM=SUM+W(L)*B(J)
130     SUM=SUM+W(L)*B(J)*W(3)
CDAVE   RESI=W(MM)-SUM
        RESI=W(MM)*W(3)-SUM
CDAVE   NEW STATEMENT:
        W(MM)=W(MM)*W(3)
140     WRITE(12,12) II,W(MM),SUM,RESI
CDAVE   NEW STATEMENT
        W(MM)=W(MM)/W(3)
        REWIND 1
        REWIND 13
C       WRITE OUT THE FIT DATA TO DISK
        DETNBR=JDET+20
        TYPEFIT=ITYPEFIT
C       DETECTOR NUMBER (ABSOLUTE)
        WRITE BINARY(2) DETNBR
C       TYPE OF POLYNOMIAL FIT PHOTO(1),COMPTON(2)
        WRITE BINARY(2) TYPEFIT
C       REGRESSION COEFFICIENTS
        WRITE BINARY(2) (B(NCOEF),NCOEF=1,K)
C       INTERCEPT VALUE
        WRITE BINARY(2) ANS(1)
200     CONTINUE
        ACCEPT"IS THIS THE LAST SET OF POLYNOMIAL FITS?",IPOLY
        IF(IPOLY.EQ.1) GOTO 300
        GOTO 100
300     CONTINUE
        CALL RESET
        END
```

Subroutine CORRE:

```
C
C     ..................................................
C
C     SUBROUTINE CORRE
C           P32 IN THE IBM SCIENTIFIC SOFTWARE DOCUMENT
C     PURPOSE
C        COMPUTE MEANS, STANDARD DEVIATIONS, SUMS OF CROSS-PRO-
C        DUCTS OF DEVIATIONS, AND CORRELATION COEFFICIENTS
C
C     USAGE
C        ****NOTE:IN ALL OTHER PROGRAMS D=B,B=D****
C        CALL CORRE (N,M,IO,X,XBAR,STD,RX,R,B,D,T)
C
C     DESCRIPTION OF PARAMETERS
C        N     -NUMBER OF OBSERVATIONS. N MUST BE > OR = TO 2.
C        M     -NUMBER OF VARIABLES. M MUST BE > OR = TO 1.
C        IO    -OPTION CODE FOR INPUT DATA
C               0 IF DATA ARE TO BE READ IN FROM INPUT DEVICE IN
C                 THE SPECIAL SUBROUTINE NAMED DATA. (SEE SUBROU-
C                 TINES USED BY THIS SUBROUTINE BELOW.)
C               1 IF ALL DATA ARE ALREADY IN CORE.
C        X     -IF IO=0, THE VALUE OF X IS 0.0
C               IF IO=1, X IS THE INPUT MATRIX (N BY M) CONTAINING
C                 DATA.
C        XBAR  -OUTPUT VECTOR OF LENGTH M CONTAINING MEANS.
C        STD   -OUTPUT VECTOR OF LENGTH M CONTAINING STANDARD
C               DEVIATIONS.
C        RX    -OUTPUT MATRIX (M X M) CONTAINING SUMS OF CROSS-
C               PRODUCTS OF DEVIATIONS FROM MEANS.
C        R     -OUTPUT MATRIX (ONLY UPPER TRIANGULAR PORTION OF
C               THE SYMMETRIC MATRIX OF M BY M) CONTAINING CORRE-
C               LATION COEFFICIENTS. (STORAGE MODE OF 1)
C        ****NOTE:IN ALL OTHER PROGRAMS D=B,B=D****
C        B     -OUTPUT VECTOR OF LENGTH M CONTAINING THE DIAGONAL
C               OF THE MATRIX SUMS OF CROSS-PRODUCTS OF
C               DEVIATIONS FROM MEANS.
C        D     -WORKING VECTOR OF LENGTH M.
C        ****NOTE:IN ALL OTHER PROGRAMS D=B,B=D****
C        T     -WORKING VECTOR OF LENGTH M.
C
C     REMARKS
C        CORRE WILL NOT ACCEPT A CONSTANT VECTOR.
C
C     SUBROUTINES AND FUNCTION SUBPROGRAMS REQUIRED
C        DATAM(M,D) - THIS SUBROUTINE MUST BE PROVIDED BY THE USER.
C                     (1) IF IO=0, THIS SUBROUTINE IS EXPECTED TO
C                         FURNISH AN OBSERVATION IN VECTOR D FROM
C                         AN EXTERNAL INPUT DEVICE.
C                     (2) IF IO=1, THIS SUBROUTINE IS NOT USED
C                         BY CORRE BUT MUST EXIST IN JOB DECK. IF
C                         USER HAS NOT  SUPPLIED A SUBROUTINE NAMED
C                         DATA, THE FOLLOWING IS SUGGESTED.
C                              SUBROUTINE DATAM
C                              RETURN
C                              END
C
C     METHOD
C        PRODUCT-MOMENT CORRELATION COEFFICIENTS ARE COMPUTED.
C
C     ..................................................
C
      SUBROUTINE CORRE(N,M,IO,X,XBAR,STD,RX,R,B,D,T,JDET,ITYPEFIT)
```

```
      DIMENSION X(1),XBAR(10),STD(10),RX(100),R(55),B(10),
     X  D(10),T(10)
C
C     ..................................................
C
C     IF A DOUBLE PRECISION VERSION OF THIS ROUTINE IS DESIRED,
C     THE C IN COLUMN 1 SHOULD BE REMOVED FROM THE DOUBLE PRE-
C     CISION STATEMENT WHICH FOLLOWS.
C
      DOUBLE PRECISION XBAR,STD,RX,R,B,T
C
C     THE C MUST ALSO BE REMOVED FROM DOUBLE PRECISION STATE-
C     MENTS APPEARING IN OTHER ROUTINES USED IN CONJUNCTION
C     WITH THIS ROUTINE.
C
C     THE DOUBLE PRECISION VERSION OF THIS SUBROUTINE MUST ALSO
C     CONTAIN DOUBLE PRECISION FORTRAN FUNCTIONS. SQRT AND ABS
C     IN STATEMENT 220 MUST BE CHANGED TO DSQRT AND DABS.
C
C     ..................................................
C
C     INITIALIZATION
C
      DO 100 J=1,M
      B(J)=0.0
100   T(J)=0.0
      K=(M*M+M)/2
      DO 102 I=1,K
102   R(I)=0.0
      FN=N
      L=0
C
      IF(IO) 105,127,105
C
C     DATA ARE ALREADY IN CORE
C
105   DO 108 J=1,M
      DO 107 I=1,N
      L=L+1
107   T(J)=T(J)+X(L)
      XBAR(J)=T(J)
108   T(J)=T(J)/FN
C
      DO 115 I=1,N
      JK=0
      L=I-N
      DO 110 J=1,M
      L=L+N
      D(J)=X(L)-T(J)
110   B(J)=B(J)+D(J)
      DO 115 J=1,M
      DO 115 K=1,J
      JK=JK+1
115   R(JK)=R(JK)+D(J)*D(K)
      GOTO 205
C
C     READ OBSERVATIONS AND CALCULATE TEMPORARY
C     MEANS FROM THESE DATA IN T(J)
C
127   IF(N-M) 130,130,135
130   KK=N
      GOTO 137
135   KK=M
137   DO 140 I=1,KK
      CALL DATAM(M,D,JDET,ITYP,FIT)
      DO 140 J=1,M
```

```
      T(J)=T(J)+D(J)
      L=L+1
140   RX(L)=D(J)
      FKK=KK
      DO 150 J=1,M
      XBAR(J)=T(J)
150   T(J)=T(J)/FKK
C
C     CALCULATE SUMS OF CROSS-PRODUCTS OF DEVIATIONS
C     FROM TEMPORARY MEANS FOR M OBSERVATIONS.
C
      L=0
      DO 180 I=1,KK
      JK=0
      DO 170 J=1,M
      L=L+1
170   D(J)=RX(L)-T(J)
      DO 180 J=1,M
      B(J)=B(J)+D(J)
      DO 180 K=1,J
      JK=JK+1
180   R(JK)=R(JK)+D(J)*D(K)
C
      IF(N-KK) 205,205,185
C
C     READ THE REST OF OBSERVATIONS ONE AT A TIME, SUM THE
C     OBSERVATION, AND CALCULATE SUMS OF CROSS-PRODUCTS OF
C     DEVIATIONS FROM TEMPORARY MEANS
C
185   KK=N-KK
      DO 200 I=1,KK
      JK=0
      CALL DATAM(M,D,JDET,ITYPEFIT)
      DO 190 J=1,M
      XBAR(J)=XBAR(J)+D(J)
      D(J)=D(J)-T(J)
190   B(J)=B(J)+D(J)
      DO 200 J=1,M
      DO 200 K=1,J
      JK=JK+1
200   R(JK)=R(JK)+D(J)*D(K)
C
C     CALCULATE MEANS
C
205   JK=0
      DO 210 J=1,M
      XBAR(J)=XBAR(J)/FN
C
C     ADJUST SUMS OF CROSS-PRODUCTS OF DEVIATIONS
C     FROM TEMPORARY MEANS.
C
      DO 210 K=1,J
      JK=JK+1
210   R(JK)=R(JK)-B(J)*B(K)/FN
C
C     CALCULATE CORRELATION COEFFICIENTS
C
      JK=0
      DO 220 J=1,M
      JK=JK+J
220   STD(J)= DSQRT(DABS(R(JK)))
      DO 230 J=1,M
      DO 230 K=J,M
      JK=J+(K*K-K)/2
      L=M*(J-1)+K
      RX(L)=R(JK)
```

```
         L=M*(K-1)+J
         RX(L)=R(JK)
         IF(STD(J)*STD(K)) 225,222,225
222      R(JK)=0.0
         GOTO 230
225      R(JK)=R(JK)/(STD(J)*STD(K))
230      CONTINUE
C
C     CALCULATE STANDARD DEVIATIONS
C
         FN=SQRT(FN-1.0)
         DO 240 J=1,M
240      STD(J)=STD(J)/FN
C
C        COPY THE DIAGONAL OF THE MATRIX OF SUMS OF CROSS-PRODUCTS
C        OF DEVIATIONS FROM MEANS.
C
         L=-M
         DO 250 I=1,M
         L=L+M+1
250      B(I)=RX(L)
         RETURN
         END
```

Subroutine DATAM:

```
C
C       .....................................................
C
C       SAMPLE INPUT SUBROUTINE -DATAM
C           P452 IN THE IBM SCIENTIFIC SOFTWARE DOCUMENT
C
C       PURPOSE
C           READ AN OBSERVATION (M DATA VALUES)FROM INPUT DEVICE.
C           THIS SUBROUTINE IS CALLED BY THE SUBROUTINE CORRE AND
C           MUST BE PROVIDED BY THE USER. IF SIZE AND LOCATION
C           OF DATA FIELDS ARE DIFFERENT FROM PROBLEM TO PROBLEM
C           , THIS SUBROUTINE MUST BE RECOMPILED WITH A PROPER
C           FORMAT STATEMENT.
C
C       USAGE
C           CALL DATAM (M,D)
C
C       DESCRIPTION OF PARAMETERS
C          M     -THE NUMBER OF VARIABLES IN AN OBSERVATION
C          D     -OUTPUT VECTOR OF LENGTH M CONTAINING THE OBSER-
C                 VATION DATA.
C
C       REMARKS
C           THE TYPE OF CONVERSION SPECIFIED IN THE FORMAT MUST
C           BE EITHER F OR E.
C
C       SUBROUTINES AND FUNCTION SUBPROGRAMS REQUIRED
C           NONE
C       .....................................................
C
CVAR    SUBROUTINE DATAM(M,D)
        SUBROUTINE DATAM(M,D,JDET,ITYPEFIT)
C
        DIMENSION D(10)
C
C       READ AN OBSERVATION FROM INPUT DEVICE
CDL     AN OBSERVATION HERE REFERS TO THE CALIBRATION DATA FOR
CDL     ONE DETECTOR, STANDARD THICKNESS,SALINE CONCENTRATION,
CDL     AND KVP.
CDL     INPUT THE DATA FROM THE DETECTOR DATA FILE
CVAR    READ BINARY(1) (D(I),I=1,M)
        CALL EXPTPTS(JDET,D,ITYPEFIT)
C
C       INPUT DATA ARE WRITTEN ON LOGICAL TAPE 13 FOR THE RESIDU-
C       AL ANALYSIS PERFORMED IN THE SAMPLE MULTIPLE REGRESSION
C       PROGRAM.
C
CDL     NOW WRITE THIS OBSERVATION TO CHANNEL 13 FOR TEMPORARY
CDL     STORAGE.
        WRITE BINARY(13) (D(I),I=1,M)
        RETURN
        END
```

Subroutine EXPTPTS:

```
      SUBROUTINE EXPTPTS(JDET,D,ITYPEFIT)
C     PURPOSE: TO READ IN DATA FROM THE COMPRESSED DATA FILE
C     AND TO COMPUTE THE LINE INTEGRAL VARIABLES NEEDED FOR
C     THE POLYNOMIAL FIT OF THE POINTS IN THESIS WE ASSUME A
C     FIT OF THE FORM:
C     (MUP*X)/LN(IH)=A1(LN(IS)/LN(IH))+A2(LN(IS))+A3(LN(IH))+
C       A4(LN(IS)*LN(IS))/LN(IH)+A5
      DIMENSION D(10),AIRON(210),TANT(210)
      PI=3.14159
C     READ IN THE DATA POINT OFF OF THE DISK
C     IRON DATA
100   READ BINARY(1) AIRON
C     TANTALUM DATA
      READ BINARY(1) TANT
C     CHECK TO SEE IF THIS DATA IS VALID FOR THE FIT
      IR=AIRON(JDET)*50.0
      IF(IR.GT.0) IR=1
      JTA=TANT(JDET)*50.0
      IF(JTA.GT.0) JTA=1
      IF(IR*JTA) 100,100,125
125   CONTINUE
C     THE DATA READ IN IS GOOD
C     USE THE ABOVE ORDER OF THE POLYNOMIAL TERMS IN THE VAR-
C     IABLE ORDER (EXCEPT THE DEPENDENT VARIABLE)
C     ASSUMPTIONS: SEE LAB BOOKS 8 AND 9
C     LUCITE THICKNESS=0.148178815CM
C     1.4=1.261471185CM H2O
C     2.8=2.685417185CM H2O
C     5.7=5.556061185CM H2O
C     11.4=11.26516119CM H2O
C     CALIBRATIONS PERFORMED AT 24DEGC. DENSITY CORRECTION
C     OBTAINED FROM BAUMEISTER AND MARKS.
C     COMPUTETHE EFFECTIVE THICKNESS.
C     IF(AIRON(3)-TANT(3)) 500,130,500
      IF(AIRON(3)-1.5E0) 131,131,133
131   THK=1.26147
      GOTO 145
133   IF(AIRON(3)-2.9E0) 134,134,136
134   THK=2.68542
      GOTO 145
136   IF(AIRON(3)-5.8E0) 137,137,139
137   THK=5.55606
      GOTO 145
139   IF(AIRON(3)-11.5E0) 140,140,500
140   THK=11.2652
145   TKPLEX=0.148179
C     FIND OUT WHAT KIND OF FIT THIS IS (PHOTO(1),COMPTON(2))
      IF(ITYPEFIT-1) 500,150,175
150   CONTINUE
C     PHOTOELECTRIC FIT. CROSS SECTIONS:(@20DEGC)
C     IF(AIRON(2)-TANT(2)) 500,153,500
      IF(AIRON(2)-0.01E0) 154,154,156
154   CXSAL=0.02937
      GOTO 170
156   IF(AIRON(2)-0.26E0) 157,157,159
157   CXSAL=0.0429025
      GOTO 170
159   IF(AIRON(2)-0.51E0) 160,160,162
160   CXSAL=0.057473
      GOTO 170
162   IF(AIRON(2)-0.76E0) 163,163,165
163   CXSAL=0.06936
```

```
      GOTO 170
165   IF(AIRON(2)-1.01E0) 166,166,500
166   CXSAL=0.08774
170   CXPLEX=2.31330E-2
      GOTO 200
175   CONTINUE
C     COMPTON FIT. CROSS SECTIONS:(@20DEGC)
      IF(AIRON(2)-0.01E0) 176,176,178
176   CXSAL=0.177103
      GOTO 195
178   IF(AIRON(2)-0.26E0) 179,179,181
179   CXSAL=0.183008
      GOTO 195
181   IF(AIRON(2)-0.51E0) 182,182,184
182   CXSAL=0.18888
      GOTO 195
184   IF(AIRON(2)-0.76E0) 185,185,187
185   CXSAL=0.194095
      GOTO 195
187   IF(AIRON(2)-1.01E0) 188,188,500
188   CXSAL=0.20133
195   CXPLEX=2.05466E-1
200   CONTINUE
C     FIND THE STANDARD-DETECTOR ANGLE
C     COMPUTE THE ABSOLUTE NBR OF THE DETECTOR
      JFNUM=JDET+20
      CALL PHI1ANG(JFNUM,PHI)
      ANG=AIRON(4)*(PI/180)+PHI
C     WRITE(10)"TANT(JDET)=",TANT(JDET)
C     WRITE(10)"AIRON(JDET)=",AIRON(JDET)
C     WRITE(10)"AIRON(3)=",AIRON(3)
C     WRITE(10)"ANG=",ANG
C     WRITE(10)"THK=",THK
C     WRITE(10)"CXSAL=",CXSAL
C     WRITE(10)"CXPLEX=",CXPLEX
C     WRITE(10)"TKPLEX=",TKPLEX
C     COMPUTE THE LINE INTEGRAL(CORRECTED TO 24DEGC)
      SIGMAX=(CXSAL*(0.99732/0.99823)*THK+CXPLEX*TKPLEX)/COS(ANG)
C     WRITE(10)"SIGMAX=",SIGMAX
C     NOW COMPUTE THE VARIABLES
      D(1)=TANT(JDET)/AIRON(JDET)
      D(2)=TANT(JDET)
      D(3)=AIRON(JDET)
      D(4)=(TANT(JDET)*TANT(JDET))/AIRON(JDET)
      D(5)=AIRON(JDET)*AIRON(JDET)
      D(6)=(TANT(JDET)*TANT(JDET)*TANT(JDET))/AIRON(JDET)
      D(7)=SIGMAX/AIRON(JDET)
      RETURN
500   TYPE"I/O ERROR: SPECIFICATIONS DON'T MATCH, OR NO FIT"
      TYPE"TYPE GIVEN"
      STOP
      END
```

Subroutine PHI1ANG:

```
      SUBROUTINE PHI1ANG(JFNUM,PHI)
C
C
C PURPOSE
C  TO DETERMINE THE RELATIVE ANGLE BETWEEN THE DETECTOR IN QUES-
C  TION AND THE CENTERLINE OF THE SCANNER.
C METHOD
C  BASED ON THE MANUFACTURING SPECIFICATIONS FOR THE DETECTOR
C  GEOMETRY.  REFERENCE: PAGE 7.019 IN THE LAB NOTEBOOK.
C
C  ALL ARITHMETIC IS PERFORMED IN RADIANS: P9-4 DGC FORTRAN.
C  DETERMINE THE GEOMETRY PARAMETERS
      N=128
      ALAMBDA=0.069341
      A=24.750
C  IN THIS COMPUTATION:
C  DETECTOR 1 CORRESPONDS TO POSITIVE PHI
C  DETECTOR 256 CORRESPONDS TO NEGATIVE PHI
C  THE PROGRAM PHIANG IS SLIGHTLY DIFFERENT FROM PHI1ANG
      R=(N+0.75-JFNUM)*ALAMBDA
      GAMMA=R/A
C  USE THE SIN INVERSE STATEMENT FUNCTION
C  SIN X=((A/R)/1)=(OPP/HYP);OPP=A/R,HYP=1
C  ADJACENT=SQRT(HYP**2-OPP**2)
C          =SQRT(1-OPP**2)
C  TAN=OPP/ADJ=OPP/(SQRT(1-OPP**2))
C  X=ATAN2(OPP/ADJ)
C       SININV(OPP)=ATAN2(OPP,(SQRT(1-(ABS(OPP))**2)))
      PHI=ATAN2(GAMMA,(SQRT(1-(ABS(GAMMA))**2)))
C       PHI=SININV(GAMMA)
C  NOW CHANGE THE SIGN (FOR CONSISTENCY) OF PHI SO THAT IT
C  CORRESPONDS TO THE SIGN OF PHI IN NDEFAN. AFTER THE CHANGE
C  WE ONLY HAVE TO ADD THE ANGLE PHI TO THE TABLE ANGLE TO
C  GIVE THE RELATIVE ANGLE OF THE STANDARD WRT THE DETECTOR IN
C  QUESTION.
      PHI=PHI*(-1.0)
C  PHI COMPUTED FOR THIS DETECTOR: THEREFORE
      RETURN
      END
```

Subroutine ORDER:

```
C
C     ..................................................
C
C     SUBROUTINE ORDER
C           P36 IN THE IBM SCIENTIFIC SOFTWARE DOCUMENT
C     PURPOSE
C        CONSTRUCT FROM A LARGER MATRIX OF CORRELATION COEFFI-
C        CIENTS A SUBSET MATRIX OF INTERCORRELATIONS AMONG INDE-
C        PENDENT VARIABLES AND A VECTOR OF INTERCORRELATIONS
C        OF INDEPENDENT VARIABLES WITH DEPENDENT VARIABLE.
C        THIS SUBROUTINE IS NORMALLY USED IN THE PERFORMANCE
C        OF MULTIPLE AND POLYNOMIAL REGRESSION ANALYSES.
C
C     USAGE
C        CALL ORDER (M,R,NDEP,K,ISAVE,RX,RY)
C
C     DESCRIPTION OF PARAMETERS
C        M      -NUMBER OF VARIABLES AND ORDER OF MATRIX R.
C        R      -INPUT MATRIX CONTAINING CORRELATION COEFFICIENTS
C                THIS SUBROUTINE EXPECTS ONLY UPPER TRIANGULAR
C                PORTION OF THE SYMMETRIC MATRIX TO BE STORED
C                (BY COLUMN) IN R. (STORAGE MODE OF 1)
C        NDEP   -THE SUBSCRIPT NUMBER OF THE DEPENDENT VARIABLE.
C        K      -NUMBER OF INDEPENDENT VARIABLES TO BE INCLUDED
C                IN THE FORTHCOMING REGRESSION. K MUST BE GREATER
C                THAN OR EQUAL 1.
C        ISAVE -INPUT VECTOR OF LENGTH K+1 CONTAINING, IN AS-
C                CENDING ORDER, THE SUBSCRIPT NUMBERS OF K INDEP-
C                ENDENT VARIABLES TO BE INCLUDED IN THE FORTH-
C                COMING REGRESSION.
C                UPON RETURNING TO THE CALLING ROUTINE, THIS VEC-
C                TOR CONTAINS, IN ADDITION, THE SUBSCRIPT NUMBER
C                OF THE DEPENDENT VARIABLE IN K+1 POSITION.
C        RX     -OUTPUT MATRIX (K X K)CONTAINING INTER-
C                CORRELATIONS AMONG INDEPENDENT VARIABLES TO BE
C                USED IN FORTHCOMING REGRESSION.
C        RY     -OUTPUT VECTOR OF LENGTH K CONTAINING INTERCOR-
C                RELATIONS OF INDEPENDENT VARIABLES WITH DEPENDENT
C                VARIABLES.
C
C     REMARKS
C        NONE
C
C     SUBROUTINES AND FUNCTION SUBPROGRAMS REQUIRED
C        NONE
C
C     METHOD
C        FROM THE SUBSCRIPT NUMBERS OF THE VARIABLES TO BE IN-
C        CLUDED IN THE FORTHCOMING REGRESSION, THE SUBROUTINE
C        CONSTRUCTS THE MATRIX RX AND THE VECTOR RY.
C
C        ..................................................
C
      SUBROUTINE ORDER(M,R,NDEP,K,ISAVE,RX,RY)
      DIMENSION R(55),ISAVE(10),RX(100),RY(10)
C
C     ..................................................
C
C     IF A DOUBLE PRECISION VERSION OF THIS ROUTINE IS DESIRED
C     THE C IN COLUMN 1 SHOULD BE REMOVED FROM THE DOUBLE
C     PRECISION STATEMENT WHICH FOLLOWS.
C
```

```
      DOUBLE PRECISION R,RX,RY
C
C     THE C MUST ALSO BE REMOVED FROM DOUBLE PRECISION STATE-
C     MENTS APPEARING IN OTHER ROUTINES USED IN CONJUNCTION
C     WITH THIS ROUTINE.
C
C     ..................................................
C
C     COPY INTERCORRELATIONS OF INDEPENDENT VARIABLES
C     WITH DEPENDENT VARIABLE.
C
      MM=0
      DO 130 J=1,K
      L2=ISAVE(J)
      IF(NDEP-L2) 122,123,123
122   L=NDEP+(L2*L2-L2)/2
      GOTO 125
123   L=L2+(NDEP*NDEP-NDEP)/2
125   RY(J)=R(L)
C
C     COPY A SUBSET MATRIX OF INTERCORRELATIONS AMONG
C     INDEPENDENT VARIABLES.
C
      DO 130 I=1,K
      L1=ISAVE(I)
      IF(L1-L2) 127,128,128
127   L=L1+(L2*L2-L2)/2
      GOTO 129
128   L=L2+(L1*L1-L1)/2
129   MM=MM+1
130   RX(MM)=R(L)
C
C     PLACE THE SUBSCRIPT NUMBER OF THE DEPENDENT
C     VARIABLE IN ISAVE(K+1)
C
      ISAVE(K+1)=NDEP
      RETURN
      END
```

Subroutine MINV:

```
C
C     ..................................................
C
C     SUBROUTINE MINV
C           P118 IN THE IBM SCIENTIFIC SOFTWARE DOCUMENT
C     PURPOSE
C        INVERT A MATRIX
C
C     USAGE
C        CALL MINV(A,N,D,L,M)
C
C     DESCRIPTION OF PARAMETERS
C        A     -INPUT MATRIX, DESTROYED IN COMPUTATION AND REPLACED
C               BY RESULTANT INVERSE.
C        N     -ORDER OF MATRIX A
C        D     -RESULTANT DETERMINANT
C        L     -WORK VECTOR OF LENGTH N.
C        M     -WORK VECTOR OF LENGTH N.
C
C     REMARKS
C        MATRIX A MUST BE A GENERAL MATRIX
C
C     SUBROUTINES AND FUNCTION SUBPROGRAMS REQUIRED
C        NONE
C
C     METHOD
C        THE STANDARD GAUSS-JORDAN METHOD IS USED. THE DETERMINANT
C        IS ALSO CALCULATED. A DETERMINANT OF ZERO INDICATES THAT
C        THE MATRIX IS SINGULAR.
C
C     ..................................................
C
      SUBROUTINE MINV(A,N,D,L,M)
      DIMENSION A(100),L(10),M(10)
C
C     ..................................................
C
C     IF A DOUBLE PRECISION VERSION OF THIS ROUTINE IS DESIRED,
C     THE C IN COLUMN 1 SHOULD BE REMOVED FROM THE DOUBLE PRE-
C     CISION STATEMENT WHICH FOLLOWS.
C
      DOUBLE PRECISION A,D,BIGA,HOLD
C
C     THE C MUST ALSO BE REMOVED FROM DOUBLE PRECISION STATE-
C     MENTS APPEARING IN OTHER ROUTINES USED IN CONJUNCTION
C     WITH THIS ROUTINE.
C
C     THE DOUBLE PRECISION VERSION OF THIS SUBROUTINE MUST ALSO
C     CONTAIN DOUBLE PRECISION FORTRAN FUNCTIONS. ABS IN STATE-
C     MENT 10 MUST BE CHANGED TO DABS.
C
C     ..................................................
C
C     SEARCH FOR LARGEST ELEMENT
C
      D=1.0
      NK=-N
      DO 80 K=1,N
      NK=NK+N
      L(K)=K
      M(K)=K
      KK=NK+K
```

```
      BIGA=A(KK)
      DO 20 J=K,N
      IZ=N*(J-1)
      DO 20 I=K,N
      IJ=IZ+I
      IF(DABS(BIGA)-DABS(A(IJ))) 15,20,20
C10   IF(DABS(BIGA)-DABS(A(IJ))) 15,20,20
15    BIGA=A(IJ)
      L(K)=I
      M(K)=J
20    CONTINUE
C
C     INTERCHANGE ROWS
C
      J=L(K)
      IF(J-K) 35,35,25
25    KI=K-N
      DO 30 I=1,N
      KI=KI+N
      HOLD=-A(KI)
      JI=KI-K+J
      A(KI)=A(JI)
30    A(JI)=HOLD
C
C     INTERCHANGE COLUMNS
C
35    I=M(K)
      IF(I-K) 45,45,38
38    JP=N*(I-1)
      DO 40 J=1,N
      JK=NK+J
      JI=JP+J
      HOLD=-A(JK)
      A(JK)=A(JI)
40    A(JI)=HOLD
C
C     DIVIDE COLUMN BY MINUS PIVOT (VALUE OF PIVOT ELEMENT IS
C     CONTAINED IN BIGA)
C
45    IF(BIGA) 48,46,48
46    D=0.0
      RETURN
48    DO 55 I=1,N
      IF(I-K) 50,55,50
50    IK=NK+I
      A(IK)=A(IK)/(-BIGA)
55    CONTINUE
C
C     REDUCE MATRIX
C
      DO 65 I=1,N
      IK=NK+I
      HOLD=A(IK)
      IJ=I-N
      DO 65 J=1,N
      IJ=IJ+N
      IF(I-K) 60,65,60
60    IF(J-K) 62,65,62
62    KJ=IJ-I+K
      A(IJ)=HOLD*A(KJ)+A(IJ)
65    CONTINUE
C
C     DIVIDE ROW BY PIVOT
C
      KJ=K-N
      DO 75 J=1,N
```

```
      KJ=KJ+N
      IF(J-K) 70,75,70
70    A(KJ)=A(KJ)/BIGA
75    CONTINUE
C
C     PRODUCT OF PIVOTS
C
      D=D*BIGA
C
C     REPLACE PIVOT BY RECIPROCAL
C
      A(KK)=1.0/BIGA
80    CONTINUE
C
C     FINAL ROW AND COLUMN INTERCHANGE
C
      K=N
100   K=(K-1)
      IF(K) 150,150,105
105   I=L(K)
      IF(I-K) 120,120,108
108   JQ=N*(K-1)
      JR=N*(I-1)
      DO 110 J=1,N
      JK=JQ+J
      HOLD=A(JK)
      JI=JR+J
      A(JK)=-A(JI)
110   A(JI)=HOLD
120   J=M(K)
      IF(J-K) 100,100,125
125   KI=K-N
      DO 130 I=1,N
      KI=KI+N
      HOLD=A(KI)
      JI=KI-K+J
      A(KI)=-A(JI)
130   A(JI)=HOLD
      GOTO 100
150   RETURN
      END
```

Subroutine MULTR:

```
C
C     ..................................................
C
C        SUBROUTINE MULTR
C            P37 IN THE IBM SCIENTIFIC SOFTWARE DOCUMENT
C     PURPOSE
C        PERFORM A MULTIPLE LINEAR REGRESSION ANALYSIS FOR A
C        DEPENDENT VARIABLE AND A SET OF INDEPENDENT VARIABLES
C        THIS SUBROUTINE IS NORMALLY USED IN THE PERFORMANCE OF
C        MULTIPLE AND POLYNOMIAL REGRESSION ANALYSES.
C
C     USAGE
C        CALL MULTR(N,K,XBAR,STD,D,RX,RY,ISAVE,B,SB,T,ANS)
C
C     DESCRIPTION OF PARAMETERS
C        N     -NUMBER OF OBSERVATIONS.
C        K     -NUMBER OF INDEPENDENT VARIABLES IN THIS REGRESSION.
C        XBAR  -INPUT VECTOR OF LENGTH M CONTAINING MEANS OF ALL
C               VARIABLES. M IS NUMBER OF VARIABLES IN OBSERVATIONS
C        STD   -INPUT VECTOR OF LENGTH M CONTAINING STANDARD DEVI-
C               ATIONS OF ALL VARIABLES.
C        D     -INPUT VECTOR OF LENGTH M CONTAINING THE DIAGONAL OF
C               THE MATRIX OF SUMS OF CROSS-PRODUCTS OF DEVIATIONS
C               FROM MEANS FOR ALL VARIABLES.
C        RX    -INPUT MATRIX (K X K) CONTAINING THE INVERSE OF
C               INTERCORRELATIONS AMONG INDEPENDENT VARIABLES.
C        RY    -INPUT VECTOR OF LENGTH K CONTAINING INTERCORRELA-
C               TIONS OF INDEPENDENT VARIABLES WITH DEPENDENT
C               VARIABLE.
C        ISAVE-INPUT VECTOR OF LENGTH K+1 CONTAINING SUBSCRIPTS
C              OF INDEPENDENT VARIABLES IN ASCENDING ORDER. THE
C              SUBSCRIPT OF THE DEPENDENT VARIABLE IS STORED IN
C              THE LAST, K+1, POSITION.
C        B     -OUTPUT VECTOR OF LENGTH K CONTAINING REGRESSION
C               COEFFICIENTS.
C        SB    -OUTPUT VECTOR OF LENGTH K CONTAINING STANDARD
C               DEVIATIONS OF REGRESSION COEFFICIENTS
C        T     -OUTPUT VECTOR OF LENGTH K CONTAINING T-VALUES.
C        ANS   -OUTPUT VECTOR OF LENGTH 10 CONTAINING THE FOLLOWING
C               INFORMATION.
C               ANS(1)  INTERCEPT
C               ANS(2)  MULTIPLE CORRELATION COEFFICIENT
C               ANS(3)  STANDARD ERROR OF ESTIMATE
C               ANS(4)  SUM OF SQUARES ATTRIBUTABLE TO REGRESSION
C                       (SSAR)
C               ANS(5)  DEGREES OF FREEDOM ASSOCIATED WITH SSAR
C               ANS(6)  MEAN SQUARE OF SSAR
C               ANS(7)  SUM OF SQUARES OF DEVIATIONS FROM REGRES-
C                       SION (SSDR)
C               ANS(8)  DEGREES OF FREEDOM ASSOCIATED WITH SSDR
C               ANS(9)  MEAN SQUARE OF SSDR
C               ANS(10) F-VALUE
C
C     REMARKS
C        N MUST BE GREATER THAN K+1.
C
C     SUBROUTINES AND FUNCTION SUBPROGRAMS REQUIRED
C        NONE
C
C     METHOD
C        THE GAUSS-JORDAN METHOD IS USED IN THE SOLUTION OF THE
C        NORMAL EQUATIONS. REFER TO W.W. COOLEY AND P.R. LOHNES,
```

```
C       "MULTIVARIATE PROCEEDURES FOR THE BEHAVIORAL SCIENCES",
C       JOHN WILEY AND SONS, 1962, CHAPTER 3, AND 8. OSTLE,
C       "STATISTICS IN RESEARCH", THE IOWA STATE COLLEGE PRESS,
C       1954, CHAPTER 8.
C
C       ..................................................
C
        SUBROUTINE MULTR(N,K,XBAR,STD,D,RX,RY,ISAVE,B,SB,T,ANS)
        DIMENSION XBAR(10),STD(10),D(10),RX(100),RY(10)
     X  ,ISAVE(10),B(10),
     X            SB(10),T(10),ANS(10)
C
C       ..................................................
C
C       IF A DOUBLE PRECISION VERSION OF THIS ROUTINE IS DESIRED
C       , THE C IN COLUMN 1 SHOULD BE REMOVED FROM THE DOUBLE
C       PRECISION STATEMENT WHICH FOLLOWS.
C
        DOUBLE PRECISION XBAR,STD,D,RX,RY,B,SB,T,ANS,RM,BO,SSAR,
     X                   SSDR,SY,FN,FK,SSARM,SSDRM,F
C
C       THE C MUST ALSO BE REMOVED FROM DOUBLE PRECISION STATE-
C       MENTS APPEARING IN OTHER ROUTINES USED IN CONJUCTION WITH
C       THIS ROUTINE.
C
C       THE DOUBLE PRECISION VERSION OF THIS SUBROUTINE MUST ALSO
C       CONTAIN DOUBLE PRECISION FORTRAN FUNCTIONS, SQRT AND ABS
C       IN STATEMENTS 122,125,AND135 MUST BE CHANGED TO DSQRT AND
C       DABS.
C
C       ..................................................
C
        MM=K+1
C
C       BETA WEIGHTS
C
        DO 100 J=1,K
100     B(J)=0.0
        DO 110 J=1,K
        L1=K*(J-1)
        DO 110 I=1,K
        L=L1+I
110     B(J)=B(J)+RY(I)*RX(L)
        RM=0.0
        BO=0.0
        L1=ISAVE(MM)
C
C       COEFFICIENT OF DETERMINATION
C
        DO 120 I=1,K
        RM=RM+B(I)*RY(I)
C
C       REGRESSION COEFFICIENTS
C
        L=ISAVE(I)
        B(I)=B(I)*(STD(L1)/STD(L))
C
C       INTERCEPT
C
120     BO=BO+B(I)*XBAR(L)
        BO=XBAR(L1)-BO
C
C       SUM OF SQUARES ATTRIBUTABLE TO REGRESSION
C
        SSAR=RM*D(L1)
C
```

```
C       MULTIPLE CORRELATION COEFFICIENT
C
C122
        RM=DSQRT(DABS(RM))
C
C       SUM OF SQUARES OF DEVIATIONS FROM REGRESSION
C
        SSDR=D(L1)-SSAR
C
C       VARIANCE OF ESTIMATE
C
        FN=N-K-1
        SY=SSDR/FN
C
C       STANDARD DEVIATIONS OF REGRESSION COEFFICIENTS
C
        DO 130 J=1,K
        L1=K*(J-1)+J
        L=ISAVE(J)
C125
        SB(J)=DSQRT(DABS((RX(L1)/D(L))*SY))
C
C       COMPUTED T-VALUES
C
130     T(J)=B(J)/SB(J)
C
C       STANDARD ERROR OF ESTIMATE
C
C135
        SY=DSQRT(DABS(SY))
C
C       F VALUE
C
        FK=K
        SSARM=SSAR/FK
        SSDRM=SSDR/FN
        F=SSARM/SSDRM
C
        ANS(1)=BO
        ANS(2)=RM
        ANS(3)=SY
        ANS(4)=SSAR
        ANS(5)=FK
        ANS(6)=SSARM
        ANS(7)=SSDR
        ANS(8)=FN
        ANS(9)=SSDRM
        ANS(10)=F
        RETURN
        END
```

Appendix C.6 Listing of the Data File Defanning Program - TCNDEFAN

Purpose

To take the fan beam transmission data and rebin it into sets of parallel-ray data.

Program Name	Function
Main Program:	
TCNDEFAN	- to coordinate the defanning process.
Subprograms:	
TCFACC	- to check the name format.
FILNAM	- to open a new name file.
NAMMAK	- to create a new ASCII name.
FORT.LB	- FORTRAN IV mathematics library.

Main Program TCNDEFAN:

```
      DIMENSION MATRIX(256,50),LINE(256),ISHFT(256),WGT(256)
      INTEGER TABLE(256),FNAME(10)
C100  FORMAT(S15)
      DO 99 I=1,256
99    LINE(I)=0
      CALL FILNAM(FNAME)
      CALL NAMMAK(FNAME,"AL")
      CALL FOPEN(5,FNAME,512)
      CALL RDBLK(5,1,LINE,1,IER)
      IF(IER.NE.1)GO TO 900
      NSAMP=LINE(1)
      TYPE"NSAMP=",NSAMP
      NVIEW=LINE(2)
      TYPE"NVIEW=",NVIEW
      NFETH=LINE(3)
      CALL NAMMAK(FNAME,"RF")
      CALL FOPEN(3,FNAME,512)
      IF(NFETH.EQ.0)GO TO 10
C BEGIN FEATHERING
      TYPE "FEATHERING"
      CALL NAMMAK(FNAME,"SC")
      CALL FOPEN(2,"RAWDATA",512)
      DELTA=1./(NFETH+1.)
      IST=1
      ITOT=0
1     IRD=20
      IF((ITOT+20).GT.NFETH)IRD=NFETH-ITOT
      IST2=IST+NVIEW
      CALL RDBLK(3,IST,MATRIX(1,1),IRD,IER)
      IF(IER.NE.1)GO TO 900
      CALL RDBLK(3,IST2,MATRIX(1,21),IRD,IER)
      IF(IER.NE.1)GO TO 900
      DO 2 I=1,IRD
      ITOT=ITOT+1
      WT=ITOT*DELTA
      I2=I+20
      WT2=1.-WT
      DO 2 K=1,NSAMP
2     MATRIX(K,I)=IFIX(WT*MATRIX(K,I)+WT2*MATRIX(K,I2)+0.5)
      CALL WRBLK(2,IST,MATRIX(1,1),IRD,IER)
      IF(IER.NE.1)GO TO 900
      IF(ITOT.EQ.NFETH)GO TO 10
      IST=IST+IRD
      GO TO 1
C FINISHED FEATHERING--BEGIN DEFANNING
C COMPUTE TABLE
10    TYPE "COMPUTING TABLE"
      DELTH=6.28319/NVIEW
C     CONSTANTS CHANGED FOR NEW DETECTOR 8/31/77 TEW
C     FID2=3969.
C     FUDGE=0.09785*NSAMP+0.048925
      FID2=24.75**2
      FUDGE=(.069341)*NSAMP**.5+.069341*.25
      DO 3 I=1,NSAMP
C     D=0.1957*I-FUDGE
      D=.069341*I-FUDGE
      X=D/(SQRT(FID2-D*D))
      THETA=ATAN(X)
      X=THETA/DELTH
      TABLE(I)=IFIX(X+0.5)
      IF(X.LT.0.0)TABLE(I)=IFIX(X-0.5)
      XX=FLOAT(TABLE(I))-X
```

```
        IF(XX.LT.0.00)GO TO 1704
        ISHFT(I)=0
        WGT(I)=XX
        GO TO 1705
1704    ISHFT(I)=-1
        WGT(I)=1+XX
1705    CONTINUE
3       CONTINUE
C NOW DEFAN AND NORMALIZE
        TYPE "DEFANNING"
        NL=TABLE(1)
        NF=TABLE(NSAMP)
        NCOR=NF-NL+1
        IF(NCOR.LE.50)GO TO 60
        TYPE "ERROR-NCOR TOO LARGE"
        CALL RESET
        STOP
60      CALL NAMMAK(FNAME,"SK")
C       CALL FOPEN(4,FNAME,512)
        CALL FOPEN(4,"DPOF:RAWDATA",512)
        NREC=-NF+NL
        NOUT=NREC
        NTOT=NVIEW+NCOR-1
        KK=-NF
        DO 90 N=1,NTOT
        TYPE N
        KK=KK+1
        NN=N
        IF(NN.GT.NVIEW)NN=NN-NVIEW
        NREC=NREC+1
        NOUT=NOUT+1
        IF(NOUT.GT.NCOR)NOUT=NOUT-NCOR
        ICH=3
        IF(NN.LE.NFETH)ICH=2
        CALL RDBLK(ICH,NN,LINE,1,IER)
        IF(IER.NE.1)GO TO 900
        DO 91 I=1,NSAMP
        K=KK+TABLE(I)
        IF(K.LE.0)GO TO 91
        GO TO 201
200     K=K-NCOR
201     IF(K.GT.NCOR)GO TO 200
        MATRIX(I,K)=LINE(I)
91      CONTINUE
        IF(NOUT.LE.0)GO TO 90
        CALL WRBLK(4,NREC,MATRIX(1,NOUT),1,IER)
        IF(IER.NE.1)GO TO 900
90      CONTINUE
        IF(NFETH.EQ.0)GO TO 50
        CALL CLOSE(2,IER)
        IF(IER.NE.1)GO TO 900
50      CALL CLOSE(3,IER)
        IF(IER.NE.1)GO TO 900
        CALL CLOSE(5,IER)
        IF(IER.NE.1)GO TO 900
C INTERPOLATING OUT ANGULAR ERRORS
        TYPE "INTERPOLATING IN ANGLE "
        ID0=3
        ID1=1
        ID2=2
        CALL NAMMAK(FNAME,"SS")
        CALL FOPEN(5,FNAME,512)
        CALL RDBLK(4,NVIEW,MATRIX(1,1),1,IER)
        IF(IER.NE.1)GO TO 900
        CALL RDBLK(4,1,MATRIX(1,2),1,IER)
        IF(IER.NE.1)GO TO 900
```

```
        DO 1700 N=1,NVIEW
        ID3=ID0
        ID0=ID1
        ID1=ID2
        ID2=ID3
        KIN=N+1
        IF(KIN.GT.NVIEW)KIN=1
        CALL RDBLK(4,KIN,MATRIX(1,ID2),1,IER)
        IF(IER.NE.1)GO TO 900
        DO 1701 I=1,NSAMP
        IF(ISHFT(I).EQ.0)GO TO 1702
        IF(ISHFT(I).NE.(-1))TYPE "ERROR"
        IDIF=MATRIX(I,ID1)-MATRIX(I,ID0)
        X=MATRIX(I,ID0)+WGT(I)*IDIF
        GO TO 1703
1702    IDIF=MATRIX(I,ID2)-MATRIX(I,ID1)
        X=MATRIX(I,ID1)+WGT(I)*IDIF
1703    MATRIX(I,4)=IFIX(X+0.5)
        IF(X.LT.0.00)MATRIX(I,4)=IFIX(X-0.5)
1701    CONTINUE
        CALL WRBLK(5,N,MATRIX(1,4),1,IER)
        IF(IER.NE.1)GO TO 900
1700    CONTINUE
        CALL CLOSE(5,IER)
        IF(IER.NE.1)GO TO 900
        CALL CLOSE(4,IER)
        IF(IER.NE.1)GO TO 900
        CALL FOPEN(4,FNAME,512)
C END OF DEFANNING-BEGIN INTERLACING
        TYPE "INTERLACING"
        NHALF=NVIEW/2
        TYPE NVIEW,NHALF
        CALL NAMMAK(FNAME,"OT")
        CALL FOPEN(5,FNAME,512)
        DO 55 K=21,40
        DO 55 I=1,256
55      MATRIX(I,K)=0
        IFLAG=0
        ITOT=0
        ISTW=1
        IF(NF.EQ.0)GO TO 554
        NMAX=NF
        NADD=-NHALF
        ISTR=NVIEW-NF+1
51      IRD=10
        ISTR2=ISTR+NADD
        IF((ITOT+10).GT.NMAX)IRD=NMAX-ITOT
        NCHECK=2*NSAMP+1
        ITOT=ITOT+IRD
        IWR=2*IRD
        TYPE IRD,ISTR,ISTW,ISTR2,IWR
        CALL RDBLK(4,ISTR,MATRIX(1,1),IRD,IER)
        IF(IER.NE.1)GO TO 900
        CALL RDBLK(4,ISTR2,MATRIX(1,11),IRD,IER)
        IF(IER.NE.1)GO TO 900
        DO 52 I=1,IRD
        I10=I+10
        I1=19+2*I
        DO 53 K=1,NSAMP
        KE=2*K
        KO=NCHECK-2*K
        MATRIX(KE,I1)=MATRIX(K,I)
53      MATRIX(KO,I1)=MATRIX(K,I10)
52      CONTINUE
        CALL WRBLK(5,ISTW,MATRIX(1,21),IWR,IER)
        IF(IER.NE.1)GO TO 900
```

```
        ISTW=ISTW+IWR
        IF(ITOT.EQ.NMAX)GO TO 554
        ISTR=ISTR+IRD
        GO TO 51
554     IF(IFLAG.EQ.1)GO TO 54
        IFLAG=1
        ISTR=1
        NADD=NHALF
        NMAX=NHALF
        GO TO 51
C FINISHED INTERLAING
54      CALL CLOSE(5,IER)
        IF(IER.NE.1)GO TO 900
        CALL CLOSE(4,IER)
        IF(IER.NE.1)GO TO 900
        CALL RESET
        CALL NAMMAK(FNAME,"SK")
        CALL DELETE(FNAME)
        CALL NAMMAK(FNAME,"SS")
        CALL DELETE(FNAME)
        CALL NAMMAK(FNAME,"RF")
        CALL DELETE(FNAME)
C       CALL CHAIN("TCBRECON.SV")
        GOTO 901
900     TYPE "I/O ERROR ",IER
901     STOP
        END
```

Subroutine TCFACC:

See Appendix C.1.

Subroutine FILNAM:

See Appendix C.1.

Subroutine NAMMAK:

See Appendix C.1.

Appendix C.7 Listing of the Data Reconstruction Programs - TCBRECON

Purpose

To reconstruct an image from the line integral data set using the Hanning-weighted ramp-filter backprojection reconstruction method.

Program Name	Function
Main Program:	
TCBRECON	- to reconstruct an image from the transmission line integral data set.
Subprograms:	
FILNAM	- to open a new name file.
TCRSUFF	- to add a suffix to the file name.
RSTST	- to test the name of the reconstruction file with the new suffix.
TCFACC	- to check the name format.
MATFL	- to perform the backprojection operation of the reconstruction.
TOMO.LB	- tomography library.
CSP.LB	- computer special library.
FSYS.LB	- FORTRAN IV system library.
FORT.LB	- FORTRAN IV mathematics library.

Main Program TCBRECON:

```
        COMPILER NOSTACK
C       RECONSTRUCTION PROGRAM TO DO ARBITRARY SIZE MATRICES
        DIMENSION MAT(4096),D1(513),ICOS(2),ISIN(2),ISTRT(2)
        DOUBLE PRECISION THETA,DNPA,DV,DS,DC,DPI
0)      INTEGER G2(-1100:1100),G3(2,1005),G4(5000),FNAME(20),FNAME2(
        COMMON/RPARM/NANG,NA
C FIND PARAMETERS
        DPI=3.14159265358979D0
        PI=DPI
        NELT=1000       ;DEFINE ARRAY LENGTH
        MATMAX=64       ;MAXIMUM ARRAY SIZE IN ONE PASS
        CALL FOPEN(5,"DPOF:RAWDATA",512)
89      CONTINUE
        CALL FILNAM(FNAME)
        CALL NAMMAK(FNAME,"AL")
        CALL FOPEN(4,FNAME,512)
        CALL RDBLK(4,1,G4,1,IER)
        IF(IER.NE.1)TYPE "ERROR ON READ .AL-- ",IER
        NSAMP=G4(1)
        NVIEW=G4(2)
        CALL CLOSE(4,IER)
        IF(IER.NE.1)TYPE "ERROR ON CLOSE .AL-- ",IER
        NPT=2*NSAMP
        NANG=NVIEW/2
        CALL NAMMAK(FNAME,"OT")
        CALL FOPEN(3,FNAME,512)
        TYPE NPT,NANG
        CALL TCFACC("FILTER GAIN",XMULT,"F")
C CALCULATE RAMP FILTER
        NELTG=NELT+20
        DO 1 N=1,NELTG
        G2(-N)=0
1       G2(N)=0
        X1=-4*XMULT/(PI*PI)
        G2(0)=XMULT+0.5
        DO 2 N=1,NELTG,2
        XN=N
        G2(N)=X1/(XN*XN)-0.5
        IF(G2(N).NE.0)GO TO 2
        NXTNT=N
        GO TO 500
2       G2(-N)=G2(N)
500     TYPE "FIRST ZERO FILTER ELEMENT IS NO. ",NXTNT
        TYPE "FILTER MAXIMUM = ",G2(0)
        CALL TCFACC("MATRIX SIZE",MS,"I")
        IF(MS.LE.64) MS=64
        NLINE=MATMAX**2/MS
        TYPE "NUMBER OF LINES/MATRIX = ",NLINE
        MATELT=NLINE*MS
        NMAT=MS/NLINE
        IF(NMAT*NLINE.NE.MS) NMAT=NMAT+1
        TYPE "NUMBER OF INTERMEDIATE MATRICES = ",NMAT
        DMS2=(MS-1.)/2
        NBLK=MATMAX**2/256
C       ACCEPT "CENTER OF RECONSTRUCTION MATRIX-X,Y ",MX,MY
        MX=0
        MY=0
C       ACCEPT "ZOOM FACTOR ",ZOOM
        ZOOM=2.5
        CALL TCFACC("FILTERED DATA GAIN",FDGAIN,"F")
        DNPA=3.14159265358979D0/DFLOAT(NANG)
        TYPE "GAINS : ",XMULT,ZOOM,FDGAIN
```

```
        NDSTRT=2
        NDEND=NPT+1
        THETA=-DNPA
C ZEROING RECONSTRUCTION MATRIX
        DO 600 J=1,MATELT
600     MAT(J)=0
        DO 610 J=1,NMAT
        CALL WRBLK(5,NBLK*(J-1),MAT,NBLK,IER)
        IF(IER.NE.1)TYPE "ERROR ON CLEAR ",IER
610     CONTINUE
C BEGIN RECONSTRUCTION
        DO 90 NA=1,NANG
        THETA=THETA+DNPA
        DS=DSIN(THETA)
        DC=DCOS(THETA)
        CA=DC
        SA=DS
C READ IN DATA SHIFTED TO THE RIGHT
        DO 501 NP=1,1000
501     G4(NP)=0
        IRD=2*NA-1
        CALL RDBLK(3,IRD,G4(2),2,IER)
        IF(IER.NE.1)TYPE "ERROR ON READ-- ",IRD,IER
C CALCULATE PARAMETERS FOR CONVOLUTION
        CNT=MX*CA-MY*SA+(NPT+3)/2
        TMP=ZOOM*DMS2*(ABS(CA)+ABS(SA))
        NENDO=CNT+TMP+3
        NBEGO=CNT-TMP-2
        NP2=NPT+2
        IF(NENDO.GT.NP2)NENDO=NP2
        IF(NBEGO.LT.1)NBEGO=1
        CALL CONV(G4,G2(0),NDSTRT,NDEND,NBEGO,NENDO,2,G3)
C CONVERT FILTERED DATA TO REALS
        DO 31 I=NBEGO,NENDO
        CALL DWFL(G3(1,I),DV)
31      D1(I)=DV
C HANNING WEIGHTING,GAIN,SHIFT,AND LOCATE MIN
        KEND=NENDO-2
        XMIN=0.
        DO 32 I=NBEGO,KEND
        D1(I)=FDGAIN*(D1(I)+2.*D1(I+1)+D1(I+2))
32      XMIN=AMIN1(XMIN,D1(I))
        MIN=1-XMIN
        XMIN=MIN+0.5
C COMPENSATE FOR NEG'S,INTERPOLATE,CONVERT TO INTGRS,AND DECOMPENSAT
        K=0
        KEN=KEND-1
        DO 34 I=NBEGO,KEN
        K=K+1
        G4(K)=D1(I)+XMIN
        G4(K)=G4(K)-MIN
        DIF=(D1(I+1)-D1(I))/10.
        G=D1(I)+XMIN
        DO 35 J=1,9
        G=G+DIF
        K=K+1
        G4(K)=G
35      G4(K)=G4(K)-MIN
34      CONTINUE
        NPROJ=K+1
        G4(NPROJ)=D1(KEND)+XMIN
        G4(NPROJ)=G4(NPROJ)-MIN
C CALCULATE BACKPROJECTION PARAMETERS
        CALL FLOW(ZOOM*DC*655360.0D0,ICOS)
        CALL FLOW(-ZOOM*DS*655360.0D0,ISIN)
        NCENT=5*NPT-10*NBEGO+6
```

```
        DV=((DBLE(MX-DMS2)*DC)-(DBLE(MY-DMS2)*DS))*10.000
        DV=NCENT+ZOOM*DV-0.500
        DVV=DV
        CALL FLOW(DV*65536.000,ISTRT)
        DO 80 JMAT=1,NMAT
        IER=1
        IF(NMAT.NE.1) CALL RDBLK(5,NBLK*(JMAT-1),MAT,NBLK,IER)
        CALL MATFL(MAT,G4(1),ICOS,ISIN,ISTRT,MS,NLINE,NPROJ)
        IF(NMAT.NE.1) CALL WRBLK(5,NBLK*(JMAT-1),MAT,NBLK,IER)
        IF(IER.NE.1) TYPE "ERROR ON INTERMEDIATE WRITE ",IER
80      CONTINUE
        TYPE NA
90      CONTINUE
        TYPE "DONE"
        CALL CLOSE(3,IER)
        IF(IER.NE.1)TYPE "ERROR ON CLOSE .OT-- ",IER
        JMAX=MAT(1)
        JMIN=MAT(1)
        DO 91 JMAT=1,NMAT
        IF(NMAT.NE.1) CALL RDBLK(5,NBLK*(JMAT-1),MAT,NBLK,IER)
        DO 91 J=1,MATELT
        JMAX=MAX0(JMAX,MAT(J))
91      JMIN=MIN0(JMIN,MAT(J))
        TYPE "RANGE OF RECONSTRUCTED VALUES: ",JMIN," TO ",JMAX
        ISUFF=2HDO
        CALL TCRSUFF(FNAME,ISUFF)
        CALL FOPEN(3,"RECON.FN")
        WRITE(3,10001) FNAME(1)
        CALL CLOSE(3,IER)
        WRITE(10,10001) FNAME(1)
10001   FORMAT(1X,S30)
        CALL FOPEN(3,FNAME)
        WRITE BINARY(3)MS,MS,JMAX,JMIN
        DO 95 JMAT=1,NMAT
        IF(NMAT.NE.1) CALL RDBLK(5,NBLK*(JMAT-1),MAT,NBLK,IER)
        WRITE BINARY(3)(MAT(J),J=1,MATELT)
95      CONTINUE
        CALL FCLOS(3)
CDAVE: HARDWIRE A STOP HERE
        GOTO 97
C POSSIBLE TASKS:
C       S=STOP
C       A=ANOTHER RECONSTRUCTION
C       T=TYPE OUT A LINE
C       D=DISPLAY ON CRT
        TYPE "WHAT NOW? S=STOP,A=ANOTHER RECON,T=TYPE LINE,D=DISPLAY
102     FORMAT(A1)
93      READ(11,102)IANS
        IF(IANS.EQ.2HS )GO TO 99
        IF(IANS.EQ.2HA )GO TO 89
        IF(IANS.EQ.2HD )GO TO 97
        TYPE "WHAT?"
        GO TO 93
97      CONTINUE
        CALL RESET
C       CALL CHAIN("FILEDISP.SV")
99      STOP
        END
```

Subroutine FILNAM:

See Appendix C.1.

Subroutine TCRSUFF:

```
        SUBROUTINE TCRSUFF(FNAME,JSUFF)
        INTEGER FNAME(20)
        INTEGER ISUF2(5)
C       FIND FIRST AVAILABLE SUFFIX FOR FILE NAME
C       USE RENAME FOR TEST OF FILE EXISTENCE
        ISUF=JSUFF
        DO 100 JSUF=1,32
        IF(JSUF.GT.10.AND.JSUF.LT.18) GO TO 90
        CALL RSTST(FNAME,ISUF,IER)
        IF(IER.EQ.1) GO TO 200
90      ISUF=ISUF+1
100     CONTINUE
150     CONTINUE
        TYPE "VALID FILENAME NOT FOUND. ENTER NEW SUFFIX"
        READ(11,1102) ISUF2(1)
        ISUF=ISUF2(1)
160     CALL RSTST(FNAME,ISUF,IER)
        IF(IER.NE.1) GO TO 150
        RETURN
200     CONTINUE
CDAVE JUMP THE NEW SUFFIX QUESTION:
        GOTO 201
        TYPE "ENTER NEW SUFFIX OF C.R. TO USE THIS ONE"
        READ(11,1102) ISUF2(1)
        ISUF=ISUF2(1)
1102    FORMAT(S2)
        IF(ISUF.NE.32) GO TO 160
CDAVE A NEW STATEMENT:
201     CONTINUE
        RETURN
        END
```

Subroutine RSTST:

```
      SUBROUTINE RSTST(FNAME,ISUF,IER)
      INTEGER FNAME(20)
      CALL NAMMAK(FNAME,ISUF)
      CALL RENAME(FNAME,FNAME,IER)
      IF(IER.EQ.13) GO TO 200
      IF(IER.EQ.4) WRITE(10,1001) FNAME(1)
1001  FORMAT(1H ,S20," IS AN ILLEGAL NAME")
      IF(IER.EQ.12) WRITE(10,1002) FNAME(1)
1002  FORMAT(1H ,S20," EXISTS")
      IF(IER.NE.4.AND.IER.NE.12) WRITE(10,1003) FNAME(1),IER
1003  FORMAT(1H ,S20," EXISTS OR IS ILLEGAL. IER=",I4)
      IER=0
      RETURN
200   CONTINUE
      WRITE(10,1004) FNAME(1)
1004  FORMAT(1H ,S20," IS AVAILABLE")
      IER=1              ;OK
      RETURN
      END
```

Subroutine TCFACC:

See Appendix C.1.

Subroutine MATFL:

```
        .TITL   MATFL
        .ENT    MATFL
        .EXTD   .FRET,.CPYL
        .NOCON  1
        .MACRO  DWADD
        LDA     1,^3+1
        ADDZ    1,^2,SZC
        INC     ^1,^1
        LDA     1,^3
        ADD     1,^1
        %
        .MACRO  MOVE
MOVEI=0
        .DO     '^3'==''
        LDA     1,@^1,3         ;LOAD PARAMETER ^1
        STA     1,^2            ;STORE IN ^2
        .ENDC
        .DO     '^3'<>''
        XCH     1,2
        .DO     ^3
        LDA     2,^1,3          ;LOAD PARM ADDRESS
        LDA     2,MOVEI,2
        STA     2,^2+MOVEI
MOVEI=MOVEI+1
        .ENDC
        XCH     1,2
        .ENDC
        %
        .NREL
MAT=-167
G=MAT+1
CTHTA=G+1       ;COS THETA *2^16
STHTA=CTHTA+1   ;SIN THETA *2^16
XSTRT=STHTA+1
NCOLS=XSTRT+1
NROWS=NCOLS+1
NPROJ=NROWS+1
FS.=NPROJ+167+1

        FS.
MATFL:  JSR @.CPYL
        STA     3,STPTR
        MOVE    XSTRT,YBASE,2
        LDA     1,MAT,3
        STA     1,MLOC          ;STORE STARTING MATRIX LOCN
        LDA     1,G,3           ;STORE PROJECTION LOCATION
        STA     1,GADR
        MOVE    NPROJ,HLIM      ;SET COMPARE LIMITS
        DSZ     HLIM            ; TO 1 LESS THAN SPECIFIED
        MOVE    NROWS,YCNT
        MOVE    CTHTA,XDEL,2
        MOVE    STHTA,YDEL,2
        LDA     2,YBASE         ;LOAD INDEX
        LDA     0,YBASE+1
YLOOP:  LDA     3,STPTR         ;RESTORE POINTER
        MOVE    NCOLS,XCNT
XLOOP:  CLM     2,2
        0                       ;LOWER LIMIT
HLIM:   255.                    ;UPPER
        JMP     CYLP            ;EXIT LOOP IF OUT OF LIMITS
XLOAD:  ELDA    1,0,2
GADR=XLOAD+1
```

```
        LDA     3,@MLOC
        ADD     3,1
        STA     1,@MLOC
CYLP:   ISZ     MLOC
        DWADD   2,0,XDEL        ;INCREMENT PROJECTION POSN
        DSZ     XCNT
        JMP     XLOOP
        LDA     2,YBASE
        LDA     0,YBASE+1       ;LOAD TWO WORDS OF YBASE
        DWADD   2,0,YDEL        ;ADD DELTA Y TO BASE
        STA     2,YBASE         ; STORE RESULT
        STA     0,YBASE+1
        DSZ     YCNT
        JMP     YLOOP
        LDA     3,STPTR
        LDA     2,XSTRT,3
        LDA     0,YBASE
        STA     0,0,2
        LDA     0,YBASE+1
        STA     0,1,2
        JSR     @.FRET          ;RETURN
STPTR:  0
MLOC:   0
YBASE:  .BLK    2
XCNT:   0
YCNT:   0
XDEL:   .BLK    2
YDEL:   .BLK    2
.END
```

Appendix C.8 Listing of the Reconstructed-Image Display Programs - FILEDISP

Purpose

To display the reconstructed data file on the CRT Lexidata display.

Program Name	Function
Main Program:	
FILEDISP	- to coordinate the subprograms which read out and display the reconstructed image on the CRT.
Subprograms:	
EXP64	- to expand a 64x64 matrix into a 128x128 matrix.
EXLINE	- to expand a 64x64 matrix into a 128x128 matrix.
INTLI	- to perform in-line interpolation.
EMINORM	- to normalize a display buffer into a standard EMI number format.
BLKIO	- to perform a fast binary read/write of a block of data.
IERCH	- to note an error in the data blocks.
BLMOVE	- to move the zero in a buffer block.
CLEAR	- to clear a buffer to zero.
NAMMAK	- to create a new ASCII name.
BITSE	- to set a bit on a word.
DISP	- to display the matrix value at the proper grey level on the CRT.
LEXPA	- to display the reconstructed matrix by performing an infinite DO loop of the display process.
ALLEX	- to convert alpha characters to packed Lexidata format and put in display buffer.
WDPACK	- to pack the display buffer using temporary fill area.

WPLOAD - to load WCS with a pack instruction.

WTLOAD - to load WCS with a table look-up instruction.

SWCODE

SWTCH

WCLOAD

FORT.LB - FORTRAN IV mathematics library.

Main Program FILEDISP:

```
        DIMENSION IFNAME(20)
        DIMENSION IB(128,128),IP(40,160)
        DIMENSION IA(40)
100     TYPE "FILENAME?"
        CALL RESET
        READ(11,1101) IFNAME(1)
1101    FORMAT(S30)
        IF(IFNAME(1).NE.32) GO TO 30
        CALL FOPEN(3,"RECON.FN")
        READ(3,1101,END=9000,ERR=9000) IFNAME(1)
        CALL FCLOS(3)
30      CONTINUE
        WRITE(10,1102) IFNAME(1)
1102    FORMAT(1H ,S30)
        CALL FOPEN(1,IFNAME)
C       READ BINARY(1,END=9000,ERR=9000) MS1,MS2,JMAX,JMIN
        LEN=6400
        LUN=1
        IREAD=1
        INIT=0
        CALL BLKIO(LUN,IP,LEN,IFIN,ILIN,JBIN,IA,4,INIT)
        CALL BLKIO(LUN,IP,LEN,IFIN,ILIN,JBIN,IA,4,IREAD)
        MS1=IA(1)
        MS2=IA(2)
        JMAX=IA(3)
        JMIN=IA(4)
        CALL NAMMAK(IFNAME,"AL")
        CALL FOPEN(2,IFNAME,512)
        CALL CLEAR(IB,100)
        CALL RDBLK(2,1,IB,1,IER)
        IF(IER.NE.1) TYPE "ERROR ",IER," ON .AL FILE"
        CALL FCLOS(2)
        DO 35 J=1,40
35      IA(J)=IB(J+10,1)
        TYPE "SIZE IS ",MS1,MS2,JMAX,JMIN
62)     READ BINARY(1,END=9000,ERR=9000) ((IB(J1,J2),J1=1,MS1),J2=1,
        DO 50 J2=1,MS2
        CALL BLKIO(LUN,IP,LEN,IFIN,ILIN,JBIN,IB(1,J2),MS1,IREAD)
50      CONTINUE
        IF(MS1.EQ.64) CALL EXP64(IB)
        ACCEPT "WATER= ",WATER
        IF(WATER.LT.1E-10) GO TO 1000
C       DO 40 JX=1,128
C       DO 40 JY=1,128
C       IB(JX,JY)=(IB(JX,JY)-WATER)*1000./WATER+.5
C40     CONTINUE
        CALL EMINORM(IB,IFIX(WATER) )
        JMAX=(JMAX-WATER)*1000./WATER+.5
        JMIN=(JMIN-WATER)*1000./WATER+.5
        TYPE "RANGE IS NOW ",JMAX," TO ",JMIN
1000    CONTINUE
        ACCEPT "MAX,MIN ? ",MAX,MIN
        IF(MAX.EQ.0.AND.MIN.EQ.0) GO TO 9050
        IF(MAX.EQ.-1.AND.MIN.EQ.-1) GO TO 2000
        CALL LEXPA(IB,IP,MAX,MIN,IA)
        GO TO 1000
9000    CONTINUE
        TYPE "CANNOT READ FILE"
        WRITE (10,1001) IFNAME(1)
1001    FORMAT(1X,S20)
9050    CONTINUE
        GO TO 100
2000    CONTINUE
        TYPE "STANDARD DEVIATION NOT IMPLEMENTED"
```

```
C       CALL SQMAT(IB,IP)
        GO TO 1000
        END
```

Subroutine EXP64:

```
      SUBROUTINE EXP64(IB)
C     SUBROUTINE TO EXPAND 64 BY 64 TO 128 BY 128
      DIMENSION IB(128,128)
      TYPE "EXPANDING"
      DO 100 JBACK=1,64
      JLINE=65-JBACK
      JL2=2*JLINE-1
C     EXPAND INTO MATRIX FROM BACK TO FRONT
      CALL BLMOVE(IB(1,JLINE+1),IB(65,JLINE),64)
      CALL EXLINE(IB(1,JLINE),IB(1,JL2))
100   CONTINUE
      RETURN
      END
```

Subroutine EXLINE:

```
      SUBROUTINE EXLINE(IB,IB2)
C     SUBROUTINE TO EXPAND 64 BY 64 TO 128 BY 128
      DIMENSION IB(130),IB2(256)
C     INTLI(K1,K2,K3,K4)=(4.5+K1+K1+K1+K1+K2+K2+K3+K3+K4)/9.
      DO 100 J=1,64
      LP1=IB(J)
      LP2=IB(J+64)
      LP3=IB(J+1)
      IF(J.EQ.64) LP3=0
      LP4=IB(J+65)
      IF(J.EQ.64) LP4=0
      J2=J+J-1
      IB2(J2)=INTLI(LP1,LP2,LP3,LP4)
      IB2(J2+128)=INTLI(LP2,LP1,LP4,LP3)
      IB2(J2+1)=INTLI(LP3,LP1,LP4,LP2)
      IB2(J2+129)=INTLI(LP4,LP2,LP3,LP1)
100   CONTINUE
      RETURN
      END
```

Subroutine INTLI:

```
        .TITL   INTLI
;       ROUTINE TO PERFORM IN LINE INTERPOLATION
        .NREL
        .EXTD   .CPYL,.FRET
        .ENT    INTLI
FVAL=-167
K1=FVAL+1
K2=K1+1
K3=K2+1
K4=K3+1
.FS=K4+167+1
        .FS
INTLI:  JSR     @.CPYL
        STA     3,CPYL3
        SUB     0,0
        SUB     1,1
        LDA     2,@K1,3
        JSR     DADD
        JSR     DADD
        JSR     DADD
        JSR     DADD
        LDA     2,@K2,3
        JSR     DADD
        JSR     DADD
        LDA     2,@K3,3
        JSR     DADD
        JSR     DADD
        LDA     2,@K4,3
        JSR     DADD
        ELEF    2,4,0
        JSR     DADD            ;ROUND
        ELEF    2,9.,0          ;SET UP DIVIDE
        DIVS
        STA     1,@FVAL,3
        JSR     @.FRET
DADD:   STA     3,DADD3
        MOV     2,3             ;SET UP REGS IN STANDARD DW FORMAT
        SUB     2,2
        MOVL#   3,3,SZC
        COM     2,2             ;HIGH ORDER NEG IF LOW ORDER IS
        ADDZ    3,1,SZC
        INC     0,0
        ADD     2,0
        MOV     3,2
        LDA     3,CPYL3         ;RESTORE IN CASE ANOTHER REF
        JMP     @DADD3
DADD3:  0
CPYL3:  0
        .END
```

Subroutine EMINORM:

```
        .TITL   EMINORM
;       ROUTINE TO NORMALIZE DISPLAY BUFFER TO A STANDARD EMI NUMBER
        .NREL
        .EXTD   .FRET,.CPYL
        .ENT    EMINORM
IB=-167
IW=IB+1
.FS=IW+167+1
        .FS
EMINORM: JSR    @.CPYL
        LDA     0,@IW,3
        STA     0,WATER
        LDA     0,IB,3          ;STORE BUFFER ADDRESS
        STA     0,BUFAD
        ELEF    0,128.*128.,0
        STA     0,NPTS
NLOOP:  LDA     1,@BUFAD
        LDA     2,WATER
        SUB     2,1
        SUB     0,0
        ELEF    2,1000.,0
        MULS
        LDA     2,WATER
        DIVS
        STA     1,@BUFAD
        ISZ     BUFAD
        DSZ     NPTS
        JMP     NLOOP
        JSR     @.FRET
WATER:  0
BUFAD:  0
NPTS:   0
        .END
```

Subroutine BLKIO:

```
      SUBROUTINE BLKIO(LUN,IOBUF,LEN,IFIRST,ILAST,JBLOCK,
     X          IUBUF,LENU,IACT)
      DIMENSION IOBUF(LEN),IUBUF(LENU)
C     SUBROUTINE TO DO BLOCK TRANSFER I/O AS A REPLACEMENT FOR
C     BINARY READ/WRITE
C
C     CODES--
C     IACT=-1          FLUSH OUTPUT BUFFER
C     IACT=0           INITIALIZE POINTERS (SHOULD BE FIRST CALL)
C     IACT=1           READ FROM CURRENT FILE POSITION TO IUBUF
C     IACT=2           WRITE "      "
C
C     SCRATCH BUFFER IOBUF IS USED TO HOLD BLOCKS FOR RDBLK/WRBLK
C
      IF(IACT.NE.-1) GO TO 200
C     FLUSH OUTPUT BUFFER
      IF(ILAST.LE.1) GO TO 100
      NBLK=1+(ILAST-2)/256
      CALL WRBLK(LUN,JBLOCK,IOBUF,NBLK,IER)
      CALL IERCH(IER,"ON BLOCK FLUSH")
      JBLOCK=JBLOCK+NBLK
100   ILAST=1
      RETURN
200   IF(IACT.NE.0) GO TO 300
C     INITIALIZE
      ILAST=1
      IFIRST=1
      JBLOCK=0
      RETURN
300   IF(IACT.NE.1) GO TO 400
C     READ
      JSTART=1
      JLEFT=LENU
C     COMPUTE AVAILABLE WORDS IN BUFFER
310   IF(IFIRST.LT.ILAST) GO TO 320
C     NONE, MUST READ SOME IN
      NBLK=LEN/256
      IF(NBLK.LE.0) GO TO 910
      CALL RDBLK(LUN,JBLOCK,IOBUF,NBLK,IER,IBLK)
      IF(IER.EQ.9) NBLK=IBLK
      IF(IER.NE.9)CALL IERCH(IER,"ON BLOCK READ")
      IF(IER.EQ.9.AND.IBLK.EQ.0) GO TO 920
      JBLOCK=JBLOCK+NBLK
      ILAST=NBLK*256+1
      IFIRST=1
320   NAVAIL=ILAST-IFIRST
      NTRAN=MINO(NAVAIL,JLEFT)
      CALL BLMOVE(IOBUF(IFIRST),IUBUF(JSTART),NTRAN)
      JSTART=JSTART+NTRAN
      IFIRST=IFIRST+NTRAN
      JLEFT=JLEFT-NTRAN
      IF(JLEFT.NE.0) GO TO 310
      RETURN
400   IF(IACT.NE.2) GO TO 900
C     WRITE BUFFER
      JSTART=1
      JLEFT=LENU
C     COMPUTE AVAILABLE SPACE TO FILL
      NBLK=LEN/256
      LEN2=256*NBLK
410   NAVAIL=LEN2+1-ILAST
      IF(NAVAIL.GT.0) GO TO 420
C     WRITE OUT BUFFER
      CALL WRBLK(LUN,JBLOCK,IOBUF,NBLK,IER)
```

```
      CALL IERCH(IER,"ON BLOCK WRITE")
      JBLOCK=JBLOCK+NBLK
      ILAST=1
420   NTRAN=MINO(NAVAIL,JLEFT)
      CALL BLMOVE(IUBUF(JSTART),IOBUF(ILAST),NTRAN)
      JSTART=JSTART+NTRAN
      ILAST=ILAST+NTRAN
      JLEFT=JLEFT-NTRAN
      IF(JLEFT.GT.0) GO TO 410
      RETURN
900   STOP BAD BLKIO ACTION CODE
910   STOP BAD BLOCK SIZE COMPUTED
920   STOP ATTEMPT TO READ PAST END OF FILE
      END
```

Subroutine IERCH:

```
      SUBROUTINE IERCH(IER,ISTR)
      DIMENSION ISTR(10)
      IF(IER.NE.1) WRITE(10,1001) IER,ISTR(1)
1001  FORMAT(" I/O ERROR ",I3,1X,S40)
      RETURN
      END
```

Subroutine BLMOVE:

```
        .TITL BLMOV
;       BLMOV BUFFER TO ZERO
        .ENT BLMOV
        .EXTD   .FRET,.CPYL
BUF=-167
BUF2=BUF+1
N=BUF2+1
.FS=N+167+1
        .NREL
        .FS
BLMOV:  JSR     @.CPYL
        LDA     1,@N,3          ;LOAD COUNT
        LDA     2,BUF,3         ;LOAD ADDRESS
        LDA     3,BUF2,3        ;ADR->3
        BLM                     ;MOVE THE ZERO
        JSR     @.FRET
        .END
```

Subroutine CLEAR:

See Appendix C.1.

Subroutine NAMMAK:

See Appendix C.1.

Subroutine BITSE:

```
        .TITL BITSE
        .ENT BITSE
        .EXTD   .CPYL,.FRET
BUF=-167
IX=BUF+1
IY=IX+1
IV=IY+1
FS.=IV+167+1
        .NREL
        FS.
BITSE:  JSR     @.CPYL
        LDA     0,BUF,3
        LDA     1,@IY,3
        MOVS    1,1
        LDA     2,@IX,3
        IOR     2,1
        MOV     1,2
        ANDI    17,2
        NEG     2,2
        ADDI    17,2
        ANDI    177760,1
        IOR     2,1
        LDA     2,@IV,3
        INC#    2,2,SNR         ;TEST FOR -1
        JMP     TEST            ;YES, GO TEST
        LDA     3,ZERBT
        MOV     2,2,SZR
        LDA     3,SETBT
        XCT     3
        JSR     @.FRET
SETBT:  BTO     0,1
ZERBT:  BTZ     0,1
TEST:   SUB     2,2
        SZB     0,1
        SUBZL   2,2
        STA     2,@IV,3
        JSR     @.FRET
        .END
```

Subroutine DISP:

```
        .TITL   DISP
        .EXTD   .CPYL,.FRET
        .EXTN   .UIEX
        .ENT    DISP
USTIT=411
BUFAD=-167
NLINE=BUFAD+1
IMODE=NLINE+1
FS.=IMODE+167+1
        .NREL
        FS.
DISP:   JSR     @.CPYL
        LDA     0,@IMODE,3
        STA     0,MODE
        LDA     0,@NLINE,3
        STA     0,NL
        STA     3,HOLD3
        LDA     0,ICALLD
        MOV     0,0,SZR         ;TEST FOR INIT
        JMP     NOINIT
        SUBZL   0,0
        STA     0,ICALLD        ;RESET POINTER
        LDA     0,DEVADR
        LDA     1,DCTADR
        LDA     2,NBLK
        .SYSTM
        .IDEF
        JMP     ERCALL
        LDA     0,DEVADR
        LDA     1,BUFAD,3
        .SYSTM
        .STMAP
        JMP     ERCALL
        STA     1,MAPBUF
NOINIT: NIOC    DISDEV
        .SYSTM          ;ENABLE INTERRUPTS
        .OEBL
        JMP     ERCALL
        ADC     0,0     ;-1 TO AC0
        ESTA    0,USTIT
        LDA     0,MODE
        MOV     0,0,SNR
        JMP     NODIS
        .SYSTM          ;DISABLE ^A INTERRUPT
        .ODIS
        JMP     ERCALL
        ELEF    0,CTRLA
        ESTA    0,USTIT
        ELEF    2,TABLE,0
DSPLP:  LDA     0,0,2
        MOV     0,0,SNR
        JMP     DONE
        DOA     0,DISDEV
        INC     2,2
        JMP     DSPLP
DONE:NODIS:     JSR     @.FRET
CTRLA:  NIOC    DISDEV
        .SYSTM
        .RTN
ERCALL: .SYSTM
        .ERTN
TABLE:  3
MAPBUF: 0
        4
```

```
NL:     320
MODE:   2
        0
DISDEV=60
HOLD3:  0
DEVADR: DISDEV
NBLK:   1+7
ICALLD: 0
SBIT:   100000
DCTADR: .+1+100000
        0
        -1
        ERCALL
        .END
```

Subroutine LEXPA:

```
      SUBROUTINE LEXPA(IB,IP,MAX,MIN,IA)
      DIMENSION IA(10,4)
      DIMENSION IBTEMP(256)
      DIMENSION IB(128,128),IP(40,160)
      CALL WPLOAD(IDUMMY)
      CALL WTLOAD(IDUMMY)
      CALL CLEAR(IP,40*160)
      CALL DISP(IP,159,2)
      ITITDIS=0
1000  CONTINUE
      IDGREY=0
      ISTEP=(MAX-MIN)/16.+.5
      CALL WDPACK(IB,IBTEMP,IP(1,16),MIN+ISTEP,ISTEP)
1100  CONTINUE
      CALL NEWMAX(MAX,MIN,NEW)
      IF(NEW.EQ.-1) GO TO 2000
      IF(NEW.EQ.1) GO TO 1000
      IF(IDGREY.EQ.1) GO TO 1100
      IDGREY=1
      DO 100 JG=1,16
      LEV=.01+MIN+(JG-1)/15.*(MAX-MIN)
      LINE=(16-JG)*8+17
      LEV2=IABS(LEV)
      DO 80 JDIG=1,4
      NUM=48+MOD(LEV2,10)
      IF(LEV2.NE.0) GO TO 60
      IF(JDIG.GT.1) NUM=0
      IF(LEV.LT.0) NUM=45
      LEV=IABS(LEV)
60    CONTINUE
      IF(LEV.GT.9999.OR.LEV.LT.-999) NUM=42
      LEV2=LEV2/10
      NUM=ISHFT(NUM,8)
      IGREY=1-JG
      IF(JG.LE.8) IGREY=JG-16
      CALL ALLEX(NUM,IP(1,LINE),21-JDIG,IGREY)
80    CONTINUE
      IF(JG.GE.9) GO TO 100
      LINE7=LINE+7
      DO 90 JL1=LINE,LINE7
      DO 90 JL2=33,40
      IP(JL2,JL1)=.NOT.IP(JL2,JL1)
90    CONTINUE
100   CONTINUE
      IF(ITITDIS.EQ.1) GO TO 1100
      ITITDIS=1
      DO 300 JA=1,20
      DO 300 JLINE=1,4
      JL=8*JLINE-7
      IF(JLINE.GT.2) JL=JL+128
      JC=(JA+1)/2
      JW=IA(JC,JLINE)
      IF(0.EQ.IAND(JA,1)) JW=ISHFT(JW,8)
      JW=IAND(JW,177400K)
      CALL ALLEX(JW,IP(1,JL),JA,15)
300   CONTINUE
      GO TO 1100
2000  CONTINUE
      CALL DISP(IP,0,0)
      RETURN
      END
```

Subroutine ALLEX:

```
        .TITL   ALLEX
;       CONVERT ALPHA CHARACTER TO PACKED LEXIDATA FORMAT AND PUT IN
;       DISPLAY BUFFER
;       CALL- CALL ALLEX(IALPH,IB,JX,IGREY)
;       ALPH- CHARACTER IN A1 (1H) FORMAT
;       IB- LINE OF BUFFER
;       JX- CHARACTER NUMBER IN BUFFER
;       IGREY- GREY LEVEL FOR CHARACTER
;              NEGATIVE=WHITE SURROUND
        .ENT ALLEX
        .EXTD   .CPYL,.FRET
IALPH=-167
IB=IALPH+1
JX=IB+1
IGREY=JX+1
FS.=IGREY+167+1
        .NREL
        FS.
ALLEX:  JSR     @.CPYL
        LDA     0,@JX,3
        SBI     1,0             ;CONVERT ONE INDEX TO ZERO
SS      XORI    1,0             ;TOGGLE LAST BIT TO CHANGE BYTE ADDR
        MOVZR   0,0
        MOVR    1,1     ;STORE CARRY
        ADDZL   0,0     ;SHIFT 2
        MOVL    1,1
        MOVL    0,0     ;RESTORE CARRY
        LDA     2,IB,3
        MOVZL   2,2
        ADD     0,2     ;COMPUTE BYTE POINTER
        LDA     0,@IGREY,3
        STA     0,GVAL
        MOVL#   0,0,SZC
        NEG     0,0
        STA     0,AGVAL
        LDA     1,@IALPH,3
        ANDI    77400,1
        MOVS    1,1
        ADDI    -30.,1
        MOVL#   1,1,SZC
        SUB     1,1
        ADDZL   1,1
        ADDI    CTAB,1
RN      MOVZL   1,1             ;FORM BYTE POINTER TO CHARACTER PATT
        STA     1,CPTR
        ELEF    1,8.            ;SET UP LOOP
        STA     1,NLINES
L1:     LDA     1,CPTR
        LDB     1,1             ;LOAD PATTERN
        MOVZL   1,1             ;SHIFT OVER ONE BIT
        LDA     3,GVAL          ;TEST WHITE SURROUND
        MOVL#   3,3,SZC
        COM     1,1
        LDA     0,AGVAL
        HXL     3,0
        ELEF    3,4
        STA     3,NGREY
        SUB     3,3
L2:     STB     2,1
        MOVL    0,0,SNC
        STB     2,3
        ADI     2,2
```

```
        DSZ     NGREY
        JMP     L2
        ADDI    72.,2
        ISZ     CPTR
        DSZ     NLINES
        JMP     L1
        JMP     @.FRET
GVAL:   0
CPTR:   0
AGVAL:  0
NLINES: 0
NGREY:  0
CTAB:       0   ;FUDGE
            0   ;FUDGE
            0   ;FUDGE
            0   ;FUDGE
         1004   ;ARROW
         7420   ;ARROW
         7404   ;ARROW
         1000   ;ARROW
            0   ;SPACE
            0   ;SPACE
            0   ;SPACE
            0   ;SPACE
         2004   ;!
         2004   ;!
         2000   ;!
         2000   ;!
         5012   ;"
            0   ;"
            0   ;"
            0   ;"
           12   ;#
        17412   ;#
        17412   ;#
            0   ;#
         7025   ;$
         2416   ;$
        12025   ;$
         7000   ;$
         1423   ;%
         4004   ;%
         1031   ;%
        14000   ;%
            2   ;&
         2402   ;&
        12411   ;&
        13000   ;&
         2004   ;'
            0   ;'
            0   ;'
            0   ;'
         4004   ;(
         1002   ;(
         1004   ;(
         4000   ;(
         1004   ;)
         4010   ;)
         4004   ;)
         1000   ;)
           25   ;*
         7037   ;*
         7025   ;*
            0   ;*
            4   ;+
        20377   ;+
```

```
 2004  ;+
    0  ;+
    0  ;,
    0  ;,
    4  ;,
 1000  ;,
    0  ;-
   37  ;-
    0  ;-
    0  ;-
    0  ;.
    0  ;.
    0  ;.
 2000  ;.
   20  ;/
 4004  ;/
 1001  ;/
    0  ;/
 7021  ;0
14425  ;0
11421  ;0
 7000  ;0
 2006  ;1
 2004  ;1
 2004  ;1
 2000  ;1
 7021  ;2
10014  ;2
 1001  ;2
17400  ;2
 7021  ;3
10014  ;3
10021  ;3
 7000  ;3
 4411  ;4
 4437  ;4
 4010  ;4
 4000  ;4
17401  ;5
  417  ;5
10021  ;5
 7000  ;5
 7021  ;6
  417  ;6
10421  ;6
 7000  ;6
17420  ;7
 4004  ;7
 1002  ;7
 1000  ;7
 7021  ;8
10416  ;8
10421  ;8
 7000  ;8
 7021  ;9
10436  ;9
10010  ;9
 3000  ;9
    0  ;:
    4  ;:
    0  ;:
 2000  ;:
    0  ;;
    4  ;;
    4  ;;
 1000  ;;
```

```
 4004  ;<
 1001  ;<
 1004  ;<
 4000  ;<
    0  ;=
17400  ;=
17400  ;=
    0  ;=
 1004  ;>
 4020  ;>
 4004  ;>
 1000  ;>
 7021  ;?
10010  ;?
 2000  ;?
 2000  ;?
   17  ;@
10026  ;@
12427  ;@
 4000  ;@
 2012  ;A
10421  ;A
17421  ;A
10400  ;A
 7421  ;B
10417  ;B
10421  ;B
 7400  ;B
 7021  ;C
  401  ;C
  421  ;C
 7000  ;C
 7421  ;D
10421  ;D
10421  ;D
 7400  ;D
17401  ;E
  417  ;E
  401  ;E
17400  ;E
17401  ;F
  417  ;F
  401  ;F
  400  ;F
 7021  ;G
  401  ;G
16421  ;G
 7000  ;G
10421  ;H
10437  ;H
10421  ;H
10400  ;H
 7004  ;I
 2004  ;I
 2004  ;I
 7000  ;I
10020  ;J
10020  ;J
10021  ;J
 7000  ;J
10411  ;K
 2403  ;K
 2411  ;K
10400  ;K
  401  ;L
  401  ;L
```

```
  401  ;L
17400  ;L
10433  ;M
12421  ;M
10421  ;M
10400  ;M
10421  ;N
11425  ;N
14421  ;N
10400  ;N
 7021  ;O
10421  ;O
10421  ;O
 7000  ;O
 7421  ;P
10417  ;P
  401  ;P
  400  ;P
 7021  ;Q
10421  ;Q
12411  ;Q
13000  ;Q
 7421  ;R
10417  ;R
 2411  ;R
10400  ;R
 7021  ;S
  416  ;S
10021  ;S
 7000  ;S
17404  ;T
 2004  ;T
 2004  ;T
 2000  ;T
10421  ;U
10421  ;U
10421  ;U
 7000  ;U
10421  ;V
10421  ;V
10412  ;V
 2000  ;V
10421  ;W
10421  ;W
12425  ;W
 5000  ;W
10421  ;X
 5004  ;X
 5021  ;X
10400  ;X
10421  ;Y
 5004  ;Y
 2004  ;Y
 2000  ;Y
17420  ;Z
 4004  ;Z
 1001  ;Z
17400  ;Z
 7002  ;[
 1002  ;[
 1002  ;[
 7000  ;[
    1  ;\
 1004  ;\
 4020  ;\
    0  ;\
```

```
 7010  ;]
 4010  ;]
 4010  ;]
 7000  ;]
 2016  ;^
12404  ;^
 2004  ;^
 2000  ;^
 4004  ;_
 1037  ;_
 1004  ;_
 4000  ;_
 1004  ;@
    0  ;@
    0  ;@
    0  ;@
    0  ;A
 7011  ;A
 4411  ;A
17000  ;A
  401  ;B
  407  ;B
 4411  ;B
 3400  ;B
    0  ;C
 3011  ;C
  411  ;C
 3000  ;C
 4010  ;D
 4016  ;D
 4411  ;D
 7000  ;D
    0  ;E
 7011  ;E
 3401  ;E
 7000  ;E
 2012  ;F
 1007  ;F
 1002  ;F
 1000  ;F
 3011  ;G
 4416  ;G
 4011  ;G
 3000  ;G
  401  ;H
  407  ;H
 4411  ;H
 4400  ;H
    2  ;I
    2  ;I
 1002  ;I
 3000  ;I
 2000  ;J
 2004  ;J
 2005  ;J
 1000  ;J
  401  ;K
 4405  ;K
 1405  ;K
 4400  ;K
 1002  ;L
 1002  ;L
 1002  ;L
 3000  ;L
    0  ;M
 5425  ;M
```

```
12425  ;M
12400  ;M
    0  ;N
 3411  ;N
 4411  ;N
 4400  ;N
    0  ;O
 3011  ;O
 4411  ;O
 3000  ;O
 3411  ;P
 4407  ;P
  401  ;P
  400  ;P
 7011  ;Q
 4416  ;Q
 4010  ;Q
14000  ;Q
    0  ;R
 3411  ;R
  401  ;R
  400  ;R
    0  ;S
 7001  ;S
 3010  ;S
 3400  ;S
    2  ;T
 3402  ;T
 1002  ;T
 6000  ;T
    0  ;U
 4411  ;U
 4411  ;U
 7000  ;U
    0  ;V
10421  ;V
10412  ;V
 2000  ;V
    0  ;W
10421  ;W
12433  ;W
10400  ;W
    0  ;X
10412  ;X
 2012  ;X
10400  ;X
 4411  ;Y
 4416  ;Y
 4010  ;Y
 3400  ;Y
    0  ;Z
17410  ;Z
 2002  ;Z
17400  ;Z
 4004  ;[
 2002  ;[
 2004  ;[
 4000  ;[
 2004  ;\
 2000  ;\
 2004  ;\
 2000  ;\
 1004  ;]
 2010  ;]
 2004  ;]
 1000  ;]
```

```
     0  ;^
 11015  ;^
     0  ;^
     0  ;^
 17437  ;RUBOUT
 17437  ;RUBOUT
 17437  ;RUBOUT
 17400  ;RUBOUT
.END
```

Subroutine WDPACK:

```
        .TITL   WDPACK
;       PROGRAM TO PACK DISPLAY BUFFER USING TEMPORARY FILL AREA
;       CALL -- CALL WDPACK(IB,IBTEMP,IP,ITHRESH,ISTEP)
;               IB -- DATA BUFFER (128 BY 127)
;               IBTEMP -- 128 WORD SCRATCH AREA
;               IP -- IMAGE MATRIX PORTION OF DISPLAY
;                       127 ROWS OF 32 DISPLAY WORDS, 8 SKIPPED WORD
;               ITHRESH -- THRESHOLD FOR GREY LEVEL 1
;               ISTEP -- VALUE OF EQUAL STEP BETWEEN LEVELS
        .NREL
        .ENT    WDPACK
        .EXTN   WCLOAD
        .EXTD   .CPYL,.FRET
;
WCPINS=2                        ;PACK INSTRUCTION NUMBER
;WCS PACK INSTRUCTION -- XOP1 0,0,2
;PACKS 16 INTENSITIES INTO FOUR WORDS
;ACCUMULATOR CONTENTS --
;AT END AC2 -- ADDRESS OF VECTOR OF 16 INTENSITIES. INCREMENTED BY 1
;               OF INSTR.
;       AC3 -- ADDRESS OF OUTPUT TABLE OF FOUR WORDS. UPDATED BY 4
;       AC0 -- ZERO BIT WORD OF INTENSITIES (SCRATCH)
;       AC1 -- ONE BIT (SCRATCH)
;
WCTINS=3        ;TABLE LOOK UP INSTRUCTION
;WCS TABLE LOOK UP INSTRUCTION -- XOP1 0,0,3
;       AC0 - THRESHOLD FOR LEV 1
;       AC1 - INCREMENT BETWEEN LEVELS
;       AC2 - FROM ADDR
;       AC3 - TO ADDR
;       PC+1 - NUMBER OF WORDS
;
IB=-167
IBTEMP=IB+1
IP=IBTEMP+1
ITHRESH=IP+1
ISTEP=ITHRESH+1
FS.=ISTEP+167+1
        FS.
WDPACK: JSR     @.CPYL
        STA     3,HOLD3
        LDA     0,IB,3
        STA     0,IBADR
        LDA     0,IBTEMP,3
        STA     0,IBTADR
        LDA     0,IP,3
        STA     0,IPADR
        LDA     0,@ITHRESH,3
        STA     0,THR
        LDA     0,@ISTEP,3
        STA     0,STEP
        ELEF    0,127.,0        ;SET UP 127 LINES OF DATA
        STA     0,NL0
L0:     LDA     2,IBADR         ;LOAD ADDRESSES AND CONS FOR TAB LOO
        LDA     3,IBTADR
        LDA     0,THR
        LDA     1,STEP
        XOP1    0,0,WCTINS      ;EXECUTE LOOK UP INSTR
        128.                    ;OF 128 WORDS
        STA     2,IBADR         ;STORE UPDATED INPUT ADDRESS
        ELEF    0,8.,0  ;SET UP LOOP OF 8. WORDS
        STA     0,NL1
```

```
        LDA     2,IBTADR
        LDA     3,IPADR
L1:     XOP1    0,0,WCPINS      ;EXECUTE PACK INSTR
        DSZ     NL1
        JMP     L1
        ADDI    8.,3            ;SKIP OVER 8 WORDS OF GREY SCALE
        STA     3,IPADR
        DSZ     NL0
        JMP     L0
        JSR     @.FRET          ;DONE, RETURN
IBADR:  0
IBTADR: 0
IPADR:  0
THR:    0
STEP:   0
PPTR:   0
INTPTR: 0
NL0:    0
NL1:    0
NL2:    0
P16:    16.
P4:     4.
HOLD3:  0
CALLED: 0
        .END
```

Subroutine WPLOAD:

```
        .TITL   WPLOAD
;       LOAD WCS WITH PACK INSTR
        .NREL
        .ENT    WPLOAD
        .EXTN   WCLOAD
        .EXTD   .CPYL,.FRET
;
WCLOC=.
WCINS=2                         ;INSTRUCTION NUMBER
WCORG=110                       ;LOCATION IN WCS OF CODE
;
;WCS PACK INSTRUCTION
;PACKS 16 INTENSITIES INTO FOUR WORDS
;ACCUMULATOR CONTENTS --
;AT END AC2 -- ADDRESS OF VECTOR OF 16 INTENSITIES. INCREMENTED BY 1
;               OF INSTR.
;       AC3 -- ADDRESS OF OUTPUT TABLE OF FOUR WORDS. UPDATED BY 4
;       AC0 -- ZERO BIT WORD OF INTENSITIES (SCRATCH)
;       AC1 -- ONE BIT (SCRATCH)
;       GR1 -- TWO BIT (SCRATCH)
;       GR2 -- THREE BIT (SCRATCH)
;       GR0 -- MEMORY IN REGISTER
;       GR3 -- PC
        .MACRO BITIN
        WG      AR,GR0,A,R0,L   ;SHIFT GR0 RIGHT
        WG      AR,^1,A,RL,L    ;SHIFT BIT INTO REGISTER
%
LWC:    WG      AR,AC2,A,S      ;START MEMORY READ W/ AC2
NTO GR0 WG      AR,AC2,A1,FA,L,READ     ;INCREMENT AC2 AND READ MEM
        BITIN   GR2
        BITIN   GR1
        BITIN   AC1
        BITIN   AC0
SIMPLICI@%      CNTND,T[LWC]            ;USE EXTRA LINE FOR LOOP FOR
        WG      AR,AC3,A,S              ;START MEMORY W/ AC3
ART MEM WG      AR,AC3,BAC0,A1,FA,L,S,WRIT,BMEM ;WRITE AC0,INC AC3 S
        WG      AR,AC3,BAC1,A1,FA,L,S,WRIT,BMEM
        WG      AR,AC3,BGR1,A1,FA,L,S,WRIT,BMEM
NEW AC3 WG      AR,AC3,BGR2,A1,FA,L,WRIT,BMEM   ;DONT START MEM WITH
        WG      AR,PC,A,F0,L,S          ;END INSTR
        WG      READ,LDIR,WFADR
WCEND=.
;
N=-167  ;DUMMY PARAMETER
FS.=N+167+1
        FS.
WPLOAD: JSR     @.CPYL
        EJSR    WCLOAD
        WCLOC
        WCEND
        WCORG
        WCINS
        JSR     @.FRET          ;DONE, RETURN
        .END
```

Subroutine WTLOAD:

```
        .TITL WTLOAD
;       LOAD WCS WITH TABLE LOOK UP INSTRUCTION
        .NREL
        .ENT WTLOAD
        .EXTN   WCLOAD
        .EXTD .FRET,.CPYL
;       DEFINE WCS INSTR
;       ACCUMULATORS --
;       AC0 - THRESHOLD FOR LEV 1
;       AC1 - INCREMENT BETWEEN LEVELS
;       AC2 - FROM ADDR
;       AC3 - TO ADDR
;       GR0 - MEMORY REG
;       GR1 - INTENSITY LEVEL
;       GR2 - WORD COUNT
;       GR3 - PC
WCLOC=.
WCINS=3                         ;INSTRUCTION NUMBER
WCORG=160                       ;LOCATION IN WCS OF CODE
        WG      AR,PC,A,F0,L,S  ;GET WORD COUNT
R PC    WG      AR,PC,BGR2,A1,F0,L,BMEM,READ    ;PUT INTO GR2 AND IN
WL1:    WG      AR,AC2,A,S              ;START MEMORY READ W/ AC2
        WG      AR,AC2,A1,FA,L,READ     ;READ TO GR0
        WG      AR,GR0,BAC0,AMB,FA,L    ;SUBTRACT THRESHOLD
        WG      Z,GR1,CA,FA,L,LCNT              ;-1->GR1,15->COUNT
ND2:    WG      AR,GR1,A1,FA,L,CNTND,T[WL21],F[WCL2]    ;INCR GR1,CN
WCHECK  WG      AR,GR0,BAC1,AMB,FA,L,AO,T[WCL2],F[WL2]  ;LOWER THRES
;                                       VALUE BEFORE.LOWERING
WCL2:   WG      AR,AC3,A,S              ;START MEM W/ AC3
        WG      AR,AC3,BGR1,A1,FA,L,WRIT,BMEM   ;WRITE AND INCR AC3
        WG      AR,GR2,AM1,FA,L,ALUZ,T[WEND],F[WL1]
WEND:   WG      AR,PC,A,F0,L,S
        WG      READ,LDIR,WFADR
WCEND=.
;
N=-167  ;DUMMY PARM
.FS=N+167+1
        .FS
WTLOAD: JSR     @.CPYL
        EJSR    WCLOAD
        WCLOC
        WCEND
        WCORG
        WCINS
        JMP .+1
        JSR     @.FRET
        .END
```

```
        .TITLE SWCODE
        .ENT    SWCODE
        .EXTN   WCLOAD
        .EXTD   .FRET,.CPYL
        .NREL
WCLOC=.
WCINS=1
WCORG=100
        WG      READ,CNIN
        WG      Z,ACS,BGRO,AOB,FA,L
        WG      AR,PC,A,FO,L,S
        WG      READ,LDIR,WFADR
WCEND=.
;
IVAL=-167
.FS=IVAL+167+1
        .FS
SWCODE: JSR     @.CPYL
        STA     3,HOLD3
        LDA     0,CALLED
        MOV     0,0,SZR
        JMP     NOLOAD
        SUBZL   0,0
        STA     0,CALLED
        EJSR    WCLOAD
        WCLOC
        WCEND
        WCORG
        WCINS
NOLOAD: XOP1    0,0,1
        LDA     3,HOLD3
        STA     0,@IVAL,3
        JMP     @.FRET
HOLD3:  0
CALLED: 0
        .END SWCODE
```

```
        .TITLE  SWTCH
;RETURN SWITCH SSETTINGS
        .EXTD   .FRET,.CPYL
        .ENT    SWTCH
IVAL=-167
.FS=1
        .NREL
        .FS
SWTCH:  JSR     @.CPYL
        READS   0
        STA     0,@IVAL,3
        JSR     @.FRET
        .END
```

```
        .TITL   WCLOAD
        .ENT    WCLOAD
        .NREL
WCS=1
;
WCLOAD: STA     3,HOLD3
        LDA     0,CALLED
        MOV     0,0,SZR
        JMP     NOCALL
        SUBZL   0,0
        STA     0,CALLED        ;FLAG SYSTEM ALREADY CALLED
        ELEF    WCS,0           ;NOW PUT WCS ADDRESS IN AC0
        ELEF    1,.     ;DUMMY TO AC1
        .SYSTM
        .IDEF
        JMP     .+1
NOCALL: LDA     3,HOLD3
        LDA     2,0,3   ;BUFFER LOCN
        LDA     1,1,3   ;LAST WORD
        SUB     2,1
        STA     1,COUNT
        LDA     0,2,3   ;LOAD BASE ADDRESS
        LDA     1,3,3   ;LOAD INSTRUCTION
        MOVZL   1,1     ;SHIFT LEFT
        DOA     1,WCS
        DOC     0,WCS
        ADDZL   0,0     ;SHIFT AC0 LEFT TWO
WCLD:   MOV     0,1     ;TEST OVERFLOW OF WCS
        ANDI    -1024.,1
        MOV     1,1,SZR
        JMP     LODERR
        DOA     0,WCS
        LDA     1,0,2
        DOB     1,WCS
        INC     0,0
        INC     2,2
        DSZ     COUNT
        JMP     WCLD
        JMP     4,3
LODERR: ELEF    2,6,0
        .SYSTM
        .ERTN
COUNT:  0
HOLD3:  0
CALLED: 0
        .END
```

Glossary of Terms

A/D	analog to digital convertor
aliasing	the phenomena whereby oscillations occur in the reconstructions due to an attempt to reconstruct spatial frequencies within the image which are higher than the maximum sampling frequency of the transmission measurements
'average' atomic number	that atomic number (not necessarily integer) that would correspond to the measured photoelectric cross section of the atomic mixture
beam analyser disk	the rotating disk used in the experiment which performed alternating selective filtration on the x-ray tube spectrum
CRT	cathode ray tube
CT	computerized tomography
Compton image	the reconstructed image of the Compton attenuation coefficients within the scanned slice
Compton line integral	the line integral of the Compton attenuation coefficients along the ray path measured
dark current	the current measured by the detector when the x-ray tube is off
data mapping	the operation of taking the soft and hard spectrum transmission measurements and determining Compton and photoelectric line integrals
dose	radiation energy deposited per gram of tissue
dose/energy detected	the ratio of the surface dose absorbed by the patient to the energy detected by the detector. A figure-of-merit with dimensions gm^{-1}
electron beam current	electron current accelerated onto the x-ray tube anode target
flood current	current measured by the detector when the x-ray tube is on and no target is within the beam (I_o)

fractional transmission	the ratio of the current measured from detected x-rays with the patient in the beam (I), to when there is no patient in the beam (I_o)
Gibb's phenomenon	an oscillation within the reconstructed image, similar to aliasing
Hanning-weighted ramp-filter backprojection	the standard method of tomographic reconstruction (see Appendix A)
HV	high voltage
kVp	peak kilovoltage of the bremsstrahlung x-ray spectrum
MGH	Massachusetts General Hospital
Monte Carlo method	a photon transport simulation method which simulates the individual histories of photons
photoelectric image	the reconstructed image of the photoelectric + Rayleigh attenuation coefficients within the scanned slice
photoelectric line integral	the line integral of the photoelectric + Rayleigh attenuation coefficients along the ray path measured
projection current	the current measured by the detector when the x-ray tube is on and the patient is within the beam (I)
pulse encoder	a device used on the rotating table which generates 500 logic level pulses every degree of rotation
reconstruction	a method by which x-ray transmission measurements in a scanned slice are solved simultaneously to determine the attenuation coefficients versus position within the scanned slice
ring artifact	an artifact within a reconstructed image which appears as a circle or ring
scan	the process by which transmission measurements are performed in 360° on an unknown target
sensitivity factor	a figure-of-merit developed to quantify the fraction of the transmitted and detected x-rays which are sensitive to changes in the photoelectric + Rayleigh attenuation coefficient

statistical uncertainty	uncertainty in the x-ray transmission measurement only due to Poisson counting statistics
streak artifact	an artifact within a reconstructed image which appears as a line across the image. Usually due to a detector discharge
tomochemistry	the method by which information on the 'average' atomic composition and electron density are obtained by x-ray computerized tomography
tomography	the method of x-ray transmission scanning of a slice of an unknown object
transmission measurement	see fractional transmission
Tretiak condition	the condition which states the number of angular views required in a CT scan to obtain a faithful reconstruction of the unknown object

List of Symbols

D/	the dose per energy detected. A figure-of-merit defined by Eq. (2.1B.3)
F	the fraction of the x-ray energy emitted by the x-ray tube which could have been detected by the detector which does get detected by the detector. (After losses in the filter, patient, detector inefficiencies, etc.) A figure-of-merit defined by Eq. (2.1B.4)
I	the current measured by the detector
S	the sensitivity factor. Defined in the glossary and by Eq. (2.1B.5)
Z	atomic number
μ	attenuation coefficient (macroscopic cross section)

All other symbols are defined within the text

References

A.1 R.E. Alvarez and A. Macovski, "Energy-Selective Reconstructions in X-ray Computerized Tomography", Phys. Med. Biol., 22-5, pp. 733-744, 1976.

A.2 R.E. Alvarez and A. Macovski, "X-ray Spectral Decomposition Imaging System", United States Patent 4,029,963, June 14, 1977.

A.3 D.E. Avrin, A. Macovski, and L.M. Zatz, "Clinical Application of Compton and Photo-Electric Reconstruction in Computed Tomography: Preliminary Results", Investigative Radiology, 13, pp. 217-222, 1978.

A.4 R.E. Alvarez and E. Seppi, "A Comparison of Noise and Dose in Conventional and Energy Selective Computed Tomography", IEEE Transactions on Nuclear Science, NS-26-2, 1979.

A.5 G.D. Alkhazov, A.P. Kower, and A.A. Vorolev, "Ionization Fluctuations and Resolution of Ionization Chambers and Semiconductor Detectors", Nucl. Inst. and Methods, 48, pp. 1-12, 1967.

A.6 R.E. Alvarez and A. Macovski, "Noise and Dose in Energy Dependent Computerized Tomography", Proc. Soc. Photo-Optical Instr. Engr. 96, pp. 131-137, 1976.

A.7 L.W. Anderson, W.W. Beeman, "Electric Circuits and Modern Electronics", Holt, Rinehart, and Winston, Inc., New York, 1973.

B.1 R.A. Brooks, "A Quantitative Theory of the Hounsfield Unit and Its Application to Dual Energy Scanning", Journal of Computer Assisted Tomography, 1-4, pp. 487-493, 1977.

B.2 M.J. Bergren, S.A. Johnson, J.F. Greenleaf, "A method for selective tissue and chemical element three-dimensional reconstructive imaging from radiographic film and roentgenvideo images". Digest of Papers. Optical Society of America Topical Meeting on Image Processing for 2-D and 3-D Reconstruction from Projections: Theory and Practice in Medicine and the Physical Sciences. August 4-7, Stanford, California, 1975.

B.3 R. Bracewell, "Two-Dimensional Aerial Smoothing in Radio Astronomy", Aust. J. Phys., 9, pp. 297-314, 1956.

B.4 W. Bambynek, B. Crasemann, R.W. Fink, H.U. Freund, H. Mark, C.D. Swift, R.E. Price, and P.V. Rao, "X-ray Fluorescence Yields, Auger, and Coster-Kronig Transition Probabilities", Review Modern Physics, 44, p. 716, 1972.

B.5 D.P. Boyd, "Instrumentation Considerations for Fan Beam Computerized-Tomography of the Body", High Energy Physics Laboratory Report, Stanford University, Stanford, California, 94305, 1975.

B.6 G.L. Brownell, M. Weissberger, "Split Finger Tomochemistry", Massachusetts General Hospital-Physics Research Laboratory internal report, September 1978.

B.7 G.L. Brownell, private communication, March 1980.

B.8 R. Bracewell, "The Fourier Transform and its Applications", McGraw-Hill, New York, 1965.

B.9 T.F. Budinger, G.T. Gullberg, "Three-dimensional Reconstruction in Nuclear Emission Imaging", IEEE Trans. NS-21-3, p. 2, 1974.

B.10 H.H. Barrett, W. Swindell, "Analog Reconstruction Methods for Transaxial Tomography", Proceedings of the IEEE, 65-1, January 1977.

B.11 R.B. Blackwell and J.W. Tukey, "The Measurement of Power Spectra", Dover Publications, New York, 1958.

B.12 T. Baumeister, E.A. Avallone, T. Baumeister III, "Mark's Standard Handbook for Mechanical Engineers", 8th edition, McGraw-Hill Book Co., New York, 1978.

B.13 J.W. Boag, "Ionization Chambers", in Radiation Dosimetry, volume 2, second edition, F.H. Attix, W.C. Roesch, editors, Academic Press, New York, 1966.

B.14 P.R. Bevington, "Data Reduction and Error Analysis for the Physical Sciences", McGraw-Hill, New York, 1969.

B.15 K.A. Brownlee, "Statistical Theory and Methodology in Science and Engineering", Second ed., John Wiley and Sons, New York, 1965.

B.16 R.A. Brooks, G. DiChiro, "Beam Hardening in X-ray Reconstructive Tomography", Phys. Med. Biol., 21, pp. 390-398, 1976.

B.17 J.W. Boag, "General Recombination in Ionization Chambers with Spatially Non-uniform Ionization Intensity - Two Spectra Cases", Int. J. Radiation Phys. Chem, 7, pp. 243-249, 1975.

B.18 R.B. Blackman and J.W. Tukey, "The Measurement of Power Spectra", Dover Publications, New York, 1958.

C.1 Z.H. Cho, C.M. Tsai, and G. Wilson, "Study of Contrast and Modulation Mechanisms in X-ray/Photon Transverse Axial Transmission Tomography", Phys. Med. Biol., 20-6, pp. 879-889, 1975.

C.2 A. Cormack, "Representation of a Function by its Line Integrals, with some Radiological Applications", J. Appl. Physics, 34-9, pp. 2722-2727, 1963.

C.3 A. Cormack, "Representation of a Function by its Line Integrals, with some Radiological Applications", J. Appl. Physics, 35-10, pp. 2908-2913, 1964.

C.4 D.A. Chesler, S.J. Riederer, and N.J. Pelc, "Noise Due to Photon Counting Statistics in Computed X-Ray Tomography", J. Comput. Assist. Tomogr., 1-1, pp. 64-74, 1977.

C.5 D.A. Chesler, S. Aronow, J.E. Correll, S. Riederer, and N. Pelc, "Statistical Properties and Simulation Studies of Transverse Section Algorithms", in Reconstruction Tomography in Diagnostic Radiology and Nuclear Medicine, Edited by M.M. Ter-Pergossian, University Park Press, Baltimore MD, 1977.

C.6 L.L. Carter, E.D. Cashwell, "Particle-Transport Simulation with the Monte Carlo Method", Technical Information Center, Office of Public Affairs, USERDA, 1975.

C.7 G.L. Clark, "Applied X-rays", McGraw Hill Book Company, New York, 1955.

C.8 G.L. Clark, "The Encyclopedia of X-Rays and Gamma Rays", Reinhold Publishing Corp., New York, 1963.

C.9 D.A. Chesler, "Positron Tomography and Three-Dimensional Reconstruction Techniques" in Tomographic Imaging in Nuclear Medicine, ed., G.S. Freedman, Soc. Nucl. Med., New York, 1973.

C.10 D.A. Chesler and S.J. Riederer, "Ripple Suppression During Reconstruction in Transverse Tomography", Phys. Med. Biol., 20, pp. 632-636, 1975.

C.11 "CRC Handbook of Chemistry and Physics", R.C. Weast, ed., 60th edition, CRC Press Inc., Boca Raton, Florida, 1980.

D.1 L. Dubal and U. Wiggli, "Tomochemistry of the Brain", Journal of Computer Assisted Tomography, 1-3, 1977.

D.2 G. DiChiro and R.A. Brooks, "The 1979 Nobel Prize in Physiology or Medicine", Science, 206-4422, pp. 1060-1062, 1979.

D.3 C.M. Davidson, "Alpha, Beta, and Gamma Spectroscopy", ed. K. Sieghahn, North-Holland Publishing Co., Amsterdam, 1964.

D.4 O.L. Deutsch, B.W. Murray, and G.L. Brownell, "Calculation of Scattered Signal Background in Whole Body Tomographic Imaging", Massachusetts General Hospital-Physics Research internal report, 1976.

D.5 P.J. Davis, "Interpolation and Approximation", Blaisdell Publ. Co., New York, 1963.

D.6 J.P. Den Hartog, "Advanced Strength of Materials", McGraw-Hill, New York, 1952.

D.7 C. Daniel, "Fitting Equations to Data-Computer Analysis of Multifactor Data for Scientists and Engineers", Wiley-Interscience, New York, 1971.

D.8 D.J. Drost and A. Fenster, "Experimental Dual Xenon Detectors for Quantitative CT and Spectral Artifact Correction", Med. Phys., 7-12, pp. 101-107, 1980.

D.9 N.A. Dyson, "Characteristic X-rays - A Still Developing Subject", Phys. Med. Biol., 20, pp. 1-29, 1975.

D.10 Data General, "Users Manual FORTRAN IV", document 093-000053-07, Data General Corporation, 1974.

E.1 U. Elsasser and P. Rüegsegger, "Bone Densitometry with the Aid of Computerized Transaxial Tomography", Am. J. Roentgenol., 126, pp. 1275-1277, 1976.

E.2 R. Evans, "The Atomic Nucleus", McGraw-Hill Book Company, Inc., New York, 1955.

E.3 R.M. Eisberg, "Fundamentals of Modern Physics", John Wiley and Sons, Inc., New York, 1961.

E.4 C.J. Everett, E.D. Cashwell, G.D. Turner, "A New Method of Sampling the Klein-Nishina Probability Distribution for all Incident Photon Energies Above 1 keV", Los Alamos Scientific Laboratory Report LA-4663, 1971.

F.1 A. Fenster, "Split Xenon Detector for Tomochemistry in Computed Tomography", J. Comput. Assist. Tomagr., 2, pp. 243-252, 1978.

F.2 R.W. Fink, R.C. Jopson, H. Mark, and C.D. Swift, "Atomic Fluorescence Yields", Reviews of Modern Physics, 38-3, pp. 513-540, 1966.

G.1 H.K. Genant and D. Boyd, "Quantitative Bone Mineral Analysis Using Dual Energy Computed Tomography", Invest. Radiol., 12, pp. 545-551, 1977.

G.2 R. Gordon and G.T. Herman, "Reconstruction of Pictures from Their Projections", Comm. ACM, 14, p. 552, 1971.

G.3 R. Gordon, R. Bender, and G.T. Herman, "Algebraic Reconstruction Techniques (ART) for Three-Dimensional Electronmicroscopy and X-ray Photography", J. Theo. Bio., 28, P. 471, 1970.

G.4 M. Goitein, "Three-Dimensional Density Reconstructions from a Series of Two-Dimensional Projections", Nuc. Inst. and Meth., 101, p. 509, 1971.

G.5 Glanville, "The Plastic Engineers Data Book", Industrial Press, Inc., 1971.

G.6 A. Gottschalk and R.N. Beck, "Fundamental Problems in Imaging", Charles C. Thomas, Publisher, Springfield, Ill., 1968.

H.1 G.N. Hounsfield, "Computerized Transverse Axial Scanning (Tomography): Part I. Description of System", Br. J. Radiology 46, pp. 1016-1022, 1973.

H.2 H. Hill, personal communication, March 1980.

H.3 E.J. Hall, "Radiobiology for the Radiologist", Harper and Row, Hagerstown, Maryland, 1973.

H.4 J.H. Hubbell, "Photon Mass Attenuation and Mass Energy-Absorption Coefficients for H, C, N, O, Ar and Seven Mixtures from 0.1 keV to 20 MeV", Radiation Research, 70, pp. 58-81, 1971.

H.5 W. Heitler, "The Quantum Theory of Radiation", Clarendon Press, Oxford, England, 3rd Edition, 1954.

H.6 G.T. Herman and S.W. Rowland, " SNARK 77, A Programming System for Image Reconstruction From Projections", Technical Report Number 130, State University of New York at Buffalo, Department of Computer Science, 1978.

H.7 R.W. Hamming, "Numerical Methods for Scientists and Engineers", McGraw-Hill, New York, 1962.

H.8 A.F. Henry, "Nuclear-reactor Analysis", MIT Press, Cambridge, Mass. 1975.

H.9 F.B. Hildebrand, "Advanced Calculus for Applications", Prentice-Hall Inc., Englewood Cliffs, N.J., 1962.

H.10 F.B. Hildebrand, "Introduction to Numerical Analysis", McGraw-Hill, New York, 1956.

I.1 I. Isherwood, B.R. Pullan, R.A. Rutherford, and F.A. Strang, "Electron Density and Atomic Number Determination by Computed Tomography", Br. J. Radiology, 50, pp. 613-619, 1977.

I.2 International Commission on Radiological Protection, "Report of the Task Group on Reference Man", ICRP Publication 23, Permagon Press, Oxford, England, 1975.

I.3 IBM Corporation, "System/360 Scientific Subroutine Package, Version III, Programmer's Manual", IBM Corporation, White Plains, N.Y., 1968.

J.1 B. Jacobson and J.G. Webster, "Medicine and Clinical Engineering", Prentice-Hall Inc., Englewood Cliffs, New Jersey, p. 418, 1977.

J.2 J.D. Jackson, "Classical Electrodynamics", 2nd edition, John Wiley and Sons, Inc., New York, 1975.

J.3 P.M. Joseph and R.D. Spital, "A Method for Correcting Bone Induced Artifacts in Computed Tomography Scanners", J. Computer Asst. Tomogr., 2, pp. 100-109, 1978.

J.4 P.F. Judy, "The Line Spread Function and Modulation Transfer Function of a Computed Tomographic Scanner", Med. Phys., 3-4, pp. 233-236, 1976.

K.1 F. Kelcz, P.M. Joseph, and S.K. Hilal, "Noise Considerations in Dual Energy CT Scanning", Medical Physics, 6-5, pp. 418-425, 1979.

K.2 K. Kerrfott, "RELSLIB3 Study of Amount of Iodinated Contrast Agent Required for CT Imaging", Massachusetts General Hospital-Physics Research Laboratory internal report, August 30, 1979.

K.3 G.F. Knoll, "Radiation Detection and Measurement", John Wiley and Sons, Inc., New York, 1979.

K.4 D.B. Kay, J.W. Keyes, and W. Simon, "Radionuclide Tomographic Image Reconstruction Using Fourier Transform Techniques", J. Nuc. Med., 15, p. 981, 1974.

L.1 D.B. Laning, G.L. Brownell, and D.D. Lanning, "Engineering Optimization of a Prototype Tomochemistry Scanner", Proceedings of the Topical Meeting on Computational Methods in Nuclear Engineering, Williamsburg, Virginia, April 1979.

L.2 D.B. Laning, "Experimental and Monte Carlo Studies of Patient Dose Received from Computerized Axial Tomography", S.M. Thesis, Massachusetts Institute of Technology, 1978.

L.3 P. Lorrain and D.R. Corson, "Electromagnetic Fields and Waves", W.H. Freemand and Company, San Francisco, 1970.

L.4 C.M. Lederer and V.S. Shirley, eds., "Table of Isotopes", 7th ed., Wiley-Interscience Publication, John Wiley and Sons, Inc., New York, 1978.

L.5 C. Lanczos, "Applied Analysis", Prentice-Hall, Englewood Cliffs, N.J., 1956.

L.6 W.E. Lawrence and E.E. Johnson, "Design for Limiting Explosion Damage", Chemical Engineering, January 1974.

M.1 W.D. McDavid, R.G. Waggener, M.J. Dennis, V.J. Sank, and W.H. Payne, "Estimation of Chemical Composition and Density from Computed Tomography Carried Out at a Number of Energies", Investigative Radiology, 12, pp. 189-194, 1977.

M.2 W.V. Mayneord, "Significance of the Roentgen", Acta Union Internationalis Contra Cancrum, 2, pp. 271-282, 1967.

M.3 E.C. McCullough, H.J. Baker, Jr., O.W. Houser, et al., "An Evaluation of the Quantitative and Radiation Features of a Scanning X-ray Transverse Axial Tomograph: the EMI Scanner", Radiology, 111, pp. 709-715, June 1974.

M.4 M.R. Millner, W.D. McDavid, R.G. Waggener, M.J. Dennis, W.H. Payne, and V.J. Sank, "Extraction of Information from CT Scans at Different Energies", Medical Physics, 6-1, pp. 70-71, 1979.

M.5 M.R. Millner, W.H. Payne, R.G. Waggener, W.D. McDavid, M.J. Dennis, and V.J. Sank, "Determination of Effective Energies in CT Calibration", Medical Physics, 5-6, pp. 543-543, 1978.

M.6 H.V. Malmstadt, C.G. Enke, and S.R. Crouch, "Electronic Measurements for Scientists", W.A. Benjamin Inc., Reading, Mass. 1974.

M.7 E.C. McCullough, "Photon Attenuation in Computed Tomography", Medical Physics, 2, pp. 307-320, 1975.

M.8 W.H. Marshall, R.E. Alvarez, A. Macovski, J. Healy, and L.M. Zatz, "Dual Kilovoltage at Computed Tomography: A Pre-reconstruction Method for Estimation of Effective Atomic Number and Electron Density", Neuroradiology, 16, pp. 605-606, 1978.

M.9 A. Macovski, R.E. Alvarez, J.L.-H. Chan, J.P. Stonestrom, and L.M. Zatz, "Energy Dependent Reconstruction in X-ray Computerized Tomography", Comput. Biol. Med., 6, pp. 325-336, 1976.

M.10 C.H. Macgillavry and G.D. Rieck, "International Tables for X-Ray Crystallography", Vol. III, The Kynoch Press for the International Union of Crystallography, Birmingham, England, 1962.

M.11 N. Mika, K.H. Reiss, "Tabelen zur Rontgendiagnostik, 1, Siemens Aktiengesellschaft", 1976.

M.12 W.D. McDavid, R.G. Waggener, W.H. Payne, and M.J. Dennis, "Spectral Effects on Three-dimensional Reconstruction from X-rays", Med. Phys., 2, pp. 321-324, 1975.

M.13 W.D. McDavid, R.G. Waggener, W.H. Payne, and M.J. Dennis, "Correction for Spectral Artifacts in Cross-Sectional Reconstruction from X-rays", Med. Phys., 4, pp. 54-57, 1977.

M.14 D.W. Marquardt, "An Algorithm for Least Squares Estimation of Nonlinear Parameters", Journal Society Industrial Appl. Math., 11, pp. 431-441, 1963.

M.15 W.H. Marshall, R. Alvarez, A. Macovski, and E. Seppi, "Dual Kilovoltage Applied to Computed - Tomography - Determination of Electron-Density, Effective Atomic Number and Optimum Reconstruction keV", Invest. Radiol., 14, pp. 400-401, 1979.

N.1 Department of the Navy, "Petry Formula - Design of Protective Structures", Navy Document P-51, Bureau of Yards and Docks, Washington, D.C., 1950.

0.1 W.H. Oldendorf, "Isolated flying spot detection of radiodensity discontinuities - displaying the in ernal structural pattern of a complex object", I.R.E. Transactions on Bio-medical Electronics, 8, pp. 68-72, 1961.

0.2 A.V. Oppenheim and R.W. Schafer, "Digital Signal Processing", Prentice-Hall, Englewood Cliffs, N.J., 1975.

P.1 M.E. Phelps, M.H. Gado, and E.J. Hoffmann, "Correlation of Effective Atomic Number and Electron Density with Attenuation Coefficients Measured with Polychromatic X-Rays", Radiology, 117, pp. 585-588, December 1975.

P.2 M.E. Phelps, E.J. Hoffman, M. Gado, et al., "Computerized transaxial transmission reconstruction tomography". [In] The Past, Present, and Future of Non-Invasive Brain Imaging, ed. by H. DeBlanc and J. Sorenson. New York, Society of Nuclear Medicine, Chapter 8, 1974.

P.3 W.H. Payne, W.D. McDavid, R.G. Waggener, M.J. Dennis, and V.J. Sank, "Extrapolation of Linear Attenuation Coefficients of Biological Materials from Diagnostic-Energy X-ray Levels to the Megavoltage Range", Medical Physics, 4-6, pp. 505-507, 1977.

P.4 W.J. Price, "Nuclear Radiation Detection", 2nd ed., McGraw-Hill Book Co., New York, 1964.

P.5 A. Papoulis, "The Fourier Integral and its Applications", McGraw-Hill, New York, 1962.

R.1 P. Rüegsegger, U. Elsasser, M. Anliker, H. Gnehm, H. Kind, and A. Prader, "Quantification of Bone Mineralization Using Computed Tomography", Radiology, 121, pp. 93-97, 1976.

R.2 R.A. Rutherford, B.R. Pullan, and I. Isherwood, "Measurement of Effective Atomic Number and Electron Density Using an EMI Scanner", Neuroradiology, 11, pp. 15-21, 1976.

R.3 R.A. Rutherford, B.R. Pullan, and I. Isherwood, "X-Ray Energies for Effective Atomic Number Determination", Neuroradiology, 11, pp. 23-28, 1976.

R.4 J. Radon, "Uber die Bestimmung von Funktionen durch ihre Integralwärte längs Gewisser Männigfaltigkeiten", Ber. Verk. Sächs. Akad., 69, p. 262, 1917.

R.5 G. Ramachandran and A. Lakshminarayanan, "Three-dimensional Reconstruction from Radiographs and Electron Micrographs: Application of Convolutions Instead of Fourier Transforms", Proc. Nat. Acad. Sci. U.S.A., 68-9, pp. 2236-2240, 1971.

R.6 R.A. Rutherford, B.R. Pullan, and I. Isherwood, "Calibration and Response of an EMI Scanner", Neuroradiology, 11, pp. 7-13, 1976.

R.7 S.J. Riederer, "Computer Simulation Studies in Transverse Tomography", S.M. Thesis, Massachusetts Institute of Technology, 1975.

R.8 B.R. Rossi and H.H. Staub, "Ionization Chambers and Counters - Experimental Techniques", McGraw-Hill, New York, 1949.

S.1 F.W. Spiers, "Effective Atomic Number and Energy Absorption in Tissues", Brit. J. Radiology, 19, pp. 52-63, 1946.

S.2 L. Shepp and B. Logan, "Reconstructing interior head tissue from x-ray transmission", IEEE Trans. on Nucl. Sci., pp. 128-236, February 1974.

S.3 D.L. Snyder and J.R. Cox, Jr., "An Overview of Reconstructive Tomography and Limitations Imposed by a Finite Number of Projections", Reconstruction Tomography in Diagnostic Radiology and Nuclear Medicine, University Park Press, Baltimore, Md., 1977.

S.4 E. Storm, H.I. Israel, and D.W. Lier, "Bremsstrahlung Emission Measurement from Thick Tungsten Targets in the Energy Range 12 to 300 kV", Los Alamos Scientific Laboratory Report No. LA-4624, 1971 (unpublished).

S.5 B.W. Soole, "A Method of X-ray Attenuation Analysis for Approximating the Intensity Distribution at its Point of Origin of Bremsstrahlung Excited in a Thick Target by Incident Electrons of Constant Medium Energy", Phys. Med. Biol., 21-3, pp. 369-389, 1976.

S.6 E. Storm, "Calculated Bremsstrahlung Spectra from Thick Tungsten Targets", Physical Review A, 5-6, pp. 2328-2338, 1972.

S.7 P.B. Scott and J.R. Greening, "The Determination of Saturation Currents in Free-air Ionization Chambers by Extrapolation Methods", Phys. Med. Biol., 8, pp. 51-57, 1973.

S.8 L.A. Shepp and J.A. Stein, "Simulated Reconstruction Artifacts in Computerized X-Ray Tomography", Reconstruction Tomography in Diagnostic Radiology and Nuclear Medicine, Edited by M.M. Ter-Pergossian et al., University Park Press, Baltimore, Md., 1977.

T.1 C.M. Tsai and Z.H. Cho, "Physics of Contrast Mechanism and Averaging Effect of Linear Attenuation Coefficients in a Computerized Transverse Axial Tomography (CTAT) Transmission Scanner", Phys. Med. Biol., 21-4, pp. 544-559, 1976.

T.2 P. Tothill, "The Ratio of K Characteristic to Total Radiation Emitted from a Tungsten Target X-ray Tube", Br. J. Appl. Phys. (J. Phys. D), 1, pp. 1093-1107, 1968.

T.3 P.A. Tipler, "Foundation of Modern Physics", Worth Publishers, Inc., New York, 1969.

T.4 M.M. Ter Pergossian, "A Positron-Emission Transaxial Tomograph for Nuclear Imaging (PETT)", Radiology, 114-89, 1975.

T.5 O.J. Tretiak, M. Eden, and W. Simon, "Internal Structure from X-ray Images", Proc. 8th Int. Conf. on Med. and Bio. Eng., Chicago, 1969.

T.6 Texas Instruments Inc. Engineering Staff-Semiconductor Group, "The TTL Data Book for Design Engineers", 2nd Edition, Texas Instruments Incorporated, Dallas, Tx., 1976.

T.7 S. Timoshenko and D.H. Young, "Elements of Strength of Materials", 5th Edition, D. Van Nostrand Company, New York, 1968.

V.1 W.J. Veigele and E. Briggs, "X-ray Cross Section Compilation from 0.1 keV to 1 MeV", DNA 2433F (formerly DASA 2433) Volume 1, Revision 1, KN-71-431(R), Kaman Sciences Corporation, 1971.

V.2 C.G. Veinott, "Fractional and Subfractional Horsepower Electric Motors", McGraw-Hill, New York, 1970.

V.3 A. von Engel, "Ionized Gases", pp. 112-138, Oxford University Press, Oxford, 1965.

W.1 D.R. White, "An Analysis of the Z-dependence of Photon and Electron Interactions", Phys. Med. Biol., 22-2, pp. 219-228, 1977.

W.2 D.R. White, "The Formulation of Tissue Substitute Materials using Basic Interaction Data", Phys. Med. Biol., 22-5, pp. 889-899, 1977.

W.3 D.R. White and M. Fitzgerald, "A Tabulation of the 4th Order Polynomial Coefficients Calculated to Fit the Photon Interaction Data of 69 ICRP Reference Man Tissues", Health Physics, 33, pp. 628-633, December 1977.

W.4 J. Weber and D.J. van der Berge, "The Effective Atomic Number and the Calculation of the Composition of Phantom Materials", Brit. J. Radiol., 42, pp. 378-383, 1969.

W.5 M.A. Weissberger, R.G. Zemenhof, S. Aronow, and R.M. Near, "Computed Tomography Scanning for the Measurement of Bone Mineral in the Human Spine", J. Comput. Assist. Tomography, 2, pp. 253-268, 1978.

W.6 T. Walters, personal communication, June 1978.

W.7 T. Walters, "Status of Detector Electronics", Massachusetts General Hospital-Physics Research internal report, June 5, 1978.

Y.1 M. Yaffe, A. Fenster, and H.E. Johns, "Xenon Ionization Detectors for Fan Beam Computed Tomography Scanners", J. Comput. Assist. Tomagr., 2, pp. 419-428, 1977.